4TH APPLIED SYNTHETIC BIOLOGY IN EUROPE

EDITED BY: Jean Marie François, Fayza Daboussi and Jussi Jantti
PUBLISHED IN: Frontiers in Bioengineering and Biotechnology

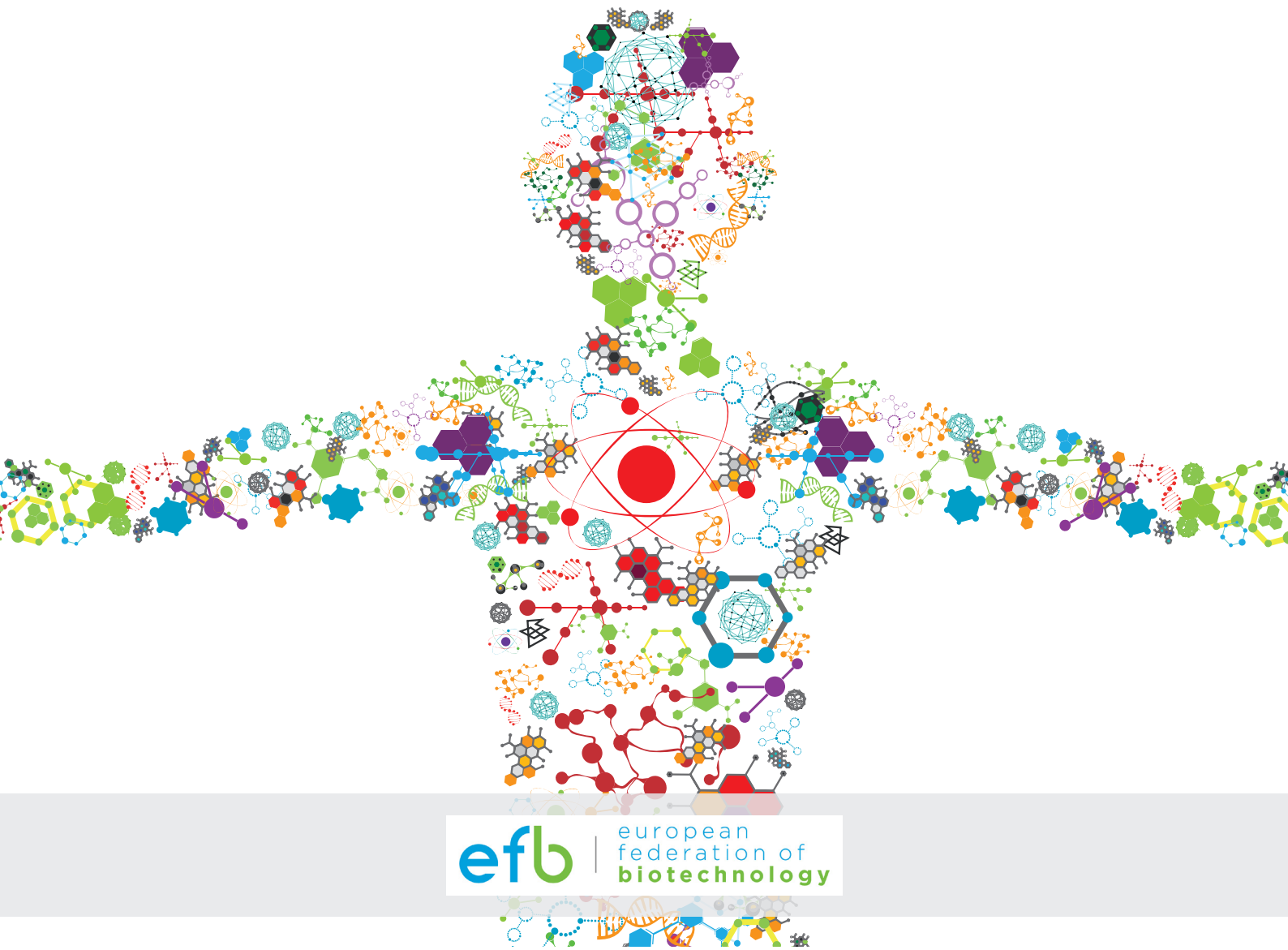

efb | european federation of biotechnology

frontiers Research Topics

ISSN 1664-8714
ISBN 978-2-88963-812-3
DOI 10.3389/978-2-88963-812-3

About Frontiers

Frontiers is more than just an open-access publisher of scholarly articles: it is a pioneering approach to the world of academia, radically improving the way scholarly research is managed. The grand vision of Frontiers is a world where all people have an equal opportunity to seek, share and generate knowledge. Frontiers provides immediate and permanent online open access to all its publications, but this alone is not enough to realize our grand goals.

Frontiers Journal Series

The Frontiers Journal Series is a multi-tier and interdisciplinary set of open-access, online journals, promising a paradigm shift from the current review, selection and dissemination processes in academic publishing. All Frontiers journals are driven by researchers for researchers; therefore, they constitute a service to the scholarly community. At the same time, the Frontiers Journal Series operates on a revolutionary invention, the tiered publishing system, initially addressing specific communities of scholars, and gradually climbing up to broader public understanding, thus serving the interests of the lay society, too.

Dedication to Quality

Each Frontiers article is a landmark of the highest quality, thanks to genuinely collaborative interactions between authors and review editors, who include some of the world's best academicians. Research must be certified by peers before entering a stream of knowledge that may eventually reach the public - and shape society; therefore, Frontiers only applies the most rigorous and unbiased reviews.
Frontiers revolutionizes research publishing by freely delivering the most outstanding research, evaluated with no bias from both the academic and social point of view. By applying the most advanced information technologies, Frontiers is catapulting scholarly publishing into a new generation.

What are Frontiers Research Topics?

Frontiers Research Topics are very popular trademarks of the Frontiers Journals Series: they are collections of at least ten articles, all centered on a particular subject. With their unique mix of varied contributions from Original Research to Review Articles, Frontiers Research Topics unify the most influential researchers, the latest key findings and historical advances in a hot research area! Find out more on how to host your own Frontiers Research Topic or contribute to one as an author by contacting the Frontiers Editorial Office: researchtopics@frontiersin.org

4TH APPLIED SYNTHETIC BIOLOGY IN EUROPE

Topic Editors:
Jean Marie François, Institut Biotechnologique de Toulouse (INSA), France
Fayza Daboussi, Institut National de la Recherche Agronomique (INRA), France
Jussi Jantti, VTT Technical Research Centre of Finland Ltd, Finland

Citation: François, J. M., Daboussi, F., Jantti, J., eds. (2020). 4th Applied Synthetic Biology in Europe. Lausanne: Frontiers Media SA. doi: 10.3389/978-2-88963-812-3

Table of Contents

frontiers in Bioengineering and Biotechnology

EDITORIAL
published: 06 May 2020
doi: 10.3389/fbioe.2020.00431

Editorial: 4th Applied Synthetic Biology in Europe

Jean Marie François[1,2]*, *Jussi Jantti*[3] *and Fayza Daboussi*[1,2]

[1] Toulouse Biotechnology Institute, Université de Toulouse, CNRS, INRA, INSA, Toulouse, France, [2] Toulouse White Biotechnology Center, UMS-INSA-INRA-CNRS, Ramonville St Agnes, France, [3] VTT Technical Research Centre of Finland, Espoo, Finland

Keywords: synthetic biology, genome engineering, metabolic engineering, evolution engineering, cell-free systems, bionanoengineering

Editorial on the Research Topic

4th Applied Synthetic Biology in Europe

The congress of Applied Synthetic Biology in Europe was the 4th of this kind to be organized under the auspices of the European Federation of Biotechnology in Toulouse from 24 to 27 October 2018. It gathered about 130 participants from all over Europe as well as some participants from Asia, Brazil, and USA. Five sessions encompassing main disciplines in Synthetic Biology were on the program, and we acknowledged receiving several contributions by many of the participants to this meeting in each of these sessions. The sessions that received the most contributions were those dealing with topics in synthetic pathways for bio (chemical) manufacturing and synthetic biology for biotechnology applications. Relevant in these reports were concerns about pathways design and reconstruction, sometimes guided by computational analysis to propose non-natural metabolic routes for maximal yield and the choice of the more appropriate microorganism as potential industrial producer. In this regard, the production of trans-cinnamate from glucose was achieved by rational engineering of L-phenylalanine accumulation in *Pseudomonas taiwensis* since this bacteria is much more tolerant than *E. coli* to this non-natural product (Otto et al.). However, toxicity of this product remains a serious bottleneck in order to reach economically viable titers and yields of *t*-cinnamate from sugars, which might be overcome by application of adaptive laboratory evolution. As a well-established microbial platform for fatty acid accumulation (Blazeck et al., 2015), the oleaginous *Yarrowia lipolytica* was engineered for *de novo* biosynthesis of odd fatty acid from inexpensive carbon source (Park et al.). The critical point in this work was to enable an endogenous supply of propionyl-CoA as the key precursor for the synthesis of these fatty acids. These authors brought this capability to the yeast cell by the expression of a modular pathway with seven enzymatic steps that employed the threonine biosynthetic route and its deamination into α-ketobutyrate. The industrial potential of this strategy will await further improvement in the specificity and activity of the decarboxylating enzyme on α-ketobutyrate as well as enhancement of carbon fluxes to propionyl-coA through metabolic engineering tools. Two other papers in this session were dedicated to implement non-natural pathways to produce bio-based products from C5 and C6 sugars at the highest yield. Bator et al. compared *in silico* and *in vivo* the synthetic capabilities of three metabolic routes, namely the xylose isomerase, the Dahms and the Weimberg pathways for xylose metabolization into a wide variety of valuable products in *Pseudomonas putida* KT2240. The computational analysis with flux balance analysis (FBA)

OPEN ACCESS

Edited and reviewed by:
Pablo Ivan Nikel,
Novo Nordisk Foundation Center for Biosustainability (DTU Biosustain), Denmark

***Correspondence:**
Jean Marie François
fran_jm@insa-toulouse.fr

Specialty section:
This article was submitted to Synthetic Biology, a section of the journal Frontiers in Bioengineering and Biotechnology

Received: *08 April 2020*
Accepted: *15 April 2020*
Published: *06 May 2020*

Citation:
François JM, Jantti J and Daboussi F (2020) Editorial: 4th Applied Synthetic Biology in Europe. Front. Bioeng. Biotechnol. 8:431. doi: 10.3389/fbioe.2020.00431

indicated highest yield of 12 out of the 14 value products by the isomerase pathway, which was confirmed *in vivo* for the production of mono-rhamnolipids and pyocyanin. While reinforcing the usefulness of FBA to guide pathway design, the limitation of these *in silico* methods is that they cannot predict best productivity and titer. Ultimately, the work showed that higher production rate and titer were obtained with the Weimberg pathway for these high value products. Product yield higher than those calculated from the stoichiometry of natural pathways can be obtained by pathway reconstruction in which loss of carbon as CO_2 is avoided, as recently shown for the construction of the "NOG" pathway (Bogorad et al., 2013) and reviewed by François et al.. Along this line, Lachaux et al. devised a cyclic pathway enabling optimal conversion of C5 and C6 carbon into glycolic acid by reallocating the function of two *E.coli kdsD* and *fsaA* genes encoding arabinose-5-P isomerase and fructose-6-P aldolase, respectively, in combination with the non-oxidative pentose pathway. Altogether, these contributions illustrate the trend of integrating systems biology, synthetic biology, and evolutionary engineering with traditional metabolic engineering to expedite the development of relevant microbial cell factories for the production of bio-based products from renewable carbon sources, as the cornerstone of the emerging Bio-Economy. However, there is still a gap to be filled in to make these strains industrially competitive and the attendant fermentation processes economically viable. Notably, better knowledge of the management of the cellular energy and redox balance by metabolic engineering as reviewed in Kalnenieks et al. for the ethanologenic bacterium *Zymomonas mobilis* and development of analytical tools for rapid screening of products yield, such as sensing and monitoring production of benzoic derivatives by mean of a biosensor (Castaño-Cerezo et al.) are important to make rapid progress in this applied field of Synthetic Biology.

Generation and investigation of biological functions can be in *in vitro* systems using cell-free systems that rests on the use of cell free protein synthesis (CFPS). Pioneered by Nirenberg and Matthaei (1961) to elucidate the genetic code, cell-free systems are gaining more and more credit in the field of Synthetic Biology as a prototype platform to engineer biological parts at levels of protein, metabolism and cell (Shimizu et al., 2006; Hodgman and Jewett, 2012; Moore et al., 2017). Cell free synthetic biology was particularly emphasized in the session "Biosciences and Bionanoengineering' with several contributions. Spice et al. reported on the synthesis and assembly of hepatitis B virus-like particles (VLP) using cell-free system prepared from *Pichia pastoris*, which can represent an alternative approach to the production of VLP for therapeutic purposes. On the other hand, Gabant and Borrero exploited cell-free protein synthesis system as a rapid method to expedite production and validation of a large set of bacteriocin, which are cataloged into a database, termed "PARAGEN1.0." Cell free system is also suggested as an alternative strategy for engineering and production of organophosphorus hydrolysing enzymes to be used to decontaminate highly toxic agricultural pesticides and chemical warfare (Thakur et al.). In addition, these authors make a thorough overview on the practice that are currently used for decontaminating environments and seawater from toxic organophosphorus compounds, emphasizing on the need to strongly enhance catalytic activity and stability of these organophosphorus hydrolysing enzymes by various bionanoengineering approaches.

Genome editing, genome engineering, and synthetic genomics are among the most disruptive technology at the heart of Synthetic Biology. A contribution to this session was a paper by Millacura et al. who report on a cell-based logic system termed ParAlleL that allows to construct complex logic circuits enable to respond to a combination of inputs. They demonstrate their concept through the construction of three simple logic circuits, a 1-bit full adder, a 1-bit subtractor, and a numeric display. Experimentally, the concept was shown by transforming *E. coli* with three out of six plasmids to make them able to survive only when precisely three antibiotics are provided. This represents an interesting way of constructing circuits from cellular populations in which logic is constructed and circuitry functionality displayed simply by the surviving cells in the presence of antibiotics. Very challenging in genetic and genome engineering is to build efficient and robust gene expression leading to high protein production, for instance. Eichmann et al. tentatively solved the problem of expression and production of so-called three difficult-to-express proteins by systematic evaluation of ribosome binding sites, N-terminal affinity tags and periplasmic translocation sequences to which was fused green fluorescent protein (GFP) to identify high producers by fluorescence activated cell screening (FACS). Large combinatorial libraries of genes were expressed and the outcome was measured in a platform monitoring expression automatically. Though yields were still low, this work unraveled that TAT-dependent signal sequence from *E. coli* YahJ for expression is recognized in the fast-growing bacterium *Vibrio natriegens*, which could be used as an industrial platform for production of recombinant proteins.

This editorial can be concluded by referring to the article by El Karoui et al. which reports on a workshop that brought together British academics and industrialists at the University of Edinburgh to discuss the future of synthetic biology. If processes that underlie all living systems can be manipulated, modified or reshaped using the tools of Synthetic Biology, then in return we need to take the public with us on this journey to create a productive dialogue about the work we can do and the impact it can have on our world and our way of life.

AUTHOR CONTRIBUTIONS

All authors listed have made a substantial, direct and intellectual contribution to the work, and approved it for publication.

REFERENCES

Blazeck, J., Hill, A., Jamoussi, M., Pan, A., Miller, J., and Alper, H.S. (2015). Metabolic engineering of *Yarrowia lipolytica* for itaconic acid production. *Metab. Eng.* 32, 66–73. doi: 10.1016/j.ymben.2015.09.005

Bogorad, I. W., Lin, T. S., and Liao, J. C. (2013). Synthetic non-oxidative glycolysis enables complete carbon conservation. *Nature* 502, 693–697. doi: 10.1038/nature12575

Hodgman, C. E., and Jewett, M. C. (2012). Cell-free synthetic biology: thinking outside the cell. *Metab. Eng.* 14, 261–269. doi: 10.1016/j.ymben.2011.09.002

Moore, S. J., Macdonald, J. T., and Freemont, P. S. (2017). Cell-free synthetic biology for *in vitro* prototype engineering. *Biochem. Soc. Trans.* 45, 785–791. doi: 10.1042/BST20170011

Nirenberg, M. W., and Matthaei, J. H. (1961). The dependence of cell-free protein synthesis in *E. coli* upon naturally occurring or synthetic polyribonucleotides. *Proc. Natl. Acad. Sci. U.S.A.* 47, 1588–1602.

Shimizu, Y., Kuruma, Y., Ying, B. W., Umekage, S., and Ueda, T. (2006). Cell-free translation systems for protein engineering. *FEBS J.* 273, 4133–4140. doi: 10.1111/j.1742-4658.2006.05431.x

Conflict of Interest: JJ was employed by company VTT Technical Research Centre of Finland.

The remaining authors declare that the research was conducted in the absence of any commercial or financial relationships that could be construed as a potential conflict of interest.

frontiers in Bioengineering and Biotechnology

ORIGINAL RESEARCH
published: 20 November 2019
doi: 10.3389/fbioe.2019.00312

Rational Engineering of Phenylalanine Accumulation in *Pseudomonas taiwanensis* to Enable High-Yield Production of *Trans*-Cinnamate

*Maike Otto[1], Benedikt Wynands[1], Christoph Lenzen[2], Melanie Filbig[2], Lars M. Blank[2] and Nick Wierckx[1]**

[1] Institute of Bio- and Geosciences (IBG-1: Biotechnology), Forschungszentrum Jülich GmbH, Jülich, Germany, [2] Institute of Applied Microbiology, Rheinisch-Westfälische Technische Hochschule (RWTH) Aachen University, Aachen, Germany

OPEN ACCESS

Edited by:
Jean Marie François,
UMS3582 Toulouse White Biotechnology (TWB), France

Reviewed by:
Jian-Ming Liu,
Technical University of Denmark, Denmark
John A. Morgan,
Purdue University, United States

***Correspondence:**
Nick Wierckx
n.wierckx@fz-juelich.de

Specialty section:
This article was submitted to Synthetic Biology, a section of the journal Frontiers in Bioengineering and Biotechnology

Received: 11 September 2019
Accepted: 23 October 2019
Published: 20 November 2019

Citation:
Otto M, Wynands B, Lenzen C, Filbig M, Blank LM and Wierckx N (2019) Rational Engineering of Phenylalanine Accumulation in Pseudomonas taiwanensis to Enable High-Yield Production of Trans-Cinnamate. Front. Bioeng. Biotechnol. 7:312. doi: 10.3389/fbioe.2019.00312

Microbial biocatalysis represents a promising alternative for the production of a variety of aromatic chemicals, where microorganisms are engineered to convert a renewable feedstock under mild production conditions into a valuable chemical building block. This study describes the rational engineering of the solvent-tolerant bacterium *Pseudomonas taiwanensis* VLB120 toward accumulation of L-phenylalanine and its conversion into the chemical building block *t*-cinnamate. We recently reported rational engineering of *Pseudomonas* toward L-tyrosine accumulation by the insertion of genetic modifications that allow both enhanced flux and prevent aromatics degradation. Building on this knowledge, three genes encoding for enzymes involved in the degradation of L-phenylalanine were deleted to allow accumulation of 2.6 mM of L-phenylalanine from 20 mM glucose. The amino acid was subsequently converted into the aromatic model compound *t*-cinnamate by the expression of a phenylalanine ammonia-lyase (PAL) from *Arabidopsis thaliana*. The engineered strains produced *t*-cinnamate with yields of 23 and 39% Cmol Cmol^{-1} from glucose and glycerol, respectively. Yields were improved up to 48% Cmol Cmol^{-1} from glycerol when two enzymes involved in the shikimate pathway were additionally overexpressed, however with negative impact on strain performance and reproducibility. Production titers were increased in fed-batch fermentations, in which 33.5 mM *t*-cinnamate were produced solely from glycerol, in a mineral medium without additional complex supplements. The aspect of product toxicity was targeted by the utilization of a streamlined, genome-reduced strain, which improves upon the already high tolerance of *P. taiwanensis* VLB120 toward *t*-cinnamate.

Keywords: *Pseudomonas*, metabolic engineering, *trans*-cinnamic acid, L-phenylalanine, rational engineering, glycerol, glucose

INTRODUCTION

Trans-cinnamate is an aromatic compound naturally occurring in plants, where it serves as central intermediate for the biosynthesis of a large number of substances, including coumarins, flavonoids, and phenylpropanoids (Chemler and Koffas, 2008; Vogt, 2010). It is widely used in industry for flavoring, pharmaceuticals, and cosmetics (Fausta et al., 1999; De et al., 2011; Vargas-Tah and Gosset, 2015) and can serve as precursor for bio-based drop-in chemicals such as styrene (McKenna and Nielsen, 2011) or for value-added chemicals such as the stilbene pinosylvin (van Summeren-Wesenhagen and Marienhagen, 2015). Commercial production currently happens from petroleum-based, non-renewable feedstocks in processes that demand high amounts of energy and release toxic by-products (Bruckner, 2010; Tietze et al., 2015). This comes along with increasing apprehension on global climate change and depleting aromatic fossil resources. Hence, there are both environmental and economic drivers for alternative synthesis routes.

Microbial production by whole-cell biocatalysis represents a less environmentally demanding alternative to the common and well-established petrochemical processes (Hatti-Kaul et al., 2007; Becker and Wittmann, 2012; Cho et al., 2015; Kallscheuer et al., 2019). Herein, microbes can be supplied with renewable feedstocks (e.g., glucose, glycerol, or lignin, Kohlstedt et al., 2018; Johnson et al., 2019), and metabolic conversion enables the synthesis of diverse products under mild production conditions, either via native enzymes (Hosseinpour Tehrani et al., 2019) or by heterologous expression of foreign genes (Kallscheuer et al., 2019). In plants, *t*-cinnamate is formed through deamination of the amino acid L-phenylalanine by phenylalanine ammonia-lyase (PAL) (Cochrane et al., 2004; Huang et al., 2010), and can be further converted into the *cis*-isoform by photoisomerization (Salum and Erra-Balsells, 2013). While only the *trans*-isoform is involved in biosynthesis pathways in plants (Salum and Erra-Balsells, 2013), *cis*-cinnamate displays higher anti-bacterial activities (Chen et al., 2011). The heterologous synthesis of this enzyme in various microorganisms, including *Escherichia coli* (Vargas-Tah et al., 2015; Bang et al., 2018) or *Streptomyces lividans* (Noda et al., 2011) enabled *t*-cinnamate production. Product toxicity is a limiting factor for the efficiency of many microbial production process with these hosts (McKenna and Nielsen, 2011). From a biochemical engineering perspective, it is important to "begin with the end in mind" when developing microbial production strains (Straathof et al., 2019), and product toxicity is one important aspect for this.

Bacteria of the genus *Pseudomonas* are considered as promising alternative host to produce aromatics such as *t*-cinnamate. Their robust growth behavior and metabolic versatility recently enabled the synthesis of many different industrially relevant compounds, including a variety of aromatics (Nijkamp et al., 2007; Kuepper et al., 2015; Wynands et al., 2018), rhamnolipids (Tiso et al., 2017), terpenes (Mi et al., 2014), or prodiginines (Domröse et al., 2015). This is in particular due to their high stress tolerance, which has been extensively investigated in the past (Kusumawardhani et al., 2018). Pseudomonads are able to thrive under both endogenous and exogenous oxidative stress, enabled by their particular central carbon metabolism architecture (Chavarría et al., 2013; Nikel et al., 2015). Furthermore, they are equipped with a variety of native tolerance mechanisms that allow growth in the presence of highly toxic compounds (Sardessai and Bhosle, 2002; Segura et al., 2012). For this, Pseudomonads are able to adapt the composition of the inner and outer membrane to lower the permeability for substrates and they can increase their production of energy to fuel energy-consuming tolerance mechanisms (Isken and de Bont, 1998; Ramos et al., 2002; Belda et al., 2016). Some strains of *Pseudomonas* additionally express solvent efflux pumps that can actively extrude toxic compounds from the inner membrane (Kieboom et al., 1998) and degrade solvents such as toluene (Ramos et al., 2002) or styrene (Velasco et al., 1998). Additional transporters confer higher resistance to further aromatic molecules like *p*-hydroxybenzoate or *p*-coumarate (Verhoef et al., 2010; Calero et al., 2018). The native capabilities of *Pseudomonas* species thus form a strong basis for a biocatalytic process for *t*-cinnamate synthesis by expanding process options due to reduced product toxicity.

To further exploit its potential as industrial production strain, we recently enhanced the bioprocess features of the solvent-tolerant strain *Pseudomonas taiwanensis* VLB120 by successive feature reduction (Wynands et al., 2019). The deletion of redundant genomic elements such as proviral segments, genes for biofilm formation and flagella expression and the megaplasmid pSTY resulted in strains with 15% enhanced growth rates and increased biomass yields, thereby improving the overall performance of the strain under bioprocess conditions. In addition, genes encoding for the efflux pump TtgGHI located on the pSTY plasmid were re-integrated into the chromosome of the genome-reduced chassis (GRC) strains to maintain tolerance enabled by this efflux pump. These modifications, in combination with inherent tolerance traits, make the engineered strains promising hosts to efficiently synthesize aromatic compounds like *t*-cinnamate, as well as potential hydrophobic derivatives such as styrene or stilbenes.

The potential of *Pseudomonas* species for *t*-cinnamate production has been demonstrated in a strain of *P. putida* S12 by the expression of PAL from *Rhodosporidium toruloides* (Nijkamp et al., 2005). Here, enhanced precursor supply was realized by mutagenesis and subsequent selection on the toxic analog *m*-fluoro-phenylalanine, leading to the production of 5 mM *t*-cinnamate with a yield of 6.7% Cmol Cmol^{-1}. However, although genomic analysis of this strain provided leads to enhance the flux through the shikimate pathway in *P. taiwanensis* VLB120 (Wynands et al., 2018), the genetic rearrangements enabling the enhanced flux specifically toward L-phenylalanine have not been determined. We recently reported a study on phenol production from L-tyrosine in *P. taiwanensis* VLB120, where 22 mutations in 50 different strains delivered a comprehensive insight on the rational engineering of L-tyrosine accumulation (Wynands et al., 2018). In the most productive strain, five genes involved in the degradation of aromatic intermediates and the gene *pykA* were deleted to increase the precursor supply for the synthesis of aromatic amino acids. The flux through the shikimate pathway

was further enhanced by genomic modifications of genes at their native chromosomal locus resulting in a strain able to accumulate up to 2.8 mM of L-tyrosine from 20 mM glucose.

The aim of this study was to build on this knowledge to redirect the enhanced flux to L-tyrosine in *P. taiwanensis* GRC3 Δ5Δ*pykA*-tap (Wynands, 2018) toward L-phenylalanine, given the close relation of their biosynthesis pathways, and thereby expanding the potential product range. Furthermore, the superior tolerance of the streamlined *P. taiwanensis* GRC toward high concentrations of *t*-cinnamate was assessed. Routes involved in L-phenylalanine degradation were deleted, leading to L-phenylalanine accumulation. Titers were further increased by an additional overexpression of feedback-resistant versions of the bottleneck enzymes AroG and PheA. Heterologous expression of a PAL from *Arabidopsis thaliana* in the engineered strains then enabled the production of *t*-cinnamate. In a completely minimal medium, the plasmid-free chassis strains produced up to 6.3 mM of *t*-cinnamate from glycerol, which corresponds to a yield of 48% Cmol Cmol^{-1}. Cultivation in fed-batch fermentations resulted in titers of around 33.5 mM, which is the highest reported titer of microbially produced *t*-cinnamate in a cultivation medium without complex supplements. The engineered strains can further serve as efficient platform to produce various products from L-phenylalanine and *t*-cinnamate, including styrene, benzoate, or plant polyphenols such as pinosylvin.

MATERIALS AND METHODS

Bacterial Strains, Plasmids, and Cultivation Conditions

Strains and plasmids used in this study can be found in **Tables 1**, **2**. For cloning purposes, *E. coli* and *Pseudomonas* cells were cultivated at 37 or 30°C, respectively, either in liquid LB medium containing 5 g L^{-1} sodium chloride or on solid LB agar plates [additionally containing 1.5% (w/v) agar]. After tri- or four-parental mating procedures, Pseudomonads were isolated on cetrimide agar (Sigma Aldrich) plates supplemented with 10 mL L^{-1} glycerol. Kanamycin (50 μg mL^{-1}) or gentamicin (20 μg mL^{-1}) was added to cultures or plates when necessary.

During production and toxicity experiments in shake flasks and well plates, liquid cultures of *P. taiwanensis* were grown in mineral salt medium (MSM) adapted from Hartmans et al. (1989) at pH 7.0 without the addition of antibiotics. The medium's standard phosphate buffer capacity was increased to 5-fold (111.5 mM K_2HPO_4 and 68 mM NaH_2PO_4). Glucose or glycerol were added as sole carbon source at indicated concentrations. Main cultures were inoculated at an OD_{600} of 0.2, from seed cultures grown in MSM containing glucose as carbon source. Production experiments were performed in 500 mL Erlenmeyer flasks with a culture volume of 50 mL, which were cultivated in a rotary shaker with a frequency of 200 rpm and a throw of 50 mm. Toxicity assays were performed in 96-round low-well plates with a filling volume of 200 μL in the System Duetz® cultivation system (EnzyScreen, Leiden, Netherlands) with a shaking frequency of 225 rpm. OD_{600} values were calculated from the measured green values using a calibration. Phenylalanine accumulation was analyzed in 24-square deep-well plates with a filling volume of 5 mL and a shaking frequency of 225 rpm, and growth was monitored in the Growth profiler® system.

Plasmid Construction and Genomic Modification

For plasmid construction, DNA fragments were PCR amplified using the Q5 high-fidelity polymerase (New England Biolabs, New Ipswich, USA) with corresponding overhangs to enable subsequent Gibson assembly (Gibson et al., 2009) with the HiFi DNA assembly master mix (New England Biolabs, New Ipswich, USA). Primers were ordered from Eurofins Genomics (Ebersberg, Germany). The gene sequences for *aroG*^{fbr} (from *E. coli* K12 W3110) and AtPAL (from *A. thaliana*) were codon-optimized for *P. taiwanensis* VLB120 using the online tool OPTIMIZER (Puigbo et al., 2007) and ordered as synthetic DNA fragments from Thermo Fisher Scientific (Waltham, USA). The gene *pheA*^{T310I} was amplified from genomic DNA of strain *P. putida* S12palM12. pEMG-based plasmids were transformed into *E. coli* DH5α λpir cells, pBG-based plasmids were transformed into *E. coli* PIR2. Correct plasmid assembly was verified by Sanger sequencing performed by Eurofins Genomics (Ebersberg, Germany). Integration at the *attTn7*-site was achieved by patch-mating of the *E. coli* donor strain holding the respective pBG-plasmid, the helper strain *E. coli* HB101 pRK2013, DH5α λpir pTNS1 providing the required transposase and the recipient *Pseudomonas taiwanensis* strain as described by Wynands et al. (2018). After the mating procedure, *Pseudomonas* were isolated on Cetrimide agar containing gentamicin and correct integration was confirmed by colony PCR using the OneTaq Quick-Load Master Mix (New England Biolabs, New Ipswich, USA).

Genomic deletions and point mutations were realized using the I-SceI-based method developed by Martínez-García and de Lorenzo (2011) using a streamlined protocol adapted by Wynands et al. (2018). Successful deletions were verified by colony PCR using the OneTaq quick-Load Master Mix (New England Biolabs, New Ipswich, USA).

Fed-Batch in Controlled Bioreactors

Fermentations were carried out in fed-batch operation mode in DASbox® mini-bioreactors using the DASware control software (Eppendorf, Hamburg, Germany). The reactors were set up of 385 ml glass vessels, two Rushton-type impellers driven by direct overhead drives, feeding lines for acid, base, and carbon source, a temperature sensor, an EasyFerm Plus K8 120 pH-sensor (Hamilton Company, Reno, NV, USA) and an InPro® 6800 series O_2 sensor (Mettler-Toledo International Inc., Columbus, OH, USA). The starting volume was 100 mL and the temperature was maintained at 30°C. Gas supply was provided via headspace with a starting gas flow rate of 6 sL h^{-1}. The initial agitation frequency was 500 rpm. The dO_2 was controlled with a cascade, keeping the concentration of diluted oxygen at 35% by first increasing the agitation speed up to 1,200 rpm, then increasing the oxygen concentration in the air supply to a maximum of 80% and subsequently increasing the gas flow rate. pH 7 was maintained by automatic addition of 5% NH_3 or 1 M H_2SO_4.

TABLE 1 | Plasmids.

Plasmid	Description	References
pEMG	Km^R, oriR6K, lacZα with two flanking I-SceI sites	Martínez-García and de Lorenzo, 2011
pSW-2	Gm^R, oriRK2, *xylS*, Pm→ I-SceI	Martínez-García and de Lorenzo, 2011
pEMG-*pobA*	pEMG bearing flanking sequences of *pobA*, *pobA* deletion delivery vector	Wynands et al., 2018
pEMG-*hpd*	pEMG bearing flanking sequences of *hpd*, *hpd* deletion delivery vector	Wynands et al., 2018
pEMG-*quiC*	pEMG bearing flanking sequences of *quiC*, *quiC* deletion delivery vector	Wynands et al., 2018
pEMG-*quiC1*	pEMG bearing flanking sequences of *quiC1*, *quiC1* deletion delivery vector	Wynands et al., 2018
pEMGu-PVLB_13075	pEMGu bearing flanking sequences of *quiC2*, *quiC2* deletion delivery vector	Wynands et al., 2018
pEMG-*pykA*	pEMG bearing flanking sequences of *pykA*, *pykA* deletion delivery vector	Wynands et al., 2018
pEMGu-*trpE*^{P290S}	pEMGu bearing flanking sequences of *trpE*^{P290S}, P290S substitution delivery vector	Wynands et al., 2018
pEMGg-*aroF-1*^{P148L}	pEMGg bearing flanking sequences of *aroF-1*^{P148L}, P148L substitution delivery vector	Wynands et al., 2018
pEMGg-*pheA*^{T310I}	pEMGg bearing flanking sequences of *pheA*^{T310I}, T310I substitution delivery vector	Wynands et al., 2018
pEMG-*phhAB*	pEMG bearing flanking sequences of *phhAB*, *phhAB* deletion delivery vector	This study
pEMG-*katG*	pEMG bearing flanking sequences of *katG*, *katG* deletion delivery vector	This study
pEMG-PVLB_10925	pEMG bearing flanking sequences of PVLB_10925, PVLB_10925 deletion delivery vector	This study
pBG_{14d}-*msfgfp*	Km^R Gm^R, ori R6K, Tn7L and Tn7R extremes, P_{14d}-BCD2–*msfgfp* fusion	Zobel et al., 2015
pBG_{14f}-*msfgfp*	Km^R Gm^R, ori R6K, Tn7L and Tn7R extremes, P_{14f}-BCD2–*msfgfp* fusion	Zobel et al., 2015
pBG_{14g}-*msfgfp*	Km^R Gm^R, ori R6K, Tn7L and Tn7R extremes, P_{14g}-BCD2–*msfgfp* fusion	Zobel et al., 2015
pBG_{14d}-*aroG*^{fbr}-*pheA*^{T310I}	Km^R Gm^R, ori R6K, Tn7L and Tn7R extremes, P_{14d}-BCD2–*aroG*^{fbr} fusion, *aroG*^{fbr} from *E.coli* K12 W3110, *pheA*^{T310I} from *P. putida* S12palM12	This study
pBG_{14g}*AtPAL*-*aroG*^{fbr}-*pheA*^{T310}	Km^R Gm^R, ori R6K, Tn7L and Tn7R extremes, P_{14g}-BCD2–*aroG*^{fbr} fusion, *aroG*^{fbr} from *E.coli* K12 W3110, *pheA*^{T310I} from *P. putida* S12palM12, *PAL2* from *A. thaliana* codon optimized for *P. taiwanensis* VLB120	This study
pBG_{14f}-*AtPAL*	Km^R Gm^R, ori R6K, Tn7L and Tn7R extremes, P_{14f}-BCD2–At-PAL fusion, *PAL2* from *A. thaliana* codon optimized for *P. taiwanensis* VLB120	This study

Cells were grown in MSM according to Hartmans et al. (1989), where the addition of mineral salts stock was increased by 2-fold ($MgCl_2.6H_2O$ 0.2 g L^{-1}, $ZnSO_4.7H_2O$ 0.004 g L^{-1}, $CaCl_2.2H_2O$ 0.002 g L^{-1}, $FeSO_4.7H_2O$ 0.01 g L^{-1}, $Na_2MoO_4.2H_2O$ 0.0004 g L^{-1}, $CuSO_4.5H_2O$ 0.0004 g L^{-1}, $CoCl_2.6H_2O$ 0.0008 g L^{-1}, $MnCL_2.2H_2O$ 0.002 g L^{-1}). The initial batch medium contained either 20 mM of glucose or 40 mM of glycerol as sole carbon source. The reactors were operated in a dO_2-controlled fed-batch mode. When glucose or glycerol was depleted, the dO_2 signal rapidly increased as a result of metabolic arrest. A dO_2 signal >70 triggered a feed pump, resulting in a feed shot of 5 mM of glucose or 10 mM of glycerol per trigger initiation.

Analytical Methods

Optical densities of liquid cultures were measured at 600 nm using an Ultrospec 10 Cell Density Meter (GE Healthcare, Illinois, USA).

Samples taken from the cultures were centrifuged at 13,000 rpm for 2–5 min and the supernatant was analyzed by HPLC. Aromatics quantification was performed using a Beckman System Gold 126 Solvent Module with a 168 diode 201 array detector (Beckman Coulter, Brea, USA) and an ISAspher 100-5 C18 BDS reversed-phase 202 column (ISERA, Düren, Germany) at 30°C and a flow rate of 0.8 mL min^{-1}. Elution took place with a gradient starting at 90% H_2O containing 0.1% (v/v) TFA and 10% methanol. This ratio was held for 2 min, followed by gradual increase to 100% methanol over the course of 8 min. After 2 min at 100% methanol, initial ratios were reached again within 1 min and held constant for further 2 min. UV detection was conducted at a wavelength of 245 nm. L-phenylalanine and L-tyrosine quantification shown in **Figure 3** was performed with the same column and elution setup as mentioned before, in a Dionex Ultimate 3000 HPLC system, where detection took place with a Corona Veo charged aerosol detector (Thermo Fisher Scientific, Waltham, MA, USA). Glucose, gluconate and glycerol analysis was performed using a Beckman System Gold 126 Solvent Module with a System Gold 166 UV-detector (Beckman Coulter, Brea, USA) and Smartline RI Detector 2300 (KNAUER, Berlin, Germany) on a MetabAAC column (ISERA, Düren, Germany). Elution took place with 5 mM H_2SO_4 at an isocratic flow of 0.5 mL min^{-1} and a temperature of 30°C for 20 min. Glucose and glycerol were analyzed using the RI detector, gluconate concentrations were determined with the UV detector at a wavelength of 210 nm. Due to co-elution of glucose and gluconate, glucose concentrations were determined by subtraction of the gluconate concentration.

RESULTS AND DISCUSSION

Enhanced *Trans*-Cinnamate Tolerance of Streamlined *P. taiwanensis* Chassis Strains

Product toxicity vastly influences the efficiency of a microbial production process. Cellular stress induced by toxic compounds leads to decreased production rates or complete growth arrest, thereby limiting feasible product titers and yields (Sardessai and Bhosle, 2002; McKenna and Nielsen, 2011; Kusumawardhani et al., 2018). Compared to hydrophobic

TABLE 2 | Bacterial strains.

Strain	Description	References
E. coli		
DH5α λpir	*E44, ΔlacU169 (ΦlacZΔM15), recA1, endA1, hsdR17, thi-1, gyrA96, relA1, λpir phage lysogen;* host for oriV(R6K) vectors	de Lorenzo and Timmis, 1994
PIR2	*F⁻ Δlac169 rpoS(Am) robA1 creC510 hsdR514 endA reacA1 uidA(ΔMlui)::pir,* host for oriV(R6K) vectors	Invitrogen
HB101 pRK2013	*F⁻ mcrB mrr hsdS20(rB⁻ mB ⁻) recA13 leuB6 ara⁻14 proA2 lacY1 galK2 xyl-5 mtl-1 rpsL20(Sm^R) gln V44* λ⁻ bearing pRK2013	Boyer and Roulland-Dussoix, 1969
DH5α λpir pTNS1	DH5α λpir bearing plasmid pTNS1	de Lorenzo Lab
P. taiwanensis		
VLB120	Wildtype	Panke et al., 1998
VLB120ΔpSTY	ΔpSTY	Wynands et al., 2019
GRC1	ΔpSTY, Δprophage1/2, Δprophage3, Δprophage4, Δflag1, Δflag2, Δlap1, Δlap2, Δlap3	Wynands et al., 2019
GRC2	ΔpSTY, Δprophage1/2::*ttgGHI*, Δprophage3, Δprophage4, Δflag1, Δflag2, Δlap1, Δlap2, Δlap3	Wynands et al., 2019
GRC3	ΔpSTY, Δprophage1/2::*VWGHI*, Δprophage3, Δprophage4, Δflag1, Δflag2, Δlap1, Δlap2, Δlap3	Wynands et al., 2019
GRC3 Δ5Δ*pykA*-tap	GRC3 with Δ*pobA*, Δ*hpd*, Δ*quiC*, Δ*quiC1*, Δ*quiC2*, Δ*pykA, trpE*^{P290S}, *aroF-1*^{P148L}, *pheA*^{T310I}	Wynands, 2018
GRC3 Δ5Δ*pykA*-tap Δ*phhAB*	GRC3 Δ5Δ*pykA*-tap with Δ*phhAB*	This study
GRC3 Δ5Δ*pykA*-tap Δ*phhAB*Δ*katG*	GRC3 Δ5Δ*pykA*-tap with Δ*phhAB,* Δ*katG*	This study
GRC3 Δ5Δ*pykA*-tap Δ*phhAB*ΔPVLB_10925	GRC3 Δ5Δ*pykA*-tap with Δ*phhAB,* ΔPVLB_10925	This study
GRC3 Δ8Δ*pykA*-tap	GRC3 Δ5Δ*pykA*-tap with Δ*phhAB,* Δ*katG,* ΔPVLB_10925	This study
GRC3 Δ8Δ*pykA*-tap *attTn7*::P$_{14g}$*AtPAL-aroG*^{fbr}*-pheA*^{T310}	GRC3 Δ8Δ*pykA*-tap with P$_{14g}$*AtPAL- aroG*^{fbr}*-pheA*^{T310} chromosomally integrated at site *attTn7*	This study
GRC3 Δ8Δ*pykA*-tap *attTn7*::P$_{14f}$*AtPAL*	GRC3 Δ8Δ*pykA*-tap with P$_{14f}$*AtPAL* chromosomally integrated at site *attTn7*	This study
GRC3 Δ5Δ*pykA*-tap *attTn7*::P$_{14d}$-*aroG*^{fbr}*-pheA*^{T310}	GRC3 Δ5Δ*pykA*-tap with P$_{14d}$-*aroG*^{fbr}*-pheA*^{T310I} chromosomally integrated at site *attTn7*	This study
GRC3 Δ5Δ*pykA*-tap Δ*phhAB* *attTn7*::P$_{14d}$-*aroG*^{fbr}*-pheA*^{T310}	GRC3 Δ5Δ*pykA*-tapΔ*phhAB* with P$_{14d}$-*aroG*^{fbr}*-pheA*^{T310} chromosomally integrated at site *attTn7*	This study
GRC3 Δ5Δ*pykA*-tap Δ*phhAB*Δ*katG* *attTn7*::P$_{14d}$-*aroG*^{fbr}*-pheA*^{T310}	GRC3 Δ5Δ*pykA*-tapΔ*phhAB*Δ*katG* with P$_{14d}$-*aroG*^{fbr}*-aheA*^{T310} chromosomally integrated at site *attTn7*	This study
GRC3 Δ5Δ*pykA*-tap Δ*phhAB*ΔPVLB_10925 *attTn7*::P$_{14d}$-*aroG*^{fbr}*-pheA*^{T310}	GRC3 Δ5Δ*pykA*-tapΔ*phhAB*Δ*PVLB_10925* with P$_{14d}$-*aroG*^{fbr}*-pheA*^{T310} chromosomally integrated at site *attTn7*	This study
GRC3 Δ8Δ*pykA*-tap *attTn7*::P$_{14d}$-*aroG*^{fbr}*-pheA*^{T310}	GRC3 Δ5Δ*pykA*-tapΔ*phhAB*Δ*katG*Δ*PVLB_10925* with P$_{14d}$-*aroG*^{fbr}*-pheA*^{T310} chromosomally integrated at site *attTn7*	This study

aromatics such as styrene, *t*-cinnamate is mildly toxic at neutral pH and it exhibits a different mode of action. Increasing concentrations of *t*-cinnamate lead to enhanced osmotic stress in cell cultures, but will also cause the inhibition of specific enzymes and disturb cellular processes, resulting in growth defects (Olasupo et al., 2003; Guzman, 2014). Growth of *E. coli*, for example, is heavily impaired at concentrations above 2.7 mM (400 mg L^{-1}) and completely inhibited at >5.4 mM (800 mg L^{-1}) when *t*-cinnamate is added at the beginning of cultivation (Olasupo et al., 2003; McKenna and Nielsen, 2011). This necessitates the addition of expensive complex supplements such as yeast extract or casamino acids or a biotransformation approach with late PAL induction at high cell densities to allow for sufficient accumulation of the precursor L-phenylalanine (Noda et al., 2011; Bang et al., 2018).

These problems can be avoided by the utilization of robust, natively stress-resistant host strains such as *Pseudomonas taiwanensis* VLB120. As shown in **Figure 1A**, the wildtype can grow in the presence of 30 mM (4.4 g L^{-1}) *t*-cinnamate in MSM with a rate of 0.24 ± 0.01 h^{-1}. *P. taiwanensis* VLB120 is equipped with particular mechanisms that enable this superior tolerance toward a variety of toxic compounds. While RND-type efflux pumps mainly act on hydrophobic aromatic solvents and a number of antibiotics (Terán et al., 2003; Köhler et al., 2013; Volmer et al., 2014), an ABC transporter (Ttg2ABC) was recently identified as crucial for *p*-coumarate tolerance, the hydroxylated derivative of *t*-cinnamate (Calero et al., 2018). Furthermore, chaperone upregulation is observed as response to protein misfolding (Segura et al., 2012).

To further exploit the native potential of *P. taiwanensis* VLB120 as microbial cell factory, we recently engineered a

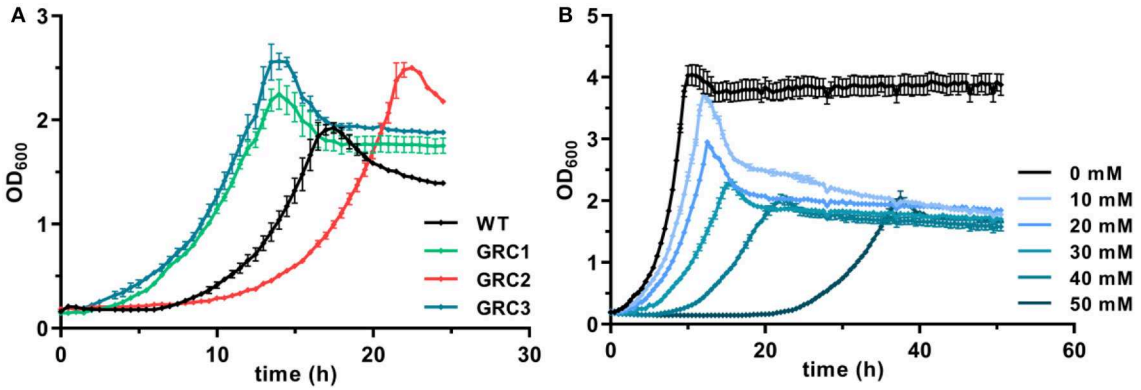

FIGURE 1 | Enhanced growth of genome-reduced *Pseudomonas taiwanensis* chassis strains in the presence of *t*-cinnamate. **(A)** Growth of the *P. taiwanensis* VLB120 wildtype and the three genome-reduced chassis strains in the presence of 30 mM of *t*-cinnamate in mineral salts medium (MSM) containing 20 mM of glucose. **(B)** Growth of *P. taiwanensis* GRC3 at increasing *t*-cinnamate concentrations (0–50 mM) in MSM. Growth was monitored in the Growth Profiler®, error bars represent the standard error of the mean ($n = 3$).

genome-reduced variant of this strain which exhibited higher growth rates and enhanced biomass formation (Wynands et al., 2019). The benefit of genome reduction for potential aromatics production strains is underlined by the tolerance test in the presence of 30 mM *t*-cinnamate (**Figure 1A**). The streamlined strains GRC1 and GRC3 had a reduced lag phase in the presence of high *t*-cinnamate concentrations, while the growth rate remains similar to the wildtype. In addition, the GRC strains reached higher final OD_{600} values compared to the wildtype. This is particularly important to improve the efficiency of a microbial production process by reducing the overall process time and lowering the amount of substrate needed to generated and maintain the biomass. The only exception is strain *P. taiwanensis* GRC2, which grew slower and with a longer lag phase than the wildtype. In contrast to GRC1 and 3, GRC2 constitutively expresses *ttgGHI* genes that encode a solvent-efflux pump. Although this constitutive expression greatly increases the fitness of GRC2 in the presence of hydrophobic solvents such as toluene, it causes a fitness reduction in the absence of solvents (Wynands et al., 2019). This drawback is absent in the other two strains, where the whole *ttg* operon is absent (GRC1), or the regulatory genes *ttgVW* are included to induce the pump in response to solvents (GRC3). The similar performance of GRC1 and GRC3 in the presence of *t*-cinnamate indicates that this aromatic acid does not induce expression of the *ttgGHI*, nor does the TtgGHI pump contribute to cinnamate tolerance. Given this similar performance, and in light of the potential to use a *t*-cinnamate-producing strain as platform for a variety of further industrially relevant hydrophobic aromatics, the strain GRC3 was chosen as host to maintain the possibility of solvent efflux by TtgGHI. As shown in **Figure 1B**, *P. taiwanensis* GRC3 can grow in the presence of *t*-cinnamate concentrations of up to 50 mM (7.4 g L^{-1}), which is 10-fold higher than MIC for *E. coli*. The native tolerance potential of *P. taiwanensis* VLB120 in combination with improved bioprocess features obtained by streamlining of this strain hence set an ideal starting point for an efficient microbial production process of *t*-cinnamate.

Rational Engineering of L-phenylalanine Production

t-cinnamate is the deamination product of L-phenylalanine and the enhanced supply of this precursor in microbial chassis strains is thus crucial to allow efficient production. A variety of approaches toward L-phenylalanine overproduction were reported over the last years, delivering highly productive strains of e.g., *E. coli* (63 g L^{-1} from glucose) (Ding et al., 2016) or *Corynebacterium glutamicum* (16 g L^{-1} from glucose) (Zhang et al., 2015). Biosynthesis of L-phenylalanine and L-tyrosine both starts with the conversion of chorismate into prephenate, which then branches via phenylpyruvate to L-phenylalanine or via 4-hydroxyphenylpyruvate to L-tyrosine. Popular strategies aim to deregulate a 3-deoxy-D-arabino-heptolusonate-7-phosphate (DAHP) synthase (e.g., AroG, AroF, or AroH) or the chorismate mutase/prephenate dehydratase (PheA) activity and to increase the availability of the precursors phosphoenolpyruvate (PEP) and erythrose-4-phosphate (E4P) (Rodriguez et al., 2014; Ding et al., 2016; Huccetogullari et al., 2019). Pseudomonads have the catabolic potential to degrade a high number of aromatic compounds. This ability is a key feature applied for many biotechnological aspects such as the metabolism of complex substrates (Xu et al., 2018), but it also increases the difficulty of manufacturing aromatic amino acid accumulation in this species. We recently reported a study describing the rational engineering of *P. taiwanensis* VLB120 to produce phenol via the aromatic amino acid L-tyrosine (Wynands et al., 2018). The deletion of five genes (*pobA*, *hpd*, *quiC*, *quiC1*, *quiC2*) associated to the degradation of shikimate pathway-derived compounds resulted in strains unable to catabolize L-tyrosine, L-phenylalanine, *p*-hydroxybenzoate, and 3-dehydroshikimate to ensure aromatics accumulation. The flux toward L-tyrosine was subsequently enhanced by the insertion of point mutations into the native locus of genes in the shikimate pathway, resulting in enzymes with amino acid substitutions ($TrpE^{P290S}$, $AroF\text{-}1^{P148L}$, $PheA^{T310I}$). The deletion of *pykA* (encoding for a pyruvate kinase) additionally reduced the flux of PEP toward

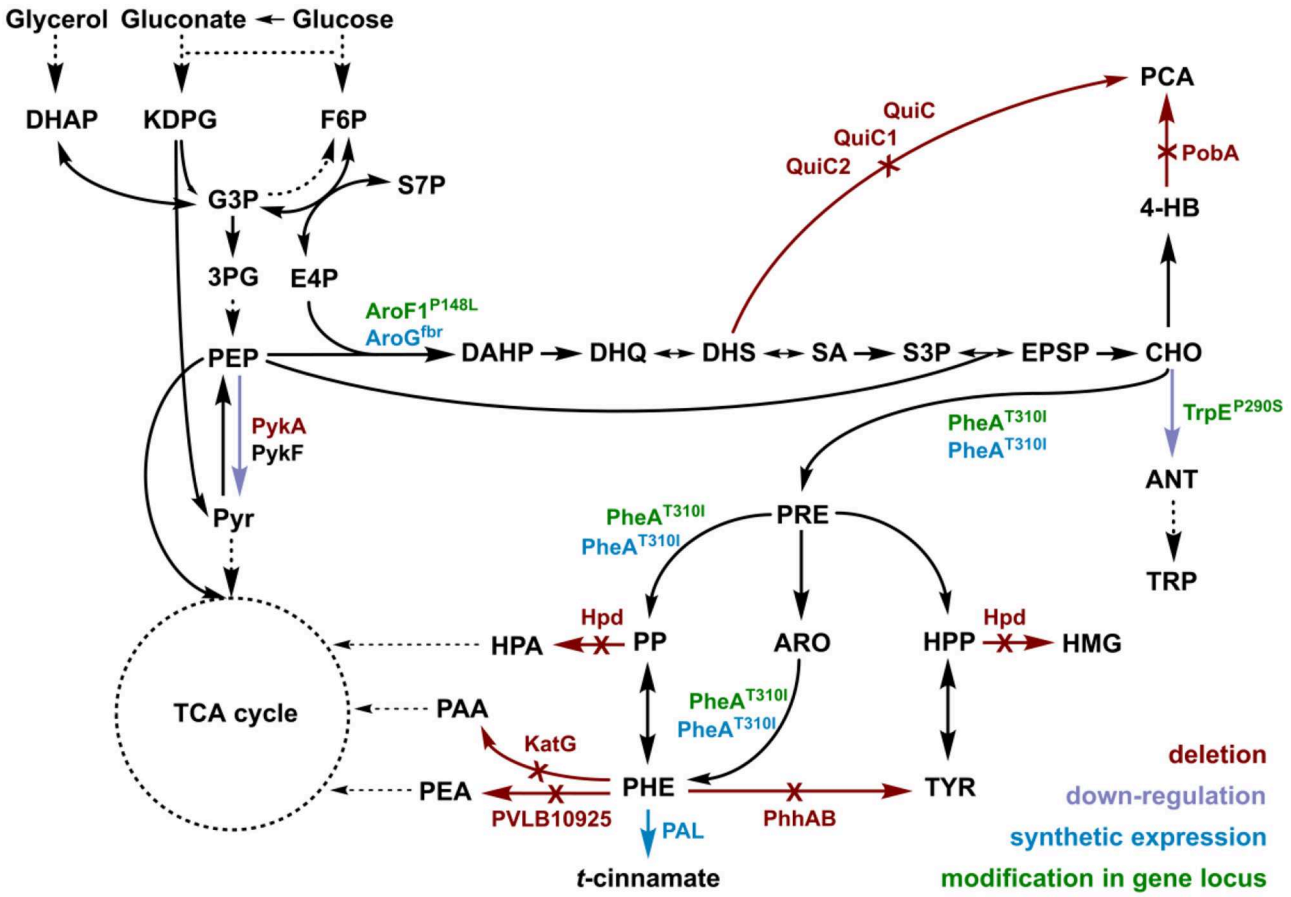

FIGURE 2 | Genomic modifications introduced into strain *P. taiwanensis* GRC3 to enable accumulation of L-phenylalanine and subsequent deamination to *t*-cinnamate. Red arrows and annotations indicate gene deletions, purple arrows represent enzymatic downregulation, green annotations highlight point mutations introduced into the native gene locus, and blue tags and arrows represent the overexpression of heterologous genes. DAHP, dihydroxyacetone phosphate; KDPG, 2-keto-3-deoxy-6-phosphogluconate; F6P, fructose-6-phosphate; G3P, glyceraldehyde-3-phosphate; 3PG, 3-phosphoglycerat; S7P, seduheptulose-7-phosphate; PEP, phosphoenolpyruvate; PYR, pyruvate; E4P, erythrose-4-phosphate; DAHP, 3-deoxy-D-arabinoheptulosonate-7-phosphate; DHQ, 3-dehydroquinate; DHS, 3-dehydroshikimate; SA, shikimate; S3P, shikimate-3-phosphate; EPSP, 5-enolpyruvyl-shikimate-5-phosphate; CHO, chorismate; 4-HB, 4-hydroxybenzoate; PCA, protocatechuate; ANT, anthranilate; TRP, tryptophan; PRE, prephenate; PP, phenylpyruvate; HPP, 4-hydroxyphenylpyruvate; ARO, arogenate; TYR, tyrosine; PHE, phenylalanine; HMG, homogentisate; PAA, 2-phenylacetamide; PEA, phenylethylamine; PykA/PykF, pyruvate kinase isozymes; QuiC/QuiC1/QuiC2, 3-dehydroshikimate dehydratase isozymes; PobA, 4-hydroxybenzoate 3-monooxygenase; Hpd, 4-hydroxyphenylpyruvate dioxygenase; AroF-1^{P148L}/AroG^{fbr}, DAHP synthase isozymes; TrpE^{P290S}, anthranilate synthase (component I); PheA^{T310I}, bi-functional chorismate mutase/prephenate dehydratase; PhhAB, phenylalanine 4-monooxygenase; KatG, catalase-peroxidase; PVLB_10925, aromatic-L-amino-acid decarboxylase; PAL, phenylalanine ammonia-lyase.

pyruvate, thereby increasing the precursor pool for the shikimate pathway. An introduction of these mutations in the genome-reduced strains of *P. taiwanensis* VLB120 led to the efficient production of phenol from L-tyrosine (Wynands et al., 2019). As shown in **Figure 3**, the strain *P. taiwanensis* GRC3 Δ5Δ*pykA*-tap accumulates 2.85 ± 0.02 mM of tyrosine from 20 mM of glucose, which is comparable to the non-genome-reduced strain. Three genes involved in phenylalanine catabolism were subsequently deleted from the chromosome of *P. taiwanensis* GRC3 Δ5Δ*pykA*-tap: (i) *phhAB* encoding for phenylalanine-4-monooxygenase involved in the conversion of phenylalanine to tyrosine (Herrera et al., 2010), (ii) PVLB_10925, putatively encoding an aromatic-L-amino-acid decarboxylase responsible for the decarboxylation into phenylethylamine, and (iii) *katG*, putatively coding for a catalase-peroxidase which converts phenylalanine into phenyl acetamide (**Figure 2**).

Pseudomonads possess a variety of transporters that allow export and import of aromatic amino acids. Transcriptome analysis of a *Pseudomonas putida* strain with increased flux toward tyrosine revealed that upon increased intracellular aromatic amino acid levels, amino acid exporters are upregulated, while uptake systems are downregulated (Wierckx et al., 2008). Aromatics accumulation shown in **Figure 3** displays extracellular concentrations, indicating enhanced efflux of both tyrosine and phenylalanine.

The deletion of *phhAB* led to the accumulation of 2.22 ± 0.02 mM of phenylalanine and 0.29 ± 0.01 mM tyrosine after 50 h (**Figure 3**). This indicates that about 88% of L-tyrosine

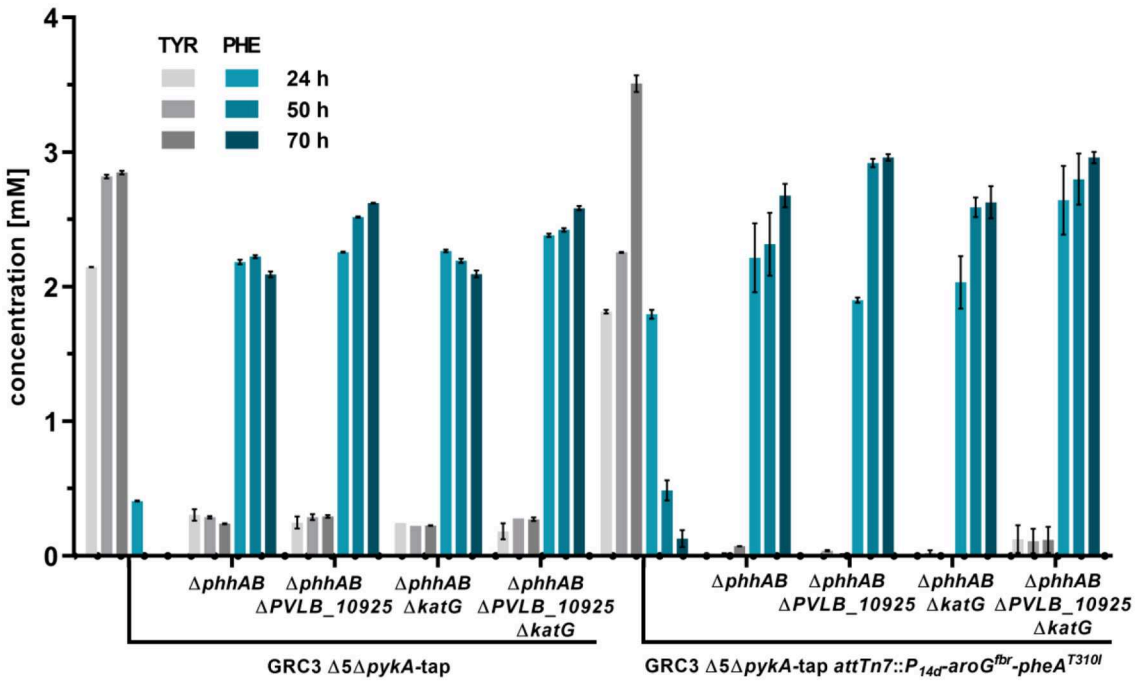

FIGURE 3 | L-phenylalanine and L-tyrosine accumulation of *P. taiwanensis* GRC3 Δ5Δ*pykA*-tap and subsequent mutants with deletions to prevent L-phenylalanine degradation and additional overexpression of AroG^{fbr} and PheA^{T310I}. The strains were cultivated in MSM containing 20 mM glucose in a System Duetz® shaker. Error bars represent the standard error of the mean ($n = 3$).

accumulating due to the enhanced flux toward prephenate in strain *P. taiwanensis* GRC3 Δ5Δ*pykA*-tap is stemming from L-phenylalanine. In most microorganisms, L-phenylalanine cannot be converted into L-tyrosine in which case it is solely synthesized from prephenate (Guroff and Ito, 1965). In *Pseudomonas* however, the pathway via L-phenylalanine seems to be a major route for L-tyrosine formation under the given conditions (Wierckx et al., 2009). As described for other *Pseudomonas* species, Xanthomonads and *Alcalignes* (Ahmad et al., 1990), this diversity of aromatic amino acid metabolism account for the flexibility of the organism to cope with a variety of end product analogs (Fiske et al., 1983). The concentration of L-phenylalanine in the culture of *P. taiwanensis* GRC3 Δ5Δ*pykA*-tapΔ*phhAB* was slightly reduced after 70 h, indicating that other pathways involved in L-phenylalanine degradation were still active in this strain. The subsequent deletion of gene PVLB_10925 prevented this degradation, resulting instead in a further increase of the final titer to 2.62 ± 0.00 mM L-phenylalanine. The deletion of *katG* had no influence on phenylalanine accumulation and the strain shows a similar production pattern as the strain without a deletion. Indeed, as the progenitor strain *P. taiwanensis* GRC3 Δ5Δ*pykA*-tap was already not able to grow on L-phenylalanine and L-tyrosine (Wynands et al., 2018), this confirms that catabolic pathways are either not active (*katG*) or not connected to the central carbon metabolism (PVLB_10925) under the applied conditions, even though this strain contains the genetic inventory for the full degradation of the resulting 2-phenylacetamide and phenylethylamine. This is underlined by similar observations in an L-phenylalanine overproducing strain of *P. putida* DOT-T1E (Molina-Santiago et al., 2016).

L-Tyrosine and L-phenylalanine production could be increased further by the additional overexpression of AroG^{fbr}, a feedback inhibition resistant versions of the DAHP synthase from *E. coli* K12 W3110 (Kikuchi et al., 1997) and PheA^{T310I} from *P. putida* S12palM12 (Nijkamp et al., 2005). The coding genes were integrated chromosomally at the *attTn7*-site and expressed under the control of the constitutive promoter P_{14g} (Zobel et al., 2015). Overexpression in the tyrosine-accumulating strain *P. taiwanensis* GRC3 Δ5Δ*pykA*-tap led to tyrosine titers of about 3.5 ± 0.11 mM after 70 h. Transient L-phenylalanine accumulation was observed with this strain, further underlining the high flux through PhhAB. Upon overexpression of *aroG*^{fbr} and *pheA*^{T310I} in strains with deletions of *phhAB*, *katG* and PVLB_10925, the resulting strain GRC3 Δ8Δ*pykA*-tap *attTn7*::P_{14d}-*aroG*^{fbr}-*pheA*^{AT31I} (Δ8 = eight deletions of pathways involved in aromatics degradation) accumulated 3.0 ± 0.07 mM of L-phenylalanine after 70 h. Also, L-tyrosine production was reduced, likely due to PheA^{T310I} increasing the flux of prephenate toward L-phenylalanine.

Production of *t*-cinnamate From Glucose and Glycerol in Shake Flasks

The L-phenylalanine-accumulating strain *P. taiwanensis* GRC3 Δ8Δ*pykA*-tap was subsequently used as host for the production of *t*-cinnamate. The deamination of L-phenylalanine into *t*-cinnamate was achieved using the PAL2 enzyme from *A.*

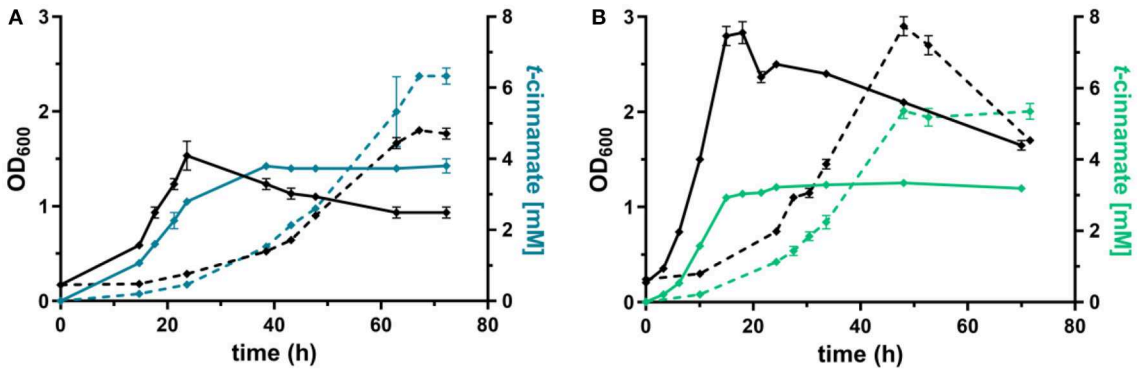

FIGURE 4 | Shake flask cultivations of *P. taiwanensis* GRC3 Δ8Δ*pykA*-tap with varying heterologous expression modules. **(A)** Growth (black lines) and t-cinnamate production (blue lines) by *P. taiwanensis* GRC3 Δ8Δ*pykA*-tap *attTn7*::P_{14g}*AtPAL- aroG*^{fbr}*-pheA*^{T310} in MSM containing 20 mM glucose (solid line) or 40 mM of glycerol (dotted line). **(B)** Growth (black lines) and *t*-cinnamate production (green lines) by *P. taiwanensis* GRC3 Δ8Δ*pykA*-tap *attTn7*::P_{14f}*AtPAL* in MSM containing 20 mM glucose (solid line) or 40 mM of glycerol (dotted line). Error bars represent the standard error of the mean ($n = 3$).

thaliana. While four genes encoding PAL have been identified in *A. thaliana* (Cochrane et al., 2004), PAL2 displayed the highest specific activity when expressed in *E. coli* (McKenna and Nielsen, 2011). In addition, it has no activity on L-tyrosine as a substrate, in contrast to a variety of other yeast PALs (Cui et al., 2008). As overexpression of *aroG*^{fbr} and *pheA*^{T310I} improved L-phenylalanine yields by 15% (**Figure 3**), combinatorial expression with PAL on the *Tn7* transposon under the control of P_{14g} was applied for *t*-cinnamate production in the strain *P. taiwanensis* GRC3 Δ8Δ*pykA*-tap *attTn7*::P_{14g}*AtPAL-aroG*^{fbr}*-pheA*^{T310}. The strain was cultivated in shake flasks in MSM containing either 20 mM of glucose or 40 mM of glycerol as sole carbon source. Glycerol is a promising alternative as feedstock for microbial production processes as abundant by-product of the bio-diesel production (Zambanini et al., 2016). When cultivated on glucose, the strain accumulated 3.80 ± 0.20 mM *t*-cinnamate, corresponding to a yield of 25.9 ± 0.1% Cmol Cmol^{-1}, with a volumetric productivity of 0.10 ± 0.00 mM h^{-1} (**Figure 4**). From glycerol, the *t*-cinnamate titer was further increased to 6.33 ± 0.12 mM, corresponding to a yield of 47.5 ± 0.9% Cmol Cmol^{-1}. As observed for the production of phenol and *p*-hydroxybenzoate (Wynands et al., 2018; Lenzen et al., 2019), metabolism of glycerol is highly beneficial for enhanced titers and yields of compounds derived from aromatic amino acids, likely due to metabolic rearrangements favoring the supply of PEP and E4P (Nikel et al., 2014; Poblete-Castro et al., 2019). The volumetric productivity on glycerol is slightly lower compared to glucose (0.09 ± 0.01 mM h^{-1}), as a result of the reduced growth rate. While this strain has a very high yield, its reliable application as a production host was problematic. When the experiment described above was repeated, the cultures displayed varying growth behavior in terms of lag-phase, growth rates, and productivity (**Figure S1**), even though the cultivation procedure remained identical. Re-transformation of the Tn7-transposon bearing the overexpression constructs and culturing of single colonies yielded the same unstable phenotype. Sequencing of the *attTn7*-regions of theses strains revealed no mutations in this sequence and verified correct integration. Likely, a combination of the extreme drain on carbon posed by the high *t*-cinnamate yield, the burden of heterologous overexpression of genes, and the production of a mildly toxic compound provide a strong selection for suppressor mutations. This impairs the reproducibility and renders the strain *P. taiwanensis* GRC3 Δ8Δ*pykA*-tap *attTn7*::P_{14g}*AtPAL-aroG*^{fbr}*-pheA*^{T310} unsuitable as reliable production host in its current form.

In contrast, *P. taiwanensis* GRC3 Δ8Δ*pykA*-tap *attTn7*::P_{14f}*AtPAL*, harboring only the PAL for L-phenylalanine deamination under the control of the weaker P_{14f} promoter, showed reliable growth and production patterns. This strain still carries feedback-resistant *aroF-1*^{P148L}, *pheA*^{T310I}, but only in their native context. The lack of *in trans* overexpression of *aroG*^{fbr} and *pheA*^{T310I} reduced *t*-cinnamate titers and yields slightly, with 3.34 ± 0.07 mM produced from glucose and 5.25 ± 0.22 mM from glycerol, which corresponds to yields of 22.8 ± 0.5 and 38.9 ± 1.6% Cmol Cmol^{-1}, respectively. To the best of our knowledge, these are still the highest yields of *t*-cinnamate produced in a microbial process using a mineral medium without the addition of complex supplements. This strain furthermore reached higher final biomass and exhibited improved volumetric productivity on glucose (0.13 ± 0.00 mM h^{-1}) and glycerol (0.11 ± 0.00 mM h^{-1}) compared to the strain additionally expressing *aroG*^{fbr} and *pheA*^{T310I}. In the course of the cultivations, no accumulation of L-phenylalanine was observed. This indicates that PAL activity is not inhibited by the concentrations of *t*-cinnamate reached in these cultures, in contrast to observations in other hosts and with PALs from different organisms (Nijkamp et al., 2005; McKenna and Nielsen, 2011; Molina-Santiago et al., 2016). Furthermore, no L-tyrosine accumulation was observed, in contrast to the phenylalanine-producing equivalent that does not express PAL (**Figure 3**), likely due to a reduction of product inhibition of the upstream metabolic enzymes as a result of efficient conversion to *t*-cinnamate.

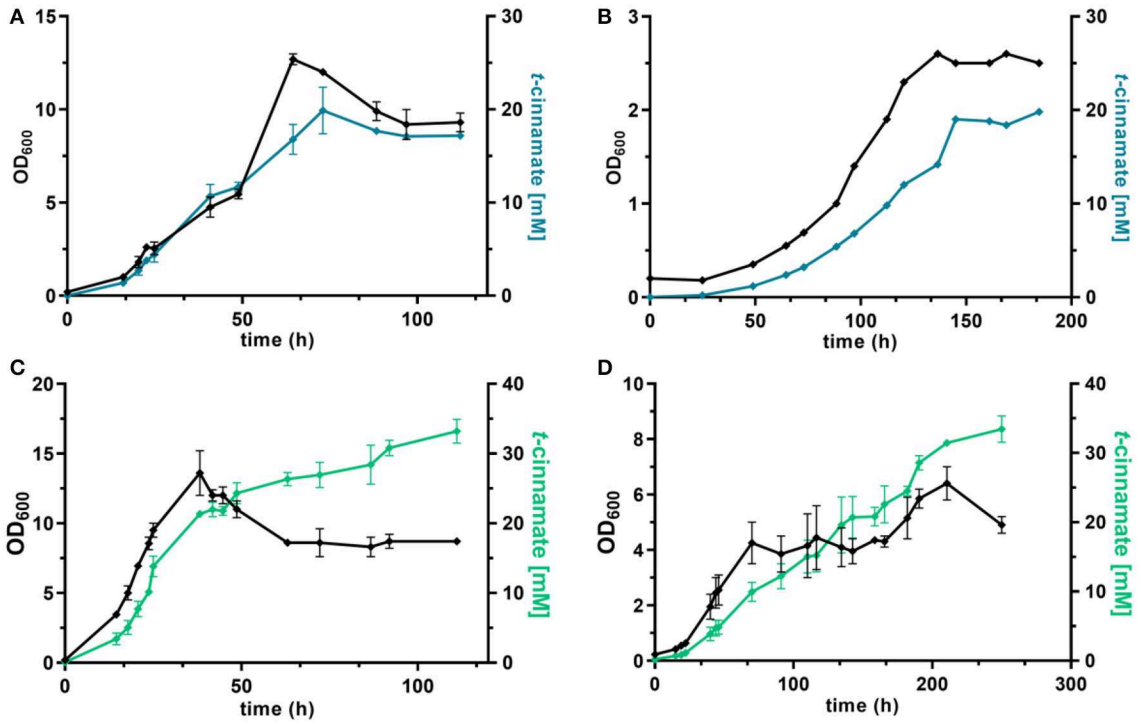

FIGURE 5 | dO_2-stat fed-batch fermentations of *t*-cinnamate producing strains of *P. taiwanensis*. Cultivations were performed in MSM, where the initial batch medium contained either glucose or glycerol as sole carbon source and the subsequent feeding solution contained solely the respective carbon source. The top graphs show growth (black lines) and *t*-cinnamate accumulation (blue lines) during fermentation of *P. taiwanensis* GRC3 Δ8Δ*pykA*-tap *attTn7::P*$_{14g}$*AtPAL- aroG*^{fbr}*-pheA*^{T310} on glucose **(A)** and glycerol **(B)**. The glycerol figure **(B)** displays data of a single reactor. The bottom graphs represent growth (black lines) and *t*-cinnamate accumulation (green lines) during fermentation of *P. taiwanensis* GRC3 Δ8Δ*pykA*-tap *attTn7::P*$_{14f}$*AtPAL* on glucose **(C)** and glycerol **(D)**. The error bars represent the standard error ($n = 2$).

Production in Controlled Bioreactors

In order to assess higher-level *t*-cinnamate production under more industrially relevant conditions, the strains were cultivated in fed-batch fermentations in controlled bioreactors. The fermenters were operated in a dO_2-stat fed-batch mode where carbon depletion and the resulting increase of the dO_2 due to metabolic arrest triggered the initiation of a pulse feed of either 5 mM glucose or 10 mM glycerol (Johnson et al., 2016, 2019). This feeding protocol allows controlled addition of carbon source throughout the whole fermentation process, independent from time-varying carbon demands of the cell, thereby preventing excess carbon surplus (Johnson et al., 2016). The resulting feeding trends of single reactors are exemplarily shown in **Figure S3**. Cultivation took place at pH 7 in a mineral medium without the addition of complex supplements.

Under these conditions, the strain *P. taiwanensis* GRC3 Δ8Δ*pykA*-tap *attTn7::P*$_{14g}$*AtPAL-aroG*^{fbr}*-pheA*^{T310} accumulated 17.2 ± 0.28 mM of *t*-cinnamate from glucose, corresponding to a yield of 11.2 ± 0.6% (Cmol Cmol^{-1}) and a volumetric productivity of 0.19 ± 0.20 mM h^{-1}. As shown in **Figure 5A**, the culture reaches a final OD_{600} of 12.7 after around 65 h. At this point, a decrease in biomass concentration was observed. Furthermore, there was no significant increase in *t*-cinnamate titers from this point on, in spite of the fact that the base strain GRC3 tolerated higher concentrations of *t*-cinnamate up to 50 mM (**Figure 1**). It is possible that several factors impact the lowered growth performance of the production strains in the presence of *t*-cinnamate. One factor is the overexpression of heterologous genes which leads to lowered growth rates and impaired fitness as observed in shake flask experiments (**Figure 4**). Especially the overexpression of AroG and PheA appears to lead to increased cellular stress, which in turn also lowers the growth performance in the presence of toxic compounds. Furthermore, experiments regarding styrene toxicity have demonstrated a crucial difference in tolerance depending on whether a compound is added exogenously to the medium or produced intracellularly (Lian et al., 2016).

Fed-batch fermentations using glycerol as carbon source further underline complications using the phenotypically unstable strain *P. taiwanensis* GRC3 Δ8Δ*pykA*-tap *attTn7::P*$_{14g}$*AtPAL-aroG*^{fbr}*-pheA*^{T310} (**Figure 5B**; **Figure S2**). During fermentations, cultures in duplicate reactors showed different growth behavior while stemming from the same pre-culture. The cultures showed differences in lag-phase, growth rate and productivity. The final titers remained comparable, likely as a result of product inhibition as described before. **Figure 5B** shows a single fermentation on glycerol as an example. Here, the strain produced up to 19.8 mM *t*-cinnamate, with a yield

TABLE 3 | Comparison of *t*-cinnamate titer, yield, and volumetric productivity of strains *P. taiwanensis* GRC3 Δ8Δ*pykA*-tap *attTn7*::P_{14g}AtPAL- aroG^{fbr}-pheA^{T310} and GRC3 Δ8Δ*pykA*-tap *attTn7*::P_{14f}*AtPAL* in shake flask cultivations and fed-batch fermentations.

		GCR3 Δ8Δ*pykA trpE*^{P290S} *aroF-1*^{P148L} *pheA*^{T310I} (tap)	
		***attTn7*::P_{14g}*AtPAL-aroG*^{fbr}*-pheA*^{T310}**	***attTn7*::P_{14f}*AtPAL***
Shake flask glucose	Final titer [mM]	3.8 ± 0.20	3.3 ± 0.07
	Yield (% Cmol Cmol^{-1})	25.9 ± 0.1	22.8 ± 0.5
	Productivity (mM h^{-1})	0.10 ± 0.00	0.13 ± 0.00
Shake flask glycerol	Final titer [mM]	6.3 ± 0.12	5.4 ± 0.22
	Yield (% Cmol Cmol^{-1})	47.5 ± 0.9	38.9 ± 1.6
	Productivity (mM h^{-1})	0.09 ± 0.01	0.11 ± 0.00
Fed-batch glucose	Final titer [mM]	17.2 ± 0.3	33.2 ± 2.4
	Yield (% Cmol Cmol^{-1})	11.2 ± 0.6	21.4 ± 1.1
	Productivity (mM h^{-1})	0.19 ± 0.20	0.30 ± 0.02
Fed-batch glycerol	Final titer [mM]	19.8 ($n = 1$)	33.5 ± 2.7
	Yield (% Cmol Cmol^{-1})	47.8 ($n = 1$)	36.1 ± 0.08
	Productivity (mM h^{-1})	0.13 ($n = 1$)	0.15 ± 0.00

of 47.8% Cmol and a volumetric productivity of 0.13 mM h^{-1}. The extended lag phase observed during glycerol assimilation (Poblete-Castro et al., 2019) might even increase the occurrence of suppressor mutations by induction of the SOS response.

As observed for shake flask cultivations, reproducibility and stable production was restored in a strain overexpressing solely PAL for L-phenylalanine conversion. The strain *P. taiwanensis* GRC3 Δ8Δ*pykA*-tap *attTn7*::P_{14f}*AtPAL* produced up to 33.2 ± 2.4 mM *t*-cinnamate from glucose (**Figure 5C**) and 33.5 ± 2.7 mM from glycerol (**Figure 5D**) in a fed-batch fermentation. While the productivity throughout the whole cultivation of *P. taiwanensis* GRC3 Δ8Δ*pykA*-tap *attTn7*::P_{14f}*AtPAL* on glucose was 0.30 ± 0.02 mM h^{-1}, increasing concentrations of *t*-cinnamate impaired the strain's fitness and productivity. The volumetric productivity within the first 25 h is 0.55 ± 0.08 mM h^{-1}, which is reduced after 38 h to 0.16 ± 0.04 mM h^{-1}. At the same time, a drop in OD_{600} was observed at concentrations above 20 mM *t*-cinnamate. As production continued and cells were still viable at this point as indicated by the ongoing substrate consumption, this drop in OD_{600} values hints toward an increased cumulative burden on the cell. The drop in OD_{600} was not caused by biofilm formation, likely due to the deletion of the biofilm-associated *lap* genes in the GRC3 strain. Membrane adaptation is a key mechanisms of *Pseudomonas* to cope with environmental stress. Membrane active substances and certain environmental conditions cause adaptations such as *cis*- to *trans*-isomerization of fatty acids to increase membrane rigidity and lead to the formation of outer membrane vesicles to facilitate biofilm formation (Eberlein et al., 2018). In addition, many porins as well as import and export pumps are differentially expressed under stress, altering membrane permeability (Volkers et al., 2006; Ramos et al., 2015). The importance of membrane structure on similar compounds such as *p*-coumarate has recently been demonstrated (Calero et al., 2018) and can likely be partially be transferred to *t*-cinnamate tolerance.

As enzyme inhibition of different PALs by *t*-cinnamate has been observed in various studies (Nijkamp et al., 2007; McKenna and Nielsen, 2011), the decrease in productivity could also be linked to this effect. However, no L-phenylalanine accumulation was observed over the course of the fermentations, indicating that the precursor was completely converted by the PAL. Furthermore, no L-tyrosine accumulation was observed during fermentations.

In contrast to the strain overexpressing AroG^{fbr} and PheA^{T310I}, experiments with strain *P. taiwanensis* GCR3 Δ8Δ*pykA*-tap *attTn7*::P_{14f}*AtPAL* are highly reproducible. While an additional expression of AroG^{fbr} and PheA^{T310I} led to higher yields in shake flasks, solely PAL expression in the L-phenylalanine-overproducing chassis strains enables both higher titers and volumetric productivities in fed-batch fermentations (**Table 3**). To the best of our knowledge, these are the highest *t*-cinnamate yields reported for a microbial production process. While titers of 6.5 g L^{-1} (43.9 mM) have been reported in fed-batch fermentations of *t*-cinnamate-producing strains of *E. coli* (Bang et al., 2018), these processes required the addition of yeast extract in the initial batch medium and casamino acid in the feeding solution. The utilization of these engineered *P. taiwanensis* GRC strains enables growth without the addition of complex supplements. However, tolerance mechanisms for *t*-cinnamate remain to be further investigated and exploited to enhance titers and thus the feasibility of microbial *t*-cinnamate synthesis.

CONCLUSION

In this study, we describe the rational engineering of *P. taiwanensis* VLB120 towards efficient *t*-cinnamate production. The plasmid-free strain bearing no auxotrophies synthesized *t*-cinnamate from glucose or glycerol, with yields of up to 48% Cmol Cmol^{-1} in shake flask cultivations. Titers were increased up to 33.35 mM in fed-batch fermentations using glycerol as sole carbon source. As product titers achieved in this study impair fitness and productivity of

the chassis strains, the native tolerance features of *Pseudomonas* allowing enhanced *t*-cinnamate tolerance require further investigation and enhancement to increase process efficiency. One promising target is the ABC transporter Ttg2ABC, an extrusion pump involved in *p*-coumarate tolerance (Calero et al., 2018). An overexpression of this pump might deliver enhanced tolerance toward *t*-cinnamate, its regulation however remains to be investigated. Fine-tuning of additional *aroG* and *pheA* overexpression, e.g., by using weaker or inducible promoters, could furthermore avoid the observed growth defects while still maintaining the high yields achieved with this setup. Overall, the results underline the high potential of *Pseudomonas* species to produce chemical building blocks using aromatic amino acids as precursors. The establishment of efficient microbial production of the model compound *t*-cinnamate will in future serve as foundation to expand the product collection of this versatile species, ranging from bulk chemicals such as styrene (Lee et al., 2019) to specialty compounds such as stilbenes (van Summeren-Wesenhagen and Marienhagen, 2015).

DATA AVAILABILITY STATEMENT

All datasets generated for this study are included in the article/**Supplementary Material**.

AUTHOR CONTRIBUTIONS

NW conceived and supervised the study with the help of LB. MO and MF performed the experiments with support of BW and CL. BW provided the GRC strains with deletions for L-tyrosine accumulation and deletion vectors. MO wrote the manuscript with the help of BW and NW. All authors read and approved the manuscript.

FUNDING

MO, BW, CL, and NW were funded by the German Research Foundation (DFG) through the Emmy Noether program (WI 4255/1-1).

ACKNOWLEDGMENTS

We kindly acknowledge Eppendorf AG for assistance regarding scripting of automated feed protocols.

SUPPLEMENTARY MATERIAL

The Supplementary Material for this article can be found online at: https://www.frontiersin.org/articles/10.3389/fbioe.2019.00312/full#supplementary-material

REFERENCES

Ahmad, S., Weisburg, W. G., and Jensen, R. A. (1990). Evolution of aromatic amino acid biosynthesis and application to the fine-tuned phylogenetic positioning of enteric bacteria. *J. Bacteriol.* 172, 1051–1061. doi: 10.1128/jb.172.2.1051-1061.1990

Bang, H. B., Lee, K., Lee, Y. J., and Jeong, K. J. (2018). High-level production of *trans*-cinnamic acid by fed-batch cultivation of *Escherichia coli*. *Process Biochem.* 68, 30–36. doi: 10.1016/j.procbio.2018.01.026

Becker, J., and Wittmann, C. (2012). Bio-based production of chemicals, materials and fuels – *Corynebacterium glutamicum* as versatile cell factory. *Curr. Opin. Biotechnol.* 23, 631–640. doi: 10.1016/j.copbio.2011.11.012

Belda, E., van Heck, R. G. A., José Lopez-Sanchez, M., Cruveiller, S., Barbe, V., Fraser, C., et al. (2016). The revisited genome of *Pseudomonas putida* KT2440 enlightens its value as a robust metabolic chassis. *Environ. Microbiol.* 18, 3403–3424. doi: 10.1111/1462-2920.13230

Boyer, H. W., and Roulland-Dussoix, D. (1969). A complementation analysis of the restriction and modification of DNA in *Escherichia coli*. *J. Mol. Biol.* 41, 459–472. doi: 10.1016/0022-2836(69)90288-5

Bruckner, R. (2010). *Organic Mechanisms: Reactions, Stereochemistry and Synthesis, 3rd Edn*, ed M. Harmata. Berlin: Springer. doi: 10.1007/978-3-642-03651-4

Calero, P., Jensen, S. I., Bojanovič, K., Lennen, R. M., Koza, A., and Nielsen, A. T. (2018). Genome-wide identification of tolerance mechanisms toward *p*-coumaric acid in *Pseudomonas putida*. *Biotechnol. Bioeng.* 115, 762–774. doi: 10.1002/bit.26495

Chavarría, M., Nikel, P. I., Pérez-Pantoja, D., and de Lorenzo, V. (2013). The Entner-Doudoroff pathway empowers *Pseudomonas putida* KT2440 with a high tolerance to oxidative stress. *Environ. Microbiol.* 15, 1772–1785. doi: 10.1111/1462-2920.12069

Chemler, J. A., and Koffas, M. A. (2008). Metabolic engineering for plant natural product biosynthesis in microbes. *Curr. Opin. Biotechnol.* 19, 597–605. doi: 10.1016/j.copbio.2008.10.011

Chen, Y.-L., Huang, S.-T., Sun, F.-M., Chiang, Y.-L., Chiang, C.-J., Tsai, C.-M., et al. (2011). Transformation of cinnamic acid from *trans*- to *cis*-form raises a notable bactericidal and synergistic activity against multiple-drug resistant *Mycobacterium tuberculosis*. *Eur. J. Pharm. Sci.* 43, 188–194. doi: 10.1016/j.ejps.2011.04.012

Cho, C., Choi, S. Y., Luo, Z. W., and Lee, S. Y. (2015). Recent advances in microbial production of fuels and chemicals using tools and strategies of systems metabolic engineering. *Biotechnol. Adv.* 33, 1455–1466. doi: 10.1016/j.biotechadv.2014.11.006

Cochrane, F. C., Davin, L. B., and Lewis, N. G. (2004). The *Arabidopsis* phenylalanine ammonia lyase gene family: kinetic characterization of the four PAL isoforms. *Phytochemistry* 65, 1557–1564. doi: 10.1016/j.phytochem.2004.05.006

Cui, J. D., Jia, S. R., and Sun, A. Y. (2008). Influence of amino acids, organic solvents and surfactants for phenylalanine ammonia lyase activity in recombinant *Escherichia coli*. *Lett. Appl. Microbiol.* 46, 631–635. doi: 10.1111/j.1472-765X.2008.02364.x

de Lorenzo, V., and Timmis, K. N. (1994). [31] Analysis and construction of stable phenotypes in Gram-negative bacteria with Tn5- and Tn10-derived minitransposons. *Methods Enzymol.* 235, 386–405. doi: 10.1016/0076-6879(94)35157-0

De, P., Baltas, M., and Bedos-Belval, F. (2011). Cinnamic acid derivatives as anticancer agents - a review. *Curr. Med. Chem.* 18, 1672–1703. doi: 10.2174/092986711795471347

Ding, D., Liu, Y., Xu, Y., Zheng, P., Li, H., Zhang, D., et al. (2016). Improving the production of L-phenylalanine by identifying key enzymes through multi-enzyme reaction system *in vitro*. *Sci. Rep.* 6:32208. doi: 10.1038/srep32208

Domröse, A., Klein, A. S., Hage-Hülsmann, J., Thies, S., Svensson, V., Classen, T., et al. (2015). Efficient recombinant production of prodigiosin in *Pseudomonas putida*. *Front. Microbiol.* 6:972. doi: 10.3389/fmicb.2015.00972

Eberlein, C., Baumgarten, T., Starke, S., and Heipieper, H. J. (2018). Immediate response mechanisms of Gram-negative solvent-tolerant bacteria to cope with environmental stress: cis-trans isomerization of unsaturated fatty acids and outer membrane vesicle secretion. *Appl. Microbiol. Biotechnol.* 102, 2583–2593. doi: 10.1007/s00253-018-8832-9

Fausta, N., Mirella, N., di Felice, M., and Scaccini, C. (1999). Benzoic and cinnamic acid derivatives as antioxidants: structure–activity relation. *J. Agric. Food Chem.* 47, 1453–1459. doi: 10.1021/jf980737w

Fiske, M. J., Whitaker, R. J., and Jensen, R. A. (1983). Hidden overflow pathway to L-phenylalanine in *Pseudomonas aeruginosa*. *J. Bacteriol.* 154, 623–631.

Gibson, D. G., Young, L., Chuang, R.-Y., Venter, J. C., Hutchison, C. A., and Smith, H. O. (2009). Enzymatic assembly of DNA molecules up to several hundred kilobases. *Nat. Methods* 6, 343–345. doi: 10.1038/nmeth.1318

Guroff, G., and Ito, T. (1965). Phenylalanine hydroxylation by *Pseudomonas* species (ATCC 11299a). *J. Biol. Chem.* 240, 142–146.

Guzman, J. D. (2014). Natural cinnamic acids, synthetic derivatives and hybrids with antimicrobial activity. *Molecules* 19, 19292–19349. doi: 10.3390/molecules191219292

Hartmans, S., Smits, J. P., Van Der Werf, M. J., Volkering, F., and De Bont, J. A. M. (1989). 2-Phenylethanol in the styrene-degrading metabolism of styrene oxide and 2-phenylethanol in the styrene-degrading *Xanthobacter* strain 124X. *Appl. Environ. Microbiol.* 55, 2850–2855.

Hatti-Kaul, R., Törnvall, U., Gustafsson, L., and Börjesson, P. (2007). Industrial biotechnology for the production of bio-based chemicals - a cradle-to-grave perspective. *Trends Biotechnol.* 25, 119–124. doi: 10.1016/j.tibtech.2007.01.001

Herrera, M. C., Duque, E., RodrÃ-guez-Herva, J. J., FernÃ¡ndez-Escamilla, A. M., and Ramos, J. L. (2010). Identification and characterization of the PhhR regulon in *Pseudomonas putida*. *Environ. Microbiol.* 12, 1427–1438. doi: 10.1111/j.1462-2920.2009.02124.x

Hosseinpour Tehrani, H., Geiser, E., Engel, M., Hartmann, S. K., Hossain, A. H., Punt, P. J., et al. (2019). The interplay between transport and metabolism in fungal itaconic acid production. *Fungal Genet. Biol.* 125, 45–52. doi: 10.1016/j.fgb.2019.01.011

Huang, J., Gu, M., Lai, Z., Fan, B., Shi, K., Zhou, Y.-H., et al. (2010). Functional analysis of the *Arabidopsis* PAL gene family in plant growth, development, and response to environmental stress. *Plant Physiol.* 153, 1526–1538. doi: 10.1104/pp.110.157370

Huccetogullari, D., Luo, Z. W., and Lee, S. Y. (2019). Metabolic engineering of microorganisms for production of aromatic compounds. *Microb. Cell Fact.* 18:41. doi: 10.1186/s12934-019-1090-4

Isken, S., and de Bont, J. A. M. (1998). Bacteria tolerant to organic solvents. *Extremophiles* 2, 229–238. doi: 10.1007/s007920050065

Johnson, C. W., Salvachúa, D., Khanna, P., Smith, H., Peterson, D. J., and Beckham, G. T. (2016). Enhancing muconic acid production from glucose and lignin-derived aromatic compounds via increased protocatechuate decarboxylase activity. *Metab. Eng. Commun.* 3, 111–119. doi: 10.1016/j.meteno.2016.04.002

Johnson, C. W., Salvachúa, D., Rorrer, N. A., Black, B. A., Vardon, D. R., St. John, P. C., et al. (2019). Innovative chemicals and materials from bacterial aromatic catabolic pathways. *Joule* 3, 1523–1537. doi: 10.1016/j.joule.2019.05.011

Kallscheuer, N., Classen, T., Drepper, T., and Marienhagen, J. (2019). Production of plant metabolites with applications in the food industry using engineered microorganisms. *Curr. Opin. Biotechnol.* 56, 7–17. doi: 10.1016/j.copbio.2018.07.008

Kieboom, J., Dennis, J. J., Zylstra, G. J., and de Bont, J. A. (1998). Active efflux of organic solvents by *Pseudomonas putida* S12 is induced by solvents. *J. Bacteriol.* 180, 6769–6772.

Kikuchi, Y., Tsujimoto, K., and Kurahashi, O. (1997). Mutational analysis of the feedback sites of phenylalanine-sensitive 3-deoxy-D-arabino-heptulosonate-7-phosphate synthase of *Escherichia coli*. *Appl. Environ. Microbiol.* 63, 761–762.

Köhler, K. A., Rückert, C., Schatschneider, S., Vorhölter, F. J., Szczepanowski, R., Blank, L. M., et al. (2013). Complete genome sequence of *Pseudomonas* sp. strain VLB120 a solvent tolerant, styrene degrading bacterium, isolated from forest soil. *J. Biotechnol.* 168, 729–730. doi: 10.1016/j.jbiotec.2013.10.016

Kohlstedt, M., Starck, S., Barton, N., Stolzenberger, J., Selzer, M., Mehlmann, K., et al. (2018). From lignin to nylon: cascaded chemical and biochemical conversion using metabolically engineered *Pseudomonas putida*. *Metab. Eng.* 47, 279–293. doi: 10.1016/j.ymben.2018.03.003

Kuepper, J., Dickler, J., Biggel, M., Behnken, S., Jäger, G., Wierckx, N., et al. (2015). Metabolic engineering of *Pseudomonas putida* KT2440 to produce anthranilate from glucose. *Front. Microbiol.* 6:1310. doi: 10.3389/fmicb.2015.01310

Kusumawardhani, H., Hosseini, R., and de Winde, J. H. (2018). Solvent tolerance in bacteria: fulfilling the promise of the biotech era? *Trends Biotechnol.* 36, 1025–1039. doi: 10.1016/j.tibtech.2018.04.007

Lee, K., Bang, H. B., Lee, Y. H., and Jeong, K. J. (2019). Enhanced production of styrene by engineered *Escherichia coli* and *in situ* product recovery (ISPR) with an organic solvent. *Microb. Cell Fact.* 18:79. doi: 10.1186/s12934-019-1129-6

Lenzen, C., Wynands, B., Otto, M., Bolzenius, J., Mennicken, P., Wierckx, N., et al. (2019). High-yield production of 4-hydroxybenzoate from glucose or glycerol by an engineered *Pseudomonas taiwanensis* VLB120. *Front. Bioeng. Biotechnol.* 7:130. doi: 10.3389/fbioe.2019.00130

Lian, J., McKenna, R., Rover, M. R., Nielsen, D. R., Wen, Z., and Jarboe, L. R. (2016). Production of biorenewable styrene: utilization of biomass-derived sugars and insights into toxicity. *J. Ind. Microbiol. Biotechnol.* 43, 595–604. doi: 10.1007/s10295-016-1734-x

Martínez-García, E., and de Lorenzo, V. (2011). Engineering multiple genomic deletions in Gram-negative bacteria: analysis of the multi-resistant antibiotic profile of *Pseudomonas putida* KT2440. *Environ. Microbiol.* 13, 2702–2716. doi: 10.1111/j.1462-2920.2011.02538.x

McKenna, R., and Nielsen, D. R. (2011). Styrene biosynthesis from glucose by engineered *E. coli*. *Metab. Eng.* 13, 544–554. doi: 10.1016/j.ymben.2011.06.005

Mi, J., Becher, D., Lubuta, P., Dany, S., Tusch, K., Schewe, H., et al. (2014). *De novo* production of the monoterpenoid geranic acid by metabolically engineered *Pseudomonas putida*. *Microb. Cell Fact.* 13:170. doi: 10.1186/s12934-014-0170-8

Molina-Santiago, C., Cordero, B. F., Daddaoua, A., Udaondo, Z., Manzano, J., Valdivia, M., et al. (2016). *Pseudomonas putida* as a platform for the synthesis of aromatic compounds. *Mircobiology* 162, 1535–1543. doi: 10.1099/mic.0.000333

Nijkamp, K., van Luijk, N., de Bont, J. A. M., and Wery, J. (2005). The solvent-tolerant *Pseudomonas putida* S12 as host for the production of cinnamic acid from glucose. *Appl. Microbiol. Biotechnol.* 69, 170–177. doi: 10.1007/s00253-005-1973-7

Nijkamp, K., Westerhof, R. G., Ballerstedt, H., De Bont, J. A., and Wery, J. (2007). Optimization of the solvent-tolerant *Pseudomonas putida* S12 as host for the production of *p*-coumarate from glucose. *Appl. Microbiol. Biotechnol.* 74, 617–624. doi: 10.1007/s00253-006-0703-0

Nikel, P. I., Chavarría, M., Fuhrer, T., Sauer, U., and de Lorenzo, V. (2015). *Pseudomonas putida* KT2440 strain metabolizes glucose through a cycle formed by enzymes of the Entner-Doudoroff, Embden-Meyerhof-Parnas, and pentose phosphate pathways. *J. Biol. Chem.* 290, 25920–25932. doi: 10.1074/jbc.M115.687749

Nikel, P. I., Kim, J., and de Lorenzo, V. (2014). Metabolic and regulatory rearrangements underlying glycerol metabolism in *Pseudomonas putida* KT2440. *Environ. Microbiol.* 16, 239–254. doi: 10.1111/1462-2920.12224

Noda, S., Miyazaki, T., Miyoshi, T., Miyake, M., Okai, N., Tanaka, T., et al. (2011). Cinnamic acid production using *Streptomyces lividans* expressing phenylalanine ammonia lyase. *J. Ind. Microbiol. Biotechnol.* 38, 643–648. doi: 10.1007/s10295-011-0955-2

Olasupo, N. A., Fitzgerald, D. J., Gasson, M. J., and Narbad, A. (2003). Activity of natural antimicrobial compounds against *Escherichia coli* and *Salmonella enterica* serovar *Typhimurium*. *Lett. Appl. Microbiol.* 37, 448–451. doi: 10.1046/j.1472-765X.2003.01427.x

Panke, S., Witholt, B., Schmid, A., and Wubbolts, M. G. (1998). Towards a biocatalyst for (S)-styrene oxide production: characterization of the styrene degradation pathway of *Pseudomonas* sp. strain VLB120. *Appl. Environ. Microbiol.* 64, 2032–2043.

Poblete-Castro, I., Wittmann, C., and Nikel, P. I. (2019). Biochemistry, genetics and biotechnology of glycerol utilization in *Pseudomonas* species. *Microb. Biotechnol.* 1–22. doi: 10.1111/1751-7915.13400

Puigbo, P., Guzman, E., Romeu, A., and Garcia-Vallve, S. (2007). OPTIMIZER: a web server for optimizing the codon usage of DNA sequences. *Nucleic Acids Res.* 35, W126–W131. doi: 10.1093/nar/gkm219

Ramos, J.-L., Sol Cuenca, M., Molina-Santiago, C., Segura, A., Duque, E., Gómez-García, M. R., et al. (2015). Mechanisms of solvent resistance mediated by interplay of cellular factors in *Pseudomonas putida*. *FEMS Microbiol. Rev.* 39, 555–566. doi: 10.1093/femsre/fuv006

Ramos, J. L., Duque, E., Gallegos, M.-T., Godoy, P., Ramos-Gonzalez, M. I., Rojas, A., et al. (2002). Mechanisms of solvent tolerance in Gram-negative bacteria. *Annu. Rev. Microbiol.* 56, 743–768. doi: 10.1146/annurev.micro.56.012302.161038

Rodriguez, A., Martínez, J. A., Flores, N., Escalante, A., Gosset, G., and Bolivar, F. (2014). Engineering *Escherichia coli* to overproduce aromatic amino acids and derived compounds. *Microb. Cell Fact.* 13:126. doi: 10.1186/s12934-014-0126-z

Salum, M. L., and Erra-Balsells, R. (2013). High purity *cis*-cinnamic acid preparation for studying physiological role of *trans*-cinnamic and *cis*-cinnamic acids in higher plants. *Environ. Control Biol.* 51, 1–10. doi: 10.2525/ecb.51.1

Sardessai, Y., and Bhosle, S. (2002). Tolerance of bacteria to organic solvents. *Res. Microbiol.* 153, 263–268. doi: 10.1016/S0923-2508(02)01319-0

Segura, A., Molina, L., Fillet, S., Krell, T., Bernal, P., Muñoz-Rojas, J., et al. (2012). Solvent tolerance in Gram-negative bacteria. *Curr. Opin. Biotechnol.* 23, 415–421. doi: 10.1016/j.copbio.2011.11.015

Straathof, A. J. J., Wahl, S. A., Benjamin, K. R., Takors, R., Wierckx, N., and Noorman, H. J. (2019). Grand research challenges for sustainable industrial biotechnology. *Trends Biotechnol.* 37, 1042–1050. doi: 10.1016/j.tibtech.2019.04.002

Terán, W., Felipe, A., Segura, A., Rojas, A., Ramos, J.-L., and Gallegos, M.-T. (2003). Antibiotic-dependent induction of *Pseudomonas putida* DOT-T1E TtgABC efflux pump is mediated by the drug binding repressor TtgR. *Antimicrob. Agents Chemother.* 47, 3067–3072. doi: 10.1128/AAC.47.10.3067-3072.2003

Tietze, L.-F., Eicher, T., Diederichsen, U., Speicher, A., and Schützenmeister, N. (2015). *Reactions and Syntheses : In the Organic Chemistry Laboratory, 1st Edn*, eds J. Fischer and D. P. Rotella. Weinheim: Wiley VCH.

Tiso, T., Zauter, R., Tulke, H., Leuchtle, B., Li, W.-J., Behrens, B., et al. (2017). Designer rhamnolipids by reduction of congener diversity: production and characterization. *Microb. Cell Fact.* 16:225. doi: 10.1186/s12934-017-0838-y

van Summeren-Wesenhagen, P. V., and Marienhagen, J. (2015). Metabolic engineering of *Escherichia coli* for the synthesis of the plant polyphenol pinosylvin. *Appl. Environ. Microbiol.* 81, 840–849. doi: 10.1128/AEM.02966-14

Vargas-Tah, A., and Gosset, G. (2015). Production of cinnamic and *p*-hydroxycinnamic acids in engineered microbes. *Front. Bioeng. Biotechnol.* 3:116. doi: 10.3389/fbioe.2015.00116

Vargas-Tah, A., Martínez, L. M., Hernández-Chávez, G., Rocha, M., Martínez, A., Bolívar, F., et al. (2015). Production of cinnamic and *p*-hydroxycinnamic acid from sugar mixtures with engineered *Escherichia coli*. *Microb. Cell Fact.* 14:6. doi: 10.1186/s12934-014-0185-1

Velasco, A., Alonso, S., García, J. L., Perera, J., and Díaz, E. (1998). Genetic and functional analysis of the styrene catabolic cluster of *Pseudomonas* sp. strain Y2. *J. Bacteriol.* 180, 1063–1071.

Verhoef, S., Ballerstedt, H., Volkers, R. J. M., de Winde, J. H., and Ruijssenaars, H. J. (2010). Comparative transcriptomics and proteomics of *p*-hydroxybenzoate producing *Pseudomonas putida* S12: novel responses and implications for strain improvement. *Appl. Microbiol. Biotechnol.* 87, 679–690. doi: 10.1007/s00253-010-2626-z

Vogt, T. (2010). Phenylpropanoid biosynthesis. *Mol. Plant* 3, 2–20. doi: 10.1093/mp/ssp106

Volkers, R. J. M., de Jong, A. L., Hulst, A. G., van Baar, B. L. M., de Bont, J. A. M., and Wery, J. (2006). Chemostat-based proteomic analysis of toluene-affected *Pseudomonas putida* S12. *Environ. Microbiol.* 8, 1674–1679. doi: 10.1111/j.1462-2920.2006.01056.x

Volmer, J., Neumann, C., Bühler, B., and Schmid, A. (2014). Engineering of *Pseudomonas taiwanensis* VLB120 for constitutive solvent tolerance and increased specific styrene epoxidation activity. *Appl. Environ. Microbiol.* 80, 6539–6548. doi: 10.1128/AEM.01940-14

Wierckx, N., Ruijssenaars, H. J., de Winde, J. H., Schmid, A., and Blank, L. M. (2009). Metabolic flux analysis of a phenol producing mutant of *Pseudomonas putida* S12: verification and complementation of hypotheses derived from transcriptomics. *J. Biotechnol.* 143, 124–129. doi: 10.1016/j.jbiotec.2009.06.023

Wierckx, N. J., Ballerstedt, H., de Bont, J. A., de Winde, J. H., Ruijssenaars, H. J., and Wery, J. (2008). Transcriptome analysis of a phenol-producing *Pseudomonas putida* S12 construct: genetic and physiological basis for improved production. *J. Bacteriol.* 190, 2822–2830. doi: 10.1128/JB.01379-07

Wynands, B. (2018). *Engineering of Pseudomonas taiwanensis VLB120 for the sustainable production of hydroxylated aromatics* (dissertation). RWTH Aachen University, Aachen, Germany.

Wynands, B., Lenzen, C., Otto, M., Koch, F., Blank, L. M., and Wierckx, N. (2018). Metabolic engineering of *Pseudomonas taiwanensis* VLB120 with minimal genomic modifications for high-yield phenol production. *Metab. Eng.* 47, 121–133. doi: 10.1016/j.ymben.2018.03.011

Wynands, B., Otto, M., Runge, N., Preckel, S., Polen, T., Blank, L. M., et al. (2019). Streamlined *Pseudomonas taiwanensis* VLB120 chassis strains with improved bioprocess features. *ACS Synth. Biol.* 8, 2036–2050. doi: 10.1021/acssynbio.9b00108

Xu, R., Zhang, K., Liu, P., Han, H., Zhao, S., Kakade, A., et al. (2018). Lignin depolymerization and utilization by bacteria. *Bioresour. Technol.* 269, 557–566. doi: 10.1016/j.biortech.2018.08.118

Zambanini, T., Sarikaya, E., Kleineberg, W., Buescher, J. M., Meurer, G., Wierckx, N., et al. (2016). Efficient malic acid production from glycerol with *Ustilago trichophora* TZ1. *Biotechnol. Biofuels* 9:67. doi: 10.1186/s13068-016-0483-4

Zhang, C., Zhang, J., Kang, Z., Du, G., and Chen, J. (2015). Rational engineering of multiple module pathways for the production of L-phenylalanine in *Corynebacterium glutamicum*. *J. Ind. Microbiol. Biotechnol.* 42, 787–797. doi: 10.1007/s10295-015-1593-x

Zobel, S., Benedetti, I., Eisenbach, L., de Lorenzo, V., Wierckx, N., and Blank, L. M. (2015). Tn7-based device for calibrated heterologous gene expression in *Pseudomonas putida*. *ACS Synth. Biol.* 4, 1341–1351. doi: 10.1021/acssynbio.5b00058

Conflict of Interest: The authors declare that the research was conducted in the absence of any commercial or financial relationships that could be construed as a potential conflict of interest.

frontiers in Bioengineering and Biotechnology

ORIGINAL RESEARCH
published: 17 January 2020
doi: 10.3389/fbioe.2019.00480

Comparison of Three Xylose Pathways in *Pseudomonas putida* KT2440 for the Synthesis of Valuable Products

Isabel Bator[1], *Andreas Wittgens*[2,3,4], *Frank Rosenau*[2,3,4], *Till Tiso*[1] *and Lars M. Blank*[1]*

[1] iAMB - Institute of Applied Microbiology, ABBt – Aachen Biology and Biotechnology, RWTH Aachen University, Aachen, Germany, [2] Institute for Pharmaceutical Biotechnology, Ulm-University, Ulm, Germany, [3] Ulm Center for Peptide Pharmaceuticals, Ulm, Germany, [4] Max-Planck-Institute for Polymer Research Mainz, Synthesis of Macromolecules, Mainz, Germany

Pseudomonas putida KT2440 is a well-established chassis in industrial biotechnology. To increase the substrate spectrum, we implemented three alternative xylose utilization pathways, namely the Isomerase, Weimberg, and Dahms pathways. The synthetic operons contain genes from *Escherichia coli* and *Pseudomonas taiwanensis*. For isolating the Dahms pathway in *P. putida* KT2440 two genes (PP_2836 and PP_4283), encoding an endogenous enzyme of the Weimberg pathway and a regulator for glycolaldehyde degradation, were deleted. Before and after adaptive laboratory evolution, these strains were characterized in terms of growth and synthesis of mono-rhamnolipids and pyocyanin. The engineered strain using the Weimberg pathway reached the highest maximal growth rate of 0.30 h^{-1}. After adaptive laboratory evolution the lag phase was reduced significantly. The highest titers of 720 mg L^{-1} mono-rhamnolipids and 30 mg L^{-1} pyocyanin were reached by the evolved strain using the Weimberg or an engineered strain using the Isomerase pathway, respectively. The different stoichiometries of the three xylose utilization pathways may allow engineering of tailored chassis for valuable bioproduct synthesis.

Keywords: ***Pseudomonas putida*, xylose, metabolic engineering, rhamnolipid, phenazine, pyocyanin, flux balance analysis, heterologous production**

OPEN ACCESS

Edited by:
Jean Marie François, UMS3582 Toulouse White Biotechnology (TWB), France

Reviewed by:
Antoine Danchin, INSERM U1016 Institut Cochin, France
Mingfeng Cao, University of Illinois at Urbana-Champaign, United States

***Correspondence:**
Lars M. Blank
lars.blank@rwth-aachen.de

Specialty section:
This article was submitted to Synthetic Biology, a section of the journal Frontiers in Bioengineering and Biotechnology

Received: *04 September 2019*
Accepted: *23 December 2019*
Published: *17 January 2020*

Citation:
Bator I, Wittgens A, Rosenau F, Tiso T and Blank LM (2020) Comparison of Three Xylose Pathways in Pseudomonas putida KT2440 for the Synthesis of Valuable Products. Front. Bioeng. Biotechnol. 7:480. doi: 10.3389/fbioe.2019.00480

INTRODUCTION

For the establishment of a circular bioeconomy, the chemical industry has to overcome the massive and ever-increasing use of fossil resources and the concomitant production of environmental pollutions including greenhouse gases. The alternative is CO_2 as carbon source, either directly or fixed via chemocatalysis or plants (Olah et al., 2009; Goeppert et al., 2012). CO_2-fixation though cannot only proceed under natural conditions, there are also many synthetic approaches to convert CO_2 to valuable products. The conversion of CO_2 mainly results in the production of biomass in microbes and is well-studied. Hence, it immediately becomes clear that the knowledge about CO_2-fixation pathways can be utilized to redirect the metabolic flow into the production of chemicals using the synthetic biology arsenal. On the one hand cell-free systems are used to fix CO_2 via multienzyme cascades (Schwander et al., 2016; Satagopan et al., 2017), on the other hand

engineered autotrophic microbes are used for the production of chemicals based on CO_2 (Lan and Liao, 2011; Angermayr et al., 2012). If the usage of non-autotrophic microbes is desired for the production of multi-carbon compounds via CO_2-fixation, either existing pathways (e.g., the Calvin cycle) or newly designed pathways have to be introduced into the cells (Guadalupe-Medina et al., 2013; Antonovsky et al., 2016; Bouzon et al., 2017; Schada von Borzyskowski et al., 2018), with the outcome of alternative stoichiometries (Liebal et al., 2018). CO_2-fixation via plants is a common choice as lignocellulosic biomass is abundant and does not compete immediately with food applications. Lignocellulosic biomass contains about 25–50% hemicellulose (Saha, 2003). In addition to glucose, the pentose xylose is a dominant building block in hemicellulose. For example, bagasse fibers consist of ∼23% xylose (Lee, 1997). While wheat straw and corn stover are industrially used as carbon source for bioethanol production (Larsen et al., 2008; Maas et al., 2008; Zhao et al., 2018), exemplifying the feasibility of the alternatives, most other microbes than yeast are still on the experimental scale.

The well-characterized chassis *Pseudomonas putida* KT2440 is known for its versatile metabolism, the richness of cofactors, and high solvent tolerance (Ramos et al., 1995; Nelson et al., 2002; Blank et al., 2010; Tiso et al., 2014). Further, the genome is sequenced and well-annotated (Nelson et al., 2002; Belda et al., 2016; Winsor et al., 2016; Nogales et al., 2019). The structure of the central carbon metabolism and the fluxes on different carbon sources are well-studied for *P. putida* KT2440 (Sudarsan et al., 2014). Further, many tools for genomic engineering are available (Martínez-García and de Lorenzo, 2011; Poblete-Castro et al., 2012; Nikel and de Lorenzo, 2018). Besides, its non-pathogenicity contributes to it being a chassis relevant for production of valuable products (Nelson et al., 2002; Tiso et al., 2014; Loeschcke and Thies, 2015; Wittgens and Rosenau, 2018).

However, *P. putida* KT2440 lacks the capability to metabolize xylose. Microbial assimilation of xylose has so far been observed by three different metabolic pathways: An isomerase and two oxidative pathways called Weimberg and Dahms. The Isomerase pathway is characterized by the presence of a xylose isomerase and xylulokinase. The resulting intermediate xylulose is subsequently phosphorylated to xylulose-5-phosphate and introduced into the pentose phosphate pathway. The Isomerase pathway is originally found in prokaryotes, such as *Escherichia coli* and *Bacillus subtilis* (David and Weismeyer, 1970; Wilhelm and Hollenberg, 1985). The oxidative pathways start with the oxidation of xylose to xylonate. This step is often catalyzed by a periplasmic dehydrogenase. A xylonate dehydratase then converts xylonate into 2-keto-3-deoxy-xylonate. The resulting intermediate is dehydrated to α-ketoglutaric semialdehyde in case of the Weimberg pathway. In case of the Dahms pathway, α-ketoglutaric semialdehyde is split by an aldolase into pyruvate and glycolaldehyde. While pyruvate is directly converted to acetyl-CoA in the central carbon metabolism, glycolaldehyde is further metabolized in several steps to 2-phosphoglycerate (Franden et al., 2018). 2-Phosphoglycerate is then converted in glycolysis. In the Weimberg pathway, an additional oxidation step from α-ketoglutaric semialdehyde to 2-oxoglutarate is present. The latter metabolite is converted in the tricarboxylic acid (TCA) cycle (**Figure 1**). The Weimberg pathway was reported for example to be present in *P. fragi*, *Haloferax volcanii*, and *Caulobacter crescentus* (Weimberg, 1961; Stephens et al., 2007; Johnsen et al., 2009). The genes of the latter species were already heterologously expressed in different organisms to establish the Weimberg pathway (Meijnen et al., 2009; Radek et al., 2014; Rossoni et al., 2018). Recently, also *P. taiwanensis* VLB120 was found to be a native xylose-consumer using the Weimberg pathway (Köhler et al., 2015). The Dahms pathway was first found to be present in an unclassified *Pseudomonas* strain (Dahms, 1974). Some of the genes of *C. crescentus* were also heterologously expressed to establish the Dahms pathway in *E. coli*, because *E. coli* harbors a gene coding for an aldolase, which catalyzes the last step of the Dahms pathway (Choi et al., 2017; Cabulong et al., 2018).

P. putida KT2440 has already been engineered to utilize xylose via the Isomerase pathway (Le Meur et al., 2012; Dvorák and de Lorenzo, 2018). Furthermore, *P. putida* S12 was equipped successfully with xylose metabolism genes to establish the Isomerase and the Weimberg pathway (Meijnen et al., 2008, 2009). In the studies mentioned above, growth via the Isomerase pathway was rather slow. This phenomenon occurred because most of the substrate was oxidized to the dead-end product xylonate. Further, xylose transport was reported to be inefficient in *P. putida* KT2440. By implementing adaptive laboratory evolution (ALE) growth on xylose could be improved (Meijnen et al., 2008). Using a different approach, Dvorák and de Lorenzo additionally inserted the proton-coupled symporter XylE, also achieving improved growth (Dvorák and de Lorenzo, 2018).

So far, metabolic engineering approaches were limited to metabolic alterations in order to synthesize a target compound based on a previously determined substrate. We here propose to exploit the metabolic potential of microbes for the production of chemicals by electing for the substrate of choice the most suited degradation pathway. Pseudomonads are suitable hosts for the heterologous production of several products, e.g., surfactants, aromatics, terpenoids, and phenazines besides others (Wittgens et al., 2011, 2018; Loeschcke and Thies, 2015; Schmitz et al., 2015b; Tiso et al., 2017; Wynands et al., 2018). However, the usage of xylose for the synthesis of valuable chemicals with *P. putida* KT2440 has not been reported so far.

In this work, we aimed at engineering a chassis, which can be used for the production of desired secondary metabolites using xylose. First, we investigated the theoretical potential for the synthesis of valuable products using the different xylose pathways via flux balance analysis (FBA). Second, we implemented the three different xylose pathways into *P. putida* KT2440 and optimized growth by ALE. Third, we used these strains for the synthesis of mono-rhamnolipids and pyocyanin, a derivative of phenazines. We demonstrate efficient growth on xylose via the oxidative pathways. The results show that using xylose pathways having different stoichiometries leads to differences in substrate consumption, growth, and production rates, as well as in biomass and product yields. We propose to use different xylose degradation pathways in dependence of product needs.

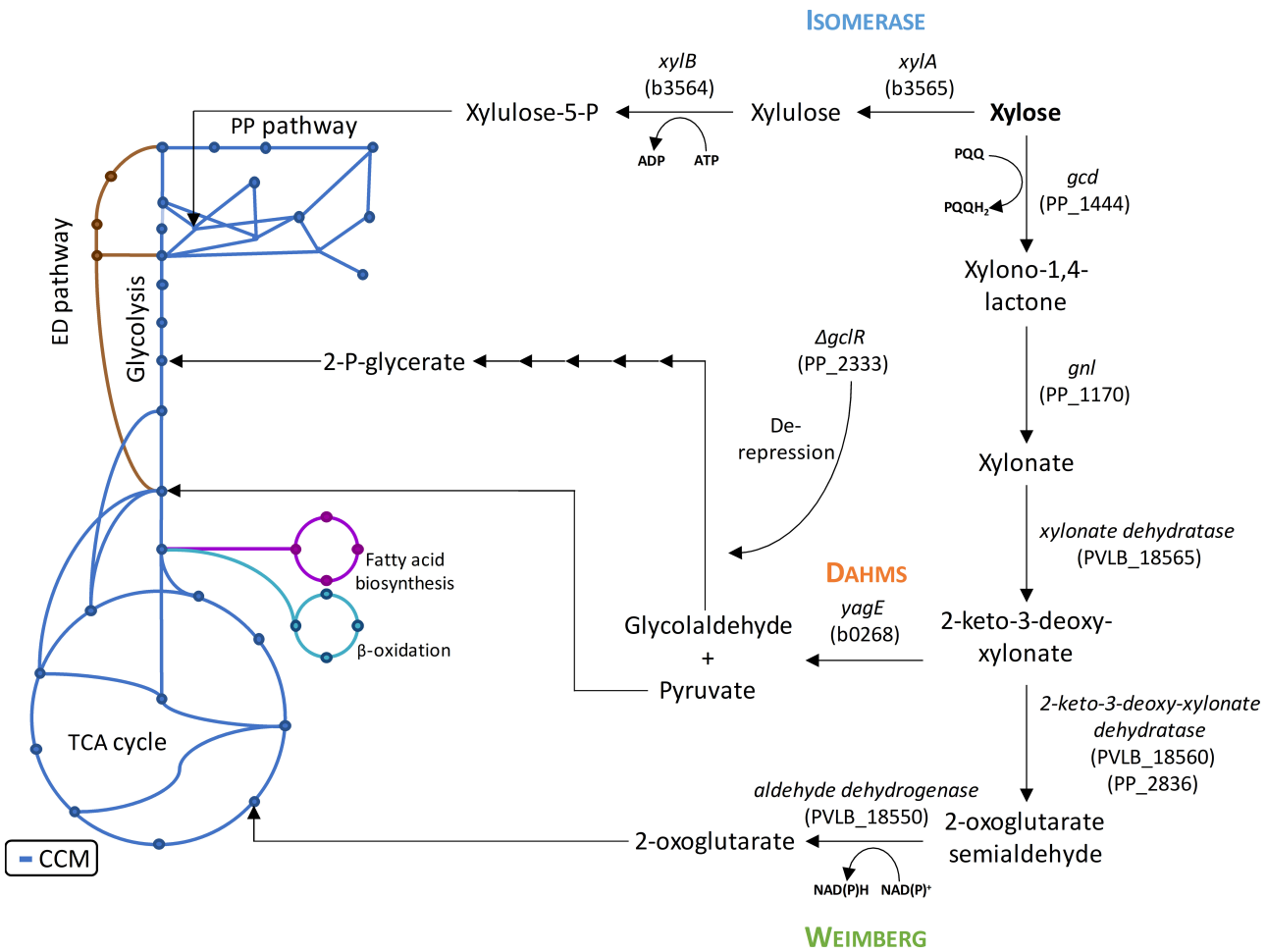

FIGURE 1 | Introduction of xylose metabolism pathways into the central carbon metabolism of *P. putida* KT2440 with the presumed endogenous enzymes and heterologous enzymes from *E. coli* DH5α and *P. taiwanensis* VLB120. The blue lines indicate the central carbon metabolism based on (Sudarsan et al., 2014). The PP numbers represent the locus tag in *P. putida* KT2440, the PVLB numbers represent the locus tag in *P. taiwanensis* VLB120, and the b numbers represent the locus tag in *E. coli* K12, of which *E. coli* DH5α is derived from. ADP, adenosine diphosphate; ATP, adenosine triphosphate; NAD^+, nicotinamide adenine dinucleotide; NADH, reduced nicotinamide adenine dinucleotide; PQQ, pyrroloquinoline quinone; $PQQH_2$, reduced pyrroloquinoline quinone.

MATERIALS AND METHODS

Bacterial Strains, Media, and Growth Conditions

For strain maintenance and cloning experiments, the strains *P. putida* KT2440 (DSM6125, ATCC47054), *E. coli* DH5α (New England Biolabs, Ipswich, MA, USA), and *E. coli* PIR2 (ThermoFisher Scientific, Waltham, MA, USA) were routinely cultivated in LB medium containing 10 g L^{-1} peptone, 5 g L^{-1} yeast extract, and 10 g L^{-1} NaCl. *P. putida* was cultivated at 30°C and *E. coli* at 37°C. If required, 50 μg mL^{-1} kanamycin or 30 μg mL^{-1} gentamycin were added to the medium to avoid loss of plasmid. After mating procedures, *P. putida* strains were selected on cetrimide agar (Sigma-Aldrich, St. Louis, MO, USA). Growth and production experiments were performed using M9 minimal medium with a final composition (per L) of 8.5 g $Na_2HPO_4x2H_2O$, 3 g KH_2PO_4, 0.5 g NaCl, 1 g NH_4Cl, 2 mM $MgSO_4$, 4.87 mg $FeSO_4x7H_2O$, 4.12 mg $CaCl_2x2H_2O$, 1.5 mg $MnCl_2x4H_2O$, 1.87 mg $ZnSO_4x7H_2O$, 0.3 mg H_3BO_3, 0.25 mg $Na_2MoO_4x2H_2O$, 0.15 mg $CuCl_2x2H_2O$, 0.84 mg $Na_2EDTAx2H_2O$ (Sambrook and Russell, 2001), and 10 g glucose for pre-cultures or 10 g xylose for main cultures. Growth experiments were performed in 500 mL shake flasks with 10% filling volume at 200 rpm and in 24-deep well-plates (SystemDuetz; Enzyscreen B.V., Heemstede, The Netherlands) with 1 mL filling volume at 300 rpm.

^{13}C-Labeling Experiments

Strains for the isotope labeling experiments were grown under the conditions stated above. The medium contained 50% of 1-^{13}C labeled xylose (99% purity, Sigma-Aldrich, St. Louis, MO, USA). When the culture reached pseudo-steady state, samples with defined amounts of biomass (0.3 mg) were taken, hydrolyzed, and derivatized according to Schmitz et al. (2015a). The MS

data were processed with iMS2Flux (Poskar et al., 2012), which enables the correction of the data for the presence of naturally occurring isotopes and the determination of the fractional labeling of selected amino acids. The fractional labeling indicates the fraction of ^{13}C-labeled carbon atoms.

Plasmid and Strain Construction

The genes for xylose utilization were amplified from genomic DNA of *E. coli* DH5α and *P. taiwanensis* VLB120 (isolated with High Pure PCR Template Preparation Kit, Roche Holding, Basel, Switzerland). Plasmid construction of pBT-Isomerase, pBT-Weimberg, and pBT-Dahms was planned with NEBuilder Assembly online tool and performed with NEBuilder HiFi DNA Assembly (New England Biolabs, Ipswich, MA, USA) (Gibson et al., 2009). The expression vector pBT including the constitutive P_{tac} promoter (Koopman et al., 2010) was linearized with XbaI (New England Biolabs, Ipswich, MA, USA) prior to assembly. DNA fragments for Gibson Assembly were amplified using Q5 High-Fidelity DNA Polymerase (New England Biolabs, Ipswich, MA, USA) according to the manual. All used primers with their nucleotide sequences are listed in the supplemental information (**Supplementary Table 1**). For pBT-Isomerase, the operon *xylAB* (b3565 and b3564 from *E. coli* DH5α) was amplified using primers IB-27 and IB-28 and cloned into the linearized pBT vector by Gibson Assembly. To generate pBT-Weimberg, an operon from *P. taiwanensis* VLB120 was used. The first two genes (PVLB_18555 and PVLB_18550), originally on antisense strand, were amplified using primers IB-63 and IB-64 and the following two genes (PVLB_18560 and PVLB_18565) were amplified using primers IB-65 and IB-66. Afterwards, the linearized pBT vector and both amplified fragments were assembled in one reaction. After that, pBT-Weimberg was used as template for pBT-Dahms. The backbone including PVLB_18555 and PVLB_18550 was amplified from pBT-Weimberg with primers IB-67 and IB-74. Amplification of gene PVLB_18565 from *P. taiwanensis* VLB120 was performed using primers IB-68 and IB-124 and the gene for the aldolase *yagE* (b0268 from *E. coli* DH5α) was amplified using the primers IB-118 and IB-125 to create a synthetic operon. All fragments were assembled via Gibson reactions. In a final step to obtain pBT-Dahms, the putative dehydratase PVLB_18550 was deleted from the assembled vector. Therefore, the vector was amplified with primers IB-93 and IB-94. Subsequently, the amplified vector was self-ligated using T4 Polynucleotide Kinase, T4 DNA Ligase, and T4 DNA Ligase Reaction Buffer (all New England Biolabs GmbH, Ipswich, MA, USA) according to the manual.

The resulting plasmids, pBT-Isomerase, pBT-Weimberg, and pBT-Dahms, were transferred individually into chemically competent *E. coli* PIR2 cells using heat shock according to Hanahan (1983). Transformants were selected on LB agar with kanamycin. Positive colonies were verified via colony PCR using OneTaq 2x Master Mix with Standard Buffer (New England Biolabs, Ipswich, MA, USA). The efficiency of colony PCR was increased by lysis of cell material with alkaline polyethylene glycol according to Chomczynski and Rymaszewski (2006). Plasmids were validated by Sanger sequencing performed by Eurofins (Brussels, Belgium). Subsequently, plasmids were isolated with Monarch Plasmid Miniprep Kit (New England Biolabs, Ipswich, MA, USA) and transferred via electroporation in competent *P. putida* cells according to Choi et al. (2006). Electroporation was performed using a GenePulser Xcell (Biorad, Hercules, CA, USA) using a cuvette with a 2 mm gap and the settings 2.5 kV, 200 Ω, and 25 μF. Plasmids pBT-Isomerase and pBT-Weimberg were transferred individually in *P. putida* KT2440 and *P. putida* KT2440 Δ*gcd*. Plasmid pBT-Dahms was transferred individually in *P. putida* KT2440, *P. putida* KT2440 ΔPP_2836, and *P. putida* KT2440 Δ*gclR* ΔPP_2836. Harboring of the plasmids was verified via colony PCR using primers IB-5 and IB-35 (as above).

Deletion mutants were obtained using the I-*Sce*I-based system developed by Martínez-García and de Lorenzo (2011). Briefly, 700 bp upstream and downstream flanking regions of the target sites, named TS1 and TS2 regions, were amplified from the genomic DNA of *P. putida* KT2440 and cloned into the non-replicative pEMG vector by Gibson Assembly. The resulting plasmids, pEMG-*gcd* and pEMG-PP_2836, were transferred individually into chemically competent *E. coli* PIR2 cells using heat shock as described above. Afterwards, the plasmids were verified by Sanger sequencing and transferred from the *E. coli* PIR2 strains into the required *Pseudomonas* strains via triparental mating according to Wynands et al. (2018). The I-*Sce*I-encoding plasmid pSW-2 was used and no 3-methylbenzoate for induction of I-*Sce*I expression was needed according to Wynands et al. (2018). Positive colonies with loss of kanamycin resistance were verified for targeted deletion by colony PCR using OneTaq 2x Master Mix with Standard Buffer. To obtain marker-free and pure clones, the recombinant strains were cured of pSW-2 plasmid by re-inoculation in LB medium without gentamycin and verified again by colony PCR. In this study, the gene for glucose dehydrogenase (PP_1444) was deleted in the wild type, resulting in *P. putida* KT2440 Δ*gcd*. The gene for the putative 2-keto-3-deoxy-xylonate dehydratase (PP_2836) was deleted in the wild type and *P. putida* KT2440 Δ*gclR* (Li et al., 2019), resulting in *P. putida* KT2440 ΔPP_2836 and *P. putida* KT2440 Δ*gclR* ΔPP_2836.

To demonstrate the production of secondary metabolites, two target molecules, rhamnolipids and phenazines, were chosen. For the production of mono-rhamnolipids, the mini-Tn7 delivery transposon vector (pBG) developed by Zobel et al. (2015), which inserts a synthesis module in a single genomic locus of the chromosome, was used. Therefore, plasmid pBG14ffg with a stronger constitutive, synthetic promoter than pBG14g (Sebastian Köbbing, RWTH Aachen University, personal communication) was used as backbone and amplified with primers SK06 and SK07. The genes enabling rhamnolipid production *rhlAB* from *P. aeruginosa* were amplified with primers SK08 and SK09 and cloned into the amplified backbone by Gibson Assembly. The resulting mini-Tn7 vector pSK02 was integrated into the genome of xylose consuming strains via homologous recombination according to Zobel et al. (2015). The integration of the rhamnolipid synthesis module into the *att*Tn7 site was verified by colony PCR as described above. Mono-rhamnolipid producing clones were identified using cetrimide-blood agar plates (7.5% (v/v) sheep blood;

Fiebig-Naehrstofftechnik, Idstein-Niederauroff, Germany). If rhamnolipid synthesis occurred, a halo around the colony was visible, because of their hemolytic activity. The 10 clones showing the largest halos were selected for experiments in minimal medium with 10 g L^{-1} xylose to quantitatively examine rhamnolipid production. Subsequently, the best three producers of each strain were subjected to replicate experiments and out of these the best was chosen for further characterization and is described in this study.

Phenazine production was achieved by plasmid-based expression. Plasmid pJNN_*phzA1-G1,M,S* (modified from Schmitz et al., 2015b) was transferred into competent xylose consuming strains via electroporation according to Choi et al. (2006). Harboring of the plasmid was confirmed via colony PCR as described above. Based on Schmitz et al. (2015b), five clones were used to inoculate 1 mL minimal medium containing antibiotics and 10 g L^{-1} xylose at a starting OD_{600} of 0.1 and induced with 0.1 mM salicylate to induce phenazine synthesis. If phenazine synthesis occurred, a blue color, which is typical for pyocyanin production, was observed. The best three producers of each strain were subjected to replicate experiments and out of these the best was chosen for further characterization and is described in this study.

All used strains in this study are listed in **Table 1**.

Adaptive Laboratory Evolution

For adaptation to xylose, the different xylose-consuming strains were grown in M9 minimal medium containing 10 g L^{-1} xylose. OD_{600} was measured daily and the cells were sequentially transferred to fresh medium with a starting OD_{600} of 0.1. The sub-culturing was carried out 30 times for the isomerase-strain, 17 times for the Weimberg-strain, and 26 times for the Dahms-strain. The inhomogeneous culture was streaked out on LB-agar to obtain single isolates, which were subsequently tested for adaption to xylose in a 96-well-plate in a Growth Profiler 960 (Enzyscreen B.V., Heemstede, The Netherlands).

Analytical Methods

Analysis of Bacterial Growth

The optical density at 600 nm (OD_{600}) was measured using an Ultrospec 10 cell density meter (Amersham Biosciences, UK). A correlation between OD_{600} and cell dry weight (CDW) was established. An OD_{600} of 1.0 corresponds with a cell dry weight of 369 mg L^{-1}.

Analysis of Xylose and Xylonate

Xylose and xylonate concentrations in the supernatant were analyzed in a Beckmann Coulter System Gold High Performance Liquid Chromatography (HPLC) (Beckmann Coulter, Brea, CA, USA) with a Metab-AAC 300 × 7.8 mm separation column (particle size: 10 µm, ISERA GmbH, Düren, Germany), a UV detector 166 (Beckmann Coulter, Brea, CA, USA) at 210 nm and a refractory index detector (RI 2300, Knauer GmbH, Berlin, Germany). Elution was performed with 5 mM H_2SO_4 at a flow rate of 0.5 ml min^{-1} at 40°C.

TABLE 1 | Bacterial strains used in this study.

Strains and plasmids	Characteristics	References or sources
E. coli		
DH5α	*supE44*, Δ*lacU169* (*Φ80lacZ*ΔM15), *hsdR17* (r_{K-} m_{K+}), *recA1*, *endA1*, *thi-1*, *gyrA96*, *relA1*	Hanahan, 1985
DH5αλ.pir	λ*pir* lysogen of DH5α; host for oriV(R6K) vectors	de Lorenzo and Timmis, 1994
PIR2	F^-, Δ*lac169*, *rpoS*(*Am*), *robA1*, *creC510*, *hsdR514*, *endA*, *recA1* *uidA*(Δ*MluI*)::*pir*; host for *oriV*(R6K) vectors	ThermoFisher Scientific
HB101 pRK2013	Sm^R, *hsdR-M*$^+$, *proA2*, *leuB6*, *thi-1*, *recA*; harboring plasmid pRK2013	Ditta et al., 1980
DH5α pSW-2	DH5α harboring plasmid pSW-2 encoding I-*Sce*I nuclease, tool for genomic deletion	Martínez-García and de Lorenzo, 2011
PIR2 pEMG-PP_2836	PIR2 harboring plasmid pEMG-PP_2836	This study
PIR2 pEMG-*gcd*	PIR2 harboring plasmid pEMG-*gcd*	This study
DH5αλ.pir pTnS-1	DH5αλ*pir* harboring plasmid pTnS-1	Choi et al., 2005
DH5α pBT	DH5α harboring plasmid pBT; expression vector; containing the constitutive *tac* promoter	Koopman et al., 2010
DH5α pBT-Isomerase	DH5α harboring plasmid pBT; containing the *xylAB* genes from *E. coli* DH5α	This study
DH5α pBT-Weimberg	DH5α harboring plasmid pBT; containing the PVLB18550/18555/18560/18565 genes from *P. taiwanensis* VLB120	This study
DH5α pBT-Dahms	DH5α harboring plasmid pBT; containing the PVLB18555/18565 genes from *P. taiwanensis* VLB120 and *yagE* gene from *E. coli* DH5α	This study
PIR2 pBG14ffg	PIR2 harboring Tn7 delivery vector pBG14ffg; containing BCD2-*msfgfp* fusion	Köbbing et al., in preparation
DH5αλ.pir pSK02	DH5αλ.pir harboring Tn7 delivery vector pSK02 for chromosomal integration; containing *rhlAB* genes from *P. aeruginosa* PA01	This study
DH5α pJNN_*phzA1-G1,M,S*	DH5α harboring plasmid pJNN_*phzA1-G1,M,S;* containing *phzA1-G1,M,S* genes from *P. aeruginosa* PA01	Schmitz
P. taiwanensis		
VLB120	Wild type	Panke et al., 1998
P. putida		
KT2440	Wild type	Bagdasarian et al., 1981
KT2440 Δ*gcd*	Δ*gcd*	This study
KT2440 Δ*gclR*	Δ*gclR*	Li et al., 2019
KT2440 ΔPP_2836	ΔPP_2836	This study
KT2440 Δ*gclR* ΔPP_2836	Δ*gclR*, ΔPP_2836	This study

(Continued)

TABLE 1 | Continued

Strains and plasmids	Characteristics	References or sources
KT2440 pIso	Wild type harboring plasmid pBT-Isomerase	This study
KT2440 Δ*gcd* pIso	Δ*gcd* harboring plasmid pBT-Isomerase	This study
KT2440 pWeim	Wild type harboring plasmid pBT-Weimberg	This study
KT2440 Δ*gcd* pWeim	Δ*gcd* harboring plasmid pBT-Weimberg	This study
KT2440 pDahms	Wild type harboring plasmid pBT-Dahms	This study
KT2440 ΔPP_2836 pDahms	ΔPP_2836 harboring plasmid pBT-Dahms	This study
KT2440 Δ*gclR* pDahms	Δ*gclR* harboring plasmid pBT-Dahms	This study
KT2440ΔΔ pDahms	Δ*gclR*, ΔPP_2836 harboring plasmid pBT-Dahms	This study
EM42 Δ*gcd* pSEVA2213_*xylABE*	EM42 Δ*gcd* harboring plasmid pSEVA2213_*xylABE*	Dvorák and de Lorenzo, 2018
KT2440 pWeim2	Isolate of *P. putida* KT2440 pWeim after 17th transfer from laboratory evolution on xylose	This study
KT2440ΔΔ pDahms2	Isolate of *P. putida* KT2440ΔΔ pDahms after 26th transfer from laboratory evolution on xylose	This study
KT2440 pIso_RL	*P. putida* KT2440 pIso with *attTn7::Pffg-rhlAB*	This study
KT2440 pIso2_RL	*P. putida* EM42 Δ*gcd* pSEVA2213_*xylABE* with *attTn7::Pffg-rhlAB*	This study
KT2440 pWeim_RL	*P. putida* KT2440 pWeim with *attTn7::Pffg-rhlAB*	This study
KT2440 pWeim2_RL	*P. putida* KT2440 pWeim2 with *attTn7::Pffg-rhlAB*	This study
KT2440ΔΔ pDahms_RL	*P. putida* KT2440ΔΔ pDahms with *attTn7::Pffg-rhlAB*	This study
KT2440ΔΔ pDahms2_RL	*P. putida* KT2440ΔΔ pDahms2 with *attTn7::Pffg-rhlAB*	This study
KT2440 pIso_PZ	*P. putida* KT2440 pIso harboring plasmid pJNN_*phzA1-G1,M,S*	This study
KT2440 pIso2_PZ	*P. putida* EM42 Δ*gcd* pSEVA2213_*xylABE* harboring plasmid pJNN_*phzA1-G1,M,S*	This study
KT2440 pWeim_PZ	*P. putida* KT2440 pWeim harboring plasmid pJNN_*phzA1-G1,M,S*	This study
KT2440 pWeim2_PZ	*P. putida* KT2440 pWeim2 harboring plasmid pJNN_*phzA1-G1,M,S*	This study
KT2440ΔΔ pDahms_PZ	*P. putida* KT2440ΔΔ pDahms harboring plasmid pJNN_*phzA1-G1,M,S*	This study
KT2440ΔΔ pDahms2_PZ	*P. putida* KT2440ΔΔ pDahms2 harboring plasmid pJNN_*phzA1-G1,M,S*	This study

Analysis of Rhamnolipids

Reversed-phase chromatography was performed for analyzing mono-rhamnolipid concentrations based on a method developed earlier (Behrens et al., 2016; Tiso et al., 2016). For sample preparation, the supernatant was mixed 1:1 with acetonitrile and stored at 4°C overnight. Subsequently, the mixture was centrifuged at 16,500 g for 2 min. All samples were filtered with Phenex RC syringe filters (0.2 μm, Ø 4 mm, Phenomenex, Torrance, USA). The HPLC system Ultimate 3000 with a Corona Veo Charged Aerosol Detector (Thermo Fisher Scientific, Waltham, MA, USA) was used. For separation, a NUCLEODUR C18 Gravity 150 × 4.6 mm column (particle size: 3 mm, Macherey-Nagel GmbH & Co. KG, Düren, Germany) was used. The flow rate was set to 1 ml min^{-1} and the column oven temperature was set to 40°C. Acetonitrile (A) and 0.2% (v/v) formic acid in ultra-pure water (B) were used as running buffers. The method started with a ratio of 70% buffer A: 30% buffer B and a linear gradient was applied to reach a ratio of 80:20% in 8 min. The acetonitrile fraction was increased linearly from 80 to 100% between 9 and 10 min and decreased linearly to 70% between 11 and 12.5 min. The measurement was stopped after 15 min.

Analysis of Phenazines

The concentration of phenazines was determined in a spectrophotometer Cary 60 (Agilent, Santa Clara, CA, USA) by analyzing the blue phenazine derivative pyocyanin. Samples were centrifuged at 16,500 g for 2 min. Afterwards, the supernatant was vortexed and pyocyanin was measured at 691 nm. For quantification, Lambert-Beer's law with an extinction coefficient of 4.31 mM^{-1} cm^{-1} for pyocyanin was used (Filloux and Ramos, 2014).

Analysis of Proteinogenic Amino Acids

^{13}C-labeling pattern of proteinogenic amino acids were determined by gas chromatography coupled with mass spectrometry (GC-MS) as described in Schmitz et al. (2015a). A Trace GC Ultra coupled to an ISQ single quadrupole mass spectrometer with a TriPlus RSH autosampler (all Thermo Fisher Scientific, Waltham, MA, USA) was used. For separation, a TraceGOLD TG-5SilMS capillary column (length: 30 mm, inner diameter: 0.25 mm, film thickness: 0.25 μm, Thermo Fisher Scientific, Waltham, MA, USA) was used. A sample volume of 2 μL was injected at 270°C with a split ratio of 1:50. The flow rate of the carrier gas helium was set to 1 mL min^{-1} and the oven temperature was kept constant for 1 min at 140°C. The temperature was increased with a gradient of 10°C min^{-1} to 310°C and then kept constant for 1 min. The temperature of the transfer line and the ion source were both set to 280°C. Ionization was performed by electron impact ionization at −70 eV. All raw data were analyzed using Xcalibur (Thermo Fisher Scientific, Waltham, MA, USA).

Flux Balance Analysis

For the prediction of product yields, the genome-scale model of *P. putida* KT2440, *i*JN1411, was used (Nogales et al., 2017). All simulations were carried out in MATLAB (version R2017b, the Mathworks, Inc., Natick, MA, USA) using the COBRA toolbox (Schellenberger et al., 2011), with the linear programming solver

of Gurobi[1]. First, the existing model network was extended by the xylose utilization pathways as well as the biosynthesis routes to the desired products, e.g., mono-rhamnolipids, pyocyanin, and ethylene glycol, using reaction information from KEGG (Ogata et al., 1999). Subsequently, the evaluation of the respective product yields for the usage of the three xylose utilization pathways and their combination was performed. Here, the uptake of xylose for all investigated cases was set to 10 mmol g_{CDW}^{-1} h^{-1} and the uptake of other carbon sources (e.g., glucose) was set to zero. The production of the target molecule was used as objective function in the extended model.

RESULTS

Alternative Xylose Utilization Pathways for Maximal Product Yield

With FBA one can compute the maximal product yield in different scenarios (e.g., growth, maintenance coefficients, aeration). Here, the genome-scale model *P. putida* KT2440 *i*JN1411 (Nogales et al., 2017) was modified by introducing the alternative xylose utilization pathways. In addition, various synthesis reactions for valuable products according to Werpy and Petersen (2004) and chemicals we are working on were introduced into *i*JN1411.

The maximal product yields of 12 of the 14 metabolites computed on xylose were produced by the Isomerase pathway (**Table 2**). The exceptions of maximal yields of metabolites are such products that are directly synthesized from intermediates of the Weimberg and Dahms pathway. For example, the intermediate 2-oxoglutarate of the Weimberg pathway is an interesting metabolite, because it is introduced into the TCA cycle without carbon loss. The direct conversion of 2-oxoglutarate into glutamate (or proline, OH-proline, etc.) would thus benefit from the Weimberg pathway. This was also computed by FBA with a maximal product yield of 1 mmol $mmol^{-1}$ for the Weimberg pathway, and only 0.83 and 0.75 mmol $mmol^{-1}$ for the Isomerase and the Dahms pathway, respectively. The intermediate glycolaldehyde, using the Dahms pathway for xylose degradation, itself is a relevant chemical for industrial applications and a precursor for ethylene glycol synthesis. Ethylene glycol can neither be synthesized via the Isomerase nor the Weimberg pathway, while the maximal product yield of the Dahms pathway is 1 mmol $mmol^{-1}$. Consequently, the Dahms pathway is a favorable pathway to produce glycols out of xylose. In case of the Isomerase pathway, xylulose-5-phosphate is part of the pentose phosphate pathway and the intermediate erythrose-4-phosphate is a starting metabolite for aromatics synthesis via the shikimate pathway. This explains that the Isomerase pathway has the highest yield for the production of the here synthesized aromatic compound pyocyanin (0.27 mmol $mmol^{-1}$). Moreover, the highest maximal mono-rhamnolipid yield is also possible via the Isomerase pathway (0.14 mmol $mmol^{-1}$) and lower yields for the Weimberg and the Dahms pathway (0.08 and 0.12 mmol $mmol^{-1}$) were computed. This is due to CO_2 production using the TCA cycle for the Weimberg pathway and converting glycolaldehyde in several steps to 2-phosphoglycerate for the Dahms pathway, also releasing one CO_2. In addition, the maximal product yields for all possible combinations of the xylose pathways (Isomerase + Weimberg, Isomerase + Dahms, Weimberg + Dahms, and Isomerase + Weimberg + Dahms) were computed. In general, it was observed that always one of the pathways in the combinations is favored and is thus exclusively used. Interestingly, and contrary to the above, the combination of the Weimberg and the Dahms pathways resulted in higher maximal product yields for nine of the 14 metabolites (**Table 2**) compared to the single pathway strains. Thus, in **Table 2** only the combined activities of the latter pathways are also listed. In summary, the *in silico* study indicates that the strain equipped with the Isomerase pathway is best-suited for a range of chemicals including the production of the here chosen metabolites mono-rhamnolipids and pyocyanin. The Weimberg and Dahms pathways are favored in niche applications (**Table 2**), when xylose is the sole carbon and energy source.

TABLE 2 | FBA computed maximal product yield of valuable products for three different xylose utilization pathways (Isomerase, Weimberg, and Dahms) and the combination of the Weimberg (W) and the Dahms (D) pathway.

Products	Maximal product yield ($mmol_{product}/mmol_{xylose}$)				
	Isomerase	Weimberg	Dahms	Weimberg + Dahms	
Acetoin	**0.83**	0.5	0.75	0.75	100% D
Di-rhamnolipids	**0.12**	0.07	0.1	0.1	19% W, 81% D
Ethylene glycol	0	0	**1**	**1**	100% D
Fumaric acid	**1.67**	1	1.32	1.38	25% W, 75% D
Gluconic acid	**0.83**	0.5	0.64	0.68	27% W, 73% D
Glutamate	0.83	**1**	0.75	**1**	100% W
Glycerol	**0.81**	0.56	0.47	n.d.[a]	–
HAA	**0.17**	0.1	0.15	0.15	6% W, 94% D
Malic acid	**1.67**	1	1.32	1.38	25% W, 75% D
Succinic acid	**1.04**	1	1	1	100% W
Sorbitol	**0.77**	0.5	0.56	0.63	50% W, 50% D
Threonine	**0.83**	0.5	0.75	0.75	100% D
Mono-rhamnolipids	**0.14**	0.08	0.12	0.12	14% W, 86% D
Pyocyanin	**0.27**	0.19	0.17	0.23	63% W, 37% D

[a]*Due to constraints in the model, the maximal yield for glycerol cannot be computed for the combination of the Weimberg and the Dahms pathway.*
For the combined pathways, also the percentage of the used pathway is indicated.
The bold values indicate the highest maximal product yield.

The Oxidative Pathways Enable Efficient Xylose Utilization

A genome analysis using BLAST showed that *P. putida* KT2440 possesses genes (Altschul et al., 1990), which might encode enzymes needed in xylose utilization, but a complete pathway seems to be absent, indeed correlating with no-growth on this sugar (**Figure 2A**). All genes required for the Isomerase,

[1]www.gurobi.com

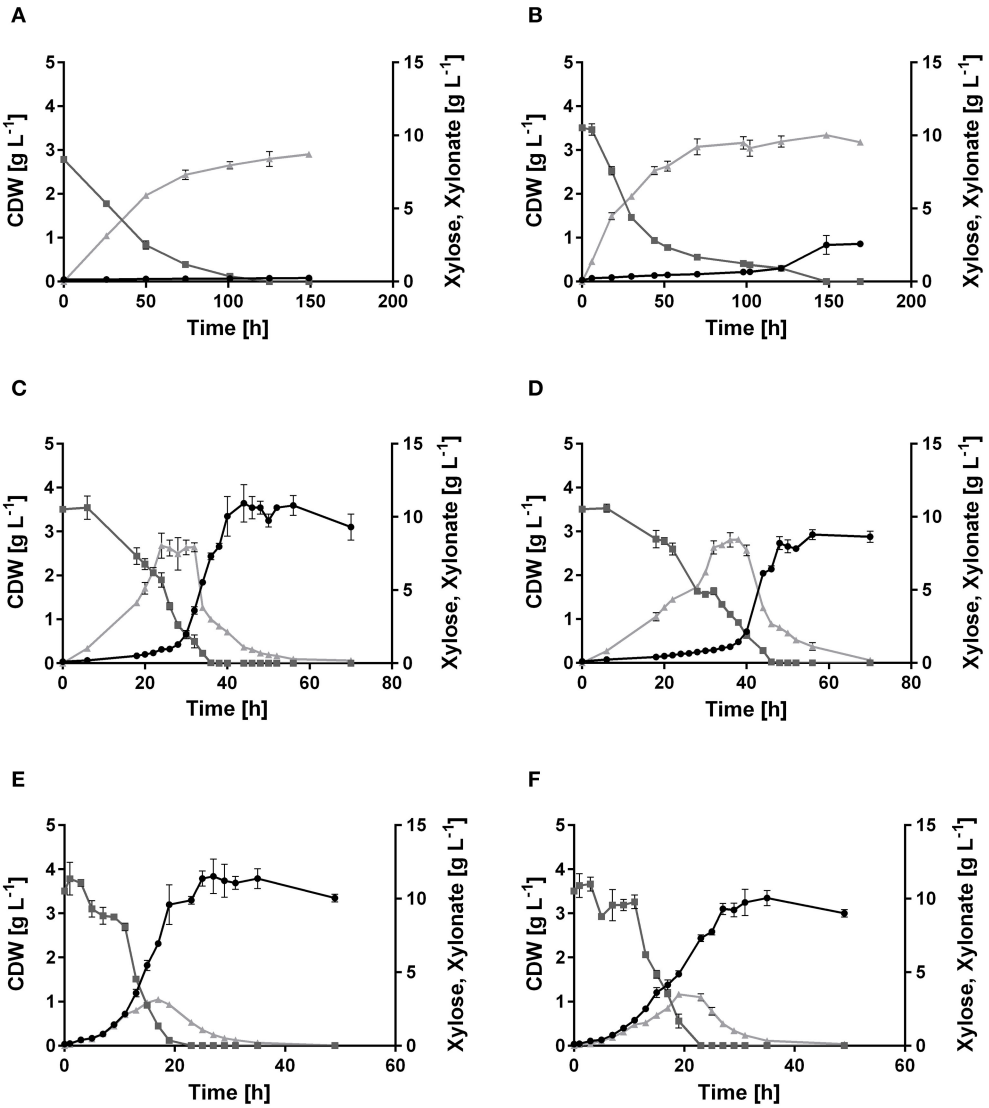

FIGURE 2 | Growth of *P. putida* KT2440, its derivate xylose consuming strains, and the xylose-adapted strains in minimal medium containing 10 g L^{-1} xylose. Consumption of xylose (■, dark gray), formation of xylonate (▲, light gray), and cell dry weight (•, black) of **(A)** *P. putida* KT2440, **(B)** *P. putida* KT2440 pIso, **(C)** *P. putida* KT2440 pWeim, **(D)** *P. putida* KT2440ΔΔ pDahms, **(E)** *P. putida* KT2440 pWeim2, and **(F)** *P. putida* KT2440ΔΔ pDahms2. Error bars indicate deviation from the mean ($n = 3$).

Weimberg, and Dahms pathways were compared to the genome of *P. putida* KT2440. No homologs for the genes *xylA* and *xylB* from *E. coli* for the Isomerase pathway are present. Additionally, no homologs for the genes PVLB_18565 from *P. taiwanensis* and *yagE* from *E. coli* for the Weimberg pathway and the Dahms pathway, respectively, are present. In contrast, homologous genes of the Weimberg pathway from *P. taiwanensis* are present (homologs to PVLB_18550, PVLB_18555, and PVLB_18560 with sequence identities of 68–72%). HPLC analysis revealed that xylose was consumed by non-growing *P. putida* KT2440, however xylose was converted into the dead-end product xylonate (**Figure 2A**). Xylonate synthesis proceeds likely via the gene products of *gcd* (PP_1444) and *gnl* (PP_1170) that are besides for glucose also active for xylose and its lactone derivative (**Figure 1**).

In order to engineer *P. putida* for the utilization of xylose, *P. putida* was equipped with a plasmid for the Isomerase pathway and designated *P. putida* KT2440 pIso. After inoculation, strain *P. putida* KT2440 pIso showed little growth (**Figure 2B**) with a maximal growth rate of 0.02 h^{-1} and a substrate consumption rate of 0.47 mmol L^{-1} h^{-1} (**Table 3**). In addition, pBT-Isomerase was introduced into *P. putida* KT2440 Δ*gcd*. This strain is unable to produce the dead-end product xylonate and thus more substrate should be available for biomass formation, as it was reported previously in a study with *P. putida* S12 (Meijnen et al., 2008). The resulting *P. putida* KT2440 Δ*gcd* pIso showed no

TABLE 3 | Growth characteristics of wild type, recombinant, and evolved *P. putida* KT2440 strains on xylose.

Strain	Growth rate μ (h^{-1})[a]	Lag phase (h)	Substrate consumption rate (mmol L^{-1} h^{-1})[b]
P. putida KT2440	–	–	0.45 ± 0.00[c]
P. putida KT2440 pIso	0.02 ± 0.00	100 ± 0	0.47 ± 0.00
P. putida KT2440 pWeim	0.30 ± 0.02	24 ± 0	1.94 ± 0.00
P. putida KT2440ΔΔ pDahms	0.21 ± 0.02	34 ± 0	1.46 ± 0.00
P. putida KT2440 pWeim2	0.21 ± 0.00	3 ± 0	3.05 ± 0.00
P. putida KT2440ΔΔ pDahms2	0.21 ± 0.01	3 ± 0	3.05 ± 0.00

[a] *The growth rate was determined during the exponential phase.*
[b] *The substrate consumption rate was determined until xylose is depleted. For the wild type, the whole cultivation time was used as reference.*
[c] *For the wild type, the substrate consumption rate is considered as substrate conversion rate, because it is not able to grow on xylose.*
Values are the arithmetic mean of biological triplicates. The deviation indicates the standard deviation from the mean (n = 3).

improved growth compared to *P. putida* KT2440 pIso (data not shown). Nevertheless, these results suggest that the cloned genes *xylAB* from *E. coli* are functionally expressed in *P. putida* KT2440 and allow slow growth of the recombinant strain.

In order to establish the oxidative Weimberg pathway in *P. putida* KT2440, the plasmid pBT-Weimberg was transferred into *P. putida* KT2440 resulting in *P. putida* KT2440 pWeim. Interestingly, *P. putida* KT2440 pWeim showed efficient growth with a maximal growth rate of 0.30 h^{-1} and a strong accumulation of xylonate (**Figure 2C**). This led to a long lag phase of ∼24 h (**Table 3**). We define the lag phase as a phase before growth was observed due to homogenous adaptation. The growth of a small phenotypic subpopulation on the new carbon source due to heterogenous adaptation described by Kotte et al. (2014) is not considered. The observed lag phase indicates a bottleneck in the conversion of xylonate to 2-keto-3-deoxy-xylonate or in the transport from the periplasm to the cytoplasm. Further, the substrate consumption rate was about 4-fold higher (1.94 mmol L^{-1} h^{-1}) in comparison to *P. putida* KT2440 pIso (**Table 3**). These results show that the xylose operon from *P. taiwanensis* is functionally expressed in *P. putida* KT2440 and results in efficient growth. To verify that the glucose dehydrogenase (Gcd) features a side-activity for xylose in *P. putida* KT2440, the plasmid pBT-Weimberg was introduced into *P. putida* KT2440 Δ*gcd* yielding *P. putida* KT2440 Δ*gcd* pWeim. After inoculation, no growth was observed (data not shown). This behavior confirms the assumption that Gcd is active for xylose because xylose needs to be converted to xylonate to establish the Weimberg pathway (**Figure 1**).

Moreover, the expression of genes encoding the Dahms pathway was targeted. Therefore, the plasmid for the Dahms pathway was introduced into wild type yielding *P. putida* KT2440 pDahms. As described before, genome analysis revealed that a homologous gene of PVLB_18560 is present (PP_2836). By comparison with genes expressing xylose-metabolizing enzymes from *C. crescentus*, PVLB_18560 is assumed to encode a dehydratase, which converts 2-keto-3-deoxy-xylonate to α-ketoglutaric semialdehyde (**Figure 1**). As a result, it is assumed that the product of the homologous gene PP_2836 in *P. putida* KT2440 is likely to catalyze this reaction. To verify this hypothesis, the plasmid pBT-Dahms was also transferred into *P. putida* KT2440 ΔPP_2836 yielding *P. putida* KT2440 ΔPP_2836 pDahms. *P. putida* KT2440 pDahms reached an OD_{600} of 8.2 after 74 h, while *P. putida* KT2440 ΔPP_2836 pDahms stopped growing after 48 h (final OD_{600} of 2.0). The latter strain showed cell clumping after 74 h, which implies stress. We speculated that low optical density and cell-clumping are caused by an accumulation of the toxic intermediate glycolaldehyde. These findings strongly indicate that PP_2836 encodes a 2-keto-3-deoxy-xylonate dehydratase. In order to overcome the toxic effect of glycolaldehyde, strain *P. putida* KT2440 Δ*gclR* was used. The glyoxylate carboligase oxidase pathway is active in this mutant, thus avoiding glycolaldehyde accumulation (Li et al., 2019). The plasmid pBT-Dahms was introduced into *P. putida* KT2440 Δ*gclR* ΔPP_2836 resulting in *P. putida* KT2440ΔΔ pDahms. In comparison to *P. putida* KT2440 ΔPP_2836 pDahms, strain *P. putida* KT2440ΔΔ pDahms indeed grew to higher cell densities, which led to the conclusion that the genes encoding the enzymes for the Dahms pathway are successfully expressed and the prevention of glycolaldehyde accumulation leads to efficient growth. The growth of *P. putida* KT2440ΔΔ pDahms was further examined and a maximal growth rate of 0.21 h^{-1} and a substrate consumption rate of 1.46 mmol L^{-1} h^{-1} was observed (**Table 3**). Further, accumulation of xylonate occurred as in the case of the Weimberg strain. Thereby, a lag phase of ∼34 h results (**Figure 2D**).

As stated above, it was observed that not only a long lag phase occurs when the Isomerase pathway is used, but also when the oxidative pathways are used. Regulatory mechanisms are assumed as a cause, but in the case of the oxidative pathways, the used route for metabolization is different. There, the xylose gets oxidized to xylonate via xylono-1,4-lactone by the enzymes encoded by *gcd* and *gnl*. It is assumed that these enzymes are active for xylose, but with a lower specificity and thus, the conversion is slower than for glucose and a long lag phase is the result. Further, accumulation of xylonate was observed, which indicates a bottleneck in xylonate conversion or transport.

Adaptive Laboratory Evolution Improves Growth on Xylose

It was shown that all xylose metabolism plasmids are functionally expressed resulting in weak growth for the Isomerase pathway and efficient growth for the Weimberg and Dahms pathways, respectively. However, the lag phase of all strains was relatively long. To optimize growth, ALE was applied. For each of the strains, *P. putida* KT2440 pIso, *P. putida* KT2440 pWeim, and *P. putida* KT2440ΔΔ pDahms, two parallel cultures were

sequentially transferred to fresh minimal medium with xylose as the sole carbon source (**Figure 3A**). The performance of *P. putida* KT2440 pWeim and *P. putida* KT2440ΔΔ pDahms was improved after 17 and 26 transfers corresponding to ∼115 and 160 generations, respectively. The number of generations was calculated based on the starting OD_{600} and the end OD_{600} of every transfer. Afterwards, 24 isolates were obtained from the culture broth and up to six from each culture were randomly selected and tested for growth on xylose in comparison to the initial strains. In **Figure 3B** five isolates in comparison to the initial strain *P. putida* KT2440 pWeim are shown. The adaptation toward xylose is not similar for all isolates, as some isolates still had a longer lag phase, suggesting that an isolation step to obtain the best growing strain is required. Hereafter, the best isolates were designated as *P. putida* KT2440 pWeim2 and *P. putida* KT2440ΔΔ pDahms2. The adaptation of *P. putida* KT2440 pIso to xylose was problematic because the strain did not grow anymore after several transfers.

The colonies showing the best performance (*P. putida* KT2440 pWeim2 and *P. putida* KT2440ΔΔ pDahms2) were characterized in detail regarding their growth behavior. Both showed improved growth compared to the initial strains. The lag phase of *P. putida* KT2440 pWeim2 was shortened from ∼24 to 3 h (**Figure 2E**). However, the maximal growth rate of the strain was 0.21 h^{-1}. Hence, the lag phase was 1.5-fold reduced compared to the initial strain (**Table 3**). For *P. putida* KT2440ΔΔ pDahms2, the lag phase was shortened from ∼34 to 3 h (**Figure 2F**). The growth rate remained the same with a value of 0.21 h^{-1} (**Table 3**). Further, the substrate consumption rate was 3 mmol L^{-1} h^{-1} for both evolved strains, which is about 1.6- and 2-fold higher than the consumption rates of their initial strains.

To identify possible mutations, which are responsible for the reduced lag phase and xylonate accumulation, the plasmids of *P. putida* KT2440 pWeim2 and *P. putida* KT2440ΔΔ pDahms2 were isolated and sequenced. Mutations in the promoter, xylose genes, replication initiator protein, origin of replication, and antibiotic resistance of the plasmids carried by strains *P. putida* KT2440 pWeim2 and *P. putida* KT2440ΔΔ pDahms2 could be excluded. Hence, mutations in coding regions in the genome are expected and will be analyzed in the future.

The Deletion of PP_2836 Enables the Exclusive Usage of the Dahms Pathway

To demonstrate that the isolated Weimberg or Dahms pathway are present in the engineered strains, growth experiments with 1-^{13}C labeled xylose as substrate were performed. Afterwards, the labeling patterns of the proteinogenic amino acids were analyzed. Since xylose is metabolized via different routes using the Weimberg or the Dahms pathway, the labeling pattern is well-distinguishable (**Figure 4**). Xylose is converted in several steps to 2-oxoglutarate via the Weimberg pathway, which is a direct precursor of glutamate, glutamine, and proline. This would lead to 1-^{13}C labeled glutamate, glutamine and proline. In the central carbon metabolism, 2-oxoglutarate is further processed via the TCA cycle and the labeling is removed via CO_2 generation. Furthermore, in the case of the Dahms pathway, xylose is converted into pyruvate and glycolaldehyde. Since pyruvate is a precursor for the amino acids alanine, lysine, and valine, they are fractionally labeled. Pyruvate is also converted to acetyl-CoA in the central carbon metabolism, removing the labeled carbon atom by CO_2 generation.

For these experiments, *P. putida* KT2440 pWeim und *P. putida* KT2440ΔΔ pDahms were used. As seen before, deletion of the gene PP_2836 entails a completely different growth behavior, which indicates that the deletion of PP_2836 is necessary to establish the Dahms pathway. It is assumed that xylose is utilized via both pathways simultaneously (Weimberg and Dahms) in a strain that still harbors PP_2836 and is deficient in *gclR* (to activate degradation of the intermediate glycolaldehyde, see **Figure 1**). This assumption was experimentally tested by introducing the plasmid pBT-Dahms into *P. putida* Δ*gclR*. The resulting *P. putida* Δ*gclR* pDahms was also used in the labeling experiments.

Significant distinctions of the fractional labeling with labeled xylose were observed for all three strains (**Figure 5**). For the Weimberg-strain, alanine, lysine, and valine were almost not

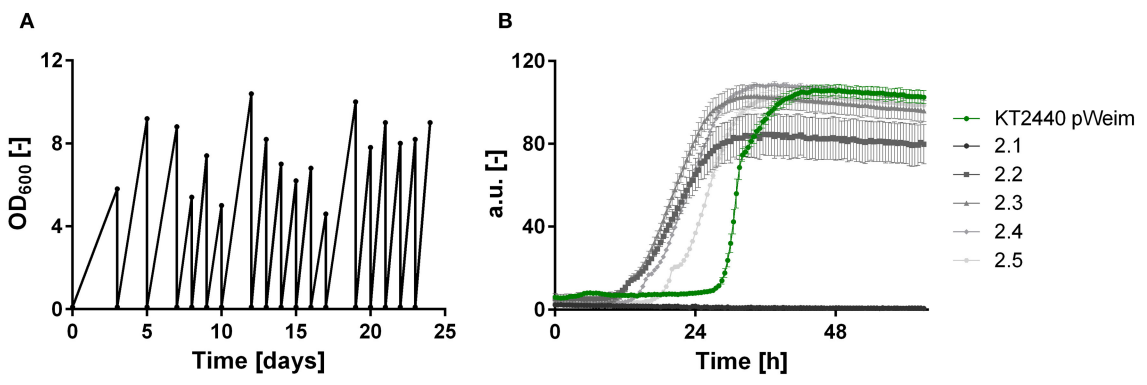

FIGURE 3 | ALE and growth characteristics of isolates of *P. putida* KT2440 pWeim on xylose. **(A)** ALE of *P. putida* KT2440 pWeim on xylose as sole carbon source. A single representative culture is shown, **(B)** Comparison of growth for *P. putida* KT2440 pWeim (•, green) and five isolates from the second ALE culture on xylose. Error bars indicate deviation from the mean ($n = 3$).

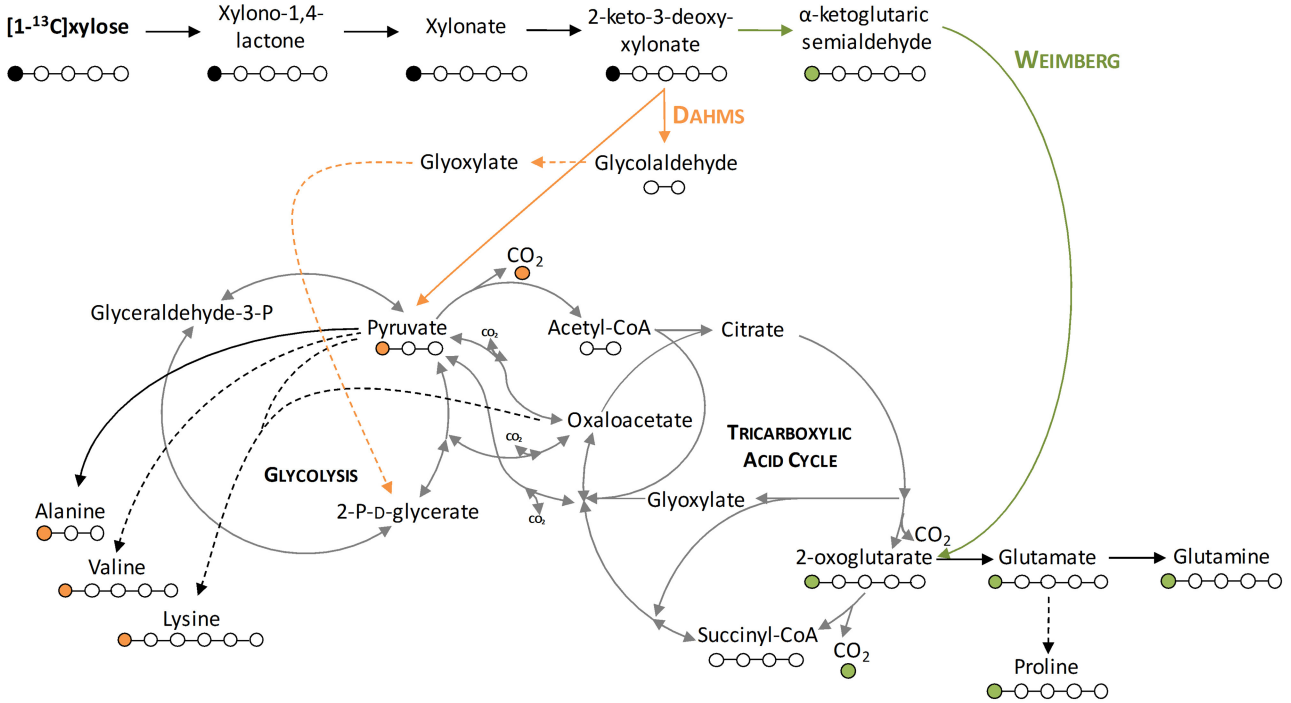

FIGURE 4 | Depiction of the labeling of metabolites resulting from labeled xylose. Shown is the stable isotope introduction into the central carbon metabolism of *P. putida* KT2440. Orange lines indicate the Dahms pathway, green lines indicate the Weimberg pathway, and dashed lines indicate several enzymatic steps. Orange dots indicate the labeling resulting from the Dahms pathway and green dots indicate the labeling resulting from the Weimberg pathway.

labeled at all while glutamate and proline showed a labeling about 0.1. This meets the expectations since 50% of 1-^{13}C-labeled xylose was used (one atom out of ten carbon atoms from two xylose molecules should be labeled). For the Dahms-strain, the fractional labeling of the amino acids, which are derived from pyruvate (alanine, lysine, and valine), is about 0.13, 0.06, and 0.07, respectively, and for glutamate and proline below 0.05. Theoretically, a fractional labeling of about 0.17 for alanine, 0.08 for lysine, and 0.1 for valine would be assumed because one out of six, ten, and twelve carbon atoms from two xylose molecules should be labeled, respectively. The observed labeling is a little bit lower than expected, but the distribution meets the expectation since again 50% of 1-^{13}C-labeled xylose was used. For more quantitative statements, metabolic flux analysis has to be performed in order to involve fluxes through the central carbon metabolism. Further, as described above the labeling is removed when CO_2 is generated. However, via anaplerotic reactions the labeled CO_2 can be reincorporated and ultimately result in labeled glutamate and proline. Nevertheless, both strains showed a distinct labeling pattern, which indicates that the Weimberg and Dahms pathways are truly used in isolation.

Moreover, for *P. putida* KT2440 Δ*gclR* pDahms it was determined that the fractional labeling of glutamate and proline was about 0.1 as in the case of the Weimberg-strain and that the labeling of alanine, lysine, and valine was in between the values of the Weimberg- and the Dahms-strain. These results show that the fractional labeling is a combination of the single fractional labelings of the Weimberg and the Dahms pathway. Thus, it is suggested that the Weimberg and the Dahms pathway are active simultaneously in this strain. Consequently, the above stated declaration that PP_2836 encodes a dehydratase is verified. The deletion of this gene is necessary to obtain a strain, which solely uses the Dahms pathway.

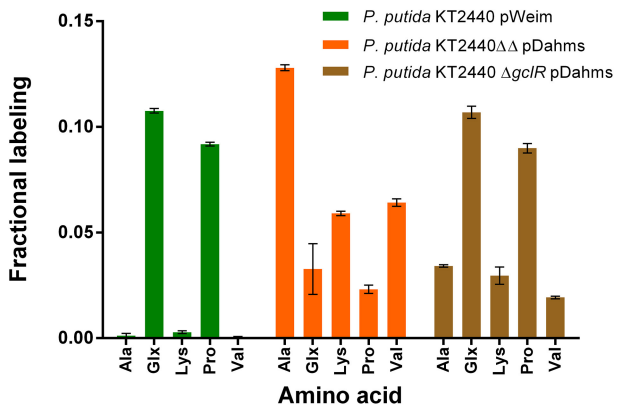

FIGURE 5 | Fractional labeling of amino acids during growth in minimal medium containing 50% 1-^{13}C-xylose. Error bars indicate deviation from the mean of three technical replicates from one growth experiment ($n = 3$). Ala, alanine; Glx, glutamate and deaminated glutamine; Lys, lysine; Pro, proline; Val, valine.

Variations in Xylose Metabolization Networks Lead to Specialized Microbial Cell Factories

Different stoichiometries of the pathways have an influence on the production yield of specific metabolites. In order to show this dependency, two secondary metabolites (rhamnolipids and phenazines) were chosen for heterologous synthesis in efficient xylose metabolizers. Exemplarily, strains with the individual pathways (Isomerase, Weimberg, and Dahms) were chosen and the production of the initial strains and the adapted strains was investigated. For the production of rhamnolipids, the rhamnolipid synthesis module was integrated as single copy into the genome of all xylose utilizing strains. *P. putida* KT2440 EM42 Δ*gcd* pSEVA2213_*xylABE* (Dvorák and de Lorenzo, 2018) was used as optimized strain using the Isomerase pathway because no evolved *P. putida* strain using the Isomerase pathway was generated. The rhamnolipid producers were designated *P. putida* KT2440 pIso_RL, *P. putida* KT2440 pWeim_RL, *P. putida* KT2440ΔΔ pDahms_RL, *P. putida* KT2440 pIso2_RL, *P. putida* KT2440 pWeim2_RL, and *P. putida* KT2440ΔΔ pDahms2_RL.

P. putida KT2440 pIso_RL, utilizing the Isomerase pathway for xylose degradation, showed only little rhamnolipid production (47 mg L^{-1}) after 96 h, because most of the xylose was converted to the dead-end product xylonate. While *P. putida* KT2440 pIso2_RL produced seven times more mono-rhamnolipids after 54 h (**Figure 6A**), although the cells were clumped and did not reach high optical densities. On the contrary, the strains with the Weimberg and Dahms pathways reached higher rhamnolipid titers. *P. putida* KT2440 pWeim_RL produced 13 times more mono-rhamnolipids than *P. putida* KT2440 pIso_RL in less time (54 h) and the evolved strain with the rhamnolipid production module *P. putida* KT2440 pWeim2_RL produced even more mono-rhamnolipids after 30 h (720 mg L^{-1}). Further, *P. putida* KT2440ΔΔ pDahms_RL and *P. putida* KT2440ΔΔ pDahms2_RL produced six times more mono-rhamnolipids after 54 h (290 mg L^{-1}) and 13 times more mono-rhamnolipids after 30 h (620 mg L^{-1}), respectively. Besides, differences in the substrate consumption were observed. While *P. putida* KT2440 pWeim2_RL and *P. putida* KT2440ΔΔ pDahms_RL consumed all of the provided xylose, xylose and xylonate in the cultures of the other rhamnolipid-producing strains was detected after growth stopped (**Supplementary Figure 1**). Hence, the ratio of the amount of product synthesized and the amount of substrate consumed (yield) is considered. *P. putida* KT2440 pIso2_RL had the highest yield (78 mg g^{-1}), while *P. putida* KT2440 pWeim2_RL and *P. putida* KT2440ΔΔ pDahms2_RL reached comparable yields, however, 1.4-fold lower than *P. putida* KT2440 pIso2_RL (**Figure 6C**). As expected, the evolved and optimized strains showed a higher rhamnolipid concentration and yield than their initial xylose utilizing strains (**Figures 6A,C**).

The synthesis of phenazines was achieved by transferring plasmid pJNN_*phzA1-G1,S,M* into all initial xylose utilizing strains and the optimized or evolved strains. The pyocyanin producers were named *P. putida* KT2440 pIso_PZ, *P. putida* KT2440 pWeim_PZ, *P. putida* KT2440ΔΔ pDahms_PZ, *P. putida* KT2440 pIso2_PZ, *P. putida* KT2440 pWeim2_PZ, and *P. putida* KT2440ΔΔ pDahms2_PZ. All strains produced pyocyanin in a similar range (∼15–20 mg L^{-1}, **Figure 6B**), but in a different period, except the strains using the Isomerase pathway. *P. putida* KT2440 pIso_PZ produced around three times less (6 mg L^{-1}) pyocyanin and *P. putida* KT2440 pIso2_PZ produced roughly two times more (30 mg L^{-1}) pyocyanin in comparison to the evolved strain using the Dahms pathway. Pyocyanin was harvested at the same time points as mono-rhamnolipids. Furthermore, as observed in rhamnolipid production experiments, differences in substrate consumption were recognized. *P. putida* KT2440 pIso_PZ converted even more xylose to xylonate than in the rhamnolipid production experiments, which could then not be used for pyocyanin production. Further, less xylose was consumed than in the rhamnolipid production experiment (**Supplementary Figure 1**). Consequently, the yield was determined and *P. putida* KT2440 pIso2_PZ showed the best yield (20 mg g^{-1}) (**Figure 6D**). Furthermore, the evolved strains reached higher yields than their initial strains (*P. putida* KT2440 pWeim2_PZ: 3.2 mg g^{-1}, *P. putida* KT2440ΔΔ pDahms2_PZ: 2.5 mg g^{-1}). It was confirmed that the evolved and optimized strains could reach higher product titers and yields than their initial strains, also in case of pyocyanin production (**Figures 6B,D**). This can be explained by the adaptation toward the novel substrate xylose for *P. putida* KT2440 pWeim2 and *P. putida* KT2440ΔΔ pDahms2. In case of *P. putida* KT2440 pIso2 the production of xylonate is prevented by deletion of the glucose dehydrogenase in comparison to *P. putida* KT2440 pIso and consequently more carbon is available for the production of pyocyanin. Conspicuously, growth was slower for the phenazine-producing strains compared to the rhamnolipid-producing strains and consequently the total consumption of xylose was lower. This might be due to the metabolic burden through the usage of kanamycin to avoid loss of the plasmid harboring the phenazine synthesis genes during cultivation. Further, product toxicity might be a cause for the xylose leftovers. In accordance to the computed data in 3.1., *P. putida* KT2440 pIso2 harboring the rhamnolipid or phenazine genes showed in both scenarios the best yield (**Figure 6**).

DISCUSSION

In this study, we integrated three bacterial xylose utilization pathways—Isomerase, Weimberg, and Dahms—in *P. putida* KT2440, to compare *in silico* and *in vivo* the synthesis capacities of these alternative degradation pathways. While other studies focus on heterologous production with *P. putida* KT2440, we aimed at showing the production of various products (i.e., mono-rhamnolipids and pyocyanin) from xylose. Further, we wanted to emphasize that computational analysis can guide strain design, reaching higher yields.

FBA indicates strong preferences for alternative pathways depending on the product of choice due to different stoichiometries. It was determined that mainly the Isomerase

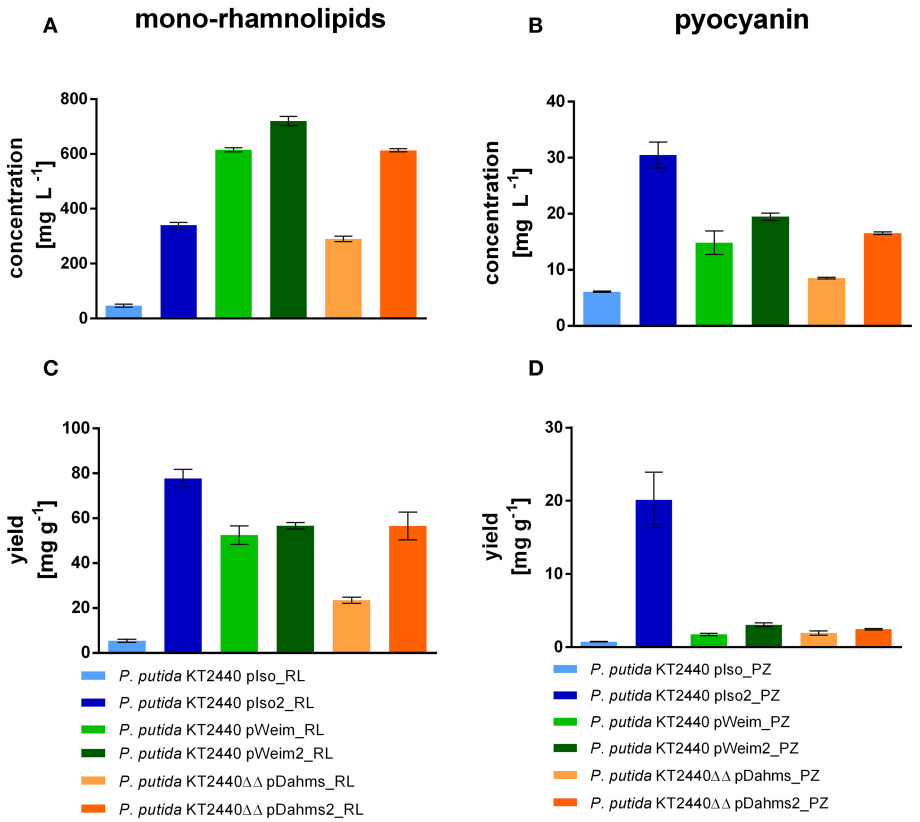

FIGURE 6 | Mono-rhamnolipid and pyocyanin production from xylose by engineered *P. putida* strains. The minimal medium contained 10 g L^{-1} xylose. Shown are the product titers of mono-rhamnolipids **(A)**, the product titers of pyocyanin **(B)**, the yield of mono-rhamnolipids on xylose **(C)**, and the yield of pyocyanin on xylose **(D)**. Error bars indicate deviation from the mean ($n = 3$).

pathway is preferred, however the Weimberg and Dahms pathways are favored in niche applications, when for example intermediates of the pathways are precursor for the products. To show this dependency, the xylose pathways and synthesis pathways were integrated in *P. putida* KT2440. In the course of isolating the Dahms pathway, two genes (PP_2836 and PP_4283) were deleted. After successful pathway implementation, the synthesis capacities for mono-rhamnolipids and pyocyanin were investigated. The resulting data matched the computed data. The approach of *in silico* metabolic network design driven by the product of choice, adds another degree of freedom for metabolic engineering.

The computed maximal product yield for both synthesized metabolites, mono-rhamnolipids and pyocyanin, was produced by the Isomerase pathway. In both cases, this was confirmed *in vivo* (**Figure 6**). While the highest rhamnolipid titer (700 mg L^{-1}) was reached by the evolved strain using the Weimberg pathway, the highest yield (78 mg g^{-1}) was reached by the strain using the Isomerase pathway. The highest pyocyanin titer (30 mg L^{-1}) and yield (20 mg g^{-1}) were also reached by the strain using the Isomerase pathway. Taken together, it was shown that the reached yields are dependent on the metabolization route and hence the stoichiometries of the pathway, which can be determined *in silico*.

Many studies deal with the heterologous production by *P. putida* KT2440. Production of biosurfactants, such as hydroxyalkanoyloxy alkanoates (HAA), mono-rhamnolipids, and di-rhamnolipids (Tiso et al., 2017; Wittgens et al., 2017, 2018), terpenoids (zeaxanthin and β-carotene) (Beuttler et al., 2011; Loeschcke et al., 2013), amino acid-derived compounds (e.g., phenazines) (Schmitz et al., 2015b), polyketides/non-ribosomal peptides (e.g., flaviolin, prodigiosin) (Gross et al., 2006; Loeschcke et al., 2013; Domröse et al., 2015), and *N*-methylglutamate (Mindt et al., 2018) was demonstrated. These examples show how diverse the production spectrum in *P. putida* KT2440 can be. To create sustainable production processes in times of high environmental pollution, one searches for alternative substrates (Vanholme et al., 2013). The concept of using xylose or other C_5 sugars for platform chemicals was already considered before (Werpy and Petersen, 2004). For example, HAA and terpenoids are benefitting from the Isomerase pathway as acetyl-CoA is the precursor (**Table 2**). Prodigiosin synthesis involves the precursors pyruvate, proline, and malonyl-CoA (Williamson et al., 2006), favoring a combination of the Isomerase and the Weimberg pathway. The Weimberg pathway would be beneficial for synthesis of *N*-methylglutamate. The attempt of using xylose as renewable source for the production

of metabolites was already considered in several studies, where *P. taiwanensis* VLB120 was used for the synthesis of monorhamnolipids, phenol, and 4-hydroxybenzoate (Tiso et al., 2017; Wynands et al., 2018; Lenzen et al., 2019). *P. taiwanensis* VLB120 utilizes xylose via the Weimberg pathway natively (Köhler et al., 2015), but engineering of the strain and enabling xylose utilization via the Isomerase pathway could enhance product yield on substrate due to the superior stoichiometry.

While the integration of the xylose pathways worked *in vivo*, we observed strong differences between the oxidative and the Isomerase pathway operations. Pseudomonades using the three xylose pathways natively were reported (Hochster, 1955; Dahms, 1974; Köhler et al., 2015), indicating that these pathways are compatible with the Pseudomonades metabolic network. Notably, we did not find any report suggesting the presence of two of the xylose pathways. The implementation of the Isomerase pathway in *P. putida* was shown before (Meijnen et al., 2008; Le Meur et al., 2012; Dvorák and de Lorenzo, 2018; Wang et al., 2019). In accordance to our results, only weak growth was observed in two studies (Meijnen et al., 2008; Dvorák and de Lorenzo, 2018), which was improved by rational or non-rational engineering. In another study, growth on xylose via the Weimberg pathway in *P. putida* was shown to be immediately efficient (Meijnen et al., 2009), matching our results. As already considered by Wang et al. (2019), xylose metabolization seems to be metabolically demanding for *P. putida* KT2440 using the isomerase route and might be the reason for the discrepancies. But how can this difference between the Isomerase pathway and the oxidative pathways be explained? The consideration of other carbon sources indicates that the usage of oxidative pathways is likely to have an advantage for *Pseudomonas* species. The metabolization of the C_5 sugar arabinose proceeds in *E. coli* via the Isomerase pathway (Laikova, 2001), whereas in other *Pseudomonas* species the utilization of arabinose happens via oxidative steps to form the intermediate pentonic acid (Lockwood and Nelson, 1946; Weimberg and Doudoroff, 1955). In the case of galacturonic acid the utilization starts with an isomerase reaction in *E. coli* (Ashwell et al., 1960). Whereas, in *Pseudomonas* species the first enzyme is a dehydrogenase, which catalyzes an oxidation reaction (Kilgore and Starr, 1959; Richard and Hilditch, 2009). There might be two explanations why *Pseudomonas* favors oxidative pathways. First, the conversion of the substrate into an intermediate acid prevents other microbes from using this substrate, which is an advantage in terms of survival. Consequently, the environment is acidified due to the resulting intermediate acid, which creates a further advantage for propagation. *P. putida* KT2440 is a soil bacterium and is able to cope with extreme conditions, such as nutrient limitation, temperature shifts, and pH changes, in contrast to enterobacteria that occur in nutrient-rich niches (Martins Dos Santos et al., 2004; Reva et al., 2006). Second, the energy metabolism is more flexible, because the dehydrogenases have different redox cofactors. This can be explained using glucose as an example. In general, the redox metabolism is balanced and therefore, the rates of reduction and oxidation of the redox cofactors have to be highly similar (Blank et al., 2010). The electrons, which are released during oxidation of glucose and gluconate, are used to reduce PQQ and FAD^+ and are feeding directly the electron transport chain. There, PQQ is directly reoxidized by transferring the electrons to ubiquinone in the inner membrane (Ebert et al., 2011; Tiso et al., 2014). The transport of glucose over the membrane costs two ATP per molecule, while only one proton and one sodium ion are necessary for the transport of gluconate and ketogluconate, respectively. Therefore, *P. putida* KT2440 saves energy using the oxidative pathway and does not require additional cofactor regeneration systems.

However, a prolonged lag phase was observed for all three engineered strains. *P. putida* KT2440 pIso had the longest lag phase with 100 h, *P. putida* KT2440 pWeim had a lag phase of 24 h, and *P. putida* KT2440ΔΔ pDahms had a lag phase of 34 h (**Table 3**). To identify possible bottlenecks, the plasmids were sequenced after ALE. Interestingly, no mutations in the xylose utilization genes and other encoding areas of the vectors could be detected. Different studies showed that mutations in the replication initiation protein or in the antibiotic resistance cassette could enhance growth by lowering the plasmid copy number, and subsequently reducing the need of resources for the synthesis of kanamycin resistance (Jakob et al., 2013; Mi et al., 2016). A second possible bottleneck could be the transport of xylonate from the periplasm to the cytoplasm. *P. putida* KT2440 harbors the transporter GntT (PP_3417), enabling the transport of gluconate from the periplasm into the cytoplasm (Porco et al., 1997). Such a transporter is characterized for *E. coli*. A conceivable possibility would be, that this transporter might be active for xylonate, but due to its high-affinity toward gluconate it might operate slower for xylonate. Another option could be that a slow, low-affinity transporter is used instead. To improve the growth performance and reduce the lag phase, ALE was implemented. Interestingly, the lag phase was reduced significantly, while the growth rates did not increase and in one case even decreased during ALE. This can be explained by positive selection for a reduced lag phase and negative selection for the growth rate. The fast-adapting cells does not have stringently the highest growth rate. After reduction of the lag phase, it can be selected for increased growth rates now. While laboratory evolution is an easy method to increase the overall fitness of a population in laboratory scale, the design of the ALE approach for adaptation of the population is not trivial. Conditions such as time point of transfer, passage size, and growth phase can alter in ALE studies (Charusanti et al., 2010; LaCroix et al., 2015). Batch cultivation and continuous (chemostat) cultivation are the mostly used ALE techniques (Dragosits and Mattanovich, 2013; Gresham and Dunham, 2014; LaCroix et al., 2017). Of these, regularly transferred batch cultures are more popular because effort and costs are rather low. However, this method has several limitations due to varying conditions (LaCroix et al., 2017). Further, this method is slower than an automated ALE because the transfer is usually done on a daily basis. While in automated ALE processes, several parameters, including the optical density and growth rate, are monitored online. If the growth rate increases over the course of the ALE, the passage frequency can automatically be increased. Additionally, cultures probably reach the stationary phase in batch cultivations, which then results in an improved survival in

stationary phase or decreased lag phase (Wiser and Lenski, 2015). Thus, it is not surprising that the batch cultivations for adaptation used in this study resulted in a shortage of the lag phase.

The here presented alternative pathways for xylose utilization open another degree of freedom in the design and metabolic engineering of the production strain. Dependent on the product of interest, the experimenter can compute the best network design considering three different stoichiometries for xylose use. The general applicability of this approach is outlined here, while as an outlook the detailed single strain optimization and the co-consumption of carbon sources *in silico* and *in vivo* should be worked on.

DATA AVAILABILITY STATEMENT

All datasets generated for this study are included in the article/**Supplementary Material**.

AUTHOR CONTRIBUTIONS

IB performed all molecular engineering and characterization experiments, analyzed the data, prepared figures, conducted the *in silico* experiments, and wrote the manuscript. TT provided guidance on *P. putida* biotechnology and edited the manuscript. TT, AW, and FR discussed the data and critically revised the manuscript. LB advised on all experiments, analyzed and discussed data, and edited the manuscript.

FUNDING

The scientific activities of the Bioeconomy Science Center were financially supported by the Ministry of Culture and Science within the framework of the NRW Strategieprojekt BioSC (No. 313/323-400-00213). The GC-MS/MS was funded by the German Research Foundation DFG (Förderkennzeichen: INST 2221018-1 FUGG). Furthermore, the authors are grateful to the Fachagentur Nachwachsende Rohstoffe e.V. (FNR; Förderkennzeichen: 22013314), the Ministry of Science, Research and the Arts of Baden-Württemberg (MWK; Förderkennzeichen: 7533-10-5-186A and 7533-10-5-190) and the EU project Horizon 2020 AD GUT (ID: 686271) for providing financial support.

ACKNOWLEDGMENTS

We thank Prof. de Lorenzo [Systems and Synthetic Biology Program, Centro Nacional de Biotecnología (CNB-CSIC)] for providing *P. putida* EM42 Δ*gcd* pSEVA2213_*xylABE*, Dr. Simone Schmitz (RWTH Aachen University) and Prof. Agler-Rosenbaum (Leibniz Institute for Natural Product Research and Infection Biology, Hans-Knöll-Institute) for providing plasmid pJNN_*phzA1-G1*,*M*,*S*, Sebastian Köbbing (RWTH Aachen University) for providing plasmid pBG14ffg, and Wing-Jin Li (RWTH Aachen University) for providing *P. putida* KT2440 Δ*gclR*. We kindly acknowledge Hans M. Böhne and Sebastian Kruth for their experimental help.

SUPPLEMENTARY MATERIAL

The Supplementary Material for this article can be found online at: https://www.frontiersin.org/articles/10.3389/fbioe.2019.00480/full#supplementary-material

REFERENCES

Altschul, S. F., Gish, W., Miller, W., Myers, E. W., and Lipman, D. J. (1990). Basic local alignment search tool. *J. Mol. Biol.* 215, 403–410. doi: 10.1016/S0022-2836(05)80360-2

Angermayr, S. A., Paszota, M., and Hellingwerf, K. J. (2012). Engineering a cyanobacterial cell factory for production of lactic acid. *Appl. Environ. Microbiol.* 78, 7098–7106. doi: 10.1128/AEM.01587-12

Antonovsky, N., Gleizer, S., Noor, E., Zohar, Y., Herz, E., Barenholz, U., et al. (2016). Sugar synthesis from CO_2 in *Escherichia coli*. *Cell* 166, 115–125. doi: 10.1016/j.cell.2016.05.064

Ashwell, G., Wahba, A. J., and Hickman, J. (1960). Uronic acid metabolism in bacteria. I. Purification and properties of uronic acid isomerase in *Escherichia coli*. *J. Biol. Chem.* 235, 1559–1565.

Bagdasarian, M., Lurz, R., Rückert, B., Franklin, F. C. H., Bagdasarian, M. M., Frey, J., et al. (1981). Specific-purpose plasmid cloning vectors II. Broad host range, high copy number, RSF 1010-derived vectors, and a host-vector system for gene cloning in *Pseudomonas*. *Gene* 16, 237–247. doi: 10.1016/0378-1119(81)90080-9

Behrens, B., Baune, M., Jungkeit, J., Tiso, T., Blank, L. M., and Hayen, H. (2016). High performance liquid chromatography-charged aerosol detection applying an inverse gradient for quantification of rhamnolipid biosurfactants. *J. Chromatogr. A* 1455, 125–132. doi: 10.1016/j.chroma.2016.05.079

Belda, E., van Heck, R. G., José Lopez-Sanchez, M., Cruveiller, S., Barbe, V., Fraser, C., et al. (2016). The revisited genome of *Pseudomonas putida* KT2440 enlightens its value as a robust metabolic chassis. *Environ. Microbiol.* 18, 3403–3424. doi: 10.1111/1462-2920.13230

Beuttler, H., Hoffmann, J., Jeske, M., Hauer, B., Schmid, R. D., Altenbuchner, J., et al. (2011). Biosynthesis of zeaxanthin in recombinant *Pseudomonas putida*. *Appl. Microbiol. Biotechnol.* 89, 1137–1147. doi: 10.1007/s00253-010-2961-0

Blank, L. M., Ebert, B. E., Buehler, K., and Bühler, B. (2010). Redox biocatalysis and metabolism: molecular mechanisms and metabolic network analysis. *Antioxid. Redox Signal.* 13, 349–394. doi: 10.1089/ars.2009.2931

Bouzon, M., Perret, A., Loreau, O., Delmas, V., Perchat, N., Weissenbach, J., et al. (2017). A synthetic alternative to canonical one-carbon metabolism. *ACS Synth. Biol.* 6, 1520–1533. doi: 10.1021/acssynbio.7b00029

Cabulong, R. B., Lee, W. K., Bañares, A. B., Ramos, K. R. M., Nisola, G. M., Valdehuesa, K. N. G., et al. (2018). Engineering *Escherichia coli* for glycolic acid production from D-xylose through the Dahms pathway and glyoxylate bypass. *Appl. Microbiol. Biotechnol.* 102, 2179–2189. doi: 10.1007/s00253-018-8744-8

Charusanti, P., Conrad, T. M., Knight, E. M., Venkataraman, K., Fong, N. L., Xie, B., et al. (2010). Genetic basis of growth adaptation of *Escherichia coli* after deletion of *pgi*, a major metabolic gene. *PLoS Genet.* 6, 1–13. doi: 10.1371/journal.pgen.1001186

Choi, K. H., Gaynor, J. B., White, K. G., Lopez, C., Bosio, C. M., Karkhoff-Schweizer, R. A., et al. (2005). A Tn7-based broad-range bacterial cloning and expression system. *Nat. Methods* 2, 443–448. doi: 10.1038/nmeth765

Choi, K. H., Kumar, A., and Schweizer, H. P. (2006). A 10-min method for preparation of highly electrocompetent *Pseudomonas aeruginosa* cells: application for DNA fragment transfer between chromosomes and plasmid transformation. *J. Microbiol. Methods* 64, 391–397. doi: 10.1016/j.mimet.2005.06.001

Choi, S. Y., Kim, W. J., Yu, S. J., Park, S. J., Im, S. G., and Lee, S. Y. (2017). Engineering the xylose-catabolizing Dahms pathway for

production of poly(d-lactate-co-glycolate) and poly(d-lactate-co-glycolate-co-d-2-hydroxybutyrate) in *Escherichia coli*. *Microb. Biotechnol.* 10, 1353–1364. doi: 10.1111/1751-7915.12721

Chomczynski, P., and Rymaszewski, M. (2006). Alkaline polyethylene glycol-based method for direct PCR from bacteria, eukaryotic tissue samples, and whole blood. *Biotechniques* 40, 454–458. doi: 10.2144/000112149

Dahms, S. A. (1974). 3-Deoxy-D-pentulosonic acid aldolase and its role in a new pathway of D-xylose degradation. *Biochem. Biophys. Res. Commun.* 60, 1433–1439. doi: 10.1016/0006-291X(74)90358-1

David, J. D., and Weismeyer, H. (1970). Control of xylose metabolism in *Escherichia coli*. *BBA Gen. Subj.* 201, 497–499. doi: 10.1016/0304-4165(70)90171-6

de Lorenzo, V., and Timmis, K. N. (1994). Analysis and construction of stable phenotypes in gram-negative bacteria with Tn5- and Tn10-derived minitransposons. *Methods Enzymol.* 235, 386–405. doi: 10.1016/0076-6879(94)35157-0

Ditta, G., Stanfield, S., Corbin, D., and Helinski, D. R. (1980). Broad host range DNA cloning system for Gram-negative bacteria: Construction of a gene bank of *Rhizobium meliloti*. *Proc. Natl. Acad. Sci. U.S.A.* 77, 7347–7351. doi: 10.1073/pnas.77.12.7347

Domröse, A., Klein, A. S., Hage-Hülsmann, J., Thies, S., Svensson, V., Classen, T., et al. (2015). Efficient recombinant production of prodigiosin in *Pseudomonas putida*. *Front. Microbiol.* 6, 1–10. doi: 10.3389/fmicb.2015.00972

Dragosits, M., and Mattanovich, D. (2013). Adaptive laboratory evolution - principles and applications for biotechnology. *Microb. Cell Fact.* 12, 1–17. doi: 10.1186/1475-2859-12-64

Dvorák, P., and de Lorenzo, V. (2018). Refactoring the upper sugar metabolism of *Pseudomonas putida* for co-utilization of cellobiose, xylose, and glucose. *Metab. Eng.* 48, 94–108. doi: 10.1016/j.ymben.2018.05.019

Ebert, B. E., Kurth, F., Grund, M., Blank, L. M., and Schmid, A. (2011). Response of *Pseudomonas putida* KT2440 to increased NADH and ATP demand. *Appl. Environ. Microbiol.* 77, 6597–6605. doi: 10.1128/AEM.05588-11

Filloux, A., and Ramos, J.-L. (2014). *Pseudomonas Methods and Protocols*. New York, NY: Springer.

Franden, M. A., Jayakody, L. N., Li, W. J., Wagner, N. J., Cleveland, N. S., Michener, W. E., et al. (2018). Engineering *Pseudomonas putida* KT2440 for efficient ethylene glycol utilization. *Metab. Eng.* 48, 197–207. doi: 10.1016/j.ymben.2018.06.003

Gibson, D. G., Young, L., Chuang, R. Y., Venter, J. C., Hutchison, C. A., and Smith, H. O. (2009). Enzymatic assembly of DNA molecules up to several hundred kilobases. *Nat. Methods* 6, 343–345. doi: 10.1038/nmeth.1318

Goeppert, A., Czaun, M., Surya Prakash, G. K., and Olah, G. A. (2012). Air as the renewable carbon source of the future: An overview of CO_2 capture from the atmosphere. *Energy Environ. Sci.* 5, 7833–7853. doi: 10.1039/c2ee21586a

Gresham, D., and Dunham, M. J. (2014). The enduring utility of continuous culturing in experimental evolution. *Genomics* 104, 399–405. doi: 10.1016/j.ygeno.2014.09.015

Gross, F., Luniak, N., Perlova, O., Gaitatzis, N., Jenke-Kodama, H., Gerth, K., et al. (2006). Bacterial type III polyketide synthases: Phylogenetic analysis and potential for the production of novel secondary metabolites by heterologous expression in pseudomonads. *Arch. Microbiol.* 185, 28–38. doi: 10.1007/s00203-005-0059-3

Guadalupe-Medina, V., Wisselink, H. W., Luttik, M. A., De Hulster, E., Daran, J. M., Pronk, J. T., et al. (2013). Carbon dioxide fixation by Calvin-cycle enzymes improves ethanol yield in yeast. *Biotechnol. Biofuels* 6, 1–12. doi: 10.1186/1754-6834-6-125

Hanahan, D. (1983). Studies on transformation of *Escherichia coli* with plasmids. *J. Mol. Biol.* 166, 557–580. doi: 10.1016/S0022-2836(83)80284-8

Hanahan, D. (1985). "Techniques for transformation of *E. coli*," in DNA Cloning: A Practical Approach, ed D. M. Glover (Oxford: IRL Press), 109–135.

Hochster, R. M. (1955). The formation of phosphorylated sugars from D-xylose by extracts of *Pseudomonas hydrophila*. *Can. J. Microbiol.* 1, 346–363. doi: 10.1139/m55-047

Jakob, F., Lehmann, C., Martinez, R., and Schwaneberg, U. (2013). Increasing protein production by directed vector backbone evolution. *AMB Expr.* 3:39. doi: 10.1186/2191-0855-3-39

Johnsen, U., Dambeck, M., Zaiss, H., Fuhrer, T., Soppa, J., Sauer, U., et al. (2009). D-xylose degradation pathway in the halophilic archaeon *Haloferax volcanii*. *J. Biol. Chem.* 284, 27290–27303. doi: 10.1074/jbc.M109.003814

Kilgore, W. W., and Starr, M. P. (1959). Uronate oxidation by phytopathogenic pseudomonads. *Nature* 183, 1412–1413. doi: 10.1038/1831412a0

Köhler, K. A. K., Blank, L. M., Frick, O., and Schmid, A. (2015). D-Xylose assimilation via the Weimberg pathway by solvent-tolerant *Pseudomonas taiwanensis* VLB120. *Environ. Microbiol.* 17, 156–170. doi: 10.1111/1462-2920.12537

Koopman, F., Wierckx, N., de Winde, J. H., and Ruijssenaars, H. J. (2010). Identification and characterization of the furfural and 5-(hydroxymethyl)furfural degradation pathways of *Cupriavidus basilensis* HMF14. *Proc. Natl. Acad. Sci. U.S.A.* 107, 4919–4924. doi: 10.1073/pnas.0913039107

Kotte, O., Volkmer, B., Radzikowski, J. L., and Heinemann, M. (2014). Phenotypic bistability in *Escherichia coli*'s central carbon metabolism. *Mol. Syst. Biol.* 10, 1–11. doi: 10.15252/msb.20135022

LaCroix, R. A., Palsson, B. O., and Feist, A. M. (2017). A model for designing adaptive laboratory evolution experiments. *Appl. Environ. Microbiol.* 83, 1–14. doi: 10.1128/AEM.03115-16

LaCroix, R. A., Sandberg, T. E., O'Brien, E. J., Utrilla, J., Ebrahim, A., Guzman, G. I., et al. (2015). Use of adaptive laboratory evolution to discover key mutations enabling rapid growth of *Escherichia coli* K-12 MG1655 on glucose minimal medium. *Appl. Environ. Microbiol.* 81, 17–30. doi: 10.1128/AEM.02246-14

Laikova, O. (2001). Computational analysis of the transcriptional regulation of pentose utilization systems in the gamma subdivision of Proteobacteria. *FEMS Microbiol. Lett.* 205, 315–322. doi: 10.1111/j.1574-6968.2001.tb10966.x

Lan, E. I., and Liao, J. C. (2011). Metabolic engineering of cyanobacteria for 1-butanol production from carbon dioxide. *Metab. Eng.* 13, 353–363. doi: 10.1016/j.ymben.2011.04.004

Larsen, J., Østergaard Petersen, M., Thirup, L., Li, H. W., and Iversen, F. K. (2008). The IBUS process - Lignocellulosic bioethanol close to a commercial reality. *Chem. Eng. Technol.* 31, 765–772. doi: 10.1002/ceat.200800048

Le Meur, S., Zinn, M., Egli, T., Thöny-Meyer, L., and Ren, Q. (2012). Production of medium-chain-length polyhydroxyalkanoates by sequential feeding of xylose and octanoic acid in engineered *Pseudomonas putida* KT2440. *BMC Biotechnol.* 12, 1–12. doi: 10.1186/1472-6750-12-53

Lee, J. (1997). Biological conversion of lignocellulosic biomass to ethanol. *J. Biotechnol.* 56, 1–24. doi: 10.1016/S0168-1656(97)00073-4

Lenzen, C., Wynands, B., Otto, M., Bolzenius, J., Mennicken, P., Wierckx, N., et al. (2019). High-yield production of 4-hydroxybenzoate from glucose or glycerol by an engineered *Pseudomonas taiwanensis* VLB120. *Front. Bioeng. Biotechnol.* 7:130. doi: 10.3389/fbioe.2019.00130

Li, W., Jayakody, L. N., Franden, M. A., Wehrmann, M., Daun, T., Hauer, B., et al. (2019). Laboratory evolution reveals the metabolic and regulatory basis of ethylene glycol metabolism by *Pseudomonas putida* KT2440. *Environ. Microbiol.* 21:3669–3682. doi: 10.1111/1462-2920.14703

Liebal, U. W., Blank, L. M., and Ebert, B. E. (2018). CO 2 to succinic acid – Estimating the potential of biocatalytic routes. *Metab. Eng. Commun.* 7, 1–10. doi: 10.1016/j.mec.2018.e00075

Lockwood, L. B., and Nelson, G. E. (1946). The oxidation of pentoses by *Pseudomonas*. *J. Bacteriol.* 52, 581–586.

Loeschcke, A., Markert, A., Wilhelm, S., Wirtz, A., Rosenau, F., Jaeger, K.-E., et al. (2013). TREX: a universal tool for the transfer and expression of biosynthetic pathways in bacteria. *ACS Synth. Biol.* 2, 22–33. doi: 10.1021/sb3000657

Loeschcke, A., and Thies, S. (2015). *Pseudomonas putida* - a versatile host for the production of natural products. *Appl. Microbiol. Biotechnol.* 99, 6197–6214. doi: 10.1007/s00253-015-6745-4

Maas, R. H., Bakker, R. R., Boersma, A. R., Bisschops, I., Pels, J. R., de Jong, E., et al. (2008). Pilot-scale conversion of lime-treated wheat straw into bioethanol: quality assessment of bioethanol and valorization of side streams by anaerobic digestion and combustion. *Biotechnol. Biofuels* 1, 1–13. doi: 10.1186/1754-6834-1-14

Martínez-García, E., and de Lorenzo, V. (2011). Engineering multiple genomic deletions in Gram-negative bacteria: analysis of the multi-resistant antibiotic profile of *Pseudomonas putida* KT2440. *Environ. Microbiol.* 13, 2702–2716. doi: 10.1111/j.1462-2920.2011.02538.x

Martins Dos Santos, V. A. P., Heim, S., Moore, E. R. B., Strätz, M., and Timmis, K. N. (2004). Insights into the genomic basis of niche specificity of *Pseudomonas putida* KT2440. *Environ. Microbiol.* 6:1264–1286. doi: 10.1111/j.1462-2920.2004.00734.x

Meijnen, J.-P., de Winde, J. H., and Ruijssenaars, H. J. (2008). Engineering *Pseudomonas putida* S12 for efficient utilization of D-xylose and L-arabinose. *Appl. Environ. Microbiol.* 74, 5031–5037. doi: 10.1128/AEM.00924-08

Meijnen, J.-P., de Winde, J. H., and Ruijssenaars, H. J. (2009). Establishment of oxidative D-xylose metabolism in *Pseudomonas putida* S12. *Appl. Environ. Microbiol.* 75, 2784–2791. doi: 10.1128/AEM.02713-08

Mi, J., Sydow, A., Schempp, F., Becher, D., Schewe, H., Schrader, J., et al. (2016). Investigation of plasmid-induced growth defect in *Pseudomonas putida*. *J. Biotechnol.* 231, 167–173. doi: 10.1016/j.jbiotec.2016.06.001

Mindt, M., Walter, T., Risse, J. M., and Wendisch, V. F. (2018). Fermentative production of *N*-methylglutamate from glycerol by recombinant *Pseudomonas putida*. *Front. Bioeng. Biotechnol.* 6:159. doi: 10.3389/fbioe.2018.00159

Nelson, K. E., Weinel, C., Paulsen, I. T., Dodson, R. J., Hilbert, H., Martins dos Santos, V. A. P., et al. (2002). Complete genome sequence and comparative analysis of the metabolically versatile *Pseudomonas putida* KT2440. *Environ. Microbiol.* 4, 799–808. doi: 10.1046/j.1462-2920.2002.00366.x

Nikel, P. I., and de Lorenzo, V. (2018). *Pseudomonas putida* as a functional chassis for industrial biocatalysis: From native biochemistry to trans-metabolism. *Metab. Eng.* 50, 142–155. doi: 10.1016/j.ymben.2018.05.005

Nogales, J., Gudmundsson, S., Duque, E., Ramos, J. L., and Palsson, B. O. (2017). Expanding the computable reactome in *Pseudomonas putida* reveals metabolic cycles providing robustness. *bioRxiv [Preprint]* 1–34. doi: 10.1101/139121

Nogales, J., Mueller, J., Gudmundsson, S., Canalejo, F. J., Duque, E., Monk, J., et al. (2019). High-quality genome-scale metabolic modelling of Pseudomonas putida highlights its broad metabolic capabilities. *Environ. Microbiol.* doi: 10.1111/1462-2920.14843

Ogata, H., Goto, S., Sato, K., Fujibuchi, W., Bono, H., and Kanehisa, M. (1999). KEGG: Kyoto encyclopedia of genes and genomes. *Nucleic Acids Res.* 27, 29–34. doi: 10.1093/nar/27.1.29

Olah, G. A., Goeppert, A., and Prakash, G. K. (2009). Chemical recycling of carbon dioxide to methanol and dimethyl ether: from greenhouse gas to renewable, environmentally carbon neutral fuels and synthetic hydrocarbons. *J. Org. Chem.* 74, 487–498. doi: 10.1021/jo801260f

Panke, S., Witholt, B., Schmid, A., and Wubbolts, M. G. (1998). Towards a biocatalyst for (*S*)-styrene oxide production: Characterization of the styrene degradation pathway of *Pseudomonas* sp. strain VLB120. *Appl. Environ. Microbiol.* 64, 2032–2043. doi: 10.1128/AEM.64.6.2032-2043.1998

Poblete-Castro, I., Becker, J., Dohnt, K., dos Santos, V. M., and Wittmann, C. (2012). Industrial biotechnology of *Pseudomonas putida* and related species. *Appl. Microbiol. Biotechnol.* 93, 2279–2290. doi: 10.1007/s00253-012-3928-0

Porco, A., Peekhaus, N., Bausch, C., Tong, S., Isturiz, T., and Conway, T. (1997). Molecular genetic characterization of the *Escherichia coli gntT* gene of GntI, the main system for gluconate metabolism. *J. Bacteriol.* 179, 1584–1590. doi: 10.1128/jb.179.5.1584-1590.1997

Poskar, C. H., Huege, J., Krach, C., Franke, M., Shachar-Hill, Y., and Junker, B. H. (2012). iMS2Flux - a high-throughput processing tool for stable isotope labeled mass spectrometric data used for metabolic flux analysis. *BMC Bioinformatics* 13:295. doi: 10.1186/1471-2105-13-295

Radek, A., Krumbach, K., Gätgens, J., Wendisch, V. F., Wiechert, W., Bott, M., et al. (2014). Engineering of *Corynebacterium glutamicum* for minimized carbon loss during utilization of D-xylose containing substrates. *J. Biotechnol.* 192, 156–160. doi: 10.1016/j.jbiotec.2014.09.026

Ramos, J. L., Duque, E., Huertas, M. J., and Haïdour, A. (1995). Isolation and expansion of the catabolic potential of a *Pseudomonas putida* strain able to grow in the presence of high concentrations of aromatic hydrocarbons. *J. Bacteriol.* 177, 3911–3916. doi: 10.1128/jb.177.14.3911-3916.1995

Reva, O. N., Weinel, C., Weinel, M., Böhm, K., Stjepandic, D., Hoheisel, J. D., et al. (2006). Functional genomics of stress response in *Pseudomonas putida* KT2440. *J. Bacteriol.* 188, 4079–4092. doi: 10.1128/JB.00101-06

Richard, P., and Hilditch, S. (2009). D-galacturonic acid catabolism in microorganisms and its biotechnological relevance. *Appl. Microbiol. Biotechnol.* 82, 597–604. doi: 10.1007/s00253-009-1870-6

Rossoni, L., Carr, R., Baxter, S., Cortis, R., Thorpe, T., Eastham, G., et al. (2018). Engineering *Escherichia coli* to grow constitutively on D-xylose using the carbon-efficient Weimberg pathway. *Microbiol.* 164, 287–298. doi: 10.1099/mic.0.000611

Saha, B. C. (2003). Hemicellulose bioconversion. *J. Ind. Microbiol. Biotechnol.* 30, 279–291. doi: 10.1007/s10295-003-0049-x

Sambrook, J., and Russell, D. W. (2001). *Molecular Cloning, 3rd Edn.* New York, NY: Cold Spring Harbor Laboratory Press.

Satagopan, S., Sun, Y., Parquette, J. R., and Tabita, F. R. (2017). Synthetic CO_2-fixation enzyme cascades immobilized on self-assembled nanostructures that enhance CO_2/O_2 selectivity of RubisCO. *Biotechnol. Biofuels* 10, 1–14. doi: 10.1186/s13068-017-0861-6

Schada von Borzyskowski, L., Carrillo, M., Leupold, S., Glatter, T., Kiefer, P., Weishaupt, R., et al. (2018). An engineered Calvin-Benson-Bassham cycle for carbon dioxide fixation in *Methylobacterium extorquens* AM1. *Metab. Eng.* 47, 423–433. doi: 10.1016/j.ymben.2018.04.003

Schellenberger, J., Que, R., Fleming, R. M., Thiele, I., Orth, J. D., Feist, A. M., et al. (2011). Quantitative prediction of cellular metabolism with constraint-based models: the COBRA Toolbox v2.0. *Nat. Protoc.* 6, 1290–1307. doi: 10.1038/nprot.2011.308

Schmitz, A., Ebert, B. E., and Blank, L. M. (2015a). "GC-MS-based determination of mass isotopomer distributions for ^{13}C-based metabolic flux analysis," in *Hydrocarbon and Lipid Microbiology Protocols*, eds. T. J. McGenity, K. N. Timmis, and B. N. Fernandez (Berlin: Springer), 223–243.

Schmitz, S., Nies, S., Wierckx, N., Blank, L. M., and Rosenbaum, M. A. (2015b). Engineering mediator-based electroactivity in the obligate aerobic bacterium *Pseudomonas putida* KT2440. *Front. Microbiol.* 6, 1–13. doi: 10.3389/fmicb.2015.00284

Schwander, T., Von Borzyskowski, L. S., Burgener, S., Cortina, N. S., and Erb, T. J. (2016). A synthetic pathway for the fixation of carbon dioxide *in vitro*. *Science (80-)* 354, 900–904. doi: 10.1126/science.aah5237

Stephens, C., Christen, B., Fuchs, T., Sundaram, V., Watanabe, K., and Jenal, U. (2007). Genetic analysis of a novel pathway for D-xylose metabolism in *Caulobacter crescentus*. *J. Bacteriol.* 189, 2181–2185. doi: 10.1128/JB.01438-06

Sudarsan, S., Dethlefsen, S., Blank, L. M., Siemann-Herzberg, M., and Schmid, A. (2014). The functional structure of central carbon metabolism in *Pseudomonas putida* KT2440. *Appl. Environ. Microbiol.* 80, 5292–5303. doi: 10.1128/AEM.01643-14

Tiso, T., Sabelhaus, P., Behrens, B., Wittgens, A., Rosenau, F., Hayen, H., et al. (2016). Creating metabolic demand as an engineering strategy in *Pseudomonas putida* – Rhamnolipid synthesis as an example. *Metab. Eng. Commun.* 3, 234–244. doi: 10.1016/j.meteno.2016.08.002

Tiso, T., Wierckx, N., and Blank, L. M. (2014). "Non-pathogenic *Pseudomonas* as platform for industrial biocatalysis," in *Industrial Bocatalysis*, ed. P. Grunwald (Hoboken: Pan Stanford), 323–372.

Tiso, T., Zauter, R., Tulke, H., Leuchtle, B., Li, W.-J., Behrens, B., et al. (2017). Designer rhamnolipids by reduction of congener diversity: production and characterization. *Microb. Cell Fact.* 16:225. doi: 10.1186/s12934-017-0838-y

Vanholme, B., Desmet, T., Ronsse, F., Rabaey, K., Van Breusegem, F., De Mey, M., et al. (2013). Towards a carbon-negative sustainable bio-based economy. *Front. Plant Sci.* 4:174. doi: 10.3389/fpls.2013.00174

Wang, Y., Horlamus, F., Henkel, M., Kovacic, F., Schläfle, S., Hausmann, R., et al. (2019). Growth of engineered *Pseudomonas putida* KT2440 on glucose, xylose, and arabinose: hemicellulose hydrolysates and their major sugars as sustainable carbon sources. *GCB Bioenergy* 11, 249–259. doi: 10.1111/gcbb.12590

Weimberg, R. (1961). Pentose oxidation by *Pseudomonas fragi*. *J. Biol. Chem.* 236, 629–635.

Weimberg, R., and Doudoroff, M. (1955). The oxidation of L-arabinose by *Pseudomonas saccharophila*. *J. Biol. Chem.* 217, 607–624.

Werpy, T., and Petersen, G. (2004). *Top Value Added Chemicals From Biomass: Volume I - Results of Screening for Potential Candidates From Sugars and Synthesis Gas*. Golden, CO: US-DoE (U.S. Department of Energy).

Wilhelm, M., and Hollenberg, C. P. (1985). Nucleotide sequence of the *Bacillus subtilis* xylose isomerase gene: extensive homology between the *Bacillus* and *Escherichia coli* enzyme. *Nucleic Acids Res.* 13, 5717–5722. doi: 10.1093/nar/13.15.5717

Williamson, N. R., Fineran, P. C., Leeper, F. J., and Salmond, G. P. (2006). The biosynthesis and regulation of bacterial prodiginines. *Nat. Rev. Microbiol.* 4, 887–899. doi: 10.1038/nrmicro1531

Winsor, G. L., Griffiths, E. J., Lo, R., Dhillon, B. K., Shay, J. A., and Brinkman, F. S. L. (2016). Enhanced annotations and features for comparing thousands of *Pseudomonas* genomes in the *Pseudomonas* genome database. *Nucleic Acids Res.* 44, 646–653. doi: 10.1093/nar/gkv1227

Wiser, M. J., and Lenski, R. E. (2015). A comparison of methods to measure fitness in *Escherichia coli*. *PLoS ONE* 10:e0126210. doi: 10.1371/journal.pone.0126210

Wittgens, A., Kovacic, F., Müller, M. M., Gerlitzki, M., Santiago-Schübel, B., Hofmann, D., et al. (2017). Novel insights into biosynthesis and uptake of rhamnolipids and their precursors. *Appl. Microbiol. Biotechnol.* 101, 2865–2878. doi: 10.1007/s00253-016-8041-3

Wittgens, A., and Rosenau, F. (2018). On the road towards tailor-made rhamnolipids: current state and perspectives. *Appl. Microbiol. Biotechnol.* 102, 8175–8185. doi: 10.1007/s00253-018-9240-x

Wittgens, A., Santiago-Schuebel, B., Henkel, M., Tiso, T., Blank, L. M., Hausmann, R., et al. (2018). Heterologous production of long-chain rhamnolipids from *Burkholderia glumae* in *Pseudomonas putida*—a step forward to tailor-made rhamnolipids. *Appl. Microbiol. Biotechnol.* 102, 1229–1239. doi: 10.1007/s00253-017-8702-x

Wittgens, A., Tiso, T., Arndt, T. T., Wenk, P., Hemmerich, J., Müller, C., et al. (2011). Growth independent rhamnolipid production from glucose using the non-pathogenic *Pseudomonas putida* KT2440. *Microb. Cell Fact.* 10, 1–17. doi: 10.1186/1475-2859-10-80

Wynands, B., Lenzen, C., Otto, M., Koch, F., Blank, L. M., and Wierckx, N. (2018). Metabolic engineering of *Pseudomonas taiwanensis* VLB120 with minimal genomic modifications for high-yield phenol production. *Metab. Eng.* 47, 121–133. doi: 10.1016/j.ymben.2018.03.011

Zhao, Y., Damgaard, A., and Christensen, T. H. (2018). Bioethanol from corn stover – a review and technical assessment of alternative biotechnologies. *Prog. Energy Combust. Sci.* 67, 275–291. doi: 10.1016/j.pecs.2018.03.004

Zobel, S., Benedetti, I., Eisenbach, L., De Lorenzo, V., Wierckx, N., and Blank, L. M. (2015). Tn7-Based device for calibrated heterologous gene expression in *Pseudomonas putida*. *ACS Synth. Biol.* 4:1341–1351. doi: 10.1021/acssynbio.5b00058

Conflict of Interest: The authors declare that the research was conducted in the absence of any commercial or financial relationships that could be construed as a potential conflict of interest.

frontiers in Bioengineering and Biotechnology

ORIGINAL RESEARCH
published: 22 January 2020
doi: 10.3389/fbioe.2019.00484

De novo Biosynthesis of Odd-Chain Fatty Acids in *Yarrowia lipolytica* Enabled by Modular Pathway Engineering

Young-kyoung Park[1]*, *Rodrigo Ledesma-Amaro*[2]* and *Jean-Marc Nicaud*[1]

[1] Université Paris-Saclay, INRAE, AgroParisTech, Micalis Institute, Jouy-en-Josas, France, [2] Imperial College Centre for Synthetic Biology and Department of Bioengineering, Imperial College London, London, United Kingdom

Microbial oils are regarded as promising alternatives to fossil fuels as concerns over environmental issues and energy production systems continue to mount. Odd-chain fatty acids (FAs) are a type of valuable lipid with various applications: they can serve as biomarkers, intermediates in the production of flavor and fragrance compounds, fuels, and plasticizers. Microorganisms naturally produce FAs, but such FAs are primarily even-chain; only negligible amounts of odd-chain FAs are generated. As a result, studies using microorganisms to produce odd-chain FAs have had limited success. Here, our objective was to biosynthesize odd-chain FAs *de novo* in *Yarrowia lipolytica* using inexpensive carbon sources, namely glucose, without any propionate supplementation. To achieve this goal, we constructed a modular metabolic pathway containing seven genes. In the engineered strain expressing this pathway, the percentage of odd-chain FAs out of total FAs was higher than in the control strain (3.86 vs. 0.84%). When this pathway was transferred into an obese strain, which had been engineered to accumulate large amounts of lipids, odd-chain fatty acid production was 7.2 times greater than in the control (0.05 vs. 0.36 g/L). This study shows that metabolic engineering research is making progress toward obtaining efficient cell factories that produce odd-chain FAs.

Keywords: odd-chain fatty acids, propionyl-CoA, *Yarrowia lipolytica*, metabolic engineering, Golden Gate assembly, synthetic biology

OPEN ACCESS

Edited by:
Fayza Daboussi,
Institut National de la Recherche Agronomique (INRA), France

Reviewed by:
Jiazhang Lian,
Zhejiang University, China
Carol Sze Ki Lin,
City University of Hong Kong, Hong Kong

***Correspondence:**
Young-kyoung Park
youngkyoung.park@inra.fr
Rodrigo Ledesma-Amaro
r.ledesma-amaro@imperial.ac.uk

Specialty section:
This article was submitted to Synthetic Biology, a section of the journal Frontiers in Bioengineering and Biotechnology

Received: *31 August 2019*
Accepted: *27 December 2019*
Published: *22 January 2020*

Citation:
Park Y, Ledesma-Amaro R and Nicaud J-M (2020) De novo Biosynthesis of Odd-Chain Fatty Acids in Yarrowia lipolytica Enabled by Modular Pathway Engineering. Front. Bioeng. Biotechnol. 7:484. doi: 10.3389/fbioe.2019.00484

INTRODUCTION

Microbial oils (lipids and fatty acid-derived products) are regarded as promising alternatives to fossil fuels in the face of growing concerns over environmental issues and energy production. To lessen the cost of producing microbial oils, considerable effort has been dedicated to enhancing production yield (Dulermo and Nicaud, 2011; Tai and Stephanopoulos, 2013; Qiao et al., 2015); using low-cost carbon substrates (Papanikolaou et al., 2013; Lazar et al., 2014; Guo et al., 2015; Ledesma-Amaro and Nicaud, 2016); and targeting high-value lipids (Xue et al., 2013; Xie et al., 2015). Odd-chain fatty acids (FAs), a type of valuable lipid, are a product with potential because they can be used in a variety of applications. Notably, research has revealed that odd-chain FAs with chain lengths of 15 and 17 carbons may have functional importance for nutrition and medical field. For example, *cis*-9-heptadecenoic acid has anti-inflammatory effects and can help treat psoriasis, allergies, and autoimmune diseases (Degwert et al., 1998). Pentadecanoic acid and heptadecanoic

acid can be used as biomarkers of food intake in dietary assessments, the risk of coronary heart disease (CHD), and the risk of type II diabetes mellitus (Forouhi et al., 2014; Jenkins et al., 2015; Pedersen et al., 2016; Pfeuffer and Jaudszus, 2016). The chemical properties and potential biological activities of odd-chain FAs are now being more extensively studied (Rezanka and Sigler, 2009), so it is possible that novel nutritional and pharmaceutical applications could soon be discovered. In addition, odd-chain FAs and their derivatives are precursors for manufacturing substances such as pesticides, flavor and fragrance compounds, hydraulic fluids, plasticizers, coatings, and other industrial chemicals (Fitton and Goa, 1991; Avis, 2000; Clausen et al., 2010; Köckritz et al., 2010). Despite the broad range of applications for FAs, studies aiming to produce odd-chain FAs using microorganisms have had limited success because microorganisms produce a much greater proportion of even-chain FAs than odd-chain FAs.

Generally, *de novo* fatty acid synthesis in microorganisms begins with the condensation of acetyl-CoA and malonyl-CoA (**Figure 1A**). Then, the elongation step occurs: long-chain FAs are synthesized in a reaction catalyzed by fatty acid synthase (FAS). The resulting acyl-CoA products are esterified to generate lysophosphatidic acid (LPA), then phosphatidic acid (PA), and finally diacylglycerol (DAG) before forming triacylglycerol (TAG), the compound in which the lipids are stored. For odd-chain FAs, propionyl-CoA could be converted from propionate is a primer for the fatty acid synthesis. The condensation of both propionyl-CoA and malonyl-CoA results in the formation of 3-oxovaleryl-ACP, which is the launching point for odd-chain FA synthesis. This five-carbon compound goes through elongation, where two carbons are added in each cycle. Then odd-chain FAs can be synthesized as described in **Figure 1B**. However, most microorganisms require the presence of propionate in the medium to produce odd-chain FAs. Wu and San have shown that *E. coli* can produce odd-chain FAs—namely undecanoic acid (C11:0), tridecanoic acid (C13:0), and pentadecanoic acid (C15:0)—if grown with propionate-supplemented medium (Wu and San, 2014). They introduced a propionyl-CoA synthetase (*prpE*) from *Salmonella enterica* and acyl-ACP thioesterases (TEs) from *Umbellularia californica* and *Ricinus communis*. Additionally, propionate supplementation has allowed various yeasts (e.g., *Yarrowia lipolytica*, *Rhodotorula glutinis*, *Cryptococcus curvatus*, and *Kluyveromyces polysporus*) to produce odd-chain FAs (Zheng et al., 2012; Kolouchová et al., 2015). More recently, in *Y. lipolytica*, metabolic engineering and the optimization of propionate feeding helped boost the production of odd-chain FAs, namely heptadecenoic acid (C17:1) (Park et al., 2018).

Therefore, to date, most studies have been focused on processes that involve propionate supplementation. However, due to the high cost (Poirier et al., 1995; Aldor et al., 2002) and toxic effects of propionate (Fontanille et al., 2012; Park and Nicaud, 2019), it is crucial to find alternative pathways for generating propionyl-CoA to be able to produce odd-chain FAs on large scales. There have been a few studies in which odd-chain FAs have been produced using glucose. Tseng and Prather have shown that, in *E. coli*, the production of very short odd-chain FAs (i.e., propionate, trans-2-pentenoate, and valerate) can be increased through the upregulation of threonine biosynthesis (Tseng and Prather, 2012). Another study demonstrated that the overexpression of threonine biosynthesis in *E. coli* resulted in increased levels of odd-chain FAs (mainly C15:0): from 0.006 to 0.246 g/L. This study further modified the experimental strain by replacing the native β-ketoacyl-ACP synthase (encoded by *FabH*) with one from *Bacillus subtilis* (encoded by *FabHI*) so that there was a biochemical preference for propionyl-CoA over acetyl-CoA (Lee et al., 2013). However, to date, no one has reported the *de novo* production of odd-chain FAs in *Y. lipolytica* or in any other yeasts without propionate supplementation. Consequently, we need more research on metabolic engineering approaches for producing odd-chain FAs in this group of microorganisms.

Of the several microbial hosts used in such systems, the oleaginous yeast *Y. lipolytica* is the most studied and has been engineered to produce large amounts of lipids and lipid derivatives, such as ricinoleic acid (Beopoulos et al., 2014), conjugated linoleic acids (Imatoukene et al., 2017), cyclopropane FAs (Czerwiec et al., 2019), and cocoa butter-like oils (Papanikolaou et al., 2003). *Y. lipolytica* can naturally grow in a broad range of substrates and has been further engineered to use even more substrates (Ledesma-Amaro et al., 2016). In addition,

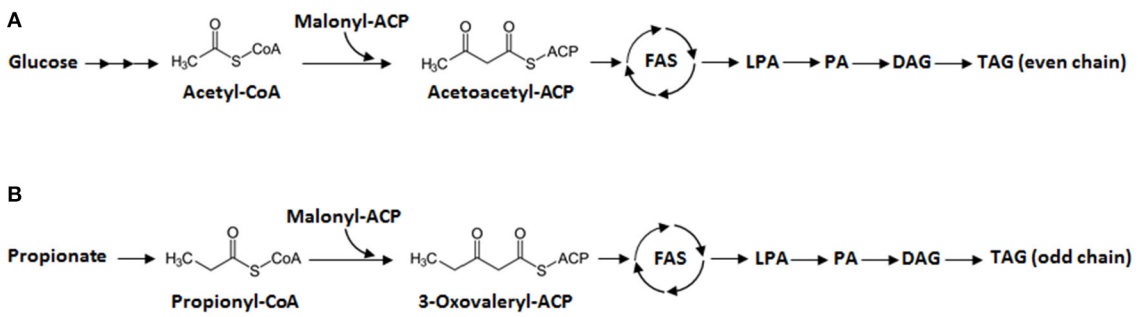

FIGURE 1 | Lipid synthesis in *Y. lipolytica*. **(A)** Synthesis of even-chain fatty acids (FAs) from glucose. **(B)** Synthesis of odd-chain FAs from propionate. First, there is elongation of fatty acyl-CoA by fatty acid synthase (FAS). Second, the resulting even- or odd-chain fatty acyl-CoA is transformed into lysophosphatidic acid (LPA), phosphatidic acid (PA), and diacylglycerol (DAG), in that order, before finally forming triacylglycerol (TAG).

many different synthetic biology tools have been created for and applied in *Y. lipolytica*, such as Gibson assembly, Golden Gate assembly, TALEN editing, and CRISPR/Cas9 editing [please see the recent review by Larroude et al. (2018) for more details]. These tools used in tandem with genetic and metabolic engineering strategies have boosted the capacities of *Y. lipolytica*, making the yeast into a promising host for biotechnological production processes.

The objective of this study was to biosynthesize odd-chain FAs *de novo* from glucose without propionate supplementation. We constructed a modular metabolic pathway for synthesizing propionyl-CoA from oxaloacetate in *Y. lipolytica* and confirmed that accumulation of odd-chain FAs was increased. We also investigated whether it could be competitive to produce odd-chain FAs from propionyl-CoA via the methylcitrate pathway using the engineered strain. Additionally, we overexpressed the pyruvate dehydrogenase (PDH) complex in the cytosol to see if it could improve the conversion of α-ketobutyrate to propionyl-CoA. This work demonstrates that our metabolic engineering strategy for directing metabolic fluxes through specific pathways can enhance odd-chain FA production.

MATERIALS AND METHODS

Strains and Media

Media and growth conditions for *E. coli* were previously described by Sambrook and Russell (2001); those for *Y. lipolytica* were previously described by Barth and Gaillardin (1997). Rich medium (YPD) and minimal glucose medium (YNB) were prepared as described elsewhere (Milckova et al., 2004). The YNB contained 0.17% (w/v) yeast nitrogen base (without amino acids and ammonium sulfate, YNBww), 0.5% (w/v) NH_4Cl, 50 mM KH_2PO_4-Na_2HPO_4 (pH 6.8), and 2% (w/v) glucose. To complement strain auxotrophies, 0.1 g/L of uracil or leucine was added as necessary. To screen for hygromycin resistance, 250 μg/ml of hygromycin was added to the YPD. Solid media were prepared by adding 1.5% (w/v) agar.

Construction of Plasmids and Strains (*E. coli* and *Y. lipolytica*)

We used standard molecular genetic techniques (Sambrook and Russell, 2001). Restriction enzymes were obtained from New England Biolabs (Ipswich, MA, USA). PCR amplification was performed in an Eppendorf 2720 Thermal Cycler with either Q5 High-Fidelity DNA Polymerase (New England Biolabs) or GoTaq DNA polymerases (Progema, WI, USA). PCR fragments were purified using a PCR Purification Kit (Macherey-Nagel, Duren, Germany), and plasmids were purified with a Plasmid Miniprep Kit (Macherey-Nagel).

The plasmids used in this study were constructed using Golden Gate assembly, as described in Celinska et al. (2017). The genes in the A, T, and H module were obtained via PCR using the genomic DNA of *Y. lipolytica* W29. Internal BsaI recognition sites were removed via PCR using the primers listed in **Supplementary Table 1**. The plasmids for each module included the Zeta sequence, the *URA3 ex* marker, and gene expression cassettes containing the *TEF1* promoter and *LIP2* terminator.

For the cytosolic PDH complex, all the genes were synthesized and cloned in the plasmid pUC57 by GenScript Biotech (New Jersey, US). Cytosolic *PDX1* was cloned into the expression plasmid (JME2563) using the BamHI and AvrII restriction sites. The other four genes were cloned into two plasmids (JME4774 and JME4775) using Golden Gate assembly.

To disrupt *PHD1*, the cassettes were constructed to include a promoter (*pPHD1*), a marker (*URA3* or *LEU2*), and a terminator (*TPHD1*), which allowed the ORF gene to be removed via homologous recombination, as described in Papanikolaou et al. (2013).

Gene expression and disruption cassettes were prepared by NotI digestion and transformed into *Y. lipolytica* strains using the lithium acetate method, as described previously (Barth and Gaillardin, 1997). Gene integration and disruption were verified via colony PCR using the primers listed in **Supplementary Table 1**. The replicative plasmid harboring the *Cre* gene (JME547; **Table 1**) was used for marker rescue (Fickers et al., 2003). After transformation with the *Cre* expression plasmid, the loss of the marker gene was verified on YNB with/without uracil. The loss of the replicative plasmid was checked using replica plating on YPD with/without hygromycin after culturing on YPD for 24 h. To construct the prototrophic strain, a *LEU2* fragment from plasmid JMP2563 was transformed. All the strains and plasmids used in this study are listed in **Table 1**.

Culture Conditions for the Lipid Biosynthesis Experiments

The lipid biosynthesis experiments were carried out in minimal media, and the cultures were prepared as follows: an initial pre-culture was established by inoculating 10 mL of YPD medium in 50 mL Erlenmeyer flasks. Then, the pre-culture was incubated overnight at 28°C and 180 rpm. The resulting cell suspension was washed with sterile distilled water and used to inoculate 50 mL of minimal medium YNBD6 containing 0.17% (w/v) yeast nitrogen base (without amino acids and ammonium sulfate, YNBww, Difco), 0.15% (w/v) NH_4Cl, 50 mM KH_2PO_4-Na_2HPO_4 buffer (pH 6.8), and 6% (w/v) glucose. This medium had been placed in 250 mL Erlenmeyer flasks. The cultures were then incubated at 28°C and 180 rpm.

Lipid Determination

Lipids were extracted from 10 to 20 mg of freeze-dried cells and converted into FA methyl esters (FAMEs) using the procedure described by Browse et al. (1986). The FAMEs were then analyzed using gas chromatography (GC), which was carried out with a Varian 3900 instrument equipped with a flame ionization detector and a Varian FactorFour vf-23ms column, where the bleed specification at 260°C is 3 pA (30 m, 0.25 mm, 0.25 μm). The FAMEs were identified via comparisons with commercial standards (FAME32, Supelco) and quantified using the internal standard method, which involves the addition of 100 μg of commercial dodecanoic acid (Sigma-Aldrich). Commercial odd-chain FAs (Odd Carbon Straight Chains Kit containing 9 FAs, OC9, Supelco) were converted into their FAMEs using the same method employed with the yeast samples. They were then

TABLE 1 | The plasmids and strains used in this study.

Strain	Description	Abbreviation	References
Plasmid			
GGE0004	TOPO-P2-*TEF1*		Celinska et al., 2017
GGE0009	TOPO-P3-*TEF1*		Celinska et al., 2017
GGE0014	TOPO-T1-*LIP2*		Celinska et al., 2017
GGE0015	TOPO-T2-*LIP2*		Celinska et al., 2017
GGE0020	TOPO-T1-3-*LIP2*		Celinska et al., 2017
GGE0021	TOPO-T2-3-*LIP2*		Celinska et al., 2017
GGE0028	pSB1C3		Celinska et al., 2017
GGE0029	pSB1A3		Celinska et al., 2017
GGE0038	TOPO-ZetaDOWN-NotI		Celinska et al., 2017
GGE0067	TOPO-ZetaUP-NotI		Celinska et al., 2017
GGE0081	TOPO-T3-*LIP2*		Celinska et al., 2017
GGE0082	TOPO-P1-*TEF1*		Celinska et al., 2017
GGE0085	TOPO-M-*URA3* ex		Celinska et al., 2017
GGE0376	TOPO-*AAT2*		This study
GGE0377	TOPO-*THR1*		This study
GGE0378	TOPO-*THR4*		This study
GGE0379	pJET-*ILV1*		This study
GGE0380	TOPO-*HOM3*		This study
GGE0381	TOPO-*HOM2*		This study
GGE0382	pJET-*HOM6*		This study
JME0547	pUC-*Cre*		Fickers et al., 2003
JME0740	pGEM-T-*PHD1* PUT		Papanikolaou et al., 2013
JME1811	pGEM-T-*PHD1* PLT		Papanikolaou et al., 2013
JME2563	JMP62-*LEU2*ex-pTEF1		Dulermo et al., 2017
JME4478	GGV-*URA3* ex-pTEF1-*AAT2*	Module A	This study
JME4479	GGV-*URA3* ex-pTEF1-*THR1*-pTEF-*THR4*-pTEF-*ILV1*	Module T	This study
JME4632	GGV-*URA3* ex-pTEF1-*HOM3*-pTEF1-*HOM2*-pTEF1-*HOM6*	Module H	This study
JME4774	GGV-*URA3* ex-pTEF1-yl*PDA1*-pTEF1-yl*PDB1*	Module P	This study
JME4775	GGV-*URA3* ex-pTEF1-yl*LPD1*-pTEF1-yl*LAT1*	Module P	This study
JME4776	JMP62-*LEU2* ex-pTEF1-yl*PDX1*	Module P	This study
Y. lipolytica			
JMY195	MATa *ura3-302 leu2-270 xpr2-322*	WT	Barth and Gaillardin, 1997
JMY2900	JMY195 *URA3 LEU2*	WT	Dulermo et al., 2014
JMY7201	JMY195 + GGV-*AAT2-URA3* ex	WT-A	This study
JMY7202	JMY195 + GGV-*AAT2*	WT-A	This study
JMY7639	JMY195 + GGV-*AAT2-URA3* ex + *LEU2*	WT-A	This study
JMY7203	JMY195 + GGV-*AAT2* + GGV-*THR1-THR4-ILV1-URA3* ex	WT-AT	This study
JMY7204	JMY195 + GGV-*AAT2* + GGV-*THR1-THR4-ILV1*	WT-AT	This study
JMY7353	JMY195 + GGV-*AAT2* + GGV-*THR1-THR4-ILV1* +GGV-*HOM3-HOM2-HOM6-URA3* ex	WT-ATH	This study
JMY7357	JMY195 + GGV-*AAT2* + GGV-*THR1-THR4-ILV1* +GGV-*HOM3-HOM2-HOM6-URA3* ex + *LEU2*	WT-ATH	This study
JMY7374	JMY195 + GGV-*AAT2* + GGV-*THR1-THR4-ILV1* +GGV-*HOM3-HOM2-HOM6-URA3* ex + *phd1*::*LEU2* ex	WT-ATH *phd1Δ*	This study
JMY7828	JMY195 + GGV-*AAT2* + GGV-*THR1-THR4-ILV1* +GGV-*HOM3-HOM2-HOM6*	WT-ATH	This study
JMY7640	JMY195 + GGV-*THR1-THR4-ILV1-URA3* ex	WT-T	This study
JMY7643	JMY195 + GGV-*THR1-THR4-ILV1-URA3* ex + *LEU2*	WT-T	This study
JMY7646	JMY195 + GGV-*HOM3-HOM2-HOM6-URA3* ex	WT-H	This study
JMY7649	JMY195 + GGV-*HOM3-HOM2-HOM6-URA3* ex + *LEU2*	WT-H	This study
JMY7824	Y195ATH+ylPDHcyto	WT-ATHP	This study
JMY3501	*Δpox1-6 Δtgl4* pTEF-*DGA2-LEU2*ex pTEF-*GPD1-URA3*ex	Obese	Lazar et al., 2014

(Continued)

TABLE 1 | Continued

Strain	Description	Abbreviation	References
JMY3820	*Δpox1-6 Δtgl4* pTEF-*DGA2* pTEF-*GPD1*	Obese	Lazar et al., 2014
JMY7206	JMY3820 + GGV-*AAT2-URA3* ex	Obese-A	This study
JMY7207	JMY3820 + GGV-*AAT2*	Obese-A	This study
JMY7208	JMY3820 + GGV-*AAT2* + GGV-*THR1-THR4-ILV1-URA3* ex	Obese-AT	This study
JMY7267	JMY3820 + GGV-*AAT2* + GGV-*THR1-THR4-ILV1*	Obese-AT	This study
JMY7412	MY3820 + GGV-*AAT2* + GGV-*THR1-THR4-ILV1* + GGV-*HOM3-HOM2-HOM6-URA3* ex + *LEU2*	Obese-ATH	This study
JMY7413	MY3820 + GGV-*AAT2* + GGV-*THR1-THR4-ILV1* + GGV-*HOM3-HOM2-HOM6*	Obese-ATH	This study
JMY7414	JMY7413 + *phd1::LEU2* ex	Obese-ATH *phd1Δ*	This study
JMY7417	JMY7413 + *phd1::LEU2* ex + *URA3*	Obese-ATH *phd1Δ*	This study
JMY7826	Y3820ATH+ylPDHcyto	Obese-ATHP	This study

identified using GC and compared with the odd-chain FAs from the yeast samples.

To determine dry cell weight (DCW), 2 mL of the culture was taken from the flasks, washed, and lysophilized in a pre-weighed tube. The differences in mass corresponded to the mg of cells found in 2 mL of culture.

RESULTS

Modular Pathway Engineering Was Used for Odd-Chain Fatty Acid Synthesis

Propionyl-CoA is a key primer in the synthesis of odd-chain FAs. It can be synthesized using β-oxidation from direct precursors, propionate, or long-chain FAs. It can also be created from other metabolites via several metabolic pathways, such as the citramalate/2-ketobutyrate pathway, the aspartate/2-ketobutyrate pathway, the methylmalonyl-CoA pathway, the 3-hydroxypropionate pathway, and the isoleucine or valine degradation pathway (**Supplementary Figure 1**; Han et al., 2013; Lee et al., 2013). Here, we tested if the overexpression of the α-ketobutyrate pathway—which produces threonine as an intermediate—could increase levels of propionyl-CoA in *Y. lipolytica*. As shown in **Figure 2A**, the pathway eventually forms the amino acids aspartate, homoserine, and threonine from oxaloacetate. Then, threonine is deaminated to generate α-ketobutyrate, a reaction catalyzed by threonine dehydratase. Alpha-ketobutyrate is directly or sequentially converted into propionyl-CoA by the pyruvate dehydrogenase (PDH) complex or pyruvate oxidase, respectively. The upregulation of threonine has previously been used to boost propionyl-CoA availability in *E. coli*. Lee et al. showed that levels of odd-chain FAs could be increased by introducing the threonine biosynthesis pathway (which creates α-ketobutyrate from aspartate semialdehyde), especially when mutated homoserine dehydrogenase (*thrA**, reduced feedback inhibition) was also expressed (Lee et al., 2013). The percentage of odd-chain FAs out of total FAs increased from <1 to 18% by overexpressing the threonine pathway in *E. coli*. The predominant odd-chain FA produced was pentadecanoic acid (C15:0).

In this study, we enhanced the extended threonine biosynthesis pathway (the aspartate/α-ketobutyrate pathway)—from oxaloacetate to α-ketobutyrate—by overexpressing seven genes (**Figure 2A**). There were three modules (**Figures 2A,C**): the aspartate synthesis module (module A), which included *AAT2*; the homoserine synthesis module (module H), which included *HOM3*, *HOM2*, and *HOM6*; and the threonine synthesis module (module T), which included *THR1*, *THR4*, and *ILV1*. While threonine and α-ketobutyrate (module T) are synthesized in the mitochondria in *S. cerevisiae*, the same may not be true in *Y. lipolytica*. While the locations of the relevant enzymes are as yet unknown in *Y. lipolytica*, predictive analyses (**Supplementary Table 4**) suggest enzyme location may differ between *S. cerevisiae* and *Y. lipolytica*. Because the module T enzymes were predicted to occur in the cytoplasm in *Y. lipolytica*, we used the original sequence of each gene in this study, as described in **Supplementary Table 3**. However, more research is needed to confirm enzyme locations in *Y. lipolytica*. The genes in each module were cloned into one plasmid using Golden Gate assembly (**Figure 2B**). They were expressed under the constitutive promoter p*TEF1*, and the expression cassette of each module was randomly integrated into the genome. Each module (A, T, and H) in the pathway was overexpressed in *Y. lipolytica* both individually and in tandem. The strain with the full modular pathway (ATH) was constructed by removing and reusing the *URA3* marker (**Supplementary Figure 2**). We verified gene integration using colony PCR with the primer set of promoters and the ORF gene (**Supplementary Table 1**).

The Engineered Strain Could Produce Odd-Chain Fatty Acids Using Glucose as Its Sole Carbon Source

To determine whether the modular metabolic pathway was effective in producing odd-chain FAs, we evaluated the performance of the engineered strains overexpressing the individual modules and the entire pathway. The strains

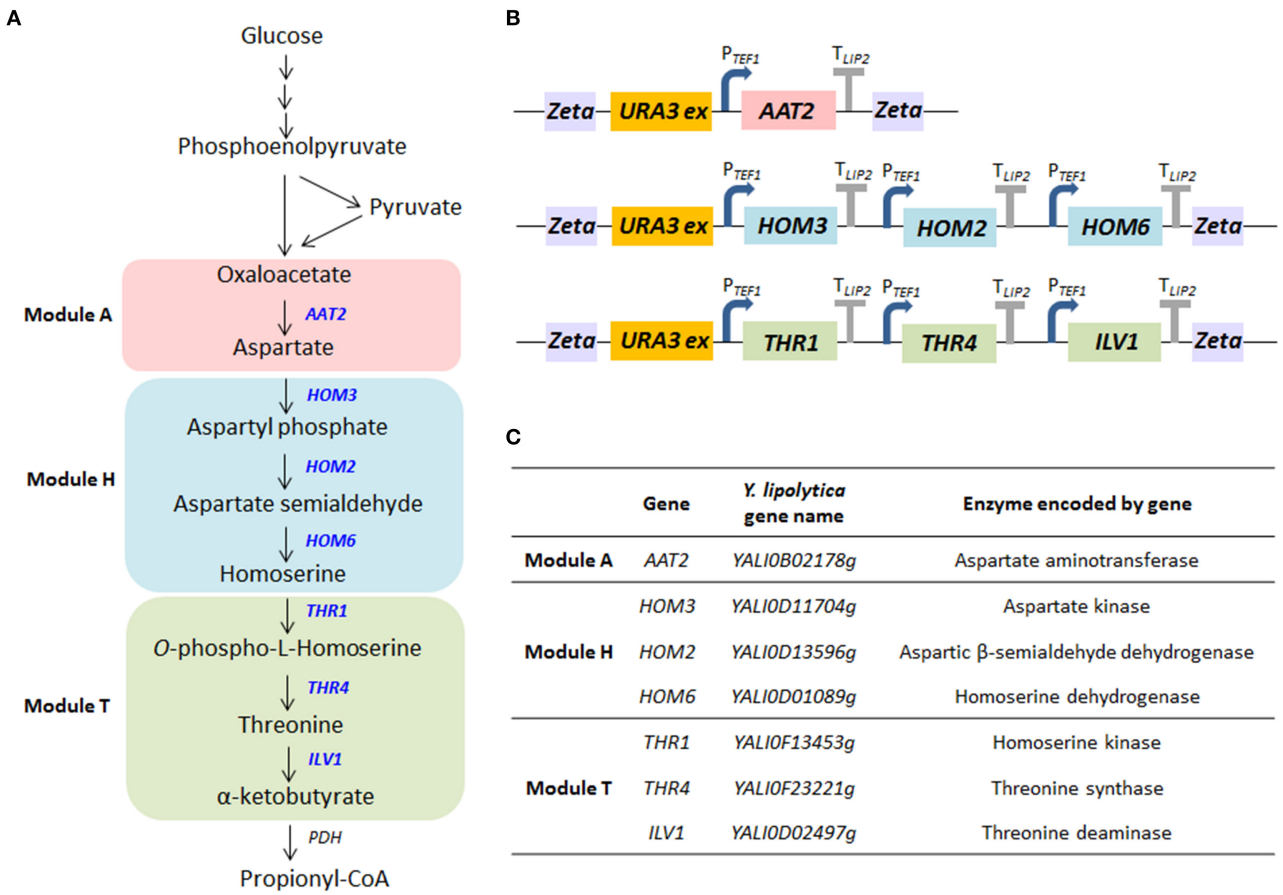

	Gene	*Y. lipolytica* gene name	Enzyme encoded by gene
Module A	*AAT2*	*YALI0B02178g*	Aspartate aminotransferase
Module H	*HOM3*	*YALI0D11704g*	Aspartate kinase
	HOM2	*YALI0D13596g*	Aspartic β-semialdehyde dehydrogenase
	HOM6	*YALI0D01089g*	Homoserine dehydrogenase
Module T	*THR1*	*YALI0F13453g*	Homoserine kinase
	THR4	*YALI0F23221g*	Threonine synthase
	ILV1	*YALI0D02497g*	Threonine deaminase

FIGURE 2 | The biosynthetic pathway for propionyl-CoA. **(A)** The metabolic pathway by which propionyl-CoA is synthesized from glucose. The genes overexpressed in this study are shown in blue. Pyruvate produced by glycolysis is converted to oxaloacetate by pyruvate carboxylase, and oxaloacetate is converted to threonine through the biosynthesis of aspartate and homoserine. Threonine deaminase subsequently generates α-ketobutyrate from threonine. Then, α-ketobutyrate is converted to propionyl-CoA by the pyruvate dehydrogenase (PDH) complex. **(B)** Structure of the multigene modules encoding enzymes in the aspartate/α-ketobutyrate pathway that were constructed in this study. Each gene expression cassette included the native *TEF1* promoter and *LIP2* terminator. **(C)** The genes included in the modules and the enzymes they encode.

were cultivated in YNBD6 medium under nitrogen limitation conditions (C/N = 60), which have been found to positively influence lipid synthesis (Beopoulos et al., 2012; Ledesma-Amaro et al., 2016). For the WT-A strain, which overexpressed *AAT2*, and the WT-T strain, which overexpressed *THR*1, *THR4*, and *ILV1*, total lipid content (%, g/g DCW) was lower than in the wild-type (WT) strain; the percentage of odd-chain FAs out of total FAs was similar (**Table 2**). For the WT-H strain, which overexpressed *HOM3*, *HOM2*, and *HOM6*, this percentage was slightly greater (1.91%) than that in the WT strain (0.84%) (**Table 2** and **Figure 3A**). For the WT-ATH strain, which overexpressed the entire pathway, odd-chain FA synthesis was significantly greater, odd-chain FA content (%, g/g DCW) was 3.8 times higher, and odd-chain FA titers (g/L) were 3.6 times higher than in the WT strain; the percentage of odd-chain FAs out of total FAs was 3.86%, which was 4.6 times higher than the value seen in the WT strain. These results indicate that the engineered aspartate/α-ketobutyrate pathway can supply propionyl-CoA; they also show that the full pathway is needed for effective odd-chain FA synthesis.

WT-ATH primarily produced C17:1 FAs (**Figure 3B**). This profile resembles that of an engineered *Y. lipolytica* strain that received propionate supplementation (Park et al., 2018). This finding implies that enhancing carbon flux through the α-ketobutyrate pathway can boost propionyl-CoA availability and odd-chain FA synthesis the same way that propionate supplementation can.

Odd-Chain Fatty Acid Production Was Significantly Improved in a Lipid-Accumulating Strain

Once we had determined that the strain overexpressing the full modular pathway produced more odd-chain FAs, we wanted to boost their accumulation. Previously, we had engineered a *Y. lipolytica* strain, JMY3501, to accumulate large amounts of lipids (Lazar et al., 2014). We eliminated lipid degradation and

TABLE 2 | Fatty acid (FA) production in the wild-type (WT) strain and the engineered strains after growth on YNBD6 medium for 120 h.

Strain	DCW (g/L)	Lipid content %		Odd-chain FA /Total FA (%)	Lipid titer (g/L)	
		Total FA	Odd-chain FA		Total FA	Odd-chain FA
WT	18.65 ± 0.15	19.13 ± 2.22	0.16 ± 0.00	0.84 ± 0.09	3.571 ± 0.442	0.029 ± 0.000
WT-A	17.30 ± 0.15	16.60 ± 1.05	0.14 ± 0.01	0.87 ± 0.03	2.873 ± 0.207	0.025 ± 0.003
WT-T	16.50 ± 0.00	14.41 ± 0.21	0.15 ± 0.00	1.03 ± 0.01	2.378 ± 0.035	0.024 ± 0.001
WT-H	16.30 ± 0.55	10.96 ± 0.09	0.21 ± 0.03	1.91 ± 0.21	1.788 ± 0.075	0.034 ± 0.005
WT-ATH	16.90 ± 0.25	15.73 ± 0.95	0.61 ± 0.13	3.86 ± 0.57	2.656 ± 0.121	0.103 ± 0.020

The values represent the means and standard deviations for two independent experiments. DCW, dry cell weight.

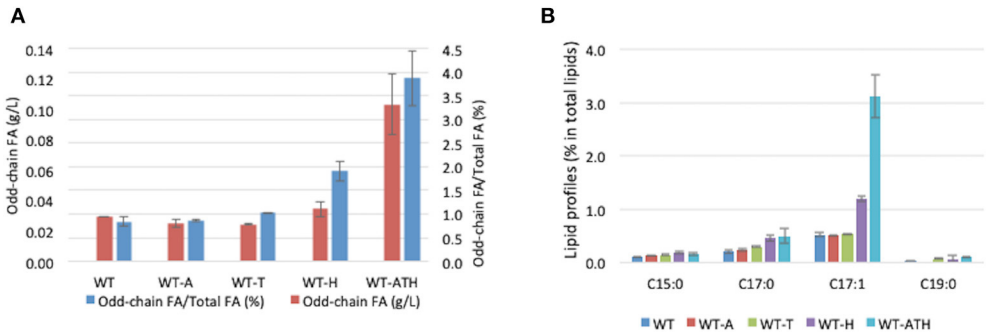

FIGURE 3 | Odd-chain fatty acid production and profiles for the wild-type and engineered strains. **(A)** Odd-chain fatty acid (FA) titers (g/L) and the percentage of odd-chain FAs relative to total FAs in the wild-type (WT) and engineered strains. **(B)** Odd-chain FA profiles (percentage of each FA out of total FAs) of the WT strain and engineered strains. WT, control strain; WT-A, strain expressing module A; WT-T, strain expressing module T; WT-H, strain expressing module H; WT-ATH, strain expressing the full pathway (all three modules). The results represent the means and standard deviations for two independent experiments.

remobilization in this obese strain by deleting the *POX* (*POX1-6*) genes (Beopoulos et al., 2008) as well as the *TGL4* gene, which encodes a triglyceride lipase (Dulermo et al., 2013). In addition, we overexpressed *DGA2*, which encodes the major acyl-CoA:diacylglycerol acyltransferase (Beopoulos et al., 2012), and *GPD1*, which encodes glycerol-3-phosphate dehydrogenase, in order to push and pull TAG biosynthesis (Dulermo and Nicaud, 2011; Tai and Stephanopoulos, 2013). Therefore, using JMY3501, we built a new obese strain that overexpressed our full modular pathway. It was called the obese-ATH strain. We then studied lipid production under the same conditions as before. As expected, total lipid accumulation was 2.29-fold greater in the obese-ATH strain than in the WT-ATH strain (**Tables 2**, **3**). Interestingly, the obese-ATH strain also accumulated more odd-chain FAs: the percentage of odd-chain FAs out of total FAs was 5.64% in the obese-ATH strain vs. 3.86% in the WT-ATH strain. The obese-ATH strain produced 0.36 g/L of odd-chain FAs, which is 7.2 times greater than the amount produced by the regular obese strain. The obese-ATH strain and the WT-ATH strain differed in their even-chain FA profiles (**Table 4**). The obese-ATH had slightly higher levels of C16:0 and slightly lower levels of C18:1, a common pattern seen in strains with the obese background regardless of the carbon source (Lazar et al., 2014; Ledesma-Amaro et al., 2016).

The Disruption of *PHD1* in the Methylcitrate Cycle Did Not Increase Odd-Chain Fatty Acid Production

In a previous study, we inactivated *PHD1*, the gene that encodes 2-methylcitrate dehydratase, which catalyzes the conversion of 2-methyl citrate to 2-methyl-*cis*-aconitate in the methylcitrate cycle; we showed that the resulting higher levels of propionyl-CoA could be used to synthesize greater amounts of odd-chain FAs (Park et al., 2018). To investigate whether the inhibition of the methylcitrate cycle—via the deletion of *PHD1*—could further improve the accumulation of odd-chain FAs, we disrupted the *PHD1* gene in both the WT-ATH strain and the obese-ATH strain. The two *phd1*Δ strains displayed higher total lipid content compared to their relative controls (**Supplementary Table 2**), a result that was also demonstrated in Papanikolaou et al. (2013); however, they also displayed lower percentages of odd-chain FAs out of total FAs (**Figure 4**). This latter negative effect was significantly more pronounced in the obese-ATH *phd1*Δ strain than in the WT-ATH *phd1*Δ strain. For the obese-ATH *phd1*Δ strain, this figure dropped by 50%, and levels of odd-chain FAs were 67% of those seen in the relative control (0.24 vs. 0.36 g/L). These results suggest that disrupting the methylcitrate cycle does not provide the benefits seen previously (Park et al., 2018) when strains are already overexpressing the aspartate/α-ketobutyrate pathway.

TABLE 3 | Fatty acid (FA) production in the obese strain and the obese-ATH strain after growth on YNBD6 medium for 120 h.

Strain	DCW (g/L)	Lipid content %		Odd-chain FA /Total FA (%)	Lipid titer (g/L)	
		Total FA	Odd-chain FA		Total FA	Odd-chain FA
Obese	19.20 ± 0.04	37.11 ± 0.14	0.25 ± 0.00	0.68 ± 0.01	7.125 ± 0.012	0.049 ± 0.001
Obese-ATH	17.62 ± 0.03	36.02 ± 0.39	2.03 ± 0.05	5.64 ± 0.06	6.347 ± 0.058	0.358 ± 0.009

The values represent the means and standard deviations for two independent experiments. DCW, dry cell weight.

TABLE 4 | Comparison of the lipid profiles (% of each FA) of the WT-ATH strain and the obese-ATH strain.

Strain	C15:0	C16:0	C16:1	C17:0	C17:1	C18:0	C18:1	C18:2	C19:0
WT-ATH	0.16 ± 0.03	8.31 ± 0.75	6.13 ± 0.00	0.50 ± 0.14	3.11 ± 0.40	5.96 ± 0.68	61.31 ± 2.43	11.02 ± 0.26	0.10 ± 0.00
Obese-ATH	0.40 ± 0.00	13.07 ± 0.01	7.25 ± 0.11	0.76 ± 0.00	4.26 ± 0.06	5.00 ± 0.17	50.12 ± 0.27	14.11 ± 0.16	0.22 ± 0.13

The values represent the means and standard deviations for two independent experiments.

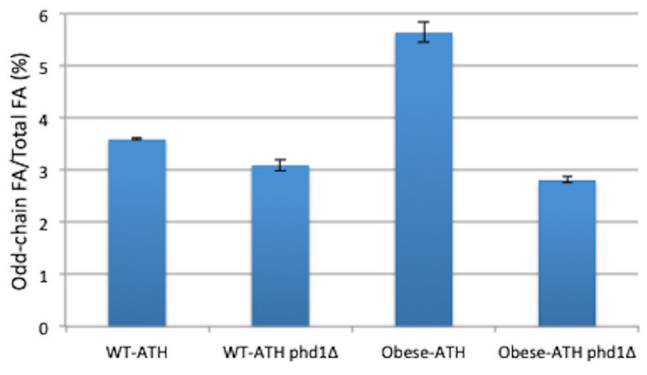

FIGURE 4 | Odd-chain fatty acid production in the *PHD1*-disrupted strains. The percentage of odd-chain fatty acids (FAs) relative to total FAs in the *PHD1*-disrupted strains and their respective controls. The results represent the means and standard deviations for two independent experiments.

The action of 2-methylcitrate dehydratase is restricted to the mitochondria. Consequently, disabling this enzyme does not directly improve cytosolic levels of propionyl-CoA. In the previous studies showing that the disruption of *PHD1* boosted odd-chain FA synthesis (Papanikolaou et al., 2013; Park et al., 2018), there was also propionate supplementation. Taken together, these findings suggest that, when the methylcitrate cycle is disrupted, the overexpression of the aspartate/α-ketobutyrate pathway has a weaker effect on propionyl-CoA levels than does propionate supplementation.

Overexpression of the Cytosolic Pyruvate Dehydrogenase (PDH) Complex Improved Lipid Synthesis but Reduced Odd-Chain Fatty Acid Production

The PDH complex consists of three main catalytic components: E1 (pyruvate dehydrogenase, encoded by *PDA1* and *PDB1*), E2 (dihydrolipoamide acetyltransferase, encoded by *LAT1*), and E3 (dihydrolipoamide dehydrogenase, encoded by *LPD1*). There is a fourth component (protein X, encoded by *PDX1*) that binds to and positions E3 relative to E2. In *Y. lipolytica*, the PDH complex is found in mitochondria and catalyzes the pathway from pyruvate to acetyl-CoA. A few studies have examined the functional expression of the PDH complex in *Y. lipolytica*. One study attempted to overexpress the direct pathway from pyruvate to acetyl-CoA in a coordinated manner (Markham et al., 2018), and another study showed that the individual overexpression of *PDA1* (shared subunits with α-ketoglutarate dehydrogenase) improved α-ketoglutarate production (Guo et al., 2014).

Here, we wanted to redirect the aspartate/α-ketobutyrate pathway to produce propionyl-CoA via the PDH complex, which has already been shown to be possible in *E. coli* (Danchin et al., 1984; Tseng and Prather, 2012; Lee et al., 2013). The PDH complex was built so it could be associated with the full modular pathway (ATH) and could provide a pool of propionyl-CoA in the cytosol where lipid synthesis takes place. The mitochondrial targeting sequences (MTSs) of each gene were predicted using MitoProt (Claros and Vincens, 1996), and the gene sequences used in this study are described in **Supplementary Table 3**. We then created the obese-ATHP strain by overexpressing the cytosolic PDH subunits in the obese-ATH strain. Next, to explore lipid accumulation dynamics, the strain was grown in YNBD6 with lipoic acid, which is required for cytosolic PDH activity in yeast (Kozak et al., 2014). Compared to the control strain, the obese-ATHP strain had significantly lower levels of odd-chain FAs (a 3.8 times lower percentage of odd-chain FAs out of total FAs); however, total lipid levels were higher (**Table 5**). The increase in lipid production might have resulted from the increased levels of cytosolic acetyl-CoA resulting from the overexpression of the PDH complex. A similar strategy was utilized in *Saccharomyces cerevisiae*, where PDH was introduced into the cytosol and was found to increase levels of acetyl-CoA (Kozak et al., 2014; Lian et al., 2014) and of the target compound of interest. Since acetyl-CoA is a key precursor in the production of both even- and odd-chain FAs, increasing levels of acetyl-CoA promotes lipid synthesis in general. However, the substantially lower levels of odd-chain FAs in the obese-ATHP strain implies that the PDH complex shows greater specificity for pyruvate than for α-ketobutyrate. The higher Km value of α-ketobutyrate

TABLE 5 | Fatty acid (FA) production in the obese-ATH strain and the obese-ATHP strain after growth on YNBD6 medium for 120 h.

Strain	DCW (g/L)	Lipid content %		Odd-chain FA /Total FA (%)	Lipid titer (g/L)	
		Total FA	Odd-chain FA		Total FA	Odd-chain FA
Obese-ATH	15.68 ± 0.02	29.23 ± 0.01	1.59 ± 0.03	5.44 ± 0.10	4.582 ± 0.010	0.249 ± 0.005
Obese-ATHP	15.25 ± 0.25	33.89 ± 1.06	0.48 ± 0.03	1.42 ± 0.03	5.171 ± 0.246	0.073 ± 0.005

The values represent the means and standard deviations for two independent experiments. DCW, dry cell weight.

compared to that of pyruvate has been seen elsewhere, such as in *E. coli* (Bisswanger, 1981), *Neurospora crassa* (Harding et al., 1970), and mammalian cells (Bremer, 1969). Therefore, it is important to explore enzyme engineering strategies that modify substrate specificity or that introduce other enzymes that can convert acetyl-CoA to propionyl-CoA with a view to further improving odd-chain FA production via a threonine-based upregulation strategy.

DISCUSSION

In this study, we developed a synthetic biological strategy for the *de novo* production of odd-chain FAs in *Y. lipolytica*. It is important to note that the wild-type *Y. lipolytica* strain produces only negligible amounts of odd-chain FAs even though it has an excellent capacity to accumulate large quantities of lipids. Several studies have shown that propionate supplementation can increase the production of odd-chain FAs (Fontanille et al., 2012; Kolouchová et al., 2015; Park et al., 2018). However, research has yet to explore the *de novo* production of odd-chain FAs from sugars in *Y. lipolytica*.

The overexpression of the aspartate/α-ketobutyrate pathway (from oxaloacetate to homoserine and threonine) via Golden Gate assembly resulted in higher levels of odd-chain FAs being produced from glucose. The best strain generated a level of odd-chain FAs, 0.36 g/L in flask that is the highest to date to be achieved in *Y. lipolytica* without propionate supplementation. Furthermore, it is comparable to the levels seen in a previous study of ours that employed propionate supplementation, where odd-chain FAs titers were 0.14 and 0.57 g/L in the wild-type strain and the obese strain, respectively (Park et al., 2018). To further increase the amount of propionyl-CoA produced via the overexpression of threonine synthesis, we constructed a cytosolic pyruvate dehydrogenase (PDH) complex. Because of the lower specificity of the PDH complex for α-ketobutyrate vs. pyruvate, the engineered strain generated lower levels of propionyl-CoA than did the relative control; however, the increased levels of acetyl-CoA in the engineered strain led to larger amounts of total FAs. This study is the first to describe the functional expression of the native PDH complex in the cytosol in *Y. lipolytica*, an approach that could also be employed to produce acetyl-CoA-derived compounds, such as polyhydroxybutyrates, isoprenoids, sterols, polyketides, polyphenols, alkanes, and alkenes (Nielsen, 2014).

Before the approach described here can be applied at industrial scales, certain issues must be resolved. It is necessary to perform research in which combinatorial pathway analysis (Lütke-Eversloh and Stephanopoulos, 2008), targeted-proteomics analysis (Redding-Johanson et al., 2011), and genome-scale metabolic network modeling (Xu et al., 2011) are used to identify bottlenecks and enhance metabolic fluxes to propionyl-CoA and odd-chain FAs. The results of the PDH overexpression experiment suggest that acetyl-CoA is a competitive precursor to propionyl-CoA in odd-chain FA synthesis and is also a precursor in lipid synthesis. Therefore, better balancing the pools of acetyl-CoA and propionyl-CoA could be key in further increasing odd-chain FA content. One way to improve odd-chain FA synthesis is to introduce enzymes—such as CoA transferase—that redirect CoA moieties from acetyl-CoA to propionyl-CoA (Yang et al., 2012) or that have greater specificity for 3-oxovaleryl-ACP than for acetoacetyl-CoA (Slater et al., 1998). Overall, this work has shown that applying synthetic biological engineering strategies in *Y. lipolytica* to improve odd-chain FA production could be useful in a wide range of pharmaceutical and industrial contexts.

DATA AVAILABILITY STATEMENT

The raw data supporting the conclusions of this article will be made available by the authors, without undue reservation, to any qualified researcher.

AUTHOR CONTRIBUTIONS

YP, RL-A, and J-MN planned the study. YP designed and carried out the experiments and drafted the manuscript. All the authors revised and approved the final manuscript.

FUNDING

YP was the recipient of a Ph.D. scholarship from the Kwanjeong Educational Foundation (KEF).

SUPPLEMENTARY MATERIAL

The Supplementary Material for this article can be found online at: https://www.frontiersin.org/articles/10.3389/fbioe.2019.00484/full#supplementary-material

REFERENCES

Aldor, I. S., Kim, S. W., Jones Prather, K. L., and Keasling, J. D. (2002). Metabolic engineering of a novel propionate-independent pathway for the production of poly(3-hydroxybutyrate-co-3-hydroxyvalerate) in recombinant *Salmonella enterica* serovar typhimurium. *Appl. Environ. Microbiol.* 68, 3848–3854. doi: 10.1128/AEM.68.8.3848-3854.2002

Avis, T. J. (2000). Synthesis and biological characterization of (Z)-9-heptadecenoic and (Z)-6-methyl-9-heptadecenoic acids: fatty acids with antibiotic activity produced by *Pseudozyma flocculosa*. *J. Chem. Ecol.* 26, 987–1000. doi: 10.1023/A:1005464326573

Barth, G., and Gaillardin, C. (1997). Physiology and genetics of the dimorphic fungus *Yarrowia lipolytica*. *FEMS Microbiol. Rev.* 19, 219–237. doi: 10.1111/j.1574-6976.1997.tb00299.x

Beopoulos, A., Haddouche, R., Kabran, P., Dulermo, T., Chardot, T., and Nicaud, J. M. (2012). Identification and characterization of DGA2, an acyltransferase of the DGAT1 acyl-CoA:diacylglycerol acyltransferase family in the oleaginous yeast *Yarrowia lipolytica*. New insights into the storage lipid metabolism of oleaginous yeasts. *Appl. Microbiol. Biotechnol.* 93, 1523–1537. doi: 10.1007/s00253-011-3506-x

Beopoulos, A., Mrozova, Z., Thevenieau, F., Le Dall, M. T., Hapala, I., Papanikolaou, S., et al. (2008). Control of lipid accumulation in the yeast *Yarrowia lipolytica*. *Appl. Environ. Microbiol.* 74, 7779–7789. doi: 10.1128/AEM.01412-08

Beopoulos, A., Verbeke, J., Bordes, F., Guicherd, M., Bressy, M., Marty, A., et al. (2014). Metabolic engineering for ricinoleic acid production in the oleaginous yeast *Yarrowia lipolytica*. *Appl. Microbiol. Biotechnol.* 98, 251–262. doi: 10.1007/s00253-013-5295-x

Bisswanger, H. (1981). Substrate specificity of the pyruvate dehydrogenase complex from *Escherichia coli*. *J. Biol. Chem.* 256, 815–822.

Bremer, J. (1969). Pyruvate dehydrogenase, substrate specificity and product inhibition. *Eur. J. Biochem.* 8, 535–540. doi: 10.1111/j.1432-1033.1969.tb00559.x

Browse, J., McCourt, P. J., and Somerville, C. R. (1986). Fatty acid composition of leaf lipids determined after combined digestion and fatty acid methyl ester formation from fresh tissue. *Anal. Biochem.* 152, 141–145. doi: 10.1016/0003-2697(86)90132-6

Celinska, E., Ledesma-Amaro, R., Larroude, M., Rossignol, T., Pauthenier, C., and Nicaud, J. M. (2017). Golden Gate Assembly system dedicated to complex pathway manipulation in *Yarrowia lipolytica*. *Microb. Biotechnol.* 10, 450–455. doi: 10.1111/1751-7915.12605

Claros, M. G., and Vincens, P. (1996). Computational method to predict mitochondrially imported proteins and their targeting sequences. *Eur. J. Biochem.* doi: 10.1111/j.1432-1033.1996.00779.x

Clausen, C. A., Coleman, R. D., and Yang, V. W. (2010). Fatty acid–based formulations for wood protection against mold and sapstain. *For. Prod. J.* 60, 301–304. doi: 10.13073/0015-7473-60.3.301

Czerwiec, Q., Idrissitaghki, A., Imatoukene, N., Nonus, M., Thomasset, B., Nicaud, J. M., et al. (2019). Optimization of cyclopropane fatty acids production in *Yarrowia lipolytica*. *Yeast* 36, 143–151. doi: 10.1002/yea.3379

Danchin, A., Dondon, L., and Daniel, J. (1984). Metabolic alterations mediated by 2-ketobutyrate in *Escherichia coli* K12. *MGG Mol. Gen. Genet.* 193, 473–478. doi: 10.1007/BF00382086

Degwert, J., Jacob, J., and Steckel, F., Inventors. (1998). *Use of Cis-9-Heptadecenoic Acid for trEating Psoriasis and Allergies*. Hamburg: Beiersdorf AG.

Dulermo, R., Brunel, F., Dulermo, T., Ledesma-Amaro, R., Vion, J., Trassaert, M., et al. (2017). Using a vector pool containing variable-strength promoters to optimize protein production in *Yarrowia lipolytica*. *Microb. Cell Fact.* 16, 1–11. doi: 10.1186/s12934-017-0647-3

Dulermo, R., Gamboa-Meléndez, H., Dulermo, T., Thevenieau, F., and Nicaud, J. M. (2014). The fatty acid transport protein Fat1p is involved in the export of fatty acids from lipid bodies in *Yarrowia lipolytica*. *FEMS Yeast Res.* 14, 883–896. doi: 10.1111/1567-1364.12177

Dulermo, T., and Nicaud, J. M. (2011). Involvement of the G3P shuttle and β-oxidation pathway in the control of TAG synthesis and lipid accumulation in *Yarrowia lipolytica*. *Metab. Eng.* 13, 482–491. doi: 10.1016/j.ymben.2011.05.002

Dulermo, T., Tréton, B., Beopoulos, A., Gnankon, A. P. K., Haddouche, R., and Nicaud, J. M. (2013). Characterization of the two intracellular lipases of *Y. lipolytica* encoded by *TGL3* and *TGL4* genes: new insights into the role of intracellular lipases and lipid body organisation. *Biochim. Biophys. Acta.* 1831, 1486–1495. doi: 10.1016/j.bbalip.2013.07.001

Fickers, P., Le Dall, M. T., Gaillardin, C., Thonart, P., and Nicaud, J. M. (2003). New disruption cassettes for rapid gene disruption and marker rescue in the yeast *Yarrowia lipolytica*. *J. Microbiol. Methods* 55, 727–737. doi: 10.1016/j.mimet.2003.07.003

Fitton, A., and Goa, K. L. (1991). Azelaic acid: a review of its pharmacological properties and therapeutic efficacy in acne and hyperpigmentary skin disorders. *Drugs* 41, 780–798. doi: 10.2165/00003495-199141050-00007

Fontanille, P., Kumar, V., Christophe, G., Nouaille, R., and Larroche, C. (2012). Bioconversion of volatile fatty acids into lipids by the oleaginous yeast *Yarrowia lipolytica*. *Bioresour. Technol.* 114, 443–449. doi: 10.1016/j.biortech.2012.02.091

Forouhi, N. G., Koulman, A., Sharp, S. J., Imamura, F., Kröger, J., Schulze, M. B., et al. (2014). Differences in the prospective association between individual plasma phospholipid saturated fatty acids and incident type 2 diabetes: the EPIC-InterAct case-cohort study. *Lancet Diabetes Endocrinol.* 2, 810–818. doi: 10.1016/S2213-8587(14)70146-9

Guo, H., Madzak, C., Du, G., Zhou, J., and Chen, J. (2014). Effects of pyruvate dehydrogenase subunits overexpression on the α-ketoglutarate production in *Yarrowia lipolytica* WSH-Z06. *Appl. Microbiol. Biotechnol.* 98, 7003–7012. doi: 10.1007/s00253-014-5745-0

Guo, Z., Duquesne, S., Bozonnet, S., Cioci, G., Nicaud, J. M., Marty, A., et al. (2015). Development of cellobiose-degrading ability in *Yarrowia lipolytica* strain by overexpression of endogenous genes. *Biotechnol. Biofuels* 8, 1–16. doi: 10.1186/s13068-015-0289-9

Han, J., Hou, J., Zhang, F., Ai, G., Li, M., Cai, S., et al. (2013). Multiple propionyl coenzyme a-supplying pathways for production of the bioplastic poly(3-Hydroxybutyrate-co-3-Hydroxyvalerate) in *Haloferax mediterranei*. *Appl. Environ. Microbiol.* 79, 2922–2931. doi: 10.1128/AEM.03915-12

Harding, R. W., Caroline, D. F., and Wagner, R. P. (1970). The pyruvate dehydrogenase fraction complex from the mitochondrial of *Neurospora crassa*. *Arch. Biochem. Biophys.* 138, 653–661. doi: 10.1016/0003-9861(70)90393-0

Imatoukene, N., Verbeke, J., Beopoulos, A., Idrissi Taghki, A., Thomasset, B., Sarde, C. O., et al. (2017). A metabolic engineering strategy for producing conjugated linoleic acids using the oleaginous yeast *Yarrowia lipolytica*. *Appl. Microbiol. Biotechnol.* 101, 4605–4616. doi: 10.1007/s00253-017-8240-6

Jenkins, B., West, J. A., and Koulman, A. (2015). A review of odd-chain fatty acid metabolism and the role of pentadecanoic acid (C15:0) and heptadecanoic acid (C17:0) in health and disease. *Molecules* 20, 2425–2444. doi: 10.3390/molecules20022425

Köckritz, A., Blumenstein, M., and Martin, A. (2010). Catalytic cleavage of methyl oleate or oleic acid. *Eur. J. Lipid Sci. Technol.* 112, 58–63. doi: 10.1002/ejlt.200900103

Kolouchová, I., Schreiberová, O., Sigler, K., Masák, J., and Rezanka, T. (2015). Biotransformation of volatile fatty acids by oleaginous and non-oleaginous yeast species. *FEMS Yeast Res.* 15, 1–8. doi: 10.1093/femsyr/fov076

Kozak, B. U., van Rossum, H. M., Luttik, M. A. H., Akeroyd, M., Benjamin, K. R., Wu, L., et al. (2014). Engineering acetyl coenzyme A supply: functional expression of a bacterial pyruvate dehydrogenase complex in the cytosol of *Saccharomyces cerevisiae*. *mBio* 5, 1–11. doi: 10.1128/mBio.01696-14

Larroude, M., Rossignol, T., Nicaud, J. M., and Ledesma-Amaro, R. (2018). Synthetic biology tools for engineering *Yarrowia lipolytica*. *Biotechnol. Adv.* 36, 2150–2164. doi: 10.1016/j.biotechadv.2018.10.004

Lazar, Z., Dulermo, T., Neuvéglise, C., Crutz-Le Coq, A. M., and Nicaud, J. M. (2014). Hexokinase-A limiting factor in lipid production from fructose in *Yarrowia lipolytica*. *Metab. Eng.* 26, 89–99. doi: 10.1016/j.ymben.2014.09.008

Ledesma-Amaro, R., Lazar, Z., Rakicka, M., Guo, Z., Fouchard, F., Coq, A. M. C., et al. (2016). Metabolic engineering of *Yarrowia lipolytica* to produce chemicals and fuels from xylose. *Metab. Eng.* 38, 115–124. doi: 10.1016/j.ymben.2016.07.001

Ledesma-Amaro, R., and Nicaud, J. M. (2016). Metabolic engineering for expanding the substrate range of *Yarrowia lipolytica*. *Trends Biotechnol.* 34, 798–809. doi: 10.1016/j.tibtech.2016.04.010

Lee, G. J., Haliburton, J. R., Hu, Z., and Schirmer, A. W., Inventors. (2013). *Production of Odd Chain Fatty Acid Derivatives in Recombinant Microbial Cells*. San Francisco, CA: LS9, INC.

Lian, J., Si, T., Nair, N. U., and Zhao, H. (2014). Design and construction of acetyl-CoA overproducing *Saccharomyces cerevisiae* strains. *Metab. Eng.* 24, 139–149. doi: 10.1016/j.ymben.2014.05.010

Lütke-Eversloh, T., and Stephanopoulos, G. (2008). Combinatorial pathway analysis for improved L-tyrosine production in *Escherichia coli*: identification of enzymatic bottlenecks by systematic gene overexpression. *Metab. Eng.* 10, 69–77. doi: 10.1016/j.ymben.2007.12.001

Markham, K. A., Palmer, C. M., Chwatko, M., Wagner, J. M., Murray, C., Vazquez, S., et al. (2018). Rewiring *Yarrowia lipolytica* toward triacetic acid lactone for materials generation. *Proc. Natl. Acad. Sci. U. S. A* 115, 2096–2101. doi: 10.1073/pnas.1721203115

Milckova, K., Roux, E., Athenstaedt, K., Andrea, S., Daum, G., Chardot, T., et al. (2004). Lipid accumulation, lipid body formation, and acyl coenzyme a oxidases of the yeast *Yarrowia lipolytica*. *Appl. Environ. Microbiol.* 70, 3918–3924. doi: 10.1128/AEM.70.7.3918-3924.2004

Nielsen, J. (2014). Synthetic biology for engineering acetyl coenzyme a metabolism in yeast. *mBio* 5, 14–16. doi: 10.1128/mBio.02153-14

Papanikolaou, S., Beopoulos, A., Koletti, A., and Thevenieau, F. (2013). Importance of the methyl-citrate cycle on glycerol metabolism in the yeast *Yarrowia lipolytica*. *J. Biotechnol.* 168, 303–314. doi: 10.1016/j.jbiotec.2013.10.025

Papanikolaou, S., Muniglia, L., Chevalot, I., Aggelis, G., and Marc, I. (2003). Accumulation of a cocoa-butter-like lipid by *Yarrowia lipolytica* cultivated on agro-industrial residues. *Curr. Microbiol.* 46, 124–130. doi: 10.1007/s00284-002-3833-3

Park, Y. K., Dulermo, T., Ledesma-Amaro, R., and Nicaud, J. M. (2018). Optimization of odd chain fatty acid production by *Yarrowia lipolytica*. *Biotechnol. Biofuels* 11, 1–12. doi: 10.1186/s13068-018-1154-4

Park, Y. K., and Nicaud, J. M. (2019). Screening a genomic library for genes involved in propionate tolerance in *Yarrowia lipolytica*. *Yeast*. doi: 10.1002/yea.3431. [Epub ahead of print].

Pedersen, H. K., Gudmundsdottir, V., Nielsen, H. B., Hyotylainen, T., Nielsen, T., Jensen, B. A. H., et al. (2016). Human gut microbes impact host serum metabolome and insulin sensitivity. *Nature* 535, 376–381. doi: 10.1038/nature18646

Pfeuffer, M., and Jaudszus, A. (2016). Pentadecanoic and Heptadecanoic acids: multifaceted odd-chain fatty acids. *Adv. Nutr.* 7, 730–734. doi: 10.3945/an.115.011387

Poirier, Y., Nawrath, C., and Somerville, C. (1995). Production of polyhydroxyalkanoates, a family of biodegradable plastics and elastomers, in Bacteria and Plants. *Nat. Biotechnol.* 13, 142–150. doi: 10.1038/nbt0295-142

Qiao, K., Imam Abidi, S. H., Liu, H., Zhang, H., Chakraborty, S., Watson, N., et al. (2015). Engineering lipid overproduction in the oleaginous yeast *Yarrowia lipolytica*. *Metab. Eng.* 29, 56–65. doi: 10.1016/j.ymben.2015.02.005

Redding-Johanson, A. M., Batth, T. S., Chan, R., Krupa, R., Szmidt, H. L., Adams, P. D., et al. (2011). Targeted proteomics for metabolic pathway optimization: application to terpene production. *Metab. Eng.* 13, 194–203. doi: 10.1016/j.ymben.2010.12.005

Rezanka, T., and Sigler, K. (2009). Odd-numbered very-long-chain fatty acids from the microbial, animal, and plant kingdoms. *Pro. Lipid. Res.* 48, 206–238. doi: 10.1016/j.plipres.2009.03.003

Sambrook, J., and Russell, D. W. (2001). *Molecular Cloning. A Laboratory Manual*, *3rd Edn*. Cold Spring Harbor, NY:Cold Spring Harbor Laboratory Press.

Slater, S., Houmiel, K. L., Tran, M., Mitsky, T. A., Taylor, N. B., Padgette, S. R., et al. (1998). Multiple β-ketothiolases mediate Poly(β-Hydroxyalkanoate) copolymer synthesis in *Ralstonia eutropha*. *J. Bacteriol.* 180, 1979–1987. doi: 10.1128/JB.180.8.1979-1987.1998

Tai, M., and Stephanopoulos, G. (2013). Engineering the push and pull of lipid biosynthesis in oleaginous yeast *Yarrowia lipolytica* for biofuel production. *Metab. Eng.* 15, 1–9. doi: 10.1016/j.ymben.2012.08.007

Tseng, H. C., and Prather, K. L. J. (2012). Controlled biosynthesis of odd-chain fuels and chemicals via engineered modular metabolic pathways. *Proc. Natl. Acad. Sci. U. S. A* 109, 17925–17930. doi: 10.1073/pnas.1209002109

Wu, H., and San, K. Y. (2014). Engineering *Escherichia coli* for odd straight medium chain free fatty acid production. *Appl. Microbiol. Biotechnol.* 98, 8145–8154. doi: 10.1007/s00253-014-5882-5

Xie, D., Jackson, E. N., and Zhu, Q. (2015). Sustainable source of omega-3 eicosapentaenoic acid from metabolically engineered *Yarrowia lipolytica*: from fundamental research to commercial production. *Appl. Microbiol. Biotechnol.* 99, 1599–1610. doi: 10.1007/s00253-014-6318-y

Xu, P., Ranganathan, S., Fowler, Z. L., Maranas, C. D., and Koffas, M. A. G. (2011). Genome-scale metabolic network modeling results in minimal interventions that cooperatively force carbon flux towards malonyl-CoA. *Metab. Eng.* 13, 578–587. doi: 10.1016/j.ymben.2011.06.008

Xue, Z., Sharpe, P. L., Hong, S. P., Yadav, N. S., Xie, D., Short, D. R., et al. (2013). Production of omega-3 eicosapentaenoic acid by metabolic engineering of *Yarrowia lipolytica*. *Nat. Biotechnol.* 31, 734–740. doi: 10.1038/nbt.2622

Yang, Y., Brigham, C. J., Song, E., Jeon, J., Rha, C. K., and Sinskey, A. J. (2012). Biosynthesis of poly (3-hydroxybutyrate- co−3- hydroxyvalerate) containing a predominant amount of 3-hydroxyvalerate by engineered *Escherichia coli* expressing propionate-CoA transferase. *J. Appl. Microbiol.* 13, 815–823. doi: 10.1111/j.1365-2672.2012.05391.x

Zheng, Y., Chi, Z., Ahring, B. K., and Chen, S. (2012). Oleaginous yeast *Cryptococcus curvatus* for biofuel production: ammonia's effect. *Biomass and Bioenergy* 37, 114–121. doi: 10.1016/j.biombioe.2011.12.022

Conflict of Interest: The authors declare that the research was conducted in the absence of any commercial or financial relationships that could be construed as a potential conflict of interest.

frontiers in Bioengineering and Biotechnology

REVIEW
published: 12 November 2019
doi: 10.3389/fbioe.2019.00327

Metabolic Engineering of Bacterial Respiration: High vs. Low P/O and the Case of *Zymomonas mobilis*

Uldis Kalnenieks, Elina Balodite and Reinis Rutkis*

Institute of Microbiology and Biotechnology, University of Latvia, Riga, Latvia

Respiratory chain plays a pivotal role in the energy and redox balance of aerobic bacteria. By engineering respiration, it is possible to alter the efficiency of energy generation and intracellular redox state, and thus affect the key bioprocess parameters: cell yield, productivity and stress resistance. Here we summarize the current metabolic engineering and synthetic biology approaches to bacterial respiratory metabolism, with a special focus on the respiratory chain of the ethanologenic bacterium *Zymomonas mobilis*. Electron transport in *Z. mobilis* can serve as a model system of bacterial respiration with low oxidative phosphorylation efficiency. Its application for redox balancing and relevance for improvement of stress tolerance are analyzed.

Keywords: respiratory chain, metabolic engineering, energy coupling, redox balance, stress resistence, *Zymomonas mobilis*

OPEN ACCESS

Edited by:
Jean Marie François, UMS3582 Toulouse White Biotechnology (TWB), France

Reviewed by:
Jian-Ming Liu, Technical University of Denmark, Denmark
Ralf Takors, University of Stuttgart, Germany

****Correspondence:***
Uldis Kalnenieks
kalnen@lanet.lv

Specialty section:
This article was submitted to Synthetic Biology, a section of the journal Frontiers in Bioengineering and Biotechnology

Received: *30 August 2019*
Accepted: *28 October 2019*
Published: *12 November 2019*

Citation:
Kalnenieks U, Balodite E and Rutkis R (2019) Metabolic Engineering of Bacterial Respiration: High vs. Low P/O and the Case of Zymomonas mobilis. Front. Bioeng. Biotechnol. 7:327. doi: 10.3389/fbioe.2019.00327

INTRODUCTION

During the last few decades a vast body of evidence on the structure, function and regulation of microbial electron transport chains has accumulated, enabled by the rapid advancement of omics techniques and molecular cloning tools. Research has focussed on deciphering of particular electron pathways in several model microorganisms, establishing their physiological role, and understanding the principles of their regulation. Transcriptional regulation in *Escherichia coli* in response to variation of available electron acceptors perhaps is the best known success story (for reviews, see Spiro and Guest, 1991; Unden and Bongaerts, 1997; Green and Paget, 2004). Here we briefly discuss how this wealth of theoretical knowledge can be used for industrial applications in the present era of metabolic engineering and synthetic biology. Generally speaking, microbial aerobic electron transport chains represent a promising, yet at the same time, challenging target for rational metabolic engineering, since their activities transcend several key cellular processes, like the catabolic ATP yield, maintenance of intracellular redox balance, production of reactive oxygen species (ROS), and protection against oxidative stress. In the present minireview we attempted to systematize the strategies of respiratory chain engineering, based on their impact on the cellular energy and reducing equivalent balance. We did not review the biotechnological applications of bacterial anaerobic respiration, electron transport chains of extremophiles, as well as bioelectrochemistry—interaction of bacterial electron transport with electrodes. Instead of trying to embrace all aspects of microbial electron transport, we here focussed on a few current biotechnology workhorses, showing how the metabolic engineering of their respiration had yielded predictable (or sometimes, not so predictable) effects on their growth and production. Some emphasis was put on low energy-coupling electron transport and the bacterium *Zymomonas mobilis* as a representative of the energetically uncoupled respiration.

RESPIRATORY ENGINEERING TO IMPROVE FERMENTATIVE CATABOLISM

Microbial respiration represents a major sink of reducing equivalents and a source of energy (ATP) for the cellular metabolism. However, if the target compound of a bioprocess is produced by a redox-balanced fermentative pathway, then respiration, by interfering with the cellular redox and energy balance, causes a decrease of product yield, to mention Pasteur effect as a classical example (for a review, see Barnett and Entian, 2005). NADH supply of reactions, producing the desired target compound of fermentative catabolism, often represents a bottleneck (Zhao et al., 2017), especially under aerobic or microaerobic conditions (Bennett and San, 2017). Removing oxygen from the growth medium seems a straightforward approach for turning off the unwanted respiration and fueling more NADH into the fermentative catabolism. However, prolonged maintenance of a strict anoxic condition may be a challenging task. It may complicate, for example, long-term directed evolution experiments, like those aimed at engineering of the *E. coli* fermentative metabolism (Portnoy et al., 2008), where complete absence of oxygen is essential. On the other hand, many yeast species performing ethanol fermentation require limited presence of oxygen (Visser et al., 1990), often within a certain narrow concentration range for optimum ethanol yield (Acevedo et al., 2017). From the technical point of view, keeping low, steady, micro-aerobic oxygen levels in bioreactors (especially for larger volumes) may be difficult, due to the sensitivity of oxygen mass transfer coefficient to the agitation rate, insufficient responsiveness of the dissolved oxygen probe and spatial in homogeneities (Wu et al., 2015a).

Decreasing the activity of electron transport chain itself represents a viable alternative way to downregulate respiration, so that the cells would behave similar to that of anoxic or microaerobic environment even in the presence of oxygen excess (Bennett and San, 2017). Such a metabolic engineering strategy of limiting the use of oxygen by the cell itself would be useful also under some co-cultivation settings, e.g., when an end-product of fermentative catabolism of one microorganism species is used as a substrate for aerobic metabolism of the second, co-cultivated species. Decreasing of respiration may be achieved by respiratory inhibitors, keeping in mind that inhibitor effects may serve as a proof of principle, yet are hardly applicable to industrial bioprocesses. Thus, Acevedo et al. (2017), using rotenone, the inhibitor of the mitochondrial NADH dehydrogenase complex I, demonstrated an increase of aerobic ethanol yield from xylose in the yeast *Scheffersomyces stipitis*. Cyanide at submillimolar concentrations was shown to improve growth and ethanol yield in aerobic culture of ethanologenic bacterium *Zymomonas mobilis* (Kalnenieks et al., 2000).

Not surprisingly, construction and study of respiratory knock-out mutants nowadays has become the dominating approach to the downregulation of microbial respiration, and has brought positive results. In *E. coli*, removal of all its terminal oxidases, followed by adaptive evolution, yielded strains able to produce lactate as a fermentation product from glucose and to undergo mixed-acid fermentation during aerobic growth (Portnoy et al., 2008). For *Corynebacterium glutamicum*, another important biotechnological producer, a respiratory chain mutant lacking both the cytochrome *bd* branch and the cytochrome bc_1-aa_3 branch was constructed (Koch-Koerfges et al., 2013), and its ability of fermentative growth without aerobic respiration was demonstrated. The mutant retained only 2% of the wild type oxygen consumption rate and displayed fermentative catabolism with L-lactate as major and acetate and succinate as minor products. In aerobically grown *Klebsiella pneumoniae* knocking out of its NADH dehydrogenase complex I (*nuo*) improved 2,3-butanediol production (Zhang et al., 2018). In the ethanol-producing, facultatively anaerobic bacterium *Z. mobilis* inactivation of its Type II respiratory NADH dehydrogenase (*ndh*) largely improved growth and ethanol yield under aerobic conditions (Kalnenieks et al., 2008; Hayashi et al., 2011, 2012; see below).

Some metabolic engineering studies have attempted fine-tuning of the respiration rate in *E. coli*. In order to mimic microaerobic metabolism of *E. coli* under condition of excessive aeration, Zhu et al. (2011) manipulated respiration rate of cells by externally adding various amount of coenzyme Q_1 to a strain lacking the *ubiCA* genes necessary for quinone biosynthesis. They demonstrated that synthesis of fermentation products, like lactate and ethanol, varied inversely with the added amount of Q_1. In the further study (Wu et al., 2015a), a nearly theoretical yield of lactate production was achieved under fully aerobic conditions by introducing a tunable pathway competing with biosynthesis of the precursors of coenzyme Q_8. This regulatory strategy was named by authors "metabolic transistor" (Wu et al., 2015b), allowing to control a large flux (electron transport) by a small change in the availability of one of the electron transport components (Q_8). An approach somewhat similar to that of Zhu et al. (2011) has been applied to *Lactococcus lactis*, in which the activity of respiratory chain naturally depends on externally added hemin, the precursor of the cytochrome heme cofactors (Liu et al., 2017). The authors constructed a multiple dehydrogenase knock-out strain of *L. lactis* with its respiratory chain as the only remaining NADH sink, and showed how the external control of respiration rate by hemin affected its growth and the degree of reduction of the synthesized products (acetoin vs. butanediol).

Bacterial respiratory chains can be engineered to control NADH/NAD^+ ratio and reducing equivalent fluxes also under anaerobic conditions. For enhancing NADH-dependent fermentative production in some strict anaerobes, the activity of electron transport chain could be used to generate NADH at the expense of other reduced cofactors, e.g., ferredoxin. This approach recently was demonstrated in *Clostridium thermocellum* (Lo et al., 2017), and in the extreme thermophile *Caldicellulosiruptor bescii* (Williams-Rhaesa et al., 2018), in which conversion of pyruvate to acetyl-CoA proceeds largely via pyruvate:ferredoxin oxidoreductase. By overexpressing Rnf, the membrane bound energy-conserving ferredoxin:NAD^+ oxidoreductase, NADH flux to the NADH-dependent ethanol synthesis could be improved, leading to a substantial increase

of ethanol production in both these bacteria, and a concomitant decrease of production of unwanted side-products.

Notably, some recent works on modification of respiratory NADH dehydrogenase activity in aerobic or facultatively anaerobic bacteria reported unexpected, NADH dehydrogenase-dependent metabolic shifts under strictly anaerobic conditions, which at present seem difficult to explain. Under aerobic conditions, manipulating the activity of either the NADH dehydrogenase complex I (*nuo*) or the Type II NADH dehydrogenase (*ndh*) was shown to affect the intracellular NADH/NAD^+ ratio, and accordingly, the catabolic product spectrum in a fairly predictable manner, as reported for several bacteria, e.g., *Bacillus subtilis* (Gyan et al., 2006), *E. coli* (Liu Q. et al., 2014), *K. pneumoniae* (Zhang et al., 2018), and *Streptococcus agalactiae* (Lencina et al., 2018). Yet, for example in *C. glutamicum*, overexpression of the *ndh* gene under oxygen-deprived conditions also substantially decreased the NADH/NAD^+ ratio, at the same time increasing the glucose consumption rate (Tsuge et al., 2015). Here "oxygen-deprived conditions" referred to <0.01 ppm oxygen, and importantly, no alternative terminal electron acceptors were present in the medium. Similarly, Hayashi et al. (2015) found a strong dependence of NADH/NAD^+ ratio on the Ndh activity in complemented *Z. mobilis ndh* mutant strains under strictly anaerobic conditions. No electron acceptors alternative to oxygen are known for this bacterium. Steinsiek et al. (2014) noted that inactivation of the NADH dehydrogenase complex I (*nuo*) in *E. coli* affected not only its aerobic metabolism, but induced significant metabolic response also under anaerobic conditions, and without alternative external electron acceptors—again, conditions where the respiratory chain should not be active. They observed genes coding for TCA cycle enzymes being upregulated, and higher amounts of succinate being synthesized by the mutant. At the same time, they noted a substantial shift of the ArcA phosphorylation pattern in the *nuo* mutant relative to the parent strain. Earlier Perrenoud and Sauer (2005) demonstrated that ArcA-dependent transcriptional regulation controls TCA cycle in *E. coli* not only under (micro)aerobic, but also under fully anaerobic conditions. Yun et al. (2005) reported higher lactate and formate yields in *E. coli ndh* mutant and *ndh nuo* double mutant under strictly anaerobic conditions. Apparently, more research is needed to understand these anaerobic effects and their possible relation to the global regulatory mechanisms linking respiratory chain to the central metabolism. At the same time, it is important to take them into account for practical respiratory engineering.

IMPROVING RESPIRATORY ENERGY-COUPLING

The classical work of Bauchop and Elsden (1960) provided evidence that on average one mole of ATP could fuel synthesis of slightly above 10_{gdrywt} of bacterial biomass. With a few exceptions, this value (Y_{ATP}) was found to be roughly similar for different microorganisms (Stouthamer, 1977). The apparent Y_{ATP} is far from being a true "biological constant" for all growth conditions, since it depends on cellular maintenance energy requirements and energy-spilling reactions (Russell and Cook, 1995). Yet, primarily it is the variation of energy generation efficiency, but not that of Y_{ATP}, that underlies the observed vast differences of microbial growth yields. Regarding aerobic catabolism, the efficiency of energy generation is determined by the stoichiometry of oxidative phosphorylation (Calhoun et al., 1993). The stoichiometry of oxidative phosphorylation (P/O) is the molar ratio between the generated ATP macroergic phosphate bonds and the oxygen atoms reduced to water by the respiratory chain (Hinkle, 2005). The mechanistic (maximum) P/O value for each particular case can be estimated from the known proton motive stoichiometries of the respiratory complexes and H^+-ATP synthase, keeping in mind that the real values are lower due to proton leaks and slips in the energy-coupling mechanisms. Typically, the bacterial electron transport chains are branched, and for electrons traveling from NADH via the respiratory complexes to oxygen, their contribution to energy coupling strongly depends on the particular pathway that the electrons take. For example, in *E. coli* electron transport chain (for a review, see Unden and Bongaerts, 1997) the stoichiometry of proton translocation per one transported electron (H^+/e) may vary between 1 and 4 (accordingly, H^+/O varies between 2 and 8). Assuming the proton/ATP stoichiometry of the H^+-ATP synthase close to 3 (Kashket, 1982), the theoretical lower and upper limits for P/O in *E. coli* appear to be 0.67 and 2.67, respectively. In reality, *E. coli* and most other bacteria with branched respiratory chains tend to employ their energetically most efficient and less efficient electron transport branches simultaneously, resulting in a submaximal net energy coupling efficiency, which is hard to measure directly under *in vivo* condition. A metabolic network model with a growth rate-dependent biomass composition, used for simulation of *E. coli* chemostat cultivations on several carbon substrates at different dilution rates, has yielded an estimate of P/O close to 1.5 (Taymaz-Nikerel et al., 2010). Thermodynamic analysis suggests that the submaximal P/O values, typically in the range of 1.0–1.5, indicate a tradeoff between metabolic energy conservation and energy dissipation, ultimately directed toward maximization of the microbial growth rate (Westerhoff et al., 1983; Molenaar et al., 2009; Werner et al., 2010).

From a practical point of view, increasing of P/O represents a metabolic engineering strategy for improving microbial biomass yield (**Figure 1**). For increase of P/O, the electron transport branches with low coupling efficiency have to be inactivated, and/or those with high efficiency have to be overexpressed. Biomass yield (and in some cases, e.g., in lactic acid bacteria, also multiple stress tolerance; Zotta et al., 2013) can thus be improved, which is desirable for cost-efficient biomass production of starter cultures, for the net productivity of bioconversions, and for the production of biomass-related compounds such as proteins, storage polymers and vitamins (Minohara et al., 2002; Brooijmans et al., 2007; Pedersen et al., 2012; Richhardt et al., 2013; Liu Q. et al., 2014).

Apart from biomass, high P/O ratio has been shown to push the synthesis of various products via pathways that consume (or at least, do not produce) ATP (de Kok et al., 2012). This takes

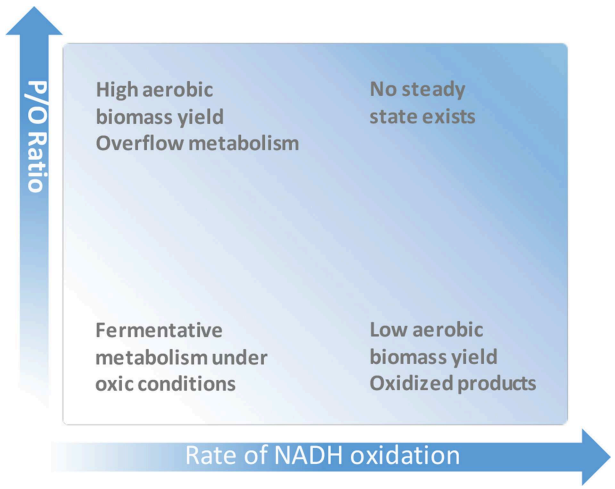

FIGURE 1 | Dependence of microbial growth and production on the energetical efficiency of respiration.

place because the energetically efficient respiration minimizes the amount of carbon substrate that has to be oxidized to generate ATP for needs of growth and maintenance. Given that the carbon source is not limiting and its uptake is rapid enough, the high P/O may facilitate production of incompletely oxidized compounds, either target products or, sometimes, undesired inhibitory metabolites. This phenomenon is known as "overflow metabolism" (Neijssel and Tempest, 1976; **Figure 1**). Enhancing product synthesis by elevating P/O has been a strategy of quite a few metabolic engineering projects. In most cases, elevation of P/O is achieved by knocking out the energetically least efficient terminal oxidase (typically cytochrome *bd*), and thus redirecting electron flow to energetically more efficient terminal oxidase(s). Poly-γ-glutamic acid (γ-PGA), a multifunctional biopolymer with various applications, is an example of a product, for which ATP supply is essential for its biosynthesis. By elimination of the cytochrome *bd* branch in *Bacillus licheniformis* respiratory chain, Cai et al. (2018) reached an increase of γ-PGA yield by almost 20%. Efficient supply of ATP is critical also for production of riboflavin. In a fed-batch culture of riboflavin-producing *B. subtilis* a 30% higher riboflavin titer was accumulated by the *cyd* mutant compared to the control strain (Zamboni et al., 2003), apparently because of redirection of the electron flow to the proton-pumping aa_3 terminal oxidase. Similar approach was used for improving of N-acetylglucosamine production in *B. subtilis* (Liu Y. et al., 2014) and lysine yield in *C. glutamicum* (Kabus et al., 2007). Liu Q. et al. (2014) demonstrated that inactivation of the cytochrome *bd*-II terminal oxidase and/or the type II (energy non-coupling) respiratory NADH dehydrogenase results in a several-fold increase of poly(3-hydroxybutyrate) accumulation in an *E. coli* recombinant producer strain.

However, under some natural conditions, and also in numerous bioprocess setups it may be preferable for bacteria to have respiration with low rather than high P/O.

INCREASING RESPIRATION RATE WHILE DECREASING ENERGY-COUPLING EFFICIENCY

Low P/O is preferable when oxidation of NAD(P)H is needed for a rapid regeneration of $NAD(P)^+$ and/or consumption of oxygen, without producing of extra ATP (**Figure 1**). Thus, the free-living nitrogen-fixing bacteria *Azotobacter vinelandii* demonstrate the utility of rapid, low-P/O respiration as one of possible means to protect their nitrogenase complex from dioxygen by keeping the intracellular oxygen concentration low (Poole and Hill, 1997). It was shown that the activity of the low energy-coupling cytochrome *bd* terminal oxidase (Kelly et al., 1990) in combination with an energy non-coupling NADH:UQ oxidoreductase (Bertsova et al., 2001) is critical for *A. vinelandii* ability to fix nitrogen while growing under conditions of air saturation. In bioprocesses, energetically uncoupled respiration is useful for avoiding production of unneeded biomass and overflow metabolites, while enabling conversion of reduced substrate into more oxidized product(s). The obligately aerobic alpha-proteobacterium *Gluconbacter oxydans* belonging to the family of acetic acid bacteria is a relevant example. Due to its numerous periplasmic membrane-bound dehydrogenases that incompletely oxidize sugars, sugar alcohols, and other compounds, *G. oxydans* has been used for decades as a biocatalyst for bioconversions (Deppenmeier et al., 2002). It oxidizes a variety of substrates and transfers the electrons via ubiquinone to the quinol oxidases bo_3 and *bd*. Although the energetically more efficient, proton-pumping bo_3 represents its major terminal oxidase activity (Richhardt et al., 2013), due to some reason the proton pumping stoichiometry of the *G. oxydans* respiratory chain is more than two-fold lower than that of aerobically cultivated *E. coli* bearing analogous major terminal oxidase.

Seeking to relate the overflow metabolism phenomenon in the model microorganisms *E. coli* and *S. cerevisiae* to their respiratory capacity, Vemuri et al. (2006a, 2007) demonstrated that overexpression of plant non-coupling alternative terminal oxidases, and/or the energy non-coupling, soluble water-forming NADH oxidase from *Streptococcus mutans* reduces the overflow metabolism, decreases the biomass yield, and shifts catabolism toward more oxidized products. In *E. coli* overexpression of streptococcal NADH oxidase was shown to raise the TCA cycle flux and to elevate the $NADPH/NADP^+$ ratio (Holm et al., 2010). In combination with the deletion of *arcA* gene it dramatically reduced acetate accumulation and hence improved capacity of recombinant *E. coli* to overexpress heterologous proteins (Vemuri et al., 2006b). Expression of the soluble water-forming NADH oxidases (*nox*) of *Streptococci* or *Lactococci*, which do not contribute to energy coupling, has been widely applied in metabolic engineering projects for enhancing respiration, lowering its energy-coupling efficiency, and decreasing the intracellular $NADH/NAD^+$ ratio. Overexpression of *noxE* from *L. lactis* in *Saccharomyces cerevisiae* has been shown to shift catabolism toward more oxidized products, like acetaldehyde, acetate, and acetoin (Heux et al., 2006). NoxE overexpression prevents accumulation of reduced byproducts,

such as glycerol and xylitol, yet improves ethanol yield during xylose fermentation by engineered *S. cerevisiae* (Zhang et al., 2017), as well as improves oxidative and osmotic stress tolerance of *S. cerevisiae* aerobic batch culture on glucose (Shi et al., 2016). The same oxidase has been overexpressed in *E. coli* (Balagurunathan et al., 2018) and in *L. lactis* (Bongers et al., 2005) to increase acetaldehyde yield at the expense of more reduced products of sugar catabolism. Bacterial soluble NADH oxidases are recently used also for *in vitro* metabolic pathways, reconstituted with isolated enzymes, as the means for recycling NADH (Nowak et al., 2015; Taniguchi et al., 2017).

In a broader sense, the metabolic engineering strategy for uncoupling of energy metabolism is not confined merely to manipulating the electron transport modules. A decrease of the energy-coupling efficiency can be achieved also by targeting the proton-dependent ATPase in order to disrupt oxidative phosphorylation, or to stimulate ATP hydrolysis. Following this approach, one can achieve energetical uncoupling in combination with overflow metabolism. Indeed, several studies have reported a decrease of biomass yield, growth rate, and intracellular ATP/ADP ratio, an increase of glycolytic and respiratory rates, and a rise of acetate production (overflow) in ATPase-deficient *E. coli* mutants (Jensen and Michelsen, 1992; Noda et al., 2006). Noda et al. (2006) observed activation of the low energy-coupling modules in the electron transport chain of such mutant: the type II NADH dehydrogenase and cytochrome *bd* terminal oxidase were upregulated. The reason for that might be the need for rapid regeneration of NAD^+ to keep the rate of glycolysis high, while at the same time investing less into proton motive force generation, since it no more could drive ATP synthesis. A similar shift in respiratory chain composition and an onset of acetate overflow were reported by Schuhmacher et al. (2014) in a wild type *E. coli*, grown under phosphate limiting condition. Notably, these physiological effects of phosphate limitation, resembling the ATPase knock-out phenotype, correspond to earlier *in vitro* findings with membrane preparations (Turina et al., 2004; D'Alessandro et al., 2008); and reconstituted liposome systems (D'Alessandro et al., 2011), indicating that H^+-ATPases of *E. coli* and *Rhodobacter capsulatus* at low phosphate and ADP concentrations decouple ATP hydrolysis from transmembrane proton translocation. Causey et al. (2003) employed the acetate overflow effect for metabolic engineering of an acetate-producing *E. coli*. By inactivating the H^+-ATP synthase along with disruption of the TCA cycle and elimination of native fermentative pathways, they obtained a strain, which synthesized acetate as its major product, reaching 86% of the theoretical maximum yield. Apart from *E. coli*, a somewhat similar response to inactivation of ATP synthase has been documented in other biotechnologically important bacteria, like *C. glutamicum* and *Bacillus subtillis* (Santana et al., 1994; Koch-Koerfges et al., 2012).

Alternatively, instead of disrupting oxidative phosphorylation, one can decrease the energetic efficiency of metabolism just by stimulating futile hydrolysis of ATP. In their pioneering work (Koebmann et al., 2002a,b) overexpressed the F_1 part of H^+-ATPase, which could be used as an universal module for metabolic engineering of intracellular ATP hydrolysis without interfering with any particular metabolic reaction. In *E. coli* and *L. lactis* overexpression of F_1 led to a decrease of growth rate and intracellular energy level, and (depending on the strain and culture growth phase) also stimulated glycolytic flux to a various degree, decoupling it from anabolism. Using this approach Liu et al. (2016) demonstrated that futile hydrolysis of ATP could enhance product synthesis via pathways that generate ATP. By overexpressing of F_1 in *L. lactis* strain engineered for acetoin production they managed to improve the product yield and productivity at the expense of biomass formation. As noted by Holm et al. (2010), the metabolic effects of overexpression of the F_1 part of H^+-ATPase and those of the soluble water-forming NADH oxidase had much in common. In both cases for *E. coli* the result was an elevated glucose consumption and reduced growth rate and biomass yield, although the acetate overflow was seen only with F_1, but not with Nox.

Finally, since majority of bacterial electron transport chains are branched (for a review, see Poole and Cook, 2000), in principle it should be possible to decrease P/O also by inactivation of the energetically efficient electron transport branch(es), while leaving the less efficient, low-coupling ones active. However, in several cases inactivation of the energetically efficient routes has resulted in a drop of the bulk activity of mutant respiratory chain, actually causing poor growth and an elevation of overflow metabolism. Reported examples are the *E. coli* strains with linear electron transport chains (Steinsiek et al., 2014), or aa_3 knock-out mutant of *B. subtilis* (Zamboni and Sauer, 2003), bearing the least energetically efficient electron transport components, yet accumulating more acetate than the respective wild types. Hence, turning a natural bacterial respiratory chain with an average P/O value into a low-P/O and high-rate one often implies complex genetic modifications and fine-tuning, including knocking out the high-coupling modules and concerted overexpression of low-coupling respiratory chain constituents. Obviously, the best alternative to such complex genetic engineering might be employing bacterial respiratory chains with a naturally low P/O, whenever possible. *L. lactis* is one of such bacteria, bearing a low energy-coupling, inducible respiratory chain, suitable for oxidizing surplus NADH, while little affecting cellular ATP production (Liu et al., 2017). Notably, although NoxE from this bacterium has been expressed in several microorganisms to elevate their respiration rate (see above), its own inducible respiratory chain proved to be more efficient than NoxE for regeneration of its own intracellular NAD^+ pool and for its oxidative stress protection. The ethanol-producing alpha-proteobacterium *Z. mobilis* is another prominent example of aerobic metabolism with a naturally uncoupled respiration.

Zymomonas mobilis: AN EXAMPLE OF UNCOUPLED ENERGY METABOLISM

Zymomonas mobilis is a facultatively anaerobic bacterium with a very rapid and efficient homoethanol fermentation pathway (Rogers et al., 1982), involving the Entner-Doudoroff (E-D) glycolysis, pyruvate decarboxylase, and two alcohol dehydrogenase isoenzymes (Sprenger, 1996). Under anaerobic

or microaerobic conditions up to 98% of substrate carbon is incorporated in ethanol. Metabolic engineering of *Z. mobilis* has largely focussed on biofuel production from variety of renewable substrates, as well as on increasing its stress-resistance (Zhang et al., 1995; Mohagheghi et al., 2015; Yang et al., 2016; Charoensuk et al., 2017; for recent reviews, see Wang et al., 2018; Xia et al., 2019). Fermentative catabolism in *Z. mobilis* is loosely linked to its anabolism and growth, and proceeds with a high rate, both during the exponential growth phase, or under non- or slowly-growing conditions (Belaich and Senez, 1965). With respect to its metabolism, *Z. mobilis* somewhat resembles lactic acid bacteria (Sauer et al., 2017), also having high carbon substrate uptake rates with low biomass formation in combination with simple central metabolic pathways, leading to a limited number of metabolites. However, the aerobic energy metabolism in *Z. mobilis* seems to stand further away from the "bacterial mainstream," than that of lactic acid bacteria.

In contrast to the inducible electron transport of lactic acid bacteria, which requires hemin to be present in growth media (Brooijmans et al., 2007; Koebmann et al., 2008), *Z. mobilis* bears a constitutive respiratory chain. It consists of the Type II NADH dehydrogenase (*ndh*), coenzyme Q_{10}, and the cytochrome *bd* terminal oxidase (*cydAB*) as the established major electron carriers (**Figure 2**), together with respiratory FAD-dependent D-lactate dehydrogenase (Ldh), PQQ-dependent glucose dehydrogenase (Gdh), a putative cytochrome *c* peroxidase (PerC), and some other minor or still unidentified constituents (Strohdeicher et al., 1990; Kalnenieks et al., 1998; Sootsuwan et al., 2008). The cytochrome *bd* seems to be the only terminal oxidase, which is encoded in the *Z. mobilis* genome (Seo et al., 2005; Yang et al., 2009), and has been detected spetroscopically (Kalnenieks et al., 1998; Sootsuwan et al., 2008). *Z. mobilis*, like *G. oxydans* (Hanke et al., 2012) and some *Acetobacter* species, possesses a "dead-end" cytochrome bc_1 branch, apparently lacking a terminal cytochrome *c* oxidase, hence its function in electron transport remains obscure. The cytochrome *c* peroxidase seems more likely to function as a quinol peroxidase (Balodite et al., 2014), than to terminate the bc_1 electron transport branch, as suggested by Charoensuk et al. (2011). Nevertheless, *Z. mobilis* mutant strain with inactivated cytochrome *b* subunit of the bc_1 complex shows a distinct respiratory phenotype (Strazdina et al., 2012), best seen in mutant membrane preparations as an increase of antimycin-resistance of oxygen consumption and alteration of cytochrome *bd* reduction kinetics with NADH. In *G. oxydans* its bc_1-deficient strain shows a growth defect under acidic conditions, while in the wild type the *qcrABC* genes are upregulated under oxygen limitation (Hanke et al., 2012). Further research might reveal novel roles for the bc_1 complex in these alpha-proteobacteria and perhaps, put forward new ideas for their respiratory metabolic engineering.

For some reasons, the energetic efficiency of *Zymomonas* respiration in aerated culture is significantly lower than reported for other bacteria, e.g., *L. lactis*, with a similar dominating electron transport pathway from Ndh to CydAB (Brooijmans et al., 2007; Rutkis et al., 2014, 2016), which makes it quite unique among the producer microorganisms. Unlike such prominent facultatively anaerobic workhorses of biotechnology as *E. coli* and *B. subtilis*, aeration does not improve *Z. mobilis* biomass yield (Belaich and Senez, 1965; for a review, see Kalnenieks, 2006). Study of respiratory knock-out mutants (Strazdina et al., 2012; Rutkis et al., 2014) did not indicate presence of any putative low energy-coupling electron transport branch, to which one might ascribe the overall low energetic efficiency. Oxidative phosphorylation has been reported in non-growing cells and cell membrane vesicles, and cells are capable of ATP synthesis with artificially induced proton gradient (Kalnenieks et al., 1993). Yet, the proton-dependent ATPase in *Z. mobilis* under aerobic growth conditions operates in the direction of ATP hydrolysis (Rutkis et al., 2014). This is possibly because of some

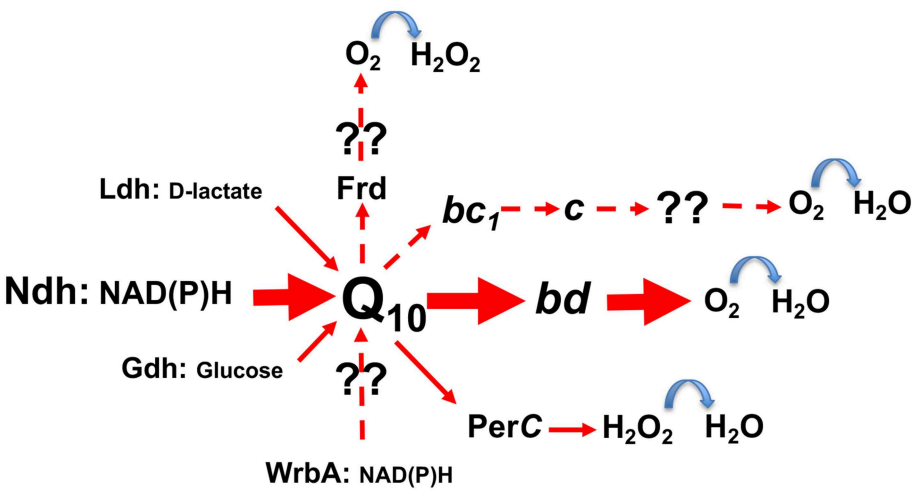

FIGURE 2 | The scheme of electron transport pathways in *Zymomonas mobilis* respiratory chain. Hypothetical pathways are shown with dashed arrows. Frd, putative fumarate reductase; WrbA, putative type IV NAD(P)H:quinone oxidoreductase; for other abbreviations see text.

intrinsic deficiency of proton motive force maintenance, or due to an unidentified proton leakage pathway in growing cells. Being an active sink of reducing equivalents, respiration lowers the ethanol yield, since it withdraws NADH from the alcohol dehydrogenase reaction. Hence, respiration causes accumulation of acetaldehyde, the inhibitory metabolic precursor of ethanol, which contributes to the poor aerobic growth of this bacterium, at the same time being a valuable target product of *Z. mobilis* aerobic bioprocess (Wecker and Zall, 1987). From the practical point of view, respiratory chain of *Z. mobilis* is well-suited for oxidation of NADH (and NADPH, since its Ndh has a good affinity for both cofactors) without stimulation of biomass growth. Aerobic acetaldehyde production by *Z. mobilis* so far is the best reported application of its respiratory potential. Recently, acetaldehyde-producing strains were developed, that reach 70% of the theoretical maximum acetaldehyde yield (Kalnenieks et al., 2019), as well as strains with the acetaldehyde-generating pyruvate decarboxylase reaction relocated to periplasm, in order to mitigate toxic effect of acetaldehyde on cell interior (Balodite et al., 2019).

It is not obvious, what are the physiological function(s) of *Z. mobilis* respiration in nature. Possibly, the respiratory chain might be accelerating glucose consumption by lowering the intracellular NADH/NAD^+ ratio (Rutkis et al., 2016), like it has been shown previously for *C. glutamicum* (Tsuge et al., 2015). Rutkis et al. demonstrated that an active respiratory chain is advantageous for reaching higher initial glucose uptake rate in non-growing cells, thus improving their survival, when glucose is available in small amounts and for restricted periods of time (most likely, that is what happens during the natural life cycle of this bacterium).

Respiratory chain apparently plays some role in the protection of *Z. mobilis* against oxic, high temperature, inhibitor and salt stresses. Cytochrome *c* peroxidase (*perC*) knock-out mutant of the thremotolerant strain TISTR 548 shows impaired growth at elevated temperature (37 and 39°C) (Charoensuk et al., 2011). Hypersensitivity to hydrogen peroxide (although, not as pronounced as in catalase-deficient strain) is another phenotypic trait of *Z. mobilis perC* mutants (Charoensuk et al., 2011; Balodite et al., 2014). In their recent work with TISTR 548, Charoensuk et al. (2017) presented results of transposon mutagenesis, followed by the mutant screening for the loss of thermotolerance. They identified 26 knock-out mutations, deleterious for thermotolerance, most of which were related to biosynthesis and maintenance of cell membranes and envelope. Yet, among the mutated genes there was the flavoprotein WrbA, a new type (type IV) of NAD(P)H:quinone oxidoreductase (Patridge and Ferry, 2006), thought to function as a protector against oxidative stress. Martien et al. (2019) noted upregulation of all respiratory chain components following exposure of a strictly anaerobic culture of *Z.mobilis* Zm4 to vigorous aeration, and suggested that the activity of PerC and cytochrome *bd* limits the toxic effects of oxygen. Interestingly, Ndh activity was shown to confer advantage for *Z. mobilis* aerobic growth and flocculation on minimal media (Jones-Burrage et al., 2019). Upregulation of *ndh* and some other oxidoreductase genes were observed under lignocellulose inhibitor stress (Chang et al., 2018). Hayashi et al. (2015) demonstrated positive impact of Ndh activity on *Z. mobilis* salt stress resistance. Likewise, activity of respiratory chain is positively correlated with acetic acid tolerance in *Acetobacter pasteurianus* (Wu et al., 2017), with multiple stress tolerance of *Lactobacillus plantarum* (Zotta et al., 2013), and with resistance of *E. coli* to critically high growth temperatures (Murata et al., 2018). Details of the mechanisms behind these general stress-protective effects, however, largely remain obscure and require further study.

Paradoxically, turning off *Z. mobilis* respiration also appears to be beneficial for its aerobic growth. The *Z. mobilis ndh* knock-out mutant shows improved aerobic growth and ethanol synthesis on rich growth medium (Kalnenieks et al., 2008; Hayashi et al., 2011, 2012), which partly can be explained by the decrease of acetaldehyde accumulation. At the same time, inactivation of the *ndh* gene elicits an adaptive response at the level of the electron transport chain and several oxidative stress protection systems (Strazdina et al., 2012). In particular, the mutant bears higher activity of respiratory D-lactate dehydrogenase (Ldh). Hayashi et al. (2011, 2012) analyzed a set of spontaneous *Z. mobilis* respiratory mutants with Ndh-deficiency, and observed their improved aerobic growth and ethanol synthesis at elevated temperature (39°C). Recently Strazdina et al. (2018) demonstrated that the elevated Ldh activity of the *ndh* strain is crucial for its temperature-resistance. Inactivation of *ldh* against the Ndh-deficient background renders the non-respiring double mutant more temperature sensitive than the *ndh* strain, bringing it back to the level of the wild type. The protective function of the respiratory Ldh at elevated temperature needs further examination, in order to establish what specific electron pathway(s) starting from Ldh might be involved in *Z. mobilis* thermotolerance.

CONCLUSIONS AND OUTLOOK

Engineering of respiratory chain represents a potent lever to modify metabolism of biotechnological producer microorganisms. Rational metabolic engineering of culture growth and product synthesis, based on targeted modification of bacterial respiratory chain branches has been proven successful in numerous cases. At the same time, engineering of electron pathways can elicit complex responses, particularly concerning physiology of stress resistance, which may be difficult to explain within the present picture of electron transport. Modification of respiratory chain components can cause unpredicted effects on growth, catabolism and intracellular redox balance. Some effects, observed under strictly anaerobic conditions, possibly indicate gaps in our understanding of anaerobic electron transport pathways. Apparently, in order to uncover the full potential of respiratory metabolic engineering, more basic research on the structure and regulatory interactions between electron transport and the rest of microbial metabolism is needed. For broadening our knowledge of the alternative physiological roles of respiration, bacteria like *Z. mobilis*, which do not use their respiration for energy generation, might be helpful as experimental model systems.

AUTHOR CONTRIBUTIONS

All authors listed have made a substantial, direct and intellectual contribution to the work, and approved it for publication.

FUNDING

The present work was funded by the Latvian ERDF project 1.1.1.1/16/A/185 and by Latvian Council of Science project lzp-2018/2-0123.

REFERENCES

Acevedo, A., Conejeros, R., and Aroca, G. (2017). Ethanol production improvement driven by genome-scale metabolic modeling and sensitivity analysis in *Scheffersomyces stipitis*. *PLoS ONE* 12:e0180074. doi: 10.1371/journal.pone.0180074

Balagurunathan, B., Tan, L., and Zhao, H. (2018). Metabolic engineering of *Escherichia coli* for acetaldehyde overproduction using pyruvate decarboxylase from *Zymomonas mobilis*. *Enz. Microb. Technol.* 109, 58–65. doi: 10.1016/j.enzmictec.2017.09.012

Balodite, E., Strazdina, I., Galinina, N., McLean, S., Rutkis, R., Poole, R. K., et al. (2014). Structure of the *Zymomonas mobilis* respiratory chain: oxygen affinity of electron transport and the role of cytochrome *c* peroxidase. *Microbiology* 160, 2045–2052. doi: 10.1099/mic.0.081612-0

Balodite, E., Strazdina, I., Martynova, J., Galinina, N., Rutkis, R., Lasa, Z., et al. (2019). Translocation of *Zymomonas mobilis* pyruvate decarboxylase to periplasmic compartment for production of acetaldehyde outside the cytosol. *Microbiol.Open* 8:e809. doi: 10.1002/mbo3.809

Barnett, J. A., and Entian, K. D. (2005). A history of research on yeasts 9: regulation of sugar metabolism. *Yeast* 22, 835–894. doi: 10.1002/yea.1249

Bauchop, T., and Elsden, S. R. (1960). The growth of microorganisms in relation to their energy supply. *J. Gen. Microbiol.* 23, 457–469. doi: 10.1099/00221287-23-3-457

Belaich, J. P., and Senez, J. C. (1965). Influence of aeration and pantothenate on growth yields of *Zymomonas mobilis*. *J. Bacteriol.* 89, 1195–1200.

Bennett, G. N., and San, K. Y. (2017). Strategies for manipulation of oxygen utilization by the electron transfer chain in microbes for metabolic engineering purposes. *J. Ind. Microbiol. Biotechnol.* 44, 647–658. doi: 10.1007/s10295-016-1851-6

Bertsova, Y. V., Bogachev, A. V., and Skulachev, V. P. (2001). Noncoupled NADH: ubiquinone oxidoreductase of *Azotobacter vinelandii* is required for diazotrophic growth at high oxygen concentrations. *J. Bacteriol.* 183, 6869–6874. doi: 10.1128/JB.183.23.6869-6874.2001

Bongers, R. S., Hoefnagel, M. H. N., and Kleerebezem, M. (2005). High-level acetaldehyde production in *Lactococcus lactis* by metabolic engineering. *Appl. Environ. Microbiol.* 71, 1109–1113. doi: 10.1128/AEM.71.2.1109-1113.2005

Brooijmans, R. J. W., Poolman, B., Schuurman-Wolters, G. K., De Vos, W. M., and Hugenholtz, J. (2007). Generation of a membrane potential by *Lactococcus lactis* through aerobic electron transport. *J. Bacteriol.* 189, 5203–5209. doi: 10.1128/JB.00361-07

Cai, D., Chen, Y., He, P., Wang, S., Mo, F., Li, X., et al. (2018). Enhanced production of poly-γ-glutamic acid by improving ATP supply in metabolically engineered *Bacillus licheniformis*. *Biotechnol. Bioeng.* 115, 2541–2553. doi: 10.1002/bit.26774

Calhoun, M. W., Oden, K. L., Gennis, R. B., de Mattos, M. J. T., and Neijssel, O. M. (1993). Energetic efficiency of *Escherichia coli*: effects of mutations in components of the aerobic respiratory chain. *J. Bacteriol.* 175, 3020–3025. doi: 10.1128/jb.175.10.3020-3025.1993

Causey, T. B., Zhou, S., Shanmugam, K. T., and Ingram, L. O. (2003). Engineering the metabolism of *Escherichia coli* W3110 for the conversion of sugar to redox-neutral and oxidized products: homoacetate production. *Proc. Natl. Acad. Sci. U.S.A.* 100, 825–832. doi: 10.1073/pnas.0337684100

Chang, D., Yu, Z., Ul Islam, Z., French, W. T., Zhang, Y., and Zhang, H. (2018). Proteomic and metabolomic analysis of the cellular biomarkers related to inhibitors tolerance in *Zymomonas mobilis* ZM4. *Biotechnol. Biofuels* 11:283. doi: 10.1186/s13068-018-1287-5

Charoensuk, K., Irie, A., Lertwattanasakul, N., Sootsuwan, K., Thanonkeo, P., and Yamada, M. (2011). Physiological importance of cytochrome c peroxidase in ethanologenic thermotolerant *Zymomonas mobilis*. *J. Mol. Microbiol. Biotechnol.* 20, 70–82. doi: 10.1159/000324675

Charoensuk, K., Sakurada, T., Tokiyama, A., Murata, M., Kosaka, T., Thanonkeo, P., et al. (2017). Thermotolerant genes essential for survival at a critical high temperature in thermotolerant ethanologenic *Zymomonas mobilis* TISTR 548. *Biotechnol. Biofuels* 10:204. doi: 10.1186/s13068-017-0891-0

D'Alessandro, M., Turina, P., and Melandri, B. A. (2008). Intrinsic uncoupling in the ATP synthase of *Escherichia coli*. *Biochim. Biophys. Acta* 1777, 1518–1527. doi: 10.1016/j.bbabio.2008.09.011

D'Alessandro, M., Turina, P., and Melandri, B. A. (2011). Quantitative evaluation of the intrinsic uncoupling modulated by ADP and Pi in the reconstituted ATP synthase of *Escherichia coli*. *Biochim. Biophys. Acta* 1807, 130–143. doi: 10.1016/j.bbabio.2010.08.011

de Kok, S., Kozak, B. U., Pronk, J. T., and van Maris, A. J.A. (2012). Energy coupling in *Saccharomyces cerevisiae*: selected opportunities for metabolic engineering. *FEMS Yeast Res.* 12, 387–397. doi: 10.1111/j.1567-1364.2012.00799.x

Deppenmeier, U., Hoffmeister, M., and Prust, C. (2002). Biochemistry and biotechnological applications of *Gluconobacter* strains. *Appl. Microbiol. Biotechnol.* 60, 233–242. doi: 10.1007/s00253-002-1114-5

Green, J., and Paget, M. S. (2004). Bacterial redox sensors. *Nat. Rev. Microbiol.* 2, 954–967. doi: 10.1038/nrmicro1022

Gyan, S., Shiohira, Y., Sato, I., Takeuchi, M., and Sato, T. (2006). Regulatory loop between redox sensing of the NADH/NAD ratio by Rex (YdiH) and oxidation of NADH by *NADH* dehydrogenase Ndh in *Bacillus subtilis*. *J. Bacteriol.* 188, 7062–7071. doi: 10.1128/JB.00601-06

Hanke, T., Richhardt, J., Polen, T., Sahm, H., Bringer, S., and Bott, M. (2012). Influence of oxygen limitation, absence of the cytochrome bc_1 complex and low pH on global gene expression in *Gluconobacter oxydans* 621H using DNA microarray technology. *J. Biotechnol.* 157, 359–372. doi: 10.1016/j.jbiotec.2011.12.020

Hayashi, T., Furuta, Y., and Furukawa, K. (2011). Respiration-deficient mutants of *Zymomonas mobilis* show improved growth and ethanol fermentation under aerobic and high temperature conditions. *J. Biosci. Bioeng.* 111, 414–419. doi: 10.1016/j.jbiosc.2010.12.009

Hayashi, T., Kato, T., and Furukawa, K. (2012). Respiratory chain analysis of *Zymomonas mobilis* mutants producing high levels of ethanol. *Appl. Environ. Microbiol.* 78, 5622–5629. doi: 10.1128/AEM.00733-12

Hayashi, T., Kato, T., Watakabe, S., Song, W., Aikawa, S., and Furukawa, K. (2015). The respiratory chain provides salt stress tolerance by maintaining a low NADH/NAD^+ ratio in *Zymomonas mobilis*. *Microbiology* 161, 2384–2394. doi: 10.1099/mic.0.000195

Heux, S., Cachon, R., and Dequin, S. (2006). Cofactor engineering in *Saccharomyces cerevisiae*: expression of a H_2O-forming NADH oxidase and impact on redox metabolism. *Metab. Eng.* 8, 303–314. doi: 10.1016/j.ymben.2005.12.003

Hinkle, P. C. (2005). P/O ratios of mitochondrial oxidative phosphorylation. *Biochim. Biophys. Acta* 1706, 1–11. doi: 10.1016/j.bbabio.2004.09.004

Holm, A. K., Blank, L. M., Oldiges, M., Schmid, A., Solem, C., Jensen, P. R., et al. (2010). Metabolic and transcriptional response to cofactor perturbations in *Escherichia coli*. *J. Biol. Chem.* 285, 17498–17506. doi: 10.1074/jbc.M109.095570

Jensen, P. R., and Michelsen, O. (1992). Carbon and energy metabolism of atp mutants of *Escherichia coli*. *J. Bacteriol.* 174, 7635–7641. doi: 10.1128/jb.174.23.7635-7641.1992

Jones-Burrage, S. E., Kremer, T. A., and McKinlay, J. B. (2019). Cell aggregation and aerobic respiration are important for *Zymomonas mobilis* ZM4 survival in an aerobic minimal medium. *Appl. Environ. Microbiol.* 85:e00193-19. doi: 10.1128/AEM.00193-19

Kabus, A., Niebisch, A., and Bott, M. (2007). Role of cytochrome *bd* oxidase from *Corynebacterium glutamicum* in growth and lysine production. *Appl. Environ. Microbiol.* 73 861–868. doi: 10.1128/AEM.01818-06

Kalnenieks, U. (2006). Physiology of *Zymomonas mobilis*: some unanswered questions. *Adv. Microb. Physiol.* 51, 73–117. doi: 10.1016/S0065-2911(06)51002-1

Kalnenieks, U., Balodite, E., Strähler, S., Strazdina, I., Rex, J., Pentjuss, A., et al. (2019). Improvement of acetaldehyde production in zymomonas mobilis by engineering of its aerobic metabolism. *Front. Microbiol.* 10:2533. doi: 10.3389/fmicb.2019.02533

Kalnenieks, U., de Graaf, A. A., Bringer-Meyer, S., and Sahm, H. (1993). Oxidative phosphorylation in *Zymomonas mobilis*. *Arch. Microbiol.* 160, 74–79. doi: 10.1007/BF00258148

Kalnenieks, U., Galinina, N., Bringer-Meyer, S., and Poole, R. K. (1998). Membrane D-lactate oxidase in *Zymomonas mobilis*: evidence for a branched respiratory chain. *FEMS Microbiol. Lett.* 168, 91–97. doi: 10.1016/S0378-1097(98)00424-8

Kalnenieks, U., Galinina, N., Strazdina, I., Kravale, Z., Pickford, J. L., Rutkis, R., et al. (2008). NADH dehydrogenase deficiency results in low respiration rate and improved aerobic growth of *Zymomonas mobilis*. *Microbiology* 154, 989–994. doi: 10.1099/mic.0.2007/012682-0

Kalnenieks, U., Galinina, N., Toma, M. M., and Poole, R. K. (2000). Cyanide inhibits respiration yet stimulates aerobic growth of *Zymomonas mobilis*. *Microbiology* 146, 1259–1266. doi: 10.1099/00221287-146-6-1259

Kashket, E. R. (1982). Stoichiometry of the H^+-ATPase of growing and resting, aerobic *Escherichia coli*. *Biochemistry* 21, 5534–5538. doi: 10.1021/bi00265a024

Kelly, M. J., Poole, R. K., Yates, M. G., and Kennedy, C. (1990). Cloning and mutagenesis of genes encoding the cytochrome bd terminal oxidase complex in *Azotobacter vinelandii*: mutants deficient in the cytochrome *d* complex are unable to fix nitrogen in air. *J. Bacteriol.* 172, 6010–6019. doi: 10.1128/jb.172.10.6010-6019.1990

Koch-Koerfges, A., Kabus, A., Ochrombel, I., Marin, K., and Bott, M. (2012). Physiology and global gene expression of a *Corynebacterium glutamicum* ΔF_1F_o-ATP synthase mutant devoid of oxidative phosphorylation. *Biochim. Biophys. Acta* 1817, 370–380. doi: 10.1016/j.bbabio.2011.10.006

Koch-Koerfges, A., Pfelzer, N., Platzen, L., Oldiges, M., and Bott, M. (2013). Conversion of *Corynebacterium glutamicum* from an aerobic respiring to an aerobic fermenting bacterium by inactivation of the respiratory chain. *Biochim. Biophys. Acta* 1827, 699–708. doi: 10.1016/j.bbabio.2013.02.004

Koebmann, B., Blank, L. M., Solem, C., Petranovic, D., Nielsen, L. K., and Jensen, P. R. (2008). Increased biomass yield of *Lactococcus lactis* during energetically limited growth and respiratory conditions. *Biotechnol. Appl. Biochem.* 33, 25–33. doi: 10.1042/BA20070132

Koebmann, B. J., Solem, C., Pedersen, M. B., Nilsson, D., and Jensen, P. R. (2002a). Expression of genes encoding F_1-ATPase results in uncoupling of glycolysis from biomass production in *Lactococcus lactis*. *Appl. Environ. Microbiol.* 68, 4274–4282. doi: 10.1128/AEM.68.9.4274-4282.2002

Koebmann, B. J., Westerhoff, H. V., Snoep, J. L., Nilsson, D., and Jensen, P. R. (2002b). The glycolytic flux in *Escherichia coli* is controlled by the demand for ATP. *J. Bacteriol.* 184, 3909–3916. doi: 10.1128/jb.184.14.3909-3916.2002

Lencina, A. M., Franza, T., Sullivan, M. J., Ulett, G. C., Ipe, D. S., Gaudu, P., et al. (2018). Type 2 NADH dehydrogenase is the only point of entry for electrons into the *Streptococcus agalactiae* respiratory chain and is a potential drug target. *mBio* 9, e01034–e01018. doi: 10.1128/mBio.01034-18

Liu, J., Kandasamy, V., Würtz, A., Jensen, P. R., and Solem, C. (2016). Stimulation of acetoin production in metabolically engineered *Lactococcus lactis* by increasing ATP demand. *Appl. Microbiol. Biotechnol.* 100, 9509–9517. doi: 10.1007/s00253-016-7687-1

Liu, J., Wang, Z., Kandasami, V., Lee, S. Y., Solem, C., and Jensen, P. R. (2017). Harnessing the respiration machinery for high-yield production of chemicals in metabolically engineered *Lactococcus lactis*. *Metabol. Eng.* 44, 22–29. doi: 10.1016/j.ymben.2017.09.001

Liu, Q., Lin, Z., Zhang, Y., Li, Y., Wang, Z., and Chen, T. (2014). Improved poly(3-hydroxybutyrate) production in *Escherichia coli* by inactivation of cytochrome *bd*-II oxidase or/and NDH-II dehydrogenase in low efficient respiratory chains. *J. Biotechnol.* 192, 170–176. doi: 10.1016/j.jbiotec.2014.09.021

Liu, Y., Zhu, Y., Ma, W., Shin, H., Li, J., Liu, L., et al. (2014). Spatial modulation of key pathway enzymes by DNA-guided scaffold system and respiration chain engineering for improved N-acetylglucosamine production by *Bacillus subtilis*. *Metabol. Eng.* 24, 61–69. doi: 10.1016/j.ymben.2014.04.004

Lo, J., Olson, D. G., Murphy, S. J. L., Tian, L., Hon, S., Lanahan, A., et al. (2017). Engineering electron metabolism to increase ethanol production in *Clostridium thermocellum*. *Metabol. Eng.* 39, 71–79. doi: 10.1016/j.ymben.2016.10.018

Martien, J. I., Hebert, A. S., Stevenson, D. M., Regner, M. R., Khana, D. B., Coon, J. J., et al. (2019). Systems-level analysis of oxygen exposure in *Zymomonas mobilis*: implications for isoprenoid production. *mSystems* 4, e00284–e00218. doi: 10.1128/mSystems.00284-18

Minohara, S., Sakamoto, J., and Sone, N. (2002). Improved H^+/O ratio and cell yield of *Escherichia coli* with genetically altered terminal quinol oxidases. *J. Biosci. Bioeng.* 93, 464–469. doi: 10.1016/S1389-1723(02)80093-7

Mohagheghi, A., Linger, J. G., Yang, S., Smith, H., Dowe, N., Zhang, M., et al. (2015). Improving a recombinant *Zymomonas mobilis* strain 8b through continuous adaptation on dilute acid pretreated corn stover hydrolysate. *Biotechnol. Biofuels* 8:55. doi: 10.1186/s13068-015-0233-z

Molenaar, D., van Berlo, R., de Ridder, D., and Teusink, B. (2009). Shifts in growth strategies reflect tradeoffs in cellular economics. *Mol. Syst. Biol.* 5:323. doi: 10.1038/msb.2009.82

Murata, M., Ishii, A., Fujimoto, H., Nishimura, K., Kosaka, T., Mori, H., et al. (2018). Update of thermotolerant genes essential for survival at a critical high temperature in *Escherichia coli*. *PLoS ONE* 13:e0189487. doi: 10.1371/journal.pone.0189487

Neijssel, O. M., and Tempest, D. W. (1976). The regulation of carbohydrate metabolism in *Klebsiella aerogenes* NCTC 418 organisms, growing in chemostat culture. *Arch. Microbiol.* 106, 251–258. doi: 10.1007/BF00446531

Noda, S., Takezawa, Y., Mizutani, T., Asakura, T., Nishiumi, E., Onoe, K., et al. (2006). Alterations of cellular physiology in *Escherichia coli* in response to oxidative phosphorylation impaired by defective F_1-ATPase. *J. Bacteriol.* 188, 6869–6876. doi: 10.1128/JB.00452-06

Nowak, C., Beer, B., Pick, A., Roth, T., Lommes, P., and Sieber, V. (2015). A water-forming NADH oxidase from *Lactobacillus pentosus* suitable for the regeneration of synthetic biomimetic cofactors. *Front. Microbiol.* 6:957. doi: 10.3389/fmicb.2015.00957

Patridge, E. V., and Ferry, J. G. (2006). WrbA from *Escherichia coli* and *Archaeoglobus fulgidus* is an NAD(P)H: quinone oxidoreductase. *J. Bacteriol.* 188, 3498–3506. doi: 10.1128/JB.188.10.3498-3506.2006

Pedersen, M. B., Gaudu, P., Lechardeur, D., Petit, M.-A., and Gruss, A. (2012). Aerobic respiration metabolism in lactic acid bacteria and uses in biotechnology. *Annu. Rev. Food Sci. Technol.* 3, 37–58. doi: 10.1146/annurev-food-022811-101255

Perrenoud, A., and Sauer, U. (2005). Impact of global transcriptional regulation by ArcA, ArcB, Cra, Crp, Cya, Fnr, and Mlc on glucose catabolism in *Escherichia coli*. *J. Bacteriol.* 187, 3171–3179. doi: 10.1128/JB.187.9.3171-3179.2005

Poole, R. K., and Cook, G. M. (2000). "Redundancy of aerobic respiratory chains in bacteria? Routes, reasons and regulation," in *Advances in Microbial Physiology, Vol. 43,* ed R. K. Poole (London: Academic Press), 165–224. doi: 10.1016/S0065-2911(00)43005-5

Poole, R. K., and Hill, S. (1997). Respiratory protection of nitrogenase activity in *Azotobacter vinelandii* – roles of the terminal oxidases. *Biosci. Rep.* 17, 303–317. doi: 10.1023/A:1027336712748

Portnoy, V. A., Herrgard, M. J., and Palsson, B. O. (2008). Aerobic fermentation of D-glucose by an evolved cytochrome oxidase-deficient *Escherichia coli* strain. *Appl. Environ. Microbiol.* 74, 7561–7569. doi: 10.1128/AEM.00880-08

Richhardt, J., Luchterhand, B., Bringer, S., Büchs, J., and Bott, M. (2013). Evidence for a key role of cytochrome bo_3 oxidase in respiratory energy metabolism of *Gluconobacter oxydans*. *J. Bacteriol.* 195, 4210–4220. doi: 10.1128/JB.00470-13

Rogers, P. L., Lee, K. J., Skotnicki, M. L., and Tribe, D. E. (1982). Ethanol production by *Zymomonas mobilis*. *Adv. Biochem. Eng.* 23, 37–84. doi: 10.1007/3540116982_2

Russell, J. B., and Cook, G. M. (1995). Energetics of bacterial growth: balance of anabolic and catabolic reactions. *Microbiol. Rev.* 59, 48–62.

Rutkis, R., Galinina, N., Strazdina, I., and Kalnenieks, U. (2014). The inefficient aerobic energetics of *Zymomonas mobilis*: identifying the bottleneck. *J. Basic Microbiol.* 54, 1–8. doi: 10.1002/jobm.201300859

Rutkis, R., Strazdina, I., Balodite, E., Lasa, Z., Galinina, N., and Kalnenieks, U. (2016). The low energy-coupling respiration in *Zymomonas mobilis* accelerates flux in the Entner- Doudoroff pathway. *PLoS ONE* 11:e0153866. doi: 10.1371/journal.pone.0153866

Santana, M., Ionescu, M. S., Vertes, A., Longin, R., Kunst, F., Danchin, A., et al. (1994). *Bacillus subtilis* F_0F_1 ATPase: DNA sequence of the atp operon and characterization of atp mutants, *J. Bacteriol.* 176 6802–6811. doi: 10.1128/jb.176.22.6802-6811.1994

Sauer, M., Russmayer, H., Grabherr, R., Peterbauer, C. K., and Marx, H. (2017). The efficient clade: lactic acid bacteria for industrial chemical production. *Trends Biotechnol.* 35, 756–769. doi: 10.1016/j.tibtech.2017.05.002

Schuhmacher, T., Löffler, M., Hurler, T., and Takors, R. (2014). Phosphate limited fed-batch processes: impact on carbon usage and energy metabolism in *Escherichia coli*. *J. Biotechnol.* 190, 96–104. doi: 10.1016/j.jbiotec.2014.04.025

Seo, J.-S., Chong, H., Park, H. S., Yoon, K.-O., Jung, C., Kim, J. J., et al. (2005). The genome sequence of the ethanologenic bacterium *Zymomonas mobilis* ZM4. *Nat. Biotechnol.* 23, 63–68. doi: 10.1038/nbt1045

Shi, X., Zou, Y., Chen, Y., Zheng, C., and Ying, H. (2016). Overexpression of a water-forming NADH oxidase improves the metabolism and stress tolerance of *Saccharomyces cerevisiae* in aerobic fermentation. *Front. Microbiol.* 7:1427. doi: 10.3389/fmicb.2016.01427

Sootsuwan, K., Lertwattanasakul, N., Thanonkeo, P., Matsushita, K., and Yamada, M. (2008). Analysis of the respiratory chain in ethanologenic *Zymomonas mobilis* with a cyanide-resistant *bd*-type ubiquinol oxidase as the only terminal oxidase and its possible physiological roles. *J. Mol. Microbiol. Biotechnol.* 14, 163–175. doi: 10.1159/000112598

Spiro, S., and Guest, J. R. (1991). Adaptive responses to oxygen limitation in *Escherichia coli*. *TIBS* 16, 310–314. doi: 10.1016/0968-0004(91)90125-F

Sprenger, G. (1996). Carbohydrate metabolism in *Zymomonas mobilis*: a catabolic highway with some scenic routes. *FEMS Microbiol. Lett.* 145, 301–307. doi: 10.1111/j.1574-6968.1996.tb08593.x

Steinsiek, S., Stagge, S., and Bettenbrock, K. (2014). Analysis of *Escherichia coli* mutants with a linear respiratory chain. *PLoS ONE* 9:e87307. doi: 10.1371/journal.pone.0087307

Stouthamer, A. H. (1977). Energetic aspects of the growth of micro-organisms. *Symp. Soc. Gen. Microbiol.* XXVII, 285–315.

Strazdina, I., Balodite, E., Lasa, Z., Rutkis, R., Galinina, N., and Kalnenieks, U. (2018). Aerobic catabolism and respiratory lactate bypass in Ndh-negative *Zymomonas mobilis*. *Metabol. Eng. Commun.* 7:e00081. doi: 10.1016/j.mec.2018.e00081

Strazdina, I., Kravale, Z., Galinina, N., Rutkis, R., Poole, R. K., and Kalnenieks, U. (2012). Electron transport and oxidative stress in *Zymomonas mobilis* respiratory mutants. *Arch. Microbiol.* 194, 461–471. doi: 10.1007/s00203-011-0785-7

Strohdeicher, M., Neuß, B., Bringer-Meyer, S., and Sahm, H. (1990). Electron transport chain of *Zymomonas mobilis*. Interaction with the membrane-bound glucose dehydrogenase and identification of ubiquinone 10. *Arch. Microbiol.* 154, 536–543. doi: 10.1007/BF00248833

Taniguchi, H., Okano, K., and Honda, K. (2017). Modules for in vitro metabolic engineering: pathway assembly for bio-based production of value-added chemicals. *Synth. Syst. Biotechnol.* 2, 65–74. doi: 10.1016/j.synbio.2017.06.002

Taymaz-Nikerel, H., Borujeni, A. E., Verheijen, P. J., Heijnen, J. J., and van Gulik, W. M. (2010). Genome-derived minimal metabolic models for *Escherichia coli* MG1655 with estimated *in vivo* respiratory ATP stoichiometry. *Biotechnol. Bioeng.* 107, 369–381. doi: 10.1002/bit.22802

Tsuge, Y., Uematsu, K., Yamamoto, S., Suda, M., Yukawa, H., and Inui, M. (2015). Glucose consumption rate critically depends on redox state in *Corynebacterium glutamicum* under oxygen deprivation. *Appl. Microbiol. Biotechnol.* 99, 5573–5582. doi: 10.1007/s00253-015-6540-2

Turina, P., Giovannini, D., Gubellini, F., and Melandri, B. A. (2004). Physiological ligands ADP and P_i modulate the degree of intrinsic coupling in the ATP synthase of the photosynthetic bacterium *Rhodobacter capsulatus*. *Biochemistry* 43, 11126–11134. doi: 10.1021/bi048975+

Unden, G., and Bongaerts, J. (1997). Alternative respiratory pathways of *Escherichia coli*: energetics and transcriptional regulation in response to electron acceptors. *Biochim. Biophys. Acta* 1320, 217–234. doi: 10.1016/S0005-2728(97)00034-0

Vemuri, G. N., Altman, E., Sangurdekar, D. P., Khodursky, A. B., and Eiteman, M. A. (2006a). Overflow metabolism in *Escherichia coli* during steady-state growth: transcriptional regulation and effect of the redox ratio. *Appl. Environ. Microbiol.* 72, 3653–3661. doi: 10.1128/AEM.72.5.3653-3661.2006

Vemuri, G. N., Eiteman, M. A., and Altman, E. (2006b). Increased recombinant protein production in *Escherichia* coli strains with overexpressed water-forming NADH oxidase and a deleted ArcA regulatory protein. *Biotechnol. Bioeng.* 94, 538–542.doi: 10.1002/bit.20853

Vemuri, G. N., Eiteman, M. A., McEwen, J. E., Olsson, L., and Nielsen, J. (2007). Increasing NADH oxidation reduces overflow metabolism in *Saccharomyces cerevisiae*. *Proc. Natl. Acad. Sci. U.S.A.* 104, 2402–2407. doi: 10.1073/pnas.0607469104

Visser, W., Scheffers, W. A., Batenburg-van der Vegte, W. H., and van Dijken, J. P. (1990). Oxygen requirements of yeasts. *Appl. Environ. Microbiol.* 56, 3785–3792.

Wang, X., He, Q., Yang, Y., Wang, J., Haning, K., Hu, Y., et al. (2018). Advances and prospects in metabolic engineering of *Zymomonas mobilis*. *Metab. Eng.* 50, 57–73. doi: 10.1016/ j.ymben.2018.04.001

Wecker, M. S. A., and Zall, R. R. (1987). Production of acetaldehyde by *Zymomonas mobilis*. *Appl. Environ. Microbiol.* 53, 2815–2820.

Werner, S., Diekert, G., and Schuster, S. (2010). Revisiting the thermodynamic theory of optimal ATP stoichiometries by analysis of various ATP-producing metabolic pathways. *J. Mol. Evol.* 71, 346–355. doi: 10.1007/s00239-010-9389-0

Westerhoff, H. V., Hellingwerf, K. J., and van Dam, K. (1983). Thermodynamic efficiency of microbial growth is low but optimal for maximal growth rate. *Proc. Natl. Acad. Sci. U.S.A.* 80, 305–309. doi: 10.1073/pnas.80.1.305

Williams-Rhaesa, A. M., Rubinstein, G. M., Scott, I. M., Lipscomb, G. L., Poole, F. L. II, Kelly, R. M., et al. (2018). Engineering redox-balanced ethanol production in the cellulolytic and extremely thermophilic bacterium, *Caldicellulosiruptor bescii*. *Metabol. Eng. Commun.* 7:e00073. doi: 10.1016/j.mec.2018.e00073

Wu, H., Bennett, G. N., and San, K. Y. (2015a). Metabolic control of respiratory levels in coenzyme Q biosynthesis-deficient *Escherichia coli* strains leading to fine-tune aerobic lactate fermentation. *Biotechnol. Bioeng.* 112, 1720–1726. doi: 10.1002/bit.25585

Wu, H., Tuli, L., Bennett, G. N., and San, K. Y. (2015b). Metabolic transistor strategy for controlling electron transfer chain activity in *Escherichia coli*. *Metab. Eng.* 28,159–168. doi: 10.1016/j.ymben.2015.01.002

Wu, X., Yao, H., Cao, L., Zheng, Z., Chen, X., Zhang, M., et al. (2017). Improving acetic acid production by overexpressing PQQ-ADH in *Acetobacter pasteurianus*. *Front. Microbiol.* 8:1713. doi: 10.3389/fmicb.2017.01713

Xia, J., Yang, Y., Liu, C. G., Yang, S., and Bai, F. W. (2019). Engineering *Zymomonas mobilis* for robust cellulosic ethanol production. *Trends Biotechnol.* 37, 960–972. doi: 10.1016/j.tibtech.2019.02.002

Yang, S., Mohagheghi, A., Franden, M. A., Chou, Y., Chen, X., Dowe, N., et al. (2016). Metabolic engineering of *Zymomonas mobilis* for 2,3-butanediol production from lignocellulosic biomass sugars. *Biotechnol. Biofuels* 9:189. doi: 10.1186/s13068-016-0606-y

Yang, S., Pappas, K. M., Hauser, L. J., Land, M. L., Chen, G. L., Hurst, G. B., et al. (2009). Improved genome annotation for *Zymomonas mobilis*. *Nat. Biotechnol.* 27, 893–894. doi: 10.1038/nbt1009-893

Yun, N. R., San, K. Y., and Bennet, G. N. (2005). Enhancement of lactate and succinate formation in adhE or pta-ackA mutants of NADH dehydrogenase-deficient *Escherichia coli*. *J. Appl. Microbiol.* 99, 1404–1412. doi: 10.1111/j.1365-2672.2005.02724.x

Zamboni, N., Mouncey, N., Hohmann, H. P., and Sauer, U. (2003). Reducing maintenance metabolism by metabolic engineering of respiration improves riboflavin production by *Bacillus subtilis*. *Metabol. Eng.* 5, 49–55. doi: 10.1016/S1096-7176(03)00007-7

Zamboni, N., and Sauer, U. (2003). Knockout of the high-coupling cytochrome aa_3 oxidase reduces TCA cycle fluxes in *Bacillus subtilis*. *FEMS Microbiol. Lett.* 226, 121–126. doi: 10.1016/S0378-1097(03)00614-1

Zhang, G. C., Turner, T. L., and Jin, Y. S. (2017). Enhanced xylose fermentation by engineered yeast expressing NADH oxidase through high cell density inoculums. *J. Ind. Microbiol. Biotechnol.* 44, 387–395. doi: 10.1007/s10295-016-1899-3

Zhang, L., Bao, W., Wei, R., Fu, S., and Gong, H. (2018). Inactivating NADH:quinone oxidoreductases affects the growth and metabolism of *Klebsiella pneumoniae*. *Biotechnol. Appl. Biochem.* 65, 857–864. doi: 10.1002/bab.1684

Zhang, M., Eddy, C., Deanda, K., Finkelstein, M., and Picataggio, S. (1995). Metabolic engineering of a pentose metabolism pathway in ethanologenic *Zymomonas mobilis*. *Science* 267, 240–243. doi: 10.1126/science.267.5195.240

Zhao, C., Zhao, Q., Li, Y., and Zhang, Y. (2017). Engineering redox homeostasis to develop efficient alcohol-producing microbial cell factories. *Microb. Cell Fact.* 16:115. doi: 10.1186/s12934-017-0728-3

Zhu, J., Sanchez, A., Bennett, G. N., and San, K. Y. (2011). Manipulating respiratory levels in *Escherichia coli* for aerobic formation of reduced chemical products. *Metab. Eng.* 13, 704–712. doi: 10.1016/j.ymben.2011.09.006

Zotta, T., Guidone, A., Ianniello, R. G., Parente, E., and Ricciardi, A. (2013). Temperature and respiration affect the growth and stress resistance of *Lactobacillus plantarum* C17. *J. Appl. Microbiol.* 115, 848–858. doi: 10.1111/jam.12285

Conflict of Interest: The authors declare that the research was conducted in the absence of any commercial or financial relationships that could be construed as a potential conflict of interest.

frontiers in Bioengineering and Biotechnology

ORIGINAL RESEARCH
published: 14 February 2020
doi: 10.3389/fbioe.2020.00072

Synthesis and Assembly of Hepatitis B Virus-Like Particles in a *Pichia pastoris* Cell-Free System

*Alex J. Spice[1,2], Rochelle Aw[1,2], Daniel G. Bracewell[3] and Karen M. Polizzi[1,2]**

[1] Department of Chemical Engineering, Imperial College London, London, United Kingdom, [2] The Imperial College Centre for Synthetic Biology, Imperial College London, London, United Kingdom, [3] Department of Biochemical Engineering, University College London, London, United Kingdom

Virus-like particles (VLPs) are supramolecular protein assemblies with the potential for unique and exciting applications in synthetic biology and medicine. Despite the attention VLPs have gained thus far, considerable limitations still persist in their production. Poorly scalable manufacturing technologies and inconsistent product architectures continue to restrict the full potential of VLPs. Cell-free protein synthesis (CFPS) offers an alternative approach to VLP production and has already proven to be successful, albeit using extracts from a limited number of organisms. Using a recently developed *Pichia pastoris*-based CFPS system, we have demonstrated the production of the model Hepatitis B core antigen VLP as a proof-of-concept. The VLPs produced in the CFPS system were found to have comparable characteristics to those previously produced *in vivo* and *in vitro*. Additionally, we have developed a facile and rapid synthesis, assembly and purification methodology that could be applied as a rapid prototyping platform for vaccine development or synthetic biology applications. Overall the CFPS methodology allows far greater throughput, which will expedite the screening of optimal assembly conditions for more robust and stable VLPs. This approach could therefore support the characterization of larger sample sets to improve vaccine development efficiency.

Keywords: cell-free protein synthesis, virus-like particles, *Pichia pastoris*, synthetic biology, hepatitis B core antigen

OPEN ACCESS

Edited by:
Jean Marie François, UMS3582 Toulouse White Biotechnology (TWB), France

Reviewed by:
Yoshihiro Shimizu, RIKEN, Japan
Navin Khanna, International Centre for Genetic Engineering and Biotechnology, India

****Correspondence:***
Karen M. Polizzi
k.polizzi@imperial.ac.uk

Specialty section:
This article was submitted to Synthetic Biology, a section of the journal Frontiers in Bioengineering and Biotechnology

Received: *30 August 2019*
Accepted: *28 January 2020*
Published: *14 February 2020*

Citation:
Spice AJ, Aw R, Bracewell DG and Polizzi KM (2020) Synthesis and Assembly of Hepatitis B Virus-Like Particles in a Pichia pastoris Cell-Free System. Front. Bioeng. Biotechnol. 8:72. doi: 10.3389/fbioe.2020.00072

INTRODUCTION

Cell-free protein synthesis was developed as early as the 1960s, where it was critical in determining the genetic code (Nirenberg and Matthaei, 1961). Over the decades, advances in synthetic biology are driving a renaissance in CFPS and it is emerging as a transformative platform technology (Carlson et al., 2012). This pique in interest is mainly due to the capacity to produce protein in a rapid and facile manner, providing benefits to multifarious applications. These include the design of *de novo* metabolic pathways (Hodgman and Jewett, 2012), personalized medicine (Ogonah et al., 2017) and biosensing (Pardee et al., 2016). CFPS has also shown distinct advantages in producing difficult-to-express proteins, such as those toxic to the cell *in vivo* (Katzen et al., 2005). Finally, due

Abbreviations: CFPS, cell-free protein synthesis; CIP, calf-intestinal alkaline phosphatase; CTD, C-terminal domain; DLS, dynamic light scattering; HBc, hepatitis B core antigen; MWCO, molecular weight cut-off; NTD, N-terminal domain; OD_{600}, optical density at 600 nm; TEM, transmission electron microscopy; VLP, virus-like particle.

to the unparalleled access to the reaction environment, optimization and characterization can be achieved with an ease that far exceeds *in vivo* systems, creating opportunities for high throughput screening and rapid prototyping.

Cell-free extracts based on a variety of host organisms are continually being developed. Arguably, extracts could be prepared from any cultivatable cell-type. The most commonly utilized systems and those which are commercially available are from *Escherichia coli* (Chen and Zubay, 1983), Chinese hamster ovary cells (CHO) (Brödel et al., 2014), wheat-germ extract (WGE) (Anderson et al., 1983; Madin et al., 2000), rabbit reticulocyte lysate (RRL) (Jackson and Hunt, 1983) and insect (Sf9) cells (Stech et al., 2014). Developing new extracts is still of great interest, unlocking access to advantageous properties of the organisms from which they are derived. The available repertoire of developed CFPS extracts is still expanding and now includes HEK293 (Bradrick et al., 2013) *Saccharomyces cerevisiae* (Gan and Jewett, 2014), *BY-2* tobacco cells (Buntru et al., 2014), *Streptomyces venezuelae* (Moore et al., 2017), *Bacillus megaterium* (Moore et al., 2018), *Vibrio natriegens* (Gan and Jewett, 2014) and most recently *Pichia pastoris* (Aw and Polizzi, 2019).

Pichia pastoris (syn. *Komagataella* spp.) has developed over the past three decades to become the most commonly utilized protein expression system after *E. coli,* for both lab and industrial-scale protein production (Bill, 2014). The popularity of *P. pastoris* largely stems from high volumetric productivity, afforded by the ability of the organism to grow to high cell densities (Darby et al., 2012). In addition, *P. pastoris* has proven to be highly versatile, with thousands of proteins successfully synthesized to date (Ahmad et al., 2014). It has also become an important expression host for the production of VLP vaccines (Wang et al., 2016).

Virus-like particles are supramolecular protein assemblies, composed of capsid-forming proteins that self-assemble, mimicking the structure of the native viruses from which they are derived (Huang et al., 2017). VLPs are non-infectious and unable to replicate, as they lack a viral genome, removing the concerns about infectivity often associated with live-attenuated or inactivated viruses. This makes VLPs exciting potential vaccine candidates, as they also display strong immunogenicity and the induction of innate and adaptive immunity in animals and humans (Roldão et al., 2010; Crisci et al., 2012). The first VLP vaccine was commercialized in 1986 and was comprised of the hepatitis B virus surface antigen, demonstrating the efficiency and potential of VLP vaccines (Gerety, 1984). In recent years there has been a shift toward engineering increased complexity, with third generation VLPs finding applications in imaging (Manchester and Singh, 2006; Schwarz and Douglas, 2015), catalysis (Patterson et al., 2014, 2015; Maity et al., 2015) and template synthesis (Wnêk et al., 2013). Additionally, VLPs are ideal for the development of platforms for heterologous antigen display, drug encapsulation and chimeric and/or hybrid VLP vaccines (Hill et al., 2017). Advances in synthetic biology are aiding these efforts by widening the repertoire of potential antigens and improving the modularity of these platforms. Despite the attractive attributes, the use of VLPs as vaccines is still hampered by issues related to their production, such as particle integrity, yield, and purification, leading to a demand for new manufacturing approaches to address these challenges (Charlton Hume et al., 2019).

Due to the ability to quickly synthesize protein, CFPS could enable portable and expeditious manufacture of vaccines in response to emerging pathogenic threats or in resource-limited areas. Cell-free systems capable of VLP production may also find use as rapid prototyping platforms for potential VLP vaccine candidates prior to full-scale industrial manufacture or wider nanotechnology applications. Of particular interest is identifying the optimal VLP assembly conditions, which are easier to establish *in vitro* due to the open nature of the reaction environment. Greater understanding of VLP assembly may help overcome issues related to architectural heterogeneity commonly associated with inconsistent product generation. Additionally, *in vivo* expression of VLPs can cause cellular toxicity that inhibits growth, such as in the case of the toxic intermediate A2 protein, which was successfully produced and incorporated into Qβ VLPs in a cell-free system (Smith et al., 2012).

A number of CFPS systems have been utilized for the production of VLPs. Hepatitis B virus core antigen VLP has been produced in extracts derived from *E. coli* (Bundy et al., 2008) and RRL (Ludgate et al., 2016). Human papillomavirus L1 VLP has been produced in *S. cerevisiae* cell-free systems (Wang et al., 2008) and Human norovirus VLP has been produced in *E. coli* cell-free systems (Sheng et al., 2017). WGE has been used extensively for the production of VLPs derived from Hepatitis B virus (Lingappa, 1994), Hepatitis C virus (Klein et al., 2004), Human immunodeficiency virus (HIV) (Lingappa et al., 1997), and Simian immunodeficiency virus (SIV) (Dooher and Lingappa, 2004; Lingappa et al., 2005).

The history of *P. pastoris* as a robust and versatile expression host able to produce VLPs from diverse origins suggests the recently developed CFPS system could be ideally suited as a high-throughput VLP manufacturing and characterization platform. The platform could be specifically suitable for the rapid optimization and validation of DNA constructs and protein variants *in vitro*, circumventing some of the lengthy cloning procedures associated with strain development, prior to full-scale industrial manufacture *in vivo*. Additionally, recombinant protein production in the *P. pastoris* CFPS system is relatively untested. Probing the capabilities of the *P. pastoris* CFPS system for complex recombinant protein production is therefore a valuable measure of the future potential of the platform for synthesis of more complex biopharmaceuticals.

As a first step toward this goal, the wild-type Hepatitis B virus core antigen (HBc) VLP was selected as a proof-of-concept, as it is one of the best characterized model VLPs. Even though there are no clinically approved native non-chimeric HBc VLP vaccines, HBc VLPs are a popular scaffold molecule for the construction of prophylactic and therapeutic vaccine candidates, many of which are currently undergoing clinical trials (Kutscher et al., 2012). HBc VLPs are an excellent platform for foreign antigen presentation due to their high amenability to foreign insertions, and efficient self-assembly (Pumpens and Grens, 2002) and therefore have been developed for the display of foreign antigens from a vast array of pathogens (Charlton Hume et al., 2019). Some of the chimeric and/or hybrid VLPs have been approved

for clinical or veterinary use; for example, against influenza (De Filette et al., 2008; Fiers et al., 2009; Kazaks et al., 2017) and malaria (Schödel et al., 1994; Sällberg et al., 2002; Nardin et al., 2004). Unlike the HBs-Ag which is an enveloped VLP, the HBc VLP is non-enveloped and therefore structurally less complex. This relative simplicity makes it a good test case for production in a cell-free system. In this study we have developed a rapid method for the production and partial purification of HBc VLPs produced in a *P. pastoris* cell-free system.

MATERIALS AND METHODS

Media and Growth Conditions

Bacterial strains were cultured in Miller lysogeny broth (LB) medium (1% peptone from casein, 0.5% yeast extract, 1% NaCl) supplemented with 37 μg ml^{-1} Kanamycin (Sigma−Aldrich, Dorset, United Kingdom). *P. pastoris* strains were cultured in a rich yeast peptone dextrose (YPD) medium (2% peptone from casein, 1% yeast extract, and 2% dextrose) and with 350 μg ml^{-1} Geneticin (VWR, Lutterworth, United Kingdom) for selection. *P. pastoris* strains were cultured in baffled glass flasks or in 50 ml Falcon tubes at a volume of no more than 20% of the total volume of the vessel starting from an OD_{600} of 0.1.

Strains

Bacterial recombinant DNA manipulation was carried out in *E. coli* strain NEB 5−α (New England Biolabs (NEB), Hertfordshire, United Kingdom). *P. pastoris (*syn. *Komagataella phaffi)* strain FHL1 was described previously (Aw and Polizzi, 2019).

Plasmid Construction

The CFPS expression plasmid was generated using the Gibson DNA assembly method as described previously (Gibson et al., 2009). The pET−28b vector (Merck UK Ltd., Hertfordshire, United Kingdom) was used as a backbone. The full-length wild-type (WT) HBc core antigen (*adw* serotype) codon-optimized for *P. pastoris* and the cricket paralysis virus (CrPV) internal ribosome entry site (IRES) sequences were synthesized by GeneArt^{TM} (Thermo Fisher Scientific, Paisley, United Kingdom). In order to make the expression constructs, desired fragments were amplified with 30 bp of homology using primers purchased from Thermo Fisher Scientific using Phusion® High Fidelity DNA polymerase (New England Biolabs). A Kozak sequence (GAAACG) was included in the primers, directly upstream of the coding region. This sequence was selected based on previously displayed efficacy in the production of recombinant proteins in *P. pastoris* and is recommended in the ThermoFisher PichiaPink^{TM} Expression System manual. The PCR reaction products were gel extracted using the Zymoclean^{TM} Gel DNA Recovery kit (Zymo Research Corporation, Irvine, CA, United States) prior to the assembly reaction. After confirmation of the correct plasmid assembly, a synthetic 50 bp polyA tail was generated using annealed primers and inserted into the vector by restriction cloning using *Xho*I and *Not*I (NEB). The plasmid material generated for CFPS reactions was extracted using the Qiagen Maxi Prep Kit (Qiagen, Crawley, United Kingdom).

Crude Extract Preparation and Coupled Cell-Free Protein Synthesis

Pichia pastoris cells were grown and extracts were prepared as previously described (Aw and Polizzi, 2019). Briefly, overnight cultures of *P. pastoris* strain FHL1 were grown in 5 ml of YPD medium and then used to inoculate 200 ml of YPD medium to an OD_{600} of 0.1. Cell growth was allowed to proceed to an OD_{600} of 18–20 at 30°C, 250 rpm. Cells were harvested, washed, homogenized and prepared using the previously described methodology (Aw and Polizzi, 2019). Cell-free protein synthesis reactions were performed by a coupled *in vitro* transcription/translation system at a volume of 50 μL at room temperature for 3 h with no shaking as previously detailed (Aw and Polizzi, 2019).

In vitro Capsid Assembly and Purification

The protocol for capsid assembly and the assembly reaction mixture was adapted from Ludgate et al., 2016. The assembly reaction mixture contained 3 μL of the product of the coupled CFPS reaction per 10 μL total assembly reaction volume and consisted of 1x restriction buffer 3 (100 mM NaCl, 50 mM Tris–HCl, 10 mM MgCl2, 1 mM dithiothreitol (DTT), pH 7.9; (NEB) supplemented with 1x complete^{TM}, mini, EDTA-free protease inhibitor cocktail (Roche, Basel, Switzerland) and 1 U μL^{-1} Murine RNase inhibitor (NEB). For reactions supplemented with exogenous phosphatase, 1 U μL^{-1} of calf intestinal alkaline phosphatase (CIP; NEB) was supplemented into the assembly reaction mixture. The reaction mixtures were incubated overnight (16 h) at 37°C. At this stage, samples were then either concentrated or the purification process continued. For concentration, Vivaspin® 500, 100 kDa MWCO centrifugal concentrators (Sartorius, Göttingen, Germany) were used according to the manufacturer's instructions and samples were buffer exchanged three times with PBS to a final volume of 50 μL.

For purification, after overnight assembly, the reaction mixture was heated at 60°C for 1 h to precipitate contaminating proteins followed by centrifugation (5000 × *g*, 10 min). After centrifugation, the supernatant was collected, and solid ammonium sulfate added to 40% saturation. The mixture was incubated on a laboratory rotator for a minimum of 2 h or overnight at 4°C. The mixture was centrifuged (10,000 × *g*, 30 min) and the resulting protein pellet resuspended in a minimal volume of phosphate-buffered saline (PBS).

SDS-PAGE Gel Analysis

Sodium dodecyl sulfate polyacrylamide gel electrophoresis (SDS–PAGE) was performed using 15% Tris–HCl SDS-PAGE gels. Protein samples were denatured by boiling for 15 min in reducing SDS sample buffer (0.0625 M Tris–HCl, pH 6.8, 2.3% (w/v) SDS, 10% (w/v) glycerol, 0.01% Bromophenol blue, 5% (v/v) β-mercaptoethanol). Molecular weight was estimated by using a pre-stained protein ladder (Pageruler,

10–170 kDa, Thermo Fisher Scientific). SDS-PAGE gels were stained using SimplyBlue^{TM} SafeStain (Invitrogen, Carlsbad, CA, United States) according to the manufacturer's instructions.

Dynamic Light Scattering (DLS) Measurements

Dynamic light scattering measurements were performed using a Malvern Zetasizer Nano ZS instrument (Malvern Instruments Ltd., Worcestershire, United Kingdom). The software utilized to collect and analyze the data was Zetasizer Series 7.13 from Malvern. Forty μL of each sample was analyzed in a 45 μL low-volume glass cuvette. All measurements were conducted at a controlled temperature of 25°C and for each sample 15 runs of 70 s were performed with three repetitions.

Transmission Electron Microscopy (TEM) Analysis

A 3.4 μL sample of purified VLP solution between 0.02–0.05 mg ml^{-1} was applied to a carbon coated copper/Formvar grid and negatively stained with 2% w/v uranyl acetate, pH 4. Images were taken by a TEMCAM XF416 (TVIPS, Oslo, Norway) camera in a CM200 (Philips, Amsterdam, Netherlands) electron microscope at an acceleration voltage of 200 kV. ImageJ software (version 1.51) (Maryland, United States) was used to process the TEM images and add scale bars.

RESULTS AND DISCUSSION

Synthesis, Assembly and Crude Purification of Hepatitis B Viral Capsids

The full-length wild-type HBc VLP was selected as a proof-of-concept due to extensive previous characterization and its use as a chassis molecule for novel vaccine designs (Pumpens and Grens, 2001). The icosahedral HBc VLP is composed of multiple copies of a single 21 kDa protein, the HBc protein. The WT HBc monomer can be divided into three distinct regions: an NTD (position 1–140) responsible for capsid assembly, a CTD (positions 149–183 or 185, depending on the strain) responsible for nucleic acid binding, and a linker region (position 140–149). The assembly domain contains the major immunodominant region, comprised of two α-helices forming the spikes on the particles. The full-length HBc forms dimers and the capsid itself is dimorphic, assembling into both the $T = 3$ (90 dimers) and $T = 4$ (120 dimers) icosahedral VLPs with diameters of 32 nm and 35 nm, respectively (Crowther, 1994; Roseman et al., 2012). In recent years, HBc VLPs have been used as a versatile chassis for both nanotechnology and vaccine applications (Chackerian, 2007; Ludwig and Wagner, 2007) primarily due to particle stability and integrity.

The full-length HBc gene (amino acids 1–183, codon-optimized for *P. pastoris*) was cloned into the pET−28b vector (Merck United Kingdom Ltd.) using the Gibson Assembly method (Gibson et al., 2009). *Pichia pastoris* CFPS reactions were performed to synthesize the HBc in a reaction volume of 50 μL at room temperature without shaking for 3 h.

During our early experiments, we found that the HBc VLPs were unable to self-assemble directly in the CFPS reaction (data not shown). Previous studies have shown that HBc VLP self-assembly *in vitro* is well known to be highly dependent on monomer concentration (Lingappa et al., 2005; Ludgate et al., 2016). When the concentration of HBc dimer exceeds a critical concentration, nearly all free dimer associates into capsid (Katen and Zlotnick, 2009). The HBc concentration required for assembly *in vitro* is high (40–80 μM) at physiological salt concentrations (Wingfield et al., 1995; Tan et al., 2013), although spontaneous self-assembly of the HBc VLP has also been shown to be triggered by increasing the salt concentration (Bundy et al., 2008). Based on the previously reported yield of luciferase produced in our system (∼4.5 μM) (Aw and Polizzi, 2019), we postulated that lack of assembly was due to low dimer concentration prohibiting capsid self-assembly. In a report describing HBc VLP production in an RRL-based CFPS system, it was shown that full-length HBc VLP assembly can be achieved at lower dimer concentrations by modulating the phosphorylation state of the CTD (Ludgate et al., 2016). We therefore aimed to recreate the capsid assembly conditions from this study to ascertain whether the HBc synthesized in our system could be induced to self-assemble into capsids, even at concentrations below the self-assembly threshold. To achieve this, we designed a synthesis, assembly and purification protocol for determining the optimum particle assembly conditions (**Figure 1**).

In order to provide adequate time for capsid assembly, the completed CFPS reactions containing HBc were diluted into the assembly reaction mixture and incubated overnight at 37°C for 16 h. Exogenous CIP, as a broad spectrum phosphatase that can also act on protein, was supplemented into selected samples to dephosphorylate the CTD of the HBc in order to modulate capsid assembly (Ludgate et al., 2016). Since the CTD undergoes non-specific RNA binding, which is modulated by its phosphorylation state, inclusion of an RNase inhibitor in the assembly reaction mixture was also essential to preserve RNA integrity (Ludgate et al., 2016). It is highly probable therefore that dephosphorylation of the CTD promotes non-specific interactions with nucleic acids, facilitating capsid assembly. It has been previously shown that a positively charged CTD interacts with negatively charged nucleic acids to enable capsid assembly at 5 nM (Klein et al., 2004) and the removal of the phosphate may contribute to increasing the local positive charge.

After incubation, centrifugation was conducted to remove aggregates and the supernatant was applied to a 100 kDa MWCO centrifugal concentrator and buffered-exchanged three times against PBS. A high MWCO membrane is frequently used in HBc VLP production as a concentration and rudimentary purification step (Kazaks et al., 2017; Wetzel et al., 2018).

Samples were taken from the retentate of the concentrator and the resultant flow-through for SDS-PAGE analysis (**Figure 2**). The HBc monomer has a molecular weight of 21 kDa, but no band of this size was observed across all samples. A band was, however, observed at approximately 40 kDa for the CIP-treated samples (green arrow) which could be indicative of the HBc dimer (42 kDa). Presence of a band at the expected size of the dimer in the CIP-treated samples suggested HBc VLP

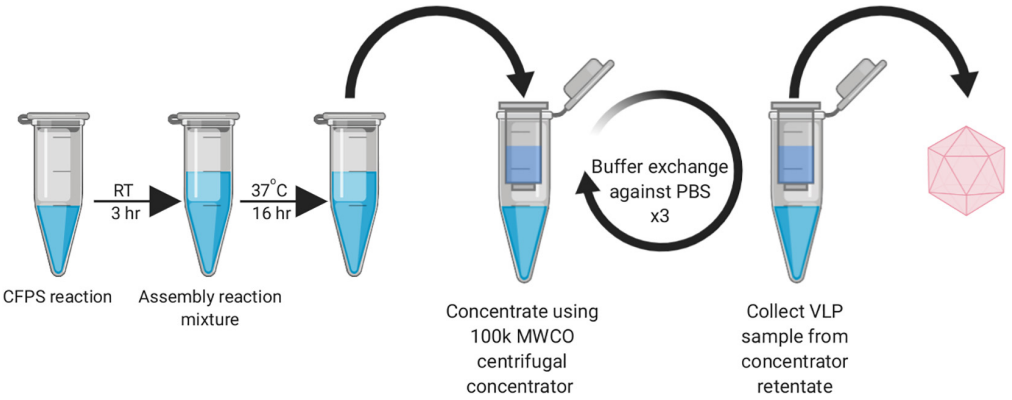

FIGURE 1 | Work-flow schematic of HBc VLP synthesis, assembly and centrifugal concentrator purification. Created with biorender.com.

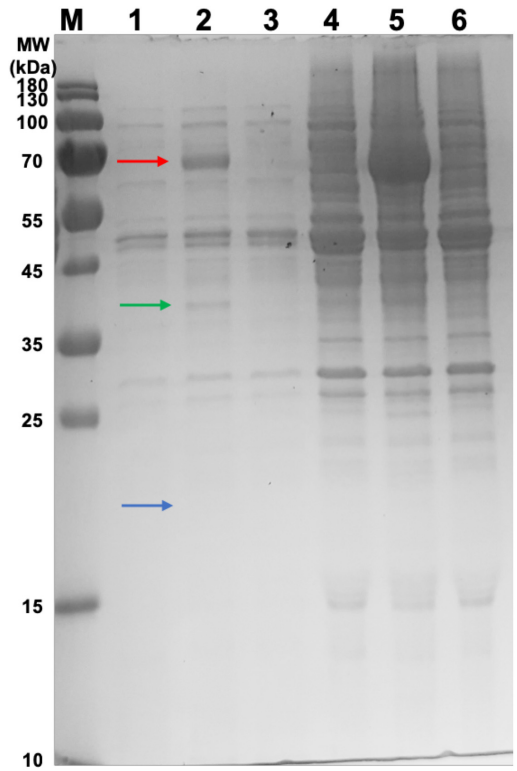

FIGURE 2 | SDS-PAGE gel of samples from the concentration of CFPS products after incubation in the assembly reaction mixture and associated flowthrough. Lane M: PageRuler pre-stained protein ladder. Lane 1, CFPS HBc retentate; Lane 2, CFPS HBc (+CIP) retentate; Lane 3, CFPS NC (no HBc template) retentate; Lane 4, CFPS HBc flowthrough; Lane 5, CFPS HBc (+CIP) flowthrough; Lane 6, CFPS NC (no HBc template) flowthrough. Red arrow indicates CIP (~70 kDa). Green arrow indicates HBc dimer (~40 kDa). Blue arrow indicates absence of band for HBc monomer (21 kDa).

assembly, though further confirmation was required. It is highly likely that the HBc monomer is not visible in the flowthrough of the untreated HBc samples due to dilution. Based on previous concentrations of luciferase produced and the molecular weight of HBc, the concentration is insufficient to meet the criteria for SDS-PAGE detection with SimplyBlue^{TM} SafeStain (Invitrogen). It is worth noting that the other prominent band found in the CIP-treated samples at approximately 70 kDa is the CIP monomer (red arrow), which is added at very high concentrations.

Characterization by DLS

To validate HBc VLP assembly, retentate samples taken after centrifugal concentration were subjected to morphological analysis. Samples of 40 μL were obtained from the concentration step and transferred to a 45 μL low-volume glass cuvette. Using DLS, the diffusion of the particles moving under Brownian motion was measured and the particles sizes of VLPs calculated. Both the CIP-treated and untreated HBc samples gave a positive result from the DLS characterization (**Figure 3**). The untreated HBc sample (**Figure 3A**) displayed a Z-average particle size of 36.89 nm. Considering our initial hypothesis that VLPs would be unable to assemble as a result of low dimer concentration, this was an unexpected result. It is possible that the concentration of monomer produced in our CFPS system is sufficient for capsid self-assembly, but only when subjected to the conditions provided by the assembly buffer. The beneficial conditions promoting capsid assembly could be the increased salt concentration of the assembly buffer, which was previously shown to trigger capsid self-assembly (Bundy et al., 2008), the inclusion of RNase inhibitor, which preserves RNA integrity thereby facilitating co-localization of free dimer, or a combination of the two. The CIP-treated HBc sample (**Figure 3B**) displayed a Z-average particle size of 37.97 nm. Both observed Z-average particle sizes are close to the reported size of the T = 4 HBc VLP (~35 nm) (Crowther, 1994; Zlotnick et al., 1996). The T = 4 capsid has been reported as the most abundant product of WT HBc produced by *in vitro* self-assembly (~95%) (Zlotnick et al., 1999).

Characterization by TEM

In order to verify that the products of our rapid synthesis, assembly and purification protocol contained correctly formed

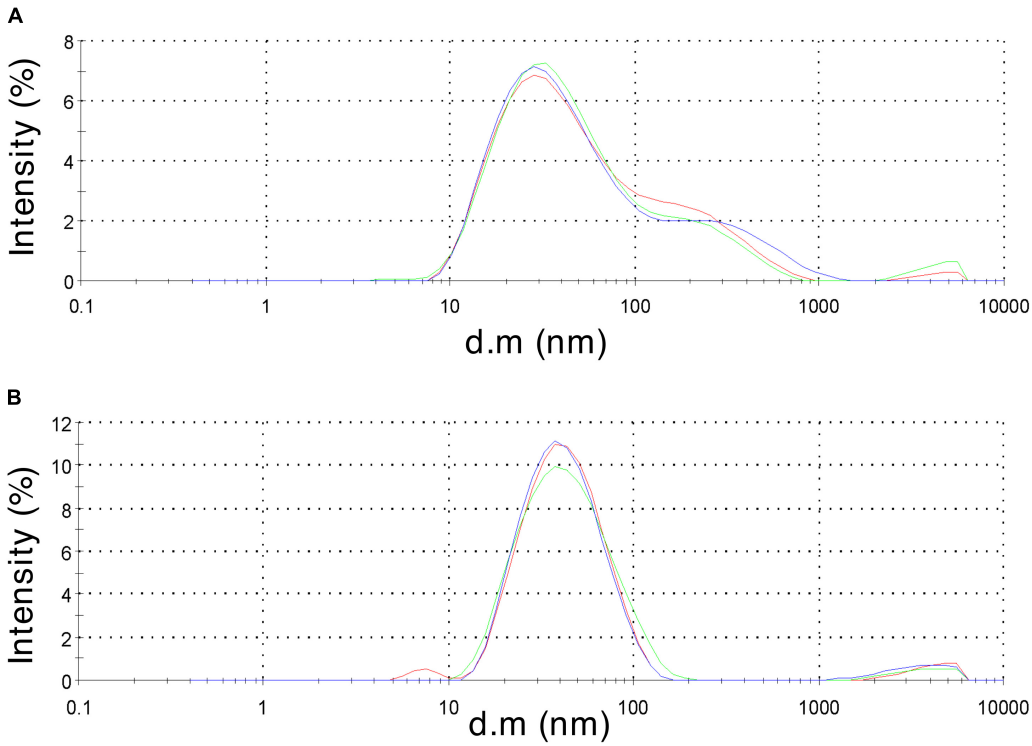

FIGURE 3 | Dynamic light scattering measurements to characterize particle size distribution of the assembled HBc VLPs. **(A)** HBc VLPs obtained from incubation in assembly buffer in the absence of CIP (untreated assembly) **(B)** HBc VLPs obtained from incubation in assembly buffer supplemented with CIP (CIP-treated assembly). Samples are displayed as intensity percentage with three technical replicates.

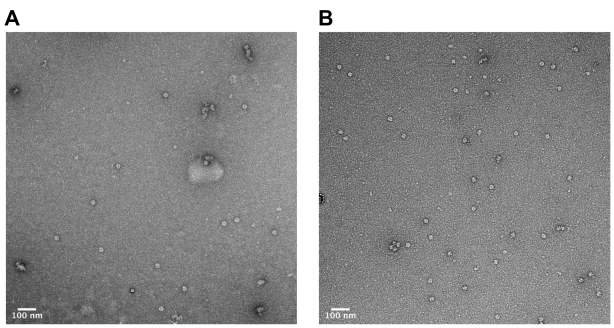

FIGURE 4 | Characterization of HBc VLPs obtained from assembly and crude purification using transmission electron microscopy (TEM). **(A)** HBc VLPs obtained from incubation in assembly buffer in the absence of CIP (untreated assembly) **(B)** HBc VLPs obtained from incubation in assembly buffer supplemented with CIP (CIP-treated assembly). Scale-bar size: 100 nm.

HBc VLPs, TEM with 2% uranyl acetate negative staining was used (**Figure 4**). The average diameter for the untreated HBc VLPs was 29.3 nm (SD = 1.4 nm, $n = 13$) and from the CIP-treated HBc VLPs the average diameter was 28.9 nm (SD = 1.8 nm, $n = 19$). The average size of particles from both samples correlate with previously reported diameters of 30.7 nm from HBc VLPs produced using *in vitro* methods (Bundy et al., 2008) and 30 nm from *in vivo* methods (Zlotnick et al., 1996). Interestingly, a greater number of fully assembled particles were visible in the CIP-treated sample relative to the untreated sample. This could explain why a faint band with a size corresponding to the dimer was visible in the SDS-PAGE analysis for the CIP-treated sample (**Figure 2**, Lane 2), but no band corresponding to the expected size of the monomer or dimer was observed for the untreated samples (HBc) (**Figure 2**, Lane 1). As previously discussed, dephosphorylation of the CTD likely boosts capsid assembly by promoting non-specific interactions with nucleic acids, facilitating capsid self-assembly. Despite this, there was no great observable difference in average particle size or morphology with both samples still displaying a proportion of partially assembled or disassembled particles, in addition to other smaller protein contaminants. It is possible the smaller contaminants are HBc monomer, CIP or host-cell protein carried through the purification. The presence of host-cell contaminants correlates with the SDS-PAGE analysis (**Figure 2**) suggesting further development of the purification protocol was needed.

Heat-Treatment and Ammonium Sulfate Purification of Assembled HBc VLPs

Once the successful synthesis and assembly of HBc VLPs was demonstrated, the next aim was to develop an improved methodology for VLP purification (**Figure 5**). We decided to develop this process using the CIP-treated samples, as the TEM characterization indicated an increased average number of

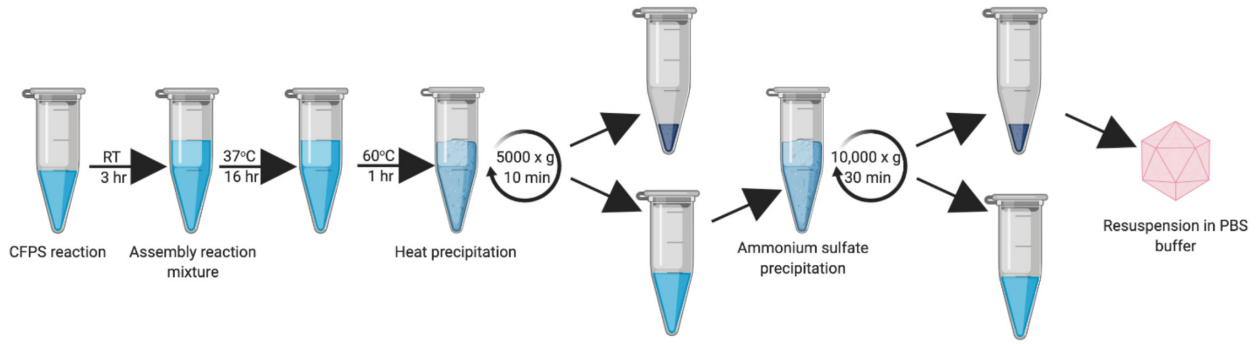

FIGURE 5 | Updated work-flow schematic of HBc VLP synthesis, assembly, heat treatment and ammonium precipitation. Created with biorender.com.

particles relative to the untreated samples. In order to keep in line with creating a simple and rapid purification process, we strived to avoid more time-consuming purification steps, such as chromatography, and those that are costly and poorly scalable for production purposes, such as ultracentrifugation. It has been reported that an efficient method of removing host-cell protein contaminants is the inclusion of a heat treatment step which is both fast and simple (Ng et al., 2006; Lee et al., 2015; Li et al., 2018). As fully-assembled HBc VLP has been shown to be highly thermostable (Ng et al., 2006; Lee and Tan, 2008), heat-labile host-cell proteins can be denatured and precipitated from solution. Toward this end, we removed the centrifugal concentrator step and included a 1 h incubation at 60°C after the initial assembly reaction in order to remove protein contaminants and improperly assembled HBc VLPs. After heating, the reaction mixture was subjected to centrifugation and the supernatant collected for ammonium sulfate precipitation.

Ammonium sulfate precipitation is a well-established method for separation of HBc VLPs and is widely used as a preparatory purification step (Palenzuela et al., 2002). Particles were precipitated by addition of solid ammonium sulfate to 40% saturation (Yang, 2005) followed by incubation at 4°C on a rotator for a minimum of 2 h. The reaction was then centrifuged, and the resultant precipitate resuspended in a minimal volume of PBS, thereby purifying and concentrating the HBc VLPs.

To validate the efficacy of our new purification method, samples were taken from the precipitate and supernatant from each step in the purification process for SDS-PAGE analysis (**Figure 6**). The initial heat treatment step, included to denature and precipitate less thermostable host-cell proteins, appears to remove a large number of contaminants as shown in Lanes 5 and 6 which correspond to the resuspended precipitates from the heat treatment of the HBc assembly reaction containing CIP and negative control. Heat treatment alone does result in sufficient purification to detect the presence of a band at approximately 20 kDa in the supernatant of the HBc assembly reaction (Lane 7), which correlates to the expected size of the HBc monomer (21 kDa). There are still a number of other protein contaminants present, including a band at 70 kDa indicative of CIP. CIP cannot be heat inactivated for removal unless heated to 80°C, which would cause dissociation of the assembled HBc VLPs

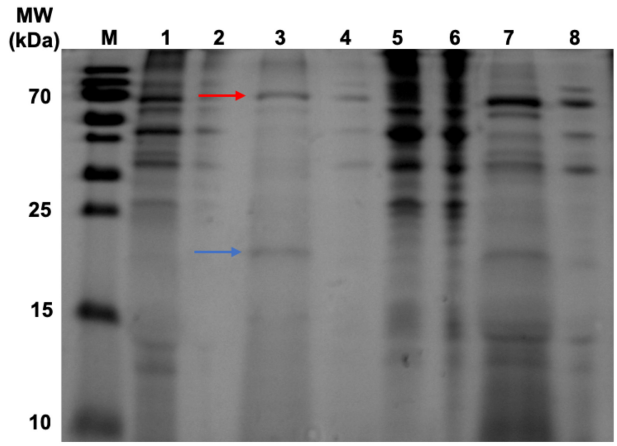

FIGURE 6 | SDS-PAGE gel displaying samples taken during heat-purification and ammonium sulfate precipitation post assembly reaction. Lanes 1–4 have undergone heat treatment then ammonium sulfate precipitation. Lanes 5–8 have undergone heat treatment only. Lane M, PageRuler pre-stained protein ladder; Lane 1, HBc (+CIP) supernatant after heat treatment and ammonium sulfate precipitation; Lane 2, Negative control (NC) (+CIP) supernatant after heat treatment and ammonium sulfate precipitation; Lane 3, HBc (+CIP) precipitate after heat treatment and ammonium sulfate precipitation; Lane 4, NC (+CIP) precipitate after heat treatment and ammonium sulfate precipitation; Lane 5, HBc (+CIP) precipitate after heat treatment only; Lane 6, NC (+CIP) after heat treatment only; Lane 7, HBc (+CIP) supernatant after heat treatment only; Lane 8, NC (+CIP) supernatant after heat treatment only. The blue arrow indicates the expected band size of the HBc monomer (21 kDa). The red arrow indicates the expected band size of the CIP protein (70 kDa).

(Li et al., 2018). Despite the presence of CIP, we note that much of the CIP is removed during the improved purification process. For example, in **Figure 7** the CIP band in lane 7 (representing CIP remaining in the sample after heat treatment alone) is much more intense relative to that of the HBc monomer than the CIP band in lane 3 (representing CIP remaining after both heat treatment and ammonium sulfate precipitation) relative to the HBc monomer.

To improve the purity of the VLPs, a number of possible strategies could be employed. The concentration of CIP used in this study was selected based on that previously reported (Ludgate et al., 2016); however, a lower concentration may still

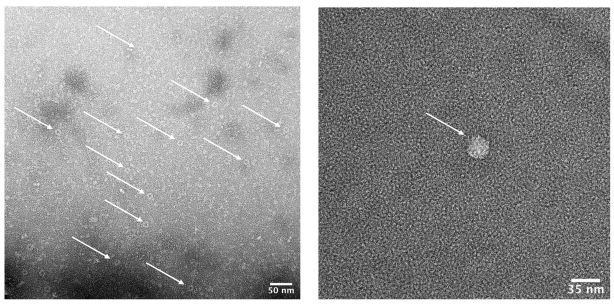

FIGURE 7 | Characterization of HBc VLPs obtained from a heat-treatment and ammonium sulfate purification method. Images generated using transmission electron microscopy (TEM). **(A)** Samples were prepared directly from material resuspended after ammonium sulfate precipitation. The arrows indicate a number of fully formed HBc VLPs. Scale-bar size: 50 nm. **(B)** Sample was prepared at a lower concentration of 5 μg ml^{-1}. Staining was preceded by three immediate washes in filtered distilled water after the sample was applied to the grid. The arrow indicates a fully formed HBc VLP. Scale-bar size: 35 nm.

be sufficient for CTD dephosphorylation to promote assembly and would reduce the amount of CIP contaminant present in the sample after purification of the HBc VLPs. Alternatively, a heat-labile alkaline phosphatase such as one derived from Shrimp (Nilsen et al., 2001) could be used instead of CIP (Mehta et al., 2009; Crawley et al., 2011), enabling its irreversible removal from the sample via heat inactivation at 65°C. This would enable removal of the phosphatase alongside the heat-labile host-cell proteins during the heat inactivation step of the purification procedure. Finally, a hexahistidine, FLAG, or other affinity purification tag could be fused to recombinantly produced CIP allowing its removal with a single chromatography step.

After adding the additional ammonium sulfate precipitation step, there are two prominent bands remaining in the HBc assembly reaction containing CIP sample (Lane 3) at the expected band size of the HBc monomer (blue arrow) and CIP protein (red arrow). It is possible that some of the CIP protein remains bound to HBc during the purification process or it may become encapsulated as the VLP forms, leading to its persistence. For example, it was recently observed that an influenza VLP contained an internal component density postulated to be encapsulated cellular components (McCraw et al., 2018). The CIP protein is also visible in the negative control sample containing CIP (Lane 4), along with other higher molecular weight contaminants.

The presence of a single band indicative of the HBc monomer in **Figure 6** compared to the observation of a band indicative of the HBc dimer in **Figure 2** could be due to a combination of factors. Firstly, there is large disparity in the total protein concentration of the samples with those in **Figure 2** having a much greater total protein concentration compared to those in **Figure 6**. It is possible, therefore, that the amount of SDS and/or beta-mercaptoethanol present in the sample to solubilize and fully denature the amount of protein was insufficient. Secondly, the HBc dimer in **Figure 2** could be due to re-dimerization of the HBc monomer between sample preparation and loading. It has previously been reported that disulfide re-oxidation can occur during SDS-PAGE (Kumar et al., 1993; Grigorian, 2005) and both the HBc monomer and dimer have been previously observed to co-occur (Storni and Bachmann, 2004).

The total protein concentration of the purified HBc VLP sample was obtained by measuring protein absorbance at 280 nm (A280) and found to be 68 μg ml^{-1}. Densitometry analysis conducted using the ImageJ software was used to estimate the yield of HBc VLP in our system at 6.4 μg ml^{-1}. This is a slight improvement on the reported yield of HBc VLP of 4 μg ml^{-1} previously produced in a WGE system (Lingappa et al., 2005). The yield is currently considerably lower in our system compared to production of HBc VLP *in vivo*, with reported yields of assembled HBc VLP in *P. pastoris* up to 3 mg per 1 g wet cell weight (Freivalds et al., 2011).

Characterization of Purified HBc VLPs by TEM

We next sought to determine whether the product of our improved purification protocol contained correctly formed HBc VLP. To achieve this, TEM with 2% uranyl acetate negative staining was performed (**Figure 7A**). A number of fully formed HBc VLPs can be observed with an overall increase in the uniformity of their morphology compared to **Figure 4**. This indicates removal of partially assembled or disassembled HBc VLPs in the developed purification scheme relative to the initial TEM analysis using the crude purification method (**Figure 4**). A number of misfolded or aggregated proteins still persist in the sample, however. Based on the SDS-PAGE analysis in **Figure 6**, we postulate that these are likely to be aggregates of CIP, as only fully formed VLPs remain in the supernatant after heat treatment (Ng et al., 2006). An additional TEM grid was prepared at a lower sample concentration of 5 μg ml^{-1}. Staining was followed by three washes in filtered distilled water for 1 min each in order to attain single particle imaging for accurate size estimation (**Figure 7B**). The wash steps were included in the staining procedure to remove excess uranyl acetate stain and led to a reduction in stain permeation of the HBc VLPs (**Figure 7B**). The observed diameter for the displayed particle was approximately 29.5 nm. The reported size correlates with previously reported diameters from HBc VLP produced using *in vitro* methods (Bundy et al., 2008), *in vivo* methods (Zlotnick et al., 1996) and our previously shown assembled particle diameter of 29.4 nm using the crude purification method.

CONCLUSION

Cell-free protein synthesis is an incredibly powerful and versatile tool in synthetic biology, which can be applied in myriad ways. We have generated a rapid HBc VLP synthesis, assembly and purification scheme demonstrating the potential of the *P. pastoris* CFPS system for the production of complex supramolecular assemblies. This approach could enable ultra-scale-down rapid prototyping of protein variants for novel vaccine technologies.

Additionally, by exploiting the open nature of the reaction environment, the conditions for assembly can be optimized, alleviating the current challenges of structural heterogeneity in VLP manufacture. We plan to expand on this work, further testing the capabilities of the system by producing VLPs of increased complexity. In future, we envision increased effectiveness in response to emerging pathogenic threats, through high-throughput vaccine development approaches.

DATA AVAILABILITY STATEMENT

All datasets generated for this study are included in the article/supplementary files.

AUTHOR CONTRIBUTIONS

AS designed and performed the experiments. RA and KP helped to design the experiments. KP and DB helped to conceive the study. All authors helped to draft the manuscript and read and approved the final manuscript.

FUNDING

This project was funded in part with UK aid from the UK government, and the UK Department of Health and Social Care is gratefully acknowledged for funding the Future Vaccine Manufacturing Research Hub through the Engineering and Physical Sciences Research Council (EPSRC, grant number: EP/R013764/1). AS would also like to thank the EPSRC Centre for Innovative Manufacturing in Emergent Macromolecular Therapies (EP/I033270/1) for Ph.D. studentship funding.

ACKNOWLEDGMENTS

The authors would like to thank Mr. Ciaran McKeown and Mr. Paul Simpson for assistance with DLS and TEM, respectively.

REFERENCES

Ahmad, M., Hirz, M., Pichler, H., and Schwab, H. (2014). Protein expression in Pichia pastoris: recent achievements and perspectives for heterologous protein production. *Appl Microbiol. Biotechnol.* 98, 5301–5317. doi: 10.1007/s00253-014-5732-5

Anderson, C. W., Straus, J. W., and Dudock, B. S. (1983). Preparation of a cell-free protein-synthesizing system from wheat germ. *Methods Enzymol.* 101, 635–644. doi: 10.1016/0076-6879(83)01044-7

Aw, R., and Polizzi, K. M. (2019). Biosensor-assisted engineering of a high-yield Pichia pastoris cell-free protein synthesis platform. *Biotechnol. Bioeng.* 116, 656–666. doi: 10.1002/bit.26901

Bill, R. M. (2014). Playing catch-up with *Escherichia coli*: using yeast to increase success rates in recombinant protein production experiments. *Front. Microbiol.* 5:85. doi: 10.3389/fmicb.2014.00085

Bradrick, S. S., Nagyal, S., and Novatt, H. (2013). A miRNA-responsive cell-free translation system facilitates isolation of hepatitis C virus miRNP complexes. *RNA* 19, 1159–1169. doi: 10.1261/rna.038810.113

Brödel, A. K., Sonnabend, A., and Kubick, S. (2014). Cell-free protein expression based on extracts from CHO cells. *Biotechnol. Bioeng.* 111, 25–36. doi: 10.1002/bit.25013

Bundy, B. C., Franciszkowicz, M. J., and Swartz, J. R. (2008). *Escherichia coli*-based cell-free synthesis of virus-like particles. *Biotechnol. Bioeng.* 100, 28–37. doi: 10.1002/bit.21716

Buntru, M., Simon, V., Holger, S., and Stefan, S. (2014). Tobacco BY-2 cell-free lysate: an alternative and highly-productive plant-based in vitro translation system. *BMC Biotechnol.* 14:37. doi: 10.1186/1472-6750-14-37

Carlson, E. D., Gan, R., Hodgman, C. E., and Jewett, M. C. (2012). Cell-free protein synthesis: applications come of age. *Biotechnol. Adv. Elsevier Inc.* 30, 1185–1194. doi: 10.1016/j.biotechadv.2011.09.016

Chackerian, B. (2007). Virus-like particles: flexible platforms for vaccine development. *Exp. Rev. Vaccines* 6, 381–390. doi: 10.1586/14760584.6.3.381

Charlton Hume, H. K., Vidigal, J., Carrondo, M. J. T., Middelberg, A. P. J., Roldão, A., and Lua, L. H. L. (2019). Synthetic biology for bioengineering virus-like particle vaccines. *Biotechnol. Bioeng.* 116, 919–935. doi: 10.1002/bit.26890

Chen, H. Z., and Zubay, G. (1983). Prokaryotic coupled transcription — translation. *Methods in Enzymol.* 101, 674–690. doi: 10.1016/0076-6879(83)01047-2

Crawley, S. W., Gharaei, M. S., Ye, Q., Yang, Y., Raveh, B., London, N., et al. (2011). Autophosphorylation activates dictyostelium myosin II Heavy Chain Kinase A by Providing a Ligand for an allosteric binding site in the α-kinase domain. *J. Biol. Chemi.* 286, 2607–2616. doi: 10.1074/jbc.M110.177014

Crisci, E., Bárcena, J., and Montoya, M. (2012). Virus-like particles: the new frontier of vaccines for animal viral infections. *Vet. Immunol. Immunopathol.* 15, 211–225. doi: 10.1016/j.vetimm.2012.04.026

Crowther, R. (1994). Three-dimensional structure of hepatitis B virus core particles determined by electron cryomicroscopy. *Cell* 77, 943–950. doi: 10.1016/0092-8674(94)90142-2

Darby, R. A. J., Cartwright, S. P., Dilworth, M. V., and Bill, R. M. (2012). Which yeast species shall I choose? *Saccharomyces cerevisiae* Versus Pichia pastoris (Review). *Methods Mol. Biol.* 866, 11–23. doi: 10.1007/978-1-61779-770-5_2

De Filette, M., Martens, W., Smet, A., Schotsaert, M., Birkett, A., Londoño-Arcila, P., et al. (2008). Universal influenza A M2e-HBc vaccine protects against disease even in the presence of pre-existing anti-HBc antibodies. *Vaccine* 26, 6503–6507. doi: 10.1016/j.vaccine.2008.09.038

Dooher, J. E., and Lingappa, J. R. (2004). Conservation of a stepwise, energy-sensitive pathway involving hp68 for assembly of primate lentivirus capsids in cells. *J. Virol.* 78, 1645–1656. doi: 10.1128/jvi.78.4.1645-1656.2004

Fiers, W., De Filette, M., El Bakkouri, K., Schepens, B., Roose, K., Schotsaert, M., et al. (2009). M2e-based universal influenza A vaccine. *Vaccine* 27, 6280–6283. doi: 10.1016/j.vaccine.2009.07.007

Freivalds, J., Dislers, A., Ose, V., Pumpens, P., Tars, K., and Kazaks, A. (2011). Highly efficient production of phosphorylated hepatitis B core particles in yeast Pichia pastoris. *Protein Exp. Purif.* 75, 218–224. doi: 10.1016/j.pep.2010.09.010

Gan, R., and Jewett, M. C. (2014). A combined cell-free transcription-translation system from Saccharomyces cerevisiae for rapid and robust protein synthesis. *Biotechnol. J* 9, 641–651. doi: 10.1002/biot.201300545

Gerety, R. J. (1984). "Newly licensed hepatitis B vaccine," in *Hepatitis B*, eds I. Millman, T. K. Eisenstein, and B. S. Blumberg, (Boston, MA: Springer).

Gibson, D. G., Lei, Y., Ray-Yuan, C., Craig Venter, J., Clyde, H. A., and Hamilton, O. S. (2009). Enzymatic assembly of DNA molecules up to several hundred kilobases. *Nat. Methods* 6, 343–345. doi: 10.1038/nmeth.1318

Grigorian, A. L. (2005). Extraordinarily stable disulfide-linked homodimer of human growth hormone. *Protein Sci.* 14, 902–913. doi: 10.1110/ps.041048805

Hill, B. D., Zak, A., Khera, E., and Wen, F. (2017). Engineering virus-like particles for antigen and drug delivery. *Curr. Protein Peptide Sci.* 19, 112–127. doi: 10.2174/1389203718666161122113041

Hodgman, C. E., and Jewett, M. C. (2012). Cell-free synthetic biology: thinking outside the cell. *Metab. Eng.* 14, 261–269. doi: 10.1016/j.ymben.2011.09.002

Huang, X., Xin, W., Jun, Z., Ningshao, X., and Qinjian, Z. (2017). *Escherichia coli*-derived virus-like particles in vaccine development. *Npj Vaccines* 2:3. doi: 10.1038/s41541-017-0006-8

Jackson, R. J., and Hunt, T. (1983). Preparation and use of nuclease-treated rabbit reticulocyte lysates for the translation of eukaryotic messenger RNA. *Methods Enzymol.* 96, 50–74. doi: 10.1016/s0076-6879(83)96008-1

Katen, S., and Zlotnick, A. (2009). The thermodynamics of virus capsid assembly. *Methods Enzymol.* 455, 395–417. doi: 10.1016/S0076-6879(08)04214-6

Katzen, F., Chang, G., and Kudlicki, W. (2005). The past, present and future of cell-free protein synthesis. *Trends Biotechnol.* 23, 150–156. doi: 10.1016/j.tibtech.2005.01.003

Kazaks, I., Na, L., Sophie, F., Alex, R., Vincenzo, C., Benjamin, B., et al. (2017). Production and purification of chimeric HBc virus-like particles carrying influenza virus LAH domain as vaccine candidates. *BMC Biotechnol.* 17:79. doi: 10.1186/s12896-017-0396-8

Klein, K. C., Polyak, S. J., and Lingappa, J. R. (2004). Unique Features of Hepatitis C Virus Capsid Formation Revealed by De Novo Cell-Free Assembly. *J. Virol.* 78, 9257–9269. doi: 10.1128/jvi.78.17.9257-9269.2004

Kumar, T. K. S., Gopalakrishna, K., Prasad, V. V. H., and Pandit, M. W. (1993). Multiple bands on the sodium dodecyl sulfate-polyacrylamide gel electrophoresis gels of proteins due to intermolecular disulfide cross-linking. *Anal Biochem.* 213, 226–228. doi: 10.1006/abio.1993.1413

Kutscher, S., Tanja, B., Claudia, D., Martin, S., and Ulrike, P. (2012). Design of therapeutic vaccines: hepatitis B as an example. *Microb. Biotechnol.* 5, 270–282. doi: 10.1111/j.1751-7915.2011.00303.x

Lee, K. W., and Tan, W. S. (2008). Recombinant hepatitis B virus core particles: association, dissociation and encapsidation of green fluorescent protein. *J. Virol. Methods* 151, 172–180. doi: 10.1016/j.jviromet.2008.05.025

Lee, M. F. X., Chan, E. S., Tan, W. S., Tam, K. C., and Tey, B. T. (2015). Negative chromatography purification of hepatitis B virus-like particles using poly(oligo(ethylene glycol) methacrylate) grafted cationic adsorbent. *J. Chromatogr. A* 1415, 161–165. doi: 10.1016/j.chroma.2015.08.056

Li, Z., Wei, J., Yang, Y., Liu, L., Ma, G., Zhang, S., et al. (2018). A two-step heat treatment of cell disruption supernatant enables efficient removal of host cell proteins before chromatographic purification of HBc particles. *J. Chromatogr. A* 158, 71–79. doi: 10.1016/j.chroma.2018.10.050

Lingappa, J. R. (1994). A eukaryotic cytosolic chaperonin is associated with a high molecular weight intermediate in the assembly of hepatitis B virus capsid, a multimeric particle. *J. Cell Biol.* 125, 99–111. doi: 10.1083/jcb.125.1.99

Lingappa, J. R., Newman, M. A., Klein, K. C., and Dooher, J. E. (2005). Comparing capsid assembly of primate lentiviruses and hepatitis B virus using cell-free systems. *Virology* 333, 114–123. doi: 10.1016/j.virol.2004.12.024

Lingappa, J. R., Rebecca, L. H., Mei, L. W., and Ramanujan, S. H. (1997). A Multistep, ATP-dependent Pathway for Assembly of Human Immunodeficiency Virus Capsids in a Cell-free System. *J. Cell Biol.* 136, 567–581. doi: 10.1083/jcb.136.3.567

Ludgate, L., Liu, K., Luckenbaugh, L., Streck, N., Eng, S., Voitenleitner, C., et al. (2016). Cell-Free Hepatitis B Virus Capsid Assembly Dependent on the Core Protein C-Terminal Domain and Regulated by Phosphorylation. *J. Virol.* 90, 5830–5844. doi: 10.1128/JVI.00394-16

Ludwig, C., and Wagner, R. (2007). Virus-like particles—universal molecular toolboxes. *Curr. Opin. Biotechnol.* 18, 537–545. doi: 10.1016/j.copbio.2007.10.013

Madin, K., Sawasaki, T., Ogasawara, T., and Endo, Y. (2000). A highly efficient and robust cell-free protein synthesis system prepared from wheat embryos: Plants apparently contain a suicide system directed at ribosomes. *Proc. Natl Acad. Sci. U.S.A.* 97, 559–564. doi: 10.1073/pnas.97.2.559

Maity, B., Fujita, K., and Ueno, T. (2015). Use of the confined spaces of apo-ferritin and virus capsids as nanoreactors for catalytic reactions. *Curr. Opin. Chem. Biol.* 25, 88–97. doi: 10.1016/j.cbpa.2014.12.026

Manchester, M., and Singh, P. (2006). Virus-based nanoparticles (VNPs): Platform technologies for diagnostic imaging. *Adv. Drug Deliv. Rev.* 58, 1505–1522. doi: 10.1016/j.addr.2006.09.014

McCraw, D. M., John, R. G., Udana, T., Mallory, M. L., Michael, T. C., Neetu, et al. (2018). Structural analysis of influenza vaccine virus-like particles reveals a multicomponent organization. *Scie. Rep.* 8, 10342. doi: 10.1038/s41598-018-28700-7

Mehta, P. A., Rebala, K. C., Venkataraman, G., and Parida, A. (2009). A diurnally regulated dehydrin from Avicennia marina that shows nucleo-cytoplasmic localization and is phosphorylated by Casein kinase II in vitro. *Plant Physiol. Biochem.* 47, 701–709. doi: 10.1016/j.plaphy.2009.03.008

Moore, S. J., Lai, H. E., Needham, H., Polizzi, K. M., and Freemont, P. S. (2017). Streptomyces venezuelae TX-TL - a next generation cell-free synthetic biology tool. *Biotechnol. J.* 12:1600678. doi: 10.1002/biot.201600678

Moore, S. J., MacDonald, J. T., Wienecke, S., Ishwarbhai, A., Tsipa, A., Aw, R., et al. (2018). Rapid acquisition and model-based analysis of cell-free transcription–translation reactions from nonmodel bacteria. *Proc. Natl. Acad. Sci. U.S.A.* 115, E4340–E4349. doi: 10.1073/pnas.1715806115

Nardin, E. H., Oliveira, G. A., Calvo-Calle, J. M., Wetzel, K., Maier, C., Birkett, A. J., et al. (2004). Phase I testing of a malaria vaccine composed of hepatitis B Virus Core Particles Expressing Plasmodium falciparum circumsporozoite epitopes. *Infect. Immun.* 72, 6519–6527. doi: 10.1128/iai.72.11.6519-6527.2004

Ng, M. Y., Tan, W. S., Abdullah, N., Ling, T. C., and Tey, B. T. (2006). Heat treatment of unclarified *Escherichia coli* homogenate improved the recovery efficiency of recombinant hepatitis B core antigen. *J. Virol. Methods* 137, 134–139. doi: 10.1016/j.jviromet.2006.06.016

Nilsen, I. W., Øverbø, K., and Olsen, R. L. (2001). Thermolabile alkaline phosphatase from Northern shrimp (Pandalus borealis): protein and cDNA sequence analyses. *Comp. Biochem. Physiol. Part BBiochem. Mol. Biol.* 129, 853–861. doi: 10.1016/s1096-4959(01)00391-8

Nirenberg, M. W., and Matthaei, J. H. (1961). The dependence of cell-free protein synthesis in *E. coli* upon naturally occurring or synthetic polyribonucleotides. *Proc. Natl. Acad. Sci. U.S.A.* 47, 1588–1602. doi: 10.1073/pnas.47.10.1588

Ogonah, O. W., Polizzi, K. M., and Bracewell, D. G. (2017). Cell free protein synthesis: a viable option for stratified medicines manufacturing? *Curr. Opin. Chem. Eng.* 18, 77–83. doi: 10.1016/j.coche.2017.10.003

Palenzuela, D. O., Núñez, L., Roca, J., Acevedo, B., Díaz, T., Benítez, J. et al., (2002). Purification of the recombinant hepatitis B core antigen, and its potential use for the diagnosis of hepatitis B virus infection. *Biotecnol. Aplicada* 19, 138–142.

Pardee, K., Green, A. A., Takahashi, M. K., Braff, D., Lambert, G., Lee, J. W., et al. (2016). Rapid, Low-Cost Detection of Zika Virus Using Programmable Biomolecular Components. *Cell* 165, 1255–1266. doi: 10.1016/j.cell.2016.04.059

Patterson, D., Edwards, E., and Douglas, T. (2015). Hybrid nanoreactors: coupling enzymes and small-molecule catalysts within virus-like particles. *Israel J. Chem.* 55, 96–101. doi: 10.1002/ijch.201400092

Patterson, D. P., McCoy, K., Fijen, C., and Douglas, T. (2014). Constructing catalytic antimicrobial nanoparticles by encapsulation of hydrogen peroxide producing enzyme inside the P22 VLP. *J. Mater. Chem. B* 2:5948. doi: 10.1039/c4tb00983e

Pumpens, P., and Grens, E. (2001). HBV Core Particles as a Carrier for B Cell/T Cell Epitopes. *Intervirology* 44, 98–114. doi: 10.1159/000050037

Pumpens, P., and Grens, E. (2002). "Artificial genes for chimeric virus-like particles," in *in Artificial DNA*, (Boca Raton, FL: CRC Press).

Roldão, A., Mellado, M. C. M., and Castilho, L. (2010). Virus-like particles in vaccine development. *Exp. Rev. Vaccines* 9, 1149–1176. doi: 10.1586/erv.10.115

Roseman, A. M., Borschukova, O., Berriman, J. A., Wynne, S. A., Pumpens, P., and Crowther, R. A. (2012). Structures of hepatitis B virus cores presenting a model epitope and their complexes with antibodies. *J. Mol. Biol.* 423, 63–78. doi: 10.1016/j.jmb.2012.06.032

Sällberg, M., Hughes, J., Jones, J., Phillips, T. R., and Milich, D. R. (2002). A malaria vaccine candidate based on a hepatitis b virus core platform. *Intervirology* 45, 350–361. doi: 10.1159/000067928

Schödel, F., Wirtz, R., Peterson, D., Hughes, J., Warren, R., and Sadoff, J. (1994). Immunity to malaria elicited by hybrid hepatitis B virus core particles carrying circumsporozoite protein epitopes. *J. Exp. Med.* 180, 1037–1046. doi: 10.1084/jem.180.3.1037

Schwarz, B., and Douglas, T. (2015). Development of virus-like particles for diagnostic and prophylactic biomedical applications. *Wiley Interdiscip. Rev.*7, 722–735. doi: 10.1002/wnan.1336

Sheng, J., Lei, S., Yuan, L., and Feng, X. (2017). Cell-free protein synthesis of norovirus virus-like particles. *RSC Adv.. R. Soc. Chem.* 7, 28837–28840. doi: 10.1039/c7ra03742b

Smith, M. T., Varner, C. T., Bush, D. B., and Bundy, B. C. (2012). The incorporation of the A2 protein to produce novel Qβ virus-like particles using cell-free protein synthesis. *Biotechnol. Prog.* 28, 549–555. doi: 10.1002/btpr.744

Sogut, I., Hatipoglu, I., Kanbak, G., and Basalp, A. (2002). Purification of the recombinant hepatitis B core antigen, and its potential use for the diagnosis of hepatitis B virus infection. *Biotecnol. Aplicada* 19, 138–142. doi: 10.1089/hyb.2011.0052

Stech, M., Quast, R. B., Sachse, R., Schulze, C., Wüstenhagen, D. A., and Kubick, S. (2014). A continuous-exchange cell-free protein synthesis system based on extracts from cultured insect cells. *PloS One* 9:e96635. doi: 10.1371/journal.pone.0096635

Storni, T., and Bachmann, M. F. (2004). Loading of MHC Class I and II Presentation Pathways by Exogenous Antigens: A Quantitative In Vivo Comparison. *J. Immunol.* 172, 6129–6135. doi: 10.4049/jimmunol.172.10.6129

Tan, Z., Maguire, M. L., Loeb, D. D., and Zlotnick, A. (2013). Genetically altering the thermodynamics and kinetics of hepatitis B virus capsid assembly has profound effects on virus replication in cell culture. *J. Virol.* 87, 3208–3216. doi: 10.1128/JVI.03014-12

Wang, M., Jiang, S., and Wang, Y. (2016). Recent advances in the production of recombinant subunit vaccines in Pichia pastoris. *Bioengineered* 7, 155–165. doi: 10.1080/21655979.2016.1191707

Wang, X., Liu, J., Zheng, Y., Li, J., Wang, H., and Zhou, Y. (2008). An optimized yeast cell-free system: Sufficient for translation of human papillomavirus 58 L1 mRNA and assembly of virus-like particles. *J. Biosci. Bioeng.* 106, 8–15. doi: 10.1263/jbb.106.8

Wetzel, D., Rolf, T., Suckow, M., Kranz, A., Barbin, A., and Chan, J. (2018). Establishment of a yeast-based VLP platform for antigen presentation. *Microb. Fact.* 17:17. doi: 10.1186/s12934-018-0868-0

Wingfield, P. T., Stahl, S. J., Williams, R. W., and Steven, A. C. (1995). Hepatitis core antigen produced in *Escherichia coli*: subunit composition, conformation analysis, and in vitro capsid assembly. *Biochemistry* 34, 4919–4932. doi: 10.1021/bi00015a003

Wnêk, M., Górzny, M. L., Ward, M. B., Wälti, C., Davies, A. G., and Brydson, R. (2013). Fabrication and characterization of gold nanowires templated on virus-like arrays of tobacco mosaic virus coat proteins. *Nanotechnology* 24:025605. doi: 10.1088/0957-4484/24/2/025605

Yang, H.-J. (2005). Expression and immunoactivity of chimeric particulate antigens of receptor binding site-core antigen of hepatitis B virus. *World J. Gastroenterol.* 11:492. doi: 10.3748/wjg.v11.i4.492

Zlotnick, A., Cheng, N., Conway, J. F., Booy, F. P., Steven, A. C., and Stahl, S. J. (1996). Dimorphism of Hepatitis B Virus Capsids Is Strongly Influenced by the C-Terminus of the Capsid Protein. *Biochemistry* 35, 7412–7421. doi: 10.1021/bi9604800

Zlotnick, A., Palmer, I., Kaufman, J. D., Stahl, S. J., Steven, A. C., and Wingfield, P. T. (1999). Separation and crystallization of T = 3 and T = 4 icosahedral complexes of the hepatitis B virus core protein. *Acta Crystallogr. Section D Biol. Crystallogr.* 55, 717–720. doi: 10.1107/s090744499801350x

Conflict of Interest: The authors declare that the research was conducted in the absence of any commercial or financial relationships that could be construed as a potential conflict of interest.

frontiers in Bioengineering and Biotechnology

REVIEW
published: 10 January 2020
doi: 10.3389/fbioe.2019.00446

Synthetic Biology Applied to Carbon Conservative and Carbon Dioxide Recycling Pathways

Jean Marie François[1,2]*, *Cléa Lachaux*[2] *and Nicolas Morin*[1,2]

[1] Toulouse Biotechnology Institute (TBI), Université de Toulouse, CNRS, INRA, INSA, Toulouse, France, [2] Toulouse White Biotechnology Center (TWB), Ramonville-Saint-Agne, France

The global warming conjugated with our reliance to petrol derived processes and products have raised strong concern about the future of our planet, asking urgently to find sustainable substitute solutions to decrease this reliance and annihilate this climate change mainly due to excess of CO_2 emission. In this regard, the exploitation of microorganisms as microbial cell factories able to convert non-edible but renewable carbon sources into biofuels and commodity chemicals appears as an attractive solution. However, there is still a long way to go to make this solution economically viable and to introduce the use of microorganisms as one of the motor of the forthcoming bio-based economy. In this review, we address a scientific issue that must be challenged in order to improve the value of microbial organisms as cell factories. This issue is related to the capability of microbial systems to optimize carbon conservation during their metabolic processes. This initiative, which can be addressed nowadays using the advances in Synthetic Biology, should lead to an increase in products yield per carbon assimilated which is a key performance indice in biotechnological processes, as well as to indirectly contribute to a reduction of CO_2 emission.

Keywords: microbial physiology, metabolic engineering, synthetic biology, carbon dioxide, bio-based products, chemicals

OPEN ACCESS

Edited by:
Jens O. Krömer, Helmholtz Centre for Environmental Research (UFZ), Germany

Reviewed by:
S. Venkata Mohan, Indian Institute of Chemical Technology (CSIR), India
Robert Mans, Delft University of Technology, Netherlands

***Correspondence:**
Jean Marie François
fran_jm@insa-toulouse.fr;
jean.marie-francois@inra.fr

Specialty section:
This article was submitted to Synthetic Biology, a section of the journal Frontiers in Bioengineering and Biotechnology

Received: *27 August 2019*
Accepted: *11 December 2019*
Published: *10 January 2020*

Citation:
François JM, Lachaux C and Morin N (2020) Synthetic Biology Applied to Carbon Conservative and Carbon Dioxide Recycling Pathways. Front. Bioeng. Biotechnol. 7:446. doi: 10.3389/fbioe.2019.00446

INTRODUCTION

The global warming is caused by the anthropogenic emission of greenhouse gases (GHGS), among which emission of carbon dioxide (CO_2) is broadly accepted by the scientific community as the most contributing factor to this climate change. While Nature has been orchestrated with a natural carbon cycle, the industrial revolution that begun in the early 19th century resulted in a rise of CO_2 emission that slowly but definitively exceeded the natural geochemical carbon cycle. According to the Keeling curve, which reports the daily carbon dioxide measurements at Mauna Loa observatory, the CO_2 emission has dramatically increased over the last 50 years, mostly due to deforestation and burning of fossil fuels (https://scripps.ucsd.edu/programs/keelingcurve/). These issues are now becoming critical for the human being, which urged the scientific community to find solutions to decrease our reliance on fossil fuels that should eventually change our life style. Biofuels and more generally biorefinery have emerged as promising solution whose purpose is to exploit microorganisms as cell factories to convert non-edible but renewable carbon sources such as lignocellulosic sugars into bioethanol as alternative energy (Duwe et al., 2019; Rosales-Calderon and Arantes, 2019) or into commodity chemicals that can replace those obtained from petrochemistry (Clark et al., 2012; Chen and Dou, 2016; Singhvi and Gokhale, 2019). In spite

of the apparent sustainability of this solution, the use of chemoorganotrophic microbes such as yeast or *E. coli* present a caveat, as CO_2 is released during the process of carbon metabolism (**Figure 1**). A wonderful alternative would be to exploit autotrophic microorganisms such as acetogenic anaerobic bacteria or microalgae (Schiel-Bengelsdorf and Durre, 2012; Scaife et al., 2015) as they have the capability to capture atmospheric CO_2. However, these biological systems are at the moment industrially inefficient, due to their slow growth, poor productivity and low energy conversion yield (Claassens, 2017). The purpose of this mini-review is to expose and discuss original strategies that have emerged recently and that have employed synthetic biology tools to rewire the carbon metabolism of heterotrophic microorganisms to achieve maximal carbon conservation during their metabolism. Basically, this endeavor can be reached by either redesigning carbon metabolism network to optimize carbon conservation or recapturing carbon loss using CO_2 fixing or carboxylating systems. Autotrophic CO_2 fixation by reductive pentose phosphate cycle (rPP also known as Calvin-Benson cycle) as well as other natural metabolic pathways that perform carbon fixation including reductive TCA cycle, 3-hydroxypropionate cycle, 3-hydroxypropionate/4-hydroxybutyrate cycle, and dicarboxylate/4-hydroxybutyrate cycle are not considered in this mini-review, since they have been extensively reviewed in previous excellent papers (Berg et al., 2010; Fuchs and Berg, 2014; Erb and Zarzycki, 2018).

REWIRING CENTRAL CARBON METABOLISM OF HETEROTROPHIC ORGANISMS FOR CARBON CONSERVATION

Complete Carbon Conservation of Sugar Metabolism by the Non-oxidative Glycolysis Pathway

Glycolysis or the Embden-Meyerhof-Parnas pathway (EMP) is a fundamental metabolic pathway in most living systems that decomposes sugars into pyruvate and recovers energy of this breakdown into ATP and reducing equivalents NADH. To fuel the cell with some essential anabolic precursors, pyruvate has to be decarboxylated into acetyl-CoA. This decarboxylation step releases carbon dioxide in the environment, resulting in 33% loss of carbon yield. This wasted CO_2 may have major impact on the overall economy of bio-based products derived from fermentable carbon sources. This 33% carbon loss due to the decarboxylation of pyruvate has been challenged recently by Liao's group (Bogorad et al., 2013) who constructed a synthetic pathway termed "the non-oxidative glycolysis (NOG)" that can overcome this carbon loss, leading to a conversion of one mole of glucose to 3 moles of acetyl-moieties (**Figure 1** and **Table 1** for the stoichiometric equation). The logic of NOG relies on the phosphorylating cleavage of sugar phosphates

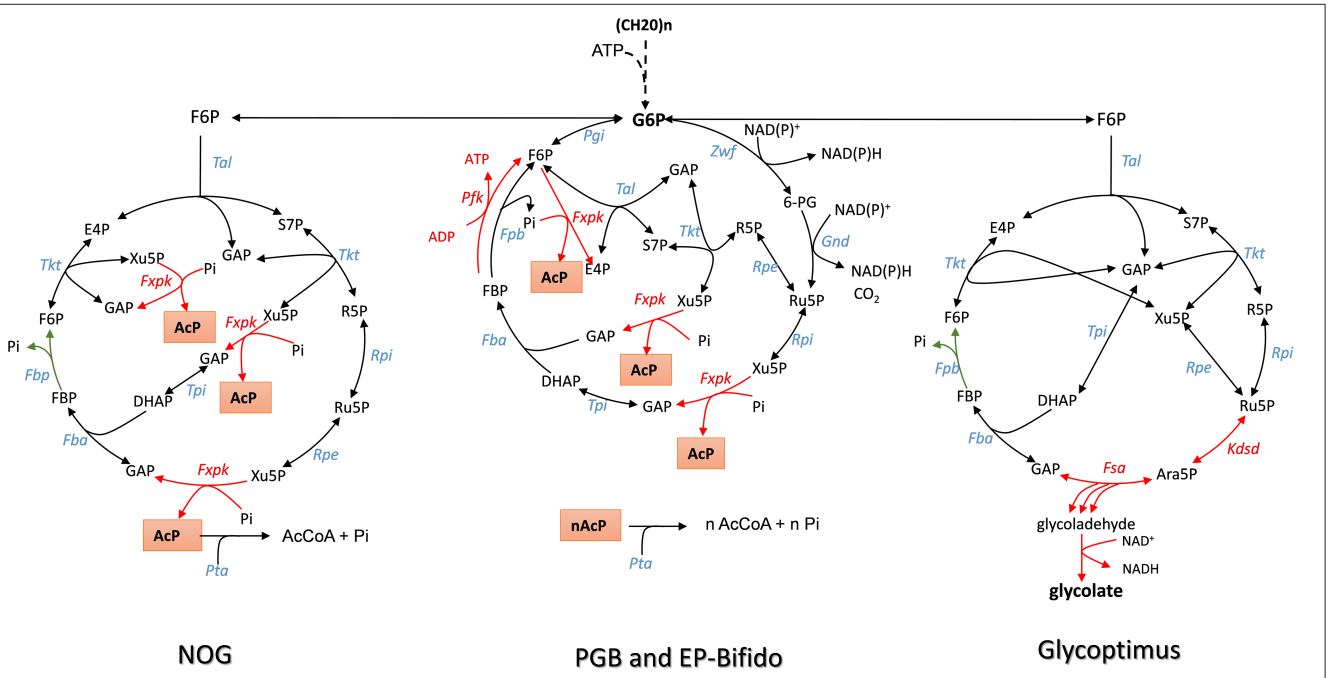

FIGURE 1 | The scheme of non–oxidative glycolysis (NOG), Embden-Pentose-Bifido (EP-Bifido), and Glycoptimus synthetic pathways. Enzymes abbreviation are Fxpk, F6P/Xu5P-phosphoketolase; Tal, transaldolase; Tkt, transketolase; Fbp, fructose-1,6- bisphosphatase; Fba, fructose1,6 bisphosphate aldolase; tpi, triose phosphate isomerase; Rpe, ribulose 5-P epimerase; Rpi, ribose 5-P isomerase; Kdsd, arabinose-5-P isomerase; Fsa, fructose-6P aldolase; Alda, glycolaldehyde dehydrogenase. Metabolites: F6P, fructose-6P; PEP, phosphoenolpyruvate; Pyr, pyruvate; E4P, erythrose-4P; S7P, sedoheptulose-7P; R5P, ribose-5P; Ru5P, ribulose-5P; X5P, xylulose-5P; GAP, glyceraldehyde-3P; DHAP, dihydroxyacetone-P; FBP, fructose-1,6-bisphosphate; AcP, acetyl-Pi, AcCoA, acetyl-CoA.

TABLE 1 | Stoichiometric equation of carbon conservative pathways described in **Figures 1–5**, and their calculated thermodynamic value*.

Pathway name	Equation	$\Delta_r G'^{O*}$ (KJ/mole)
NOG	Glucose + 1 ATP + 3 CoaSH -> 3 acetyl-CoA + 1 ADP + 1 Pi	−193.6
PGB	Glucose + 4 $NAD(P)^+$ + 2 CoASH -> 2 acetyl-CoA + $2CO_2$ + 4 NAD(P)H + 4 H^+	−204
EP-Bifido	Glucose + 2 $NAD(P)^+$ + 1 ATP + 2.5 CoASH + H_2O -> 2.5 acetyl-CoA + 1 CO_2 + 1 ADP + 1 Pi + 2 NAD(P)H + 2H^+	−180.6
rGS	Glucose + 1 NAD^+ + 1 ADP + 1 QH_2 + 1 Pi + 3 CoASH -> 3 acetyl-CoA + 1 NADH + 1 H+ + 1 ATP + 1 Quinone	−229
MCG	Glucose + 1 ADP + 1 Pi + 3 CoaSH -> 3 acetyl-CoA + 1 ATP + H_2O	−193.6
Glycoptimus	Glucose + 1 ATP + 3 NAD^+ + H_2O -> 3 glycolic acid + 1 ADP + 1 Pi + 3 NADH + 3 H^+	−139.6
MOG	Glucose + 2 HCO_3^- + 3 ATP + 3 H_2O -> 2 glyoxylate + 2 acetate + 3ADP +3 Pi	−233
Mser	Methanol + CO_2 + $2H_2O$ + 4 ATP + CoASH + NADP(H) + H^+ -> Acetyl-CoA + 4ADP + 4 Pi + $NAD(P)^+$	−153
HOB	Tetrahydrofolate+ 2 NAD(P)H + HCo_3^- + $4H_2O$ + 3ATP -> 5′-10-methylene tetrahydrofolate + 3 ADP + 3 Pi + 2 $NAD(P)^+$	−63.5

*Gibbs energy value of the reaction was calculated using eQuilibrator (at http://equilibrator.weizmann.ac.il/).

by a phosphoketolase (Fxpk), which, combined with a carbon rearrangement cycles, creates a cyclic pathway with F6P as the input molecule (**Figure 1**). The irreversibility of this pathway is ensured by the phosphoketolase reaction that cleaves Xu5P into glyceraldehyde-3-P (GAP) and AcP and by the fructose-1,6-bisphosphatase reaction (Fbp) which recycles back F6P from FBP. The carbon rearrangement also involves transaldolase (Tal) and transketolase (Tkt) and the net result of this FBP-dependent cycle is the irreversible formation of three acetyl-phosphate (AcP) molecules from one F6P molecule. As phosphoketolase also displays phosphorylating cleavage activity on F6P (Tittmann, 2014), cleaving the latter molecule into AcP and E4P, a sedoheptulose bisphosphate (SBP)-dependent network can be conceived yielding to the same solution. In this case, this cycle will not need transaldolase (*tal* gene) but will require a SBP-aldolase to condense DHAP and E4P into SBP, and a sedoheptulose phosphatase (Sbp) to recycle back S7P. Such cycle can potentially exist since Sbp is essential in the Calvin-Benson cycle, and has been identified in yeast as being implicated in ribogenesis (Clasquin et al., 2011) and in methylotrophic bacteria where it participates in the ribulose 5-monophosphate (RuMP) cycle (Stolzenberger et al., 2013).

In their Nature report, Liao and coworkers succeeded in demonstrating the *in vitro* and *in vivo* functioning of NOG (Bogorad et al., 2013). The *in vitro* system required the core of eight enzymes, which were either purchased when commercially available or produced by expression in *E. coli*. This was the case for phosphoketolase which is encoded by f*xpk* gene in *Bifidobacterium adolescensis* (Yin et al., 2005) and for some enzymes of the pentose phosphate pathway (PPP). In accordance with the pathway model, F6P initially added at 10 mM was readily and completely converted into 30 mM AcP. To validate the *in vivo* pathway, they chose to use xylose as the initial carbon substrate, as the phosphotransferase-dependent uptake and phosphorylation of glucose is not compatible with NOG and also because xylose does not cause repression of the *fbp* encoding fructose-1,6-bisphosphatase (Sedivy et al., 1984), which is needed together with the overexpression of *fxpk*. Other enzymes of the NOG pathway were natively expressed on a high copy plasmid, including *pta* and *ackA* which codes for phosphate acetyl transferase and acetate kinase, respectively, and which convert AcP into acetate. In addition, competitive fermentative pathways were disabled (i.e., deletion of *ldhA*, *pflB*, *adhE,* and *frdBC* to prevent production of lactate, formate, ethanol, and succinate) and the experiment was carried out under anaerobic condition to avoid further oxidation of acetate in the TCA cycle. Under this condition, 2.2 moles of acetate per mole of xylose were produced by the engineered *E. coli* equipped with the NOG pathway. In theory, the maximal yield that can be obtained by this conversion process should be 2.5. This yield termed the thermodynamic feasibility "Y^E" can be calculated as the ratio between the degree of reduction of the substrate γ_s to that of the product γ_p. Y^E is independent of the stoichiometry of the pathway and provides yield limits of the thermochemical process whatsoever the followed pathway or the catalyst used (Dugar and Stephanopoulos, 2011). In this case, Y^E of acetate from xylose ($\gamma_s = 20$) is 2.5 since γ_p of acetate $= 6$, whereas the stoichiometric yield "Y^{st}" is 1,66. Therefore, the efficiency of the NOG pathway which can be calculated as the ratio of Y^E to Y^{st} is 50% better than the classical EMP pathway. The fact that the *in vivo* conversion of xylose into acetate by the engineered *E. coli* expressing the NOG pathway only reached 88% of Y^E was due to some by-products formation, notably succinate.

According to the stoichiometric equation (**Table 1**), each mole of acetyl-CoA produced from glucose by NOG can be converted into acetate, which is accompanied by the production of one ATP. Therefore, a net balance of 2 ATP and 3 acetate molecules can be obtained from glucose by NOG. However, this pathway is not compatible for growth as it can generate neither the 12 metabolic building blocks nor the reducing power needed for synthetizing all cellular constituents. These features may explain why NOG has not been retained as a viable pathway during evolution. Nevertheless, in a second seminal paper published in PNAS, Liao's group succeeded in evolving a *E. coli* strain that could grow while relying on NOG for carbon catabolism (Lin et al., 2018). To achieve this challenge, they blocked glycolysis at the level of glyceraldehyde-3-P dehydrogenase and phosphoglycerate kinase by deleting the corresponding genes as well as the methylglyoxal and the Entner-Doudoroff pathways to prevent bypass of glucose into pyruvate. The glyoxylate shunt and gluconeogenesis was then upregulated to enable conversion of acetyl-CoA to metabolic intermediates required for growth,

whereas the reducing power and ATP were derived from TCA, which could be done only under aerobic condition. Since these genetic interventions could potentially generate futile cycles, notably at the level of F6P/FBP and pyruvate/ acetate, *pfkA* gene encoding the major phosphofructokinase and *poxB* encoding pyruvate oxidase were deleted. The final strain termed PHL13 contained 10 genes deletion and the 2 overexpressed genes *pck* and *fxpk* encoding PEP carboxykinase and phosphoketolase. This engineered strain was still unable to grow on glucose unless acetate was present. It was therefore subjected to evolution by serial transfer to selective media and meanwhile, a quest for the limiting enzymes in the NOG cycle was carried out by devising a clever whole-pathway assay in crude extract of the engineered strains. Practically, the assay was to measure the rate of AcP production from F6P in a crude extract augmented with a mix of all purified NOG enzymes and determine the effect of removing a particular enzyme from this mix on AcP production. This study identified phosphoketolase as the most limiting enzyme followed by transketolase and transaldolase. Therefore, these genes were expressed on a high copy plasmid that also contained genes encoding the glucose permease (*glf*) from *Zymomonas mobilis*, the glucokinase (*glk*), and a AMP-insensitive PEP-activated FBPase (*glpX*) from *E. coli* (Donahue et al., 2000). Strain PHL13 that carried out this constructed plasmid was then subjected to further adaptive laboratory evolution (Mattanovich et al., 2014; Jang et al., 2019) to get rid of its dependence to acetate and rely only on glucose for growth. After further improvement of transketolase activity by the whole-pathway assay, these authors could isolate a slow growth colony NOG21 on glucose minimal medium, which was further evolved to yield a faster growing colony NOG26. Use of ^{13}C glucose labeled on C3 and C4 confirmed that the growth was accomplished by NOG since acetate was labeled on its C1 and C2, as expected. Genome sequencing of this evolved strain unexpectedly unraveled a reduced expression of *fxpk* and *pck*. This result could be explained by a fitness response of the strain to the growth condition in order to avoid "kinetic traps" that would cause imbalance of the metabolic flux, as for instance by draining out all oxaloacetate from the TCA cycle or Xu5P from the NOG cycle. Other mutations were identified in the metabolic network such as a deletion of *pykF* encoding the major pyruvate kinase or mutation in *pts* genes, which likely reduced the PEP dependent phosphorylation of glucose, leaving thus more PEP for gluconeogenesis. All these genomic modifications likely resulted in a fine-tuning of pathway regulation that would be difficult to predict *a priori*.

From a biotechnological perspective, the potential of NOG is very limited unless this pathway is coupled with another to make compounds other than acetate. An example would be to establish a NOG- based reductive fermentation in which additional reducing agents such as molecular hydrogen is provided together with sugars. In this condition, 3 moles ethanol can be produced per mole of glucose which would increase by 50% the maximal yield from natural sugar fermentation pathway. The challenge here will be to express hydrogenase to allow the input of additional reducing equivalents. Another practical use of NOG shall be to combine with the Calvin-Benson-Bassham (CBB) cycle (Calvin, 1962) for the biosynthesis of acetyl-coA derived products, such as 1-butanol and fatty acids by autotrophic organisms (Liu et al., 2011). This metabolic rewiring could represent a 50% increase of CO_2 into acetyl-CoA over the native pathway, concomitantly reducing the requirement of RuBisCO activity to reach the same carbon yield (Tcherkez et al., 2006).

The Pentose-Bifido-Glycolysis Cycling Pathway to Solve the Lack of Reducing Power in NOG

A serious drawback of the NOG pathway is its inability to generate reducing power that is essential for the biosynthesis of added-value molecules from acetyl-CoA such as isoprene, fatty acids or polyhydroxybutyrate. A first approach to overcome this limitation was proposed by Opgenorth et al. (2016) who designed a synthetic *in vitro* pathway termed "Pentose-Bifido-Glycolysis" cycle (PBG) for the synthetic conversion of glucose into PHB via acetyl-CoA. This PBG cycle is divided in three metabolic parts. The first part is the phosphorylation of glucose into G6P which enters the cycle through the oxidative branch of the PPP and breaks down into Xu5P while producing NADPH. In a second phase, Xu5P is split into AcP and GAP by the phosphoketolase Fxpk. While AcP can be converted into acetyl-CoA by the CoA-phosphotransferase enzyme (Pta), GAP is recycled in a third phase into G6P. This occurs by the condensation of GAP and DHAP into FBP by the aldolase Fba, followed by a process involving a unique phosphofructokinase that catalyzes the ATP-dependent formation of F6P from FBP. At variance to the traditional phosphofructo-1-kinase reaction (Uyeda, 1979), this *E. coli* PFK encoded by *pfkB* was found to work reversibly and thus to regenerate ATP needed for glucose phosphorylation. This last phase enables to complete the cycle in ATP neutral manner. Accordingly, for each glucose entering the PBG cycle, two moles of acetyl-CoA, 2 moles of CO_2 and 4 moles of NADPH is produced at zero cost of ATP (**Table 1**). However, there are two caveats with this synthetic pathway design. First the phosphoketolase Fxpk can also split F6P into E4P and AcP, which could abrogate the functioning of the cycle. Secondly, there is large excess of NADPH, as the synthesis of one PHB monomer only requires one NADPH, which therefore could lead to a feedback inhibition of the pathway. To solve the first issue, these authors (Opgenorth et al., 2016) complemented the pathway with PPP enzymes, namely transketolase (Tkt), transaldolase (Tal) and ribose-5-P isomerase (Rpi) in order to recycle E4P into the cycle (**Figure 2B**). The second problem was disentangled by introducing a "NAD(P)H purge valve" to regulate the build-up of NADPH. The outcome of this sophisticated purge valve is to uncouple carbon flux from NADPH production enabling a non-stoichiometric pathway production of NADPH. The construction of this purge valve requires the presence of NAD^+-dependent glucose-6-P dehydrogenase (Zwf) and NAD^+-dependent phosphogluconate dehydrogenase (Gnd) enzymes together with their native $NADP^+$ dependent counterparts and a H_2O-forming NADH

oxidase (NoxE). While NADPH is reoxidized during PHB production, high level of NADPH would not penalize the cycle since it is taken over by the NAD^+-dependent enzymes which continue to provide the precursor acetyl-CoA while NADH is readily reoxidized by NoxE. This original cell-free system production of bio-based chemicals from glucose turned out to be quite efficient as the authors reported a maximum productivity of the PBG cycle of 0.7 g PHB/L/h with a yield of 90%. There is great hope in developing such a process at an industrial scale since cell-free system can overcome common problems afflicting *in vivo* biological systems, such as building-up toxic intermediates, low productivities due to competing pathways and undesirable byproducts (Dudley et al., 2015). However, cell-free systems require to solve major technical and economic problems including production, purification, and stability of enzymes or their potential recycling.

Another approach to disentangle the failure of the NOG pathway to generate redox power was proposed by Wang et al. (2019) through the *in vivo* construction of an "EP-Bifido" pathway. This synthetic pathway is very similar to PGB as it combines EMP and PPP pathway with the expression of phosphoketolase enzymes acting on F6P and Xu5P, but it does not employ PFK reaction to regenerate the ATP that is needed to phosphorylate glucose (**Figure 2B)**. As indicated in **Figure 1**, the major difference between NOG and the EP-Bifido is that the latter implicates the oxidative portion of the PPP, which leads to the production of NADPH. However, this metabolic process occurs at the expense of one CO_2. The remaining reaction steps share those of the NOG with notably Fbp that provides the second driving force and recycles back F6P into the cycle. In theory, this pathway design should yield 2.5 acetyl CoA per mole glucose with two moles of NAD(P)H at the cost of 1 ATP (see **Table 1**). However, it may have the capacity to achieve an even higher yield of acetyl-CoA, as this will depend on favoring G6P into PPP with respect to EMP. In theory, 2.66 moles of acetyl-CoA could be produced from 1 glucose if 66% of G6P goes through PPP. To create this EP-Bifido pathway and expect to attain this optimal carbon yield, the following genetic modifications were carried out in *E. coli*. On the one hand, *zwf* and *gnd* were overexpressed to direct glucose into the PPP together with *fxpk* encoding F6P/Xu5P phosphoketolase from *Bifidus adolescentis*. On the other hand, the engineered strain was deleted for *pfkA* encoding the major phosphofructokinase, *edd/eda* encoding enzymes of the Entner-Doudoroff and *ackA* encoding acetate kinase to avoid, respectively, ATP wasteful by FBP/F6Pcycle, the production of pyruvate that could bypass the EP-Bifido pathway and the loss of AcP into acetate. Altogether, the engineered *E. coli* strain equipped with the EF-Bifido pathway grew 3 times slower than the wild type strain, did not produce any acetate and released 50 to 70% less CO_2 than the wild type strain. The performance of the EF-Bifido pathway in acyl-CoA derived polydroxybutyrate (PHB), fatty acids or mevalonate was moreover demonstrated by showing that the yield of these products was improved by 145, 56, and 48% respectively in engineered strains as compared to the control strains (Wang et al., 2019), arguing for a biotechnological relevance of reengineering the carbon metabolism of *E. coli* with this pathway.

The Glycoptimus Pathway to Convert Sugars Into Glycolic Acid Without Carbon Loss

While the refactoring of central carbon metabolic pathway was devoted to maximal acetyl-moieties from glucose, the glycoptimus pathway deals with a rewiring of the carbon metabolism to achieve maximal yield of glycolic acid (GA) from C5 and C6 sugars without carbon loss (**Figure 1**). According to thermodynamic calculation (Dugar and Stephanopoulos, 2011), the Y^E of glycolic acid ($\gamma_p = 6$) from glucose ($\gamma s = 24$) or from pentose ($\gamma_p = 20$) should be 4 and 3.3, respectively, whereas the maximal yield Y^S based on the pathway stoichiometry is 2 from glucose and 1.66 from pentose (Dolan and Welch, 2018). Using the natural pathway, no <13 genetic modifications were executed to achieve a production of 52 g/L glycolate from glucose at a yield of 50 % of the Y^{st} (Soucaille, 2007). Further genetic modifications were proposed by Deng et al. (2018), by combining Dahms pathway with the glyoxylate shunt, enabling a yield close to 90% of the stoichiometric yield. The problem to reach the thermodynamic Y^E lies at two levels. A first one is to avoid the loss of CO_2 at the pyruvate decarboxylation step, while the second is more challenging as it requires to capture one carbon mole as CO_2. Since direct CO_2 fixation by heterotrophic system is still very complicated as experienced by Milo and coworkers in *E. coli* (Antonovsky et al., 2016), we rewired the carbon central metabolism of *E. coli* in order to overcome the loss of CO_2 during the conversion of sugars into glycolic acid. Theoretically, the proposed pathway should lead to a maximal yield of 3 GA per glucose (**Table 1**) or 2.5 GA per pentose, which is 50% higher than obtained by the natural pathway (**Figure 1**). This pathway design implicates the overexpression of *kdsD* and *fsaA* of *E. coli* which codes for an arabinose-5P (Ara5P) isomerase and a class I aldolase, respectively. Even though these two genes are endogenous to *E. coli*, this pathway is not natural in this bacteria because the Kdsd enzyme is naturally implicated in the synthesis of 2-keto-3-deoxy-octulosonate (KDO), a constituent of the outer member of cell wall lipopolysaccharide (Lim and Cohen, 1966), whereas Fsa has been initially reported as a F6P aldolase that catalyzes the aldol cleavage of F6P into dihydroxyacetone (DHA) and glyceraldehyde-3-P (GAP) (Schurmann and Sprenger, 2001). The bacterium *E. coli* also harbors an ortholog of *fsaA* termed *talC* or *fsaB* (Reizer et al., 1995) but the physiological function of these two genes is still completely unknown. In particular they are not expressed under standard—LB- culture condition (Schurmann and Sprenger, 2001). Nevertheless, Clapes' team demonstrated the remarkable originality of Fsa enzyme as a unique biocatalyst for asymmetric cross-aldol addition of glycoladehyde. They also reported that Fsa can cleave Ara5P into glycolaldehyde and GAP with a 10 fold higher affinity than F6P (Garrabou et al., 2009), which was confirmed in Lachaux et al. (2019). Therefore, the consecutive action of Kdsd and Fsa leads to

the conversion of pentose phosphate intermediate Ru5P into glycolaldehyde and GAP (**Figure 1**). While glycolaldehyde can be oxidized into glycolic acid by an aldehyde dehydrogenase encoded by *aldA* (Caballero et al., 1983), GAP is recycled into Ru5P through the non-oxidative pentose phosphate pathway (**Figure 1**). This cycling scheme may result in theory in the production of 3 moles of GA per mole of glucose, only if the lower part of the glycolysis at the level of GAP is blocked. It also cost one ATP but generates 3 moles of NADH (**Table 1**) that needs to be reoxidized to allow the continuous functioning of the cycle. The reoxidation of NADH requires an active respiratory chain which is coupled to the synthesis of ATP. This ATP provision will be useful to regenerate ATP used in glucose phosphorylation, for uptake of sugars as well as for cellular maintenance. The *in vitro* and *in vivo* function of the glycoptimus pathway was validated although the yield of GA from glucose and xylose did not exceed 30% of the maximal yield expected. Possible explanation of this poor efficiency of the pathway could be that (i) the blockage of the lower part of glycolysis by deletion of *gapA* encoding GADPH was detrimental for cell viability; (ii) all competitive pathways using the same intermediaries have not yet been dismantled in the engineered strains; and (iii) the carbon flux in the *kdsD-fsaA* pathway is not optimized yet (Lachaux et al., 2019). Finally, the reoxidation of NADH is likely to generate more ATP than needed for the functioning of the glycoptimus cycle, which may result in feedback inhibition due to accumulation of intermediates and eventually depletion of cofactors. Solving these various issues together with the development of an appropriate fermentation practice should lead to an economically viable process of glycolic acid synthesis.

The Methanol Condensation Cycle for Methanol Assimilation Without Carbon Loss

Abundant carbon sources other than sugars, such as methanol can be also exploited for the biosynthesis of added-value molecules. However, assimilation of these alternative resources also poses problem with carbon conversation. As an example, the ribulose-5- monophosphate pathway (RuMP) that is present in methylotrophic bacteria and in some yeasts such as *Pichia pastoris* (Yurimoto et al., 2002; Muller et al., 2015; Russmayer et al., 2015) is one of the three natural methanol assimilatory pathways known so far (Zhang et al., 2017) which can produce one acetyl-CoA from three formaldehydes at the expense of the decarboxylation of pyruvate. Liao's team (Bogorad et al., 2014) showed that the decarboxylation step could be avoided by combining the RuMP with phosphoketolase enzymes, leading to the production of acetyl-CoA from 2 formaldehydes through a methanol condensation cycle (MCC) as depicted in **Figure 2**. However, this MCC can only work if the thermodynamically unfavorable NAD^+-dependent methanol dehydrogenase is coupled to the reoxidation of NADH into reduced products such as ethanol, n-butanol or even higher alcohols (Bogorad et al., 2014). Remarkably, the MCC reaction is completely redox balanced and independent of ATP, and thus does not involve the phosphofructokinase enzyme of the RuMP, as well as the triose phosphate isomerase (Tpi), fructose 1,6-bisphosphate aldolase (Fba) and fructose-1,6-bisphosphatase (Fbp) of the NOG pathway. This property has been exploited to demonstrate the *in vitro* functioning of MCC to the production of ethanol or n-butanol. Therefore, a cell-free system could be potentially exploitable for larger scale production of higher alcohols with maximal yield and at high productivity if conditions for enzymes and intermediates stability are assured. In addition, this *in vitro* study pointed out the role of phosphoketolase in the robustness of the MCC, showing that its optimal running requires well-balanced levels of this enzyme with respect to the others, as a low or excessive phosphoketolase activity could trigger kinetic traps that significantly diminish rate of end-product production, due to either accumulation or depletion of intermediates metabolites in the cycle.

CARBON CONSERVATION SYNTHETIC PATHWAYS BUILDING ON CARBOXYLATING REACTIONS

Reversal of the Glyoxylate Shunt to Build C2 Compounds With Maximal Carbon Conservation

The TCA or citric acid cycle elucidated by Krebs and Johnsson in 1937 (see Krebs and Johnson, 1980 for an historical perspective or Akram, 2014 for a recent review of TCA role in intermediary metabolism) is considered as the central metabolic hub of the cell whose amphibolic nature provides intermediates for numerous metabolic functions. This cycle generates energy and reducing power needed for anabolic activities of the cell at the expense of complete oxidation of pyruvate into carbon dioxide. The glyoxylate shunt, discovered by Krebs and Kornberg in 1957 (see Dolan and Welch, 2018) for an excellent review on this pathway) avoids the decarboxylation steps of the TCA cycle and allows acetyl-CoA to be converted into a C4 carbon without carbon loss. This shunt is therefore key for organisms that grow on C2 to C4 carbon such as acetate, glycerol and malate, or on ketogenic amino acids (i.e., aspartate, glutamate). The glyoxylate shunt takes carbon away from the TCA cycle at the level of isocitrate, just before the commencement of the first decarboxylation step. This requires two specific enzymes that are the hallmark of this cycle: isocitrate lyase that cleaves isocitrate into succinate (C4) and glyoxylate (C2), and malate synthase, which condenses glyoxylate with acetyl-CoA to malate. Due to the large negative Gibbs value of the malate synthase reaction ($\Delta rG'^0 = -44$ kJ/mol), the glyoxylate cycle can only run in the acetyl-CoA condensation. However, running the cycle clockwise directly could be beneficial to supply acetyl-CoA from sugars by bypassing the decarboxylation step of pyruvate. As illustrated in **Figure 3**, a reversal of the glyoxylate shunt (rGS) in which the thermodynamically favorable PEP carboxylating reaction is implemented could generate 2 acetyl-CoA from TCA intermediates. This challenge was raised by the Liao' group according to the following strategy (Mainguet et al., 2013). At first, they demonstrated that isocitrate lyase

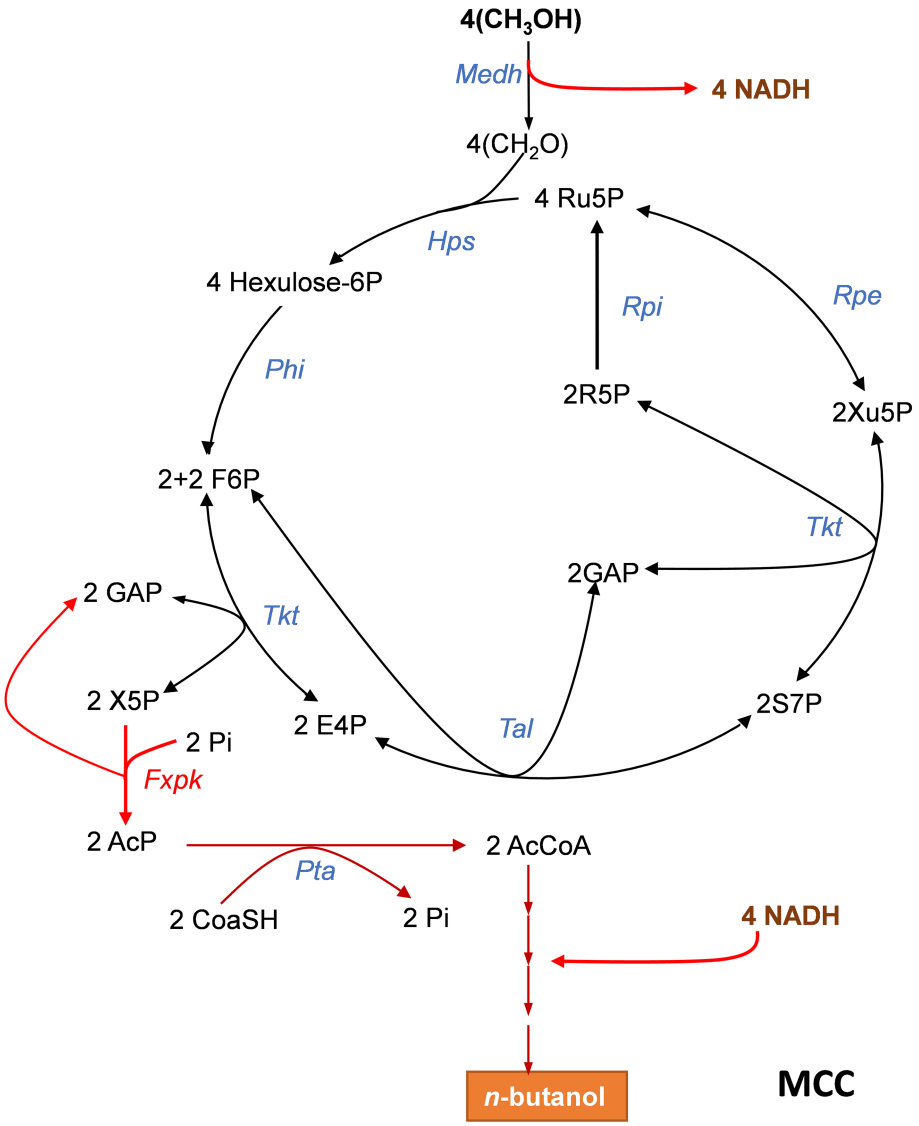

FIGURE 2 | The methanol condensation cycle (MCC) for assimilation of methanol into higher alcohol with maximal carbon conservation. The MCC is a combination of the RuMP with part of the NOG allowing to avoid pyruvate decarboxylation and to bypass ATP dependency. It results in the net production of acetyl-CoA (AcCoA) from 2 methanol. Here, it is represented the metabolic pathway leading to the production of n-butanol which requires 4 methanol. Enzymes abbreviations are: Medh, NAD^+-dependent methanol dehydrogenase; Hps, hexulose-6P synthase; Phi, phosphohexuloseisomerase; Tkt, transketolase, Fxkp, F6P/Xu5P phosphoketolase; Tal, transaldolase; Rpe, ribulose-5-P epimerase; Rpi, ribose-5-isomerase. Abbreviation for metabolites as in **Figure 1**.

(ICL) is reversible *in vivo* by showing that a *E. coli* strain made auxotroph for glutamate (glu^- strain) by deletion of *gltA* and *prpC* encoding citrate synthase was able to grow on glucose mineral medium supplemented with glyoxylate and succinate. In contrast, this glu^- strain was unable to recover growth when glyoxylate was replaced by malate, even if *dctA* gene encoding a non-glucose repressible malate importer from *B. subtilis* had been overexpressed. These results confirmed that malate synthase reaction was not reversible *in vivo*. To get around this obstacle, they wished to express an ATP-dependent malate thiokinase (Mtk) encoded by *mtkA* and *mtkB* from *Methylobacterium extorquens*. In this methanotrophic bacterium, this enzyme contributes to C1 assimilation through the serine cycle (Fei et al., 2014). This reaction step is then followed by the cleavage of malyl-CoA into glyoxylate and acetyl-CoA by a malyl-coA lyase (Mcl) naturally present in microorganisms that use the 3-hydroxypropionate cycle for autotrophic carbon dioxide fixation (Berg et al., 2007). Unfortunately, the expression of *mtkAB* and *mcl* from *Methylobacterium extorquens* expressed in a glu^- strain did not rescue growth on malate and succinate likely because Mtk was not functional. They overcame this problem by screening various putative malate thiokinase and discovered that *sucCD-2* from *Methylococcus capsulatus* annotated as encoding a succinyl-CoA synthetase (Ward et al., 2004) had very good

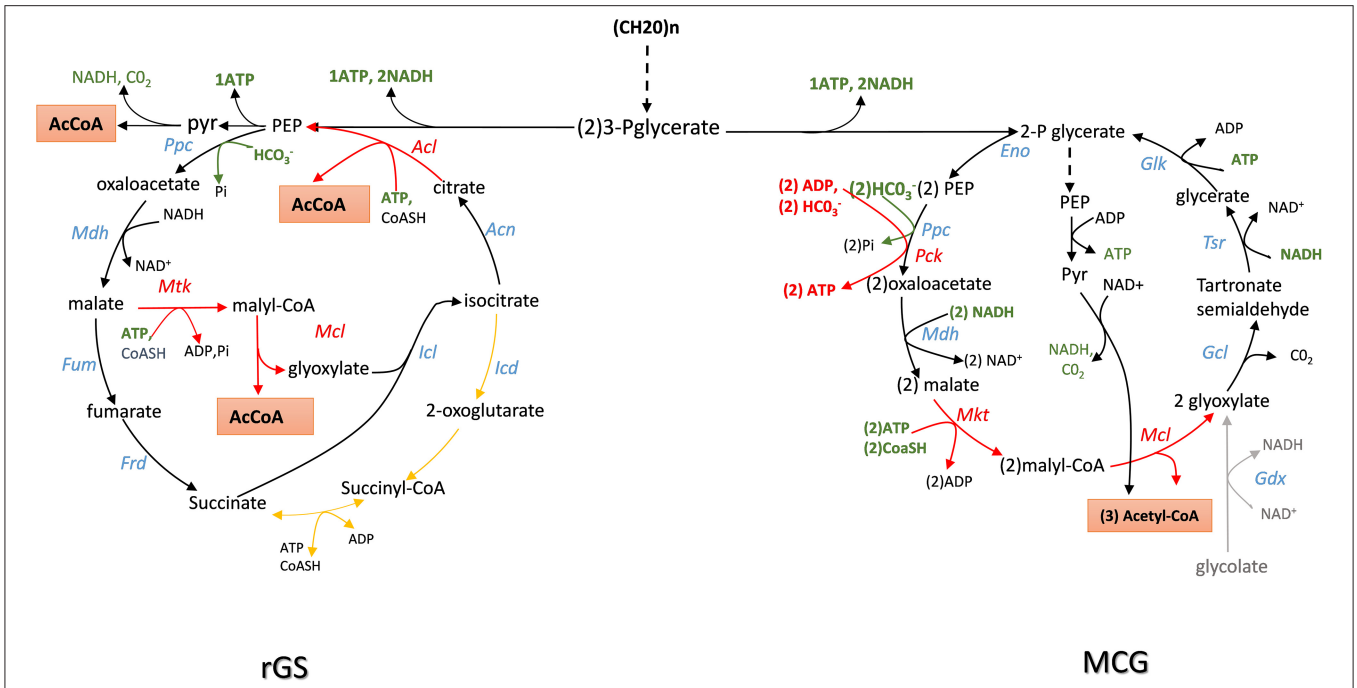

FIGURE 3 | Scheme of the reversal of glyxoylate shunt (rGS) and maly-CoA Glycerate (MGC) cycling pathway for the production of acetyl-CoA from sugars with maximal carbon conservation. Enzymes abbreviation are: Ppc, PEP carboxylase; Mdh, malate dehydrogenase; Fum, fumarase; Frd, fumarate reductase; AceA, isocitrate lyase; Aco, aconitase; Acl, acyl-CoA lyase: Mtk, malate thiokinase; Mcl, malyl-CoA lyase; Gdh, glycolate dehydrogenase; Gcl, glyoxylate carboxyligase; Tsr, tartronate semialdehyde reductase; Glk, glycerate kinase; Eno, enolase.

Mtk activity. Expression of *sucCD-2* gene with *mcl* restored the capacity of growth of a glu$^-$ strain on glucose supplemented with malate and succinate. The second important action was to recycle OAA from isocitrate that is accompanied by the release of a second molecule of acetyl-coA. This involves to reverse the aconitase and the citrate synthase reaction. While the first one is readily reversible, the conversion of citrate to OAA by citrate synthase is strongly unfavorable ($\Delta rG'^{\circ} \sim +34$ KJ/mol). It can nevertheless be obtained by expressing an ATP-dependent citrate lyase encoded by *acl* which is present in several eukaryotic cells and in some archeabacteria (Fatland et al., 2000; Verschueren et al., 2019). The *in vivo* functionality of the Acl reaction was tested in *E. coli* strain made auxotroph to aspartate (asp$^-$ strain) by deleting genes encoding all enzymes that produce its precursor OAA (ie *ppc*, *mdh*, *mqo*), as well as citrate synthase and citrate lyase (*gltA* and *citE*). As expected, the asp$^-$ strain recovered growth on a glucose minimal medium when supplemented with citrate. Although the thermodynamically unfavorable reactions were solved to potentially create a reverse glyoxylate cycle, it was also necessary to remove isocitrate dehydrogenase (*icd*) to avoid siphoning isocitrate obtained by condensation of glyoxylate and succinate into α-ketoglutarate. Then, the assembly of the complete pathway in asp$^-$ strain which was otherwise deleted for *mdh*, *mqo*, *ppc*, *icd*, and *aceB* consisted in the overexpression of Bs*dctA*, Mc*succD-2*, Rs*mcl*, and Ct*acl* genes. This strain was shown to grow on glucose supplemented with malate and succinate, demonstrating the *in vivo* function of this rGS. Until now, the complete demonstration of the "*in vivo*" reversal of the glyoxylate cycle has not been fully demonstrated. It will require to connect OAA to malate which can be easily carried out by the reversible NAD$^+$-dependent malate dehydrogenase encoded by *mdh*. However, cycling malate shall require also expression of a fumarase (Fum) and a fumarate reductase (Frd), both enzymes being preferentially active under anaerobic conditions (Lin and Iuchi, 1991; Tseng, 1997).

In theory, the integration of rGS with the central carbon metabolic pathway via the PEP carboxylase encoded by *ppc* could lead to the conversion of one mole glucose into 3 moles of acetyl-CoA, thus achieving a 50% yield increase over the native pathway. Contrary to the NOG pathway that converts glucose to 3 AcCOA at the expense of one ATP, the conversion of glucose into AcCOA by the rGS generates one extra ATP. In addition, while NOG is redox neutral, the rGS pathway results in the net production of one NADH and one reduced quinone per glucose (**Table 1**). This indicates that rGS is more energetically efficient than NOG which could be an advantage with respect to the production of acetyl-CoA derived products such as isoprenoids, fatty acids, long chain alcohols as they required reduced power and ATP (Tabata and Hashimoto, 2004; Kondo et al., 2012; Robles-Rodriguez et al., 2018).

The Malyl-CoA—Glycerate Cycling (MCG)

Like the rGS pathway, the synthetic Malyl-CoA-Glycerate (MCG) cycling pathway allows the conversion of glucose into acetyl-CoA. As depicted in **Figure 3**, this synthetic pathway relies on 6

natural reaction steps that are catalyzed by endogenous enzymes in *E. coli*, completed by the heterologous expression of *mtkAB* and *mcL* from methylotrophic bacteria. The importance of these two reaction steps in the *in vivo* functionality of the MCG was demonstrated by showing that the growth on glucose of an acetyl-COA auxotroph *E. coli* strain (Δ*aceE* Δ*poxB* Δ*plfB*) can be rescued upon the expression of *mtkAB* and *mcl* genes. Like NOG and rGS, the theoretical molar yield of acetyl-COA per glucose consumed is 3 (**Table 1**). Another interesting feature of the MCG is to be able to assimilate C2 compound such as glycolate or glyoxylate (**Figure 3**). Hence, in photosynthetic organisms, expression of MCG could improve carbon fixation in combination with the CBB cycle by re-assimilating glycolate produced by photorespiration. Also, the conversion of glucose into acetyl-CoA by the MCG is redox neutral and costs one ATP for glucose phosphorylation, unless the glycolytic PEP carboxykinase as it exists in the rumen bacterium *Actinobacillus succinogenes* (Kim et al., 2004; Leduc et al., 2005) is used instead of PPC, which would result in the production of one extra ATP.

EXPLOITING CARBOXYLATING ENZYMES FOR CO_2 FIXATION IN HETEROTROPHIC ORGANISMS

Carboxylating Enzymes as a Key Reaction in Heterotrophic Organisms for CO_2 Fixation

In an elegant paper published in 2010, Bar-Even et al. (2010) developed a constrained-based modeling approach that explored all possibilities that could be devised from a repertoire of ∼5,000 known metabolic enzymes reported in the KEGG database (https://www.genome.jp/kegg/pathway.html) to generate carbon fixation pathways that are alternative to the 5 known to date. Criteria used in their modeling were (i) the enzyme's specific activity is equal or superior to that of RuBisCO which is used as the benchmark activity; (ii) a minimal energy cost of the pathway, which corresponds to the cost in NAD(P)H, ferredoxins, $FADH_2$, and ATP in the production of one mole of products from CO_2; (iii) thermodynamic feasibility of the pathway under a plausible physiological range of metabolites concentrations; (iv) topology of the pathway, which incorporates the number of enzymatic reactions the carbon fixation pathway can make as an independent unit and (v) the compatibility or integration of this synthetic pathway with the endogenous metabolic network. According to these criteria, they identified several cycling pathways containing four to six enzymatic steps leading to the production of the C2 compound glyoxylate. Although most of them were unrealistic because thermodynamically unfeasible or using oxygen-sensitive ferredoxin-oxidoreductase enzyme, these authors found that kinetically efficient pathways absolutely require a carboxylating enzyme with high activity and affinity toward CO_2 or HCO_3^- whose reaction must be physiologically irreversible. PEP carboxylase (*ppc* gene) and pyruvate carboxylase (*pyc* gene) came at first in their listing, followed by acetyl-CoA and propionyl-CoA carboxylase. Accordingly, they designed a pathway family termed Malonyl-CoA-Oxaloacetate-Glyoxylate (MOG) cycle employing either PEP carboxylase or pyruvate carboxylase as the sole carboxylating enzyme and that has a higher carboxylating activity than the reductive pentose pathway (rPP). This MOG pathway resembles the natural C4 cycle in which the recuperation of CO_2 arising from malate decarboxylation to pyruvate by RuBisCO is replaced by a PEP or pyruvate carboxylating enzyme. The net product of MOG is the C2-carbon glyoxylate, which can be converted into GAP by the bacterial-like glycerate pathway (Eisenhut et al., 2006; Igamberdiev and Kleczkowski, 2018) (**Figure 4**). Interestingly, this pathway turns out to be thermodynamically feasible and more efficient than the rPP, although it has not been found in Nature yet. Moreover, combined with the plant natural C4-cycle, it could allow to overcome the futile CO_2 cycling that is taking place in the bundle sheath cell and which is due to malate decarboxylation coupled to reassimilation of CO_2 by RuBisCO. In addition, this coupling could result in an extra CO_2 fixation with the release of glyoxylate. Therefore, it can be anticipated that the expression of MOG in autotrophic cells may provide great advantages from a biotechnological point of view, with faster growth and increased crop yields because of additional carbon dioxide input and absence of competing oxygenation reaction that reduces carbon fixation by plants. Whether the implementation of this MOG pathway in a heterotrophic cell like *E. coli* is biotechnologically relevant is less obvious. Indeed, this implementation will require the expression of heterologous genes encoding six out of the nine reactions of this cyclic pathway (**Figure 4**), namely the malate thiokinase (*mtkAB*), the malyl-CoA lyase (*mcl*), the methylmalonyl-COA carboxytransferase (*mct*), the malonyl-CoA reductase (*mcr*), the β-alanine-pyruvate transaminase (*bapta*), and the alanine 2,3 aminomutase *(aam*). More importantly, the stoichiometry evaluation of this route from glucose indicated that it can produce 2 moles of glyoxylate and 2 moles of acetate, with the requirement of two mole of CO_2. However, while globally thermodynamically favorable and redox balanced, this reaction can occur at the expense of 3 ATP, which can be obtained by consumption of acetate, and hence resulting in the reemission of 2 moles of CO_2. Therefore, this route has likely no meaning to be expressed in a chemoorganotrophic system.

The Modified Serine Cycle Pathway in *E. coli*

In methylotrophic bacteria, the serine cycle is a natural pathway to assimilate C1 carbon such as methanol or methane into acetyl-CoA intermediate without loss of carbon (Smejkalova et al., 2010). A modified serine cycle pathway has been designed in *E. coli* to allow co-assimilation of C1-carbon such as methanol or formate with bicarbonate to generate acetyl-COA as a precursor for several bio-based products (Yu and Liao, 2018). This synthetic pathway encompasses nine enzymatic reactions for the cycle in which CO_2 is captured by the reaction catalyzed by PEP carboxylase, and four additional reaction enabling assimilation into 5–10 methylene tetrahydrofolate ($CH_2 = H_4F$). The methyl unit is afterwards transferred on serine cycle by a

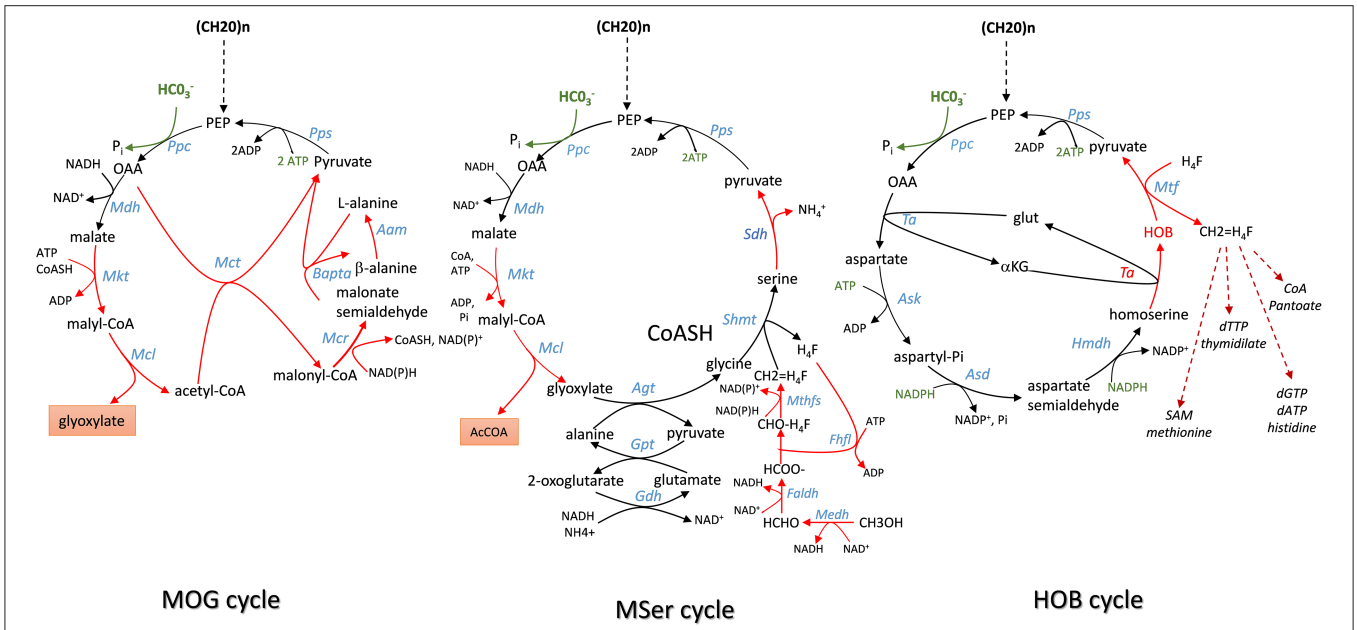

FIGURE 4 | Scheme of Malonyl-coA-Oxaloacetate- Glyoxylate (MOG), Modified Serine (MSer) and 4-hydroxy-2-oxo-butyrate (HOB) cycling pathway employing the efficient PEP carboxylase to capture Co_2 into either product or biomass. Enzymes abbreviation are: Ppc, PEP carboxylase; Mdh, malate dehydrogenase; Mtk, malate thiokinase; Mcl, malyl -CoA lyase; Mct, malonyl-CoA acetyl transferase; Mcr, malonyl CoA reductase; Bapta, β-alanine: pyruvate transaminase; Aam, alanine 2,3 aminomutase; Pps, PEP synthase; Ta, transaminase; Ask, aspartate kinase; Asd, aspartyl-Pi semialdehyde dehydrogenase; HmdH, homoserine dehydrogenase; Hmtf, hydroxymethyl transferase.

reaction involving glycine and catalyzed by serine hydroxymethyl transferase (Shmt). From these 13 enzymatic steps, seven (highlighted in red in **Figure 5**) had to be implemented using heterologous genes from various organisms, which included *S. cerevisiae* for the glyoxylate:alanine transaminase (Agt) encoded by *AGX1*, serine dehydratase (Sdh) from *Cupriavidus necator* encoded by *SdaA*, malate thiokinase (Mkt), and malyl-CoA lyase(Mcl) from *M.extorquens*. For methanol oxidation and its conversion to 5–10 methylene tetrahydrofolate, a variant of the *Cupriavidus necator* methanol dehydrogenase (Medh) with higher specific activity was used together with formate-H4F ligase (Fhlfl) and 5,10-methylene tetrahydrofolase synthase (Mthfs) from *Moorella thermoacetica*. The NAD^+-linked formadehyde dehydrogenase (Faldh) from *Pseudomonas putida* was employed to oxidize formaldehyde to formate. All these genes were carried on 3 different plasmids and transformed into *E. coli* strain HY106, which was deleted for genes to avoid byproducts formation and shortage of intermediates in the cycle. Accordingly, *aceB* and *glcB* both encoding malate synthase were deleted to avoid competitive reverse reaction catalyzed by Mkt and Mcl. The *gcl* gene encoding glyoxylate carboxyligase was deleted to prevent shortage of glyoxylate into tartronate semialdehyde, as well as *gcvP* to avoid loss of glycine by decarboxylation. Genes encoding lactate dehydrogenase (*ldhA*) and fumarate reductase (*frABCD*) were also deleted in this strain to avoid shortage of pyruvate into D-lactate and malate into succinate. As indicated in **Table 1**, co-assimilation of methanol with CO_2 needs 3 moles ATP and 1 mole reduced equivalent per mole of acetyl-CoA produced. Hence, it cannot proceed without addition of another carbon source to provide this energy and cofactors. Thus, the *in vivo* function of the complete cycle was demonstrated using C^{13}-methanol together with xylose to supply energy and PEP. In addition the pyruvate to malate flux was increased upon overexpression of *pyc* and *mdh* encoding pyruvate carboxylase and malate dehydrogenase in the engineered *E. coli* equipped with the Mser pathway. The engineered strain could produce acetate from which 33% came from methanol. When the same experiment was carried out with both C^{13} methanol and C^{13} bicarbonate, the amount of acetate produced was the same but the labeling of both C1 and C2- carbon of acetyl-moieties was enriched by 2-fold, indicating that bicarbonate has been also incorporated into acetyl moieties. To conclude, the construction of this synthetic serine cycle in *E. coli* enables the assimilation of C1 compounds such as methanol to increase the production of C2-compounds as precursor of bio-based products such as PHB, isoprenoid, fatty acids, etc. In addition, this cycle, combined with the glyoxylate shunt, is capable to support growth from pyruvate that is formed from two C1-carbon (formate or methanol) and one bicarbonate, unless the mole excess of NAD(P)H is reoxidized by respiratory chain coupled with ATP.

The HOB Pathway as an Alternative for C1-Carbon Metabolism Through CO_2 Fixation by PEP Carboxylase

Another illustration about the potential function of carboxylating enzyme to incorporate CO_2 into biomass comes from the work of Bouzon et al. (2017). These authors built a synthetic pathway

that is alternative to the ubiquitous one carbon pathway transferring C1-moities (i.e., formyl, hydroxymethyl, or methyl group) from tetrahydrofolate for the synthesis of purine nucleotides, thymidylate, methionine, or coenzyme A (**Figure 4**). These C1-moities are obtained from the pivotal intermediate 5,10-methylene tetrathydrofolate (CH_2=H_4F) produced by the condensation of tetrahydrofolate with formaldehyde that originates from serine or glycine. To replace these amino acids as C1-donor, these authors devised a cyclic pathway in which the C1 compound (in this case formaldehyde) is obtained from the aldolytic cleavage of the non-natural intermediate 2-keto-4-hydroxybutyrate (HOB). As shown in **Figure 4**, the complete cycle encompasses 8 enzymatic steps in which the C1- source is HCO_3^- that is captured by PEP carboxylase to yield OAA. Through a set of 4 natural enzymatic step, OAA is converted into homoserine which gives rise to HOB through a transaminase reaction. The best candidate for this non-natural transaminase reaction was obtained by employing an automated evolutionary technology originally developed by Marlière et al. for evolving *E. coli* possessing DNA in which thymine was replaced by the synthetic building block 5-chlorouracil (Marliere et al., 2011). The evolved transaminase was found to correspond to a variant of the alanine: pyruvate transaminase encoded by *alaC* having amino change at position 142 (Ala to Pro) and 245 (Tyr to Glu). The HOB is then cleaved into pyruvate and formaldehyde which is readily transferred into H4F by the promiscuous hydroxymethytransferase (Mtf) encoded by *panB*. The cycle is then closed by converting back pyruvate into PEP, which implicates PEP synthase. Overall, the functioning of this cycle costs two moles of NADPH and three moles of ATP per mole of CO_2 incorporated (**Table 1**). To implement this synthetic pathway that completely rewires the C1-canonical metabolism by imposing HOB as the essential metabolic intermediate, the authors banked on an evolutionary trajectory of a *E. coli* strain lacking all enzymes necessary for the natural C1- transfer moieties using an original automated evolutionary technology that is now commercialized as "Heurisko" by the company Altar (http://www.altar.bio/). The authors estimated that the CO_2 assimilated in the biomass of *E. coli* expressing this HOB pathway is about 2 times more than in wild type strain (Bouzon et al., 2017). However, being quite energy consuming, the relevance of this pathway in the production of biotechnological molecules methionine is questionable.

EXPRESSION OF THE CALVIN-BENSON CYCLE ENZYMES FOR *IN-SITU* CO_2 REINTEGRATION INTO THE CENTRAL METABOLIC NETWORK

Under anaerobic condition, sugar fermentation by the yeast *Saccharomyces cerevisiae* into ethanol generated excess of NADH, which must be reoxidized to warrant redox-cofactor balancing (Van Dijken and Scheffers, 1986). This reoxidation diverts between 4 and 10% of the sugar into glycerol, which has a significant impact on the economy of large scale yeast-based bioethanol production. To reduce or even eliminate this by-product and in the same time, to increase the ethanol yield, the group of Jack Pronk in TU Delft proposed to use CO_2 as electron acceptor for the reoxidation of this excess of NADH. A theoretical analysis indicates that the replacement of glycerol by CO_2 can increase the ethanol yield from sugar by 14% if the CO_2 is incorporated through phosphoribulokinase (PRK) and ribulose-1,5-bisphosphate carboxylase/oxygenase (RuBisCO) onto ribulose 5-P (Ru5P) (**Figure 5**). In their design, Ru5P must be produced from the non-oxidative pentose phosphate route in order to reoxidize all biosynthetic NADH and not NADPH through a transhydrogenase-type conversion NADPH-> NADH (Guadalupe-Medina et al., 2013). This clever idea was demonstrated in two elegant papers published in Biotechnology for Biofuels (Guadalupe-Medina et al., 2013; Papapetridis et al., 2018). In the first paper, the authors expressed the codon-optimized prokaryotic form II RuBisCO-encoding *cbbM* gene from *T. denitrificans* in a centromeric plasmid under the strong *TDH3* promoter and showed that RuBisCO was functional only upon co-expression of *E. coli groEL/groES* encoding chaperones whereas surprisingly *T denitrificans* chaperones encoded by *cbb02/cbbQ2* were ineffective. The *PRK* from *Spinachia oleracea* was integrated together with the *E. coli groEL/groES* gene in the yeast genome at the *CAN1* locus under the galactose-inducible *GAL1* promoter. Remarkably, expression of this minimal Calvin cycle in this engineered yeast cultivated under anaerobic chemostat condition showed a 68% reduction of glycerol production accompanied by a 10% increase of ethanol yield. Saturating the culture with CO_2 resulted in a 90% decrease of glycerol, which could be explained in part by the low affinity of form II RuBisCO for CO_2 (K_{C02} = 0.26 mM). In a second paper, the authors carried out several targeted metabolic engineering to optimize the fermentation kinetic, improving ethanol yield and reducing glycerol production. To achieve this goal, nine copies of the *cbbM* overexpression cassette along with a single expression cassette of *E. coli groEL/groES* chaperones were integrated at the *SGA1* locus using CRISPR-Cas9 tool followed by the integration at X-2 locus of the *PRK1* under the inducible anaerobic *DAN1* promoter. The resulting engineered strain expressing a more robust Calvin-Benson cycle showed significant (31%) reduction of glycerol under glucose anaerobic condition. However, the contribution of the PRK/RuBisCO pathway to NADH reoxidation decreased with increased growth rate, with a concurrent higher contribution of the glycerol pathway. Therefore, a complementary strategy was to abrogate this pathway by removal of glycerol-3-P dehydrogenase encoded by *GPD1* and *GPD2*. While *GPD1* is essential for growth of *Saccharomyces cerevisiae* under osmotic stress (Albertyn et al., 1994), loss of *GPD2* strongly affects growth under anaerobic condition (Ansell et al., 1997). Accordingly, the deletion of *GPD2* in the engineered strain bearing the Calvin cycle resulted in a 62 % decrease of glycerol and 13% increase of ethanol yield as compared to a reference strain. An additional engineering strategy was dedicated to overexpress genes encoding the transketolase and transaldolase with the aim to increase the availability of Ru5P. Indeed, this intermediate is not solely the substrate of PRK, but it is also indirectly implicated in the

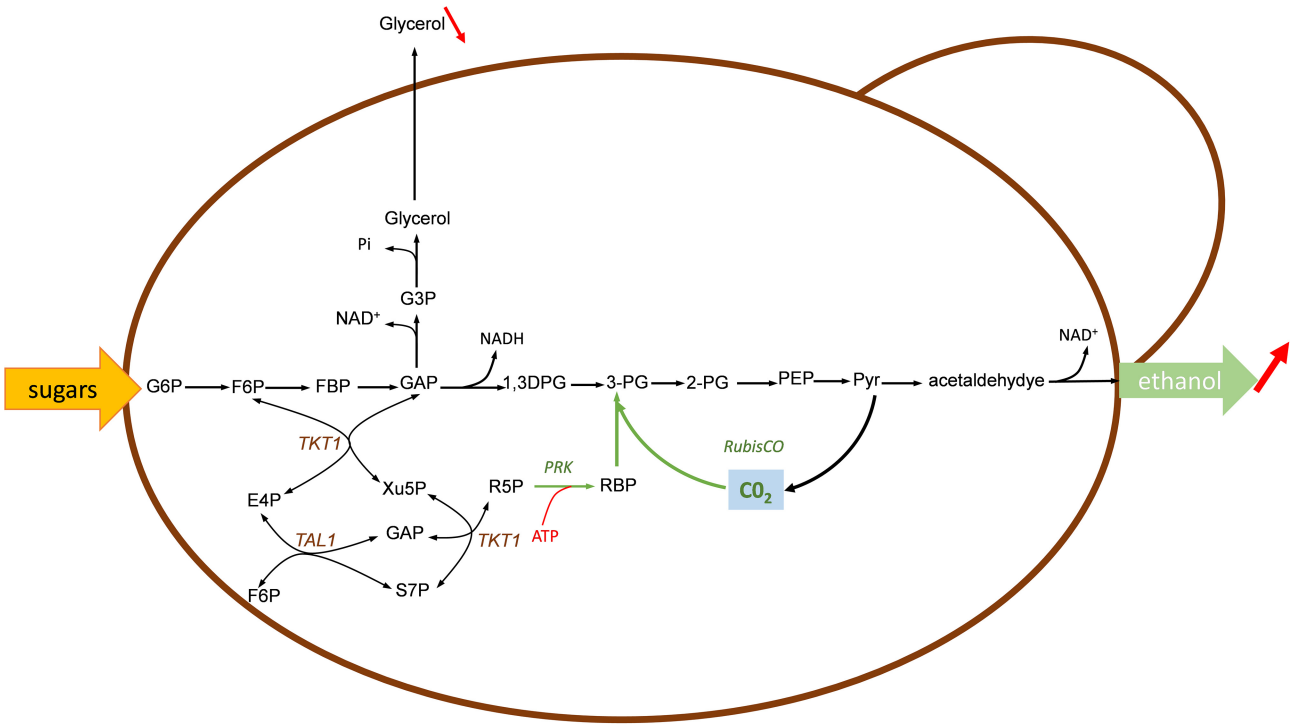

FIGURE 5 | Engineering sugars fermentation with Calvin-cycle enzymes for fixing *in-situ* CO_2 to improve bioethanol yield in yeast. In green are shown the Calvin-cycle enzymes corresponding to RuBisCO and phosphoribulose-5-P kinase (PRK). The expression of this Calvin-cycle enzymes enables the use of CO_2 as alternative electron acceptor for reoxidation of NADH, thereafter reducing glycerol production under anaerobic condition. Enzymes: RuBisCO, ribulose 1,5 bisphosphate carboxylase; PRK, phosphoribulose 5-P kinase; Tkt, transketolase; Tal, transaldolase. Metabolites abbreviation, as in **Figure 1** except: 1,3-DPG, 1,3 diphosphoglycerate; 3-PG, 3-phosphoglycerate; 2-PG, 2-phosphoglycerate; G3P, glycerol-3-P.

biosynthesis of nucleic acid, aromatic amino acids and vitamins. Thus, its depletion through PRK could be in part responsible for the poor growth of the strain expressing the Calvin cycle. In accordance with this idea, overexpression of non-oxidative PPP genes *RPEI*, *TKL1*, *TKL2*, *TAL1*, *RKI1* in the engineered strain also deleted for *GPD2* resulted in a specific growth rate that was virtually the same as the reference strain under anaerobic batch condition on glucose. Furthermore, this engineered strain achieved the best fermentation performance with an increased ethanol yield of 15% and a 90% decrease of glycerol production (Papapetridis et al., 2018).

A comparable strategy has been applied by two other research groups which have equipped a xylose-utilizing *Saccharomyces cerevisiae* with the two Calvin-cycle enzymes PRK and RuBisCO to enhance xylose fermentation with *in situ* CO_2 fixation (Li et al., 2017; Xia et al., 2017). As *S. cerevisiae* cannot naturally ferment xylose, fungal pathway consisting of a xylose reductase (XR) and xylulose dehydrogenase (XDH) or the bacterial xylose isomerase (XI) have been heterologously expressed, together with upregulation of the native pentose phosphate pathway (PPP) to achieve efficient and rapid xylose fermentation (Matsushika et al., 2009; Young et al., 2010; Oreb et al., 2012). While the XR/XDH pathway appears to be more effective for xylose fermentation rate and ethanol productivity than the XI pathway (Karhumaa et al., 2007), it leads to cofactor imbalance with a surplus of NADH that is regenerated at the cost of by-products formation such as glycerol and xylitol. Expression of the PRK-RuBisCO module should exploit this NADH surplus for recycling CO_2 that is generated during the fermentation. This strategy was developed by Xia et al. (2017) which used a previously evolutionary engineered *S. cerevisiae* SR8 strain that was able to efficiently co-ferment xylose and glucose. This engineered strain harbored the XR/XDH together with an upregulated PPP and was deleted for *PHO13* and *ALD6* as beneficial targets for xylose fermentation (Kim et al., 2013). Similarly to the work of Guadalupe-Medina et al. (2013), two copies of the *cbbM* gene encoding form-II RuBisCO from *R. rubrum* under the strong *TDH3* promoter and *groEL/groES* cassette under *TEF1* promoter were integrated in the yeast genome (notably at *ALD6* and *PHO13* locus, respectively) leading to a stable platform SR8C^{+} strain. Only RuBisCO activity was detected in yeast strain co-expressing *cbbM* and *groEL/ES*. Then, while the overexpression of PRK from *Spinacia oleracea* alone was toxic for growth on xylose but not on glucose, likely because of ATP depletion or consecutive hyperaccumulation of RuBP, expression of the PRK-RuBisCO module rescued complete growth on xylose, which was accompanied by a 24% reduction of xylitol and 10% increase of ethanol yield while glycerol yield was similar to the control strain. Moreover, it was demonstrated that this engineered *S. cerevisiae* carrying the Calvin-cycle enzymes released 7% less CO_2 than the control strain during anaerobic

xylose fermentation. In a more recent publication, Li et al. (2017) engineered a xylose-utilizing *S. cerevisiae* for co-utilization of maltose, xylose and CO_2. The rationale behind this strategy was to provide metabolite precursors, energy and reduced cofactor useful for xylose reduction by XR from maltose, which otherwise does not repress xylose fermentation. In addition, a mXR variant that preferred NADH over NADPH was co-expressed together with XR and XDH on a high copy plasmid pRS425. At variance to previous works, genes encoding form-I RuBisCO of *Ralstonia eutropha* or form-II of *R. rubrum*, PRK from *Spinacia oleracea* or *Ralstonia eutrophia* together with *E. coli groEL* and *groES* encoding chaperone were cloned in a low copy plasmid YcpLac33 and transformed into the xylose-utilizing yeast. They reported that these engineered strains grew better on a mix maltose-xylose medium than control strain. They exhibited higher ethanol productivity and yield, with the highest increase of ethanol yield (+ 15%) and sugar consumption rate (+ 63%) with the engineered strain expressing heterotrophic form-I RuBisCO. Using ^{13}C-labeled CO_2 and a metabolic flux index MFI $_{h-C02}$ (Gong et al., 2015) for relative quantification of flux ratio between the CO_2-fixing by-pass pathway and the central carbon metabolic pathway, an incorporation of 8% CO_2 into Ru5P was estimated at a rate of 390 ± 50 mg CO_2/L/h, which is a rate that is in the range of CO_2 fixation by natural autotrophic microbes (Gong et al., 2015). Altogether, these results indicated that the beneficial effect of implementing the CO_2-fixation pathway on growth and fermentation largely overcome the additional cost of ATP that is required when this pathway is expressed.

The RuBisCO-based pathway was also investigated in *E. coli* initially as a screen to find out variants of RuBisCO enzyme with higher catalytic activity and better affinity to CO_2 (Parikh et al., 2006). It was then exploited for *in situ* CO_2 assimilation in bioproduction (Zhuang and Li, 2013; Gong et al., 2015). For this purpose, the RuBisCO-encoding genes *rbcl-rbcX-rbcS* from the cyanobacterium *Synechococcus sp* PC7002 and PRK-encoding gene from *Synechococcus elongatus* were expressed on a high copy plasmid pET30a and arabinose was provided to the medium as an extra carbon source to enhance C5-phosphorylated sugar required for RuBisCO enzyme. Under this condition, the authors reported that the expression of RuBisCO alone promoted faster and complete consumption of arabinose, whereas the overexpression of PRK alone caused some growth retardation, which was explained by accumulation of RuBP. It was shown that the engineered strain expressing the Calvin-cycle was able to assimilate under anaerobic growth condition CO_2 at a rate comparable to that of the autotrophic cyanobacteria and microalgae (Gong et al., 2015). However, to overcome the co-cultivation condition, the same authors decided to enhance the non-oxidative pentose phosphate pathway by either overexpressing transketolase (*tktAB*) or by deleting glucose-6-P dehydrogenase (*zwf*) encoding gene. These genetic actions resulted in a significant decrease of CO_2 yield per glucose consumed. Genes encoding D-lactate dehydrogenase (*ldh*) and fumarate reductase (*frd*) were further deteled in this *zwf* mutant in order to favor recycling of *in situ* CO_2 into fermentation products ethanol or acetate. However, while this reduced CO_2 production proved the Calvin cycle pathway to work *in vivo*, and the expression of this cycle did not impede the growth on glucose, only 70% of carbon initially fed in the medium was recovered at the end of the fermentation. Moreover, there was no significant increase in C2-related compounds (Li et al., 2015; Yang et al., 2016). It turned out that this fermentation profile was explained by a huge accumulation of pyruvate that likely resulted from an excessive glycolytic flux at the sugar uptake and phosphorylation step leading to accumulation of NADH and concurrent reduction of pyruvate-formate lyase activity. This activity was inhibited by two concurrent actions, namely a direct inhibition by NADH and a downregulation of *pflB* encoding this enzyme due to the repression of its transcriptional activator encoded by *arcA* (Yang et al., 2016). Intriguingly, these transcriptional effects were already observed upon the simple overexpression of RuBisCO, suggesting a direct impact of the protein on the central carbon metabolism. To overcome these inhibitory problems, pyruvate decarboxylase and alcohol dehydrogenase encoding genes from *Zymomonas mobilis* were overexpressed in the Δ*zwf* Δ*ldh* Δ*frbd* mutant strain equipped with the Calvin-cycle enzymes PRK and RuBisCO. This genetic intervention resulted in a yield of C-2 compounds from glucose 20% higher than that of theoretical fermentation value, which was due to a direct *in situ* CO_2 recycling into these products by the RuBisCO system. In addition, a rate of 53 mg/L/h of CO_2 consumption was evaluated, which was in the range of rate measured for CO_2 fixation by microalgae (Gonzalez Lopez et al., 2009; Ho et al., 2012), arguing that mixotrophic fermentation can be a competitive alternative for reducing loss of CO_2 and converting it into bio-based products.

CONCLUSIONS AND OUTLOOK

The carbon management during the metabolic conversion of renewable carbon sources such as sugars by heterotrophic organisms is an attractive, yet partial, solution to combat the acute problem of continuous CO_2 emission associated with human activities. Since carbon dioxide is an intrinsic by-product of carbon metabolism ensuring the irreversibility of metabolic pathways in which it is involved, the rewiring of carbon metabolism aiming to circumvent this carbon loss must take into account this cost. However, in most of the case that were presented here, this cost can be overridden by the benefit of a higher carbon yield achieved by these refractory or synthetic pathways. This higher carbon yield is the second advantage of this carbon management since it can in principle increase the practical performance of a product per carbon consumed, which is a decisive parameter for the economic evaluation of a biotechnology process. Nonetheless, the synthetic pathways aiming at reducing carbon loss or assimilate CO_2 are still in their infancy. Substantial work is required to evaluate the potential for industrial application of some of them, such as NOG, MCG, rGS or glycoptimus, whereas others such as the MOG, MSer, and HOB will likely remain as elegant intellectual models illustrating the power of Synthetic Biology in its ability to reformat metabolic pathways.

While heterotrophic organisms are not naturally able to assimilate carbon dioxide, an attractive and complementary strategy to those developed elsewhere to capture CO_2 is to equip these organisms with the two key Calvin cycle enzymes in order to capture CO_2 produced during sugar fermentation, and meanwhile use it as an electron acceptor for NADH reoxidation. This dual function has been developed in yeast and *E. coli* and was shown to increase C2- products such as ethanol (Papapetridis et al., 2018; Tseng et al., 2018). The high concentration of carbon dioxide that prevails in industrial fermentations and their usual anaerobic to micro-aeration conditions are factors that should support the proper functioning of this capture system since RuBisCO has low affinity to CO_2 and its carboxylation activity is antagonized by oxygen. Therefore, this engineering strategy could be implemented without major investment at the industrial scale owing to the fact that GMO's legislation is modified.

Another promising strategy that is already attracting much interest is to exploit the high catalytic capacity of carboxylating enzymes such as the PEP carboxylase to capture "CO_2" *in vivo*. In addition of engineering specific pathways allowing this capture such as rGS or MCG, a great advantage of using heterotrophic organisms such as yeast or *E. coli* for CO_2 fixation is their fast growth rates and capability to reach high cell density in bioreactors, both criteria contributing to CO_2 assimilation rate that are higher than that of auxotrophic organisms. Therefore, engineering heterotrophic microbes for CO_2 fixation can be a promising avenue to both reduce CO_2 emission and in the meantime increase carbon yield as the fixed CO_2 can be easily integrated into the central carbon metabolism. To be even more efficient, the next step will be to employ other energy source than sugar for CO_2 fixation.

AUTHOR CONTRIBUTIONS

All authors listed have made a substantial, direct and intellectual contribution to the work, and approved it for publication.

ACKNOWLEDGMENTS

The authors wish to acknowledge Agence Nationale de la Recherche (ANR), Ministry of Research and Education (MENRT), and TWB for technical and financial support.

REFERENCES

Akram, M. (2014). Citric acid cycle and role of its intermediates in metabolism. *Cell Biochem. Biophys.* 68, 475–478. doi: 10.1007/s12013-013-9750-1

Albertyn, J., Hohmann, S., Thevelein, J. M., and Prior, B. A. (1994). *GPD1*, which encodes glycerol-3-phosphate dehydrogenase, is essential for growth under osmotic stress in *Saccharomyces cerevisiae*, and its expression is regulated by the high-osmolarity glycerol response pathway. *Mol. Cell. Biol.* 14, 4135–4144. doi: 10.1128/MCB.14.6.4135

Ansell, R., Granath, K., Hohmann, S., Thevelein, J. M., and Adler, L. (1997). The two isoenzymes for yeast NAD+-dependent glycerol 3-phosphate dehydrogenase encoded by GPD1 and GPD2 have distinct roles in osmoadaptation and redox regulation. *EMBO J* 16, 2179–2187.

Antonovsky, N., Gleizer, S., Noor, E., Zohar, Y., Herz, E., Barenholz, U., et al. (2016). Sugar synthesis from CO_2 in *Escherichia coli*. *Cell* 166, 115–125. doi: 10.1016/j.cell.2016.05.064

Bar-Even, A., Noor, E., Lewis, N. E., and Milo, R. (2010). Design and analysis of synthetic carbon fixation pathways. *Proc. Natl. Acad. Sci. U.S.A.* 107, 8889–8894. doi: 10.1073/pnas.0907176107

Berg, I. A., Kockelkorn, D., Buckel, W., and Fuchs, G. (2007). A 3-hydroxypropionate/4-hydroxybutyrate autotrophic carbon dioxide assimilation pathway in Archaea. *Science* 318, 1782–1786. doi: 10.1126/science.1149976

Berg, I. A., Kockelkorn, D., Ramos-Vera, W. H., Say, R. F., Zarzycki, J., Hugler, M., et al. (2010). Autotrophic carbon fixation in archaea. *Nat. Rev. Microbiol.* 8, 447–460. doi: 10.1038/nrmicro2365

Bogorad, I. W., Chen, C. T., Theisen, M. K., Wu, T. Y., Schlenz, A. R., Lam, A. T., et al. (2014). Building carbon-carbon bonds using a biocatalytic methanol condensation cycle. *Proc. Natl. Acad. Sci. U.S.A.* 111, 15928–15933. doi: 10.1073/pnas.1413470111

Bogorad, I. W., Lin, T. S., and Liao, J. C. (2013). Synthetic non-oxidative glycolysis enables complete carbon conservation. *Nature* 502, 693–697. doi: 10.1038/nature12575

Bouzon, M., Perret, A., Loreau, O., Delmas, V., Perchat, N., Weissenbach, J., et al. (2017). A synthetic alternative to canonical one-carbon metabolism. *ACS Synth. Biol.* 6, 1520–1533. doi: 10.1021/acssynbio.7b00029

Caballero, E., Baldoma, L., Ros, J., Boronat, A., and Aguilar, J. (1983). Identification of lactaldehyde dehydrogenase and glycolaldehyde dehydrogenase as functions of the same protein in *Escherichia coli*. *J. Biol. Chem.* 258, 7788–7792.

Calvin, M. (1962). The path of carbon in photosynthesis. *Science* 135, 879–889. doi: 10.1126/science.135.3507.879

Chen, R., and Dou, J. (2016). Biofuels and bio-based chemicals from lignocellulose: metabolic engineering strategies in strain development. *Biotechnol. Lett.* 38, 213–221. doi: 10.1007/s10529-015-1976-0

Claassens, N. J. (2017). A warm welcome for alternative CO_2 fixation pathways in microbial biotechnology. *Microb. Biotechnol.* 10, 31–34. doi: 10.1111/1751-7915.12456

Clark, J. H., Luque, R., and Matharu, A. S. (2012). Green chemistry, biofuels, and biorefinery. *Annu. Rev. Chem. Biomol. Eng.* 3, 183–207. doi: 10.1146/annurev-chembioeng-062011-081014

Clasquin, M. F., Melamud, E., Singer, A., Gooding, J. R., Xu, X., Dong, A., et al. (2011). Riboneogenesis in yeast. *Cell* 145, 969–980. doi: 10.1016/j.cell.2011.05.022

Deng, Y., Ma, N., Zhu, K., Mao, Y., Wei, X., and Zhao, Y. (2018). Balancing the carbon flux distributions between the TCA cycle and glyoxylate shunt to produce glycolate at high yield and titer in *Escherichia coli*. *Metab. Eng.* 46, 28–34. doi: 10.1016/j.ymben.2018.02.008

Dolan, S. K., and Welch, M. (2018). The glyoxylate shunt, 60 years on. *Annu. Rev. Microbiol.* 72, 309–330. doi: 10.1146/annurev-micro-090817-062257

Donahue, J. L., Bownas, J. L., Niehaus, W. G., and Larson, T. J. (2000). Purification and characterization of glpX-encoded fructose 1, 6-bisphosphatase, a new enzyme of the glycerol 3-phosphate regulon of *Escherichia coli*. *J. Bacteriol.* 182, 5624–5627. doi: 10.1128/JB.182.19.5624-5627.2000

Dudley, Q. M., Karim, A. S., and Jewett, M. C. (2015). Cell-free metabolic engineering: biomanufacturing beyond the cell. *Biotechnol. J.* 10, 69–82. doi: 10.1002/biot.201400330

Dugar, D., and Stephanopoulos, G. (2011). Relative potential of biosynthetic pathways for biofuels and bio-based products. *Nat. Biotechnol.* 29, 1074–1078. doi: 10.1038/nbt.2055

Duwe, A., Tippkotter, N., and Ulber, R. (2019). Lignocellulose-biorefinery: ethanol-focused. *Adv. Biochem. Eng. Biotechnol.* 166, 177–215. doi: 10.1007/10_2016_72

Eisenhut, M., Kahlon, S., Hasse, D., Ewald, R., Lieman-Hurwitz, J., Ogawa, T., et al. (2006). The plant-like C2 glycolate cycle and the bacterial-like glycerate pathway cooperate in phosphoglycolate metabolism in cyanobacteria. *Plant Physiol.* 142, 333–342. doi: 10.1104/pp.106.082982

Erb, T. J., and Zarzycki, J. (2018). A short history of RubisCO: the rise and fall (?) of Nature's predominant CO_2 fixing enzyme. *Curr. Opin. Biotechnol.* 49, 100–107. doi: 10.1016/j.copbio.2017.07.017

Fatland, B., Anderson, M., Nikolau, B. J., and Wurtele, E. S. (2000). Molecular biology of cytosolic acetyl-CoA generation. *Biochem. Soc. Trans.* 28, 593–595. doi: 10.1042/bst0280593

Fei, Q., Guarnieri, M. T., Tao, L., Laurens, L. M., Dowe, N., and Pienkos, P. T. (2014). Bioconversion of natural gas to liquid fuel: opportunities and challenges. *Biotechnol. Adv.* 32, 596–614. doi: 10.1016/j.biotechadv.2014.03.011

Fuchs, G., and Berg, I. A. (2014). Unfamiliar metabolic links in the central carbon metabolism. *J. Biotechnol.* 192(Pt B), 314–322. doi: 10.1016/j.jbiotec.2014.02.015

Garrabou, X., Castillo, J. A., Guerard-Helaine, C., Parella, T., Joglar, J., Lemaire, M., et al. (2009). Asymmetric self- and cross-aldol reactions of glycolaldehyde catalyzed by D-fructose-6-phosphate aldolase. *Angew. Chem. Int. Ed. Engl.* 48, 5521–5525. doi: 10.1002/anie.200902065

Gong, F., Liu, G., Zhai, X., Zhou, J., Cai, Z., and Li, Y. (2015). Quantitative analysis of an engineered CO_2-fixing *Escherichia coli* reveals great potential of heterotrophic CO_2 fixation. *Biotechnol. Biofuels* 8:86. doi: 10.1186/s13068-015-0268-1

Gonzalez Lopez, C. V., Acien Fernandez, F. G., Fernandez Sevilla, J. M., Sanchez Fernandez, J. F., Ceron Garcia, M. C., and Molina Grima, E. (2009). Utilization of the *cyanobacteria Anabaena* sp. ATCC 33047 in CO_2 removal processes. *Bioresour. Technol.* 100, 5904–5910. doi: 10.1016/j.biortech.2009.04.070

Guadalupe-Medina, V., Wisselink, H. W., Luttik, M. A., De Hulster, E., Daran, J. M., Pronk, J. T., et al. (2013). Carbon dioxide fixation by Calvin-Cycle enzymes improves ethanol yield in yeast. *Biotechnol. Biofuels* 6:125. doi: 10.1186/1754-6834-6-125

Ho, S. H., Chen, C. Y., and Chang, J. S. (2012). Effect of light intensity and nitrogen starvation on CO_2 fixation and lipid/carbohydrate production of an indigenous microalga Scenedesmus obliquus CNW-N. *Bioresour. Technol.* 113, 244–252. doi: 10.1016/j.biortech.2011.11.133

Igamberdiev, A. U., and Kleczkowski, L. A. (2018). The glycerate and phosphorylated pathways of serine synthesis in plants: the branches of plant glycolysis linking carbon and nitrogen metabolism. *Front. Plant Sci.* 9:318. doi: 10.3389/fpls.2018.00318

Jang, S., Kim, M., Hwang, J., and Jung, G. Y. (2019). Tools and systems for evolutionary engineering of biomolecules and microorganisms. *J. Ind. Microbiol. Biotechnol.* 46, 1313–1326. doi: 10.1007/s10295-019-02191-5

Karhumaa, K., Garcia Sanchez, R., Hahn-Hagerdal, B., and Gorwa-Grauslund, M. F. (2007). Comparison of the xylose reductase-xylitol dehydrogenase and the xylose isomerase pathways for xylose fermentation by recombinant *Saccharomyces cerevisiae*. *Microb. Cell Fact.* 6:5. doi: 10.1186/1475-2859-6-5

Kim, P., Laivenieks, M., Vieille, C., and Zeikus, J. G. (2004). Effect of overexpression of *Actinobacillus succinogenes* phosphoenolpyruvate carboxykinase on succinate production in *Escherichia coli*. *Appl. Environ. Microbiol.* 70, 1238–1241. doi: 10.1128/AEM.70.2.1238-1241.2004

Kim, S. R., Skerker, J. M., Kang, W., Lesmana, A., Wei, N., Arkin, A. P., et al. (2013). Rational and evolutionary engineering approaches uncover a small set of genetic changes efficient for rapid xylose fermentation in *Saccharomyces cerevisiae*. *PLoS ONE* 8:e57048. doi: 10.1371/journal.pone.0057048

Kondo, T., Tezuka, H., Ishii, J., Matsuda, F., Ogino, C., and Kondo, A. (2012). Genetic engineering to enhance the Ehrlich pathway and alter carbon flux for increased isobutanol production from glucose by *Saccharomyces cerevisiae*. *J. Biotechnol.* 159, 32–37. doi: 10.1016/j.jbiotec.2012.01.022

Krebs, H. A., and Johnson, W. A. (1980). The role of citric acid in intermediate metabolism in animal tissues. *FEBS Lett.* 117 (Suppl), K1–10. doi: 10.1016/0014-5793(80)80564-3

Lachaux, C., Frazao, C. R., Krauser, F., Morin, N., Walther, T., and Francois, J. (2019). A new synthetic pathway for the bioproduction of glycolic acid from lignocellulosic sugars aimed at maximal carbon conservation *Front. Bioeng. Biotechnol.* 7:359. doi: 10.3389/fbioe.2019.00359

Leduc, Y. A., Prasad, L., Laivenieks, M., Zeikus, J. G., and Delbaere, L. T. (2005). Structure of PEP carboxykinase from the succinate-producing *Actinobacillus succinogenes*: a new conserved active-site motif. *Acta Crystallogr. D Biol. Crystallogr.* 61, 903–912. doi: 10.1107/S0907444905008723

Li, Y. H., Ou-Yang, F. Y., Yang, C. H., and Li, S. Y. (2015). The coupling of glycolysis and the Rubisco-based pathway through the non-oxidative pentose phosphate pathway to achieve low carbon dioxide emission fermentation. *Bioresour. Technol.* 187, 189–197. doi: 10.1016/j.biortech.2015.03.090

Li, Y. J., Wang, M. M., Chen, Y. W., Wang, M., Fan, L. H., and Tan, T. W. (2017). Engineered yeast with a CO_2-fixation pathway to improve the bio-ethanol production from xylose-mixed sugars. *Sci. Rep.* 7:43875. doi: 10.1038/srep43875

Lim, R., and Cohen, S. S. (1966). D-phosphoarabinoisomerase and D-ribulokinase in *Escherichia coli*. *J. Biol. Chem.* 241, 4304–4315.

Lin, E. C., and Iuchi, S. (1991). Regulation of gene expression in fermentative and respiratory systems in *Escherichia coli* and related bacteria. *Annu. Rev. Genet.* 25, 361–387. doi: 10.1146/annurev.ge.25.120191.002045

Lin, P. P., Jaeger, A. J., Wu, T. Y., Xu, S. C., Lee, A. S., Gao, F., et al. (2018). Construction and evolution of an *Escherichia coli* strain relying on non-oxidative glycolysis for sugar catabolism. *Proc. Natl. Acad. Sci. U.S.A.* 115, 3538–3546. doi: 10.1073/pnas.1802191115

Liu, X., Sheng, J., and Curtiss, R III. (2011). Fatty acid production in genetically modified cyanobacteria. *Proc. Natl. Acad. Sci. U.S.A.* 108, 6899–6904. doi: 10.1073/pnas.1103014108

Mainguet, S. E., Gronenberg, L. S., Wong, S. S., and Liao, J. C. (2013). A reverse glyoxylate shunt to build a non-native route from C4 to C2 in *Escherichia coli*. *Metab. Eng.* 19, 116–127. doi: 10.1016/j.ymben.2013.06.004

Marliere, P., Patrouix, J., Doring, V., Herdewijn, P., Tricot, S., Cruveiller, S., et al. (2011). Chemical evolution of a bacterium's genome. *Angew. Chem. Int. Ed Engl.* 50, 7109–7114. doi: 10.1002/anie.201100535

Matsushika, A., Inoue, H., Kodaki, T., and Sawayama, S. (2009). Ethanol production from xylose in engineered *Saccharomyces cerevisiae* strains: current state and perspectives. *Appl. Microbiol. Biotechnol.* 84, 37–53. doi: 10.1007/s00253-009-2101-x

Mattanovich, D., Sauer, M., and Gasser, B. (2014). Yeast biotechnology: teaching the old dog new tricks. *Microb. Cell Fact.* 13:34. doi: 10.1186/1475-2859-13-34

Muller, J. E., Meyer, F., Litsanov, B., Kiefer, P., and Vorholt, J. A. (2015). Core pathways operating during methylotrophy of Bacillus methanolicus MGA3 and induction of a bacillithiol-dependent detoxification pathway upon formaldehyde stress. *Mol. Microbiol.* 98, 1089–1100. doi: 10.1111/mmi.13200

Opgenorth, P. H., Korman, T. P., and Bowie, J. U. (2016). A synthetic biochemistry module for production of bio-based chemicals from glucose. *Nat. Chem. Biol.* 12, 393–395. doi: 10.1038/nchembio.2062

Oreb, M., Dietz, H., Farwick, A., and Boles, E. (2012). Novel strategies to improve co-fermentation of pentoses with D-glucose by recombinant yeast strains in lignocellulosic hydrolysates. *Bioengineered* 3, 347–351. doi: 10.4161/bioe.21444

Papapetridis, I., Goudriaan, M., Vazquez Vitali, M., De Keijzer, N. A., Van Den Broek, M., Van Maris, A. J. A., et al. (2018). Optimizing anaerobic growth rate and fermentation kinetics in *Saccharomyces cerevisiae* strains expressing Calvin-cycle enzymes for improved ethanol yield. *Biotechnol. Biofuels* 11:17. doi: 10.1186/s13068-017-1001-z

Parikh, M. R., Greene, D. N., Woods, K. K., and Matsumura, I. (2006). Directed evolution of RuBisCO hypermorphs through genetic selection in engineered *E. coli*. *Protein Eng. Des. Sel.* 19, 113–119. doi: 10.1093/protein/gzj010

Reizer, J., Reizer, A., and Saier, M. H. Jr. (1995). Novel phosphotransferase system genes revealed by bacterial genome analysis–a gene cluster encoding a unique Enzyme I and the proteins of a fructose-like permease system. *Microbiology* 141(Pt 4), 961–971. doi: 10.1099/13500872-141-4-961

Robles-Rodriguez, C. E., Munoz-Tamayo, R., Bideaux, C., Gorret, N., Guillouet, S. E., Molina-Jouve, C., et al. (2018). Modeling and optimization of lipid accumulation by Yarrowia lipolytica from glucose under nitrogen depletion conditions. *Biotechnol. Bioeng.* 115, 1137–1151. doi: 10.1002/bit.26537

Rosales-Calderon, O., and Arantes, V. (2019). A review on commercial-scale high-value products that can be produced alongside cellulosic ethanol. *Biotechnol. Biofuels* 12:240. doi: 10.1186/s13068-019-1529-1

Russmayer, H., Buchetics, M., Gruber, C., Valli, M., Grillitsch, K., Modarres, G., et al. (2015). Systems-level organization of yeast methylotrophic lifestyle. *BMC Biol.* 13:80. doi: 10.1186/s12915-015-0186-5

Scaife, M. A., Nguyen, G. T., Rico, J., Lambert, D., Helliwell, K. E., and Smith, A. G. (2015). Establishing *Chlamydomonas reinhardtii* as an industrial biotechnology host. *Plant J.* 82, 532–546. doi: 10.1111/tpj.12781

Schiel-Bengelsdorf, B., and Durre, P. (2012). Pathway engineering and synthetic biology using acetogens. *FEBS Lett.* 586, 2191–2198. doi: 10.1016/j.febslet.2012.04.043

Schurmann, M., and Sprenger, G. A. (2001). Fructose-6-phosphate aldolase is a novel class I aldolase from *Escherichia coli* and is related to a novel group of bacterial transaldolases. *J. Biol. Chem.* 276, 11055–11061. doi: 10.1074/jbc.M008061200

Sedivy, J. M., Daldal, F., and Fraenkel, D. G. (1984). Fructose bisphosphatase of *Escherichia coli*: cloning of the structural gene (fbp) and preparation of a chromosomal deletion. *J. Bacteriol.* 158, 1048–1053.

Singhvi, M. S., and Gokhale, D. V. (2019). Lignocellulosic biomass: hurdles and challenges in its valorization. *Appl. Microbiol. Biotechnol.* 103, 9305–9320. doi: 10.1007/s00253-019-10212-7

Smejkalova, H., Erb, T. J., and Fuchs, G. (2010). Methanol assimilation in *Methylobacterium extorquens* AM1: demonstration of all enzymes and their regulation. *PLoS ONE* 5:e13001. doi: 10.1371/journal.pone.0013001

Soucaille, P. (2007). *Glycolic Acid Production by Fermentation from Renewable Resources*. France Patent Application: WO/2007/141316.

Stolzenberger, J., Lindner, S. N., Persicke, M., Brautaset, T., and Wendisch, V. F. (2013). Characterization of fructose 1,6-bisphosphatase and sedoheptulose 1,7-bisphosphatase from the facultative ribulose monophosphate cycle methylotroph Bacillus methanolicus. *J. Bacteriol.* 195, 5112–5122. doi: 10.1128/JB.00672-13

Tabata, K., and Hashimoto, S. (2004). Production of mevalonate by a metabolically-engineered *Escherichia coli*. *Biotechnol. Lett.* 26, 1487–1491. doi: 10.1023/B:BILE.0000044449.08268.7d

Tcherkez, G. G., Farquhar, G. D., and Andrews, T. J. (2006). Despite slow catalysis and confused substrate specificity, all ribulose bisphosphate carboxylases may be nearly perfectly optimized. *Proc. Natl. Acad. Sci. U.S.A.* 103, 7246–7251. doi: 10.1073/pnas.0600605103

Tittmann, K. (2014). Sweet siblings with different faces: the mechanisms of FBP and F6P aldolase, transaldolase, transketolase and phosphoketolase revisited in light of recent structural data. *Bioorg. Chem.* 57, 263–280. doi: 10.1016/j.bioorg.2014.09.001

Tseng, C. P. (1997). Regulation of fumarase (fumB) gene expression in *Escherichia coli* in response to oxygen, iron and heme availability: role of the arcA, fur, and hemA gene products. *FEMS Microbiol. Lett.* 157, 67–72. doi: 10.1111/j.1574-6968.1997.tb12754.x

Tseng, I. T., Chen, Y. L., Chen, C. H., Shen, Z. X., Yang, C. H., and Li, S. Y. (2018). Exceeding the theoretical fermentation yield in mixotrophic Rubisco-based engineered *Escherichia coli*. *Metab. Eng.* 47, 445–452. doi: 10.1016/j.ymben.2018.04.018

Uyeda, K. (1979). Phosphofructokinase. *Adv. Enzymol. Relat. Areas Mol. Biol.* 48, 193–244. doi: 10.1002/9780470122938.ch4

Van Dijken, J. P., and Scheffers, W. A. (1986). Redox balances in the metabolism of sugars by yeast. *FEMS Microbiol. Rev.* 32, 199–224. doi: 10.1111/j.1574-6968.1986.tb01194.x

Verschueren, K. H. G., Blanchet, C., Felix, J., Dansercoer, A., De Vos, D., Bloch, Y., et al. (2019). Structure of ATP citrate lyase and the origin of citrate synthase in the Krebs cycle. *Nature* 568, 571–575. doi: 10.1038/s41586-019-1095-5

Wang, Q., Xu, J., Sun, Z., Luan, Y., Li, Y., Wang, J., et al. (2019). Engineering an *in vivo* EP-bifido pathway in *Escherichia coli* for high-yield acetyl-CoA generation with low CO_2 emission. *Metab. Eng.* 51, 79–87. doi: 10.1016/j.ymben.2018.08.003

Ward, N., Larsen, O., Sakwa, J., Bruseth, L., Khouri, H., Durkin, A. S., et al. (2004). Genomic insights into methanotrophy: the complete genome sequence of *Methylococcus capsulatus* (Bath). *PLoS Biol.* 2:e303. doi: 10.1371/journal.pbio.0020303

Xia, P. F., Zhang, G. C., Walker, B., Seo, S. O., Kwak, S., Liu, J. J., et al. (2017). Recycling carbon dioxide during xylose fermentation by engineered *Saccharomyces cerevisiae*. *ACS Synth. Biol.* 6, 276–283. doi: 10.1021/acssynbio.6b00167

Yang, C. H., Liu, E. J., Chen, Y. L., Ou-Yang, F. Y., and Li, S. Y. (2016). The comprehensive profile of fermentation products during *in situ* CO2 recycling by Rubisco-based engineered *Escherichia coli*. *Microb. Cell Fact.* 15:133. doi: 10.1186/s12934-016-0530-7

Yin, X., Chambers, J. R., Barlow, K., Park, A. S., and Wheatcroft, R. (2005). The gene encoding xylulose-5-phosphate/fructose-6-phosphate phosphoketolase (xfp) is conserved among *Bifidobacterium* species within a more variable region of the genome and both are useful for strain identification. *FEMS Microbiol. Lett.* 246, 251–257. doi: 10.1016/j.femsle.2005.04.013

Young, E., Lee, S. M., and Alper, H. (2010). Optimizing pentose utilization in yeast: the need for novel tools and approaches. *Biotechnol. Biofuels* 3:24. doi: 10.1186/1754-6834-3-24

Yu, H., and Liao, J. C. (2018). A modified serine cycle in *Escherichia coli* coverts methanol and CO_2 to two-carbon compounds. *Nat. Commun.* 9:3992. doi: 10.1038/s41467-018-06496-4

Yurimoto, H., Hirai, R., Yasueda, H., Mitsui, R., Sakai, Y., and Kato, N. (2002). The ribulose monophosphate pathway operon encoding formaldehyde fixation in a thermotolerant methylotroph, *Bacillus brevis* S1. *FEMS Microbiol. Lett.* 214, 189–193. doi: 10.1111/j.1574-6968.2002.tb11345.x

Zhang, W., Zhang, T., Wu, S., Wu, A. L., Xin, F., Dong, W., et al. (2017). Guidance for engineering of synthetic methylotrophy based on methanol metabolism in methylotrophy. *RSC Adv.* 7, 4083–4091. doi: 10.1039/C6RA27038G

Zhuang, Z. Y., and Li, S. Y. (2013). Rubisco-based engineered *Escherichia coli* for *in situ* carbon dioxide recycling. *Bioresour. Technol.* 150, 79–88. doi: 10.1016/j.biortech.2013.09.116

Conflict of Interest: The authors declare that the research was conducted in the absence of any commercial or financial relationships that could be construed as a potential conflict of interest.

frontiers in Bioengineering and Biotechnology

ORIGINAL RESEARCH
published: 27 November 2019
doi: 10.3389/fbioe.2019.00359

A New Synthetic Pathway for the Bioproduction of Glycolic Acid From Lignocellulosic Sugars Aimed at Maximal Carbon Conservation

Cléa Lachaux[1,2], Cláudio J. R. Frazao[1†], Franziska Krauβer[1], Nicolas Morin[1,2], Thomas Walther[1,2†] and Jean Marie François[1,2]*

[1] Toulouse Biotechnology Institute (TBI), Université de Toulouse, CNRS, INRA, INSA, Toulouse, France, [2] TWB, Toulouse, France

OPEN ACCESS

Edited by:
Matthias Georg Steiger, Vienna University of Technology, Austria

Reviewed by:
Peter Richard, VTT Technical Research Centre of Finland Ltd, Finland
Peter J. Schaap, Wageningen University & Research, Netherlands
Kris Niño Gomez Valdehuesa, Myongji University, South Korea

***Correspondence:**
Jean Marie François
fran_jm@insta-toulouse.fr

†Present address:
Cláudio J. R. Frazao, Thomas Walther, TU Dresden, Institute of Natural Materials Technology, Dresden, Germany

Specialty section:
This article was submitted to Synthetic Biology, a section of the journal Frontiers in Bioengineering and Biotechnology

Received: *15 August 2019*
Accepted: *12 November 2019*
Published: *27 November 2019*

Citation:
Lachaux C, Frazao CJR, Krauβer F, Morin N, Walther T and François JM (2019) A New Synthetic Pathway for the Bioproduction of Glycolic Acid From Lignocellulosic Sugars Aimed at Maximal Carbon Conservation. Front. Bioeng. Biotechnol. 7:359. doi: 10.3389/fbioe.2019.00359

Glycolic acid is a two-carbon α-hydroxy acid with many applications in industrial sectors including packaging, fine chemistry, cosmetics, and pharmaceutics. Currently, glycolic acid is chemically manufactured from fossil resources. This chemical mode of production is raising some concerns regarding its use in health for personal care. Microbial production of GA stands as a remarkable challenge to meet these concerns, while responding to the increasing demand to produce bio-sourced products from renewable carbon resources. We here report on the design and expression of a novel non-natural pathway of glycolic acid in *E. coli*. The originality of this new pathway, termed "glycoptimus" relies on two pillars. On the one hand, it requires the overexpression of three naturally occurring *E. coli* genes, namely *kdsD* encoding a D-arabinose-5-P isomerase, *fsaA* encoding a class 1 aldolase that cleaves D-arabinose-5-P into glyceraldehyde-3-P and glycolaldehyde, and *aldA* coding for an aldehyde dehydrogenase that oxidizes glycoladehyde in glycolate. These three genes constitute the "glycoptimus module." On the other hand, the expression of these genes together with a reshaping of the central carbon metabolism should enable a production of glycolic acid from pentose and hexose at a molar ratio of 2.5 and 3, respectively, which corresponds to 50% increase as compared to the existing pathways. We demonstrated the '*in vivo*' potentiality of this pathway using an *E. coli* strain, which constitutively expressed the glycoptimus module and whose carbon flow in glycolysis was blocked at the level of glyceraldehyde-3-P dehydrogenase reaction step. This engineered strain was cultivated on a permissive medium containing malate and D-glucose. Upon exhaustion of malate, addition of either D-glucose, D-xylose or L-arabinose led to the production of glycolic acid reaching about 30% of the maximum molar yield. Further improvements at the level of enzymes, strains and bioprocess engineering are awaited to increase yield and titer, rendering the microbial production of glycolic acid affordable for a cost-effective industrial process.

Keywords: synthetic biology, metabolic engineering, glycolic acid, aldolase, white biotechnology

INTRODUCTION

Glycolic acid (GA) is a two-carbon α-hydroxy acid ($HOCH_2COOH$) with dual properties of both alcohol and moderately acid (pKa 3.83). It is the simplest organic acid, which finds multiple applications in the cosmetic industry to improve skin texture, in pharmaceutic industries to treat skin diseases, in textile industry as a dyeing and tanning agent, in food industry as flavor and preservative as well as for cleaning and sanitizer agent in household and industry (https://www.grandviewresearch.com/industry-analysis/glycolic-acid-industry). Polymerization of glycolic acid alone or with other acids monomer such as lactic acid yields thermoplastic resins with excellent gas barrier properties. These polymers have the capability of being hydrolysed in aqueous environments gradually and controllably, making them good candidates for packaging materials or dissolvable sutures useful for biomedical applications (Fredenberg et al., 2011; Gädda et al., 2014). This large panel of glycolic acid applications accounts for the fact that the demand for this organic acid is constantly growing from US$ ∼300 million in 2017 to US$ ∼406 million in 2023, exhibiting a CAGR of 6.83% during this forecast period (https://www.researchandmarkets.com/reports/4542547/glycolic-acid-market-forecasts-from-2018-to-2023). Even though glycolic acid can be extracted from plants such as sugarcane, pineapple, and sugar beets, it is chiefly chemically manufactured from fossil resources by carbonylation of formaldehyde at high-pressure temperature (Drent et al., 2001). Alternatively, it can be produced from the enzymatic conversion of glycolonitrile using microbial nitrilases (He et al., 2010) or by bioconversion of ethylene glycol using *Gluconobacter oxydans* as the biocatalyst (Kataoka et al., 2001; Wei et al., 2009). However, these chemo-enzymatic methods rely on known irritant and carcinogenic chemicals, making their use problematic for some applications, especially within the personal care products industry.

In addition to these health concerns, another strong impetus to develop alternative and sustainable solutions for glycolic acid production comes from environmental and societal needs to reduce our dependence on fossil-based products and to promote bio-production from renewable carbon sources using microbial cell factories (Aguilar et al., 2013). GA represents a good opportunity for such an advancement, motivated by the fact that there are no natural microbial producers to produce at high yield this platform molecule from sugars (Salusjarvi et al., 2019). Consequently, biotechnological production of this simple organic acid from renewable resources has received a substantial interest in the recent years leading to the engineering of four different routes as depicted in **Figure 1** (and reviewed in Salusjarvi et al., 2019). The glyoxylate shunt (GS) is the natural pathway, the physiological function of which is to bypass the oxidative decarboxylation of TCA cycle, thereby conserving carbon skeletons for biomass (Dolan and Welch, 2018). This bypass starts at the level of isocitrate, which is aldolytically cleaved into succinate and glyoxylate by isocitrate lyase (ICL) encoded by *aceA* in *E. coli*. The first attempt for the bioproduction of glycolic acid from D-glucose via the glyoxylate shunt in *Escherichia coli* has been patented by METEX (Soucaille, 2007). To achieve a production of *ca* 57 g/L at 45% of the theoretical yield, 13 genetic modifications have been implemented, including the overexpression of the NADPH glyoxylate reductase (GLR) encoded by *ycdW*/*ghrA*, attenuation of isocitrate dehydrogenase (IDH) and deletion of side pathways that prevent lactate and acetate production as well as to the oxidation of glycolate. Further genetic modifications brought about by Deng et al. (2018) resulted in an engineered strain able to produce 65 g/L at 90% of the theoretical yield. D-xylose and ethanol have been used as carbon source for GA production via engineering of GS pathway in *Saccharomyces cerevisiae* and *Kluyveromyces lactis* (Koivistoinen et al., 2013), whereas acetate was the carbon substrate for glycolate production by a engineered *C. glutamicum* strain for TCA cycle and GS pathway and using D-glucose for growth (Zahoor et al., 2014). However, the exploitation of GS for glycolic production presents at least two major limitations. The first one deals with the fact that the pathway has been optimized to use only D-glucose as the carbon source, either by releasing glucose repression of the glyoxylate shunt genes in *E.coli* (Gui et al., 1996) or by expressing these genes under non-repressible glucose promoter in the yeast *S. cerevisiae* (Koivistoinen et al., 2013). The second problem is related to the NADPH preference of the glyoxylate reductase enzymes, which generates redox imbalance in the cell. In *E. coli*, this problem is even reinforced if ICDH activity is attenuated since it results in a reduction of NADPH availability.

Three -non-natural- GA pathways (**Figure 1**) have been constructed and expressed in bacteria and yeast that could in part overcome the problems stated above. Firstly, the production of GA by these routes bypasses the central carbon metabolism. As such, it requires fewer enzymatic reaction steps than with the natural GS: only three enzymatic steps are required for the X1P pathway (Cam et al., 2016) while four for the R1P (Pereira et al., 2016a) and for the Dahms pathway (Cabulong et al., 2018). Lowering the number of reaction steps might have a positive effect on the production yield as it reduces the energy cost for protein synthesis and metabolic burden and reduce loss of intermediates by competitive pathways (Bilgin and Wagner, 2012). Second, GA is produced from glycolaldehyde by a NAD^+-dependent (glycol)aldehyde dehydrogenase. However, only pentose sugars can be assimilated by these non-natural pathways. In addition to this limitation, only two carbons of the C5-intermediates are utilized to produce GA whereas the three remained carbons are diverted into biomass via DHAP. To overcome in part this carbon loss, X1P and R1P pathways have been combined with GS bypass, enabling assimilation of both hexose and pentose sugars (Alkim et al., 2016; Pereira et al., 2016b). Conversion of C5 sugar to GA with high yield has been also proposed by linking part of the GS pathway with two reverse glyoxylate pathway (RGP) enzymes malate thiokinase and malyl-coA lyase through Dahms pathway to recuperate pyruvate and recycle malate into glyoxylate (Cabulong et al., 2018).

The combination of the natural glyoxylate shunt with non-natural GA producing pathways is very promising, as for instance, a conversion rate of D-xylose into GA at 92% of the theoretical yield was obtained by the Dahms-GS-RGP (Cabulong et al., 2018). However, these pathways still present

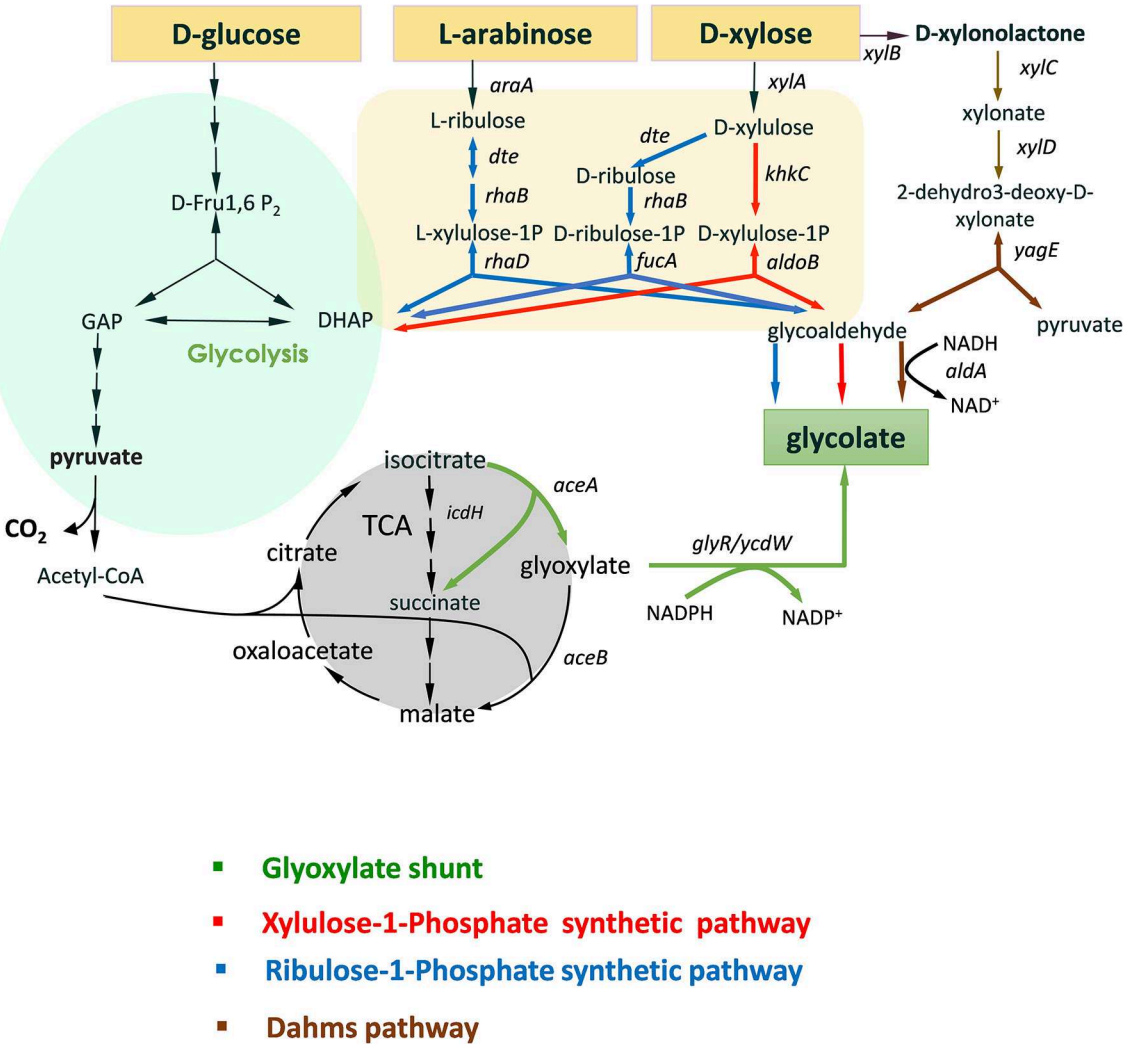

FIGURE 1 | Scheme of natural and non-natural pathways for glycolic acid production from D-glucose, D-xylose, and L-arabinose. Only the most significant genes (enzymes) are illustrated. Legend: *araA (*arabinose isomerase*); dte* (tagatose 6-P epimerase); *rhaB* (L-rhamnulokinase); *rhaD* (L-rhamno 1-phosphate aldolase); *xylA* (xylose isomerase); *fucA* (L-fuculose-1-phosphate aldolase); *khKC* (keto-hexokinase/fructose-1phosphate kinase); *aldoB* (aldolase-B); *xylB* (xylose dehydrogenase; *xylC* (xylonolactone lactonase); *xylD* (xylonate dehydratase); *yagE* (KDX aldolase); *aldA* (glycoaldehyde dehydrogenase).

some metabolic hurdles such as redox imbalance between NADH and NADPH. In addition, they do not reach the maximum energy yield (Y^E) which is the maximum amount of product that can be formed from a substrate (Dugar and Stephanopoulos, 2011). This Y^E value is pathway independent and is determined by the ratio γ_s/γ_p where γ_s and γ_p are the reduction degrees of the substrate and the product, respectively. Accordingly, it can be calculated that Y^E of glycolic acid ($\gamma_p = 6$) from D-glucose ($\gamma_S = 24$) and from pentose ($\gamma_S = 20$) would be 4 and 3.3, respectively. However, this yield can only be reached if the biological system is capable of uptaking a carbon mole as CO_2. Alternatively, if the loss of CO_2 at the level of pyruvate is prevented (see **Figure 1**), the theoretical yield of GA from D-glucose and pentose would be 3 and 2.5 moles/mole, which is 50% higher than that obtained by natural and non-natural pathways (**Table 1**). Given this postulate, the purpose of this communication was to design and validate a novel -non-natural- GA pathway enabling an efficient assimilation of pentose and hexose derived from lignocellulosic biomass into GA to reach these yields and that in the meantime solving most of the problems raised by the existing ones and notably to overcome redox imbalance.

MATERIALS AND METHODS

Chemicals and Reagents

All chemicals and solvents were purchased from Sigma-Aldrich unless otherwise stated. Restriction endonucleases and DNA-modifying enzymes were from New England Biolabs. DNA plasmid were extracted using GeneJET Plasmid Miniprep Kit

TABLE 1 | Maximal yield of glycolic acid as calculated from stoichiometric and thermodynamic rules.

Pathway	Yield of GA (mole/mole)		References
	D-xylose/L-arabinose	D-glucose	
Glyoxylate shunt (GS) pathway	1.66	2	Deng et al., 2018
Ribulose-1P pathway	1	0	Pereira et al., 2016a
Xylulose-1P pathway	1	0	Cam et al., 2016
Ribulose-1P+ GS pathways	2	2	Pereira et al., 2016a
Xylulose-1P + GS pathways	2	2	Alkim et al., 2016
Dahms-GS-RGP pathway	2	–	Cabulong et al., 2018
Glycoptimus pathway	2.5	3	This work

TABLE 2 | Plasmids used or constructed in this study.

Name	Description	Source
pET28a	Kan ^{R,} ori ColE1, Ptac	Novagen
pZA33	Cm^R, ori p15A, $P_{a1lac0-1}$	Expressys
pZA27	Kan ^{R}, ori p15A, proC	This study
pZA36	Cm ^{R}, ori p15A, P_{tac}	This study
pZA38	Cm ^{R}, ori p15A, proC	This study
pZS23	Kan ^{R}, ori pSC101, $P_{a1lac0-1}$	Expressys
pZS27	Kan ^{R}, ori pSC101, proD	This study
pA4	pZS23 aldA	This study
pA7	pZS27 aldA	This study
pKF3	pZA36 kdsD fsaA	This study
pKF6	pZS38 aldA	This study
pVT-FSAA	pET28 fsaA	This study
pVT-KDSD	pET28 kdsD	This study
pVT-ALDA	pET28 aldA	This study

(Thermo Scientific). DNA sequencing was subcontracted to Eurofins SAS (Ebersberg, Germany).

Plasmid Construction

Vectors pZA23, pZA33, pZE23, and pZS23 from Expressys® were used as they are inducible by IPTG and harbor a lightened structure of the *lacI* gene which reduces its size (2 358 to 3 764 bp) and they are modulable (easy to change replication origin, resistance marker and vector promoter by restriction/ligation). In this study, the promoter PA1lac0-1 in pZA33 has been replaced by the constitutive promoter proC and by the inducible promoter P_{tac}, generating pZA37 and pZA36, respectively. Likewise, the promoter PA1lac0-1 of pZS23 has been replaced by proD generating pZS28.

Gene cloning was carried out using NEBuilder HIFI DNA Assembly Master Mix (NEB E2621). This method enables several fragments to be assembled in a single step. The commercial mixture provided by New England Biolabs contains (a) an exonuclease, which creates 3′ single strand ends, which facilitates assembly of the fragments, which share a sequence complementarity; (b) a polymerase, which fills the empty spaces after the fragments have been assembled; and (c) a ligase, which links fragments together. The *E. coli kdsD*, *fsaA* and *aldA* genes were amplified from the genome DNA extracted from *E. coli* K12 MG1655 by PCR using primers described in **Table S1**. Fragments (*kdsD* + *fsaA or aldA*) were then inserted by HiFi assembly® into linearized beforehand pZ with primers hybridizing on either side of the MCS. All the plasmids have been verified by sequencing. The resulting plasmids bearing the *kdsD, fsaA, and aldA* genes are reported In **Table 2**.

Strain Construction and Transformation

The *E. coli* strains used in this work are listed in **Table 3**. Gene deletion (i.e., *glcD, fucA, mgsA,pfkA, ptsG*) was made by transduction using the phage P1vir. The preparation of the lysates P1vir and the transduction procedures were carried out as described in Bremer et al. (1984) with slight modifications. Strains (donor strain) from KEIO collection (Murakami et al., 2007) bearing a single deletion and a kanamycin antibiotic-resistance cassette was inoculated (200 µl of an overnight preculture made in LB) in 5 ml of LB containing 0.2% D-glucose and 5 mM $CaCl_2$ for 30 min at 37°C. Then, 100 µl of P1vir lysate ($\sim 5 \times 10^8$ phages/ml) was added to each donor culture and incubated at 37°C for 2 to 3 h until the culture was clear and the cells were completely lysed (Baba et al., 2006). The lysates were recovered by filtration using 25 mm sterile syringe filters with a 0.2 µm support membrane (Pall) and preserved at 4°C. To delete the gene of interest, the receiving strain was infected with P1vir bearing the donor gene deletion cassette having a kanamycin resistance. For this purpose, the receiving strain was previously cultivated in 5 ml LB medium at 37°C, collected by centrifugation at 1 500 g for 10 min and re-suspended in 1.5 ml of 10 mM $MgSO_4$ and 5 mM $CaCl_2$. P1vir Lysate bearing the gene deletion cassette from the donor strain was added (0.1 ml) to the receiving strain suspension and incubated for 30 min at 37°C. Then, 0.1 ml of 1 M sodium citrate was added, then 1 mL LB, and this cellular suspension was incubated of 1 h at 37°C, 200 rpm before being spread on a solid LB medium with the appropriate antibiotic. Colonies were screened by PCR to isolate successful transduction events. Removal of the antibiotic cassette was carried out by transformed of the bacteria strains with pCP20 plasmid bearing the FLP recombinase, followed by PCR checking.

The competent non-commercial strains were prepared according to the protocol of Chung et al. (1989) with minor modifications as followed. A pre-culture was made overnight in LB overnight. Fresh LB culture was then inoculate with cells at a DO_{600} of 0.1. When DO_{600} reaches about 0.5, 2 ml of culture was collected and to the resulting pellet was resuspended in 300 µl TSS buffer [$2.5\%_{(w/v)}$ PEG 3350, 1 M $MgCl_2$, $5\%_{(vol/vol)}$ DMSO]. After 10 min on ice, plasmid of interest was added to the cell suspension, which was further incubated for 30 min on ice. This step was followed by a heat shock at 42°C for 90 s. The transformed cells were put on ice for 10 min then 400 µl LB was added and the culture was incubated at 200 rpm for 1 h at 30°C. After centrifugation at 8 000 rpm for 2.5 min, the cell pellet was

TABLE 3 | *E. coli* strains used and constructed in this work.

Strain	Genotype	References
MG1655	F- λ- *ilvG- rfb*-50 *rph*-1	ATCC 407076
NEB5	*fhuA2* Δ*(argF-lacZ)U169 phoA glnV44 Φ80* Δ*(lacZ)M15 gyrA96 recA1 relA1 endA1 thi-1 hsdR17*	NEB
BL21 (DE3)	*huA2 [lon] ompT gal (λ DE3) [dcm]* Δ*hsdS)*	NEB
Screen00	MG1655 ΔtktA ΔtktB ΔglcD containing pZA36	This study
Screen09	Screen00 containing pZA36 kdsD fsaA (pKF3) and pZS23 aldA (pA4)	This study
Screen14	MG1655 ΔtktA ΔtktB ΔglcD containing pZA27	This study
Screen23	Screen00 containing pZA37 kdsD fsaA (pKF6) and pZA28aldA (pA7)	This study
WC3G gapA-	W3CG F^-, *LAM*$^-$, *gapA 10::Tn10, IN(rrnD-rrnE), rph*$^{-1}$	Ganter and Pluckthun, 1990
BW25113	F-, Δ*(araD-araB)567*, Δ*lacZ4787*(::rrnB-3), λ^-, *rph-1*, Δ*(rhaD-rhaB)568*, *hsdR514*	Baba et al., 2006
JW2771	BW25113 ΔfucA	Baba et al., 2006
JW4364	BW25113 ΔarcA	Baba et al., 2006
JW5129	BW25113 ΔmgsA	Baba et al., 2006
JW2946	BW25113 ΔglcD	Baba et al., 2006
JW2771	BW25113 ΔfucA	Baba et al., 2006
JW3887	BW25113 ΔpfkA	Baba et al., 2006
Glyco00	WC3G *gapA-10::Tn10* ΔglcD ΔarcA ΔmgsA ΔfucA ΔpfkA galP^{ProD}	This study
Glyco09	GA00 containing pZA36 kdsD fsaA (pKF3) and pZS23 aldA (pA4)	This study
Glyco23	GA00 containing pZA38 kdsD fsaA (pKF6) and pZA27 aldA (pA7)	This study

resuspended in 600 μl of LB and 150 μl were spread on a solid LB plates with the appropriate antibiotic.

Cultures Conditions

For molecular biology techniques, the bacteria strains were cultured in the LB medium (10 g/L trypton, 5 g/L yeast extracts and 5 g/L NaCl), and 5 g/L agar was added for solid medium in petri dishes. For GA production, the mineral medium M9 was used. Unless otherwise stated, it contained per liter: 18 g $Na_2HPO_4^*12H_2O$, 3 g KH_2PO_4, 0.5 g NaCl, 2 g NH_4Cl, 0.5 g $MgSO_4^*7H_2O$, 0.015 $CaCl_2^*2H_2O$, 1 ml of 0.06 M $FeCl_3$ from a 1000 × stock solution in concentrated HCl, 2 ml of 10 mM thiamine HCl stock solution, 20 g MOPS, and 1 ml of trace element solution (1000 × solution of 0.5 g $Na_2EDTA^*2H_2O$, 0.18 g $CoCl_2^*6H_2O$, 0.18 g $ZnSO_4^*7H_2O$, 0.4 g $Na_2MoO_4^*2H_2O$, 0.1 g H_3BO_3, 0.12 g $MnSO_4^*H_2O$, 0.12 g $CuCl_2$ × H_2O). The carbon source D-glucose, L-arabinose or D-xylose was added at a final concentration of 10 g/l, the pH was adjusted to 7 with acid 3-(N-morpholino) propanesulphonic (MOPS) and then filter sterilized through 0.2 μm membranes. The antibiotics ampicillin, kanamycin and chloramphenicol were added when required at concentrations of 100, 50, and 25 mg/L, respectively.

For the *E. coli* strains defective in transketolase activity *(*Δ*tktA* Δ*tktB)*, M9 medium was supplemented with 500 μM L-phenylalanine, 250 μM L-tyrosine, 200 μM L-tryptophan, 6 μM p-aminobenzoate, 6 μM p-hydroxydenzoate, and 280 μM shikimate and trace of LB (20% $_{V/V}$). For the strains defective in glyceraldehyde-3-phosphate dehydrogenase activity (Δ*gapA*), the M9 medium was completed with 0.4 g/L malic acid adjusted at pH 7 with KOH. When required, the appropriate antibiotics was added to the medium at 100 μg/mL for ampicillin, 50 μg/mL for kanamycin, or 25 μg/mL for chloramphenicol. The bacteria cultures were placed in rotatory shaker at 200 rpm and at 37°C. Growth was monitored by measuring absorbance at 600 nm with a spectrophotometer (Biochrom Libra S11).

Enzymes Production, Purification, and Assays

The *kdsD*, *fsaA,* and *aldA* genes were amplified using primers in **Table S1** and cloned in the expression vector pET28a (Novagen). The *E. coli* strain BL21 (DE3) transformed with the plasmid bearing these genes were inoculated from a pre-culture made in LB-kanamycin (50 mg/ L) in 200 mL of LB-Kanamycin at 600 nm (DO_{600}) of 0.1 at 16°C in a rotary shaker at 200 rpm. When DO_{600} reached 0.6–0.8, the expression of the protein of interest was induced by addition of IPTG at 1 mM final concentration 1 mM IPTG. After 16 h at 16°C, the culture was collected by centrifugation at 4,800 rpm for 15 min at 4°C. The cell pellet was re-suspended in 1.5 mL washing buffer (50 mM HEPES, pH 7.5; 0.3 M NaCl) and sonicated four times (30 s each) at 30% power on ice. The HIS-tagged proteins were purified using cobalt resin according to the protocol described in commercial kit (Clontech). Purification of the protein was verified by SDS-PAGE electrophoresis and protein concentration was measured by Bradford method (Bradford, 1976)

Enzymes assays were made in a Tris-Cl, 100 mM pH 7.5/10 mM $MgCl_2$ buffer at 37°C. Unless otherwise stated, KdsD activity was measured in a coupled assay in the presence of 3 mM NAD^+ and 5 mM D-Ribu-5P with 10 μg/ml of each of FsaA and AldA. FSA was measured by coupling GAP produced from cleavage of 3 mM Ara5P with the oxidation of 0.2 mM NADH at 340 nm in the presence of 1 U/ml of triose isomerase and glycerol-3-P dehydrogenase. AldA was measured in the same buffer by reduction of NAD^+ (3 mM) at 340 nm in the presence of 5 mM glycolaldehyde.

Analytical Methods

Extracellular metabolites were determined by high performance liquid chromatography (HPLC) with an Ultimate 3000 chromatograph (Dionex, Sunnyvale, USA). The HPLC system was equipped with a cation exchange column (Aminex, HPX87H; 300 × 7.8 mm, 9 μm, BioRad), an automatic injector (WPS-3000RS, Dionex), an IR detector (RID 10A, Shimadzu) and a UV detector (SPD-20A, Shimadzu). The sample injection volume was 20 μL, and the compounds were separated in an Aminex HPX-87H column protected by a Micro-Guard Cation H pre-column (BioRad, USA). The separation was performed at 35°C with 1.25 mM H_2SO_4 at 0.5 mL min^{-1} as mobile phase.

All samples were centrifuged (2 min at 10,000 g) and syringe-filtered (0.2 μm), and the resulting supernatant kept at −20°C until analysis.

Genome-Scale Modeling and Flux Balance Analysis

The iJO1366 genome-scale *E. coli* model (Orth et al., 2011) has been adapted to simulate GA production through the glycoptimus pathway. Notably, a modified *fsaA* reaction was added to the model to allow the conversion of arabinose-5P into glyceraldehyde-3P and glycolaldehyde. Parsimonious flux balance analyses (pFBA) were performed using the OptFlux software (Rocha et al., 2010), using either D-glucose, L-arabinose or D-xylose as a carbon source. For each simulation, the uptake rate of the carbon source was arbitrarily set at 10 $mmol.g_{CDW}^{-1}.h^{-1}$. Non-growth associated maintenance was set at 3.15 $mmol_{ATP}.g_{CDW}^{-1}.h^{-1}$, and reactions involved in the electron transport system were constrained to simulate a realistic P/O ratio, as previously described (Orth et al., 2011). pFBA simulations were performed using GA export as the objective function to maximize.

Statistical Methods

Statistical analyses were conducted in Microsoft Excel® using the Analysis ToolPak package. A two-tailed unpaired *t*-test was to use to compare fluorescence induction levels, in which an alpha level of $p < 0.05$ was set for significance.

RESULTS AND DISCUSSION

Pathway Design and Modeling

The pathway design that could maximally convert the lignocellulose-derived sugars D-glucose, D-xylose and L-arabinose into GA with, in theory, no loss of CO_2 is illustrated in **Figure 2**. This route relies on two key enzymatic steps that are sequentially catalyzed by an isomerase encoded by *kdsD*/*yrbH* (Meredith and Woodard, 2003), which interconverts D-Ribu-5P and D-Ara-5P, and an aldolase encoded by *fsaA* (Schurmann and Sprenger, 2001) that cleaves this intermediate into glycolaldehyde and GAP. The latter is shuttled back to D-Ribu-5P via the pentose phosphate pathway. Overall, this cyclic pathway should in theory produces 3 moles GA per mole of consumed D-glucose and 2.5 moles GA per mole of consumed pentose sugar, as confirmed by parsimonious flux balance analyses (**Table S2** and **Figure S1**). The proposed pathway is thermodynamically favorable as deduced from the sum of $\Delta_r G'^0$ of each reaction using Equilibrator (http://equilibrator.weizmann.ac.il/) (**Figure S2**). The large negative Gibbs energy results from the phosphorylation of the sugar and the oxidation of glycolaldehyde by the glycoladehyde dehydrogenase encoded by *aldA* (**Figure 2**). In addition, this metabolic pathway which we termed "glycoptimus" is redox balanced since NADH produced can be regenerated to NAD^+ via oxidative phosphorylation, leading to ATP production. This energy provision is sufficient to sustain GA production, based on the assumption that (i) 2 moles ATP are produced per mole of NADH and (ii) 2 moles of ATP are required for the active transport and phosphorylation

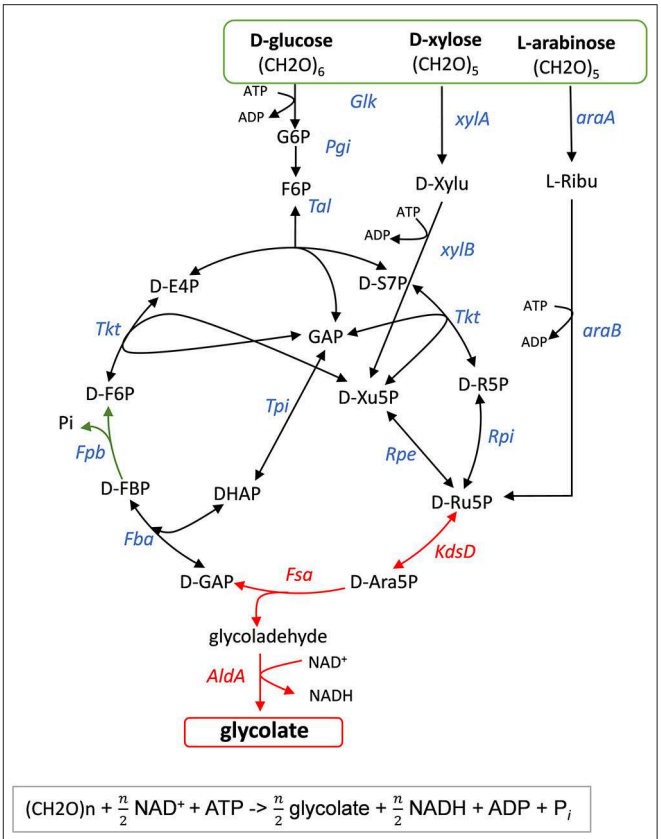

FIGURE 2 | Scheme of the glycoptimus pathway. Key steps are D-arabinose-5-phosphate isomerase (KdsD) and fructose-6-phosphate aldolase (FsaA) shown as red arrows. In green is shown the oxidation of glycoladehyde to glycolate by glycoladehyde dehydrogenase AldA. Glk, glucokinase; Pgi, phosphoglucoseiomserase, Tal, transaldolase; Tkt, transketolase; Rpi, ribose-5-P isomerase; Rpe, ribulose-5-P epimerase; Fba, fructose1,6-bisphosphate aldolase; Tpi, triose isomerase; Fbp, fructose1,6-bisphosphate phosphatase; xylA, xylose isomerase; xyB, xylulose 5-P kinase; araA, arabinose isomerase; araB, L-ribulose-5-P kinase. Stoichiometry of the glycoptimus reaction with sugar is given below.

of each mole of sugar. As flux balance analyses equilibrate redox and energetic balances, modeling of the glycoptimus pathway highlighted that optimal flux toward GA production should be accompanied with a reduction of the P/O ratio. Indeed, the model adjusts the production of ATP to the needs of the system (i.e., sugar uptake and non-growth associated maintenance). Excess of redox cofactors is therefore equilibrated by the introduction of futile cycles within the model. These results highlight the fact that an *in vivo* strategy toward a maximal GA production yield might require further process development (e.g., use of micro-aerobic conditions) to adapt oxidative phosphorylation and redox balance during the production phase. Alternatively, the introduction of additional reactions to oxidize the excess of NADH produced by AldA could be considered.

Kinetic Properties of Key Enzyme Encoded by *kdsD* and *fsaA* and *in vitro* Validation

Our rational to design this pathway arose from the fact that *E. coli* genome is endowed with *kdsD*/*yrbH* gene that encodes an Ara5P

isomerase (Meredith and Woodard, 2003). The physiological function of this enzyme is to generate D-Ara-5P from D-Ribu-5P as the first precursor in the biosynthesis of 3-deoxy-(D)-manno-octulosonate (KDO), a sugar moiety located in the lipopolysaccharide layer of most Gram-negative bacteria. We have revised the kinetic properties of the three key enzymes in the proposed pathway, namely KdsD, FsaA, and AldA, all being expressed in *E. coli* BL21 (DE3) strain as HIS-tagged fusion proteins. The enzyme KdsD was confirmed to be highly specific toward D-Ara-5P and D-Ribu-5P. However, the determined catalytic constant (k_{cat}) and Michaelis-Menten affinity constant (K_M) values for the D-Ribu-5P substrate were found to be distinct of those previously reported by Meredith and Woodard (2003). In particular, a four-fold higher K_M (D-Ribu-5P, ∼1.3 mM) and a 10-fold lower k_{cat} (D-Ribu-5P, 24 s^{-1}) were obtained in our study (**Table 4**). These differences could be ascribed to the presence of the HIS-tag at the N-terminus of the protein, which could interfere with the catalytic activity of this enzyme. For the aldolytic cleavage of D-Ara-5P into glycolaldehyde et GAP, the aldolase encoded by *fsaA* was retained based on the work of Garrabou et al. (2009) which reported a higher specificity of this enzyme to D-Ara-5P than to F6P; the latter being cleaved into dihydroxyacetone and GAP (Schurmann and Sprenger, 2001). While the physiological function of this class I aldolase in *E. coli* is still unclear, this enzyme is profitably employed as a biocatalyst for stereoselective C-C bond formation (Clapes et al., 2010). The K_M and k_{cat} determined on D-Ara-5P using purified His-tagged FsaA enzyme (named FsaA-HIS) was in the range of those obtained by Garrabou et al. (2009) (**Table 4**). Since KdsD and FsaA both catalyse reversible reactions, the feasibility of this pathway is ensured by coupling the NAD^+-dependent glycolaldehyde dehydrogenase to the oxidative phosphorylation chain (resulting in NAD^+ regeneration coupled to ATP synthesis). We thus determined the kinetic properties of the purified AldA (**Table 4**). While the K_M for glycoladehyde was similar to that reported in the original work of Caballero et al. (1983), the k_{cat} was 10-fold lower, which may be due to difference in enzyme purification and condition of enzymatic assay. Nonetheless, determination of catalytic efficiencies (expressed as k_{cat}/K_M) indicated that FsaA is most likely the rate-limiting step in the metabolic route yielding GA from D-Ribu5-P (**Table 4**).

We then validated the functioning of the glycoptimus route *in vitro* by incubating D-Ribu5-P with purified KdsD, FsaA, and AldA (**Figure 3**). Pathway validity was assessed by following the increase of absorbance at 340 nm corresponding to NADH production coupled with the stoichiometric formation of GA as confirmed by HPLC analyses. In the absence of either KdsD or FsaA, no NADH formation was observed as expected.

Growth-Based Screening of the Glycoptimus Pathway

The most direct way to show that a synthetic pathway works *in vivo* is to express the genes of that pathway in a plasmid under the dependence of an inducible promoter. Upon promoter induction with a suitable inducer, the production of the compound of interest can be monitored. However, it is also wiser to associate the implementation of a synthetic pathway with a phenotypical trait that is fully dependent of the *in vivo* functioning of the pathway. With this procedure, effects of plasmids copy number, promoter strength, RBS, position of the genes in the operon can be investigated in a combinatorial manner to find out the expression modules leading to the best production pathway. With respect to our glycoptimus pathway, we took advantage of the previous finding that an *E. coli* strain defective in transketolase encoded by *tktA* and *tktB* is unable to grow on D-xylose or L-arabinose (Josephson and Fraenkel, 1969, 1974). Expression of *kdsD-fsaA-aldA* module pathway shall restore cell growth in the aforementioned sugar substrates. With this approach (see **Figure 2**), the assimilation of D-xylose or L-arabinose will result in the formation of glycoladehyde and GAP. While the former can be oxidized into GA, GAP will be used for cell growth (see **Figure S3**). The herein proposed screening strategy shall in principle meet two criteria: (i) growth rescue of a Δ*tktA* Δ*tktB* mutant on D-xylose (or L- arabinose), and (ii) GA production correlated to growth proficiency of the mutant strain bearing the pathway. To avoid degradation of GA product, the *glcD* gene encoding the glycolate oxidase (Pellicer et al., 1996) has been also deleted from the template screening strain.

Accordingly, we initially constructed a single *kdsD-fsaA-aldA* operon under the control of the IPTG-inducible P_{lac} promoter expressed from medium- and high-copy number plasmids from the pZ collection. Unexpectedly, none of these constructs rescued growth of the MG1655Δ*tktA* Δ*tktB* Δ*glcD* on D-xylose. Upon sequencing of these plasmids, we systematically found a deletion in the P_{lac} promotor, which was due to a repeat motif of this promotor present in these pZ plasmids. This event has been recognized earlier and explained by a replication-slipping mechanism, which often occurs due to the presence of short repeat motifs in these plasmids (Kawe et al., 2009). Replacement of P_{lac} by P_{tac} was also unsuccessful, resulting instead in Tn10 transposon insertion in the *kdsD* gene. We therefore changed our strategy by expressing *aldA* separately from *kdsD-fsaA*. We found that splitting the operon in two different but compatible plasmids enabled growth rescue of the Δ*tktA* Δ*tktB* Δ*glcD* strain. Encouraged by this observation, we constructed 24 different expression systems in which combination of 3 types of vectors carrying three different but compatible replication origin and 4 different promoters (2 inducible P_{tac} and P_{lac} and 2 constitutive proC and prod, Davis et al., 2011) were attempted, while genes order of *kdsD-fsaA* and their original RBS sequences remained unchanged. These 24 different expression systems (see details on plasmid constructs for this purpose in **Table S3** and **Figure S4**) were transformed into MG1655Δ*tktA* Δ*tktB* Δ*glcD* strain. After an overnight pre-culture in M9 medium with 10 g/l of D-glucose supplemented with 0.1% (w/v) LB and 0.1% (w/v) yeast extract, the cells were collected by centrifugation, washed once with sterile water and resuspended at an initial $0D_{600}$ of 0.5 in M9 containing 10 g/L D-xylose complemented with the necessary auxotrophic requirements. After 46 h of cell cultivation during which growth was monitored (notice that growth rate of the transformants was rather low in the range of 0.03 to 0.05 $h^{-1,}$ data not shown), the supernatant was collected to

TABLE 4 | Catalytic constants of arabinose-5P isomerase (KDSD), fructose-6P aldolase (FSA), aldehyde dehydrogenase (AldA) purified from *E. coli* expressing the protein flanked of a His-tag at the N-terminus of the sequence.

Enzyme	Substrate	K_M (mM)	V_{max} (μmoles.min^{-1} mg^{-1})	k_{cat} (s^{-1})	k_{cat}/K_M ($s^{-1}.mM^{-1}$)
KdsD-His	D-ribulose-5P	1.30 ± 0.12	1.4 ± 0.17	24	18.4
FsaA-His	D-arabinose-5P	0.65 ± 0.15	0.26 ± 0.09	3.6	5.5
AldA-His	glycolaldehyde	0.21 ± 0.05	1.66 ± 0.31	52	247.5

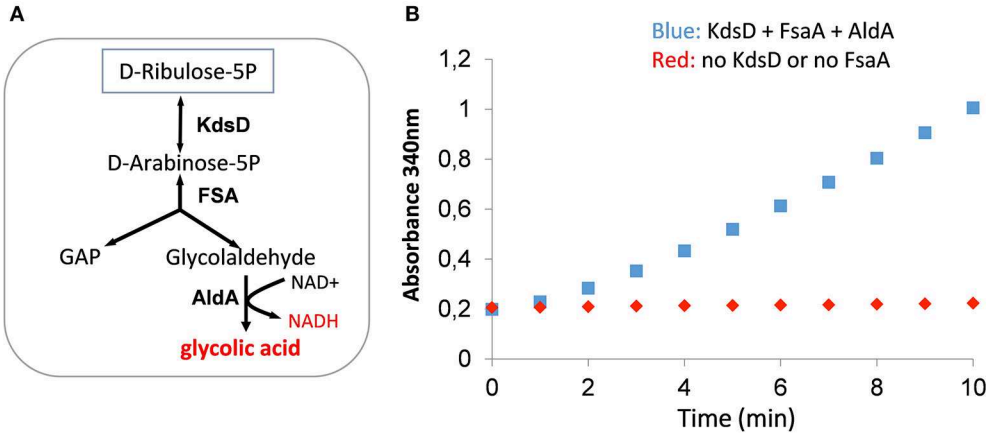

Time (min)	NADH (mM)	GA (mM)
0	0	0
10	0,2	nd
60	1,43	1,57

FIGURE 3 | *In vitro* validation of the KdsD-FsaA pathway for GA production. In **(A)** *In vitro* enzyme assay scheme for conversion of D-ribulose 5-phosphate into GA. In **(B)** is shown the NADH production resulting from the conversion of D-ribulose 5-phosphate into GA. The reaction was made in 1 ml buffer solution (100 mM Tris-HCl pH 7.5, 10 mM $Mgcl_2$, 0.1 mM $MnCL_2$, and 1 mM sodium thiamine pyrophosphate) in the presence of 5 mM D-ribulose 5-phosphate, 2 mM NAD^+, and 10 μg of each of purified KdsD, FsaA, and AldA enzyme.

measure GA produced and D-xylose consumed by HPLC. The results supported in part our assertion as the amount of GA produced was roughly correlated ($R^2 \sim 0.53$) with growth (**Figure 4A**). A slightly better correlation was obtained between GA produced and D-xylose consumed ($R^2 \sim 0.72$, see **Figure S5**), which may indicate that GA was produced in part independently to growth. Also, it was unanticipated to find a significant production of GA (4.7 mM) in strains bearing empty plasmids (namely strain Screen00 and Screen14), which otherwise hardly grew on D-xylose. A careful analysis of the exometabolome in these transformants showed the presence of D-xylulose whose accumulation was the highest in the control strains Screen00 and Screen14. Moreover, an inverse correlation could be drawn by plotting GA yield per D-xylose vs. D-xylulose yield per D-xylose (see **Figure S5B**). While these data support the notion that GA production is coupled to growth, it still does not explain where GA comes from in the non-growing strains. There is at least two possibilities, which are likely additive. On the one hand, GA could arise from the aldolytic cleavage of D-xylulose by FsaA. We indeed found a weak activity of this enzyme on D-xylulose, which exhibited a very weak affinity on this substrate (**Figure S6**). Alternatively or complementary to this possibility, part of the hyperaccumulated phosphorylated sugars that are found in the non-growing strain (up to 15 mM, data not shown) can be diverted to GA using the endogenous activity of KdsD, FsaA, or its homolog FsaB and AldA (data no shown).

From the correlation of GA produced to D-xylose consumed, it turned out that strains termed Screen09 and Screen23 were the best producers with a product yield of 0.48 mol GA/mol of D-xylose (**Figure 4B**). Interestingly, in both strains, the *kdsD-fsaA* operon and *aldA* gene were carried out in a medium- and a low-copy plasmid, respectively. While the expression system of these genes was IPTG inducible in strain Screen09, *kdsD-fsaA,* and *aldA* were driven by the constitutive promoter proD and proC, respectively. We also validated that these two strains could produce GA from L-arabinose. As shown in **Figure 5**, the production of GA on D-xylose and L-arabinose was significantly better in strain Screen09 and Screen23 than in the control strain Screen00, which showed that the module pathway driven either by an IPTG inducible (strain Screen09) or

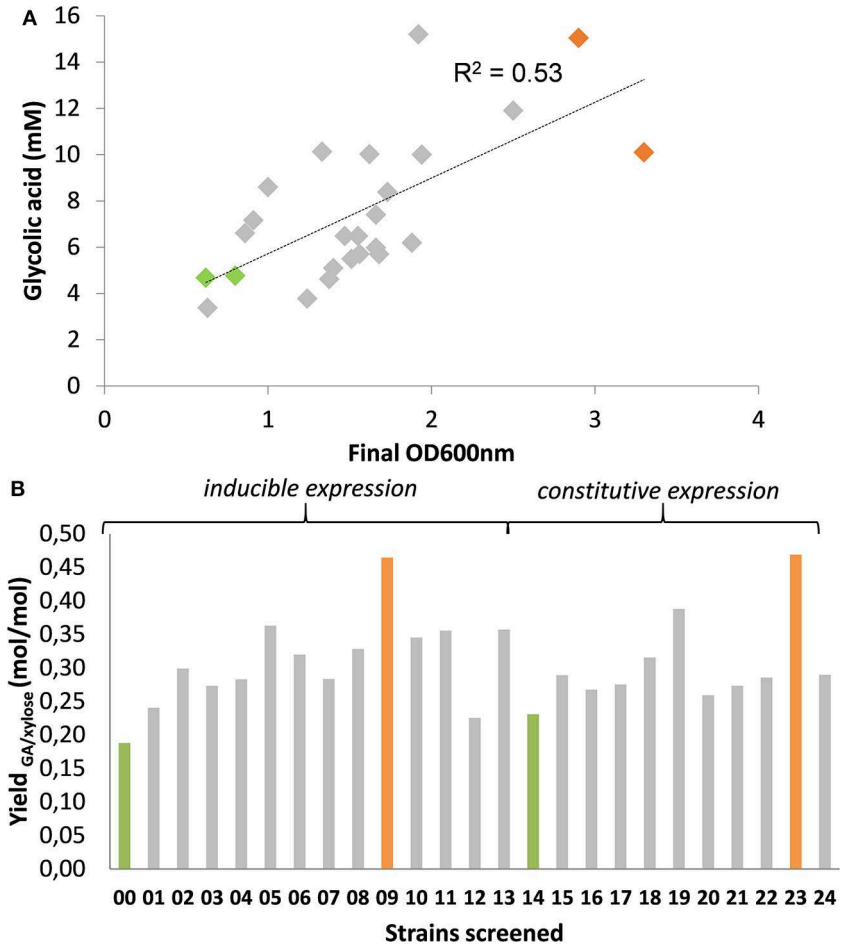

FIGURE 4 | *In vivo* screen of strains for production of GA expressing *KdsD-fsaA* + *aldA* operon. Strain MG1655 Δ*tktA* Δ*tktB* Δ*glcD* was transformed with pZS bearing various *kdsD-fsaA* + *aldA* operons as described in **Table S3**, **Figure S4** and cultivated on M9 supplemented in the presence of 1% (w:v) D-xylose. After an adaptation phase of about 16–24 h, cells were centrifuged (4,000 rpm, 5 min) and re-inoculated at DO_{600} of 0.5 in 50 mL of the same medium in 250 ml baffled shake flask. Growth was monitored at 600 nm **(A)** and after 150 h, when OD_{600} was stable, which is after 150 h, sample was taken to measure GA in the supernatant. **(B)** Results shown are the mean of two independent experiments.

by constitutive promoters (strain Screen23) was operational. In addition, although the titer of GA on D-xylose was higher than on L-arabinose, the yield was actually comparable (i.e., 0.5 mole / mole of sugar), indicating that D-xylose was better assimilated than L-arabinose.

Further Engineering of the Central Carbon Metabolism and Effect on GA Production

While the results reported above proved that the *kdsD-fsaA* + *aldA* module pathway is functional *in vivo*, we wanted to go one-step further by refactoring the central carbon metabolism to drive more carbon for GA production. Therefore, our starting *E. coli* strain was W3CG, which is defective in the lower part of glycolysis due to a *Tn10* transposon insertion into *gapA* encoding glyceraldehyde-3P dehydrogenase (Ganter and Pluckthun, 1990). The homologous gene *gapB* was found to be inactive in this strain (Tsuruno et al., 2015). Hence, this strain requires a gluconeogenic substrate such as malate in addition to D-glucose to grow. Our metabolic engineering for maximal GA production implied to delete competing but non-essential pathways for growth, as they could siphon intermediates out of the glycoptimus pathway (genetic intervention are schematically depicted in **Figure S7**). Therefore, the oxidation of glycolate into glyoxylate was abrogated by deletion of *glcD* encoding glycolate dehydrogenase (Pellicer et al., 1996). Meanwhile, *arcA*, which encodes the DNA-transcriptional regulator of the two-component system *ArcAB* implicated in redox state signaling (Malpica et al., 2006) was disrupted since it was reported to repress *aldA* (Pellicer et al., 1999). Deletion of *mgsA* encoding methylglyoxal synthase (Saadat and Harrison, 1998) and *fucA* encoding a fuculose aldolase was also carried out in the recipient strain to reduce siphoning of DHAP/GAP out of the glycoptimus pathway. We also deleted *pfkA* encoding PFK-1 isoform I, which contributes to 90% of the phosphofructokinase activity (Kotlarz et al., 1975) to avoid wasteful recycling of F6P into $F1,6P_2$. Finally, the sugar/H^+ transporter encoded by *galP* was overexpressed

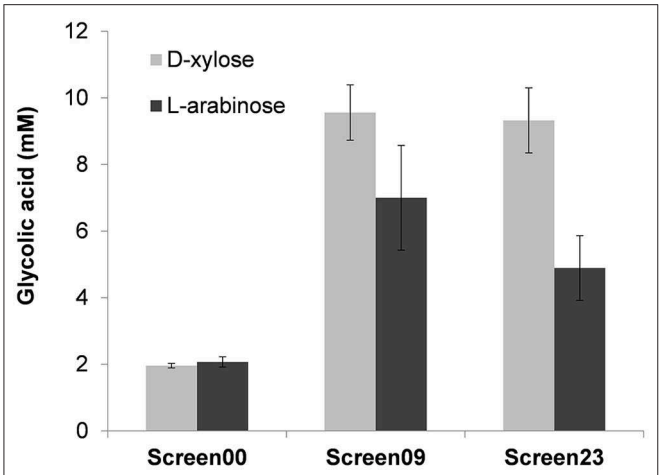

FIGURE 5 | Glycolic acid production in MG1655 Δ*tktA* Δ*tktB* Δ*glcD* on D-xylose and L-arabinose. Strain Screen09 was MG1655 Δ*tktA* Δ*tktB* Δ*glcD* transformed with the IPTG inducible operon *kdsD-fsaA* (pKF3 in pZA36) and pA4 (aldA in pZS23), whereas strain Screen23 was MG1655 Δ*tktA* Δ*tktB* Δ*glcD* transformed with pKF6 (*kdsD-fsaA* in pZA38 under constitutive promoter proC) and pA7 (*aldA* in pZS27 under constitutive promoter proD). The strains were cultivated in mineral medium M9 at 37°C in the presence of D-xylose or L-arabinose at 10 g/L. GA was determined after 46 h of growth by HPLC. The results shown are the mean ± SD of three independent experiments.

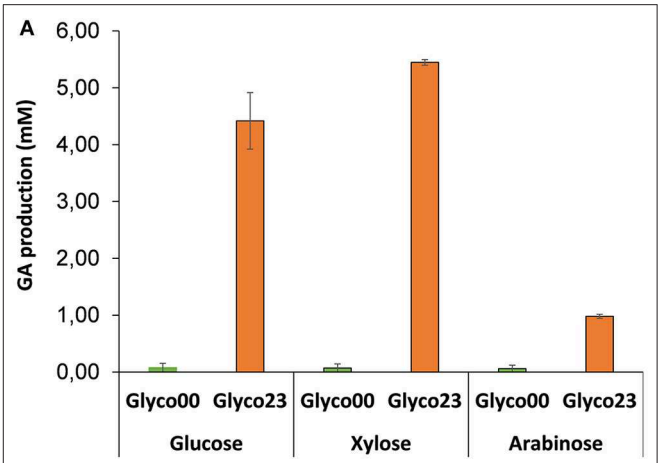

B

Sugars	Glycolic acid Yield (mol/mol) / [% of max]
Glucose	0.19 / [6.3]
Xylose	0.60 / [24]
Arabinose	0.68 / [27]

FIGURE 6 | Titer and yield of GA in strain Glyco and Glyco23 on D-xylose and L-arabinose. Strain Glyco00 corresponded to *E. coli* WC3G Δ*gapA* Δ*glcD* Δ*arcA* Δ*mgsA* Δ*fucA* Δ*pkf proD-galP*, transformed with empty vector pZA36 and pZS27 whereas pKF6 and pA7, was used to yield Glyco23 strain. The strains were preliminary cultivated in 50 ml of mineral medium M9 containing 5 g/L malate and 1 g/L D-xylose at 37°C in 250 ml shake flask at 37°C. When malate was completely consumed, 5 g/L of either D-xylose or L-arabinose was added and the culture was further incubated for 24 h. **(A)** Titer and **(B)** yield were determined after 24 of cultures. The results are the mean ± SD of two independent experiments.

by swapping its own promoter by the strong constitutive proD promoter to favor uptake of D-glucose and D-xylose (Henderson, 1990).

This engineered strain termed Glyco00 was transformed with the constitutive expression system 23 corresponding to plasmid pKF6 (*kdsD-fsaA* under proC promoter in a medium copy plasmid) and pA7 (*aldA* under proD promoter in a low copy plasmid) to yield strain Glyco23. Both the untransformed and transformed strains were firstly cultivated in mineral medium M9 in the presence of malate (5 g/L) and D-xylose (1 g/L), with a growth rate in the range of 0.07 −0.11 h^{-1}. After complete consumption of malate, D-xylose, L-arabinose or D-glucose were added at 5 g/L. GA production was monitored for 24 h. It can be seen in **Figure 6** that strain Glyco23 was able to produce GA from hexose and pentose sugars. However, the production yield was only 0.2, 0.6, and 0.68 mole GA per mole of D-glucose, D-xylose and L-arabinose, respectively (**Figure 6B**). This very low yield is not in accordance with our model. In addition, only a small amount of sugar has been consumed during the 48 h-incubation period, suggesting that the expression of the glycoptimus pathway has impaired the energetic status of the cell. Ongoing work is underway to clarify this problem. It is interesting to notice that the control strain Glyco00 did not accumulate GA, which supports the hypothesis that the production of GA seen in screen00 (see **Figure 4**) might originate from D-xylulose and/or phosphorylated sugars that were accumulated, what did not occur in Glyco00 because the pentose phosphate pathway was operational.

Several hypothesis can be drawn to optimize the carbon flux toward GA production with additional metabolic engineering. According to our model, the glucose-6P dehydrogenase encoded by *zwf*, which catalyzes the entrance of D-glucose into the pentose phosphate pathway should be deleted, as well as of *eda-edd* of the Entner-Doudoroff, as both reaction can bypass deletion of *gapA* and generate pyruvate which will then feed the TCA cycle. Additionally, sugar transport can be a valuable target for optimization. Notably, the phosphoenolpyruvate-dependent phosphotransferase (PTS) system does not induce a carbon loss *per se*, but it causes some deviation of PEP that contributes to biomass production. Loss of *PTS* function may have two significant advantages: better assimilate pentose sugars and make possible to uncouple growth and production over time. A bi-phasic process can further be developed to improve the yield. The first phase will be dedicated to the production of biomass from an affordable carbon source in C2, C3, or C4 (ex: malate) to fuel TCA cycle. Meanwhile, the second phase of the fermentation will be dedicated to the production of glycolic acid from lignocellulosic sugars. As highlighted by the flux balance analyses, this second phase could also benefit from further process development, notably by using micro-aerobic conditions to adapt oxidative phosphorylation and redox balance during the production phase. By combining further metabolic engineering and process development, it should be feasible to

reach GA production yield close to theoretical maximum yield of 3 moles of GA per mole of C6 and 2.5 moles per mole of C5.

CONCLUSION

A new non-natural pathway for GA production has been conceived, implemented and *in vivo* validated. This new pathway termed glycoptimus relies on two pillars. On the one hand, it required the overexpression of three naturally occurring *E. coli* genes, namely *kdsD*, *fsaA* and *aldA*, whose physiological role are still unclear except for *kdsD*. This synthetic pathway combined with the refactoring of the central carbon metabolism to minimize the carbon loss as CO_2 at the level of pyruvate should allow to yield theoretically 2,5, and 3 moles of GA from lignocellulosic pentose and hexose, respectively. We successfully demonstrated that this pathway was operational *in vivo*, leading to the production of GA from D-glucose, D-xylose and L-arabinose, albeit at yield that was only at 20–30% of the theoretical ones. Nevertheless, these results argued for a great potential of this microbial process in term of industrial feasibility which will require further optimisation including among others, additional metabolic and strain engineering as well as efficient coupling of NADH reoxidation and energy requirement for sugars uptake and phosphorylation. In addition to ensure stability and robustness of this synthetic pathway, bioprocess-engineering optimisation will be determinant notably because a two-stage process in which a production phase uncoupled from growth is likely the most favorable condition to be conducted to achieve high yield and titer of GA with engineered strains equipped with the glycoptimus pathway.

DATA AVAILABILITY STATEMENT

The datasets generated for this study are available on request to the corresponding author.

AUTHOR CONTRIBUTIONS

CL, CF, and FK performed the experiments. NM carried out the modeling. TW and JF provided guidance for the experimental setups and helped interpreting the results. JF and CL wrote the paper, which has been improved by TW, CF, and NM. All authors approved the final version.

FUNDING

This study was supported in part by the' Agence Nationale de la Recherche - France (Synpathic project, ANR14-CE06-0024) to JF. CL was financed by MENERT (Ministery of Research and Education) during this work.

ACKNOWLEDGMENTS

We are grateful to Miss Lucie Spina for HPLC analysis.

SUPPLEMENTARY MATERIAL

The Supplementary Material for this article can be found online at: https://www.frontiersin.org/articles/10.3389/fbioe.2019.00359/full#supplementary-material

REFERENCES

Aguilar, A., Magnien, E., and Thomas, D. (2013). Thirty years of European biotechnology programmes: from biomolecular engineering to the bioeconomy. *N. Biotechnol.* 30, 410–425. doi: 10.1016/j.nbt.2012.11.014

Alkim, C., Trichez, D., Cam, Y., Spina, L., Francois, J. M., and Walther, T. (2016). The synthetic xylulose-1 phosphate pathway increases production of glycolic acid from xylose-rich sugar mixtures. *Biotechnol. Biofuels* 9:201. doi: 10.1186/s13068-016-0610-2

Baba, T., Ara, T., Hasegawa, M., Takai, Y., Okumura, Y., Baba, M., et al. (2006). Construction of *Escherichia* coli K-12 in-frame, single-gene knockout mutants: the Keio collection. *Mol. Syst. Biol.* 2:2006.0008. doi: 10.1038/msb4100050

Bilgin, T., and Wagner, A. (2012). Design constraints on a synthetic metabolism. *PLoS ONE* 7:e39903. doi: 10.1371/journal.pone.0039903

Bradford, M. M. (1976). A rapid and sensitive method for the quantitation of microgram quantities of protein utilizing the principle of protein-dye binding. *Anal. Biochem.* 72, 248–254. doi: 10.1016/0003-2697(76)90527-3

Bremer, E., Silhavy, T. J., Weisemann, J. M., and Weinstock, G. M. (1984). Lambda placMu: a transposable derivative of bacteriophage lambda for creating lacZ protein fusions in a single step. *J. Bacteriol.* 158, 1084–1093.

Caballero, E., Baldoma, L., Ros, J., Boronat, A., and Aguilar, J. (1983). Identification of lactaldehyde dehydrogenase and glycolaldehyde dehydrogenase as functions of the same protein in *Escherichia* coli. *J. Biol. Chem.* 258, 7788–7792.

Cabulong, R. B., Lee, W. K., Banares, A. B., Ramos, K. R. M., Nisola, G. M., Valdehuesa, K. N. G., et al. (2018). Engineering *Escherichia* coli for glycolic acid production from D-xylose through the Dahms pathway and glyoxylate bypass. *Appl. Microbiol. Biotechnol.* 102, 2179–2189. doi: 10.1007/s00253-018-8744-8

Cam, Y., Alkim, C., Trichez, D., Trebosc, V., Vax, A., Bartolo, F., et al. (2016). Engineering of a synthetic metabolic pathway for the assimilation of (d)-xylose into value-added chemicals. *ACS Synth. Biol.* 5, 607–618. doi: 10.1021/acssynbio.5b00103

Chung, C. T., Niemela, S. L., and Miller, R. H. (1989). One-step preparation of competent *Escherichia* coli: transformation and storage of bacterial cells in the same solution. *Proc. Natl. Acad. Sci. U.S.A.* 86, 2172–2175. doi: 10.1073/pnas.86.7.2172

Clapes, P., Fessner, W. D., Sprenger, G. A., and Samland, A. K. (2010). Recent progress in stereoselective synthesis with aldolases. *Curr. Opin. Chem. Biol.* 14, 154–167. doi: 10.1016/j.cbpa.2009.11.029

Davis, J. H., Rubin, A. J., and Sauer, R. T. (2011). Design, construction and characterization of a set of insulated bacterial promoters. *Nucleic Acids Res.* 39, 1131–1141. doi: 10.1093/nar/gkq810

Deng, Y., Ma, N., Zhu, K., Mao, Y., Wei, X., and Zhao, Y. (2018). Balancing the carbon flux distributions between the TCA cycle and glyoxylate shunt to produce glycolate at high yield and titer in *Escherichia coli*. *Metab. Eng.* 46, 28–34. doi: 10.1016/j.ymben.2018.02.008

Dolan, S. K., and Welch, M. (2018). The Glyoxylate Shunt, 60 Years on. *Annu. Rev. Microbiol.* 72, 309–330. doi: 10.1146/annurev-micro-090817-062257

Drent, E., Mul, W., and Ruisch, B. (2001). *Process for the Carbonylation of Formaldehyde*. International Application No. PCT/EP2000/013357.

Dugar, D., and Stephanopoulos, G. (2011). Relative potential of biosynthetic pathways for biofuels and bio-based products. *Nat. Biotechnol.* 29, 1074–1078. doi: 10.1038/nbt.2055

Fredenberg, S., Wahlgren, M., Reslow, M., and Axelsson, A. (2011). The mechanisms of drug release in poly(lactic-co-glycolic acid)-based drug delivery systems–a review. *Int. J. Pharm.* 415, 34–52. doi: 10.1016/j.ijpharm.2011.05.049

Gädda, T. M., Pirttimaa, M. M., Koivistoinen, O., Richard, P., Penttilä, M., and Harlin, A. (2014). The industrial potential of bio-based glycolic acid and polyglycolic acid: (Short survey). *Appita J.* 67. Available online at: https://cris.vtt.fi/en/publications/the-industrial-potential-of-bio-based-glycolic-acid-and-polyglyco

Ganter, C., and Pluckthun, A. (1990). Glycine to alanine substitutions in helices of glyceraldehyde-3-phosphate dehydrogenase: effects on stability. *Biochemistry* 29, 9395–9402. doi: 10.1021/bi00492a013

Garrabou, X., Castillo, J. A., Guerard-Helaine, C., Parella, T., Joglar, J., Lemaire, M., et al. (2009). Asymmetric self- and cross-aldol reactions of glycolaldehyde catalyzed by D-fructose-6-phosphate aldolase. *Angew. Chem. Int. Ed Engl.* 48, 5521–5525. doi: 10.1002/anie.200902065

Gui, L., Sunnarborg, A., Pan, B., and Laporte, D. C. (1996). Autoregulation of iclR, the gene encoding the repressor of the glyoxylate bypass operon. *J. Bacteriol.* 178, 321–324. doi: 10.1128/jb.178.1.321-324.1996

He, Y. C., Xu, J. H., Su, J. H., and Zhou, L. (2010). Bioproduction of glycolic acid from glycolonitrile with a new bacterial isolate of *Alcaligenes* sp. ECU0401. *Appl. Biochem. Biotechnol.* 160, 1428–1440. doi: 10.1007/s12010-009-8607-y

Henderson, P. J. (1990). Proton-linked sugar transport systems in bacteria. *J. Bioenerg. Biomembr.* 22, 525–569. doi: 10.1007/BF00762961

Josephson, B. L., and Fraenkel, D. G. (1969). Transketolase mutants of *Escherichia coli*. *J. Bacteriol.* 100, 1289–1295.

Josephson, B. L., and Fraenkel, D. G. (1974). Sugar metabolism in transketolase mutants of *Escherichia coli*. *J. Bacteriol.* 118, 1082–1089.

Kataoka, M., Sasaki, M., Hidalgo, A. R., Nakano, M., and Shimizu, S. (2001). Glycolic acid production using ethylene glycol-oxidizing microorganisms. *Biosci. Biotechnol. Biochem.* 65, 2265–2270. doi: 10.1271/bbb.65.2265

Kawe, M., Horn, U., and Pluckthun, A. (2009). Facile promoter deletion in *Escherichia* coli in response to leaky expression of very robust and benign proteins from common expression vectors. *Microb. Cell Fact.* 8:8. doi: 10.1186/1475-2859-8-8

Koivistoinen, O. M., Kuivanen, J., Barth, D., Turkia, H., Pitkanen, J. P., Penttila, M., et al. (2013). Glycolic acid production in the engineered yeasts *Saccharomyces cerevisiae* and *Kluyveromyces lactis*. *Microb. Cell Fact.* 12:82. doi: 10.1186/1475-2859-12-82

Kotlarz, D., Garreau, H., and Buc, H. (1975). Regulation of the amount and of the activity of phosphofructokinases and pyruvate kinases in *Escherichia coli*. *Biochim. Biophys. Acta* 381, 257–268. doi: 10.1016/0304-4165(75)90232-9

Malpica, R., Sandoval, G. R., Rodriguez, C., Franco, B., and Georgellis, D. (2006). Signaling by the arc two-component system provides a link between the redox state of the quinone pool and gene expression. *Antioxid. Redox Signal.* 8, 781–795. doi: 10.1089/ars.2006.8.781

Meredith, T. C., and Woodard, R. W. (2003). *Escherichia* coli YrbH is a D-arabinose 5-phosphate isomerase. *J. Biol. Chem.* 278, 32771–32777. doi: 10.1074/jbc.M303661200

Murakami, K., Tao, E., Ito, Y., Sugiyama, M., Kaneko, Y., Harashima, S., et al. (2007). Large scale deletions in the *Saccharomyces cerevisiae* genome create strains with altered regulation of carbon metabolism. *Appl. Microbiol. Biotechnol.* 75, 589–597. doi: 10.1007/s00253-007-0859-2

Orth, J. D., Conrad, T. M., Na, J., Lerman, J. A., Nam, H., Feist, A. M., et al. (2011). A comprehensive genome-scale reconstruction of *Escherichia* coli metabolism—2011. *Mol. Syst. Biol.* 7:535. doi: 10.1038/msb.2011.65

Pellicer, M. T., Badia, J., Aguilar, J., and Baldoma, L. (1996). glc locus of *Escherichia* coli: characterization of genes encoding the subunits of glycolate oxidase and the glc regulator protein. *J. Bacteriol.* 178, 2051–2059. doi: 10.1128/jb.178.7.2051-2059.1996

Pellicer, M. T., Lynch, A. S., De Wulf, P., Boyd, D., Aguilar, J., and Lin, E. C. (1999). A mutational study of the ArcA-P binding sequences in the aldA promoter of *Escherichia coli*. *Mol. Gen. Genet.* 261, 170–176. doi: 10.1007/s004380050954

Pereira, B., Li, Z. J., De Mey, M., Lim, C. G., Zhang, H., Hoeltgen, C., et al. (2016a). Efficient utilization of pentoses for bioproduction of the renewable two-carbon compounds ethylene glycol and glycolate. *Metab. Eng.* 34, 80–87. doi: 10.1016/j.ymben.2015.12.004

Pereira, B., Zhang, H., De, M. M., Lim, C. G., Li, Z. J., and Stephanopoulos, G. (2016b). Engineering a novel biosynthetic pathway in *Escherichia* coli for production of renewable ethylene glycol. *Biotechnol. Bioeng.* 113, 376–383. doi: 10.1002/bit.25717

Rocha, I., Maia, P., Evangelista, P., Vilaca, P., Soares, S., Pinto, J. P., et al. (2010). OptFlux: an open-source software platform for *in silico* metabolic engineering. *BMC Syst. Biol.* 4:45. doi: 10.1186/1752-0509-4-45

Saadat, D., and Harrison, D. H. (1998). Identification of catalytic bases in the active site of *Escherichia coli* methylglyoxal synthase: cloning, expression, and functional characterization of conserved aspartic acid residues. *Biochemistry* 37, 10074–10086. doi: 10.1021/bi980409p

Salusjarvi, L., Havukainen, S., Koivistoinen, O., and Toivari, M. (2019). Biotechnological production of glycolic acid and ethylene glycol: current state and perspectives. *Appl. Microbiol. Biotechnol.* 103, 2525–2535. doi: 10.1007/s00253-019-09640-2

Schurmann, M., and Sprenger, G. A. (2001). Fructose-6-phosphate aldolase is a novel class I aldolase from *Escherichia coli* and is related to a novel group of bacterial transaldolases. *J. Biol. Chem.* 276, 11055–11061. doi: 10.1074/jbc.M008061200

Soucaille, P. (2007). *Glycolic Acid Production by Fermentation from Renewable Resources.* WO/2007/141316.

Tsuruno, K., Honjo, H., and Hanai, T. (2015). Enhancement of 3-hydroxypropionic acid production from glycerol by using a metabolic toggle switch. *Microb. Cell Fact.* 14:155. doi: 10.1186/s12934-015-0342-1

Wei, G., Yang, X., Gan, T., Zhou, W., Lin, J., and Wei, D. (2009). High cell density fermentation of *Gluconobacter* oxydans DSM 2003 for glycolic acid production. *J. Ind. Microbiol. Biotechnol.* 36, 1029–1034. doi: 10.1007/s10295-009-0584-1

Zahoor, A., Otten, A., and Wendisch, V. F. (2014). Metabolic engineering of *Corynebacterium glutamicum* for glycolate production. *J. Biotechnol* 192, 366–375. doi: 10.1016/j.jbiotec.2013.12.020

Conflict of Interest: The authors declare that the research was conducted in the absence of any commercial or financial relationships that could be construed as a potential conflict of interest.

frontiers in Bioengineering and Biotechnology

ORIGINAL RESEARCH
published: 07 January 2020
doi: 10.3389/fbioe.2019.00372

Development of a Biosensor for Detection of Benzoic Acid Derivatives in *Saccharomyces cerevisiae*

Sara Castaño-Cerezo[1]*, *Mathieu Fournié*[1], *Philippe Urban*[1], *Jean-Loup Faulon*[2,3] and *Gilles Truan*[1]

[1] TBI, Université de Toulouse, CNRS, INRA, INSA, Toulouse, France, [2] Micalis Institute, INRA, AgroParisTech, Université Paris-Saclay, Jouy-en-Josas, France, [3] Chemistry School, Manchester Institute of Biotechnology, The University of Manchester, Manchester, United Kingdom

4-hydroxybenzoic acid (pHBA) is an important industrial precursor of muconic acid and liquid crystal polymers whose production is based on the petrochemical industry. In order to decrease our dependency on fossil fuels and improve sustainability, microbial engineering is a particularly appealing approach for replacing traditional chemical techniques. The optimization of microbial strains, however, is still highly constrained by the screening stage. Biosensors have helped to alleviate this problem by decreasing the screening time as well as enabling higher throughput. In this paper, we constructed a synthetic biosensor, named sBAD, consisting of a fusion of the pHBA-binding domain of HbaR from *R. palustris*, the LexA DNA binding domain at the N-terminus and the transactivation domain B112 at the C-terminus. The response of sBAD was tested in the presence of different benzoic acid derivatives, with cell fluorescence output measured by flow cytometry. The biosensor was found to be activated by the external addition of pHBA in the culture medium, in addition to other carboxylic acids including *p*-aminobenzoic acid (pABA), salicylic acid, anthranilic acid, aspirin, and benzoic acid. Furthermore, we were able to show that this biosensor could detect the *in vivo* production of pHBA in a genetically modified yeast strain. A good linearity was observed between the biosensor fluorescence and pHBA concentration. Thus, this biosensor would be well-suited as a high throughput screening tool to produce, via metabolic engineering, benzoic acid derivatives.

Keywords: *p*-hydroxybenzoic acid, *p*-aminobenzoic acid, biosensor, synthetic biology, yeast

OPEN ACCESS

Edited by:
Jean Marie François, UMS3582 Toulouse White Biotechnology (TWB), France

Reviewed by:
Muralikannan Maruthamuthu, Purdue University, United States
M. Kalim Akhtar, United Arab Emirates University, United Arab Emirates

***Correspondence:**
Sara Castaño-Cerezo
castanoc@insa-toulouse.fr

Specialty section:
This article was submitted to Synthetic Biology, a section of the journal Frontiers in Bioengineering and Biotechnology

Received: *01 August 2019*
Accepted: *13 November 2019*
Published: *07 January 2020*

Citation:
Castaño-Cerezo S, Fournié M, Urban P, Faulon J-L and Truan G (2020) Development of a Biosensor for Detection of Benzoic Acid Derivatives in Saccharomyces cerevisiae. Front. Bioeng. Biotechnol. 7:372. doi: 10.3389/fbioe.2019.00372

INTRODUCTION

Synthetic biology proposes cutting-edge methodologies for using natural resources (Jullesson et al., 2015; Smanski et al., 2016; Le Feuvre and Scrutton, 2018; Schindler et al., 2018), understanding basic cellular functions (Metzger et al., 2018; Toda et al., 2018) or reprogramming cell fate (Black and Gersbach, 2018). Biosynthesis of small organic molecules by microorganisms, instead of manufacturing them from petroleum-sourced synthesized chemicals, is one of the main objectives of metabolic engineering (Khalil and Collins, 2010; Markham and Alper, 2015; Li et al., 2018). While the demand for green (sustainable) chemistry is growing steadily, there are still few examples

of successful industrial production of molecules from microorganisms. The clear bottleneck in metabolic engineering lays in the low throughput of analytical techniques used to determine products yields compared to the rate of the construction of new engineered microorganisms (Rogers and Church, 2016). To overcome this limitation, natural or synthetic biosensors are potential tools capable of correlating the concentration of a target chemical within the cell to an easily monitored output signal, such as fluorescence (Farmer and Liao, 2000; Schulman and Heyman, 2004; Dietrich et al., 2010; Liu et al., 2017; Mannan et al., 2017).

The yeast *Saccharomyces cerevisiae* is a widely used model organism and production host, due to a comprehensive collection of metabolic engineering tools and deep knowledge of its genetics accumulated over half a century. However, the development of synthetic biosensors in yeast somewhat lags behind those available for *E. coli* (Leavitt and Alper, 2015). One of the first transcription factor-based biosensors was exemplified with the NhaR system from *Pseudomonas putida.* This system could drive the transcription of β-galactosidase as a function of benzoic acid and 2-hydroxybenzoic acid concentrations in *E. coli.* The system was applied to screen active enzymes capable of converting benzaldehyde and 2-hydroxybenzoaldehyde to their carboxylic acid derivatives (van Sint Fiet et al., 2006). Since then, several successful applications of biosensors have been described in *E. coli* (Selvamani et al., 2017; Ganesh et al., 2019) and more recently in cell-free systems (Eggeling et al., 2015; Voyvodic et al., 2019). However, transferring genetic sensors between various organisms remains highly challenging. For example, the simple transfer of a tetracycline resistance gene circuit from yeast to mammalian cells required extensive optimizations such as the translation of the reporter, the DNA sequences of the heterologous proteins, the nuclear localization signal of the transcription factor and the design of the promoter (Nevozhay et al., 2013).

In yeast, one of the first designed sensing systems was used to monitor the intracellular S-adenosylmethionine concentrations (Umeyama et al., 2013). Transcriptional-based biosensors were also constructed to screen for muconic acid-producing yeast strains (Leavitt et al., 2017; Snoek et al., 2018). Other types are now implemented, using optogenetic regulation such as the blue light-activated EL222 from *Erythrobacter litoralis* that was recently reported to control, in yeast, the mitochondrial isobutanol-producing pathway (Zhao et al., 2018).

4-hydroxybenzoic acid (pHBA), a molecule produced from chorismate by chorismate lyase, is present in low amounts in bacterial cultures (Winter et al., 2014). pHBA is essential in all organisms for coenzyme Q synthesis (Tran and Clarke, 2007) but was found to inhibit yeast growth when added to the culture medium (Ando et al., 1986; Palmqvist et al., 1999; Larsson et al., 2000). pHBA-derived natural products form a large group of secondary metabolites that exhibit a wide variety of biological activities (Wang et al., 2018). Industrial uses of pHBA include manufacturing of liquid crystal polymers and thermoplastics used for space technologies (Rothschild, 2016). The alkyl esters of pHBA, namely parabens, are also widely used as preservatives in drugs, cosmetic products and food products. However, their toxicity is a major human health concern (Giulivo et al., 2016). Currently, pHBA is chemically synthesized from petroleum-derived building blocks. Biotechnology offers an alternative for pHBA production, based on the shikimate pathway (Lee and Wendisch, 2017). Recently, researchers have engineered yeast to overproduce pHBA, increasing the flux to chorismate and expressing, in the modified strain, the chorismate lyase gene (UbiC) from *E. coli* (Averesch et al., 2017).

Therefore, pHBA is a molecule for which *in vivo* biological detection is critical, and a performant pHBA biosensor could be used either to build detection kits capable of operating in various biological environments or to screen the capacity of modified strains to overproduce pHBA. In this study, we report the construction of a synthetic transcription factor (sTF) capable of sensing pHBA, *in vivo*, in *Saccharomyces cerevisiae*. We tested the transcriptional activity against the native effector of *R. palustris* HbaR and a battery of metabolites with similar structure and determine the promiscuity and binding characteristics of each of them. Last, we exemplified the activity of our newly constructed biosensor in a pHBA-producing strain.

Abbreviations: bp, base pair; pHBA, 4-hydroxybenzoic acid; pABA, 4-aminobenzoic acid; 2HBA, 2-hydroxybenzoic acid (salicylic acid); 3HBA, 3-hydroxybenzoic acid; 2NBA, 2-aminobenzoic acid (anthranilic acid); 3NBA, 3-aminobenzoic acid; 2,5DHBA, 2,5 dihydroxybenzoic acid (gentisic acid); 3,4DHBA, 3,4 dihydroxybenzoic or protocatechuic acid; CSM, Complete Supplement Mixture; SD, Synthetic Defined medium; sTF, Synthetic transcription factor; sBAD, sensor of benzoic acid derivatives; YNB, Yeast Nitrogen Base.

MATERIALS AND METHODS

Culture Conditions

The vectors described in this work were constructed in the *E. coli* DH5α strain using standard molecular biology protocols (Sambrook and Russell, 2001). The CEN.PK 2C-1 *S. cerevisiae* strain (*MATa*; *ura3-52*; *trp1-289*; *leu2-3*, *112*; *his3:1*; *MAL2-8C*; *SUC2*) was used throughout the entire study.

For the screening experiments, yeast strains were grown in synthetic medium containing 20 g/L of glucose, 6.9 g/L of yeast nitrogen base with or without pABA and Complete Supplement Mixture (CSM) drop-out minus uracil and histidine (Formedium). The different inducers were dissolved in the medium and pH was then adjusted to 5.5. All culture media were sterilized by filtration. For pHBA production, the synthetic medium without pABA and with CSM drop-out minus His, Ura, and Leu was supplemented with 76 mg/L tyrosine, phenylalanine and tryptophan.

Yeast strains were cultured as follows. A fresh yeast colony from a SD minus Ura and His agar plate containing pABA was resuspended in water to an OD_{600nm} of 0.2 and 5 μL of this solution was used to inoculate 200 μL of media. Cells were grown at 30°C in a MixMate (Eppendorf) with 900 rpm agitation for 20 h. For the pHBA production experiments, a fresh colony was resuspended in water to an OD_{600nm} of 0.2 and 50 mL of culture medium was inoculated with 400 μL of this solution. Cells were grown at 30°C with an agitation of 200 rpm in an INFORS incubator (25 mm orbital) for 65 h.

Vectors and Strains Constructions

All plasmids and strains used in this study are listed in **Supplementary Tables 1, 2**. Yeast transformation was performed using the high efficiency protocol from Gietz (2014). The *hbaR* gene from *Rhodopseudomonas palustris,* the native *ubiC* gene from *E. coli* and the modified *ARO4K226L* gene from *S. cerevisiae* were codon-optimized for *S. cerevisiae* (Twist Bioscience). All DNA sequences can be found in **Supplementary Table 3**.

The pHBA sTF was constructed using the vector FRP880 as a backbone. FRP880 was digested with *Eco*RV to remove the estradiol-sensing domain and the HbaR-sensing domain was inserted by blunt-end cloning leading to the plasmid pSCC185. To create the ySCC185-F strain, we first integrated a DNA fragment expressing mKATE2 under the control of the *TDH3* promoter into the locus 2 of chromosome X (Mikkelsen et al., 2012) and carrying the auxotrophic marker *TRP1*, yielding ySCC001. pSCC185 was then linearized with the restriction enzyme *Pac*I, integrated in the *HIS3* locus in ySCC001, yielding ySCC185. Finally, the linearized plasmid FRP795, containing a promoter with 8 LexA DNA binding domains and a *CYC1* minimal promoter controlling the expression of the mCitrine fluorescent protein was integrated in ySCC185, yielding ySCC185-F. Integrations were verified by colony PCR and by functional analysis.

To build the pHBA-overproducing strain, we used the vector pENZ030 containing two homologous arms for the integration in the *HO* locus, a *LEU2* auxotrophic marker and a bidirectional promoter formed by *TDH3* and *PGK* and flanked by *ADH1* and *ADH2* terminators. The *ubiC* ORF was cloned downstream of the *TDH3* promoter by cutting pENZ030 with *Xho*I. The *ubiC* gene was inserted in pENZ030 by isothermal assembly. The pHBA-producing strains were derived from ySCC185-F. First, the *TRP3* gene was deleted using a hygromycin resistance cassette from the vector pUG75 flanked by a 38 bp homologous region of *TRP3* yielding ySCC185-F-T. The *ARO7* gene was then deleted and its promoter used to express the *ARO4K229L* mutant (Williams et al., 2015). To construct this, the previous strain was transformed with two cassettes. The first one contained the gene encoding the *ARO4K229L* mutant with two homologous regions of 40 bp, upstream for *ARO7* and downstream for the second integration cassette. The second cassette contained the *CYC1* terminator and G418 resistance. This DNA was amplified from the vector pMRI34 and the PCR containing homologous regions for the first cassette and the end of *ARO7* gene yielding ySCC185-F-A. This last strain was used to express the *E. coli ubiC* gene, using a PCR amplified DNA fragment and the vector pENZ030-UbiC as a template, yielding ySCC185-UbiC. The control strain for the pHBA production experiments was derived from ySCC185-F-A with an integrated copy of the empty vector pENZ30 (ySCC185-30).

Flow Cytometry

Cells were incubated for 30 min with 70 μg/mL cycloheximide (prepared in DMSO), further diluted to reach a cell count between 0.5×10^6 and 1.5×10^6 cells/mL and then immediately injected into a flow cytometer MACSQuant VYB (Miltenyi Biotec, Germany). Regions were determined as a function of the mCitrine and mKate2 fluorescence. Optimal laser and filter setups for the two dyes were as follows: 488 nm laser and 525/25 Band Pass B1-filter for mCitrine, and 561 nm laser and 615/10 Band Pass Y2-filter for mKate2. The expression profile of mKate2 was measured for each sample by the MACSQuant VYB flow cytometer with the MACSQuantify TM Software (Miltenyi Biotec, Germany). A filter was applied on FSC-A/SSC-A to select homogeneous cells regarding size, shape, and cellular complexity. The mean fluorescence value of mKate2 and mCitrine was calculated and exported.

Western Blot

Protein extracts were prepared following the protocol described by Zhang et al. (2011). Briefly, 1 OD_{600nm} of pelleted cells were pre-treated with 100 μL of 2 M lithium acetate solution, left standing on ice for 5 min, followed by 5 min centrifugation at 5,000 g, 4°C. The supernatant was discarded and 100 μL of a 0.4 M solution of NaOH added. After gentle resuspension and 5 min standing on ice, samples were centrifuged 5 min at 4°C. Cell pellets were vigorously vortexed with 60 μL of a dye solution containing bromophenol-blue and supplemented with 5% β-mercaptoethanol. After denaturation at 99°C for 10 min, 10 μL of each sample was deposited on a 10% SDS page gel. Semi-dry transfer was performed on a PVDF membrane (Merck Millipore, Darmstadt, Germany) using a Trans-Blot® SD Cell BioRad apparatus (15 V at 600 mA during 30 min). Five percent powdered milk in TBS was used as a blocking agent. Mouse primary antibody anti-EGFP (Thermoscientific), and secondary anti-mouse IgG coupled with alkaline phosphatase (Thermoscientific) were diluted following instructions from the provider. Antibody incubations were performed in 5% powdered milk in TBS during 1 h. Proteins were detected by the incubation of BCIP/NBT AP substrate buffer (Sigma-Aldrich, St. Louis, MO, USA).

pHBA HPLC Analysis

Supernatants of pHBA-producing strains were collected during 3 days of batch growth. Analysis of the pHBA production was carried out on a Waters Alliance HPLC system coupled with a 996 Waters PDA detector. Twenty microliter of the culture supernatant was injected on a Xterra column (100 × 2.0 mm and 3 μm particle size) maintained at 45°C during the analysis. The mobile phases consisted in a mixture of A (H_2O with 0.1% formic acid) and B (acetonitrile with 0.1% formic acid). The flow was set at 1 mL/min with the following gradient: 0–0.1 min 100% A, 0.1–11 min 40% A and 60% B, 11–12.5 min 100% B, 12.5–13 min 100% A. Absorbance spectra from 210 to 400 nm were recorded. pHBA was quantified by its absorbance at 254 nm.

Statistical Analysis

Statistical analyses were performed using the GRAPHPAD PRISM 8.2 software.

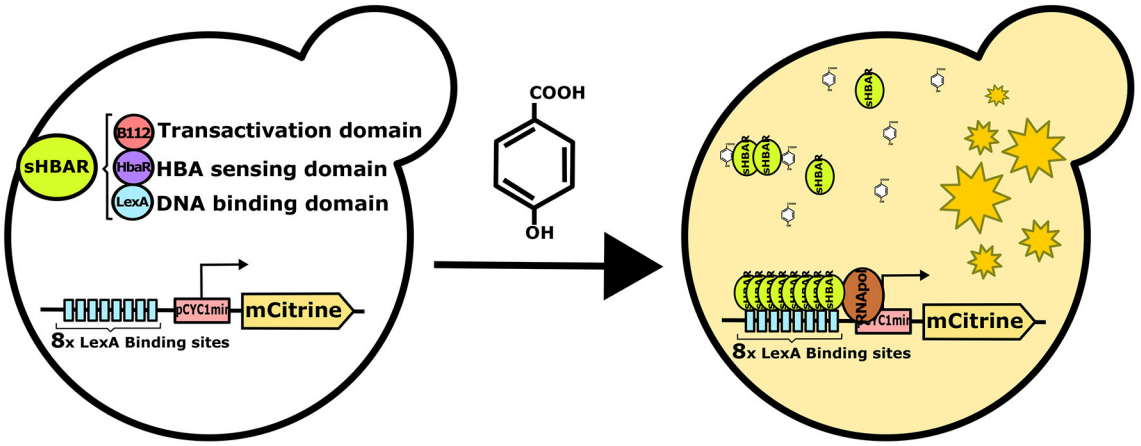

FIGURE 1 | Schematic representation the sHbaR sTF detecting pHBA *in vivo* in *S. cerevisiae*.

RESULTS AND DISCUSSION

Design and Validation of the Synthetic Transcription-Based Biosensor

The architecture chosen for the pHBA sTF was inspired by the work performed by Stelling and co-workers, in which a collection of modular tripartite sTFs, activated by estradiol, were developed (Ottoz et al., 2014). We thus designed our sTF using LexA and B112 proteins as DNA binding and transactivation domains, respectively (**Figure 1**). We cloned the ORF of the HbaR ligand binding domain from *R. palustris*, known to be specifically activated by pHBA (Egland and Harwood, 2000), between the transactivation and DNA binding domains (pSCC185, see **Supplementary Table 2**). To report the transcriptional activation of our synthetic pHBA biosensor, designated as sHbaR, we used the previously constructed vector FRP795 containing the gene encoding for the mCitrine yellow fluorescent protein downstream of the minimal *CYC1* promoter with 8 LexA DNA binding sites (Ottoz et al., 2014). The resulting strain, ySCC185-F, bears both the reporter gene and the sHbaR sTF.

To validate transcriptional activation by pHBA, the strain ySCC185-F was cultured in 96-well plates at 30°C with or without pHBA (2 mM). mCitrine fluorescence was measured at late exponential phase ($OD_{600nm} = 4$) to get the best sensitivity possible with a rather small volume of culture. As shown in **Figure 2**, the mCitrine fluorescence is 3-fold higher with pHBA compared with the control medium that did not contain the inducer. We also verified that the measured fluorescent signal is proportional to the quantity of mCitrine measured by Western Blot (**Supplementary Figure 1**). Notwithstanding the fact that a previous *in vitro* study described a sTF activated by pHBA (Yao et al., 2018), to our knowledge, sHbaR is the first biosensor that can be activated by pHBA *in vivo*, in *S. cerevisiae*.

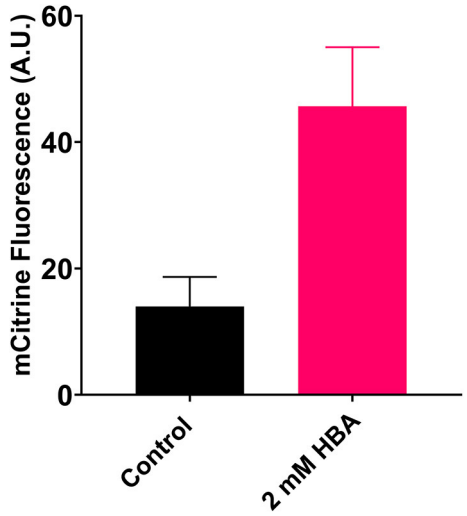

FIGURE 2 | pHBA activation of sHbaR in *S. cerevisiae*. mCitrine fluorescence was measured by flow cytometry at late exponential phase. Values are calculated as the mean of three biological replicates.

pABA Also Activates the sHbaR Sensing System

Analysis of the first experiments demonstrated that the fluorescent signal measured with the strain ySCC185-F in the absence of pHBA is greater than the signal measured without the reporter (**Supplementary Figure 2A**). This could be due either to some leakage of the synthetic promoter in the absence of the sTF or promiscuous activation of sHbaR by molecule(s) present in the medium or in the cells. In fact, promiscuity of benzoic acid-responsive natural transcription factors has been reported before, evidencing that they can respond, to different degrees, to a variety of substituted benzoic acids (but not pHBA) (Xue et al., 2014). Therefore, we hypothesized that a compound present in the synthetic medium could be also an effector of sHbaR.

The most similar metabolite to pHBA found in our synthetic media is p-aminobenzoic acid (pABA), which, according to the supplier's medium composition, is present at a final concentration of 1.46 μM. We thus analyzed if the low levels of pABA in this medium could activate sHbaR. As expected,

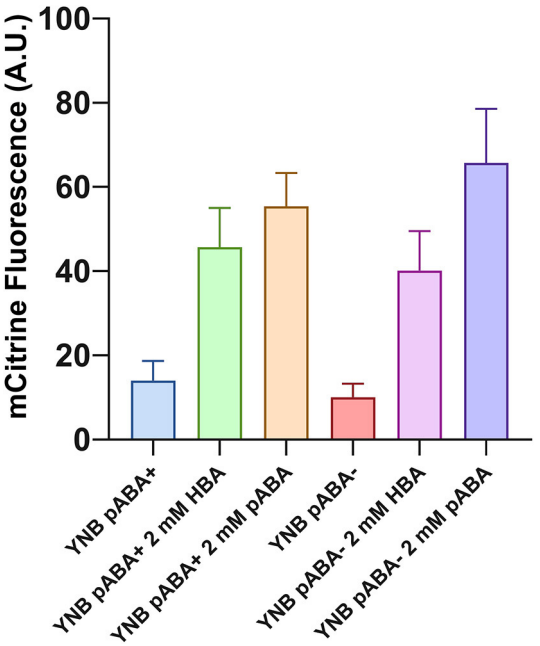

FIGURE 3 | pABA activates sHbaR. ySCC185-F was grown with YNB containing or not pABA and with the addition, in the medium, of 2 mM of pHBA or pABA. Cells were harvested in late exponential phase. Values are calculated as the mean of three biological replicates.

the fluorescence signal produced by the strain ySCC185-F is reduced by almost 30% in a synthetic medium devoid of pABA compared to the same one containing pABA (*p*-value 0.0014, **Figure 3**). This indicates that a rather small concentration of this metabolite in the growth medium indeed activates sHbaR *in vivo*. We also tested if tyrosine and phenylalanine that possess rather similar chemical structures to pHBA and that are present in the CSM at a concentration of 300 μM each could also activate sHbaR. We grew ySCC185-F with and without these amino acids and observed no difference between both conditions (**Supplementary Figure 2B**). We also supplemented each of the two amino acids to a final concentration of 2 mM and could not observe any difference in the level of fluorescence compared with the control medium (**Supplementary Figure 2B**). Since the promoter-reporter construction that we have used showed absolutely no leakage of transcription in the absence of inducers in a previous study (Ottoz et al., 2014), we thus attributed the remaining fluorescence signal to the presence of other molecules capable of activating sHbaR.

To further understand the possible competition or synergy between pABA and pHBA, we grew the strain ySCC185-F in YNB (containing or not pABA) in the presence of externally added pABA or pHBA (2 mM) (**Figure 3**). When pABA is present in the medium, the addition of 2 mM of pHBA or pABA induced, respectively, a 3- or 4-fold fluorescence increase. The same trend is observed on a synthetic medium devoid of endogenous pABA, i.e., a 4-fold augmentation of fluorescence with 2 mM pHBA and 6-fold with 2 mM pABA. We thus hypothesize that there is no competition or synergy between these two metabolites and sHbaR and that pABA is simply a better effector for sHbaR than pHBA.

Promiscuity of the Synthetic sHbaR Sensing System

Since sHbaR seems to not completely distinguish between two different substituents at the *para* position of benzoic acid, we decided to change the name of our biosensor to sBAD (previously known as sHbaR), standing for "sensor of benzoic acid derivatives." We further investigated the promiscuity of sBAD with different benzoic acid-derived chemicals at 2 mM each, in the absence of pABA in the growth medium (**Figure 4**). Interestingly, benzoic acid itself leads to a 5-fold activation of sBAD, a value comparable to the one obtained with pHBA (∼4 fold) and pABA (∼6 fold). The other three molecules substituted in the *ortho* position (2HBA (salicylic acid), 2NBA (anthranilic acid), and aspirin) were able to produce a low, but significant (2-fold) response of sBAD. A general trend for the specificity is remarkably conserved between hydroxy- or amino-substituted benzoic acid derivatives: the *para* position is the preferred one, followed by the *ortho* position and the *meta* position, which is the least potent for sBAD activation. For the rest of the tested metabolites, only those mono-substituted with a hydroxyl or amino group at the *ortho* or *para* position of the benzoic ring provided a significant increase of fluorescence compared to the control. Surprisingly, a larger substituent at the *ortho* position (aspirin, **Figure 4**H) can also activate sBAD. On the contrary, all other di-substituted benzoic acid derivatives were incapable of activating sBAD. This result indicates that sBAD has a rather tight control of the number of substituents on the aromatic ring.

It is known that the positions and the chemical properties of benzoic acid substituents influence the pK_a of the carboxylic group of the corresponding chemicals (**Supplementary Table 4**). A difference of 1.5 pH units indeed exists between the *ortho*-hydroxybenzoic acid ($pK_a = 3$) and pHBA ($pK_a = 4.6$). Thus, all tested metabolites have different pK_as and their diffusion through the plasma membrane of yeast might be slightly different. Moreover, it is known that the rates of import of benzoic acid derivatives (*p*-coumaric acid and pHBA) in *S. cerevisiae* are different (Barnhart-Dailey et al., 2019). However, as pHBA, 2HBA, pABA, 2NBA, benzoic acid, and aspirin all activate sBAD *in vivo* under the conditions tested, we assume that they are transported in the cell in order to activate the intracellular sBAD and trigger the corresponding fluorescence signal. Alternatively, the diverse responses obtained could also originate from different binding affinities of the different compounds to the sTF. As no crystal structure of the native transcription factor HbaR from *R. palustris* with its cognate binder (pHBA) is available, we can only hypothesize that the delocalization of π-electrons of the aromatic benzene ring may partly control the recognition of the inducer by the binding domain of the sBAD biosensor.

Dynamic Properties of the sBAD Sensing System

To obtain a more accurate resolution of the cellular responses and the operational dynamic range of the most active inducers, we quantified the binding affinity using dose-response curves with the yeast-expressed sBAD (**Figures 5A–D**). For the metabolites

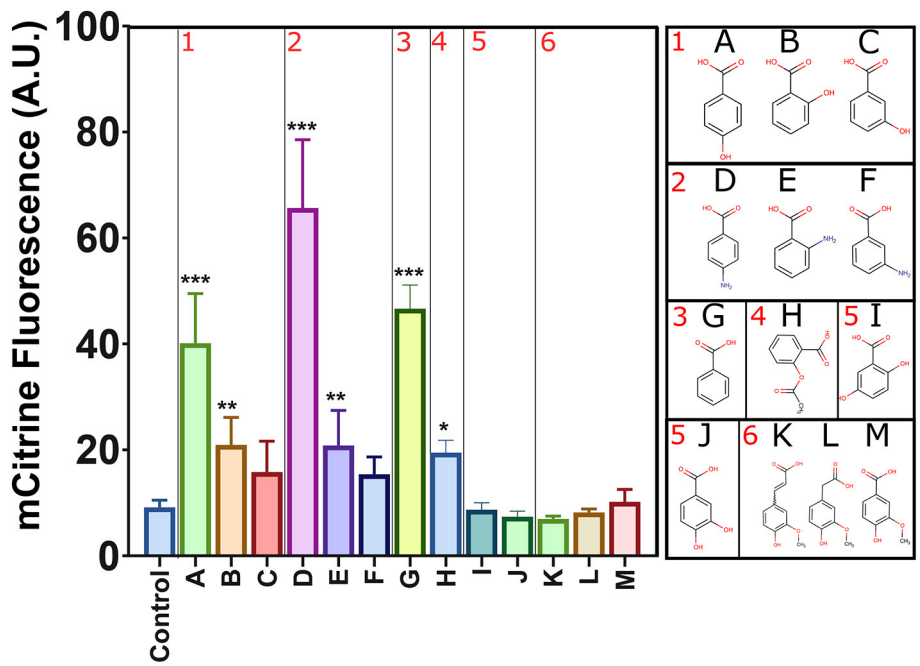

FIGURE 4 | sBAD activity with different benzoic acid derivatives. mCitrine fluorescence was measured by flow cytometry. Values are calculated as the mean of three biological replicates. The different metabolites are grouped by similarity. (1) mono hydroxybenzoic acids (A pHBA, B 2HBA, C 3HBA), (2) mono aminobenzoic acids (D pABA, E 2NBA, F 3NBA), (3) (G) benzoic acid, (4) (H) aspirin, (5) dihydroxybenzoic acids (I 2,5DHBA, J 3,4DHBA), and (6) longer radical in position 1 of the benzoic ring (K Ferulic acid, L Homovanillic acid, M Vanillic acid). Represented values are the average of the mean fluorescence measured ($n = 10$). Error bars indicate the standard deviation of the measurements ($n = 10$). Statistical tests (Dunnett's multiple comparisons test) were performed to calculate differential significance between inducers and the control condition (***$p < 0.0001$ or **$p < 0.001$ or *$p < 0.01$).

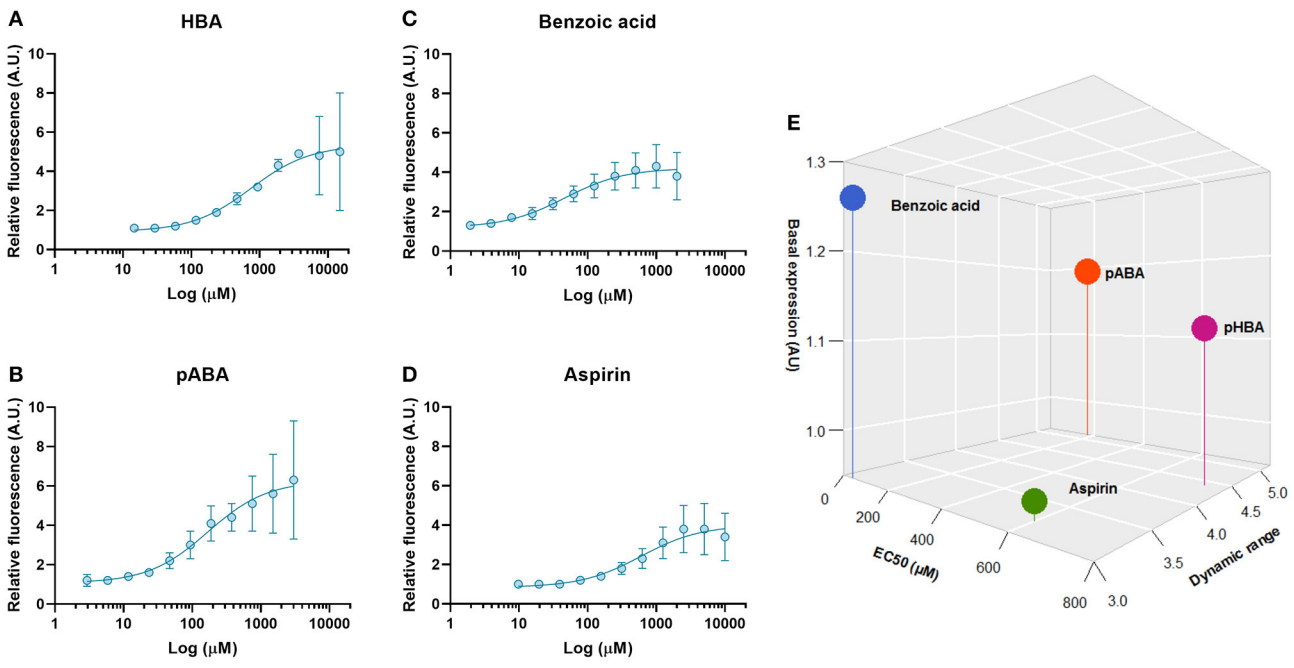

FIGURE 5 | Dose-response curves obtained with the strongest benzoic acid derivative effectors of sBAD expressed in *S. cerevisiae*. mCitrine fluorescence was measured by flow cytometry. The relative fluorescence of mCitrine was measured with cells grown at different concentration of **(A)** pHBA, **(B)** pABA, **(C)** Benzoic acid, and **(D)** Aspirin is compared with the control condition. In **(E)**, the affinity and dynamic parameters calculated from different the curves dose response are presented. Values are calculated as the mean of three biological replicates.

2HBA and 2NBA, we could not determine the different parameters since the signal never reached saturation at the highest concentrations tested (**Supplementary Figure 3**). This was probably due to some growth defect of our strain cultured with 2HBA at a concentration over 2 mM and the difficulty in dissolving 2NBA at concentrations higher than 3 mM.

In our experimental conditions, pABA and benzoic acid induced sBAD at much lower concentrations than pHBA which is supposed to be the natural inducer of HbaR in *R. palustris*. The EC50 for pHBA is 4- and 15-fold higher than the ones measured for pABA and benzoic acid, respectively (**Table 1**, **Figure 5E**). It should be noted that both the EC50 and dynamic range values were slightly smaller with aspirin than with pHBA. The biggest dynamic range was found with pABA, which in any case showed the best performance as an effector compared to the three others tested activators (**Figure 5E**). Two hypotheses can explain our results. The first one relates to the three-dimensional structure of sBAD. In our design, the effector binding domain was inserted between two other proteins, thus possibly changing the global fold of the HbaR sensing domain and consequently, the specificity or affinity of sBAD for alternate molecules such as pABA. The second hypothesis is that the native bacterial HbaR transcription factor could be promiscuous. For example, ligand promiscuity has been observed with the transcription factor XylR of *Pseudomonas putida* which regulates genes involved in the metabolism of aromatic compounds and can be activated by toluene, *m*-xylene, or benzene (Galvão and de Lorenzo, 2006). Even more interesting, the transcription factor BenM from *Acinetobacter baylyi* bears not one but two binding pockets in its structure, one for *cis,cis*-muconic acid and the second for benzoic acid (Craven et al., 2009). HbaR from *R. palustris* belongs to the CRP-FNR transcription factor family that do not display ligand promiscuity compared with the XylR-NtrC or LysR families (Egland and Harwood, 2000). It should be noted, however, that CRP from *P. putida* can be activated by cyclic AMP as well as cyclic GMP, albeit with a lower affinity (Arce-Rodríguez et al., 2012). All this information suggests that pHBA may not be the only physiological binder of HbaR in *R. palustris*.

TABLE 1 | Affinity and dynamic range parameters of sBAD with the inducers HBA, pABA, benzoic acid, and aspirin.

Metabolite	EC50 (μM)	Dynamic range
HBA	749 ± 399	4.4 ± 0.5
pABA	169 ± 81	5.2 ± 0.6
Benzoic acid	47 ± 20	3.0 ± 0.3
Aspirin	598 ± 283	3.2 ± 0.3

Reported values are calculated as the mean of three biological replicates ± SD.

In vivo Application of sBAD in pHBA-Overproducing Yeast

We next addressed whether sBAD would support real-time monitoring of *in vivo* pHBA metabolite production. To do so, we engineered the ySCC185-F strain to overproduce pHBA as previously described (Averesch et al., 2017). We first deleted the *TRP3* gene and then substituted the wild-type version of *ARO7* with the *ARO4K229L* gene. This strain named ySCC185-F-A

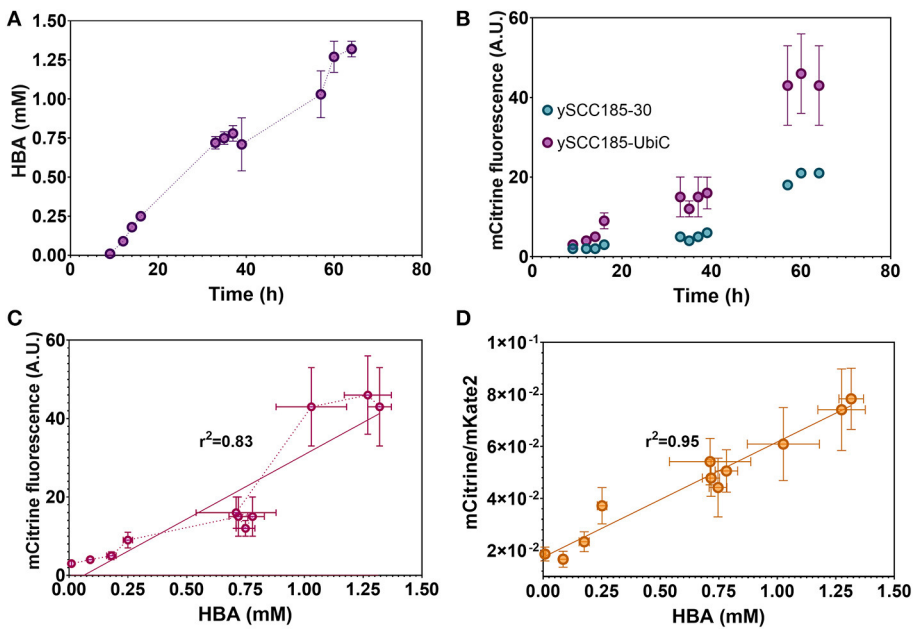

FIGURE 6 | sBAD functions in an engineered *S. cerevisiae* strain producing pHBA. **(A)** pHBA production during 65 h of growth in a medium devoid of pABA. **(B)** mCitrine fluorescence during culture in strains ySCC185-30 and ySCC185-UbiC. **(C)** Correlation between the mCitrine fluorescence and pHBA production in ySCC185-F UbiC. **(D)** Correlation between the ratio of mCitrine over mKATE2 fluorescence with pHBA production. Values are calculated as the mean of three biological replicates.

can produce higher yields of chorismate compared to the ySCC185-F strain (Averesch et al., 2017). ySCC185-F-A was then further modified to express the *ubiC* (chorismate lyase) gene from *E. coli* under the constitutive promoter *TDH3*, leading to the strain ySCC185-UbiC. We then assessed the number of cells, fluorescence of mCitrine and mKate2 (reporter of the cell number) for 65 h of cultivation with the newly constructed strains ySCC185-UbiC and ySCC185-30 (control strain). Both strains showed similar specific growth rates, indicating that the achieved level of pHBA production does not alter cell physiology (**Supplementary Table 5**). After 65 h of cultivation, the strain ySCC185-UbiC produced 1.32 mM of pHBA while the control strain ySCC185-30 did not produce any detectable amounts of it (**Figure 6A**). The production yield achieved in our strain is half of that reported by Averesch et al. (2017). This difference might be attributed to the modifications included in our parental strain (ySCC185-F) or differences in the media composition/culture conditions. Nevertheless, the concentrations reached during the cultures are in the range of detection of our biosensor, making it useful for the proof of concept of its potential use in metabolic engineering.

We then analyzed the response of sBAD to the internal production of pHBA in a medium devoid of pABA. As previously seen with ySCC185-F, a residual fluorescence signal is observed in the control strain ySCC185-30 and this signal increases with time (**Figure 6B**). However, mCitrine fluorescence is always higher with ySCC185-UbiC than with ySCC185-30. The accumulation of mCitrine after 60 h in ySCC185-30 and ySCC185-UbiC is probably due to a continuous production of the fluorescent protein, even after cell growth arrest. In fact, even the pHBA production increases after 60 h of culture while the cell count does not change anymore after 40 h (**Supplementary Figure 4**). Remarkably, there is a good linear correlation ($R^2 = 0.83$) between the mCitrine fluorescence signal and pHBA amounts produced by ySCC185-F UbiC cells (**Figure 6C**). More importantly, if we plot the ratio of the mCitrine fluorescence values (representative of sBAD activity) and the mKate2 fluorescence values (representative of the cell count) against pHBA concentrations obtained in the production experiments, the linearity of the response is even greater ($R^2 = 0.95$, **Figure 6D**, **Supplementary Figure 5**).

Therefore, our synthetic biosensor sBAD is functional and accurate enough to detect and measure the *in vivo* production of pHBA and, as such, can be used to screen for strains producing high titers of pHBA (up to 10 mM) in batch cultures. Furthermore, the capacity of sBAD may not be restricted to screening pHBA overproduction in yeast but can also be applied to pABA, benzoic acid and, to a lesser extent, other *ortho*-monosubstituted benzoic acid derivatives.

CONCLUSIONS

This work has presented the successful design, construction and characterization of an orthogonal benzoic acid derivative biosensor (sBAD) in *S. cerevisiae* using the binding domain of the bacterial HbaR from *R. palustris* linked to the LexA protein as a DNA binding domain and B112 as a transactivation domain. This biosensor system allowed us to easily monitor, in real-time, a fluorescence signal linearly correlated to extracellular concentrations of pHBA. The promiscuity of the biosensor in yeast was also analyzed and, quite unexpectedly, pABA and benzoic acid also produce responses that are even more pronounced than the one measured with pHBA, notably in terms of sensitivity and dynamic range (for pABA). The relatively strong effect of the substituent position (*para* > *ortho* > *meta*), rather than the chemical properties of the substituent itself, indicate that the physicochemical properties that govern the promiscuous recognition of benzoic acid derivatives by sBAD are non-trivial. As our output signal is easily measurable, and considering the strong linearity obtained between our reporter signals and pHBA concentrations, our biosensor opens the way to a more thorough study of its binding properties, for instance with random mutagenesis approaches. This novel biosensor for detecting benzoic acid derivatives can be considered a useful tool to improve the production of production of such derivatives by screening large populations of yeast mutants. Moreover, the strong recognition of pABA or benzoic acid by sBAD could also be used for medical sensing purposes in bodily or chemical fluids, allowing an easily measurable output signal (fluorescence) to be monitored over a range of fluid concentrations covering three orders of magnitude.

DATA AVAILABILITY STATEMENT

The datasets generated for this study are available on request to the corresponding author.

AUTHOR CONTRIBUTIONS

J-LF and GT conceived this project. SC-C designed the experiments, carried out experimental work, analyzed, and interpreted the data. MF contributed to the analysis of the data. SC-C, GT, and PU wrote the paper. All authors assisted in this process.

FUNDING

This work was supported by the Toulouse White Biotechnology consortium (pre-competitive financial support METASENS). J-LF also acknowledges funding provided by BBSRC Grant No. BB/M017702/1.

ACKNOWLEDGMENTS

We wish to thank the team of Molecular and Metabolic Engineering of Toulouse Biotechnology Institute for their support and discussions, especially to Ruben Impellizzeri. Also, Delphine Lestrade is acknowledged for her help in the use of the flow cytometer.

SUPPLEMENTARY MATERIAL

The Supplementary Material for this article can be found online at: https://www.frontiersin.org/articles/10.3389/fbioe.2019.00372/full#supplementary-material

REFERENCES

Ando, S., Arai, I., Kiyoto, K., and Hanai, S. (1986). Identification of aromatic monomers in steam-exploded poplar and their influences on ethanol fermentation by *Saccharomyces cerevisiae*. *J. Ferment. Technol.* 64, 567–570. doi: 10.1016/0385-6380(86)90084-1

Arce-Rodríguez, A., Durante-Rodríguez, G., Platero, R., Krell, T., Calles, B., and de Lorenzo, V. (2012). The Crp regulator of *Pseudomonas putida*: evidence of an unusually high affinity for its physiological effector, cAMP. *Environ. Microbiol.* 14, 702–713. doi: 10.1111/j.1462-2920.2011.02622.x

Averesch, N. J. H., Prima, A., and Krömer, J. O. (2017). Enhanced production of *para*-hydroxybenzoic acid by genetically engineered *Saccharomyces cerevisiae*. *Bioprocess Biosyst. Eng.* 40, 1283–1289. doi: 10.1007/s00449-017-1785-z

Barnhart-Dailey, M. C., Ye, D., Hayes, D. C., Maes, D., Simoes, C. T., Appelhans, L., et al. (2019). Internalization and accumulation of model lignin breakdown products in bacteria and fungi. *Biotechnol. Biofuels* 12:175. doi: 10.1186/s13068-019-1494-8

Black, J. B., and Gersbach, C. A. (2018). Synthetic transcription factors for cell fate reprogramming. *Curr. Opin. Genet. Dev.* 52, 13–21. doi: 10.1016/j.gde.2018.05.001

Craven, S. H., Ezezika, O. C., Haddad, S., Hall, R. A., Momany, C., and Neidle, E. L. (2009). Inducer responses of BenM, a LysR-type transcriptional regulator from *Acinetobacter baylyi* ADP1. *Mol. Microbiol.* 72, 881–894. doi: 10.1111/j.1365-2958.2009.06686.x

Dietrich, J. A., McKee, A. E., and Keasling, J. D. (2010). High-throughput metabolic engineering: advances in small-molecule screening and selection. *Annu. Rev. Biochem.* 79, 563–590. doi: 10.1146/annurev-biochem-062608-095938

Eggeling, L., Bott, M., and Marienhagen, J. (2015). Novel screening methods–biosensors. *Curr. Opin. Biotechnol.* 35, 30–36. doi: 10.1016/j.copbio.2014.12.021

Egland, P. G., and Harwood, C. S. (2000). HbaR, a 4-hydroxybenzoate sensor and FNR-CRP superfamily member, regulates anaerobic 4-hydroxybenzoate degradation by *Rhodopseudomonas palustris*. *J. Bacteriol.* 182, 100–106. doi: 10.1128/JB.182.1.100-106.2000

Farmer, W. R., and Liao, J. C. (2000). Improving lycopene production in *Escherichia coli* by engineering metabolic control. *Nat. Biotechnol.* 18, 533–537. doi: 10.1038/75398

Galvão, T. C., and de Lorenzo, V. (2006). Transcriptional regulators à la carte: engineering new effector specificities in bacterial regulatory proteins. *Curr. Opin. Biotechnol.* 17, 34–42. doi: 10.1016/j.copbio.2005.12.002

Ganesh, I., Kim, T. W., Na, J.-G., Eom, G. T., and Hong, S. H. (2019). Engineering *Escherichia coli* to sense non-native environmental stimuli: synthetic chimera two-component systems. *Biotechnol. Bioprocess E* 24, 12–22. doi: 10.1007/s12257-018-0252-2

Gietz, R. D. (2014). "Yeast transformation by the LiAc/SS carrier DNA/PEG method," in *Yeast Genetics: Methods and Protocols Methods in Molecular Biology*, eds. J. S. Smith and D. J. Burke (New York, NY: Springer New York), 1–12. doi: 10.1007/978-1-4939-1363-3_1

Giulivo, M., Lopez de Alda, M., Capri, E., and Barceló, D. (2016). Human exposure to endocrine disrupting compounds: their role in reproductive systems, metabolic syndrome and breast cancer. A review. *Environ. Res.* 151, 251–264. doi: 10.1016/j.envres.2016.07.011

Jullesson, D., David, F., Pfleger, B., and Nielsen, J. (2015). Impact of synthetic biology and metabolic engineering on industrial production of fine chemicals. *Biotechnol. Adv.* 33,1395–1402. doi: 10.1016/j.biotechadv.2015.02.011

Khalil, A. S., and Collins, J. J. (2010). Synthetic biology: applications come of age. *Nat. Rev. Genet.* 11, 367–379. doi: 10.1038/nrg2775

Larsson, S., Quintana-Sáinz, A., Reimann, A., Nilvebrant, N. O., and Jönsson, L. J. (2000). Influence of lignocellulose-derived aromatic compounds on oxygen-limited growth and ethanolic fermentation by *Saccharomyces cerevisiae*. *Appl. Biochem. Biotechnol.* 84–86, 617–632. doi: 10.1007/978-1-4612-1392-5_47

Le Feuvre, R. A., and Scrutton, N. S. (2018). A living foundry for synthetic biological materials: a synthetic biology roadmap to new advanced materials. *Synth. Syst. Biotechnol.* 3, 105–112. doi: 10.1016/j.synbio.2018.04.002

Leavitt, J. M., and Alper, H. S. (2015). Advances and current limitations in transcript-level control of gene expression. *Curr. Opin. Biotechnol.* 34, 98–104. doi: 10.1016/j.copbio.2014.12.015

Leavitt, J. M., Wagner, J. M., Tu, C. C., Tong, A., Liu, Y., and Alper, H. S. (2017). Biosensor-enabled directed evolution to improve muconic acid production in *Saccharomyces cerevisiae*. *Biotechnol. J.* 12:1600687. doi: 10.1002/biot.201600687

Lee, J.-H., and Wendisch, V. F. (2017). Biotechnological production of aromatic compounds of the extended shikimate pathway from renewable biomass. *J. Biotechnol.* 257, 211–221. doi: 10.1016/j.jbiotec.2016.11.016

Li, J., Zhang, L., and Liu, W. (2018). Cell-free synthetic biology for *in vitro* biosynthesis of pharmaceutical natural products. *Synth. Syst. Biotechnol.* 3, 83–89. doi: 10.1016/j.synbio.2018.02.002

Liu, Y., Liu, Y., and Wang, M. (2017). Design, optimization and application of small molecule biosensor in metabolic engineering. *Front. Microbiol.* 8:2012. doi: 10.3389/fmicb.2017.02012

Mannan, A. A., Liu, D., Zhang, F., and Oyarzún, D. A. (2017). Fundamental design principles for transcription-factor-based metabolite biosensors. *ACS Synth. Biol.* 6, 1851–1859. doi: 10.1021/acssynbio.7b00172

Markham, K. A., and Alper, H. S. (2015). Synthetic biology for specialty chemicals. *Annu. Rev. Chem. Biomol. Eng.* 6, 35–52. doi: 10.1146/annurev-chembioeng-061114-123303

Metzger, J. J., Simunovic, M., and Brivanlou, A. H. (2018). Synthetic embryology: controlling geometry to model early mammalian development. *Curr. Opin. Genet. Dev.* 52, 86–91. doi: 10.1016/j.gde.2018.06.006

Mikkelsen, M. D., Buron, L. D., Salomonsen, B., Olsen, C. E., Hansen, B. G., Mortensen, U. H., et al. (2012). Microbial production of indolylglucosinolate through engineering of a multi-gene pathway in a versatile yeast expression platform. *Metab. Eng.* 14, 104–111. doi: 10.1016/j.ymben.2012.01.006

Nevozhay, D., Zal, T., and Balázsi, G. (2013). Transferring a synthetic gene circuit from yeast to mammalian cells. *Nat. Commun.* 4:1451. doi: 10.1038/ncomms2471

Ottoz, D. S. M., Rudolf, F., and Stelling, J. (2014). Inducible, tightly regulated and growth condition-independent transcription factor in *Saccharomyces cerevisiae*. *Nucleic Acids Res.* 42:e130. doi: 10.1093/nar/gku616

Palmqvist, E., Grage, H., Meinander, N. Q., and Hahn-Hägerdal, B. (1999). Main and interaction effects of acetic acid, furfural, and p-hydroxybenzoic acid on growth and ethanol productivity of yeasts. *Biotechnol. Bioeng.* 63, 46–55. doi: 10.1002/(SICI)1097-0290(19990405)63:1<46::AID-BIT5>3.0.CO;2-J

Rogers, J. K., and Church, G. M. (2016). Genetically encoded sensors enable real-time observation of metabolite production. *Proc. Natl. Acad. Sci. U.S.A.* 113, 2388–2393. doi: 10.1073/pnas.1600375113

Rothschild, L. J. (2016). Synthetic biology meets bioprinting: enabling technologies for humans on Mars (and Earth). *Biochem. Soc. Trans.* 44, 1158–1164. doi: 10.1042/BST20160067

Sambrook, J., and Russell, D. W. (2001). *Molecular Cloning: A Laboratory Manual*. Cold Spring Harbor, NY: CSHL Press.

Schindler, D., Dai, J., and Cai, Y. (2018). Synthetic genomics: a new venture to dissect genome fundamentals and engineer new functions. *Curr. Opin. Chem. Biol.* 46, 56–62. doi: 10.1016/j.cbpa.2018.04.002

Schulman, I. G., and Heyman, R. A. (2004). The flip side: identifying small molecule regulators of nuclear receptors. *Chem. Biol.* 11, 639–646. doi: 10.1016/j.chembiol.2003.12.021

Selvamani, V., Ganesh, I., Maruthamuthu, M., Eom, G. T., and Hong, S. H. (2017). Engineering chimeric two-component system into *Escherichia coli* from *Paracoccus denitrificans* to sense methanol. *Biotechnol. Bioproc. E* 22, 225–230. doi: 10.1007/s12257-016-0484-y

Smanski, M. J., Zhou, H., Claesen, J., Shen, B., Fischbach, M. A., and Voigt, C. A. (2016). Synthetic biology to access and expand nature's chemical diversity. *Nat. Rev. Microbiol.* 14, 135–149. doi: 10.1038/nrmicro.2015.24

Snoek, T., Romero-Suarez, D., Zhang, J., Ambri, F., Skjoedt, M. L., Sudarsan, S., et al. (2018). An orthogonal and pH-tunable sensor-selector for muconic acid biosynthesis in yeast. *ACS Synth. Biol.* 7, 995–1003. doi: 10.1021/acssynbio.7b00439

Toda, S., Blauch, L. R., Tang, S. K. Y., Morsut, L., and Lim, W. A. (2018). Programming self-organizing multicellular structures with synthetic cell-cell signaling. *Science* 361, 156–162. doi: 10.1126/science.aat0271

Tran, U. C., and Clarke, C. F. (2007). Endogenous synthesis of coenzyme Q in eukaryotes. *Mitochondrion* 7 (Suppl), S62–71. doi: 10.1016/j.mito.2007.03.007

Umeyama, T., Okada, S., and Ito, T. (2013). Synthetic gene circuit-mediated monitoring of endogenous metabolites: identification of GAL11 as a novel multicopy enhancer of s-adenosylmethionine level in yeast. *ACS Synth. Biol.* 2, 425–430. doi: 10.1021/sb300115n

van Sint Fiet, S., van Beilen, J. B., and Witholt, B. (2006). Selection of biocatalysts for chemical synthesis. *Proc. Natl. Acad. Sci. U.S.A.* 103, 1693–1698. doi: 10.1073/pnas.0504733102

Voyvodic, P. L., Pandi, A., Koch, M., Conejero, I., Valjent, E., Courtet, P., et al. (2019). Plug-and-play metabolic transducers expand the chemical detection space of cell-free biosensors. *Nat. Commun.* 10:1697. doi: 10.1038/s41467-019-09722-9

Wang, S., Bilal, M., Hu, H., Wang, W., and Zhang, X. (2018). 4-Hydroxybenzoic acid-a versatile platform intermediate for value-added compounds. *Appl. Microbiol. Biotechnol.* 102, 3561–3571. doi: 10.1007/s00253-018-8815-x

Williams, T. C., Averesch, N. J. H., Winter, G., Plan, M. R., Vickers, C. E., Nielsen, L. K., et al. (2015). Quorum-sensing linked RNA interference for dynamic metabolic pathway control in *Saccharomyces cerevisiae*. *Metab. Eng.* 29, 124–134. doi: 10.1016/j.ymben.2015.03.008

Winter, G., Averesch, N. J. H., Nunez-Bernal, D., and Krömer, J. O. (2014). *In vivo* instability of chorismate causes substrate loss during fermentative production of aromatics. *Yeast* 31, 333–341. doi: 10.1002/yea.3025

Xue, H., Shi, H., Yu, Z., He, S., Liu, S., Hou, Y., et al. (2014). Design, construction, and characterization of a set of biosensors for aromatic compounds. *ACS Synth. Biol.* 3, 1011–1014. doi: 10.1021/sb500023f

Yao, Y., Li, S., Cao, J., Liu, W., Fan, K., Xiang, W., et al. (2018). Development of small molecule biosensors by coupling the recognition of the bacterial allosteric transcription factor with isothermal strand displacement amplification. *Chem. Commun. Camb. Engl.* 54, 4774–4777. doi: 10.1039/C8CC01764F

Zhang, T., Lei, J., Yang, H., Xu, K., Wang, R., and Zhang, Z. (2011). An improved method for whole protein extraction from yeast *Saccharomyces cerevisiae*. *Yeast* 28, 795–798. doi: 10.1002/yea.1905

Zhao, E. M., Zhang, Y., Mehl, J., Park, H., Lalwani, M. A., Toettcher, J. E., et al. (2018). Optogenetic regulation of engineered cellular metabolism for microbial chemical production. *Nature* 555, 683–687. doi: 10.1038/nature 26141

Conflict of Interest: The authors declare that this study received funding from Toulouse White Biotechnology. The funder was not involved in the study design, collection, analysis, interpretation of data, the writing of this article or the decision to submit it for publication.

The authors declare that the research was conducted in the absence of any commercial or financial relationships that could be construed as a potential conflict of interest.

frontiers in Bioengineering and Biotechnology

REVIEW
published: 08 November 2019
doi: 10.3389/fbioe.2019.00289

Enzymatic Bioremediation of Organophosphate Compounds—Progress and Remaining Challenges

Meghna Thakur[1], *Igor L. Medintz*[2] *and Scott A. Walper*[2]*

[1] College of Science, George Mason University, Fairfax, VA, United States, [2] Center for Bio/Molecular Sciences, U.S. Naval Research Laboratory, Washington, DC, United States

Organophosphate compounds are ubiquitously employed as agricultural pesticides and maintained as chemical warfare agents by several nations. These compounds are highly toxic, show environmental persistence and accumulation, and contribute to numerous cases of poisoning and death each year. While their use as weapons of mass destruction is rare, these never fully disappear into obscurity as they continue to be tools of fear and control by governments and terrorist organizations. Beyond weaponization, their wide-scale dissemination as agricultural products has led to environmental accumulation and intoxication of soil and water across the globe. Therefore, there is a dire need for rapid and safe agents for environmental bioremediation, personal decontamination, and as therapeutic detoxicants. Organophosphate hydrolyzing enzymes are emerging as appealing targets to satisfy decontamination needs owing to their ability to hydrolyze both pesticides and nerve agents using biologically-derived materials safe for both the environment and the individual. As the release of genetically modified organisms is not widely accepted practice, researchers are exploring alternative strategies of organophosphate bioremediation that focus on cell-free enzyme systems. In this review, we first discuss several of the more prevalent organophosphorus hydrolyzing enzymes along with research and engineering efforts that have led to an enhancement in their activity, substrate tolerance, and stability. In the later half we focus on advances achieved through research focusing on enhancing the catalytic activity and stability of phosphotriesterase, a model organophosphate hydrolase, using various approaches such as nanoparticle display, DNA scaffolding, and outer membrane vesicle encapsulation.

Keywords: organophosphate, enzyme, chemical warfare agent, bioremediation, catalysis, outer membrane vesicle, decontamination, phosphotriesterase

OPEN ACCESS

Edited by:
Jean Marie François, UMS3582 Toulouse White Biotechnology (TWB), France

Reviewed by:
Georgios Skretas, National Hellenic Research Foundation, Greece
Pasquale Stano, University of Salento, Italy

***Correspondence:**
Scott A. Walper
scott.walper@nrl.navy.mil

Specialty section:
This article was submitted to Synthetic Biology, a section of the journal Frontiers in Bioengineering and Biotechnology

Received: *29 July 2019*
Accepted: *09 October 2019*
Published: *08 November 2019*

Citation:
Thakur M, Medintz IL and Walper SA (2019) Enzymatic Bioremediation of Organophosphate Compounds—Progress and Remaining Challenges. Front. Bioeng. Biotechnol. 7:289. doi: 10.3389/fbioe.2019.00289

INTRODUCTION

Biological diversity spread across the ecological niches of the world has allowed for the evolution of cellular systems that enable the survival of microbes, plants, and animal in these highly variable environments. This has been recognized at the phenotypic level since the time of Charles Darwin's voyage on the Beagle. Today we characterize Darwinian evolutions at the genetics level recognizing

that such adaptability occurs through alterations in cellular physiology or mechanisms, many of which are the product of adapted or novel enzymatic pathways and the products they produce. Examples such as the bacteria found in arsenic contaminated aquifers or the fungi capable of growing within nuclear reactors highlight the ability of Nature to adapt to harsh environments and exploit available resources to survive (Dadachova and Casadevall, 2008; Gnanaprakasam et al., 2017; Gu et al., 2017). In addition to basic survival mechanisms, the endless quest for the raw materials necessary to sustain life has also allowed for organisms to develop metabolic pathways allowing them to scavenge, convert, and utilize an incredible range of both natural and man-made chemicals to satisfy these needs. The cellular tools of these conversions, enzymes, are capable of chemical conversions and transformations that occur incredibly fast, often at the rate of diffusion, and with a specificity and selectivity that cannot easily be rivaled using chemical catalysis. For this reason, enzymes are rapidly developing as invaluable tools in medicine as therapeutics, as agents of environmental decontamination, and as reagents that enable a diverse spectrum of commercial applications.

Historically, mankind exploited cellular processes such as fermentation for the preparation of food and drink. Today, advances and understanding in cellular and metabolic processes has allowed for an explosion in the use of purified enzymes within the food industry (Raveendran et al., 2018). Similarly, the use of enzyme-based therapeutics continues to rise as these biomolecules typically show reduced toxicity and immunogenicity compared to other chemically synthesized alternatives (Dean et al., 2017; Kumar and Abdulhameed, 2017; Yari et al., 2017). Enzymes for commercial and industrial applications is also on the rise as these biomolecules offer a sustainable path with reduced toxic waste products (Chapman et al., 2018). One area of particular interest in research and development is in the area of bioremediation and detoxification of chemicals.

Bioremediation at its most basic definition is the use of natural biological systems such as plants and microbes to degrade or consume environmental pollutants. The potential of bioremediation was recognized decades ago starting with efforts to treat wastewater using environmental isolates. The first documented success with environmental microbes was detailed in a 1975 report by Raymond et al. that describes the degradation of petroleum-derived hydrocarbons by microbial populations (Raymond et al., 1975; Dvorak et al., 2017). Expanding on these studies, researchers have sought to harness this phenomenon for other purposes, particularly environmental decontamination. Contaminants such as industrial waste products including polycyclic aromatic compounds, organic dyes, heavy metals, and polyhalogenated compounds are common contaminants in aquifers and soil as are petroleum-based hydrocarbons and pharmaceutical compounds. Fortunately, each of these have been targets of various bioremediation strategies (Singh and Walker, 2006; Yi and Crowley, 2007; Peng et al., 2008; Ben Mansour et al., 2012; Montgomery et al., 2013; Rodgers-Vieira et al., 2015; Dzionek et al., 2016; Brar et al., 2017; Dvorak et al., 2017; Ojuederie and Babalola, 2017; Wu et al., 2017; Liu et al., 2018). The adaptability and versatility of plants and microbes has enabled bioremediation as a "biologically-friendly" strategy to eliminate many of the harmful contaminants released by the everyday machinations of human society, see schematic overview in **Figure 1**. At present, bioremediation of environmental reservoirs is accomplished using primarily natural, non-engineered bacteria that have been isolated from contaminated sources and exhibit an ability to consume or convert the target contaminant as highlighted in several examples (Cologgi et al., 2011; Silar et al., 2011; Dubinsky et al., 2013; Prakash et al., 2013; Gustavsson et al., 2016). With the rise of synthetic biology and microbial engineering, future strategies may likely include engineered microbes containing novel metabolic pathways or tailored for enhanced fitness in austere environments. Despite the advantages these strategies may afford, regulations in the U.S. and across Europe limit or prohibit the use and release of genetically modified organisms into the environment. For this reason, many researchers are investigating the potential direct use of recombinant enzymes for the purpose of environmental decontamination. Often referred to as cell-free synthetic biology, these strategies offer a fine level of control where researchers can tailor reaction conditions such as enzyme concentrations, the availability of co-factors, ionic strength, and others. Of significant importance, unlike the engineered microbes from which they are derived, cell-free catalytic systems are non-replicative and are therefore less likely to be impacted by regulatory policies.

This review will focus on enzymatic systems for the bioremediation of a ubiquitous but highly dangerous group of man-made compounds collectively referred to as organophosphates (OPs). First described in the late nineteenth century, these compounds existed in relative obscurity until their potential as anti-biological agents were recognized during World War II. Since then they have rapidly evolved from chemical warfare agents (CWAs) to commercial pesticides used all over the world. As both agents of war and agricultural tools, these chemical compounds have left a lasting effect on the environment as they are contaminants of both soil and water capable of inducing illness and death to those that inadvertently encounter them. Fortunately, microbial species have rapidly evolved enzymatic processes to degrade these contaminants and researchers have developed strategies to utilize these biological catalysts for bioremediation of OP compounds. In this review we will detail many of the enzymes currently employed and studied for OP remediation describing the properties of each and efforts to develop them into products useful for environmental clean-up. Unfortunately, recombinant enzymes often suffer from issues that limit their wide-spread use as a viable material. However, as the tools and techniques of biological engineering continue to expand, the utility of enzymes as therapeutics and implements of decontamination of organophosphate compounds has been reinvigorated. This review will describe how new methods of biological engineering such as synthetic biology and cell-free synthetic biology are breathing new life into enzyme-based catalytic systems for organophosphate decontamination and neutralization. Here we pay particular attention to efforts to enhance the catalytic activity, substrate promiscuity, and

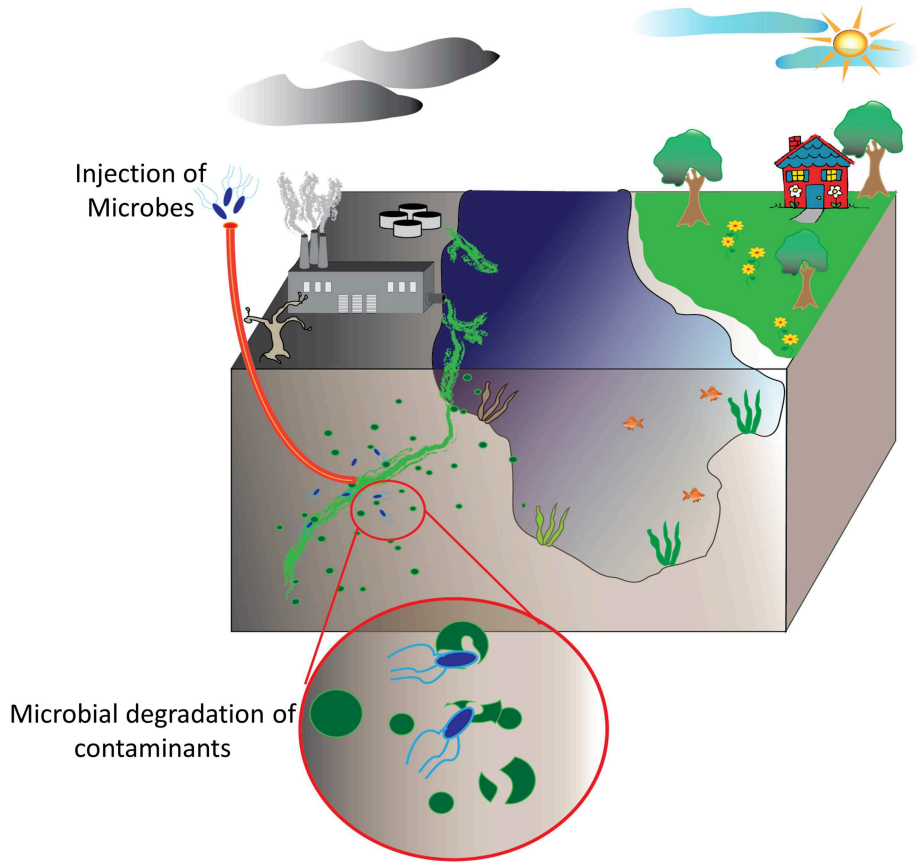

FIGURE 1 | Bioremediation of environmental pollutants. Environmental decontamination of industrial waste products and other contaminants, ideally, is realized by microbes and plant species able to convert these toxic compounds into other biomolecules that these utilize for their own metabolic functions.

stability of the more commonly used OP hydrolyzing enzymes through enzyme engineering, assembly of scaffolded cell-free systems, and through the development of microbe-based systems of bioremediation that revolve around the re-engineering of bacterial genetic circuits and cellular systems. Each of these areas highlights how the engineering of biology at the protein, system, and organism level can be utilized to address issues such as environmental contamination that affect populations around the globe.

ORGANOPHOSPHATES

Organophosphate compounds are typically phosphate esters formed from a reaction between alcohols and phosphoric acid resulting in a compound with the general structure of $O{=}P(OR)_3$. OP compounds are found in both naturally occurring biomolecules and industrial products such as pesticides including insecticides and herbicides. The first of these compounds was chemically synthesized in the late nineteenth century by Phillipe de Clemont and Wladimir Moschnin, but it was not until much later, in 1932, that Willy Lange and his student Gerde von Krueger described the cholinergic effects of these compounds (Costa, 2018; Franjesevic et al., 2019). Over the next 20 years, British and German scientists produced a suite of OP compounds that could be used as highly potent nerve agents. Later, American scientists and others adapted these chemical syntheses to manufacture OP insecticides. Chemical structures for some of the more prevalent and toxic OP compounds are shown in **Figure 2.** Toxicity of these compounds is highly variable and dependent on the chemical composition, the route of entry or exposure, and whether exposure is acute or chronic (Munro et al., 1999; Costa, 2018). While not as lethal as their CWA counterparts, OP pesticides can also be quite dangerous capable of causing illness or death. For both pesticides and CWAs, the ease and low cost of production paired with the high degree of efficacy has ensured that OP compounds continue to find use in both beneficial and nefarious applications.

OP compounds were rapidly adopted as CWAs first by the Nazis and subsequently by the British during World War II to replace the chlorine-based weapons of the previous World War. The German efforts during this time period produced the G-series of agents including sarin, cyclosarin, and soman. In parallel, the British developed a series of reagents including diisopropylfluorophosphate (DFP), VX, and VR. While diverse in chemical composition and structure, CWAs and OP pesticides function through the disruption of the enzyme

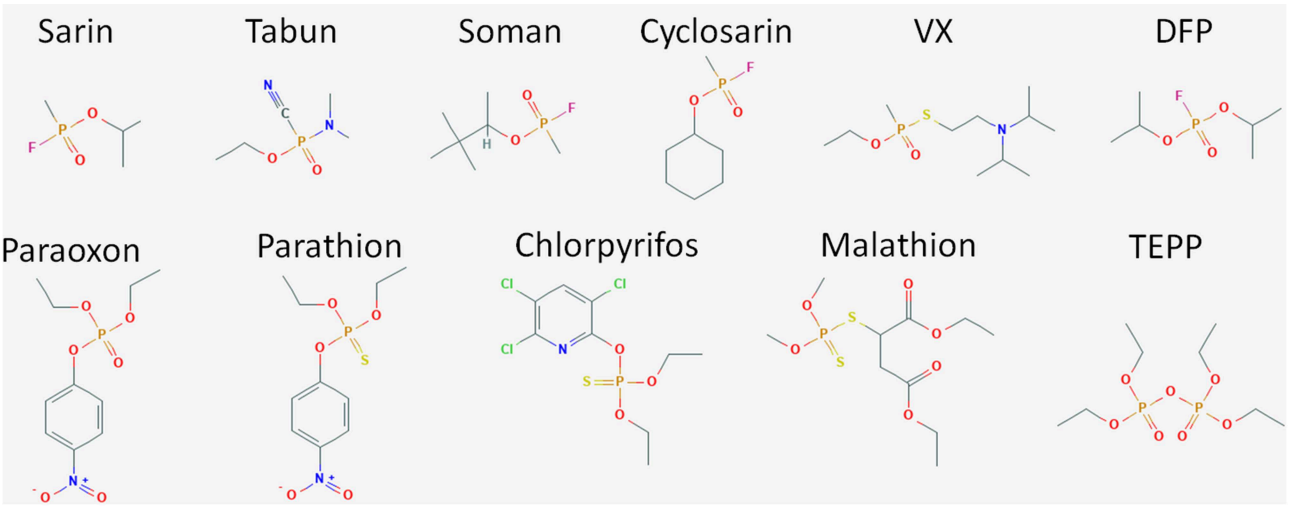

FIGURE 2 | Structure of OP compounds. The diversity of OP compounds is highlighted here in the chemical structures of some of the better known CWA nerve agents (sarin, tabun, soman, cyclosarin, VX, and DFP) and pesticides (paraoxon, parathion, chlorpyrifos, trichlorfon, dichlorvos, malathion, TEPP).

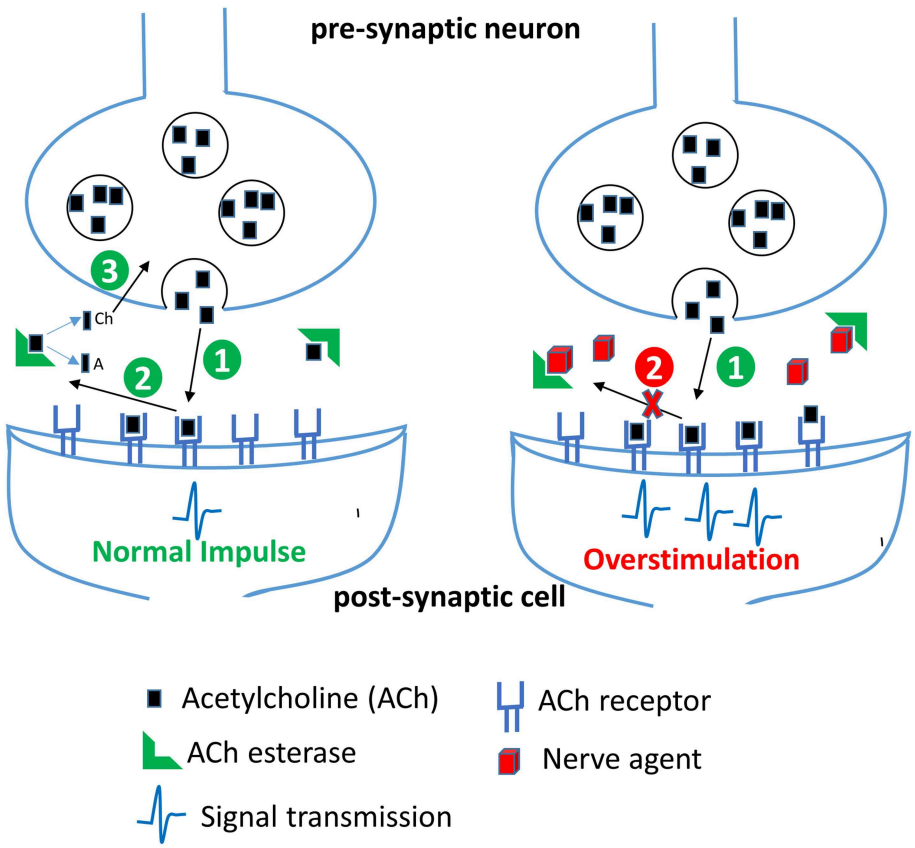

FIGURE 3 | Effect of nerve agents on central nervous system. Acetylcholine (ACh) released from the synaptic vesicles in the presynaptic neuron binds to its receptor in the postsynaptic membrane resulting in generation of a nerve impulse (step 1). In the second step, ACh dissociates from its receptor in the synaptic cleft and is rapidly broken down by the enzyme acetylcholinesterase (AChE) into acetate (A) and choline (Ch). Choline is transported back into the axon terminal and is used to make more ACh. In the presence of nerve agents, AChE is irreversibly inhibited, thereby resulting in an accumulation of ACh and a persistent stimulation of ACh receptors leading to continuous neurotransmission and an acute cholinergic syndrome.

acetylcholinesterase, a critical component of signal transduction in the neuromuscular junctions of both insects and animals, see schematic in **Figure 3**. Accumulation of acetycholine, a neurotransmitter, in the synaptic cleft leads to overstimulation of acetylcholine receptors thereby causing a cholinergic crisis characterized by anxiety, headache, convulsion, tremor and death (Jokanovic, 2018; Naughton and Terry, 2018; Sikary, 2019). Though developed during the Second World War these compounds did not see use until many years later in other conflict areas. Sarin saw widespread use by the Iraqi army during the Iran-Iraq conflicts of the 1980s resulting in the deaths of thousands despite international treaties condemning the use of CWAs. Later, in 1995, the Japanese doomsday cult Aum Shinrikyo deployed sarin gas on a Tokyo subway train killing 13 and injuring or affecting nearly 1,000 others. The same group also experimented with the production and use of the even more toxic organophosphate CWA, VX (Zurer, 1998). These compounds continue to find nefarious use today. In 2013 and again in 2017, the Syrian government bombarded cities within their own borders with sarin gas to quell a growing rebellion. OP nerve agents have also been used for assassinations as shown in the 2017 slaying of Kim Jong-nam a half-brother of the current North Korean leader and the attempt on the life of a former Russian spy, Sergei Skripal in 2018.

While governments and terrorist organizations have employed OPs as weapons of mass destruction and terror, these compounds have also seen widespread use in agriculture in both developed and developing countries. During the twenty-first century, OPs were the most widely used pesticides in the United States with as many as 36 compounds approved for domestic or agricultural use as summarized in **Supplemental Table 1** (Roberts and Reigart, 2013). It is estimated that millions of tons of these compounds are produced and dispersed each year in the U.S. alone (Atwood and Paisley-Jones, 2017). The ubiquitous utilization of these compounds leads to a high rate of human exposure and OP poisoning. It is estimated that around 3,000,000 people are exposed to OP compounds per year accounting for more than 300,000 fatalities (Bird et al., 2019). Despite the well-documented acute and chronic toxic effects, OPs are seen as vital components of commercial agriculture and pest control (Knutson and Smith, 1999; Jokanovic, 2018; Lushchak et al., 2018; Mostafalou and Abdollahi, 2018). However, in developed countries there is growing concern for the long-term use of these compounds and their environmental accumulation and toxicity. As an example, chlorpyrifos, which was first registered with the U.S. Environmental Protection Agency (EPA) in 1965, has seen a gradual shift in policy regarding its use beginning in 1996 with phase out of home use and in some agricultural products such as tomatoes. Since then the EPA has continued to examine this OP and its environmental and health effects modifying policy for its use. Mostly recently these studies and others have resulted a 2018 decision by the U.S. Ninth Circuit Court of Appeals ordering an EPA-approved ban of the compound (https://www.epa.gov/ingredients-used-pesticide-products/chlorpyrifos). Continuous studies of OP compounds and events such as the death of 25 school children in India from meals contaminated with monocrotophos, an agricultural pesticide, has led to increased public attention which in turn has fueled scientific research in methods of ensuring public safety through the development of new safer pesticides and methods of remediating OPs from the environment (Banerji et al., 2013; Than, 2013).

DECONTAMINATION OF ORGANOPHOSPHATES

The reactive nature of organophosphate compounds has allowed for the development of numerous strategies to remove and/or neutralize these materials from the environment. Typically, decontamination of organophosphates, both pesticides and CWAs, is accomplished through (1) physical removal or dilution of the material through the use of absorbents or flushing contaminated areas, (2) chemical decontamination, or (3) bioremediation using microbial species or purified enzymes (Jacquet et al., 2016). Ideally, several of these methods would be used in conjunction to detoxify target environments, equipment, and infrastructure (see **Table 1**).

Physical Decontamination

Physical decontamination of contaminated areas involves the use of incineration, sorbent materials, or simply burying or washing contaminated surfaces to minimize the risk of exposure. Unfortunately, this does not typically neutralize the material which can lead to secondary contamination particularly of soils and aquifers. Materials for this type of decontamination can span the gamut from nanoparticles to bulk use of minerals in material platforms. For example, to address aquifer contamination with OP pesticides Liu et al. developed graphene-coated silica nanoparticles capable of rapidly capturing nine different pesticides from spiked water samples (Liu et al., 2013). Other reactive materials such as cerium dioxide have shown success against both pesticides and CWAs. In laboratory trials, the research team of Lubos Vrtoch showed that cerium dioxide sorbent materials could be used to rapidly degrade both pesticides and CWAs such as VX (Janos et al., 2014). In these studies the group showed that methyl parathion, soman, and VX could be degraded in as little as 30 min after exposure using their cerium dioxide sorbent materials. Unfortunately, while cerium dioxide does have potential as a decontamination strategy studies have shown that exposure to these materials can cause immunostimulation in laboratory models and can lead to toxicity in some human cell lines (Gehlhaus et al., 2009; Mittal and Pandey, 2014).

Chemical Decontamination

Chemical reagents facilitating the hydrolysis of pesticides and CWAs as a route of decontamination are by far the most prevalent and include hydrolysis, oxidation, and reduction mechanisms. At present, materials relying on chemical hydrolysis are most commonly used for large-scale remediation of contaminated areas (Jacquet et al., 2016). Common reagents such as sodium hydroxide and hypochlorite will react with many OP compounds though both of these compounds are corrosive and not suitable for personal use or with sensitive materials

TABLE 1 | Common methods of decontamination and their application.

Method	Applications	Advantages	Disadvantages
Physical			
Incineration	Elimination of stockpiles	Ease of use and efficiency	May require transport of material (expense), potential for volatile release
Landfill, Flushing	Elimination of stockpiles	Ease of use Inexpensive	Soil and aquifer contamination
Chemical	Elimination of stockpiles, equipment and material decon (some), personnel decon (limited)	Ease of use and efficiency Rapid decon	Expensive, potentially corrosive agents damaging equipment, secondary contamination due to catalyst or agent
Bioremediation	Elimination of stockpiles, equipment and material decon, personnel decon	Bio-friendly (non-toxic) Highly efficient with limited secondary contamination	Regulatory concerns, expensive of enzyme production, stability and shelf-life (enzymes), low readiness level

(Dowling and Lemley, 1992; Tuorinsky et al., 2009; Kitamura et al., 2014). Commercial products such as Decontamination Solution 2 (DS2), BX-24, and Decontamination Formulation DF-200 are employed by U.S. and NATO forces and are highly effective against most organophosphate compounds. As with sodium hydroxide and hypochlorite both DS2 and DF-200 are composed of chemicals that limit their use for personnel or sensitive equipment due to their corrosive nature. Given warfighter and support personnel needs, personnel decontamination solutions have also been developed including the M291 Skin Decontamination Kit (SDK) and the Reactive Skin Decontamination Lotion (RSDL). These products have variable effectiveness toward organophosphate agents and neither are suitable for wound or eye decontamination. These materials and other emerging chemical decontamination strategies are thoroughly reviewed in Jacquet et al. (2016).

Decontamination agents such as DS2 and bleach are corrosive in nature and generate hazardous waste and are therefore not considered safe. This leads to a dire need for non-toxic, non-corrosive, and environmentally compatible decontamination strategies. The use of microbes and purified enzymes for decontamination has been an area that is being extensively researched and has met with success in terms of degradation of OP compounds in commercial applications.

Bioremediation

As will be discussed in subsequent sections, several enzymes have been identified in nature capable of degrading OP pesticides and CWAs (Dawson et al., 2008; Yair et al., 2008; Pizzul et al., 2009; Diao et al., 2013; Iyer et al., 2013; Geed et al., 2016; Brar et al., 2017). Several of these enzymes have been localized to the surface of microbes for evolution of substrate promiscuity and direct bioremediation of OP compounds (Richins et al., 1997; Cho et al., 2002; Zhang et al., 2004; Makkar, 2013; Alves et al., 2015, 2016, 2018; Bigley et al., 2015; Bigely et al., 2019). Cell-mediated bioremediation and biocatalysis is well-established and documented within the literature, however, application can be limited as the release of genetically-modified organisms is not currently considered a viable approach to bioremediation. Additionally, the unique role that OP compounds play as both commercial products and weapons of mass destruction necessitates remediation strategies that can also transition to therapeutic agents and personnel decontamination products.

Over the past several years, numerous successes have been realized with both the isolation of new enzymes capable of degrading OP compounds and the evolution of older enzymes to improve their utility in point-of-concern decontamination. In the subsequent sections we describe those enzymes most commonly referenced in the literature and highlight some of the new players in the field. For each of these enzymes, we also briefly discuss how scientists are attempting to further enable the use of these biological catalyst through protein engineering to increase substrate promiscuity and activity as well as other strategies to improve catalytic activity and stability.

ENZYMES FOR DECONTAMINATION

As previously mentioned, OP-intoxication occurs through the irreversible binding of OP compounds to acetylcholinesterase, an enzyme found within the neuromuscular junction, inactivating it. While acetylcholinesterase is incapable of degrading these compounds, enzyme catalysts capable of degrading OP compounds have been identified in microbial species, in squid, and even in mammals. As will be detailed below, enzymatic degradation of OP compounds occurs through nucleophilic attack of the phosphorus center of the compound mediated by a pair of divalent metal ions, a water molecule, and reactive amino acids contained within the active site of the enzyme (Aubert et al., 2004; Wymore et al., 2014). These enzymes have varying specificities for OP compounds but all follow similar mechanisms of action.

An ideal decontaminant candidate must be able to rapidly detoxify the warfare agents at a molecular level and be able to decontaminate any surface such as paint, concrete, rubber seals, asphalt, metal, plastics, clothing, and skin. Additionally, these reagents should be environmentally friendly without lasting impact on soil, vegetation, and animal life or underground water sources. Use of OP degrading enzymes for environmental decontamination present significant advantages as they can rapidly hydrolyze the nerve agents, and are environmental friendly, non-flammable, non-corrosive and can be disposed

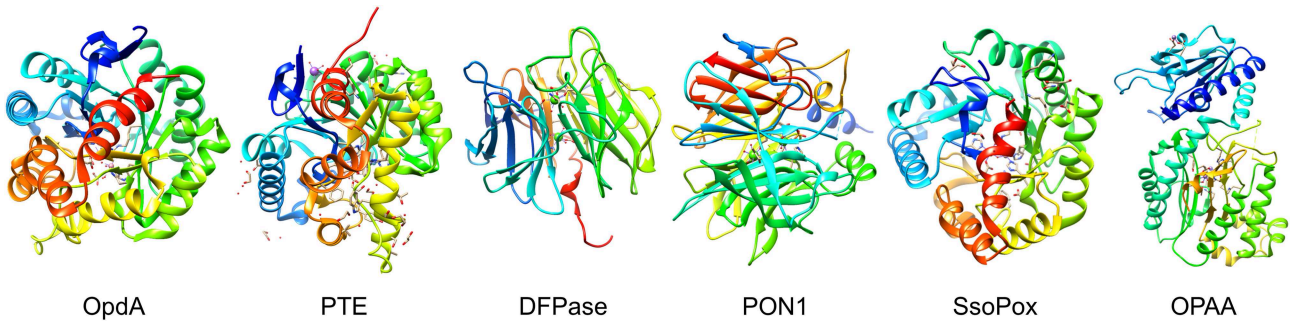

FIGURE 4 | Organophosphate hydrolyases. Representative protein structures from the Protein Data Bank (PDB) database. From left to right: Crystal structure phosphotriesterase OpdA from *Agrobacterium radiobacter* (PDB: 2D2J); crystal structure of zinc-containing phosphotriesterase (PTE) from *Pseudomonas diminuta* (PDB: 1HZY, Chain A); crystal structure of diisopropylfluorophosphatase (DFPase) from *Loligo vulgaris* (PDB: 1E1A); crystal structure of serum paraoxonase PON1 from *Oryctolagus cuniculus* (PDB: 1V04); crystal structure of phosphotriesterase-like lactonase SsoPox from *Sulfolobus solfataricus* (PDB: 2VC5, Chain A); crystal structure of organophosphate acid anhydrolase (OPAA) from *Altermonas sp.* (PDB: 3L7G, Chain A).

TABLE 2 | Summary of enzymes discussed.

Enzyme	Originating species	Structure	Metal ion	Substrates	kcat/Km $M^{-1}s^{-1}$		Notes	References
OpdA	*Agrobacterium radiobacter*	TIM barrel	Binuclear Fe^{2+}-Zn^{2+}	OPs, G-type nerve agents	Methyl-paraoxon	1.1 X 10^4	High affinity for substrates with shorter side chains	Horne et al., 2002; Yang et al., 2003
PTE	*Brevundimonas diminuta*	TIM barrel	Zn	OPs, sarin, cyclosarin and VX	DEVX	1.2 X 10^3	Metal-containing amidohydrolase superfamily	Dumas et al., 1989a; Bigely et al., 2019
					DMVX	1.9 X 10		
					malathion	3.0 X 10		
DFPase	*Loligo vulgaris*	Six-bladed β propellar	Ca^{2+}	DFP, G-type nerve agents	DFP	5.6 X 10^4	Highly specific for P-F bond hydrolysis, high pH and temperature stability	Melzer et al., 2009, 2012; Zhang et al., 2018
					GB	4.2 X 10^4		
					GF	7.2 X 10^5		
PON1	Human liver	Six-bladed propeller	Ca^{2+}	OPs, G- and V-type nerve agents	Paraoxon	0.6 X 10^4	High density lipoprotein-associated esterase/lactonase	Aharoni et al., 2004; Purg et al., 2017
Ssopox	*Sulfolobus solfataricus*	TIM barrel	Co^{2+}, Fe^{3+}	OPs	Paraoxon	4 X 10^3	Denaturation temperature 106°C	Merone et al., 2005; Elias et al., 2008
OPAA	*Alteromonas sp.*	Pita bread architecture	Mn^{2+}	G-agents- soman and cyclosarin	Paraoxon	9.36 X 10^2	Prolidases, can cleave P-F, P-O, P-CN and P-S bonds	Vyas et al., 2010; Xiao et al., 2017

OPs, Organophosphates; DEVX, Diethyl-VX; DMVX, Dimethyl-VX; DFP, Diisopropyl fluorophosphate; GB, sarin; GF, cyclosarin.

of safely and easily. Several enzymes have evolved in nature with the capability of degrading the OP compounds, see **Figure 4** for names and representative structure and **Table 2** for a summary details on each. Extensive research is being carried out to improve their efficacy and stability, thus enhancing their appeal as decontamination agents. Some of these advanced enzymes are being investigated for *in vivo* efficacy, and one of the enzyme based decontamination solutions is already in commercial use in Australia. We now briefly summarize some of the more prominent enzymes studied for OP remediation.

Diisopropylfluorophosphatase (DFPase)

Diisopropylfluorophosphatase (DFPase), isolated from the European squid *Loligo vulgaris*, catalyzes the hydrolysis of OP compounds such as diisopropylfluorophosphate (DFP) and a number of G-type nerve agents, including sarin (GB), soman (GD), cyclosarin (GF), and tabun (GA) (Hartleib and Ruterjans, 2001; Soares et al., 2018). Several structural studies on DFPase have revealed the presence of a six-bladed ß-propeller structure with two calcium ions, one required for catalysis and the other for providing structural integrity (Scharff et al., 2001; Blum and Chen, 2010; Blum et al., 2010).

Several theoretical and computational studies in agreement with the experimental results have highlighted the existence of at least two different pathways for the degradation of different OP compounds which could eventually lead to improved strategies to engineer DFPase for more efficient degradation of OP compounds (Soares et al., 2018; Zhang et al., 2018). In addition, mutational studies have also been carried out and have led to an understanding of the mechanism of action of the enzyme on substrates (Blum et al., 2006). Remarkably, in a preliminary *in vivo* study, Melzer *et al.* found that addition of pegylated DFPase minimizes lethality in rats challenged with a subcutaneous $3xLD_{50}$ dose of soman, thereby highlighting its potential for *in vivo* use (Melzer et al., 2012).

Paraoxonase (PON1)

The paraoxonase enzyme produced in the human liver is a calcium dependent enzyme able to hydrolyze aryl esters, lactones, and OPs (Rajkovic et al., 2011). Structurally, it is also described as a six-bladed propeller structure that utilize a calcium ion within its active site similar to DFPase (Gold et al., 2000; Rajkovic et al., 2011; Mackness and Mackness, 2015). Although PON1 shares identity with DFPase in the active site and tertiary structure, it shows a different substrate preference and is unable to hydrolyze bulky OPs such as DFP but does show some activity for VX (Bajaj et al., 2013; Purg et al., 2017). In addition to its activity against organophosphates, paraoxonases have been extensively studied for their anti-inflammatory, anti-oxidative, anti-atherogenic, antimicrobial, anti-diabetic, and OP-detoxifying properties. Human paraoxonase-1 (PON1) can readily hydrolyze paraoxon, a commercial OP pesticide; however, its activity toward G- and V- type nerve agents is limited to the less toxic enantiomers of these agents. As a result, the enzyme has been subjected to substantial experimental and computational characterization to enhance its catalytic efficiency and enantioselectivity (Gupta et al., 2011; Goldsmith et al., 2012; Le et al., 2015).

As the only human-derived enzyme capable of degrading OP compounds, PON1 has the greatest potential as a therapeutic to counter OP poisoning. Unfortunately, PON1 suffers from a lack of stability unless bound to a high density lipoprotein (HDL) and is further limited (as this complex) by environmental conditions and by several common biomolecules that have been shown to interact with and limit the activity of the HDL-PON1 complex (Ferretti et al., 2001; Jaouad et al., 2003; Rozenberg and Aviram, 2006; Gaidukov et al., 2009). To improve upon the potential of PON1 as therapeutic, Aharoni et al. generated a mutant version of the PON1 that exhibited a 40-fold increase in OP-degrading activity compared to the parental enzyme (Aharoni et al., 2004). This recombinant PON1 was later combined with a HDL particle (referred to as BL-3050) and tested *in vivo* in mice by the same research team (Gaidukov et al., 2009). In these studies the recombinant PON1 showed a longer half-life in mouse models and provided a significant improvement in survival rates for treated mice (87.5%) vs. non-treated controls (37.5%).

Organophosphate Hydrolase (OpdA)

One of the most efficient OP-degrading enzymes, organophosphate hydrolase (OpdA), was isolated form *Agrobacterium radiobacter* by Horne et al. in 2002 (Horne et al., 2002). The OpdA enzyme adopts an $(\alpha/\beta)_8$ barrel structure with a heterobinuclear Fe–Zn metal center and shows an enhancement in specific activity when supplemented with cobalt (Jackson et al., 2008). The enzyme can hydrolyze a wide variety of OP pesticides and has been shown to inactivate G-type nerve agents such as tabun (GA), sarin (GB), soman (GD), and ethylsarine (GE) with varying efficiencies (Dawson et al., 2008). Several mutants of OpdA with improved activity against these nerve agents have also been produced as described by Yang et al. (2003). In addition to *in vitro* studies, the *in vivo* therapeutic potential of OpdA has also been demonstrated. For instance, separate research groups showed that administration of OpdA in rats and monkeys improved survival after poisoning with highly toxic OP pesticides (Bird et al., 2008; Jackson et al., 2014). In addition to its therapeutic applications, OpdA is the only enzyme that is currently commercially employed as a bioremedier. The Australian company Orica Ltd, has marketed the OpdA-containing product Landguard™ OP-A for use in pesticide decontamination of water sources (Anderson et al., 2011; Scott et al., 2011). Studies starting in 2004 have shown that Landguard™ is able to significantly reduce OP levels in agricultural wastewater validating recombinant enzymes as a viable method of decontaminating contaminated sources at a significant scale.

Phosphotriesterase (PTE)

Phosphotriesterase (PTE), also termed organophosphate hydrolase (OPH) is a zinc-dependent bacterial enzyme that belongs to the amidohydrolase superfamily and was first identified in soil bacteria that hydrolyzed the pesticide parathion (Dumas et al., 1989a,b). The tertiary structure of the protein is an $(\alpha/\beta)_8$-barrel or TIM-barrel, in which the binuclear active site is located at the C-terminus of the protein (Vanhooke et al., 1996; Benning et al., 2001). The most commonly utilized PTE enzyme was derived from *Brevundimonas diminuta* (previously *Pseudomonas diminuta*) although homologs have been identified in other species including *Sulfolobus solfataricus* (discussed below) and *Deinococcus radiodurans* which are typically referred to as phosphotriesterase-like lactonases (PLLs) (Dumas et al., 1989a; Merone et al., 2005; Hawwa et al., 2009). The microbial substrate of PTE and PLLs has not been identified, though it likely varies between species. It is believed and has been shown in some experimental studies that these enzymes likely arose from bacterial lactonases (Chow et al., 2009; Afriat-Jurnou et al., 2012; Elias and Tawfik, 2012). PTE shows high catalytic activity toward a number of pesticides but only moderate activity toward nerve agents such as sarin, cyclosarin, and VX. The environmental persistence of V-agents such as VX has led several research teams such as those of Frank Raushel of Texas A&M University and others to invest heavily in mutational studies of this enzyme to improve activity toward VX and other substrates (Briseno-Roa et al., 2011; Tsai et al., 2012; Bigley et al., 2013, 2015; Naqvi et al., 2014; Bigely et al., 2019). Recently, Khersonsky et al. developed a

robust automated method which led to generation of PTE with a remarkable >1,000-fold improvement in nerve-agent hydrolysis (Khersonsky et al., 2018). Moving forward in that direction, Bigely et al. (2019), screened a 28,800 member six-site PTE mutant library against multiple V-agent analogs, and identified multiple variants with >1500-fold increase in k_{cat}/K_M for the hydrolysis of VX (Bigely et al., 2019).

Of the OP-degrading enzymes currently studied, PTE has some of the fastest catalytic rates and has shown the greatest promise for engineering substrate activity as described above. Early studies with direct injection of PTE as a counter-measure for OP poisoning showed some success though the half-life of enzyme was relatively low (100 min) necessitating the development of an extracorporeal reactor system to purify the blood (Masson et al., 1998). A later review by Raushel summarized some of the progress with PTE as a therapeutic in mouse models including efforts to use PTE as a pretreatment to afford some level of protection (Ghanem and Raushel, 2005). With the mutational improvement of the enzyme's stability and substrate range it is not difficult to envision PTE as a viable medical countermeasure for OP poisoning.

SsoPox

A hyperthermophilic PLL, SsoPox, was isolated from the Archaeon *Sulfolobus solfataricus* (Merone et al., 2005; Hiblot et al., 2012). SsoPox exhibits high activity toward acyl-homoserine lactones and oxo-lactones but a low phosphotriesterase activity. Similar to OP hydrolases of the amidohydrolase superfamily, the folded structure of SsoPox is an $(\alpha/\beta)_8$ barrel in which the active site resides at the C-terminal section of the structure (Hiblot et al., 2013). While SsoPox show reduced activity toward many pesticides compared to PTE and others, it is an extremely rugged enzyme exhibiting activity at temperatures up to 100°C (melting temperature is 104°C) and in the presence of several detergents and other denaturing agents (Hiblot et al., 2012). These properties make SsoPox a promising candidate for the development of field-deployable reagents for bioremediation. To further improve upon the enzyme, several groups have employed a structure-based design approach to increase the phosphotriesterase activity and improve the active site recognition for an increased range of OP substrates (Merone et al., 2010; Jacquet et al., 2017). Recently, Vitola et al. developed a biocatalytic membrane reactor (BMR) by covalently immobilizing a triple mutant of the SsoPox on polymeric membranes, leading not only to high paraoxon degradation but also long-term stability of the free enzyme (Vitola et al., 2019).

Organophosphate Acid Anhydrolase (OPAA)

The organophosphate acid anhydrolase enzymes are bacterial prolidases isolated from several species of *Alteromonas* bacteria (deFrank and Cheng, 1991). The *Alteromonas* OPAAs are dipeptidases that typically cleave dipeptide bonds in which the C-terminal residue is a proline (Cheng et al., 1999). Although not involved in the metabolism of OPs, OPAAs also show activity against a wide range of these compounds cleaving P-F, P-O, P-CN, and P-S bonds (Cheng et al., 1999). Prolidases are structurally distinct from other bacterial hydrolases such as PTE and OpdA and therefore show different OP substrate specificities and activities (Xiao et al., 2017). As with many of the other enzymes discussed here, OPAA has undergone mutagenic studies to enhance its catalytic activity and substrate specificity. Bae *et al.* showed that a series of mutations in OPAA led to significant increase in activity toward sarin and soman (Bae et al., 2018). Additionally, in these studies, the authors were able to isolate a double mutant version of OPAA that was able to show enantioselectivity for one enantiomer of sarin. The *Alteromonas* OPAA, similar to other OP enzymes, have greatest activity at biologically-relevant temperature (25–37°C) which can limit their utility in field-based applications. As has been observed with other proteins, prolidases isolated from extremophiles such as members of the *Pyrococcus* genus often show improved thermostability as shown by Theriot et al. (2011). Studying both the wild-type and mutant versions of the *Pyrococcus horikoshii* enzyme, the authors showed that these new OPAA enzymes had improved shelf-life and thermal stability compared to *Alteromonas* OPAAs making them ideal candidates for field distribution.

Other Enzymes

In addition to the above described enzymes, several proteins have been shown to possess a moonlighting OP hydrolyzing activity. For instance, senescence marker protein (SMP30) isolated from mouse liver cytosol, is capable of hydrolyzing DFP and other OPs such as sarin, soman, and tabun (Scott and Bahnson, 2011; Dutta et al., 2019). Although SMP30 can hydrolyze similar substrates like DFPase, it is not a calcium binding protein, and shows activity in the presence of Mg^{2+} and Mn^{2+} (Dutta et al., 2019). Bacterial lactonases have also shown potential as OP-degrading enzymes due to their high degree of substrate promiscuity (Draganov, 2010). Like SsoPox, other PLLs have been described in the literature as showing some potential as tools for OP bioremediation. In separate publications, Zhang et al. describe a PLL from *Geobacillus kaustophilus* referred to as GkaP (Zhang et al., 2012, 2015). This enzyme typically cleaves the 6-membered ring structures of lactones but does show some activity toward *ethyl*-paraoxon. Other enzymes capable of degrading the substrate methyl-parathion have also been described in the literature (Rani and Lalithakumari, 1994; Zhongli et al., 2001; Yang et al., 2008). These enzymes typically utilize a binuclear metal active site but show little structural similarity to phosphotriesterases (Dong et al., 2005).

Many of the enzymes presented here have a long history in the development of therapeutics, sensors, and agents for environmental and personal decontamination. As the tools of genomics and systems, synthetic, and molecular biology continue to evolve it is anticipated that more enzymes capable of degrading OP compounds will be identified in nature and evolved in the laboratory to improve their applicability. In the subsequent sections we discuss the efforts of researchers to both improve and implement these enzymes for field use. As a discussion encompassing all of the aforementioned enzymes would prove prohibitively long, we focus on efforts targeting the PTE or OPH enzymes only.

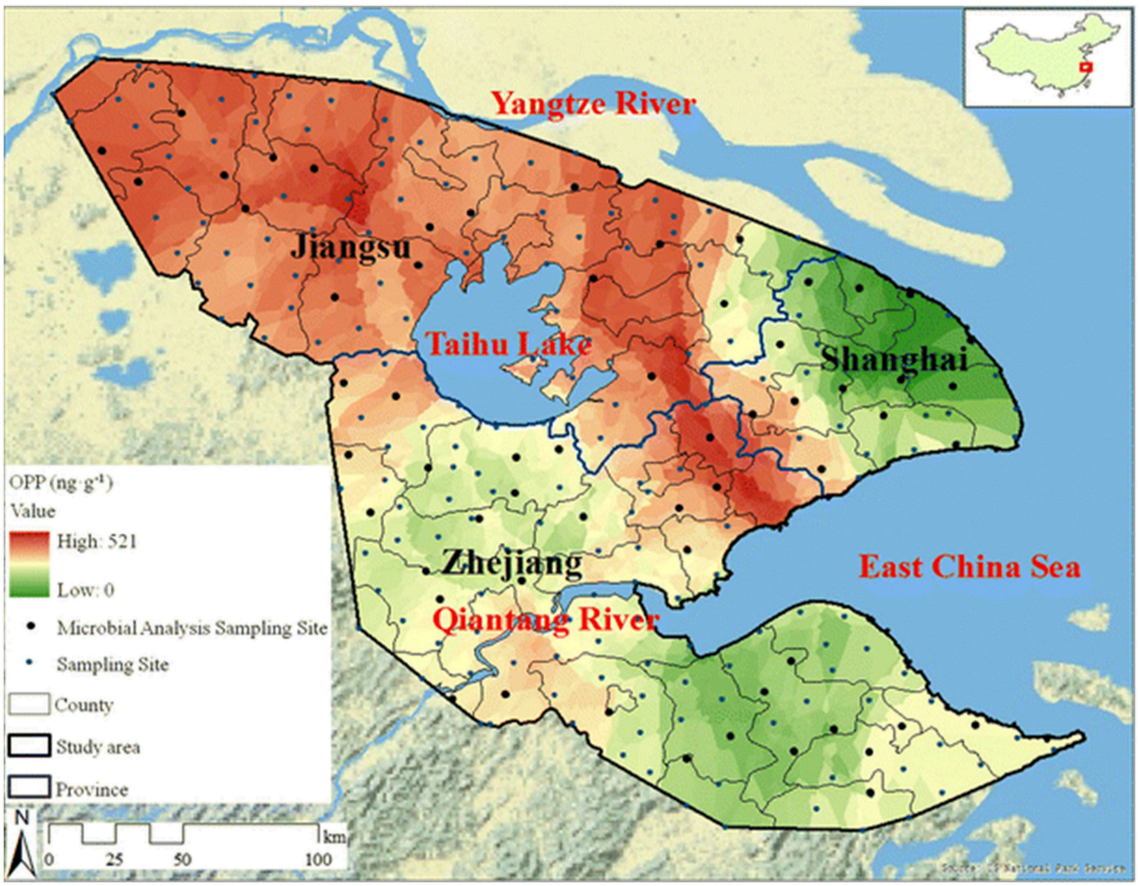

FIGURE 5 | Spatial distribution of organophosphate concentrations across the Yangtze River Delta region. Researchers tested soil samples (241 sites covering 45,800 km^2) from the Yangtze River Delta to assess the spatial distribution of OP pesticides (and others) due to agricultural use. The representative map shown here highlights 60 sites with a distribution of contamination levels. Reproduced with permission (Pan et al., 2018), Copyright Springer 2018.

RELEVANCE AND POTENTIAL FOR DEPLOYMENT

OP compounds fill two distinct and highly divergent applications in human society. At the most benign level, the compounds are used to benefit agricultural production and to control the spread of arthropod disease. At the opposing end of this spectrum, OP compounds are some of the most dangerous weapons produced by man. Though the potential for human harm is dramatically different, even widely used pesticides can be incredibly dangerous following prolonged or high concentrations of exposure. Therefore, the need to develop reliable methods to both detect and eliminate these compounds is important and relevant to both civilian and military populations. While successes have been achieved with engineering bacterial systems for decontamination and detection through mechanisms such as cell-surface localization of enzyme, the release of engineered organisms is not currently accepted by nations around the world. Cell-free synthetic biology, which can rely on cell extracts or purified recombinant enzymes, offers an avenue for utilizing the elegance of biological systems for detection and bioremediation in a non-replicating system. As will be described in the subsequent sections, enzyme-based cell-free systems have seen success as sensors, tools of bioremediation, and as potential therapeutics.

Sensors

While the use of pesticides is vital to commercial agriculture, the long half-lives and soil and water retention time of many of these organophosphate compounds necessitates environmental monitoring (Uchimiya et al., 2012; Hossain et al., 2014; Fosu-Mensah et al., 2016; Pan et al., 2018). Contamination of water sources by agricultural run-off leads to elevated concentrations of these compounds in large-scale waterways such as rivers and deltas as well as soil (Pedersen et al., 2006; Babu et al., 2011). Often, OP compounds are photodegradable or easily hydrolyzed in aerobic soils, however, as shown in a recent publication by Pan et al. and the map of the Yangtze River Delta region shown in **Figure 5,** elevated concentrations of OP compounds can easily be measured in environmental samples (Pan et al., 2018). While these effects are largely felt at the local level, the globalized agricultural economy enables contaminated food products to be distributed world-wide.

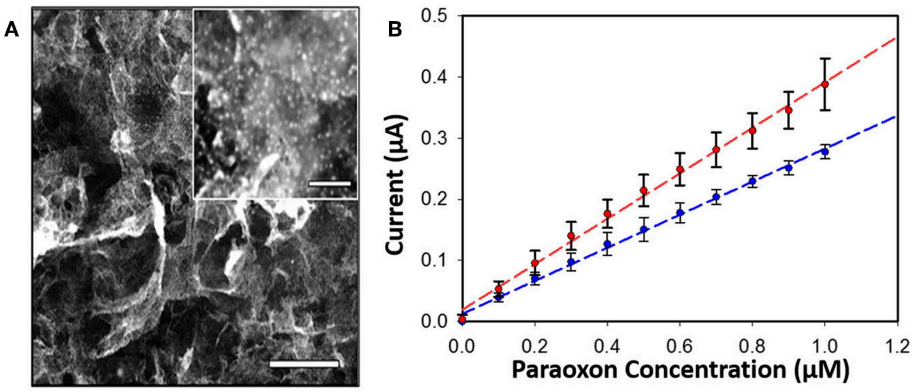

FIGURE 6 | PTE-based sensor for OP compounds. An amperometric sensor was developed that utilized PTE-coated platinum NPs laser-annealed to a graphene-coated electrode for detection of the OP pesticide paraoxon (**A**, inset show platinum particles, scale bar 200 nm). Amperometric current was monitored with and without the graphene coating **(B)** showing measurable improvement between the two systems. Reproduced with permission from Hondred et al. (2018), Copyright the American Chemical Society 2018.

The need for OP sensors touches both civilian and military walks of life. PTE-based sensors have not transitioned beyond the laboratory, however, several research groups have shown that surface-immobilized PTE is viable in sensor development (Schoning et al., 2003; Simonian et al., 2004; Andrianova et al., 2016; Hondred et al., 2017, 2018). Typically, these sensors are electrochemical in nature monitoring the formation of hydrolysis products. Schöning et al. explored a number of parameters such as immobilization strategies and reaction conditions while developing a sensor which measures small changes in pH resulting from the hydrolysis of OP compounds by PTE (Schoning et al., 2003). As another example, Andrianova et al. describe an ion-selective field-effect transistor (ISFET) that utilized immobilized PTE to detect paraoxon and methyl-paraoxon (Andrianova et al., 2016). In these studies the researchers highlighted the utility of their ISFET system in prolonged and continuous monitoring of water samples without loss of function which is relevant to the development of distributable water system sensors.

Enzyme concentration and activity in sensors is vitally important to achieving the high levels of sensitivity desired in OP detection. Often this can be accomplished through the integration of nanoparticles into the sensor platform as a scaffold for enzyme assembly. In two separate studies Hondred et al. developed a printed, graphene-based sensor to detect paraoxon and other pesticides highlighting the use of both enzymes and electrochemical detection (Hondred et al., 2017, 2018). The researchers used a variety of manufacturing techniques including the laser annealing of platinum nanoparticles (NPs) to increase enzyme loading and the overall sensitivity of the sensor as shown in **Figure 6**. In these studies they were able to show a detection limit of 3 nM for the paraoxon substrate. The benefits of combining nanostructures and enzymes in OP sensors has been realized and exploited by several other research groups whose efforts are summarized in a recent review by Sheng et al. (Xiong et al., 2018).

Improving the Utility of PTE

As discussed above for each of the OP hydrolases, protein engineering methods have led to significant improvement in the activity of the enzyme and substrate/enantio- specificity. Beyond direct modification of the amino acid sequence, immobilization of enzymes to solid supports further improves their applicability as there are often inherent benefits of improved stability and enhanced catalytic activity associated with immobilization (Mateo et al., 2007; Mohamad et al., 2015; Proschel et al., 2015; Hoarau et al., 2017). As an enzyme with significant potential as both a bioremedier and therapeutic, PTE has been attached to a range of different materials to improve its activity, long-term stability, and; therefore, viability as a deployable reagent. To illustrate the potential for increased functionality of PTE when immobilized to a solid surface, Raynes et al. cross-linked the enzyme to amyloid fibrils generated from insulin and crystallin and observed a marked improvement in thermal stability (Raynes et al., 2011). Similarly, covalently conjugating PTE to negatively charged gold nanoparticles not only decreased Km value and increased Vmax and Kcat values, but also achieved stability within a wider range of pH (2–12) and temperature (25–90°C) (Karami et al., 2016). This phenomenon of improved enzymatic and biophysical properties is not unique to PTE as highlighted in numerous review articles and recent publications (Chen M. et al., 2017; Kreuzer et al., 2017; Arsalan and Younus, 2018; Wang et al., 2018).

The enhancement of PTE activity and other enzymes at nanoparticle interfaces has been a focus of research efforts in the Medintz laboratories for several years. Focusing on semiconductor quantum dots (QDs) as the model scaffold, the team developed strategies for QD capping and PTE immobilization that led to the formation of highly active enzyme structures (Susumu et al., 2014). A subsequent study described in Breger et al., showed that the rate and efficiency of enzyme catalysis was directly affected by the size of the QD NP as shown in **Figure 7** (Breger et al., 2015a). While PTE is a highly active enzyme functioning at nearly the rate of diffusion, the team

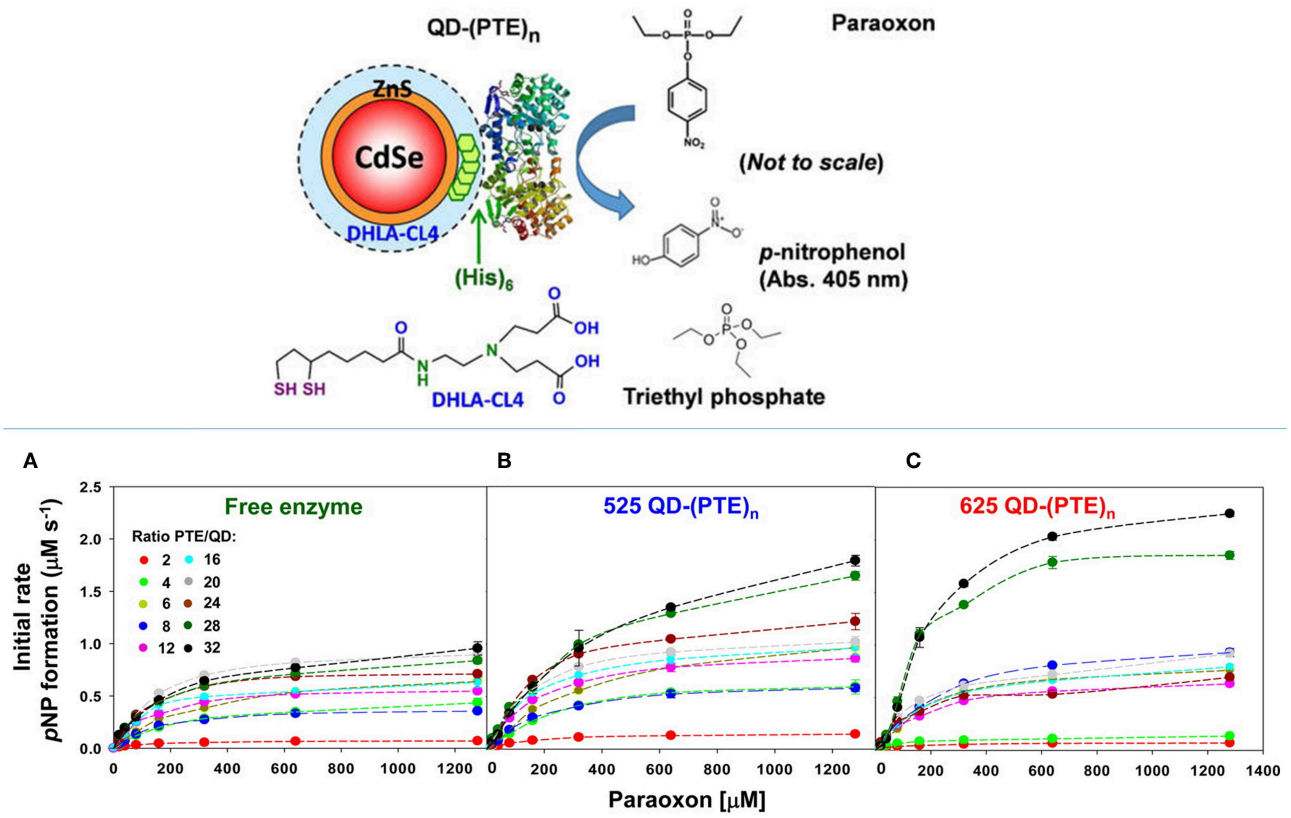

FIGURE 7 | Enhancing PTE activity using PTE-QD conjugates. Researchers have seen an increase in the catalytic activity of PTE when immobilized to the surface of QD NPs. In studies described by Breger et al., PTE was attached to CdSe NPs using an oriented assembly of the enzyme via a C-terminal His_6 amino acid sequence (schematic in the upper panel). Here the hydrolysis of paraoxon by PTE was monitored at 405 nm to assess enzyme activity for both free PTE and PTE immobilized to two QD NPs. Significant changes in the rate of initial velocity for PTE were observed when the enzyme was immobilized to 525 nm **(B)** and 625 nm **(C)** QDs. The rate of catalysis for free enzyme **(A)** was compared to each PTE-QD structure at varying ratios of nanoparticle to enzyme. In each instance the rate of reaction was markedly improved compared to the free enzyme control. Reproduced with permission (Breger et al., 2015a), Copyright American Chemical Society 2015.

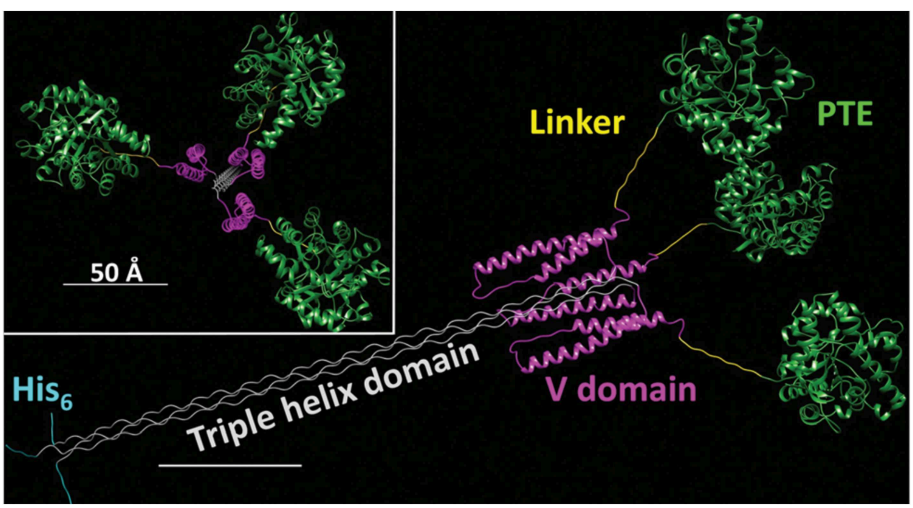

FIGURE 8 | Schematic of an Engineered PTE Triple Helix Structure—A bacterial collagen-like domain was appended to the end of PTE to force the assembly of a trimer structure with a rigid tail section that could be assembled to QDs and other NPs for the purpose of studying kinetics of this non-natural structure. Reproduced from Breger et al. (2015b) with permission from the Royal Society of Chemistry.

observed an ∼4-fold increase in the initial rate of the reaction and an increase in efficiency ∼2-fold greater than the free enzyme. Further experiments showed that this enhancement was not the result of a reduction in activation energy rather a change in the rate of dissociation of product from the enzyme active site as similarly described for the free enzyme by Caldwell et al. (1991). Expanding upon these successes, the team assembled a trimeric PTE structure by attaching a collagen-like domain to the C-terminus of this enzyme (Breger et al., 2015b). The goal here was to create a material that could be spun into a fiber for subsequent integration into textiles such as clothing. Efforts focused on both increasing the potential packing density of the enzyme as well as examining the effect on enzyme activity as the spatial positioning of the enzyme increased in relation to the QD surface as seen in the schematic of **Figure 8**. Though the overall activity of the PTE-trimer was reduced compared to monomeric PTE, the QD-assembled, trimeric structures did show enhanced activity compared to free trimer when assembled to the NPs. The authors postulated that the observed enhancement could be the result of substrate localization due to the expanded solvation shell, the increased avidity due to the trimeric structure, or the controlled orientation of the enzyme itself.

As has been shown with QDS and other abiotic scaffolds, immobilization of enzymes to solid supports is beneficial in sensor development and, in many cases, efforts to improve the kinetic and biophysical properties of the enzyme. To ensure optimum benefit from immobilization it is imperative to ensure enzyme function by carefully selecting immobilization strategies that (1) ensure the enzyme structure is not perturbed and (2) the active site of the enzyme is not occluded in any way. DNA scaffolds and DNA nanostructures can be computationally designed based on Watson-Crick base pairing to ensure consistent and reproducible display of enzymes (Proschel et al., 2015; Quin et al., 2017; Qiu et al., 2018; Sun et al., 2019). Using QDs as their solid support and PTE as their model enzyme, Breger et al. designed a strategy to conjugate the two components using a DNA linker comprised of three modified single-stranded DNA (ssDNA) oligomers (Breger et al., 2017). The goal here was to establish novel methods of QD-functionalization that potentially reduced biomolecule fouling of the QD surface while simultaneously validating a method that could be used for subsequent spatial positioning studies. Conveniently, QDs provide a simple method of biomolecular immobilization via metal affinity interaction between the shell of the QD and hexahistidine (His_6) residues at the enzyme's termini which are included for purification over nickel chelate media. The PTE was conjugated to a second ssDNA molecule and then tethered to the QD surface using a third ssDNA molecule that was complementary to the other two sequences. In these studies, the authors observed some variability in the rate enhancement between conditions but were able to conclusively show that overall enzyme activity was improved above that of free enzyme using this method of NP assembly. In a subsequent study described by Samanta et al., the research team altered their strategy using a pyramidal DNA structure as a scaffold to arrange PTE-coated QDs on the surface of the DNA cage in hopes of establishing a new hybrid scaffolding system to enhance enzyme activity (Samanta et al., 2018). Here the authors designed ssDNA oligos, each terminating with a trimeric histidine repeat that would assemble into 3-way junctions. These subunits were further combined to form a pyramidal DNA cage. The free histidine repeats were then used to assemble QDs to the cage surface through metal affinity between the QD and the terminal histidine amino acids. Subsequent attachment of PTE was accomplished as previously described using the Hi_6 tag at the C-terminus of the enzyme see **Figure 9.** As in previous efforts by the Medintz research team, variability in enzyme enhancement was observed based on the size of the QD and on the ratio of enzyme and the DNA cages. The optimized conditions in these studies showed a nearly 12.5-fold enhancement in the rates of catalysis for the DNA cage, QD-assembled enzyme compared to both free enzyme controls and PTE assembled to QD alone.

Enabling PTE Deployment

Enzymes are notoriously limited by issues of stability. Once removed from the ideal biological conditions of the cell, these intricately folded structures often unravel or collapse into non-functional amino acid chains or globules. While loss of function is expected with all biomolecules, researchers and commercial entities alike struggle to develop methods to limit loss of enzyme activity through storage formulation, direct protein engineering, and other approaches. The efficiency of remediation, rapid rates of catalysis, and environmental and biological compatibility of OP hydrolases such as of PTE make these ideal candidates for the development of commercial products. As mentioned above attaching enzymes to solid supports has been shown to improve enzyme stability and longevity. These strategies, however, are not always amenable to the development of therapeutic agents nor the wide-spread distribution of the materials due to cost of production and the potential for secondary immune response or environmental contamination. In contrast, the encapsulation of enzymes and other biomolecules has a long history in the development of therapeutics and, as will be discussed below, a future in the development of enzyme systems for bioremediation.

While the human PON1 enzyme shows catalytic activity against both V- and G-type agents, the rates of catalysis are not high enough for this enzyme to be an ideal therapeutic or prophylactic (Rajkovic et al., 2011; Le et al., 2015). In contrast, PTE catalysis of many OP compounds occurs at the rate of diffusion (Ghanem and Raushel, 2005). In a foundational publication, Pei *et al.* developed a method of PTE encapsulation targeting implementation of the enzyme as a medical counter measure (Pei et al., 1994). Here the authors permeablized murine erythrocytes which were subsequently filled with recombinant PTE using a hypotonic solution then resealed. This method yielded between 30 and 77% encapsulation depending upon the methods employed. While the PTE-filled erythrocytes were not tested *in vivo* the authors did show that hydrolysis of paraoxon could be achieved using this system and that enzyme encapsulation did not impair enzyme function. Budai et al. shifted away from natural carriers and characterized enzyme activity in synthetic stealth liposomes showing efficient hydrolysis of paraoxon in *in vitro* studies (Budai et al., 2009). In these foundational studies, the research team examined a range

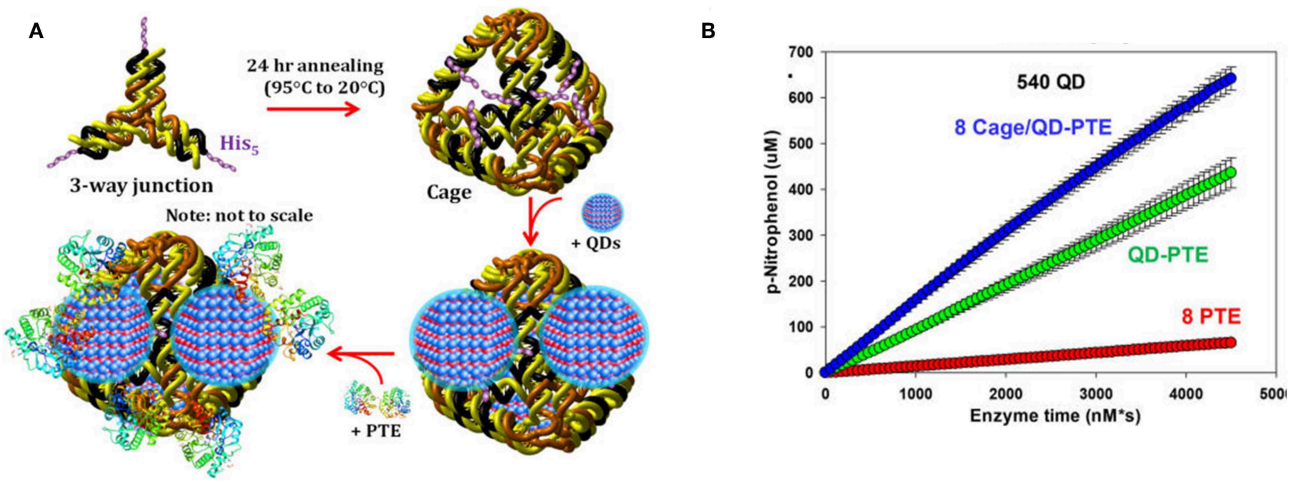

FIGURE 9 | Enhancement of PTE activity through scaffolded DNA assemblies. Pyramidal DNA cages were assembled using three-way DNA junctions that presented terminal hexahistidine sequences allowing for the positional assembly of QDs and recombinant PTE **(A)**. The initial velocity of each construct was tested in parallel **(B)** with "8 PTE" correlating to 8 free enzymes, "QD-PTE" correlating to 8 enzymes on each 540 nm QD, and "8 cage/QD-PTE" defining the assembled structure of **(A)**. Reproduced with permission (Samanta et al., 2018), Copyright the American Chemical Society 2018.

of lipid monomers and assessed overall stability of liposome-enzyme construct over 4 days in guinea pig plasma. The authors showed that the encapsulated enzyme was able to significantly out-perform the free enzyme in both plasma and controls in buffered solutions. Liposomal encapsulation has also been used for the colocalization of enzyme and other therapeutics such as atropine as described for OPAA by Petrikovics (Petrikovics et al., 2000). These studies suggest that encapsulation of enzyme could be used as pathways for *in vivo* delivery of detoxifying therapeutics, or as discussed below, vehicles for field deployment.

In addition to enzyme stability, the cost of production can often be limiting to the realization of enzyme-based tools for bioremediation. In efforts to circumvent both of these complications simultaneously, researchers at the U.S. Naval Research Laboratory explored the direct production and encapsulation of PTE in proteoliposomes produced by *Escherichia coli*. Throughout their life cycle, bacteria release fragments of their outermost membrane containing proteins, nucleic acids, and other biomolecules which have been implicated in a range of functions from pathogenesis to community communication (Deatherage et al., 2009; Schwechheimer et al., 2013). As mimics of the parental bacterium's membrane, outer membrane vesicles (OMVs) are comprised of a protein decorated lipid bilayer that affords protection to cargo proteins from environmental proteases and nucleases. To exploit these benefits, Alves et al. utilized a protein-protein ligation system to anchor PTE to the inner wall of the *E. coli* outer membrane enabling protein loading into nascent OMVs, see **Figure 10** (Alves et al., 2015). Purified directly from the bacterial culture media, these particles showed high catalytic activity toward paraoxon. In subsequent studies, the research group showed that these biological NPs conveyed significant improvements to the stability of the encapsulated PTE allowing it to undergo iterative cycles of freezing and thawing and lyophilization as shown in **Figure 11** (Alves et al., 2016). Additionally, enzyme activity was preserved under elevated temperatures, in high salt solutions that mimic seawater, and over a range of pH conditions (Alves et al., 2016, 2018). These PTE-filled OMVs were also tested in paraoxon-spiked environmental water samples, on surfaces such as painted metal coupons produced to mimic military vehicles, and on glass surfaces to demonstrate their utility in bioremediation (Alves et al., 2018). Finally, OMVs for PTE production and utilization also allowed for a simple and cost-effective method of large-scale enzyme production and dissemination. Alves et al. showed that their PTE-filled OMVs could also be easily purified from bulk growth media using an engineered His_6 affinity tag expressed on the surface of the vesicle (Alves et al., 2017). As bacteria such as the *E. coli* used here can be grown in fermenters at industrial scale, this one step purification protocol significantly reduces the burden associated with manufacture and downstream processing often associated with commercial enzyme production.

Taken as a whole and shown here with PTE, OMVs offer a highly adaptable vehicle for the design, development, and implementation of green biological tools for bioremediation. The ease of production using fermentation currently employed by large- and small-scale breweries shows the feasibility of this form of biomanufacturing. Additionally, the improvements to storage and enzyme stability has been observed with other OP-degrading enzymes such as DFPase and others (unpublished data from the Walper laboratory). Finally, OMVs offer a highly versatile platform to engineer and develop new bioremediation tools. The Walper laboratory has focused on *E. coli* as their proof-of-concept platform but other environmental species could similarly be engineered to develop bioremediation tools. As non-replicating biological particles, upstream modification of membrane channels, surface features, or others to improve functionality would likely not fall under the same regulations for environmental release currently encountered for microbial

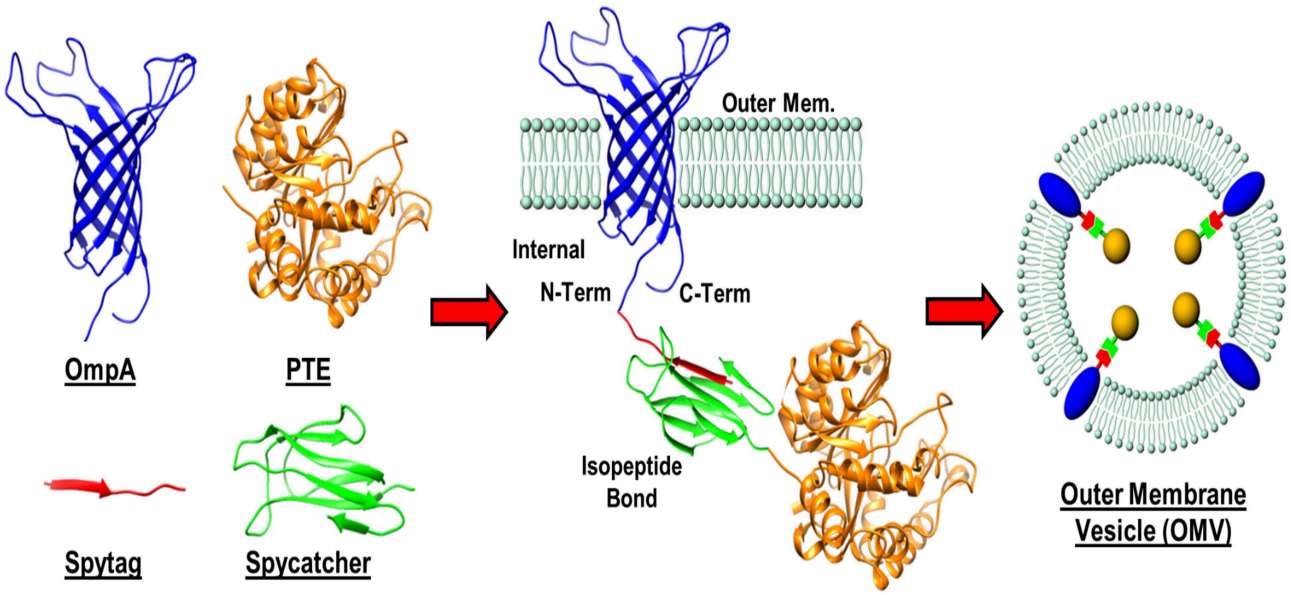

FIGURE 10 | Protein-protein ligation strategy for outer membrane vesicle (OMV) loading. A recombinant membrane protein (OmpA) presenting a SpyTag label was expressed in *E. coli* as an outer membrane anchor for a phosphotriesterase (PTE)—SpyCatcher fusion protein. Interaction between the SpyTag/SpyCatcher partners allowed for the PTE enzyme to be pulled in to nascent OMVs during formation.

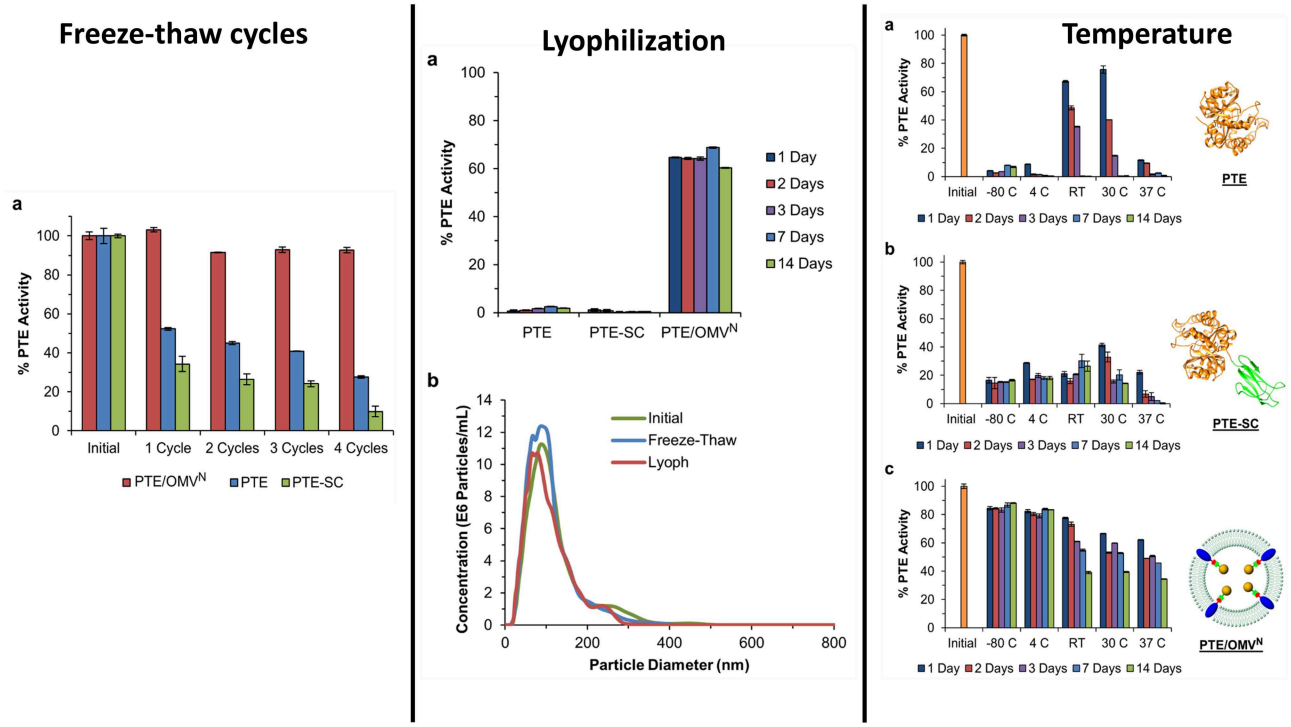

FIGURE 11 | Encapsulation of PTE within bacterial OMVs—The directed packaging of PTE within bacterial OMVs conveys improved stability to the enzymes allowing it to maintain activity over several common storage conditions such as freezing at −80°C and lyophilization and rehydration. Unlike some synthetic liposome formulations, bacterial OMVs maintain their morphology following lyophilization and rehydration (middle panel, b). Encapsulation within the vesicles also allowed the enzyme to be stored for up to 14 days over a range of conditions while maintain a high level of enzyme activity compared to controls. This figure is a combination of data sets presented in Alves et al. (2015, 2016). Both figure reproduced with permission.

species. In conclusion, the composition of bacterial membrane vesicles enables researchers to devise numerous strategies for both their functionalization and purification which will undoubtedly lead to the development of new technologies exploiting these materials as sensors and tools for environmental decontamination (Chen Q. et al., 2017; Jan, 2017; Su et al., 2017).

THE FUTURE OF ENZYMATIC SYSTEMS FOR BIOREMEDIATION AND DECONTAMINATION

The purpose of this review to was to illuminate the reader to both the need for, and successes with enzymes as tools for the bioremediation and decontamination of OP compounds. Whether used as pesticides or agents of war, these compounds have demonstrated potential to cause both acute and long-term harm to individuals and ecosystems alike. Unfortunately, with their wide-scale use in both developed and developing countries it is impossible to foresee a future in which these compounds are not released upon the world at a scale of millions of tons per annum. While chemical methods, and physical methods to some degree, can be employed for decontamination, neither of these pathways is sustainable. Therefore, it is imperative to establish green and sustainable bioremediation tools.

As we have shown here, scientists continue to make significant advances in developing enzymes as tools for environmental and personnel decontamination. In this review we very briefly describe six of the more prominent enzymes capable of degrading organophosphate compounds, however, with increasing genomic sequencing and cataloging of environmental microbes researchers will undoubtedly tease out new enzymes and novel pathways for the bioremediation of OPs and other environmental contaminants. As shown here, using the tools of molecular biology and protein design researchers have been able to significantly modify these enzymes vastly increasing the substrate binding ability and catalytic activity. These foundational studies will continue to evolve to improve both current and future OP hydrolases.

The large-scale use of enzymes as commercial products, therapeutics, and others has historically been impeded by the costs and difficulties associated with manufacture and stabilization. While these factors have historically proved as arguing points, companies such as Novozyme and others continue to demonstrate that the commercialization of enzymes in attainable and profitable. Additionally, the rapid proliferation of synthetic biology-based research efforts have led to the formation of companies such as Gingko Bioworks that focus largely on improving biomanufacturing capabilities through protein selection, gene optimization, and large-scale fermentation models. With significant financial backing in these companies and others, it is undeniable that there is a growing recognition in the potential of biological systems.

Finally, we have shown here with examples such as QD scaffolds and OMV encapsulation that downstream processing of enzyme systems offer potential mechanisms of significantly improving the applicability of enzymes as field deployable materials. In the proof-of-concept studies shown here we see significant improvements in both catalysis and stability using assembly and encapsulation platforms. These systems also offer the potential for multi-enzyme assemblies to move beyond the simple hydrolysis of substrate "A" to product "B," but rather from "A" to "D" through multi-enzyme pathways that demonstrate increased catalytic activity due to substrate channeling or proximity. These multi-enzyme pathways will be necessary to completely eliminate organophosphate compounds which are often nearly as toxic as the first hydrolysis product (Council, 1996).

In conclusion, while significant gains have been made in developing enzymes as candidate biomaterials the road ahead is still a long one. Further demonstrations in relevant environments and conditions are required to validate the potential of the materials for both personal and large-scale decontamination alike. This will require active collaborations between academy, government, and industry; each of which possesses a unique set of skills that can contribute to the realization of enzymes as tools for bioremediation and in decontamination. Unfortunately, even if all of these pieces are combined and the potential of enzymes realized, it is changes in societal and institutional perceptions of these dangerous compounds and their long-term impacts that are most needed and likely the furthest off.

AUTHOR CONTRIBUTIONS

All authors listed have made a substantial, direct and intellectual contribution to the work, and approved it for publication.

FUNDING

This work was made possible in part with funding from the Office of Naval Research (ONR), ONR Global, U.S. Naval Research Laboratory (NRL), and NRL Nanoscience Institute base funding. IM also acknowledges the National Institute of Food and Agriculture, U.S. Department of Agriculture, under award number 2016-67021-25038. SW acknowledges additional funding support from the Applied Research for Advancement of S&T Priorities Synthetic Biology for Military-relevant Environments sponsored by the Office of the Secretary of Defense.

SUPPLEMENTARY MATERIAL

The Supplementary Material for this article can be found online at: https://www.frontiersin.org/articles/10.3389/fbioe.2019.00289/full#supplementary-material

REFERENCES

Afriat-Jurnou, L., Jackson, C. J., and Tawfik, D. S. (2012). Reconstructing a missing link in the evolution of a recently diverged phosphotriesterase by active-site loop remodeling. *Biochemistry* 51, 6047–6055. doi: 10.1021/bi300694t

Aharoni, A., Gaidukov, L., Yagur, S., Toker, L., Silman, I., and Tawfik, D. S. (2004). Directed evolution of mammalian paraoxonases PON1 and PON3 for bacterial expression and catalytic specialization. *Proc. Natl. Acad. Sci. U.S.A.* 101, 482–487. doi: 10.1073/pnas.2536901100

Alves, N. J., Moore, M., Johnson, B. J., Dean, S. N., Turner, K. B., Medintz, I. L., et al. (2018). Environmental decontamination of a chemical warfare simulant utilizing a membrane vesicle-encapsulated phosphotriesterase. *ACS Appl. Mater. Interfaces* 10, 15712–15719. doi: 10.1021/acsami.8b02717

Alves, N. J., Turner, K. B., Daniele, M. A., Oh, E., Medintz, I. L., and Walper, S. A. (2015). Bacterial nanobioreactors–directing enzyme packaging into bacterial outer membrane vesicles. *ACS Appl. Mater. Interfaces* 7, 24963–24972. doi: 10.1021/acsami.5b08811

Alves, N. J., Turner, K. B., DiVito, K. A., Daniele, M. A., and Walper, S. A. (2017). Affinity purification of bacterial outer membrane vesicles (OMVs) utilizing a His-tag mutant. *Res. Microbiol.* 168, 139–146. doi: 10.1016/j.resmic.2016.10.001

Alves, N. J., Turner, K. B., Medintz, I. L., and Walper, S. A. (2016). Protecting enzymatic function through directed packaging into bacterial outer membrane vesicles. *Sci. Rep.* 6:24866. doi: 10.1038/srep24866

Anderson, B., Phillips, B., Hunt, J., Bryan, L., Shihadeh, R., and Tjeerdema, R. (2011). Pesticide and toxicity reduction using an integrated vegetated treatment system. *Environ. Toixol. Chem.* 30, 1036–1043. doi: 10.1002/etc.471

Andrianova, M. S., Gubanova, O. V., Komarova, N. V., Kuznetsov, E. V., and Kuznetsov, A. E. (2016). Development of a biosensor based on phosphotriesterase and n-Channel ISFET for detection of pesticides. *Electroanalysis* 28, 1311–1321. doi: 10.1002/elan.201500411

Arsalan, A., and Younus, H. (2018). Enzymes and nanoparticles: modulation of enzymatic activity via nanoparticles. *Int. J. Biol. Macromol.* 118, 1833–1847. doi: 10.1016/j.ijbiomac.2018.07.030

Atwood, D., and Paisley-Jones, C. (2017). *Pesticide Industry Sales and Usage 2008-2012 Market Estimates*. Washington, DC: U.S. Environmental Protection Agency.

Aubert, S. D., Li, Y., and Raushel, F. M. (2004). Mechanism for the hydrolysis of organophosphates by teh bacterial phosphotriesterase. *Biochemistry* 43, 5707–5715. doi: 10.1021/bi0497805

Babu, V., Unnikrishnan, P., Anu, G., and Nair, S. M. (2011). Distribution of organophosphorus pesticides in the bed sediments of a backwater system located in an agricultural watershed: influence of seasonal intrusion of seawater. *Arch. Environ. Contam. Toxicol.* 60, 597–609. doi: 10.1007/s00244-010-9569-3

Bae, S. Y., Myslinski, J. M., McMahon, L. R., Height, J. J., Bigley, A. N., Raushel, F. M., et al. (2018). An OPAA enzyme mutant with increased catalytic efficiency on the nerve agents sarin, soman, and GP. *Enzyme Microb. Technol.* 112, 65–71. doi: 10.1016/j.enzmictec.2017.11.001

Bajaj, P., Tripathy, R. K., Aggarwal, G., and Pande, A. H. (2013). Characterization of human paraoxonase 1 variants suggest that His residues at 115 and 134 positions are not always needed for the lactonase/arylesterase activities of the enzyme. *Protein Sci.* 22, 1799–1807. doi: 10.1002/pro.2380

Banerji, A., Bhardwaj, M., and Kotoky, A. (2013). *Contaminated School Meal Kills 25 Indian Children*. World News. Available online at: https://www.reuters.com/article/us-india-chidren-poison/contaminated-school-meal-kills-25-indian-children-idUSBRE96G0AY20130717

Ben Mansour, H., Mosrati, R., Barillier, D., Ghedira, K., and Chekir-Ghedira, L. (2012). Bioremediation of industrial pharmaceutical drugs. *Drug Chem. Toxicol.* 25, 235–240. doi: 10.3109/01480545.2011.591799

Benning, M. M., Shim, H., Raushel, F. M., and Holden, H. M. (2001). High resolution X-ray structures of differnet metal-substituted forms of phosphotriesterase from *Pseudomonas diminuta*. *Biochemistry* 40, 2712–2722. doi: 10.1021/bi002661e

Bigely, A. N., Desormeaux, E., Xiang, D. F., Bae, S. Y., Harvey, S. P., and Raushel, F. M. (2019). Overcoming the challenges of enzyme evolution to adapt phosphotriesterase for V-agent decontamination. *Biochemistry* 58, 2039–2053. doi: 10.1021/acs.biochem.9b00097

Bigley, A. N., Mabanglo, M. F., Harvey, S. P., and Raushel, F. M. (2015). Variants of phosphotriesterase for the enhanced detoxification of the chemical warfare agent VR. *Biochemistry* 54, 5502–5512. doi: 10.1021/acs.biochem.5b00629

Bigley, A. N., Xu, C., Henderson, T. J., Harvey, S. P., and Raushel, F. M. (2013). Enzymatic neutralization of the chemical warfare agent VX: evolution of phosphotriesterase for phosphorothiolate hydrolysis. *J. Am. Chem. Soc.* 135, 10426–10432. doi: 10.1021/ja402832z

Bird, S., Traub, S. J., and Grayzel, J. (2019). Organophosphate and carbamate poisoning. *UpToDate*. (accessed July 18, 2019).

Bird, S. B., Sutherland, T. D., Gresham, C., Oakeshott, J., Scott, C., and Eddleston, M. (2008). OpdA, a bacterial organophosphorus hydrolase, prevents lethality in rats after poisoning with highly toxic organophosphorus pesticides. *Toxicology* 247, 88–92. doi: 10.1016/j.tox.2008.02.005

Blum, M.-M., Lohr, F., Richard, A., Ruterjans, H., and Chen, J. C. (2006). Binding of a desinged substrate analogue to diisopropyl fluorophoshatase: implications for phosphotriesterase mechanism. *J. Am. Chem. Soc.* 2006, 12750–12757. doi: 10.1021/ja061887n

Blum, M. M., and Chen, J. C. (2010). Structural characterization of the catalytic calcium-binding site in diisopropyl fluorophosphatase (DFPase)–comparison with related beta-propeller enzymes. *Chem. Biol. Interact.* 187, 373–379. doi: 10.1016/j.cbi.2010.02.043

Blum, M. M., Tomanicek, S. J., John, H., Hanson, B. L., Ruterjans, H., Schoenborn, B. P., et al. (2010). X-ray structure of perdeuterated diisopropyl fluorophosphatase (DFPase): perdeuteration of proteins for neutron diffraction. *Acta Crystallogr. Sect. F Struct. Biol. Cryst. Commun.* 66(Pt 4), 379–385. doi: 10.1107/S1744309110004318

Brar, A., Kumar, M., Vivekanand, V., and Pareek, N. (2017). Photoautotrophic microorganisms and bioremediation of industrial effluents: current status and future prospects. *Biotech* 7:18. doi: 10.1007/s13205-017-0600-5

Breger, J. C., Ancona, M. G., Walper, S. A., Oh, E., Susumu, K., Stewart, M. H., et al. (2015a). Understanding how nanoparticle attachment enhances phosphotriesterase kinetic efficiency. *ACS Nano* 9, 8491–8503. doi: 10.1021/acsnano.5b03459

Breger, J. C., Buckhout-White, S., Walper, S. A., Oh, E., Susumu, K., Ancona, M. G., et al. (2017). Assembling high activity phosphotriesterase composites using hybrid nanoparticle peptide-DNA scaffolded architectures. *Nano Fut.* 1:011002. doi: 10.1088/2399-1984/aa6561

Breger, J. C., Walper, S. A., Oh, E., Susumu, K., Stewart, M. H., Deschamps, J. R., et al. (2015b). Quantum dot display enhances activity of a phosphotriesterase trimer. *Chem. Commun.* 51, 6403–6406. doi: 10.1039/C5CC00418G

Briseno-Roa, L., Timperley, C. M., Griffiths, A. D., and Fersht, A. R. (2011). Phosphotriesterase variants with high methylphosphonatase activity and strong negative trade-off against phosphotriesters. *Protein Eng. Des. Sel.* 24, 151–159. doi: 10.1093/protein/gzq076

Budai, M., Chapela, P., Grof, P., Zimmer, A., Wales, M. E., Wild, J. R., et al. (2009). Physicochemical characterization of stealth liposomes encapsulating an organophosphate hydrolyzing enzyme. *J. Liposome Res.* 19, 163–168. doi: 10.1080/17482940902724044

Caldwell, S. R., Newcomb, J. R., Schlecht, K. A., and Raushel, F. M. (1991). Limits of diffusion in the hydrolysis of substrates by the phosphotriesterase from *Pseudomonas diminuta*. *Biochemistry* 30, 7438–7444. doi: 10.1021/bi00244a010

Chapman, J., Ismail, A., and Dinu, C. (2018). Industrial applications of enzymes: recent advances, techniques, and outlooks. *Catalysts* 8:238. doi: 10.3390/catal8060238

Chen, M., Zeng, G., Xu, P., Lai, C., and Tang, L. (2017). How do enzymes 'meet' nanoparticles and nanomaterials? *Trends Biochem. Sci.* 42, 914–930. doi: 10.1016/j.tibs.2017.08.008

Chen, Q., Rozovsky, S., and Chen, W. (2017). Engineering multi-functional bacterial outer membrane vesicles as modular nanodevices for biosensing and bioimaging. *Chem. Commun.* 53, 7569–7572. doi: 10.1039/C7CC04246A

Cheng, T.-C., DeFrank, J. J., and Rastogi, V. K. (1999). *Alteromonas* prolidase for organophosphorus G-agen decontamination. *Chem. Biol. Int.* 119–120, 455–462. doi: 10.1016/S0009-2797(99)00058-7

Cho, C. M.-H., Mulchandani, A., and Chen, W. (2002). Bacterial cell surface display of organophosphorus hydrolase for selective screening of imprved hydorlysis for argnophosphate nerve agents. *Appl. Environ. Microbiol.* 68, 2026–2030. doi: 10.1128/AEM.68.4.2026-2030.2002

Chow, J. Y., Wu, L., and Yew, W. S. (2009). Directed evolution of a quorum-quenching lactonase from *Mycobacterium avium* subsp. paratuberculosis

K-10 in the amidohydrolase superfamily. *Biochemistry* 48, 4344–4353. doi: 10.1021/bi9004045

Cologgi, D. L., Pastirk-Lampa, S., Speers, A. M., Kelly, S. D., and Reguera, G. (2011). Extracellular reduction of uranium via *Geobacter* conductive pili as a protective cellular mechanism. *Proc. Natl. Acad. Sci. U.S.A.* 108, 15248–15252. doi: 10.1073/pnas.1108616108

Costa, L. G. (2018). Organophosphorus compounds at 80: some old and new issues. *Toxicol. Sci.* 162, 24–35. doi: 10.1093/toxsci/kfx266

Council, N. R. (1996). *Review and Evaluation of Alternative Chemical Disposal Technologies.* Washington, DC: National Academy Press.

Dadachova, E., and Casadevall, A. (2008). Ionizing radiation: how fungi cope, adapt, and exploit with the help of melanin. *Curr. Opin. Microbiol.* 11, 525–531. doi: 10.1016/j.mib.2008.09.013

Dawson, R. M., Pantelidis, S., Rose, H. R., and Kotsonis, S. E. (2008). Degradation of nerve agents by an organophosphate-degrading agent (OpdA). *J. Hazard. Mater.* 157, 308–314. doi: 10.1016/j.jhazmat.2007.12.099

Dean, S. N., Turner, K. B., Medintz, I. L., and Walper, S. A. (2017). Targeting and delivery of therapeutic enzymes. *Ther. Deliv.* 8, 577–595. doi: 10.4155/tde-2017-0020

Deatherage, B. L., Lara, J. C., Bergsbaken, T., Rassoulian Barrett, S. L., Lara, S., and Cookson, B. T. (2009). Biogenesis of bacterial membrane vesicles. *Mol. Microbiol.* 72, 1395–1407. doi: 10.1111/j.1365-2958.2009.06731.x

deFrank, J. J., and Cheng, T.-C. (1991). Purification and properties of an organophosphorus acid anhydrase from a halophilic isolate. *J. Bacteriol.* 173, 1938–1943. doi: 10.1128/jb.173.6.1938-1943.1991

Diao, J., Zhao, G., Li, Y., Huang, J., and Sun, Y. (2013). Carboxylesterase from spodoptera litura: immobilization and use for the degradation of pesticides. *Proc. Environ. Sci.* 18, 610–619. doi: 10.1016/j.proenv.2013.04.084

Dong, Y. J., Bartlam, M., Sun, L., Zhou, Y. F., Zhang, Z. P., Zhang, C. G., et al. (2005). Crystal structure of methyl parathion hydrolase from *Pseudomonas* sp. WBC-3. *J. Mol. Biol.* 353, 655–663. doi: 10.1016/j.jmb.2005.08.057

Dowling, K. C., and Lemley, A. T. (1992). "Evaluation of Organophosphorus Insecticide Hydrolysis by Conventional Means and Reactive Ion Exchange," *Pesticide Waste Management. Am. Chem. Soc.* 177–194. doi: 10.1021/bk-1992-0510.ch015

Draganov, D. I. (2010). Lactonases with organophosphatase activity: structural and evolutionary perspectives. *Chem. Biol. Interact.* 187, 370–372. doi: 10.1016/j.cbi.2010.01.039

Dubinsky, E. A., Conrad, M. E., Chakraborty, R., Bill, M., Borglin, S. E., Hollibaugh, J. T., et al. (2013). Succession of hydrocarbon-degrading bacteria in the aftermath of the deepwater horizon oil spill in the gulf of Mexico. *Environ. Sci. Technol.* 47, 10860–10867. doi: 10.1021/es401676y

Dumas, D. P., Caldwell, S. R., Wild, J. R., and Raushel, F. M. (1989a). Purification and properties of the phosphotriesterase from *Pseudomonas diminuta*. *J. Biol. Chem.* 264, 19659–19665.

Dumas, D. P., WIld, J. R., and Raushel, F. M. (1989b). Diisopropylfluorophosphate hydrolysis by a phosphotriesterase from *Pseudomonas diminuta*. *Biotechnol. Appl. Biochem.* 11, 235–243.

Dutta, R. K., Parween, F., Hossain, M. S., Dhama, N., Pandey, P., and Gupta, R. D. (2019). Comparative analysis of the metal-dependent structural and functional properties of mouse and human SMP30. *PLoS ONE* 14:e0218629. doi: 10.1371/journal.pone.0218629

Dvorak, P., Nikel, P. I., Damborsky, J., and de Lorenzo, V. (2017). Bioremediation 3.0: engineering pollutant-removing bacteria in the times of systemic biology. *Biotechnol. Adv.* 35, 845–866. doi: 10.1016/j.biotechadv.2017.08.001

Dzionek, A., Wojcieszynska, D., and Guzik, U. (2016). Natural carriers in bioremediation: a review. *Electr. J. Biotechnol.* 23, 28–36. doi: 10.1016/j.ejbt.2016.07.003

Elias, M., Dupuy, J., Merone, L., Mandrich, L., Porzio, E., Moniot, S., et al. (2008). Structural basis for natural lactonase and promiscuous phosphotriesterase activities. *J. Mol. Biol.* 379, 1017–1028. doi: 10.1016/j.jmb.2008.04.022

Elias, M., and Tawfik, D. S. (2012). Divergence and convergence in enzyme evolution: parallel evolution of paraoxonases from quorum-quenching lactonases. *J. Biol. Chem.* 287, 11–20. doi: 10.1074/jbc.R111.257329

Ferretti, G., Bacchetti, T., Marchionni, C., Caldarelli, L., and Curatola, G. (2001). Effect of glycation of high density lipoproteins on their physicochemcial properties and on paraoxonase activity. *Acta Diabetol.* 38, 163–169. doi: 10.1007/s592-001-8074-z

Fosu-Mensah, B. Y., Okoffo, E. D., Darko, G., and Gordon, C. (2016). Organophosphorus pesticide residues in soils and drinking water sources from cocoa producing areas in Ghana. *Environ. Sys. Res.* 5:10. doi: 10.1186/s40068-016-0063-4

Franjesevic, A. J., Sillart, S. B., Beck, J. M., Vyas, S., Callam, C. S., and Hadad, C. M. (2019). Resurrection and reactivation of acetylcholinesterase and butyrylcholinesterase. *Chemistry* 25, 5337–5371. doi: 10.1002/chem.201805075

Gaidukov, L., Bar, D., Yacobson, S., Naftali, E., Kaufman, O., Tabakman, R., et al. (2009). *In vivo* administration of BL-3050: highly stable engineered PON1-HDL complexes. *BMC Clin. Pharmacol.* 9:18. doi: 10.1186/1472-6904-9-18

Geed, S. R., Kureel, M. K., Shukla, A. K., Singh, R. S., and Rai, B. N. (2016). Biodegradation of malathion and evaluation of kinetic parameters using three bacterial species. *Resource Efficient Technol.* 2, S3–S11. doi: 10.1016/j.reffit.2016.09.005

Gehlhaus, M., Osier, M., Llados, F., Plewak, D., Lumpkin, M., Odin, M., et al. (2009). *Toxicology Review of Cerium Oxide and Cerium Compounds*. Washington, DC: U.S. Environmental Protection Agency.

Ghanem, E., and Raushel, F. M. (2005). Detoxification of organophosphate nerve agents by bacterial phosphotriesterase. *Toxicol. Appl. Pharmacol.* 207, 459–470. doi: 10.1016/j.taap.2005.02.025

Gnanaprakasam, E. T., Lloyd, J. R., Boothman, C., Ahmed, K. M., Choudhury, I., Bostick, B. C., et al. (2017). Microbial community structure and arsenic biogeochemistry in two arsenic-impacted aquifers in Bangladesh. *MBio* 8:e01326–17. doi: 10.1128/mBio.01326-17

Gold, R. S., Wales, M. E., Grimsley, J. K., and Wild, J. (2000). "Ancillary function of housekeeping enzymes: fortuitous degradation of environmental contaminants," in *Enzymes in Action Green Solutions for Chemical Problems,* Vol. 33, eds B. Zwanenburg, M. Mikolajczyk, and P. Kielbasinski (NATO Science Series) (Dordrecht: Springer), 263–283. doi: 10.1007/978-94-010-0924-9_13

Goldsmith, M., Ashani, Y., Simo, Y., Ben-David, M., Leader, H., Silman, I., et al. (2012). Evolved stereoselective hydrolases for broad-spectrum G-type nerve agent detoxification. *Chem. Biol.* 19, 456–466. doi: 10.1016/j.chembiol.2012.01.017

Gu, Y., J, D.V. N., Wu, L., He, Z., Qin, Y., Zhao, F. J., et al. (2017). Bacterial community and arsenic functional genes diversity in arsenic contaminated soils from different geographic locations. *PLoS ONE* 12:e0176696. doi: 10.1371/journal.pone.0189656

Gupta, R. D., Goldsmith, M., Ashani, Y., Simo, Y., Mullokandov, G., Bar, H., et al. (2011). Directed evolution of hydrolases for prevention of G-type nerve agent intoxication. *Nat. Chem. Biol.* 7, 120–125. doi: 10.1038/nchembio.510

Gustavsson, M., Hornstrom, D., Lundh, S., Belotserkovsky, J., and Larsson, G. (2016). Biocatalysis on the surface of *Escherichia coli*: melanin pigmentation of the cell exterior. *Sci. Rep.* 6:36117. doi: 10.1038/srep36117

Hartleib, J., and Ruterjans, H. (2001). High-yield expression, purification, and characterization of the recombinant diisopropylfluorophosphatase from Loligo vulgaris. *Protein Expr. Purif.* 21, 210–219. doi: 10.1006/prep.2000.1360

Hawwa, R., Larsen, S. D., Ratia, K., and Mesecar, A. D. (2009). Structure-based and random mutagenesis approaches increase the organophosphate-degrading activity of a phosphotriesterase homologue from *Deinococcus radiodurans*. *J. Mol. Biol.* 393, 36–57. doi: 10.1016/j.jmb.2009.06.083

Hiblot, J., Gotthard, G., Chabriere, E., and Elias, M. (2012). Characterisation of the organophosphate hydrolase catalytic activity of SsoPox. *Sci. Rep.* 2:779. doi: 10.1038/srep00779

Hiblot, J., Gotthard, G., Elias, M., and Chabriere, E. (2013). Differential active site loop conformations mediate promiscuous activities in the lactonase SsoPox. *PLoS ONE* 8:e75272. doi: 10.1371/journal.pone.0075272

Hoarau, M., Badieyan, S., and Marsh, E. N. G. (2017). Immobilized enzymes: understanding enzyme-surface interactions at the molecular level. *Org. Biomol. Chem.* 15, 9539–9551. doi: 10.1039/C7OB01880K

Hondred, J. A., Breger, J. C., Alves, N. J., Trammell, S. A., Walper, S. A., Medintz, I. L., et al. (2018). Printed graphene electrochemical biosensors fabricated by inkjet maskless lithography for rapid and sensitive detection of organophosphates. *ACS Appl. Mater. Interfaces* 10, 11125–11134. doi: 10.1021/acsami.7b19763

Hondred, J. A., Breger, J. C., Garland, N. T., Oh, E., Susumu, K., Walper, S. A., et al. (2017). Enhanced enzymatic activity from phosphotriesterase trimer gold

nanoparticle bioconjugates for pesticide detection. *Analyst* 142, 3261–3271. doi: 10.1039/C6AN02575G

Horne, I., Sutherland, T. D., Harcourt, R. L., Russell, R. J., and Oakeshott, J. G. (2002). Identification of an opd (organophosphate degradation) gene in an Agrobacterium isolate. *Appl. Environ. Microbiol.* 68, 3371–3376. doi: 10.1128/AEM.68.7.3371-3376.2002

Hossain, M. S., Chowdhury, M. A. Z., Pramanik, M. K., Rahman, M. A., Fakhruddin, A. N. M., and Alam, M. K. (2014). Determination of selected pesticides in water samples adjacent to agricultural fields and removal of organophosphorus insecticide chlorpyrifos using soil bacterial isolates. *Appl. Water Sci.* 5, 171–179. doi: 10.1007/s13201-014-0178-6

Iyer, R., Iken, B., and Damania, A. (2013). A comparison of organophosphate degradation genes and bioremediation applications. *Environ. Microbiol. Rep.* 5, 787–798. doi: 10.1111/1758-2229.12095

Jackson, C. J., Carville, A., Ward, J., Mansfield, K., Ollis, D. L., Khurana, T., et al. (2014). Use of OpdA, an organophosphorus (OP) hydrolase, prevents lethality in an African green monkey model of acute OP poisoning. *Toxicology* 317, 1–5. doi: 10.1016/j.tox.2014.01.003

Jackson, C. J., Foo, J. L., Kim, H. K., Carr, P. D., Liu, J. W., Salem, G., et al. (2008). In crystallo capture of a Michaelis complex and product-binding modes of a bacterial phosphotriesterase. *J. Mol. Biol.* 375, 1189–1196. doi: 10.1016/j.jmb.2007.10.061

Jacquet, P., Daude, D., Bzdrenga, J., Masson, P., Elias, M., and Chabriere, E. (2016). Current and emerging strategies for organophosphate decontamination: special focus on hyperstable enzymes. *Environ. Sci. Pollut. Res. Int.* 23, 8200–8218. doi: 10.1007/s11356-016-6143-1

Jacquet, P., Hiblot, J., Daude, D., Bergonzi, C., Gotthard, G., Armstrong, N., et al. (2017). Rational engineering of a native hyperthermostable lactonase into a broad spectrum phosphotriesterase. *Sci. Rep.* 7:16745. doi: 10.1038/s41598-017-16841-0

Jan, A. T. (2017). Outer Membrane Vesicles (OMVs) of gram-negative bacteria: a perspective update. *Front. Microbiol.* 8:1053. doi: 10.3389/fmicb.2017.01053

Janos, P., Kuran, P., Kormunda, M., Stengl, V., Grygar, T. M., Dosek, M., et al. (2014). Cerium dioxide as a new reactive sorbent for fast degradation of parathion methyl and some other organophosphates. *J. Rare Earths* 32, 360–370. doi: 10.1016/S1002-0721(14)60079-X

Jaouad, L., Milochevith, C., and Khalil, A. (2003). PON1 paraoxonase activity is reduced during HDL oxidation and is an indicator of HDL antioxidant capacity. *Free Radic. Res.* 37, 77–83. doi: 10.1080/1071576021000036614

Jokanovic, M. (2018). Neurotoxic effects of organophosphorus pesticides and possible association with neurodegenerative diseases in man: a review. *Toxicology* 410, 125–131. doi: 10.1016/j.tox.2018.09.009

Karami, R., Mohsenifar, A., Mesbah Namini, S. M., Kamelipour, N., Rahmani-Cherati, T., Roodbar Shojaei, T., et al. (2016). A novel nanobiosensor for the detection of paraoxon using chitosan-embedded organophosphorus hydrolase immobilized on Au nanoparticles. *Prep. Biochem. Biotechnol.* 46, 559–566. doi: 10.1080/10826068.2015.1084930

Khersonsky, O., Lipsh, R., Avizemer, Z., Ashani, Y., Goldsmith, M., Leader, H., et al. (2018). Automated design of efficient and functionally diverse enzyme repertoires. *Mol. Cell* 72, 178–186 e175. doi: 10.1016/j.molcel.2018.08.033

Kitamura, K., Maruyama, K., Hamano, S., Kishi, T., Kawakami, T., Takahashi, Y., et al. (2014). Effect of hypochlorite oxidation on cholinesterase-inhibition assay of acetonitrile extracts from fruits and vegetables for monitoring traces of organophosphate pesticides. *J. Toxicol. Sci.* 39, 71–81. doi: 10.2131/jts.39.71

Knutson, R. D., and Smith, E. G. (1999). *Impacts of Elmininating Organophosphates and Carbamates from Crop Production*. College Station, TX: Texas AandM University.

Kreuzer, L. P., Mannel, M. J., Schubert, J., Holler, R. P. M., and Chanana, M. (2017). Enzymatic catalysis at nanoscale: enzyme-coated nanoparticles as colloidal biocatalysts for polymerization reactions. *ACS Omega* 2, 7305–7312. doi: 10.1021/acsomega.7b00700

Kumar, S. S., and Abdulhameed, S. (2017). "Therapeutic enzymes," in *Bioresources and Bioprocess in Biotechnology,* eds S. Sugathan, N. Pradeep, and S. Abdulhameed (Singapore: Springer), 45–73. doi: 10.1007/978-981-10-3573-9

Le, Q. A., Chang, R., and Kim, Y. H. (2015). Rational design of paraoxonase 1 (PON1) for the efficient hydrolysis of organophosphates. *Chem. Commun.* 51, 14536–14539. doi: 10.1039/C5CC05857K

Liu, Q., Li, Q., Wang, N., Liu, D., Zan, L., Chang, L., et al. (2018). Bioremediation of petroleum-contaminated soil using aged refuse from landfills. *Waste Manag.* 77, 576–585. doi: 10.1016/j.wasman.2018.05.010

Liu, X., Zhang, H., Ma, Y., Wu, X., Meng, L., Guo, Y., et al. (2013). Graphene-coated silica as a highly efficient sorbent for residual organophosphorus pesticides in water. *J. Mater. Chem. A* 1, 1875–1884. doi: 10.1039/C2TA00173J

Lushchak, V. I., Matviishyn, T. M., Husak, V. V., Storey, J. M., and Storey, K. B. (2018). Pesticide toxicity: a mechanistic approach. *EXCLI J.* 17, 1101–1136. doi: 10.17179/excli2018-1710

Mackness, M., and Mackness, B. (2015). Human paraoxonase-1 (PON1): gene structure and expression, promiscuous activities and multiple physiological roles. *Gene* 567, 12–21. doi: 10.1016/j.gene.2015.04.088

Makkar, R. S. (2013). Enzyme-mediated bioremediation of organophosphates using stable yeast biocatalysts. *J. Bioremed. Biodegrad.* 4:182. doi: 10.4172/2155-6199.1000182

Masson, P., Josse, D., Lockridge, O., Viguie, N., Taupin, C., and Buhler, C. (1998). Enzymes hydrolyzing organophophates as potential scavengers against organophosphate poisoning. *J. Physiol.* 92, 357–362. doi: 10.1016/S0928-4257(99)80005-9

Mateo, C., Palomo, J. M., Fernandez-Lorente, G., Guisan, J. M., and Fernandez-Lafuente, R. (2007). Improvement of enzyme activity, stability and selectivity via immobilization techniques. *Enzyme Microb. Technol.* 40, 1451–1463. doi: 10.1016/j.enzmictec.2007.01.018

Melzer, M., Chen, J. C. H., Heidenreich, A., Gab, J., Koller, M., Kehe, K., et al. (2009). Reversed enantioselectivity of diisopropyl fluorophosphatase against organophosphorus nerve agents by rational design. *J. Am. Chem. Soc.* 131, 17226–17232. doi: 10.1021/ja905444g

Melzer, M., Heidenreich, A., Dorandeu, F., Gab, J., Kehe, K., Thiermann, H., et al. (2012). *In vitro* and *in vivo* efficacy of PEGylated diisopropyl fluorophosphatase (DFPase). *Drug Test. Anal.* 4, 262–270. doi: 10.1002/dta.363

Merone, L., Mandrich, L., Porzio, E., Rossi, M., Muller, S., Reiter, G., et al. (2010). Improving the promiscuous nerve agent hydrolase activity of a thermostable archaeal lactonase. *Bioresour. Technol.* 101, 9204–9212. doi: 10.1016/j.biortech.2010.06.102

Merone, L., Mandrich, L., Rossi, M., and Manco, G. (2005). A thermostable phosphotriesterase from the archaeon *Sulfolobus solfataricus*: cloning, overexpression and properties. *Extremophiles* 9, 297–305. doi: 10.1007/s00792-005-0445-4

Mittal, S., and Pandey, A. K. (2014). Cerium oxide nanoparticles induced toxicity in human lung cells: role of ROS mediated DNA damage and apoptosis. *Biomed. Res. Int.* 2014:891934. doi: 10.1155/2014/891934

Mohamad, N. R., Marzuki, N. H., Buang, N. A., Huyop, F., and Wahab, R. A. (2015). An overview of technologies for immobilization of enzymes and surface analysis techniques for immobilized enzymes. *Biotechnol. Biotechnol. Equip* 29, 205–220. doi: 10.1080/13102818.2015.1008192

Montgomery, M. T., Coffin, R. B., Boyd, T. J., and Osburn, C. L. (2013). Incorporation and mineralization of TNT and other anthropogenic organics by natural microbial assemblages from a small, tropical estuary. *Environ. Pollut.* 174, 257–264. doi: 10.1016/j.envpol.2012.11.036

Mostafalou, S., and Abdollahi, M. (2018). The link of organophosphorus pesticides with neurodegenerative and neurodevelopmental diseases based on evidence and mechanisms. *Toxicology* 409, 44–52. doi: 10.1016/j.tox.2018.07.014

Munro, N. B., Talmage, S. S., Griffin, G. D., Waters, L. C., Watson, A. P., King, J. F., et al. (1999). The Source, fate, and toxicity of chemical warfare agent degradation products. *Environ. Health Perspect.* 107, 933–974. doi: 10.1289/ehp.99107933

Naqvi, T., Warden, A. C., French, N., Sugrue, E., Carr, P. D., Jackson, C. J., et al. (2014). A 5000-fold increase in the specificity of a bacterial phosphotriesterase for malathion through combinatorial active site mutagenesis. *PLoS ONE* 9:e94177. doi: 10.1371/journal.pone.0094177

Naughton, S. X., and Terry, A. V. Jr. (2018). Neurotoxicity in acute and repeated organophosphate exposure. *Toxicology* 408, 101–112. doi: 10.1016/j.tox.2018.08.011

Ojuederie, O. B., and Babalola, O. O. (2017). Microbial and plant-assisted bioremediation of heavy metal polluted environments: a review. *Int. J. Environ. Res. Public Health* 14:1504. doi: 10.3390/ijerph14121504

Pan, L., Sun, J., Li, Z., Zhan, Y., Xu, S., and Zhu, L. (2018). Organophosphate pesticide in agricultural soils from the Yangtze River Delta of China: concentration, distribution, and risk assessment. *Environ. Sci. Pollut. Res. Int.* 25, 4–11. doi: 10.1007/s11356-016-7664-3

Pedersen, J. A., Yeager, M. A., and Suffey, I. H. (2006). Organophosphorus insecticides in agricultural and residental runoff: field observations and implications for total maximum daily load development. *Environ. Sci. Technol.* 40, 2120–2127. doi: 10.1021/es051677v

Pei, L., Omburo, G., McGuinn, W. D., Petrikovics, I., Dave, K., Raushel, F. M., et al. (1994). Encapsulation of phosphotriesterase within murine erythrocytes. *Toxicol. Appl. Pharmacol.* 124, 296–301. doi: 10.1006/taap.1994.1035

Peng, R. H., Xiong, A. S., Xue, Y., Fu, X. Y., Gao, F., Zhao, W., et al. (2008). Microbial biodegradation of polyaromatic hydrocarbons. *FEMS Microbiol. Rev.* 32, 927–955. doi: 10.1111/j.1574-6976.2008.00127.x

Petrikovics, I., Cheng, T.-C., Paphadjopoulos, D., Hong, K., Yin, R., DeFrank, J. J., et al. (2000). Long circulating liposomes encapsulating organophosphorus acid anhydrolase in diisopropylfluorophosphate antagonism. *Toxicol. Sci.* 57, 16–21. doi: 10.1093/toxsci/57.1.16

Pizzul, L., Castillo Mdel, P., and Stenstrom, J. (2009). Degradation of glyphosate and other pesticides by ligninolytic enzymes. *Biodegradation* 20, 751–759. doi: 10.1007/s10532-009-9263-1

Prakash, D., Gabani, P., Chandel, A. K., Ronen, Z., and Singh, O. V. (2013). Bioremediation: a genuine technology to remediate radionuclides from the environment. *Microb. Biotechnol.* 6, 349–360. doi: 10.1111/1751-7915.12059

Proschel, M., Detsch, R., Boccaccini, A. R., and Sonnewald, U. (2015). Engineering of metabolic pathways by artificial enzyme channels. *Front. Bioeng. Biotechnol.* 3:168. doi: 10.3389/fbioe.2015.00168

Purg, M., Elias, M., and Kamerlin, S. C. L. (2017). Similar active sites and mechanisms do not lead to cross-promiscuity in organophosphate hydrolysis: implications for biotherapeutic engineering. *J. Am. Chem. Soc.* 139, 17533–17546. doi: 10.1021/jacs.7b09384

Qiu, X. Y., Xie, S. S., Min, L., Wu, X. M., Zhu, L. Y., and Zhu, L. (2018). Spatial organization of enzymes to enhance synthetic pathways in microbial chassis: a systematic review. *Microb. Cell Fact.* 17:120. doi: 10.1186/s12934-018-0965-0

Quin, M. B., Wallin, K. K., Zhang, G., and Schmidt-Dannert, C. (2017). Spatial organization of multi-enzyme biocatalytic cascades. *Organ. Biomol. Chem.* 15, 4260–4271. doi: 10.1039/C7OB00391A

Rajkovic, M. G., Rumora, L., and Barisic, K. (2011). The paraoxonases 1, 2 and 3 in humans. *Biochem. Med.* 21, 122–130. doi: 10.11613/BM.2011.020

Rani, N., and Lalithakumari, D. (1994). Degradation of methyl parathion by *Pseudomonas putida*. *Can. J. Microbiol.* 40, 1000–1006. doi: 10.1139/m94-160

Raveendran, S., Parameswaran, B., Ummalyma, S. B., Abraham, A., Mathew, A. K., Madhavan, A., et al. (2018). Applications of microbial enzymes in food industry. *Food Technol. Biotechnol.* 56, 16–30. doi: 10.17113/ftb.56.01.18.5491

Raymond, J. L., Jamison, V. W., and Hudson, J. O. (1975). "Final report on beneficial stimulation of bacterial activity in ground water petroleum products," in *AlChE Symposium Series, 73* (Washington, DC: American Petroleum Institute), 390.

Raynes, J. K., Pearce, F. G., Meade, S. J., and Gerrard, J. A. (2011). Immobilization of organophosphate hydrolase on an amyloid fibril nanoscaffold: towards bioremediation and chemical detoxification. *Biotechnol. Prog.* 27, 360–367. doi: 10.1002/btpr.518

Richins, R. D., Kaneva, I., Mulchandani, A., and Chen, W. (1997). Biodegradtion of organophosphorus pesticides by surface-expressed organophosphorus hydrolase. *Nat. Biotechnol.* 15, 964–967. doi: 10.1038/nbt1097-984

Roberts, J. R., and Reigart, J. R. (2013). *Recognition and Management of Pesticide Poisonings.* Washington, DC: Environmental Protection Agency.

Rodgers-Vieira, E. A., Zhang, Z., Adrion, A. C., Gold, A., and Aitken, M. D. (2015). Identification of anthraquinone-degrading bacteria in soil contaminated with polycyclic aromatic hydrocarbons. *Appl. Environ. Microbiol.* 81, 3775–3781. doi: 10.1128/AEM.00033-15

Rozenberg, O., and Aviram, M. (2006). S-Glutathionylation regulates HDL-assocaited paraoxonase I (PON1) activity. *Biochem. Biophys. Res. Commun.* 351, 492–498. doi: 10.1016/j.bbrc.2006.10.059

Samanta, A., Breger, J. C., Susumu, K., Oh, E., Walper, S. A., Bassim, N., et al. (2018). DNA–nanoparticle composites synergistically enhance organophosphate hydrolase enzymatic activity. *ACS Appl. Nano Mater.* 1, 3091–3097. doi: 10.1021/acsanm.8b00933

Scharff, E. I., Lucke, C., Fritzsch, G., Koepke, J., Hartleib, J., Dierl, S., et al. (2001). Crystallization and preliminary X-ray crystallographic analysis of DFPase from Loligo vulgaris. *Acta Crystallogr D Biol Crystallogr* 57(Pt 1), 148–149. doi: 10.1107/S0907444900014232

Schoning, M. J., Arzdorf, M., Mulchandani, P., Chen, W., and Mulchandani, A. (2003). Towards a capacitive enzyme sensor for direct determination of organophosphorus pesticides: fundamental studies and aspects of development. *Sensors* 3, 119–127. doi: 10.3390/s30600119

Schwechheimer, C., Sullivan, C. J., and Kuehn, M. J. (2013). Envelope control of outer membrane vesicle production in Gram-negative bacteria. *Biochemistry* 52, 3031–3040. doi: 10.1021/bi400164t

Scott, C., Begley, C., Taylor, M. J., Pandey, G., Momiroski, V., French, N., et al. (2011). "Free-Enzyme Bioremediation of Pesticides," in *Pesticide Mitigation Strategies for Surface Water Quality* (Washington, DC: American Chemical Society), 155–174. doi: 10.1021/bk-2011-1075.ch011

Scott, S. H., and Bahnson, B. J. (2011). Senescence marker protein 30: functional and structural insights to its unknown physiological function. *Biomol. Concepts* 2, 469–480. doi: 10.1515/BMC.2011.041

Sikary, A. K. (2019). Homicidal poisoning in India: a short review. *J. Forensic Leg. Med.* 61, 13–16. doi: 10.1016/j.jflm.2018.10.003

Silar, P., Dairou, J., Cocaign, A., Busi, F., Rodrigues-Lima, F., and Dupret, J. M. (2011). Fungi as a promising tool for bioremediation of soils contaminated with aromatic amines, a major class of pollutants. *Nat. Rev. Microbiol.* 9:477. doi: 10.1038/nrmicro2519-c1

Simonian, A. L., Flounders, A. W., and Wild, J. R. (2004). FET-based biosensors for the direct detection of organophosphate neurotoxins. *Electroanalysis* 16, 1896–1906. doi: 10.1002/elan.200403078

Singh, B. K., and Walker, A. (2006). Microbial degradation of organophosphorus compounds. *FEMS Microbiol. Rev.* 30, 428–471. doi: 10.1111/j.1574-6976.2006.00018.x

Soares, F. V., de Castro, A. A., Pereira, A. F., Leal, D. H. S., Mancini, D. T., Krejcar, O., et al. (2018). Theoretical studies applied to the evaluation of the dfpase bioremediation potential against chemical warfare agents intoxication. *Int. J. Mol. Sci.* 19:E1257. doi: 10.3390/ijms19041257

Su, F.-H., Tabañag, I. D. F., Wu, C.-Y., and Tsai, S.-L. (2017). Decorating outer membrane vesicles with organophosphorus hydrolase and cellulose binding domain for organophosphate pesticide degradation. *Chem. Eng. J.* 308, 1–7. doi: 10.1016/j.cej.2016.09.045

Sun, Q., Tsai, S.-L., and Chen, W. (2019). Artifical scaffolds for enhanced biocatalysis. *Meth. Enzymol.* 617, 363–383. doi: 10.1016/bs.mie.2018.12.007

Susumu, K., Oh, E., Delehanty, J. B., Pinaud, F., Gemmill, K. B., Walper, S., et al. (2014). A new family of pyridine-appended multidentate polymers as hydrophilic surface ligands for preparing stable biocompatible quantum dots. *Chem. Mater.* 26, 5327–5344. doi: 10.1021/cm502386f

Than, K. (2013). *Organophosphates: A Common but Deadly Pesticide*. National Geographic. Available online at: https://www.nationalgeographic.com/news/2013/7/130718-organophosphates-pesticides-indian-food-poisoning/

Theriot, C. M., Semcer, R. L., Shah, S. S., and Grunden, A. M. (2011). Improving the catalytic activity of hyperthermophilic Pyrococcus horikoshii prolidase for detoxification of organophosphorus nerve agents over a broad range of temperatures. *Archaea* 2011:565127. doi: 10.1155/2011/565127

Tsai, P. C., Fox, N., Bigley, A. N., Harvey, S. P., Barondeau, D. P., and Raushel, F. M. (2012). Enzymes for the homeland defense: optimizing phosphotriesterase for the hydrolysis of organophosphate nerve agents. *Biochemistry* 51, 6463–6475. doi: 10.1021/bi300811t

Tuorinsky, S. D., Caneva, D. C., and Sidell, F. R. (2009). "Triage of Chemical Casualties," in *Chemical Aspects of Chemical Warfare* (Washington, DC: Walter Reed Medical Center Borden Institute), 511–526.

Uchimiya, M., Wartelle, L. H., and Boddu, V. M. (2012). Sorption of triazine and organophosphorus pesticides on soil and biochar. *J. Agric. Food Chem.* 60, 2989–2997. doi: 10.1021/jf205110g

Vanhooke, J. L., BEnning, M. M., Raushel, F. M., and Holden, H. M. (1996). Three-dimensional structure of the zinc-containing phosphotriesterase with the bound substrate analog diethyl 4-methylnezylphosphonate. *Biocehmistry* 35, 6020–6025. doi: 10.1021/bi960325l

Vitola, G., Mazzei, R., Poerio, T., Porzio, E., Manco, G., Perrotta, I., et al. (2019). Biocatalytic membrane reactor development for

organophosphates degradation. *J. Hazard. Mater.* 365, 789–795. doi: 10.1016/j.jhazmat.2018.11.063

Vyas, N. K., Nickitenko, A., Rastogi, V. K., Shah, S. S., and Quiocho, F. A. (2010). Structural insights into the dual activities of the nerve agent degrading organophosphate anhydrolase/prolidase. *Biochemistry* 49, 547–559. doi: 10.1021/bi9011989

Wang, W., Guo, N., Huang, W., Zhang, Z., and Mao, X. (2018). Immobilization of chitosanases onto magnetic nanoparticles to enahnce enzyme performance. *Catalysis* 8:401. doi: 10.3390/catal8090401

Wu, M., Li, W., Dick, W. A., Ye, X., Chen, K., Kost, D., et al. (2017). Bioremediation of hydrocarbon degradation in a petroleum-contaminated soil and microbial population and activity determination. *Chemosphere* 169, 124–130. doi: 10.1016/j.chemosphere.2016.11.059

Wymore, T., Field, M. J., Langan, P., Smith, J. C., and Parks, J. M. (2014). Hydrolysis of DFP and the nerve agent (S)-sarin by DFPase proceeds along two different reaction pathways: implications for engineering bioscavengers. *J. Phys. Chem. B* 118, 4479–4489. doi: 10.1021/jp410422c

Xiao, Y., Yang, J., Tian, X., Wang, X., Li, J., Zhang, S., et al. (2017). Biochemical basis for hydrolysis of organophosphorus by a marine bacterial prolidase. *Process Biochem.* 52, 141–148. doi: 10.1016/j.procbio.2016.10.008

Xiong, S., Deng, Y., XZHou, Y., Gong, D., Xu, Y., Yang, L., et al. (2018). Current progress in biosensors for organophosphorus pesticides based on enzyme functionalized nanostructures: a reivew. *Anal. Methods* 10, 5468–5479. doi: 10.1039/C8AY01851K

Yair, S., Ofer, B., Arik, E., Shai, S., Yossi, R., Tzvika, D., et al. (2008). Organophosphate degrading microorganisms and enzymes as biocatalysts in environmental and personal decontamination applications. *Crit. Rev. Biotechnol.* 28, 265–275. doi: 10.1080/07388550802455742

Yang, H., Carr, P. D., McLoughlin, S. Y., Liu, J. W., Horne, I., Qiu, X., et al. (2003). Evolution of an organophosphate-degarding enzyme: a comparison of natural and directed evolution. *PEDS* 16, 135–145. doi: 10.1093/proeng/gzg013

Yang, J., Yang, C., Jiang, H., and Qiao, C. (2008). Overexpression of methyl parathion hydrolase and its application in detoxification of organophosphates. *Biodegradation* 19, 831–839. doi: 10.1007/s10532-008-9186-2

Yari, M., Ghoshoon, M. B., Vakili, B., and Hasemi, Y. (2017). Therapeutic enzymes: applications and approaches to pharmacological improvement. *Curr. Pharma Biotechnol.* 18, 531–540. doi: 10.2174/1389201018666170808150742

Yi, H., and Crowley, D. E. (2007). Biostimulation of PAH degradation with plants containing high concentrations of linoleic acid. *Environ. Sci. Technol.* 41, 4382–4388. doi: 10.1021/es062397y

Zhang, H., Yang, L., Ma, Y. Y., Zhu, C., Lin, S., and Liao, R. Z. (2018). Theoretical studies on catalysis mechanisms of serum paraoxonase 1 and phosphotriesterase diisopropyl fluorophosphatase suggest the alteration of substrate preference from paraoxonase to DFP. *Molecules* 23:E1660. doi: 10.3390/molecules23071660

Zhang, J., Lan, W., Qiao, C., and Jiang, H. (2004). Bioremediation of organophosphorus pesticides by sruface-expressed carboxylesterase from mosqito on *Escherichia coli*. *Biotehcnol. Prog.* 20, 1567–1571. doi: 10.1021/bp049903c

Zhang, Y., An, J., Yang, G. Y., Bai, A., Zheng, B., Lou, Z., et al. (2015). Active site loop conformation regulates promiscuous activity in a lactonase from *Geobacillus kaustophilus* HTA426. *PLoS ONE* 10:e0115130. doi: 10.1371/journal.pone.0115130

Zhang, Y., An, J., Ye, W., Yang, G., Qian, Z. G., Chen, H. F., et al. (2012). Enhancing the promiscuous phosphotriesterase activity of a thermostable lactonase (GkaP) for the efficient degradation of organophosphate pesticides. *Appl. Environ. Microbiol.* 78, 6647–6655. doi: 10.1128/AEM.01122-12

Zhongli, C., Shunpeng, L., and Guoping, F. (2001). Isolation of methyl parathion-degrading strain M6 and cloning of the methyl parathion hydrolase gene. *Appl. Environ. Microbiol.* 67, 4922–4925. doi: 10.1128/AEM.67.10.4922-4925.2001

Zurer, P. (1998). Japanese cult used VX to slay member. *Chem. Eng. News* 76:7. doi: 10.1021/cen-v076n035.p007

Conflict of Interest: The authors declare that the research was conducted in the absence of any commercial or financial relationships that could be construed as a potential conflict of interest.

frontiers in Bioengineering and Biotechnology

ORIGINAL RESEARCH
published: 04 October 2019
doi: 10.3389/fbioe.2019.00254

Selection of High Producers From Combinatorial Libraries for the Production of Recombinant Proteins in *Escherichia coli* and *Vibrio natriegens*

Joel Eichmann[1,2], *Markus Oberpaul*[3], *Tobias Weidner*[1], *Doreen Gerlach*[3] and *Peter Czermak*[1,2,3]*

[1] Institute of Bioprocess Engineering and Pharmaceutical Technology, University of Applied Sciences Mittelhessen, Giessen, Germany, [2] Faculty of Biology and Chemistry, Justus-Liebig University of Giessen, Giessen, Germany, [3] Branch for Bioresources, Fraunhofer Institute for Molecular Biology and Applied Ecology, Giessen, Germany

OPEN ACCESS

Edited by:
Jussi Jantti,
VTT Technical Research Centre of Finland Ltd, Finland

Reviewed by:
Dae-Hee Lee,
Korea Research Institute of Bioscience and Biotechnology (KRIBB), South Korea
Antoine Danchin,
INSERM U1016 Institut Cochin, France

***Correspondence:**
Peter Czermak
peter.czermak@lse.thm.de

Specialty section:
This article was submitted to Synthetic Biology, a section of the journal Frontiers in Bioengineering and Biotechnology

Received: 15 July 2019
Accepted: 20 September 2019
Published: 04 October 2019

Citation:
Eichmann J, Oberpaul M, Weidner T, Gerlach D and Czermak P (2019) Selection of High Producers From Combinatorial Libraries for the Production of Recombinant Proteins in Escherichia coli and Vibrio natriegens. Front. Bioeng. Biotechnol. 7:254. doi: 10.3389/fbioe.2019.00254

The optimization of recombinant protein production in bacteria is an important stage of process development, especially for difficult-to-express proteins that are particularly sensitive or recalcitrant. The optimal expression level must be neither too low, which would limit yields, nor too high, which would promote the formation of insoluble inclusion bodies. Expression can be optimized by testing different combinations of elements such as ribosome binding sites and N-terminal affinity tags, but the rate of protein synthesis is strongly dependent on mRNA secondary structures so the combined effects of these elements must be taken into account. This substantially increases the complexity of high-throughput expression screening. To address this limitation, we generated libraries of constructs systematically combining different ribosome binding sites, N-terminal affinity tags, and periplasmic translocation sequences representing two secretion pathways. Each construct also contained a green fluorescent protein (GFP) tag to allow the identification of high producers and a thrombin cleavage site enabling the removal of fusion tags. To achieve proof of principle, we generated libraries of 200 different combinations of elements for the expression of an antimicrobial peptide (AMPs), an antifungal peptide, and the enzyme urate oxidase (uricase) in *Escherichia coli* and *Vibrio natriegens*. High producers for all three difficult-to-express products were enriched by fluorescence-activated cell sorting. Our results indicated that the *E. coli* ssYahJ secretion signal is recognized in *V. natriegens* and efficiently mediates translocation to the periplasm. Our combinatorial library approach therefore allows the cross-species direct selection of high-producer clones for difficult-to-express proteins by systematically evaluating the combined impact of multiple construct elements.

Keywords: Golden Gate, MoClo, protein secretion, genetic engineering, high-throughput screening, antimicrobial peptide, uricase

INTRODUCTION

Escherichia coli is one of the most common production hosts for recombinant proteins and many expression construct components are available to improve yields and facilitate protein recovery, including a variety of promoters and fusion proteins (Moore et al., 2016; Schreiber et al., 2017). Although, many recombinant proteins are strongly expressed with short production times and can be recovered as soluble products, others are difficult to express either because they are toxic to the host, resulting in low yields, or because they form insoluble inclusion bodies due to incomplete or incorrect folding (Carrió and Villaverde, 2002; Saïda, 2007). These challenges are often encountered when expressing antimicrobial peptides (AMPs), many of which require the formation of disulfide bonds for efficient folding and biological activity. In some cases inclusion bodies are produced deliberately, but the purification and refolding of insoluble proteins requires elaborate downstream processing and often limits the yield and functionality of the product (Hoffmann et al., 2018).

The folding of recombinant proteins in bacteria can also be improved by targeting the periplasm, a space between the outer and inner membrane that contains more chaperones than the cytoplasm, thus promoting folding and resulting in higher yields and less complex downstream processing steps. The oxidizing environment of the periplasm also favors the formation of disulfide bonds (Choi and Lee, 2004; Balasundaram et al., 2009). Translocation of proteins to the periplasm has been a subject to research since the very beginnings of recombinant protein expression technology (Gray et al., 1985; Oliveira et al., 1999). There are two major protein secretion pathways in bacteria. The general secretory (Sec) pathway exports unfolded proteins during or after translation (Tsirigotaki et al., 2017) whereas the twin-arginine translocation (Tat) pathway exports folded proteins. Secretion to the periplasm is achieved by adding an N-terminal signal peptide, which is cleaved off during translocation (Berks et al., 2000). Overexpression of the Tat machinery has been shown to increase the rate of recombinant protein secretion (Browning et al., 2017).

The optimization of recombinant protein production requires the appropriate combination of regulatory elements to control expression and fusion tags for purification. Translation initiation occurs at a ∼35 bp sequence upstream of the start codon, containing the Shine-Dalgarno sequence. This so called ribosome binding site strongly effects the mRNA secondary structure (Dreyfus, 1988; Gold, 1988). Expression level screening is often based on combinatorial libraries of short constitutive promoters and/or ribosome binding sites (Coussement et al., 2014; Mahr et al., 2016). Multiple platforms for fusion tag screening have also been developed for bacteria, yeasts, and animal cells. However, all require the laborious cloning of large numbers of expression constructs (Abdulrahman et al., 2009; Sinah et al., 2012; Steinmetz and Auldridge, 2017).

One of the major drawbacks of high-throughput screening is that the expression levels and fusion tags are generally considered independently (one factor at a time), for example by using the same ribosome binding site for all constructs and testing a range of fusion tags. This is disadvantageous because the rate of protein synthesis strongly depends on mRNA secondary structures, so the combination of elements used in an expression construct can have a profound effect on its performance (Punginelli et al., 2004; Espah Borujeni and Salis, 2016). To overcome this challenge, we implemented a platform to generate combinatorial libraries of ribosome binding sites, secretion signals, and fusion tags. The library included five ribosome binding sites systematically combined with the Tat-specific signal peptides ssTorA and ssNapA, as well as the ssDmsA, ssYahJ, and ssYcdB peptides that are recognized in both the Tat and Sec pathways. All signal peptides have been previously demonstrated to mediate periplasmic translocation in *E. coli* (Tullman-Ercek et al., 2007; Fisher et al., 2008). These elements were further combined with four different N-terminal affinity tags for purification: glutathione-S-transferase (GST), maltose-binding protein (MBP), the small ubiquitin-like modifier (SUMO), and thioredoxin. All four tags have been shown to improve the solubility of recombinant proteins (Young et al., 2012), and affinity chromatography methods are available based, respectively, on immobilized glutathione (Schäfer et al., 2015), amylose (Reuten et al., 2016; Han et al., 2018), SUMO-specific antibodies (Butt et al., 2005), and the formation of reversible disulfide bonds (Mambetisaeva et al., 1997; McNiff et al., 2016). All four fusion tags were also combined with an additional N-terminal His_6 tag for purification by immobilized metal affinity chromatography (IMAC) (Loughran et al., 2017), resulting in eight different purification tag versions in the library. By combing the five ribosome binding sites, five secretion signals, and eight purification tags, the library contained 200 combinations of elements in total.

Libraries were assembled for three difficult-to-express proteins. The first product was the insect metalloproteinase inhibitor (IMPI) from the greater wax moth *Galleria mellonella* (Wedde et al., 1998). This AMP is 69 amino acids in length and contains five disulfide bonds, a major challenge for bacterial expression systems. The production of soluble IMPI has been achieved in redox-engineered *E. coli* strains with an oxidizing cytoplasm that promotes disulfide bond formation (Joachim et al., 2019). Moreover, IMPI has been produced with high yields in the form of inclusion bodies, and was successfully resolubilized using the Cry4AaCter pull-down tag (Hoffmann et al., 2019). However, IMPI has yet to be expressed as a soluble product by targeting the periplasm. The second product was the antifungal peptide lucimycin from the common green bottle fly *Lucilia sericata*. This peptide is 77 amino acids in length and has been expressed as a soluble product in *E. coli*, but with low yields (Pöppel et al., 2014; Schreiber et al., 2017). The third product was the enzyme urate oxidase (uricase) also from *L. sericata*. This enzyme is localized in the Malpighian tubes (Baumann et al., 2017) and catalyzes the degradation of uric acid to 5-hydroxyisourate, which is then converted to allantoin (Ramazzina et al., 2006). It has previously been expressed in *E. coli* albeit in the form of inclusion bodies (Baumann et al., 2017). All three targets were expressed as fusion proteins containing a secretion signal, fusion tag, a green fluorescent protein (GFP) fusion partner to allow the identification of

high-producer clones by fluorescence activated cell screening (FACS), and a thrombin recognition site to cleave the fusion partners from the target protein.

Although, the expression libraries were designed for *E. coli* strain BL21, we also used them to optimize recombinant protein expression in V_{max} Express, a commercial strain of the fast-growing γ-proteobacterium *Vibrio natriegens* engineered for protein production by integrating a T7 expression cassette (Weinstock et al., 2016). This bacterium can utilize inexpensive carbon sources and has a high growth rate, making it ideal for biotechnology applications (Hoffart et al., 2017). It was recently demonstrated to be an alternative host for recombinant protein production (Schleicher et al., 2018; Becker et al., 2019). Here, we report the successful transfer of multiple expression construct elements from *E. coli* to *V. natriegens*, allowing the high-throughput screening of expression libraries and the identification of clones producing high yields of soluble recombinant proteins.

MATERIALS AND METHODS

Strains and Growth Conditions

Escherichia coli NEB 10-beta (NEB, Ipswich, Massachusetts, USA) was used for cloning and plasmid amplification. *E. coli* BL21(DE3) (Merck, Darmstadt, Germany) and *V. natriegens* V_{max} Express (SGI-DNA, La Jolla, California, USA) served as expression hosts. Unless stated otherwise, *E. coli* was grown at 37°C in LB Miller broth (LB) (Carl Roth, Karlsruhe, Germany) and Terrific Broth (TB) (Carl Roth) supplemented with 4 g/L glycerol. *V. natriegens* was cultivated in LB and TB supplemented with V2 salts (204 mM NaCl, 4.2 mM KCl, 23.14 mM $MgCl_2$) at 30°C. The following antibiotics were used for plasmid selection: ampicillin (100 μg/mL), kanamycin (35 μg/mL) and spectinomycin (*E. coli* 65 μg/mL, *V. natriegens* 50 μg/mL). Unless stated otherwise, the bacteria were cultivated in 300- or 500-mL shaking flasks with four baffles, filled with 30 or 50 mL medium, respectively, in an orbital shaker at 250 rpm. The medium was inoculated to an OD_{600} of 0.1 from glycerol stocks. Protein expression was induced at an OD_{600} of 1.0 by adding IPTG to a final concentration of 1 mM. Glycerol stocks were prepared by diluting an overnight culture with medium to reach an OD_{600} of 0.1 and cultivating as above until the OD_{600} reached 1.0. At this point, the cells were centrifuged (5,000 × *g*, 15 min, 4°C) and the pellet was resuspended in ice-cold medium supplemented with 15% (v/v) glycerol. The volume was adjusted to $OD_{600} = 5.0$ and the vials were stored at −80°C.

Library Cloning

Basic parts > 100 bp were synthesized (BioCat, Heidelberg, Germany) and subcloned in pUC57-Kan. Small basic parts were introduced into pUC57-Kan by PCR, using the Q5 Site-Directed Mutagenesis Kit (NEB). For assembly using the MoClo process, 40 fmol of each plasmid was mixed with 10 U T4 DNA Ligase (Promega, Mannheim, Germany), 2 μL of the corresponding buffer and 10 U BsaI or BbsI (NEB). The reaction mix was adjusted to a total volume of 20 μL with double-distilled water and incubated in a PCR cycler (PEQLAB, Erlangen, Germany) at 37°C for 30 min, followed by 20 cycles at 37°C (2 min) for digestion and 16°C (5 min) for ligation. After a final restriction step at 50°C for 10 min, the enzymes were heat-inactivated at 65°C for 5 min, and 10 μL of this MoClo reaction mix was introduced into competent *E. coli* NEB 10-beta cells as described below.

Preparation and Transformation of Chemically Competent *E. coli*

We inoculated 300 mL LB medium with 300 μL of an overnight culture of *E. coli* NEB 10-beta or *E. coli* BL21(DE3) cells grown at 37°C to $OD_{600} = 0.9$. The culture was transferred to sterile 50-mL centrifugation tubes and chilled on ice for 15 min. After centrifugation (5,000 × *g*, 10 min, 4°C), each pellet was resuspended in 12.5 mL 100 mM $CaCl_2$. The cells from three tubes were pooled and stored on ice for 30 min before centrifugation as above. Each pellet was resuspended in 5 mL ice-cold 100 mM $CaCl_2$ supplemented with 15% (v/v) glycerol. Aliquots of 250 μL competent cells were transferred to cryogenic vials, frozen on dry ice and stored at −80°C.

For transformation, 80 μL of the competent cell suspension was mixed with 10 μL MoClo reaction mix and incubated on ice for 15 min before a 42°C heat shock for 1 min, followed by incubation on ice for 1 min. The cells were then mixed with 1 mL LB and incubated in a ThermoMixer (Eppendorf, Hamburg, Germany) at 37°C shaking at 1,000 rpm for 1 h. The cells were plated on LB agar supplemented with the corresponding antibiotic, and incubated at 37°C overnight.

Transformation of Chemically Competent *V. natriegens*

A vial containing 50 μL of chemically competent *V. natriegens* V_{max} Express cells was thawed on ice and mixed with 200–400 ng plasmid library DNA. The cells were incubated for 30 min on ice before a 42°C heat shock for 1 min, followed by incubation on ice for 2 min. The cells were then mixed with 1 mL pre-warmed LB supplemented with V2 salts. The cells were allowed to recover in a ThermoMixer at 30°C shaking at 1,000 rpm for 2 h before streaking them on pre-warmed selection plates and incubating at 30°C overnight.

Fluorescence Microscopy

Microscope slides with cavities were filled with boiling 1% (v/v) agarose in TAE buffer and covered with a cover glass. When the agarose had cooled, the cover glass was removed and 2 μL of culture medium was added, before applying a new cover glass. Fluorescence microscopy was carried out using a Leica DMI6000 instrument (Leica Microsystems, Wetzlar, Germany) fitted with an HCX PL FLUOTAR phase contrast objective (100 x, numerical aperture 1.3), L5 filter cube (excitation filter BP 480/40 nm, dichromatic mirror 505 nm, suppression filter BP 527/30 nm), and PhotoFluor II light source (Chroma, Bellows Falls, Vermont, USA) at 470 nm. Images were captured with a DFC360FX camera (Leica Microsystems). Brightness and contrast adjustments and image cropping were carried out using Fiji software (Schindelin et al., 2012).

Fluorescence-Activated Cell Sorting

FACS was carried out using a BD FACSCalibur device (BD Bioscience, San Jose, California, USA), including standard laser and filter equipment. Phosphate buffered saline (PBS) was used as the sheath fluid (Thermo Fisher Scientific, Waltham, Massachusetts, USA). *E. coli* and *V. natriegens* cells grown as described above were sorted by FACS 4 h post-induction. For sample preparation, a small quantity of culture was suspended in PBS in a 5-mL test tube (VWR, Radnor, Pennsylvania, USA). The cell density was adjusted with PBS to achieve 2,000 ± 200 events per s. Forward-scatter (FSC) and side scatter (SSC) characteristics were applied to distinguish cells from background noise. The threshold was set on FSC to reduce background noise. Events of interest were gated, excited at 488 nm and analyzed for their fluorescence intensity using the 530/30 nm band-pass filter (FL1-H). A gate was applied to the top 5–10% of events with the highest fluorescence intensity, resulting in the sorting of 50,000 cells in exclusion mode. Subsequently, the cell suspension was concentrated from ∼150 to 1 mL using a 0.2-μm nylon filter membrane (Merck), transferred to a flask with fresh medium and incubated overnight. The following day, serial dilutions of the culture were streaked on LB agar plates. Additionally, shaking flasks with fresh medium were inoculated from the overnight cultures at an OD_{600} of 0.1, grown until the OD_{600} reached 1.0 and induced with a final concentration of 1 mM IPTG. Four hours post-induction, the fluorescence intensity of the cells was analyzed using the same settings described above.

Selection of High Producers

Each well of a 96-deep-well plate (VWR) was filled with 500 μL TB. Single clones picked from the agar plate previously streaked with sorted cells were used to inoculate the wells, and the cultures were grown overnight at 30°C shaking at 400 rpm. The following day, a new 96-deep-well plate was filled with 460 μL TB and inoculated with 20 μL of the overnight cultures. After cultivation for 3 h as above, recombinant protein expression was induced by adding 20 μL of IPTG to each well (final concentration 1 mM). Four hours post-induction, the plates were centrifuged (5,000 × *g*, 10 min, 4°C) and the pellets were resuspended in 25 μL BugBuster Master Mix (Merck) and incubated at room temperature for 20 min. Insoluble fractions were pelleted by centrifugation (5,000 × *g*, 20 min, 4°C) and the supernatants containing the soluble fractions were diluted in PBS. For the 12 clones showing the highest fluorescence in the soluble protein fraction, the production procedure was repeated in 50 mL TB in 500-mL shake flasks. Plasmids from these cultures were isolated using the NucleoSpin Plasmid EasyPure kit (Macherey-Nagel, Düren, Germany) according to the manufacturer's instructions before sequencing (Microsynth Sequlab, Göttingen, Germany).

TABLE 1 | Organisms and expression construct combinations found in the selected clones.

POI	Organism	RBS	Secretion signal	Fusion tag	Predicted T.I.R.	Frequency
IMPI	***E. coli***	**RBS3**	**ssDmsA**	**SUMO**	**84.672**	**13/18**
	E. coli	RBS5	ssDmsA	MBP	630.167	4/18
	E. coli	RBS5	ssYahJ	GST	105.563	1/18
	V. natriegens	RBS2	ssYahJ	MBP	58.806	21/21
Lucimycin	***V. natriegens***	**RBS2**	**ssYahJ**	**His-Trx**	**58.806**	**13/21**
	V. natriegens	RBS2	ssDmsA	MBP	156.860	8/21
Uricase	***V. natriegens***	**RBS5**	**ssYahJ**	**His-Trx**	**105.563**	**10/10**
	E. coli	RBS2	ssYahJ	Trx	58.806	6/11
	E. coli	RBS4	ssTorA	GST	92.231	4/11
	E. coli	RBS3	ssYahJ	His-MBP	250.485	1/11

The frequency indicates the number of clones carrying a specific combination. High producers highlighted in bold were identified as most productive clones and used for the production of the model proteins. The ribosome binding sites and secretion signal sequences are provided in the ***Supplementary Material****.*

Osmotic Shock Procedure

Pellets from 2-mL cultures (see section Strains and growth conditions) were resuspended in 1 mL osmotic shock buffer 1 (20 mM Tris-HCl, 0.25 mM EDTA, 200 g/L sucrose, pH 8.0) and incubated on ice for 10 min. After centrifugation (16,000 × *g*, 10 min, 4°C) the pellet was resuspended in 1 mL osmotic shock buffer 2 (20 mM Tris-HCl, 0.25 mM EDTA, pH 8.0) and incubated as above. After further centrifugation as above, the supernatant containing the periplasmic protein fraction was transferred to a fresh reaction tube and stored at 4°C. The remaining pellet was resuspended in 100 μL BugBuster Master Mix and incubated at room temperature for 20 min. The soluble and insoluble fractions were then separated by centrifugation (16,000 × *g*, 20 min, 4°C) and 90 μL of the supernatant containing the cytoplasmic protein fraction was transferred into a fresh tube, mixed with 810 μL PBS and stored at 4°C. The remaining supernatant was discarded, and the pellet containing the insoluble and membrane protein fraction was resuspended in 1 mL PBS.

Protein Analysis

The fluorescence intensity of each 10-μL sample of soluble protein from the periplasmic/cytoplasmic fraction was determined by mixing with 90 μL PBS, transferring to the wells of a 96-well microtiter plate and measuring the fluorescence using a Synergy HT plate reader (BioTek Instruments, Winooski, Vermont, USA) against GFP standards (Abnova, Taipei City, Taiwan), which were used to generate a standard curve. For SDS-PAGE and western blot analysis, 5–10 μL of each sample (soluble or insoluble protein in PBS) was mixed with 3.75 μL of Laemmli buffer supplemented with β-mercaptoethanol and brought to a total volume of 15 μL with double-distilled water. The sample was denatured by incubation at 95°C for 5 min and 10 μL was loaded on a 4–20% Citereon TGX Stain-Free Precast Gel (Bio-Rad, Hercules, California, USA). After running for 25 min at 250 V, gel images were captured using the ChemiDoc Imaging System (Bio-Rad). Western blots were performed using the Trans-Blot Turbo Transfer Pack and Transfer System (Bio-Rad) according to the manufacturer's instructions. Membranes were blocked with 5% bovine serum albumin (BSA) for 1 h and washed three times (5 min each) with 0.1% Tween-20 in PBS before incubation at room temperature for 2 h with the primary rat-anti-GFP 3H9 antibody

(ChromoTek, Planegg-Martinsried, Germany) diluted 1:5,000 in PBS containing 0.05% Tween-20. After washing as above, the membranes were incubated at room temperature for 2 h with the horseradish peroxidase (HRP)-conjugated secondary goat anti-rat IgG antibody (Jackson ImmunoResearch Europe, Ely, UK) and Precision Protein StrepTactin-HRP Conjugate (Bio-Rad), each diluted 1:10,000. HRP-mediated luminescence was visualized using Clarity Western ECL Substrate (Bio-Rad) according to the manufacturer's protocol. Uricase activity was determined in the soluble fractions using the Amplex Red Uricase Assay Kit (Thermo Fisher Scientific) according to the manufacturer's instructions.

RESULTS AND DISCUSSION

Expression Library Cloning Strategy

The combinatorial expression libraries were assembled in two consecutive cloning steps, starting from basic parts (the ribosomal binding sites, secretion tag sequences, and target protein sequences). Each of the basic parts was flanked by BsaI sites and housed in the cloning vector pUC57-Kan. Because the 4-bp BsaI overhang ends would result in frame shifts, two additional bases were introduced between the 5′ overhang and the coding sequences. For each of the five secretion tags, a synthetic ribosomal binding site was designed using the RBS Calculator (Salis et al., 2009; Espah Borujeni et al., 2014). Based on the promoter sequence and the coding sequence of the secretion tag, the ribosomal binding site was generated with the restriction of base numbers applying only to $(N)_{25}$CAGG or $(N)_{30}$CAGG sequences, where CAGG represents the BsaI overhang. The sites with the highest predicted translation initiation rates (TIRs) were chosen for the library (**Table S1**). Given that translational initiation depends not only on the ribosomal binding site but also on the subsequent coding sequence, the five ribosomal binding sites would lead to five different expression levels for each secretion tag. The TIR was predicted using a reverse calculation for each ribosomal binding site + secretion tag combination (**Table 1**).

The first cloning step was the assembly of basic parts in Level 1 MoClo vectors (**Figure 1A**). We used the MoClo vectors from the Waldminhaus laboratory, which carry the *ccdB* gene in addition to *lacZα* (Schindler et al., 2016). The *ccdB* gene

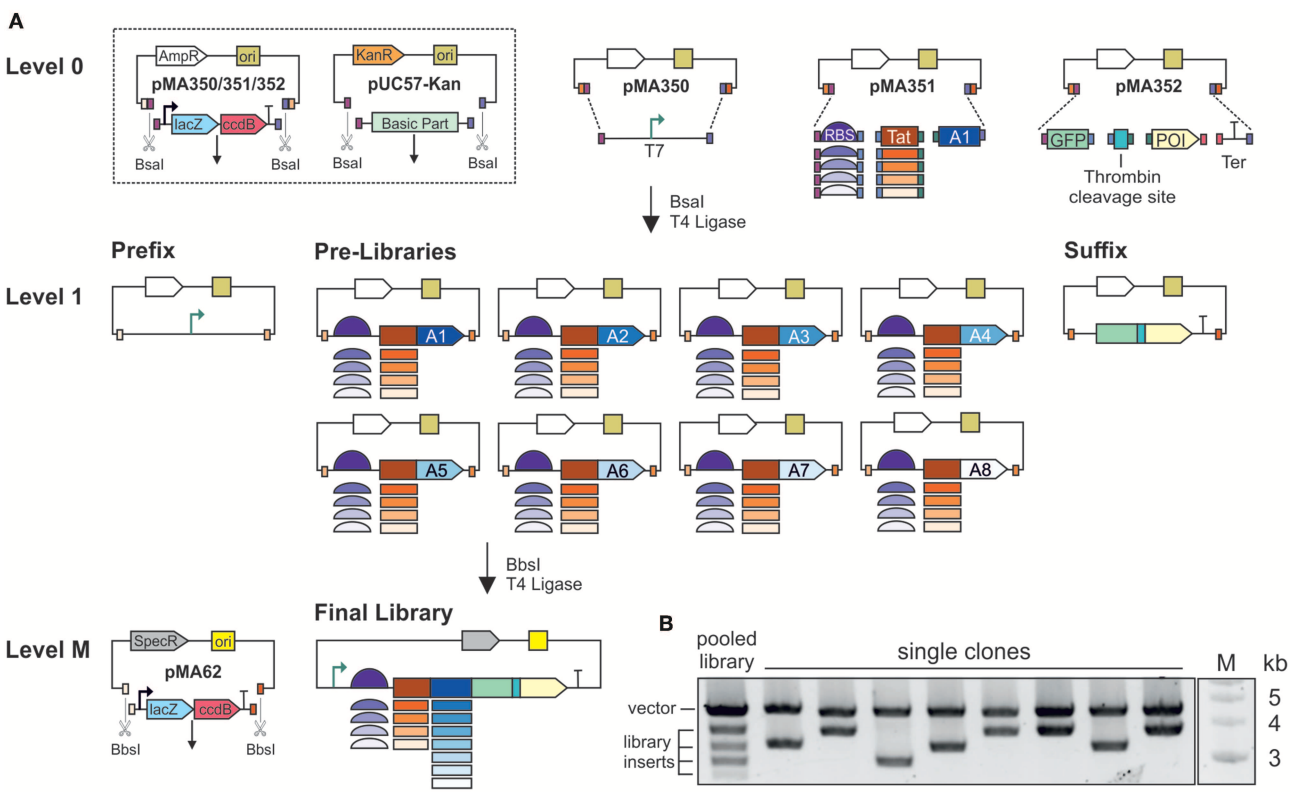

FIGURE 1 | Assembly of combinatorial expression libraries. **(A)** Schematic illustration of the MoClo assembly. Basic parts are housed in pUC57-Kan, flanked by BsaI-sites. The T7 promoter is housed in pMA350. The thrombin cleavage site, green fluorescent protein (GFP), one of the proteins of interest (POI), and the terminator (Ter) are assembled in pMA352. The five ribosome binding sites (RBS) and five secretion signals are pooled, and assembled with one of the eight affinity tags (A1–A8) as Pre-libraries in pMA351. The eight affinity tags are: A1, SUMO; A2, His_6-SUMO; A3, MBP; A4, His_6-MBP; A5, GST; A6, His_6-GST; A7, Trx; A8, His_6-Trx. In Level 1, plasmids and inserts are flanked by BbsI sites. For final library assembly, the Pre-libraries are pooled and assembled with the Prefix and Suffix. **(B)** BsaI digestion of plasmids from a pooled library, and plasmids from single clones. The upper band represents the vector backbone, and the lower bands represent the assembled expression cassettes. Inserts vary in size due to the differing sizes of the affinity tags.

encodes an inhibitor of DNA gyrase and thus kills *E. coli* cells taking up undigested or re-ligated plasmids (Bernard, 1996). This eliminates the background of undigested plasmids and increases the percentage of positive clones. Basic parts were assembled in three Level 1 vectors by Golden Gate cloning using BsaI and T4 ligase (Engler et al., 2009). The IPTG-inducible T7 promoter part, including the *lacI* repressor gene, was cloned in the first vector, pMA350, and is hereafter called *Prefix*. Pre-libraries were assembled in the second vector, pMA351. In this step, the coding sequence for one of the eight affinity tags was mixed with the five ribosomal binding sites and five secretion tags, resulting in 25 combinations. Eight Pre-libraries were prepared, one each for the eight affinity tags in the final library design. In the third vector, pMA352, we assembled the coding sequences for GFP, the thrombin cleavage site, and the protein of interest, as well as a transcriptional terminator. This building block is hereafter called *Suffix* and three versions were assembled, one for each target protein. Individual Prefix and Suffix clones were picked and verified by Sanger sequencing. Furthermore, all clones in each Pre-library (n = 110–900) were pooled and analyzed by Sanger sequencing, identifying the overlapping signals of the variable library elements.

The final libraries were assembled in vector pMA62, carrying a spectinomycin resistance gene and the IncP replication system (Werner et al., 2012; Schindler et al., 2016). Preliminary experiments revealed that this vector achieves efficient transformation and protein expression in *V. natriegens*. Equimolar amounts of all Pre-libraries were mixed in one tube with the Prefix, one of the three Suffix clones and the end-linker pMA671 for Golden Gate assembly using BbsI and T4 ligase. End-linkers with suitable overhangs serve as adapters whenever fewer than seven inserts are assembled in a MoClo reaction. Final libraries for each target protein were generated individually, and theoretically contained 200 combinations of ribosomal binding sites, secretion signals and affinity tags. For each library, 2,000–4,000 clones were pooled. Given a cloning efficiency of 80–100% at each step, there was a >99% probability that the final libraries covered all possible combinations. BsaI restriction analysis of the pooled libraries resulted in a pattern of five bands (**Figure 1B**). Given that all the ribosomal binding sites and secretion tags were similar in size, whereas the affinity tag sequences ranged from ∼300 to 1,100 bp, each of the four lower bands represent the combinations with one of the affinity tags. The upper band represents the vector backbone. BsaI test digestions of plasmids from individual clones revealed the upper band but only one the four possible lower bands.

The two-stage MoClo assembly (**Figure 1A**) was preferred to standard Golden Gate assembly, where all basic parts are assembled in a single reaction, because as the number of parts increases the efficiency of Golden Gate assembly declines and

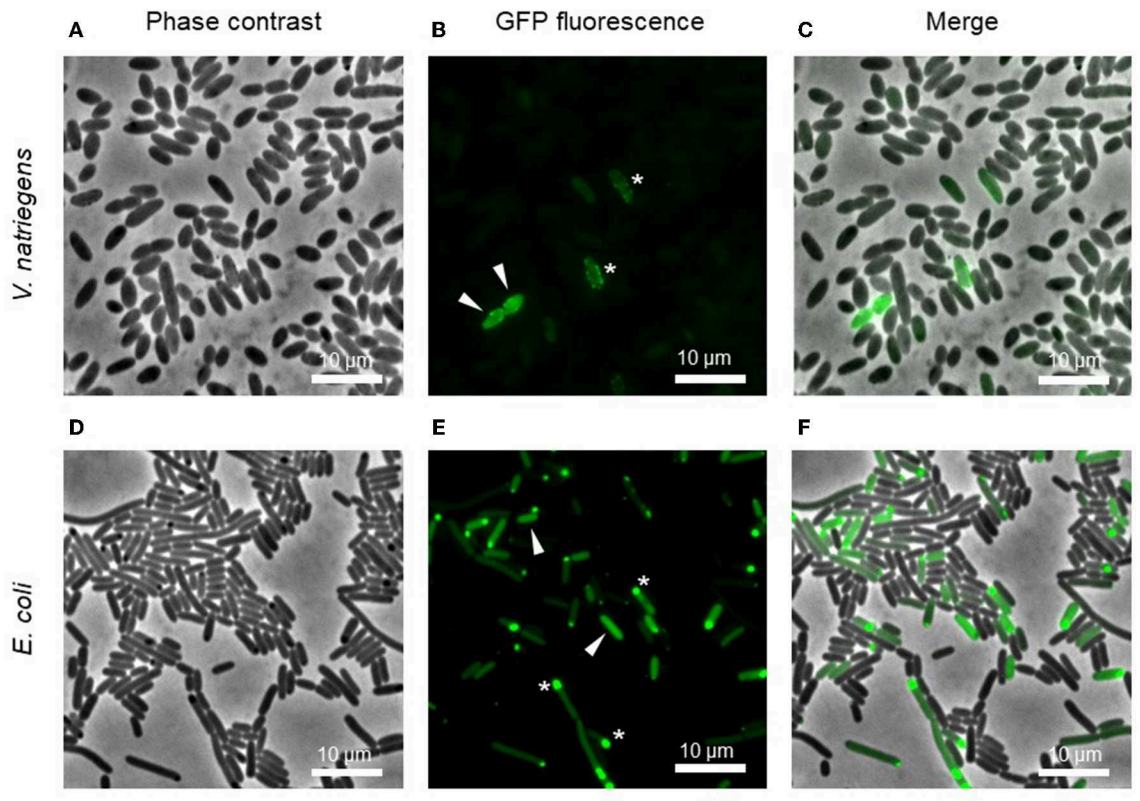

FIGURE 2 | Microscopic images of pooled cultures carrying a combinatorial expression library. Arrows indicate cells with homogeneous GFP, indicating a soluble product. Stars show GFP foci, indicating insoluble inclusion bodies. Images represent the expression of the library for IMPI production in *V. natriegens* **(A–C)** and *E. coli* **(D–F)** 4 h post-induction.

more errors are introduced (Potapov et al., 2018). When building the libraries, none of the assembly steps involved more than four parts, and accordingly we generated large numbers of colonies at low error rates. During Level 1 and Level M cloning, sequencing revealed 87, 5% of randomly picked clones to be positive (42/48). Furthermore, when multiple parts differing in size are used to generate combinatorial libraries, there is a bias toward smaller parts. By assembling the Prefix, Pre-libraries and Suffix clones, the size differences among the basic parts were minimized. In the final libraries, we found no indication that inserts from smaller Pre-libraries were overrepresented in a manner that would lead to biased screening. Furthermore, the preparation of separate Prefix, Pre-libraries and Suffix clones makes the selection of false positives during FACS less likely. In Golden Gate cloning, single parts might not be assembled, resulting in an incomplete construct, but only whole parts would be lost. During final assembly, a small but significant number of incomplete constructs will be generated. However, the incomplete construct would either lack the promoter (missing Prefix), the ribosomal binding site and start codon (missing Pre-library) or the GFP (missing Suffix). Due to the design of the library assembly method, none of these incomplete constructs would produce a strong GFP signal. Thus, clones carrying misassembled plasmids would be excluded by FACS. For future screening with other products, only the Suffix needs to be cloned. All remaining parts can be reused. The assembly of multiple Pre-libraries means that some variants can be left out if not required and others can be added. Altogether, the design and assembly of the libraries provides a high level of modularity and flexibility.

The Selection of High Producers

The final libraries for each target protein were introduced into the *E. coli* BL21(DE3) and *V. natriegens* V_{max} Express production strains, and the libraries in each case were separately pooled and stored as glycerol stocks. At the beginning of the selection pipeline, shaker flasks containing growth medium were inoculated from glycerol stocks to an OD_{600} of ∼0.1. Recombinant protein expression was induced by adding IPTG when the culture reached an OD_{600} of ∼1.0.

Fluorescence microscopy revealed the diversity of protein expression levels in the libraries (**Figure 2**). We assigned the cells to three groups. The first and largest of the groups comprised cells showing no fluorescence, indicating that the fusion protein was not expressed (or expressed at levels below the detection threshold) or was expressed but inactive, perhaps due to incomplete folding. The second group comprised cells showing homogeneous fluorescence (white arrows in **Figures 2B,E**), indicating the expression of a soluble recombinant protein. The intensity of fluorescence varied widely in this group, including cells with very strong signals representing high producers.

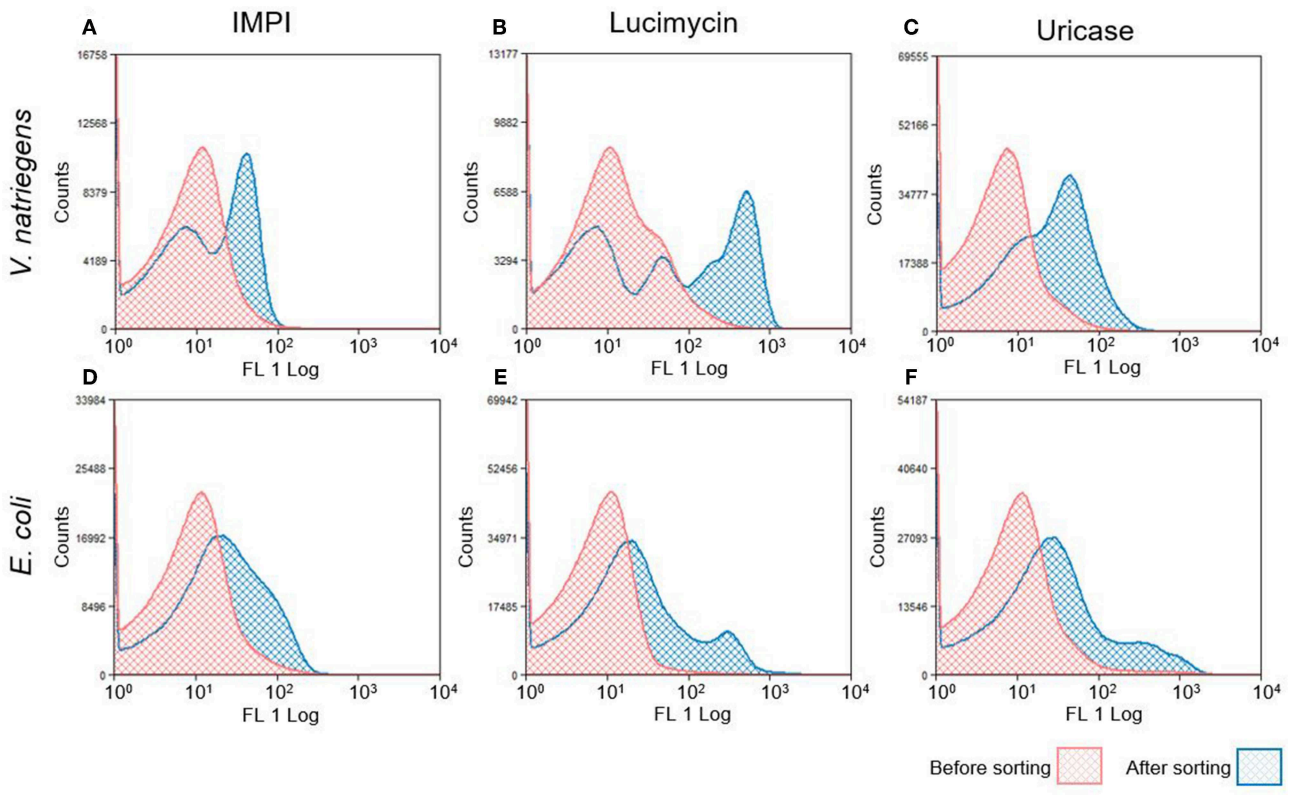

FIGURE 3 | Histograms of fluorescence distribution in *V. natriegens* **(A–C)** and *E. coli* **(D–F)** cultures expressing the combinatorial libraries. Histograms in red represent GFP distribution before FACS selection. Sorted cells were grown and protein expression was induced again, as shown in blue. The shifted peak areas with regard to increased fluorescence intensity indicate a successful enrichment of induced GFP-producing cells.

The final category comprised cells with punctate fluorescence (white stars in **Figures 2B,E**), indicating the presence of inclusion bodies.

For FACS-based selection, the cells were resuspended in PBS 4 h post-induction. Two gates were applied, the first to separate cells from background events and the second (applied to the fluorescence channel) to separate the 5–10% of cells with the highest fluorescence intensity. We sorted 50,000 cells in each of the three libraries. At a sorting rate of 30–100 events per s, these high-producer cells were separated into a large volume of PBS (100–150 mL). We therefore concentrated the suspension to 1 mL by removing the buffer using a sterile filter and a vacuum pump, and transferred the cells to a new flask for overnight incubation.

The following day, the growth and induction procedures were repeated with a culture inoculated to an OD_{600} of 0.1 from the sorted overnight culture. **Figure 3** shows the fluorescence intensity of cells before and after sorting. Most of the pre-sorting cells showed little or no fluorescence, although the *V. natriegens* population expressing lucimycin was a notable exception. After one round of cultivation and sorting, the fluorescence intensity of the *V. natriegens* cells had increased by approximately one order of magnitude for most of the cells producing IMPI and uricase, and by approximately two orders of magnitude for the cells producing lucimycin. The fluorescence of the pooled *E. coli* cultures also increased after sorting, although not to the extent observed with *V. natriegens*. In most cases, the fluorescence intensity remained similar to that in the original culture, although small subpopulations showed strong increases in fluorescence (**Figure 3B**). After two to four rounds of growth and sorting, the cells carried plasmids representing a single combination of elements from the original library. Production with this plasmid resulted in large amounts of insoluble recombinant protein (data not shown). To exploit the diversity of high producers, we therefore decided to analyze the 5–10% of cells with the highest fluorescence intensity after only one round of screening, at the cost of a higher background of less productive clones.

The workflow for the selection of high producers from libraries is shown in **Figure 4**. The day after sorting, dilutions of cells were plated on agar. Single clones were cultivated in 96-deep-well plates and protein production was induced by adding IPTG. Four hours after induction, cells were pelleted by centrifugation, and the supernatant was discarded. After lysis, the fluorescence intensity of the soluble protein fraction was measured. The top clones based on these readings were grown in shaker flasks and induced by adding IPTG. The soluble and insoluble protein fractions were analyzed by SDS-PAGE and western blot (**Figures 5–7**). Plasmids isolated from the top candidates were dispatched for sequencing to identify the basic elements.

Production of Model Peptides and Proteins

The combinations of elements resulting in the highest yield for each of the three target proteins are summarized in **Table 1**. The highest yields of IMPI were achieved in *E. coli* using the

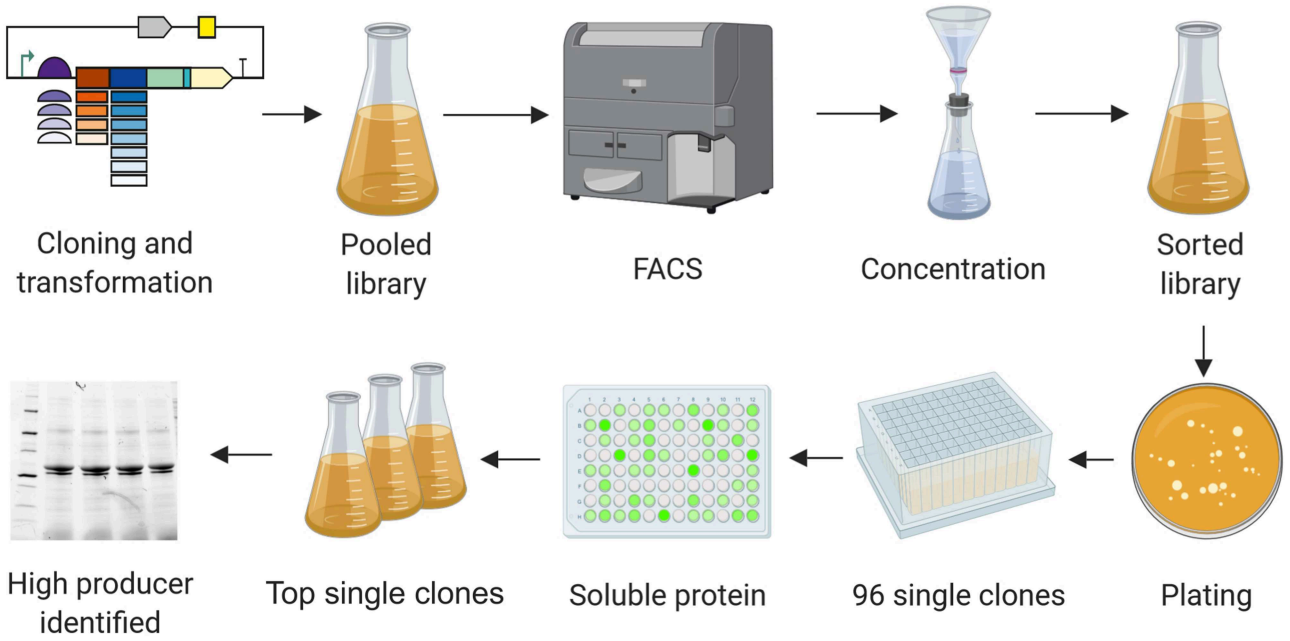

FIGURE 4 | High producer selection pipeline. Combinatorial libraries were cloned and introduced into the production strains. Cultures carrying the pooled libraries were grown and expression was induced. Cells showing the highest GFP levels were selected by FACS, resulting in a cell suspension in PBS. The cell suspension was concentrated by filtration, transferred into a flask with fresh medium and grown overnight. The resulting culture was plated on agar before transferring 96 single colonies to a 96-deep-well plate. Expression was induced for 4 h. Cells were pelleted, the soluble protein fractions were extracted, and the GFP signal was quantified. The clones showing the most intense fluorescence were cultivated in flasks and subsequently analyzed by SDS-PAGE, western blot, and Sanger sequencing. Image created with BioRender.

SUMO tag. The combination ssDmsA-MBP was present in many clones at the end of the selection pipeline but this resulted in lower yields than the SUMO fusion. Interestingly, the best combination for both lucimycin and uricase was ssYahJ-His_6-Trx in *V. natriegens*. For uricase, all clones reaching the final selection step contained this combination. For lucimycin, the combination ssDmsA-MBP was again present in many clones at the end of the selection pipeline but it achieved lower yields than ssYahJ-His_6-Trx. Only insoluble product was observed for the production of IMPI in *V. natriegens* and uricase in *E. coli*. The high-producer expression systems highlighted in **Table 1** were therefore used for the production of the three model proteins.

Production of IMPI

IMPI was produced in *E. coli* as a fusion to the SUMO tag and the product was exported to the periplasm mediated by the ssDmsA secretion signal. The soluble protein fractions from the periplasm and cytoplasm were separated by osmotic shock (**Figure 5A**). Most of the protein was located in the cytoplasm 2 and 4 h post-induction (**Figure 5B**). The protein yield in the cytoplasm did not increase further from 4 to 6 h post-induction. In contrast, the amount of protein in the periplasm doubled in this time. Six hours post-induction, about half of the soluble recombinant protein was located in the periplasm. At all times, a substantial quantity of insoluble product was detected (**Figure 5A**). IMPI contains five disulfide bonds, so translocation is likely to be accomplished by the Sec pathway, whereas the IMPI located in the cytoplasm is probably in an unfolded or incompletely folded state. Large amounts of insoluble protein result in the formation of inclusion bodies, as shown in **Figure 2**. The relatively low yield of 5–6 mg/L total soluble product must be regarded in the context of cell growth. Six hours post-induction, the cultures had reached an OD_{600} of only 7.5–8.0 but were still in the exponential growth phase. Given the large quantity of insoluble product, the yield of this expression system could be increased substantially by optimizing the cultivation and production process.

Production of Lucimycin

The antifungal peptide lucimycin was produced in *V. natriegens* with a thioredoxin tag to improve solubility and a His_6 tag for purification by IMAC. The combination of the ssYahJ secretion signal and the selected ribosome binding site resulted in a low TIR compared to other combinations, but nevertheless achieved the highest yields (**Figure 6A**). Six hours post-induction the concentration of the soluble product was ∼20 mg/L in total, about two thirds of which was found in the periplasmic fraction following the osmotic shock (**Figure 6B**). In the periplasmic fraction, a second band is visible slightly below the expected band

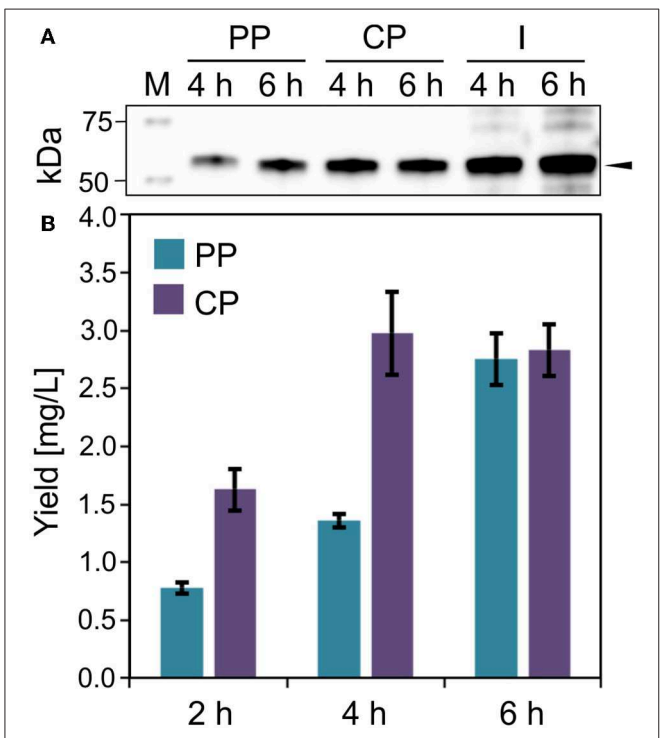

FIGURE 5 | IMPI production in *E. coli*. **(A)** Western blot (anti-GFP antibody) of soluble ssDmsA-SUMO-GFP-IMPI in the periplasmic (PP), cytoplasmic (CP), and insoluble and membrane (I) fraction 4 and 6 h post-induction. The black arrow indicates the expected band at 52.8 kDa. **(B)** Fusion protein quantification in the periplasmic and cytoplasmic fractions 2, 4, and 6 h post-induction. Error bars indicate the standard deviation.

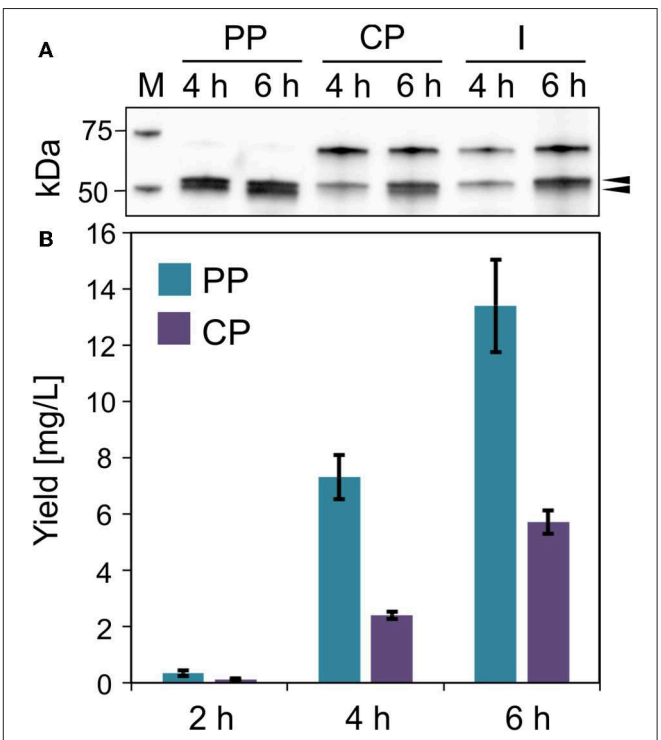

FIGURE 6 | Lucimycin production in *V. natriegens*. **(A)** Western blot (anti-GFP antibody) of soluble ssYahJ-His-Trx-GFP-lucimycin in the periplasmic (PP), cytoplasmic (CP), and insoluble and membrane (I) fraction 4 and 6 h post-induction. The upper black arrow indicates the expected band at 53.2 kDa, the lower arrow indicates the putative mature protein after the cleavage of the secretion signal. **(B)** Fusion protein quantification in the periplasmic and cytoplasmic fractions 2, 4, and 6 h post-induction. Error bars indicate the standard deviation.

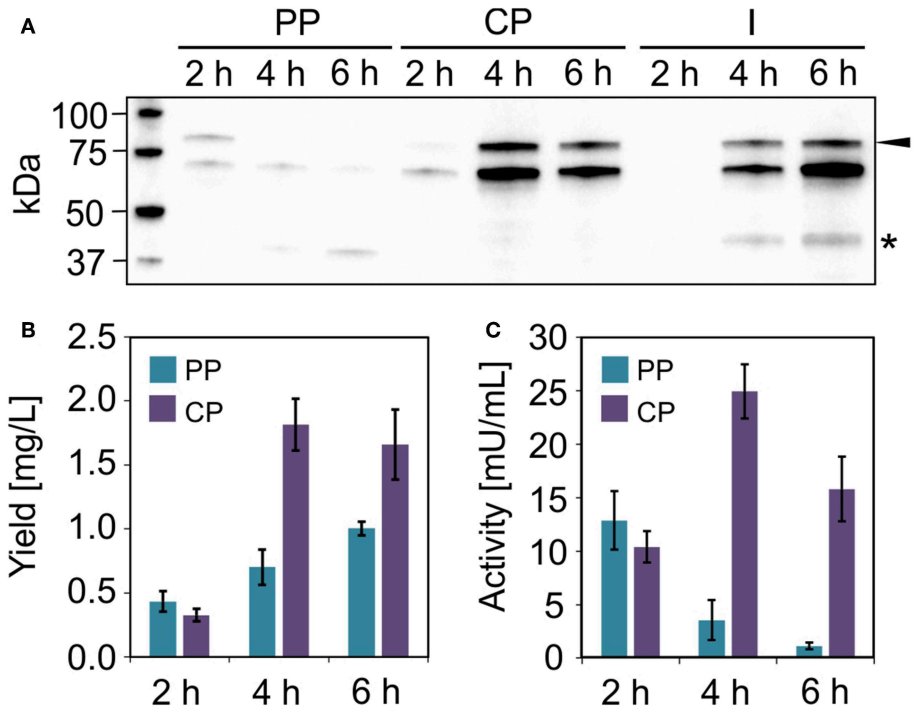

FIGURE 7 | Uricase production in *V. natriegens*. **(A)** Western blot (anti-GFP antibody) of soluble ssYahJ-His-Trx-GFP-uricase in the periplasmic (PP), cytoplasmic (CP), and insoluble and membrane (I) fraction 2, 4, and 6 h post-induction. The black arrow indicates the expected band at 83.6 kDa. The star indicates a putative product resulting from incomplete translation. **(B)** Fusion protein quantification in the periplasmic and cytoplasmic fractions 2, 4, and 6 h post-induction. Error bars indicate the standard deviation. **(C)** Uricase activity in the periplasmic and cytoplasmic fractions 2, 4, and 6 h post-induction. Error bars indicate the standard deviation.

at 53.2 kDa in the western blot (**Figure 6A**). The Sec and Tat translocation machineries cleave N-terminal secretion signals at the C-terminal Ala-x-Ala motif (Freudl, 2018). The removal of the secretion signal could explain the presence of the lower band. The product yield increased continually during production, and the quantity of insoluble was moderate. As for the production of IMPI in *E. coli*, the optimization of the production process could significantly increase the yields of lucimycin.

Production of Uricase

We were unable to identify any *E. coli* clones that achieved the production of substantial quantities of the model enzyme uricase as a soluble protein. However, moderate yields were observed when the enzyme was expressed in *V. natriegens* using the same ssYahJ-His_6-Trx combination that achieved the highest yields of lucimycin, albeit with a different ribosome binding site and thus a higher TIR. Even so, the production and localization of the enzyme differed from lucimycin (**Figure 7**). The uricase fusion protein accumulated mostly in the cytoplasmic fraction, but only 2 h post-induction substantial uricase activity was also detected in the periplasmic fraction (**Figure 7C**). The highest yield and activity were detected 4 h post-induction, and the amount of insoluble product increased over time (**Figures 7A,B**). Two unexpected bands were observed in the western blot after 4 and 6 h. The dominant band slightly below the 75 kDa marker is likely to reflect non-specific antibody binding. Similar patterns were detected in all *V. natriegens* samples (see **Figure 6A**). The lower band between the 37 and 50 kDa markers may reflect the incomplete translation of the fusion protein, resulting in a truncated product, including GFP and N-terminal fusion tags, but missing the majority of the uricase. This would explain the increasing yield of uricase in the periplasmic fraction over time even though the activity in this fraction decreases. Translation is often interrupted by the presence of rare codons. The sequences were originally codon optimized for *E. coli*, and further analysis revealed some codons that are rarely used in *V. natriegens*. The codon CCC for proline is one example (Lee et al., 2016), and it is found at the beginning of the uricase fusion protein sequence. Replacing rare codons to match *V. natriegens* codon preferences would therefore be a starting point for the improvement of uricase production.

CONCLUSIONS

One of the major challenges during expression screening is the formation of insoluble inclusion bodies. These often contain large quantities of active protein, leading to strong GFP signals that cannot be distinguished from the homogeneous fluorescence of soluble proteins during FACS. This issue could be addressed by including a biosensor for inclusion body formation. The transcriptomic response to inclusion body formation has been investigated, and

offers multiple starting points (Baig et al., 2014). The expression of a second fluorescent marker in the presence of inclusion bodies would allow such cells to be excluded, resulting in the specific gating of cells expressing soluble recombinant proteins.

We confirmed that *V. natriegens* is a suitable host for recombinant protein production, especially in the case of uricase. Although, uricases from other species have been produced successfully in *E. coli* (Nakagawa et al., 1995; Shaaban et al., 2015), this is not the case for *L. sericata* uricase and we were similarly unable to identify any *E. coli* clones that produced this enzyme in significant amounts. In contrast, *V. natriegens* produced large amounts of the enzyme in a soluble form.

We found that many of the functional elements in *E. coli* expression constructs could also be used in *V. natriegens*, including the ssYahJ secretion signal. Most of the lucimycin product was detected in the *V. natriegens* periplasmic fraction, and the presence of an additional smaller product indicated the cleavage of the secretion signal (**Figure 6A**). In *E. coli*, proteins fused to thioredoxin can be released from the cytoplasm by osmotic shock (Ajouz et al., 1998), but it is unclear whether this also occurs in *V. natriegens*. We expected to detect most of the Trx-uricase fusion protein in the periplasm (**Figure 7**) so it is unclear why the same fusion protein combination leads to the periplasmic localization of lucimycin. The abundance of insoluble uricase indicates incomplete or incorrect folding of the large fusion protein. Given that only folded proteins are translocated by the Tat pathway, an incompletely folded protein would be expected to remain in the cytoplasm. Together with the finding that ssYahJ was the major secretion tag selected in *V. natriegens* and other high producers (data not shown), we propose that ssYahJ is recognized as a secretion signal in *V. natriegens*. To validate these results, the ssYahJ tag needs to be systematically investigated in *V. natriegens* in the absence of thioredoxin.

Taken together, the screening resulted in the identification of high producers for three difficult-to-express products in *E. coli* and *V. natriegens*. These will serve as a starting point to improve yields by optimizing the production process, including medium development and scaled-up fermentation in bioreactors. We found that the MoClo system allowed the efficient construction of combinatorial libraries containing both regulatory and coding elements. The high modularity of this screening platform will facilitate the identification of additional elements and proteins of interest, and can serve as a blueprint for novel combinatorial library screening methods in microbial and eukaryotic expression systems.

DATA AVAILABILITY STATEMENT

All datasets generated for this study are included in the manuscript/**Supplementary Files**.

AUTHOR CONTRIBUTIONS

JE conceived, designed and performed all experiments, wrote the manuscript, and coordinated its preparation. MO established the FACS and cell concentration methods, and helped during all sorting experiments. DG and TW helped to draft and revise the manuscript. PC helped to draft and revise the manuscript, and supervised the research. All authors have given their approval for this final version of the manuscript.

FUNDING

This work was financially supported by the Hessian Ministry of Education and Art within the Hessen initiative for supporting economic and scientific excellence (LOEWE). Part of the work was funded by the German Ministry of Education and Research (BMBF) via the project 4-IN.

ACKNOWLEDGMENTS

We wish to thank Torsten Waldminghaus (Synmikro, Marburg, Germany) for providing the MoClo vectors, Jens Glaeser (Evotec International GmbH, Göttingen, Germany) for providing the FACS equipment, and technical and scientific advice, Sebastian Hausner and Jan Zitzmann for helping with cloning and data analysis, respectively, and Florian Scholz for excellent technical advice. We are grateful to Howard Salis (Pennsylvania State University, PA, USA) for help with the RBS Calculator. The authors thank Richard M. Twyman for manuscript editing.

SUPPLEMENTARY MATERIAL

The Supplementary Material for this article can be found online at: https://www.frontiersin.org/articles/10.3389/fbioe.2019.00254/full#supplementary-material

REFERENCES

Abdulrahman, W., Uhring, M., Kolb-Cheynel, I., Garnier, J.-M., Moras, D., Rochel, N., et al. (2009). A set of baculovirus transfer vectors for screening of affinity tags and parallel expression strategies. *Anal. Biochem.* 385, 383–385. doi: 10.1016/j.ab.2008.10.044

Ajouz, B., Berrier, C., Garrigues, A., Besnard, M., and Ghazi, A. (1998). Release of thioredoxin via the mechanosensitive channel MscL during osmotic downshock of *Escherichia coli* cells. *J. Biol. Chem.* 273, 26670–26674. doi: 10.1074/jbc.273.41.26670

Baig, F., Fernando, L. P., Salazar, M. A., Powell, R. R., Bruce, T. F., and Harcum, S. W. (2014). Dynamic transcriptional response of *Escherichia coli* to inclusion body formation. *Biotechnol. Bioeng.* 111, 980–999. doi: 10.1002/bit.25169

Balasundaram, B., Harrison, S., and Bracewell, D. G. (2009). Advances in product release strategies and impact on bioprocess design. *Trends Biotechnol.* 27, 477–485. doi: 10.1016/j.tibtech.2009.04.004

Baumann, A., Skaljac, M., Lehmann, R., Vilcinskas, A., and Franta, Z. (2017). Urate Oxidase produced by *Lucilia sericata* medical maggots is localized in Malpighian tubes and facilitates allantoin production. *Insect Biochem. Mol. Biol.* 83, 44–53. doi: 10.1016/j.ibmb.2017.02.007

Becker, W., Wimberger, F., and Zangger, K. (2019). *Vibrio natriegens*: an alternative expression system for the high-yield production of isotopically labeled proteins. *Biochemistry* 58, 2799–2803. doi: 10.1021/acs.biochem.9b00403

Berks, B. C., Sargent, F., and Palmer, T. (2000). The Tat protein export pathway. *Mol. Microbiol.* 35, 260–274. doi: 10.1046/j.1365-2958.2000.01719.x

Bernard, P. (1996). Positive selection of recombinant DNA by CcdB. *Biotechniques* 21, 320–323. doi: 10.2144/96212pf01

Browning, D. F., Richards, K. L., Peswani, A. R., Roobol, J., Busby, S. J. W., and Robinson, C. (2017). *Escherichia coli* "TatExpress" strains super-secrete human growth hormone into the bacterial periplasm by the Tat pathway. *Biotechnol. Bioeng.* 114, 2828–2836. doi: 10.1002/bit.26434

Butt, T. R., Edavettal, S. C., Hall, J. P., and Mattern, M. R. (2005). SUMO fusion technology for difficult-to-express proteins. *Protein Expr. Purif.* 43, 1–9. doi: 10.1016/j.pep.2005.03.016

Carrió, M. M., and Villaverde, A. (2002). Construction and deconstruction of bacterial inclusion bodies. *J. Biotechnol.* 96, 3–12. doi: 10.1016/S0168-1656(02)00032-9

Choi, J. H., and Lee, S. Y. (2004). Secretory and extracellular production of recombinant proteins using *Escherichia coli*. *Appl. Microbiol. Biotechnol.* 64, 625–635. doi: 10.1007/s00253-004-1559-9

Coussement, P., Maertens, J., Beauprez, J., van Bellegem, W., and de Mey, M. (2014). One step DNA assembly for combinatorial metabolic engineering. *Metab. Eng.* 23, 70–77. doi: 10.1016/j.ymben.2014.02.012

Dreyfus, M. (1988). What constitutes the signal for the initiation of protein synthesis on *Escherichia coli* mRNAs? *J. Mol. Biol.* 204, 79–94. doi: 10.1016/0022-2836(88)90601-8

Engler, C., Gruetzner, R., Kandzia, R., and Marillonnet, S. (2009). Golden gate shuffling: a one-pot DNA shuffling method based on type IIs restriction enzymes. *PLoS ONE* 4:e5553. doi: 10.1371/journal.pone.0005553

Espah Borujeni, A., Channarasappa, A. S., and Salis, H. M. (2014). Translation rate is controlled by coupled trade-offs between site accessibility, selective RNA unfolding and sliding at upstream standby sites. *Nucleic Acids Res.* 42, 2646–2659. doi: 10.1093/nar/gkt1139

Espah Borujeni, A., and Salis, H. M. (2016). Translation initiation is controlled by RNA folding kinetics via a ribosome drafting mechanism. *J. Am. Chem. Soc.* 138, 7016–7023. doi: 10.1021/jacs.6b01453

Fisher, A. C., Kim, J.-Y., Perez-Rodriguez, R., Tullman-Ercek, D., Fish, W. R., Henderson, L. A., et al. (2008). Exploration of twin-arginine translocation for expression and purification of correctly folded proteins in *Escherichia coli*. *Microb. Biotechnol.* 1, 403–415. doi: 10.1111/j.1751-7915.2008.00041.x

Freudl, R. (2018). Signal peptides for recombinant protein secretion in bacterial expression systems. *Microb. Cell Fact.* 17:52. doi: 10.1186/s12934-018-0901-3

Gold, L. (1988). Posttranscriptional regulatory mechanisms in *Escherichia coli*. *Annu. Rev. Biochem.* 57, 199–233. doi: 10.1146/annurev.bi.57.070188.001215

Gray, G. L., Baldridge, J. S., McKeown, K. S., Heyneker, H. L., and Chang, C. N. (1985). Periplasmic production of correctly processed human growth hormone in *Escherichia coli*: natural and bacterial signal sequences are interchangeable. *Gene* 39, 247–254. doi: 10.1016/0378-1119(85)90319-1

Han, Y., Guo, W., Su, B., Guo, Y., Wang, J., Chu, B., et al. (2018). High-level expression of soluble recombinant proteins in *Escherichia coli* using an HE-maltotriose-binding protein fusion tag. *Protein Expr. Purif.* 142, 25–31. doi: 10.1016/j.pep.2017.09.013

Hoffart, E., Grenz, S., Lange, J., Nitschel, R., Müller, F., Schwentner, A., et al. (2017). High substrate uptake rates empower *Vibrio natriegens* as production host for industrial biotechnology. *Appl. Environ. Microbiol.* 83:e01614–17. doi: 10.1128/AEM.01614-17

Hoffmann, D., Ebrahimi, M., Gerlach, D., Salzig, D., and Czermak, P. (2018). Reassessment of inclusion body-based production as a versatile opportunity for difficult-to-express recombinant proteins. *Crit. Rev. Biotechnol.* 38, 729–744. doi: 10.1080/07388551.2017.1398134

Hoffmann, D., Eckhardt, D., Gerlach, D., Vilcinskas, A., and Czermak, P. (2019). Downstream processing of Cry4AaCter-induced inclusion bodies containing insect-derived antimicrobial peptides produced in *Escherichia coli*. *Protein Expr. Purif.* 155, 120–129. doi: 10.1016/j.pep.2018.12.002

Joachim, M., Maguire, N., Schäfer, J., Gerlach, D., and Czermak, P. (2019). Process intensification for an insect antimicrobial peptide elastin-like polypeptide fusion produced in redox-engineered *Escherichia coli*. *Front. Bioeng. Biotechnol.* 7:150. doi: 10.3389/fbioe.2019.00150

Lee, H. H., Ostrov, N., Wong, B. G., Gold, M. A., Khalil, A., and Church, G. M. (2016). *Vibrio natriegens*, a new genomic powerhouse. *bioRxiv* 058487. doi: 10.1101/058487

Loughran, S. T., Bree, R. T., and Walls, D. (2017). Purification of polyhistidine-tagged proteins. *Methods Mol. Biol.* 1485, 275–303. doi: 10.1007/978-1-4939-6412-3_14

Mahr, R., Boeselager, R. F., von, Wiechert, J., and Frunzke, J. (2016). Screening of an *Escherichia coli* promoter library for a phenylalanine biosensor. *Appl. Microbiol. Biotechnol.* 100, 6739–6753. doi: 10.1007/s00253-016-7575-8

Mambetisaeva, E. T., Martin, P. E., and Evans, W. H. (1997). Expression of three functional domains of connexin 32 as thioredoxin fusion proteins in *Escherichia coli* and generation of antibodies. *Protein Expr. Purif.* 11, 26–34. doi: 10.1006/prep.1997.0761

McNiff, M. L., Haynes, E. P., Dixit, N., Gao, F. P., and Laurence, J. S. (2016). Thioredoxin fusion construct enables high-yield production of soluble, active matrix metalloproteinase-8 (MMP-8) in *Escherichia coli*. *Protein Expr. Purif.* 122, 64–71. doi: 10.1016/j.pep.2016.02.012

Moore, S. J., Lai, H.-E., Kelwick, R. J. R., Chee, S. M., Bell, D. J., Polizzi, K. M., et al. (2016). EcoFlex: a multifunctional MoClo kit for *E. coli* synthetic biology. *ACS Synth. Biol.* 5, 1059–1069. doi: 10.1021/acssynbio.6b00031

Nakagawa, S., Oda, H., and Anazawa, H. (1995). High cell density cultivation and high recombinant protein production of *Escherichia coli* strain expressing uricase. *Biosci. Biotechnol. Biochem.* 59, 2263–2267. doi: 10.1271/bbb.59.2263

Oliveira, J. E., de Soares, C. R., Peroni, C. N., Gimbo, E., Camargo, I. M., Morganti, L., et al. (1999). High-yield purification of biosynthetic human growth hormone secreted in *Escherichia coli* periplasmic space. *J. Chromatogr. A* 852, 441–450. doi: 10.1016/S0021-9673(99)00613-5

Pöppel, A.-K., Koch, A., Kogel, K.-H., Vogel, H., Kollewe, C., Wiesner, J., et al. (2014). Lucimycin, an antifungal peptide from the therapeutic maggot of the common green bottle fly *Lucilia sericata*. *Biol. Chem.* 395, 649–656. doi: 10.1515/hsz-2013-0263

Potapov, V., Ong, J. L., Kucera, R. B., Langhorst, B. W., Bilotti, K., Pryor, J. M., et al. (2018). Comprehensive profiling of four base overhang ligation fidelity by T4 DNA ligase and application to DNA assembly. *ACS Synth. Biol.* 7, 2665–2674. doi: 10.1021/acssynbio.8b00333

Punginelli, C., Ize, B., Stanley, N. R., Stewart, V., Sawers, G., Berks, B. C., et al. (2004). mRNA secondary structure modulates translation of Tat-dependent formate dehydrogenase N. *J. Bacteriol.* 186, 6311–6315. doi: 10.1128/JB.186.18.6311-6315.2004

Ramazzina, I., Folli, C., Secchi, A., Berni, R., and Percudani, R. (2006). Completing the uric acid degradation pathway through phylogenetic comparison of whole genomes. *Nat. Chem. Biol.* 2, 144–148. doi: 10.1038/nchembio768

Reuten, R., Nikodemus, D., Oliveira, M. B., Patel, T. R., Brachvogel, B., Breloy, I., et al. (2016). Maltose-binding protein (MBP), a secretion-enhancing tag for mammalian protein expression systems. *PLoS ONE* 11:e0152386. doi: 10.1371/journal.pone.0152386

Saïda, F. (2007). Overview on the expression of toxic gene products in *Escherichia coli*. *Curr. Prot. Protein Sci.* Chapter 5, Unit 5.19. doi: 10.1002/0471140864.ps0519s50

Salis, H. M., Mirsky, E. A., and Voigt, C. A. (2009). Automated design of synthetic ribosome binding sites to control protein expression. *Nat. Biotechnol.* 27, 946–950. doi: 10.1038/nbt.1568

Schäfer, F., Seip, N., Maertens, B., Block, H., and Kubicek, J. (2015). Purification of GST-tagged proteins. *Meth. Enzymol.* 559, 127–139. doi: 10.1016/bs.mie.2014.11.005

Schindelin, J., Arganda-Carreras, I., Frise, E., Kaynig, V., Longair, M., Pietzsch, T., et al. (2012). Fiji: an open-source platform for biological-image analysis. *Nat. Methods* 9, 676–682. doi: 10.1038/nmeth.2019

Schindler, D., Milbredt, S., Sperlea, T., and Waldminghaus, T. (2016). Design and assembly of DNA sequence libraries for chromosomal insertion in bacteria based on a set of modified MoClo vectors. *ACS Synth. Biol.* 5, 1362–1368. doi: 10.1021/acssynbio.6b00089

Schleicher, L., Muras, V., Claussen, B., Pfannstiel, J., Blombach, B., Dibrov, P., et al. (2018). *Vibrio natriegens* as host for expression of multisubunit membrane protein complexes. *Front. Microbiol.* 9:2537. doi: 10.3389/fmicb.2018.02537

Schreiber, C., Müller, H., Birrenbach, O., Klein, M., Heerd, D., Weidner, T., et al. (2017). A high-throughput expression screening platform to

optimize the production of antimicrobial peptides. *Microb. Cell Fact.* 16:29. doi: 10.1186/s12934-017-0637-5

Shaaban, M. I., Abdelmegeed, E., and Ali, Y. M. (2015). Cloning, expression, and purification of recombinant uricase enzyme from *Pseudomonas aeruginosa* Ps43 using *Escherichia coli*. *J. Microbiol. Biotechnol.* 25, 887–892. doi: 10.4014/jmb.1410.10041

Sinah, N., Williams, C. A., Piper, R. C., and Shields, S. B. (2012). A set of dual promoter vectors for high throughput cloning, screening, and protein expression in eukaryotic and prokaryotic systems from a single plasmid. *BMC Biotechnol.* 12:54. doi: 10.1186/1472-6750-12-54

Steinmetz, E. J., and Auldridge, M. E. (2017). Screening fusion tags for improved recombinant protein expression in *E. coli* with the Expresso® solubility and expression screening system. *Curr. Prot. Protein Sci.* 90, 5.27.1-5.27.20. doi: 10.1002/cpps.39

Tsirigotaki, A., Geyter, J., de Šoštaric, N., Economou, A., and Karamanou, S. (2017). Protein export through the bacterial Sec pathway. *Nat. Rev. Microbiol.* 15, 21–36. doi: 10.1038/nrmicro.2016.161

Tullman-Ercek, D., DeLisa, M. P., Kawarasaki, Y., Iranpour, P., Ribnicky, B., Palmer, T., et al. (2007). Export pathway selectivity of *Escherichia coli* twin arginine translocation signal peptides. *J. Biol. Chem.* 282, 8309–8316. doi: 10.1074/jbc.M610507200

Wedde, M., Weise, C., Kopacek, P., Franke, P., and Vilcinskas, A. (1998). Purification and characterization of an inducible metalloprotease inhibitor from the hemolymph of greater wax moth larvae, *Galleria mellonella*. *Eur. J. Biochem.* 255, 535–543. doi: 10.1046/j.1432-1327.1998.2550535.x

Weinstock, M. T., Hesek, E. D., Wilson, C. M., and Gibson, D. G. (2016). *Vibrio natriegens* as a fast-growing host for molecular biology. *Nat. Methods* 13, 849–851. doi: 10.1038/nmeth.3970

Werner, S., Engler, C., Weber, E., Gruetzner, R., and Marillonnet, S. (2012). Fast track assembly of multigene constructs using Golden Gate cloning and the MoClo system. *Bioeng. Bugs* 3, 38–43. doi: 10.4161/bbug.3.1.18223

Young, C. L., Britton, Z. T., and Robinson, A. S. (2012). Recombinant protein expression and purification: a comprehensive review of affinity tags and microbial applications. *Biotechnol. J.* 7, 620–634. doi: 10.1002/biot.201100155

Conflict of Interest: The authors declare that the research was conducted in the absence of any commercial or financial relationships that could be construed as a potential conflict of interest.

frontiers in Bioengineering and Biotechnology

BRIEF RESEARCH REPORT
published: 06 September 2019
doi: 10.3389/fbioe.2019.00213

PARAGEN 1.0: A Standardized Synthetic Gene Library for Fast Cell-Free Bacteriocin Synthesis

Philippe Gabant and Juan Borrero†*

Syngulon, Seraing, Belgium

OPEN ACCESS

Edited by:
Jean Marie François, UMS3582 Toulouse White Biotechnology (TWB), France

Reviewed by:
Dzung B. Diep, Norwegian University of Life Sciences, Norway
Dae-Hee Lee, Korea Research Institute of Bioscience and Biotechnology (KRIBB), South Korea

****Correspondence:***
Philippe Gabant
pgabant@syngulon.com

†Present address:
Juan Borrero, Sección Departamental de Nutrición y Ciencia de los Alimentos (Facultad de Veterinaria), Universidad Complutense de Madrid, Madrid, Spain

Specialty section:
This article was submitted to Synthetic Biology, a section of the journal Frontiers in Bioengineering and Biotechnology

Received: *27 June 2019*
Accepted: *22 August 2019*
Published: *06 September 2019*

Citation:
Gabant P and Borrero J (2019) PARAGEN 1.0: A Standardized Synthetic Gene Library for Fast Cell-Free Bacteriocin Synthesis. Front. Bioeng. Biotechnol. 7:213. doi: 10.3389/fbioe.2019.00213

The continuous emergence of microbial resistance to our antibiotic arsenal is widely becoming recognized as an imminent threat to global human health. Bacteriocins are antimicrobial peptides currently under consideration as real alternatives or complements to common antibiotics. These peptides have been much studied, novel bacteriocins are regularly reported and several genomic databases on these peptides are currently updated. Despite this, to our knowledge, a physical collection of bacteriocins that would allow testing and comparing them for different applications does not exist. Rapid advances in synthetic biology in combination with cell-free protein synthesis technologies offer great potential for fast protein production. Based on the amino acid sequences of the mature peptide available in different databases, we have built a bacteriocin gene library, called PARAGEN 1.0, containing all the genetic elements required for *in vitro* cell-free peptide synthesis. Using PARAGEN 1.0 and a commercial kit for cell-free protein synthesis we have produced 164 different bacteriocins. Of the bacteriocins synthesized, 54% have shown antimicrobial activity against at least one of the indicator strains tested, including Gram-positive and Gram-negative bacteria representing commonly used lab strains, industrially relevant microorganisms, and known pathogens. This bacteriocin collection represents a streamlined pipeline for selection, production, and screening of bacteriocins as well as a reservoir of ready-to-use antimicrobials against virtually any class of relevant bacteria.

Keywords: antimicrobial peptides, bacteriocins, cell-free extracts, *in vitro* synthesis, synthetic biology

The remarkable health benefits that have been achieved with antibiotics are being questioned by the rapid increase of resistant bacteria. World Health Organization's new Global Antimicrobial Surveillance System (GLASS) study shows an antibiotic resistance occurrence among 500,000 people with suspected bacterial infections throughout 22 countries (WHO, 2015). Hence a growing list of infections like pneumonia, tuberculosis and foodborne diseases are becoming sometimes impossible to treat as antibiotics are not so effective (WHO, 2015). The antibiotic resistance crisis has been attributed to an excessive as well as abusive use of antibiotics, and also as the consequence in the decrease of new drug development by the pharmaceutical industry due to reduced economic incentives and demanding regulatory requirements (Cooper and Shlaes, 2011; White, 2011). Moreover, it has been shown that the consumption of broad-spectrum antibiotics may damage

the human commensal microbiota which has major roles in the host's health (Blaser, 2011; Willing et al., 2011; Lange et al., 2016). Consequently, the development of new antimicrobial agents that may be used in different settings (clinic, food industry, animal feed, etc.) has become crucial.

Antimicrobial peptides (AMPs) have been described as "evolutionarily ancient weapons against microbial infections" (Zasloff, 2002). AMPs are produced by all organisms, including human beings, and play an essential role in innate immunity. They are key elements of the innate immune system which deliver immediately effective and non-specific defenses against infections. Among the large variety of AMPs, there is a subgroup known as bacteriocins which are small peptides, produced by bacteria and ribosomally synthesized. Bacteriocins, which were discovered in 1925 (Gratia and Fredericq, 1946), exhibit strong activity against their target strains. This activity has often been found in the nanomolar range, making them in some cases more potent than their antibiotic analogs (Mathur et al., 2013; Ming et al., 2015). Another interesting feature is that, compared to antibiotics, most bacteriocins are only active against a narrow spectrum of bacteria close related to the producer. A few years ago, this narrow inhibition spectrum was considered as a major bottleneck, however today we know that big disruptions in the gut microbiota caused by broad spectrum antibiotics are coupled to immunological, metabolic, and neurological disorders in the host. Therefore, it is believed that targeting specific bacteria instead of the whole microbiome is more efficient and less intrusive (Mills et al., 2017).

Bacteriocins are an heterogenous group with a wide range of sizes, structures, modes of action, activity spectra, and target cell receptors. Their classification undergoes continuous modifications because of new developments regarding their structures and modes of action but they may be broadly divided into class I (post-translationally modified) class II (heat-stable, <10 kDa, unmodified) and class III (thermo-labile, >10 kDa) groups (Álvarez-Sieiro et al., 2016). Along with categorizing bacteriocins based on their modifications, they may be subdivided. The unmodified (class II) bacteriocins can be divided into four groups according to the classification by Álvarez-Sieiro et al. (2016). These subclasses are peptides that contain a YGNGV motif (in which N represents any amino acid; the class IIa peptides); two-peptide bacteriocins (class IIb peptides); leaderless bacteriocins (class IIc peptides); and unmodified, linear, non-pediocin-like, single-peptide bacteriocins that do not belong to other subclasses (class IId peptides).

Since the early 2000s, the successfulness of bacteriocins against unwelcome microorganisms has opened unumbered opportunities for innovative research, and currently, research on these AMPs is rapidly gaining importance. Bacteriocins on their own have shown a great potential mainly in food preservation and biomedical applications, and as a matter of fact, over 60% of the bacteriocin-related patents granted are related to these two areas. However, the use of bacteriocins in other alternative fields is growing, and there are many examples of bacteriocins for veterinary use, cosmetic use and bacteriocins applied on production–purification systems along with recombinant proteins or molecular modifications in the producer strains (López-Cuellar et al., 2016).

Since 2008, pharmaceutical companies have only introduced four new antibiotics, compared to the 16 approved from 1983 to 1987 and, for more than 40 years there have been no releases of new classes of antibiotics to treat Gram-negative bacilli. Meanwhile, the number of new bacteriocins is rapidly increasing and it is believed that more than 99% of bacteria can produce at least one bacteriocin, although most of which are still not identified (Riley and Wertz, 2002). Only from year 2004 to 2015, there have been published 429 scientific articles and 245 granted patents related to bacteriocins and these numbers are increasing to almost one bacteriocin related publication per day (López-Cuellar et al., 2016). In an effort to centralize all this information, there are several bacteriocin sequence data repository websites (http://bactibase.hammamilab.org/main.php, http://bagel4.molgenrug.nl/) regularly updated with the most relevant features of the new bacteriocins described. Moreover, in the last years there has been an increasing number of web servers hosting bioinformatic software acting as bacteriocin genome mining tools allowing the research community to identify bacteriocins and other antimicrobial peptides in genome/metagenome sequences (http://bactibase.hammamilab.org/main.php, http://bagel4.molgenrug.nl/, https://antismash.secondarymetabolites.org/#!/start). Despite a clear interest in exploring the full potential of these peptides and the enormous amount of information on bacteriocins provided by researcher groups from all over the world, application of their potential remains to be explored. As with other molecules, the more information there is, the more difficult it is to choose the right candidate for a specific application.

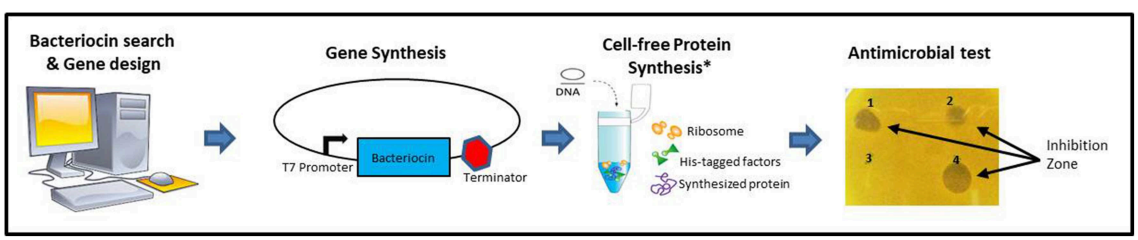

FIGURE 1 | Schematic description of the methodology used in the construction of PARAGEN 1.0. *Image from PURExpress® *in vitro* Protein Synthesis Kit (New England Biolabs).

We have identified that the availability of a physical collection of bacteriocin genes designed in a standardized format allowing a rapid production of peptides would boost innovation in the AMPs research community. This new resource should also allow for the first time to test and compare different bacteriocins, make combinations to analyse and characterize potential synergistic effects between unrelated bacteriocins as well as compare biochemical properties. Academic and industrial researchers would be able then to choose and select the right bacteriocin from this collection, tailored for each specific application.

Bacteriocin production and purification is not an easy task and is considered as one of the main bottlenecks for their use at industrial scale (Deraz et al., 2007; Jozala et al., 2008, 2015; Bali et al., 2014). Bacteriocins traditionally have been purified from their native producing strains, however this consists in a time-consuming and laborious procedure which often results in low yields of bacteriocin (Rodríguez et al., 2003). On top of that, collecting all bacteriocin producing strains described and purifying their active peptides is an almost impossible task. Other methods such as the heterologous production of bacteriocins in other microorganisms (bacteria or yeast) and in plants has been shown as a useful technology for producing higher concentrations of these peptides (Sánchez et al., 2008; Borrero et al., 2011, 2018). Nevertheless, only a few bacteriocins have been successfully produced by heterologous hosts since this approach is laborious and time consuming. Moreover, the risk that the bacteriocin will be produced at a yield not reaching the standard request of industrial processes is still quite high. There are alternatives to the use of microorganisms as peptide producers and with the recent advances in the field of Synthetic Biology, it is now possible to synthesize peptides both by chemical synthesis and by using cell-free extracts for *ex-vivo* protein production (Hols et al., 2019). Since its first application in deciphering genetic codes (Nirenberg and Matthaei, 1961) cell-free protein synthesis (CFPS) has become a key method for the obtention of recombinant proteins in order to match the rising demands for simple, inexpensive, and efficient protein production (Carlson et al., 2012; Hodgman and Jewett, 2012). The recent growing attention to crude extract CFPS is motivated mainly, but not only, by the unique benefit that barrier-free cell-free systems enable direct and fast access to enzymes and reaction conditions.

The peptidic nature of bacteriocins and the fact that they are ribosomally synthesized (Field et al., 2012) make them ideal candidates for production by CFPS. With the cell-free system there is no need of signal peptides or leader sequences attached to the bacteriocins and of dedicated transporter systems to secrete the mature and active peptide, as the bacteriocin is synthesized outside the cell. Moreover, with this technology the potential toxicity to the host is also excluded and there is no need to coproduce the immunity protein. This major technological locket could be overcome in most cases by working with cell-free extracts which is by design an abiotic technology. With these advantages in mind we have constructed a physical collection of bacteriocins: PARAGEN 1.0: a standardized synthetic gene library allowing to produce a broad set of bacteriocins in parallel.

A schematic description of the methodology used is shown in **Figure 1**. A list of class II bacteriocins was obtained from the two major genomic bacteriocin databases: BAGEL4 (van Heel et al., 2018) and BACTIBASE (Hammami et al., 2010). The aminoacidic sequence of the mature/active peptide of each bacteriocin was determined based on the information provided by these databases and, in some cases, going to the original publications and/or sequences found at the NCBI database (Database resources of the National Center for Biotechnology Information, 2015). All aminoacidic sequences were reverse-translated and codon optimized for *Escherichia coli* (www.bioinformatics.org/sms2/rev_trans.html). The nucleotide sequences were included in a vector backbone containing the T7 promoter region, a start codon (ATG) a stop codon (TAA) and a T7 terminator region. Recombinant vectors were constructed and amplified in *E. coli* DH10B standard strain and used as templates for cell-free protein synthesis using PURExpress® *in vitro* Protein Synthesis Kit (New England Biolabs). All bacteriocins synthesized were tested on petri dishes for antimicrobial activity against a set of 12 different indicators including Gram-positive and Gram-negative bacteria (**Table 1**). Bacteriocins showing a halo of inhibition against at least one of the indicators were considered as positive **(Supplementary Material)**. A total of 128 bacteriocins were synthesized, 23 belonging to the class IIa (18%), 15 belonging to the class IIb (12%), 15 belonging to the class IIc (12%), 50 belonging to the class IId (39%), and 25 belonging to the class III (20%) (**Figure 2**). Regarding their antimicrobial activity, 74% of the class IIa, 67% of the class IIb, 100% of the class IIc, 38% of the class IId and 32% of the class III bacteriocins showed activity against at least one of the indicators tested. The remaining bacteriocins (59 out of 128) did not show activity against any of the indicators tested **(Supplementary Material)**. However, we cannot conclude that these 59 bacteriocins are inactive as, most likely, they are just not active against the 12 indicators used in this work. Hence, a further analysis with a larger number of targets should be done. Other tests such as protease and pH stability of these peptides are currently being done in the lab.

TABLE 1 | Strains used as indicators to test the antimicrobial activity of the bacteriocins from PARAGEN 1.0.

Strain	Gram
Escherichia coli DH10B	–
Bacillus cereus ATCC 14579	+
Bacillus subtilis 168	+
Enterococcus faecalis Si0159	+
Enterococcus faecium ATCC 19434	+
Lactococcus lactis IL1403	+
Listeria monocytogenes ATCC 19115	+
Pediococcus pentosaceus HELA	+
Staphylococcus aureus aureus ATCC 6538	+
Staphylococcus epirdermidis ATCC 12228	+
Streptococcus mutans UA159	+
Streptococcus pyogenes ATCC 12344	+

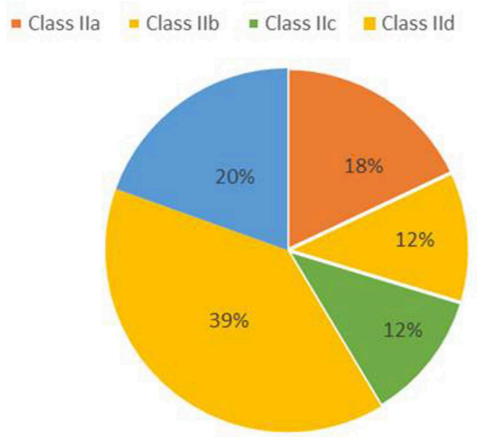

	Number of Bacteriocins	% Active Bacteriocins
Class IIa	23	74%
Class IIb	15	67%
Class IIc	15	100%
Class IId	50	38%
Class III	25	32%
Total	128	54%

FIGURE 2 | Description of bacteriocins in PARAGEN 1.0. From the total, 18% are class IIa peptides; 12% are considered class IIb, 12% belong to class IIc, 39% are class IId and 20% are class III bacteriocins. Among bacteriocins from class IIa, 74% were active; 67% from class IIb were active, all bacteriocins from class IIc were active (100%), 38% and 32% of bacteriocins from class IId and class III, respectively, showed antimicrobial activity against one or more indicators.

As shown in this work, synthetic production of bacteriocins with cell-free systems is a viable alternative to bacterial production as it allows very rapidly the synthesis and screening of a large numbers of bacteriocins in the same experiment. Further efforts need to be done in order to reduce the cost of this system, optimize and increase peptide production. There is also a need on finding a method to quantify the production of active bacteriocin in order to fully compare antimicrobial activities. Several authors have already used cell-free as platform for the production for both single proteins but also for proteins produced through complex metabolic pathways (Koch et al., 2018). Some class I bacteriocins such as microcin J25 have been modified and produced in their active conformation *ex-vivo* (Yan et al., 2012), therefore we strongly believe that the production of class I bacteriocins should be possible soon with this technology.

To our knowledge, PARAGEN 1.0 is the largest collection of active native bacteriocins ready to be tested and it keeps growing since we are constantly adding new peptides to it. We are already working in a second library of non-natural bacteriocins (PARAGEN 2.0) consisting on chimeras of different bacteriocins or variants with single or multiple amino acid modifications. The possibilities that cell-free systems offer for bacteriocin production are almost unlimited and we believe that PARAGEN might be a useful tool for gaining knowledge of the precise modes of action of bacteriocins and more generally antimicrobial peptides, allowing the production of more active and more stable variants. This would contribute to speed up the screening for natural antimicrobial activities and the design of tailor-made bacteriocins for their applications in food industries and in medicine.

DATA AVAILABILITY

All datasets generated for this study are included in the manuscript/**Supplementary Files**.

AUTHOR CONTRIBUTIONS

PG and JB have contributed equally to the design and implementation of the research, to the analysis of the results and to the writing of the manuscript.

FUNDING

The construction of the PARAGEN 1.0 collection was funded by a Research Grant from the Waloon Region, Recherche Industrielle: PARAGEN convention n°7627.

SUPPLEMENTARY MATERIAL

The Supplementary Material for this article can be found online at: https://www.frontiersin.org/articles/10.3389/fbioe.2019.00213/full#supplementary-material

REFERENCES

Álvarez-Sieiro, P., Montalbán-López, M., Mu, D., and Kuipers, O. P. (2016). Bacteriocins of lactic acid bacteria: extending the family. *Appl. Microbiol. Biotechnol*, 100, 2939–2951. doi: 10.1007/s00253-016-7343-9

Bali, V., Panesar, P. S., and Bera, M. B. (2014). Trends in utilization of agroindustrial byproducts for production of bacteriocins and

their biopreservative applications. *Crit. Rev. Biotechnol.* 8551, 1–11. doi: 10.3109/07388551.2014.947916

Blaser, M. (2011). Antibiotic overuse: stop the killing of beneficial bacteria. *Nature* 476, 393–394. doi: 10.1038/476393a

Borrero, J., Jiménez, J. J., Gútiez, L., Herranz, C., Cintas, L. M., and Hernández, P. E. (2011). Protein expression vector and secretion signal peptide optimization to drive the production, secretion, and functional expression of the bacteriocin enterocin A in lactic acid bacteria. *J. Biotechnol.* 156, 76–86. doi: 10.1016/j.jbiotec.2011.07.038

Borrero, J., Kelly, E., O'Connor, P. M., Kelleher, P., Scully, C., Cotter, P. D., et al. (2018). Plantaricyclin A, a novel circular bacteriocin produced by *Lactobacillus plantarum* NI326: purification, characterization, and heterologous production. *Appl. Environ. Microbiol.* 84, e01801–e01817. doi: 10.1128/AEM.01801-17

Carlson, E. D., Gan, R., Hodgman, C. E., and Jewett, M. C. (2012). Cell-free protein synthesis: applications come of age. *Biotechnol. Adv.* 30, 1185–1194. doi: 10.1016/j.biotechadv.2011.09.016

Cooper, M. A., and Shlaes, D. (2011). Fix the antibiotics pipeline. *Nature* 472:32. doi: 10.1038/472032a

Database resources of the National Center for Biotechnology Information (2015). *Nucleic Acids Res.* 44, 7–19. doi: 10.1093/nar/gkv1290

Deraz, S., Plieva, F. M., Galaev, I. Y., Karlsson, E. N., and Mattiasson, B. (2007). Capture of bacteriocins directly from non-clarified fermentation broth using macroporous monolithic cryogels with phenyl ligands. *Enzyme Microb. Technol.* 40, 786–793. doi: 10.1016/j.enzmictec.2006.06.024

Field, D., Begley, M., O'Connor, P. M., Daly, K. M., Hugenholtz, F., Cotter, P. D., et al. (2012). Bioengineered nisin A derivatives with enhanced activity against both Gram positive and Gram negative pathogens. *PLoS ONE.* 7:e46884. doi: 10.1371/journal.pone.0046884

Gratia, A., and Fredericq, P. (1946). Diversite' des souches antibiotiques de *E. coli* et e 'tendue variable de leur champs d'action. *Comptes Rendus Soc. Biol.* 140, 1032–1033.

Hammami, R., Zouhir, A., Le Lay, C., Ben Hamida, J., and Fliss, I. (2010). BACTIBASE second release: a database and tool platform for bacteriocin characterization. *BMC Microbiol.* 10:22. doi: 10.1186/1471-2180-10-22

Hodgman, C. E., and Jewett, M. C. (2012). Cell-free synthetic biology: thinking outside the cell. *Metab. Eng.* 14, 261–269. doi: 10.1016/j.ymben.2011.09.002

Hols, P., Ledesma-García, L., Gabant, P., and Mignolet, J. (2019). Mobilization of microbiota commensals and their bacteriocins for therapeutics. *Trendsc Microbiol.* 27, 690–702 doi: 10.1016/j.tim.2019.03.007

Jozala, A. F., De Lencastre Novaes, L. C., Mazzola, P. G., Oliveira-Nascimento, L., Vessoni Penna, T. C., Teixeira, J. A., et al. (2015). Low-cost purification of nisin from milk whey to a highly active product. *Food Bioprod. Process.* 93, 115–121. doi: 10.1016/j.fbp.2013.12.003

Jozala, A. F., Lopes, A. M., Mazzola, P. G., Magalhães, P. O., Vessoni Penna, T. C., and Pessoa, A. (2008). Liquid-liquid extraction of commercial and biosynthesized nisin by aqueous two-phase micellar systems. *Enzyme Microb. Technol.* 42, 107–112. doi: 10.1016/j.enzmictec.2007.08.005

Koch, M., Faulon, J. L., and Borkowski, O. (2018). Models for cell-free synthetic biology: make prototyping easier, better and faster. *Front. Bioeng. Biotechnol.* 6:182. doi: 10.3389/fbioe.2018.00182

Lange, K., Buerger, M., Stallmach, A., and Bruns, T. (2016). Effects of antibiotics on gut microbiota. *Digest. Dis.* 34, 260–268. doi: 10.1159/000443360

López-Cuellar, M. D. R., Rodríguez-Hernández, A. I., and Chavarría-Hernández, N. (2016). LAB bacteriocin applications in the last decade. *Biotechnol. Biotechnol. Equip.* 30, 1039–1050. doi: 10.1080/13102818.2016.1232605

Mathur, H., O'Connor, P. M., Hill, C., Cotter, P. D., and Ross, R. P. (2013). Analysis of anti-*Clostridium difficile* activity of thuricin CD, vancomycin, metronidazole, ramoplanin, and actagardine, both singly and in paired combinations. *Antimicrob. Agents Chemother.* 57, 2882–2886. doi: 10.1128/AAC.00261-13

Mills, S., Ross, R. P., and Hill, C. (2017). Bacteriocins and bacteriophage; a narrow-minded approach to food and gut microbiology. *FEMS Microbiol. Rev.* 41(Supp_1), S129–S153. doi: 10.1093/femsre/fux022

Ming, L., Zhang, Q., Yang, L., and Huang, J. A. (2015). Comparison of antibacterial effects between antimicrobial peptide and bacteriocins isolated from *Lactobacillus plantarum* on three common pathogenic bacteria. *Int. J. Clin. Exp. Med.* 8, 5806–5811.

Nirenberg, M. W., and Matthaei, J. H. (1961). The dependence of cell-free protein synthesis in *E. coli upon naturally occurring or synthetic polyribonucleotides. Proc. Natl. Acad. Sci. U.S.A.* 47, 1588–1602. doi: 10.1073/pnas.47.10.1588

Riley, M. A., and Wertz, J. E. (2002). Bacteriocins: evolution, ecology, and application. *Annu. Rev. Microbiol.* 56,117–137. doi: 10.1146/annurev.micro.56.012302.161024

Rodríguez, J. M., Martínez, M. I., Horn, N., and Dodd, H. M. (2003). Heterologous production of bacteriocins by lactic acid bacteria. *Int. J. Food Microbiol.* 80, 101–116. doi: 10.1016/S0168-1605(02)00153-8

Sánchez, J., Borrero, J., Gómez-Sala, B., Basanta, A., Herranz, C., Cintas, L. M., et al. (2008). Cloning and heterologous production of hiracin JM79, a Sec-dependent bacteriocin produced by Enterococcus hirae DCH5, in lactic acid bacteria and Pichia pastoris. *Appl. Environ. Microbiol.* 74, 2471–2479. doi: 10.1128/AEM.02559-07

van Heel, A. J., de Jong, A., Song, C., Viel, J. H., Kok, J., and Kuipers, O. P. (2018). BAGEL4: a user-friendly Web server to thoroughly mine RiPPs and bacteriocins. *Nucleic Acids Res.* 46, 278–281. doi: 10.1093/nar/gky383

White, A. R. (2011). Effective antibacterials: at what cost? The economics of antibacterial resistance and its control. *J. Antimicrob. Chemother.* 66, 1948–1953. doi: 10.1093/jac/dkr260

WHO (2015). *Global Antimicrobial Resistance Surveillance System Report*. Manual for Early Implementation. Geneva: World Health Organisation.

Willing, B. P., Russell, S. L., and Finlay, B. B. (2011). Shifting the balance: antibiotic effects on host–microbiota mutualism. *Nature Rev. Microbiol.* 9, 233–243. doi: 10.1038/nrmicro2536

Yan, K. P., Li, Y., Zirah, S., Goulard, C., Knappe, T. A., Marahiel, M. A., et al. (2012). Dissecting the maturation steps of the lasso peptide microcin J25 *in vitro*. *ChemBioChem.* 13, 1046–1052. doi: 10.1002/cbic.201200016

Zasloff, M. (2002). Antimicrobial peptides of multicellular organisms. *Nature* 415, 389–395. doi: 10.1038/415389a

Conflict of Interest Statement: PG and JB were employed by company Syngulon S.A.

frontiers in Bioengineering and Biotechnology

PERSPECTIVE
published: 07 August 2019
doi: 10.3389/fbioe.2019.00175

Future Trends in Synthetic Biology—A Report

Meriem El Karoui[1]*, *Monica Hoyos-Flight*[2] and *Liz Fletcher*[1]

[1] SynthSys-Centre for Synthetic and Systems Biology, School of Biological Sciences, University of Edinburgh, Edinburgh, United Kingdom, [2] Innogen Institute, School of Social and Political Sciences, University of Edinburgh, Edinburgh, United Kingdom

Leading researchers working on synthetic biology and its applications gathered at the University of Edinburgh in May 2018 to discuss the latest challenges and opportunities in the field. In addition to the potential socio-economic benefits of synthetic biology, they also examined the ethics and security risks arising from the development of these technologies. Speakers from industry, academia and not-for-profit organizations presented their vision for the future of the field and provided guidance to funding and regulatory bodies to ensure that synthetic biology research is carried out responsibly and can realize its full potential. This report aims to capture the collective views and recommendations that emerged from the discussions that took place. The meeting was held under the Chatham House Rule (i.e., a private invite-only meeting where comments can be freely used but not attributed) to promote open discussion; the findings and quotes included in the report are therefore not attributed to individuals. The goal of the meeting was to identify research priorities and bottlenecks. It also provided the opportunity to discuss how best to manage risk and earn public acceptance of this emerging and disruptive technology.

Keywords: synthetic biology, biosystem, future trends and developments, biodesign automation, responsible research and innovation (RRI)

OPEN ACCESS

Edited by:
Jean Marie François, UMR5504 Laboratoire d'Ingénierie des Systèmes Biologiques et des Procédés (LISBP), France

Reviewed by:
Vijai Singh, Indrashil University, India
Chris John Myers, The University of Utah, United States

***Correspondence:**
Meriem El Karoui
Meriem.Elkaroui@ed.ac.uk

Specialty section:
This article was submitted to Synthetic Biology, a section of the journal Frontiers in Bioengineering and Biotechnology

Received: *28 May 2019*
Accepted: *08 July 2019*
Published: *07 August 2019*

Citation:
El Karoui M, Hoyos-Flight M and Fletcher L (2019) Future Trends in Synthetic Biology—A Report. Front. Bioeng. Biotechnol. 7:175. doi: 10.3389/fbioe.2019.00175

INTRODUCTION

Synthetic Biology offers innovative approaches for engineering new biological systems or re-designing existing ones for useful purposes (see **Figure 1**). It has been described as a disruptive technology at the heart of the so-called Bioeconomy, capable of delivering new solutions to global healthcare, agriculture, manufacturing, and environmental challenges (Cameron et al., 2014; Bueso and Tangney, 2017; French, 2019). However, despite successes in the production of some high value chemicals and drugs, there is a perception that synthetic biology is still not yet delivering on its promise.

Moreover, there are some concerns from governments that synthetic biology expands the pool of agents of concern, which increases the need to develop detection, identification and monitoring systems, and proactively build countermeasures against chemical and biological threats (Wang and Zhang, 2019). The participation of representatives from various government organizations

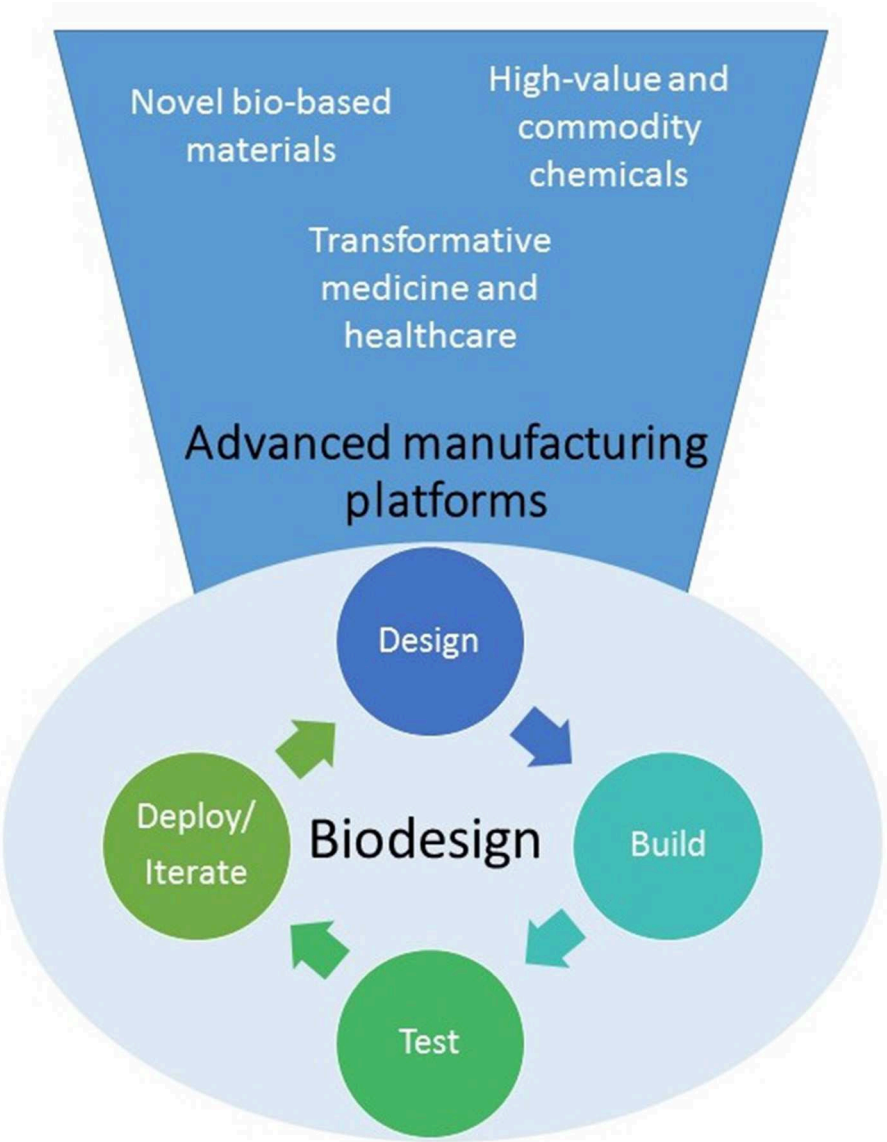

FIGURE 1 | Synthetic biology is developing into a biodesign platform where it will be possible to apply the "design-build-test-iterate (or deploy)" to predictably create cells or organisms able to produce a wide variety of novel molecules, materials or even cells for multiple applications.

at this meeting is testament to their commitment to maintaining an active dialogue with the synthetic biology community. In this way, they aim to keep abreast of the changing nature of threats and provide the best advice to government about investment in science and technology and the introduction or amendment of regulatory processes.

The cost of DNA sequencing and synthesis have decreased dramatically (Carlson, 2014; Kosuri and Church, 2014) and we have access to more genetic information and more powerful genetic engineering capabilities than ever before. Critical investments in infrastructure are bearing fruit and, as is described below, synthetic biology is increasingly becoming, at least part of, the solution to many of our present and future needs in medicine, food and energy production, remediation, manufacturing, and national security. So what is the potential of synthetic biology and what challenges does it still face to realize this?

ADVANCES IN SYNTHETIC BIOLOGY: THE STATE OF PLAY

Small Molecules: Production on Demand a Reality

Despite the lack of predictability in biology, and current technical constraints that limit data collection and analyses, we

can now produce small molecules on demand using synthetic biology approaches.

Probably the most impressive examples come from the Foundry at the Broad Institute of MIT and Harvard. When the Defense Advanced Research Projects Agency (DARPA) put the MIT-Broad Institute Foundry's design capabilities to the test, its researchers were able to deliver 6 out of 10 molecules of interest to the US Department of Defense in 90 days. This "pressure test" confirms the potential of synthetic biology to address shortages of key compounds quickly (Casini et al., 2018).

Indeed, many labs can now design and construct relatively complex gene networks capable of generating a wide variety of "designer" molecules in a range of host cells; however, this is often a slow iterative process of trial and error.

As yet, very few small molecules in medicine are manufactured using a synthetic biology process; it remains very difficult to engineer microbes to carry out processes that Nature did not intend. This is to be expected: the performance of microbes is "good enough" from an evolutionary perspective. Microbes evolved to address the specific needs and challenges of their natural environments not those of industrial fermenters and bioreactors. Gene Transfer from one system to another may sound easy but in practice is hard work and rarely generates sufficient reward (i.e., increased yield) to justify the investment made. The application of automation and artificial intelligence (e.g., in designing and building plasmids) may help to reduce the time and cost—and improve return on investment—in the future (Zhang et al., 2018).

"Scale up is product specific – we need more synthetic biology in the production process"

Plants make alternative production platforms. Improvements in mining plant genomes and the development of effective transient expression systems have enabled large-scale production of, for example, vaccines in tobacco plants in just a few weeks (Dirisala et al., 2017; Emmanuel et al., 2018). Directing the production of synthetic biological materials to plant chloroplasts also shows promise (Boehm and Bock, 2019).

The photosynthetic reducing power generated in plant chloroplasts can be harnessed for the light-driven synthesis of bioactive molecules such as dhurrin, which protects plants against insects (Gnanasekaran et al., 2016).

However, underlying all these platforms is a knowledge gap in our understanding in how nature works. This makes it very hard to apply the design/build/test/learn cycles used in conventional engineering to the production of synthetic biological materials whatever the production platform (yeast, bacteria, plants, or human cells) if the platform itself is not well-understood (Sauro et al., 2006).

What we need now are instruments able to measure and characterize outputs, assisted by progress in robotics and automation, and the application of machine learning approaches to analyse the data generated. This will help us to generate more robust models of biological systems, so we can improve experimental design for future engineering strategies.

"We can do 'build'. 'Test' is the challenge when we want to learn from the iterative design process"

Healthcare: Reimagining Medicine

Synthetic biology is driving significant advances in biomedicine, which will lead to transformational improvements in healthcare. Already, patients are benefiting from so-called CAR (for chimeric antigen receptor) technology, which engineers the immune cells (T-cells) of the patient to recognize and attack cancer cells (June et al., 2018).

Genetically engineered viruses are being used to correct defective genes in patients with inherited diseases such as Severe Combined Immune Deficiency (SCID) or epidermolysis bullosa (Dunbar et al., 2018).

The ability to reprogramme somatic cells from patients into induced pluripotent stem cells is furthering our understanding of their disease, reducing the use of animals in research, and paving the way for the development of personalized medicines and cell therapies. In principle at least, we could engineer a patient's own cells to multiply, differentiate into different cell types and even self-assemble into new tissues, or even organs, to repair those damaged through disease or injury (Davies and Cachat, 2016; Satoshi et al., 2018).

Work on new vectors that are able to deliver large genetic loads to target tissues is helping to produce more efficient therapeutics and vaccines that will have fewer side effects and a smaller risk of resistance. Furthermore, optimizing antibody or vaccine production, or example, so that they are in an edible format (e.g., plant based), could greatly reduce the cost and increase the speed of vaccine production in an epidemic.

"We have the tools but need the creativity to make stuff that can't be made without synthetic biology"

In the next few years, genetically engineering pigs to be virus resistant and have human-like immune profiles could make xenotransplantation a clinical reality (Burkard et al., 2018). Engineering the microbiome is expected to lead to the development of synthetic probiotics (Dou and Bennett, 2018).

The synthetic biology initiative known as Human Genome Project-write (HGP-write) has set its sights even higher, rallying scientists to build entire human chromosomes (Boeke et al., 2016). Concerns have been raised about the ethics of creating "synthetic humans" and indeed the scientific and commercial value of such a project. More recently, HGP-write champions have proposed a more focused project to build a virus-resistant chromosome, making at least 400,000 changes to the human genome to remove DNA sequences that viruses use to hijack cells and replicate (Dolgin, 2018).

One of the many exciting opportunities that synthetic biology offers medicine is in the production of theranostic cell lines that can sense a disease state and produce an appropriate therapeutic response (Teixeira and Fussenegger, 2019). Several obstacles need to be overcome to achieve this goal: first, to expand the range of molecules that can be recognized by cellular "sensors" as inputs; and second, to better understand the genetic control factors that

regulate gene expression in space and time so we can engineer better activator systems.

"At present we need pills because we can't swallow a chemistry kit"

Metabolomics is shedding light on many disease biomarkers. Because some biomarkers are shared between seemingly unrelated diseases, an accurate diagnosis will require the detection of multiple markers to provide a more unique "disease fingerprint." Work in whole cell and cell free systems to develop sensors of multiple disease-specific biomarkers could assist in earlier detection of disease and prognostic monitoring.

To expand the range of biologically detectable molecules, it is possible to design metabolic pathways that transform currently undetectable molecules of interest (e.g., hippuric acid, the prostate cancer biomarker) into molecules for which sensors already exist (in this case benzoic acid) (Libis et al., 2016).

Cybergenetics is an emerging field that is developing experimental tools for the computer control of cellular processes at the gene level in real time. Cybergenetic control can be achieved by interfacing living cells with a digital computer that switches on or off the embedded "genetic switch" using light (optogenetics) or chemicals (Gabriele et al., 2018; Maysam et al., 2019). Such systems could help to maintain cellular homeostasis by monitoring the state of the body and triggering an appropriate response upon the detection of dysregulation; for example, they could trigger the release of insulin when blood glucose levels rise as detected by a wireless diagnostic tool (Ye et al., 2011).

Advanced Materials: Inspired by Nature, Improved by Synthetic Biology

Synthetic biology offers the opportunity to create responsive and multifunctional materials (Le Feuvre and Scrutton, 2018). The integration of biochemical components from living systems with inorganic components can lead to new materials that are able to sense the environment (or internal signals) and change their properties. These features could be particularly useful for improving protective clothing or building materials.

An issue when using microbes to produce composite materials is regulating the assembly of these materials to achieve specific desired properties. By understanding how microbes communicate with each other, it is possible to make them work better together and combine them with other production systems so that the properties of materials can be tailored for particular functions.

Interestingly, rather than modifying, or improving existing protein-based materials, an alternative approach involves using computational techniques to design completely novel proteins that self-assemble into predicted shapes (Ljubetič et al., 2017). Such "programmable" proteins open up even further opportunities for synthetic biology not only for materials science but also for medicine and chemistry.

"The tools are there, we just don't know what we want to make"

TACKLING THE CHALLENGES

Regardless of the research areas involved, there are some common challenges for the community to address.

Design With the End in Mind

There was consensus that while the production of small molecules using synthetically engineered cells at the bench is becoming more tractable, these processes often do not translate well into mass production. Scalability needs to be incorporated into the initial design process by including features, for example, that reduce toxicity of the molecule to the production host or "chassis" and/or by introducing modifications that favor its extraction. Careful consideration of the right chassis could also greatly improve yields and significantly reduce cost of production.

"Nature has developed its own ways to concentrate and solubilise chemicals... we are not learning from this"

Expanding the Host Repertoire

The number of microbes that are currently in use for the production of synthetic biological materials is only a tiny fraction of the total diversity that exists in Nature; only ten microbes are "domesticated" for industrial use. To identify the most appropriate chassis, it is worth turning to nature to identify species that have unique metabolic networks suited to host particular types of chemical reactions. For example, the soil bacterium *Pseudomonas putida*, which has adapted to harsh environmental conditions, is ideally suited to host redox-intensive reactions (Pablo and de Lorenzo, 2018). A treasure trove of, as yet, unexplored natural products, with novel and beneficial properties, exist in the plant kingdom. In addition, as noted above, plants are naturally excellent production hosts and it is now possible to "plug and play" combinations of plant pathways to generate novel molecules (Sainsbury and Lomonossoff, 2014; Evangelos and O'connor, 2016).

Developing a Universal Production System

To circumvent the problem of the impact of different host chassis on synthetic gene circuits, researchers would benefit from a universal synthetic expression system that permits the testing of new constructs. This would aid in the identification of optimal production platforms and decrease the need for organism-specific technologies. Combining this technology with DNA editing techniques, such as CRISPR/Cas9, will make the establishment of host production platforms and the generation of complex biosynthetic products easier and faster. One articulation of this could be in cell-free formats, in which the essential cellular machinery is reconstituted *in vitro* and used as a manufacturing platform (Villarreal and Tan, 2017; Koch et al., 2018).

"We need to reduce the burden of synthetic networks on endogenous circuits"

Move to Cell-Free Environments

Cell-free environments, interfaced with semiconductors, offer a powerful route for flexible and controllable production systems.

For example, nanoparticles made of semiconductor materials or quantum dots can be used to enhance enzyme activity in a cell free environment with a minimal set of ingredients. Multistep enzymatic pathways can be tethered to nanoparticle surfaces and, by avoiding the diffusion effect that takes place in cells, reaction rates can be increased 100-fold (Wang et al., 2017). This approach can be used to access non-natural materials and circumvents the potential issue of toxicity in cells (as well as the regulatory issues of genetically modified cells).

Research on silicon chips containing immobilized genes and cell lysates allows detailed examination of gene expression in space and time. When the compartments in which DNA-driven reactions take place are linked, with materials flowing into and diffusing between the compartments, it is possible to recreate oscillating protein expression patterns and protein gradients akin to those observed in cells (Karzbrun et al., 2014). Gene expression in these "artificial cells" can be controlled with electrodes that prevent the assembly of proteins by ribosomes. By standardizing outputs, this strategy is improving the predictability of engineered genetic circuits.

Systems Modeling, Standards, and Metrology

Whatever the system being explored, a robust model of that biological system is needed if predictable modifications of genetic circuits are to be designed and implemented with any confidence. To create such models, large sets of data arising from measuring multiple parameters of cell behavior under different conditions are essential (Fletcher et al., 2016).

There is great expectation that improvements in high-throughput data measurement and collection systems will generate exactly the large data sets needed. These can be analyzed using artificial intelligence or a machine learning approach to optimize the design of synthetic biological products and move away from the inefficient trial and error process (Decoene et al., 2018).

Finally, agreement on standards of design, assembly, data transfer, data measurement and regulatory rules, as well as on the language that is used, will help to improve the interdisciplinary and international collaborations that are required to drive the field forward. This is challenging for a community with such diverse interests and perspectives, and where data sharing, curating and quality control is not common practice.

However, without some form of agreed standards, many of the products and processes of synthetic biology will not translate well to industrial settings dependent on reproducible processes and beholden to exacting regulatory requirements.

Typically, academic researchers are driven by a need to understand the complexity of nature (and publish their work in high impact journals). Standardization and scaling up production are important, but have less of an academic pull than discovering a new product. Access to funding, industrial partnerships, and academic recognition are examples of potential incentives for carrying out this type of research.

"Standards restrict flexibility but enable interoperability"

TACKLING RISK

Synthetic biology is an example of a dual-use technology: it promises numerous beneficial applications, but it can also cause harm. This has led to fears that it could, intentionally or unintentionally, harm humans or damage the environment. For example, there is huge value in our ability to engineer viruses to be more effective and specific shuttles for gene therapies of devastating inherited disorders; however, engineering viruses may also lead to the creation of even more deadly pathogens by those intent on harm.

"Synthetic biology should be regarded as an extension of earlier developments and technologies"

Some would argue that synthetic biology poses an existential risk and needs to be treated with extreme caution. However, many new technological advances across the decades have met similar concerns. The uncertainty and remote possibility of such risks could hamper the development of useful technology. Scientists, their host institutions and funding bodies should (and indeed already do) consider whether the research planned could be misused. Measures that reduce the likelihood of misuse and its consequences should be implemented and clearly communicated. The synthetic biology community needs to be aware of, and respond to, these challenges by engaging in horizon scanning exercises as well as open dialogue with regulatory bodies and the media.

"Don't avoid risk – manage it"

Being more open about risks, and how they are controlled, provides an opportunity to shift discourse toward the benefits of synthetic biology in addressing urgent global needs, such as the production of biofuels, food security and more effective medicines, and potentially improve public acceptance.

"The questions should not be 'what's the next big thing for synthetic biology' but 'where is the greatest unmet need'."

Despite the efforts by individual countries to establish synthetic biology research roadmaps, broader, international agreement on common standards (and red lines) across the field may help establish trust and to advance the best pre-competitive research into useful applications.

Meeting participants highlighted the importance of training in responsible research conduct and ethics. Given students' future role as science ambassadors and influencers, their training should not only convey skills and knowledge but also awareness and critical thinking about the prospects and potential for dual use of synthetic biology. All researchers must remain vigilant regardless

of the many pressures and distractions of running a successful research lab; they may not have specialist training in identifying the risks of misuse but they are the people best placed to maintain informed oversight of risks.

One example of current synthetic biology research with potential dual use is gene drive technology, which can be used to propagate a particular suite of genes throughout a population. The benefits of using gene drive technology include the eradication of disease-carrying insect populations and the elimination of invading pest species but it has raised concerns about the unintended ecological impacts of reducing or eliminating a population (Callaway, 2018; Collins, 2018).

Similar release concerns surround research that is harnessing the ability of pathogens to target particular tissues in the body or particular chemicals in the environment, which could greatly aid efforts to deliver targeted therapies or clean-up contaminated sites. To date, such large-scale release for environmental bioremediation interventions has not been possible.

> *"We need to mind the gap between R&D scale up and communications . . . . One bad blog can kill a commercial product"*

There was consensus that the need for regulation over this community remains important. Regulation needs to keep up to speed with the emerging technologies and should focus on the product rather than the process used to create it (Tait et al., 2017). Unsuitable regulatory frameworks (as well as unfavorable public perception) could discourage private sector investment in synthetic biology.

Open and balanced two-way communication between researchers, funders, companies and governments and the public will be vital. Consumers and activists may have no interest in the difference between making a chemical (e.g., a flavor or fragrance) synthetically and one made using genetically modified bacteria but they may instinctively distrust the latter.

CONCLUSIONS AND RECOMMENDATIONS

The short talks presented at this 2-day meeting suggest that synthetic biology is at the cusp of many major breakthroughs and that it is perhaps timely to re-define the meaning of "success" in synthetic biology.

There are many hurdles to overcome but the potential for synthetic biology to deliver solutions to many global challenges—improving healthcare, limiting environmental damage, and creating a wide variety of more sustainable processes—is great.

Meeting participants suggested that as a community they should support the measures listed below to help synthetic biology move beyond the proof-of-concept stage and to ensure that potential risks are minimized and dialog with the public can be optimized.

- Larger and longer investment in better big data management and processing (Artificial Intelligence and Machine Learning) systems, and in fundamental research on biosystems modeling, chassis development, and genome mining.
- Support standardization initiatives; while arguably not attractive academically, the community needs to agree and support efforts toward creating interoperability around biosystem modeling, and standards around DNA design (if not DNA bioparts). Without some degree of "standardization" the ability to pool data and models, essential for improving accuracy and reproducibility, will be challenging.
- The creation and funding (ideally internationally) of a "Grand Challenge," such as the development of generic sensors or the creation of protein-based electronic components, could help focus the community toward a target goal.
- Improve the assessment, communication, and management of risk and harm among all audiences.
- Ensure that early career researchers are trained in responsible research conduct and ethics as well as being cognizant of existing rules and regulations around GM (regionally dependent) and the issue of misuse and harm.
- Coordinate the efforts of academia, government and industry through focused meetings that foster interdisciplinary collaborations around shared objectives.
- Improve platforms for knowledge sharing and recognize the value of failures.

The workshop highlighted just how much more we have to learn from Nature itself. Synthetic biology is giving us insights of the criteria and processes that underpin all living systems; in turn, we can take this insight and design and use it to build a "better biology." However, we need to take the public with us on this journey, create meaningful and considered dialogue about the work we may do and the impact it might have on our world.

AUTHOR'S NOTE

The meeting was hosted by the UK Center for Mammalian Synthetic Biology (the Center), based at the University of Edinburgh. The Center is building expertise in cell engineering tool generation, whole-cell modeling, computer-assisted design and construction of DNA and high-throughput phenotyping to enable synthetic biology for medicine and healthcare. The Centre's research will not only advance basic understanding of mammalian biology and pathology but also generate products and services for near-term commercial exploitation by the pharmaceutical and drug testing industries, such as diagnostics, novel therapeutics, protein-based drugs, and regenerative medicines. The Center is funded through the Research Council's UK "Synthetic Biology for Growth" programme and by the Biological and Biotechnology Sciences Research Council (BBSRC), the Engineering and Physical Sciences Research Council and the Medical Research Council.

AUTHOR CONTRIBUTIONS

This is a meeting report and was drafted by MH-F with support from ME and LF.

ACKNOWLEDGMENTS

We are grateful to all colleagues that contributed to discussions at the workshop held in Edinburgh in May 2018 and whose views helped inform this report. We also gratefully acknowledge sponsorship for this workshop from the Office of Naval Research Global and the UK Centre for Mammalian Synthetic Biology (BBSRC Grant BB/M018040/1).

REFERENCES

Boehm, C. R., and Bock, R. (2019). Recent advances and current challenges in synthetic biology of the plastid genetic system and metabolism. *Plant Physiol.* 179, 794–802. doi: 10.1104/pp.18.00767

Boeke, J. D., Church, G., Hessel, A., Kelley, N. J., Arkin, A., Cai, Y., et al. (2016). Genome engineering: the genome project-write. *Science* 8, 126–127. doi: 10.1126/science.aaf6850

Bueso, Y. F., and Tangney, M. (2017). Synthetic biology in the driving seat of the bioeconomy. *Trends Biotechnol.* 35, 373–378. doi: 10.1016/j.tibtech.2017.02.002

Burkard, C. G., Opriessnig, T., Mileham, A. J., Stadejek, T., Ait-Ali, T., Lillico, S. G., et al. (2018). Pigs lacking the scavenger receptor cysteine-rich domain 5 of CD163 are resistant to porcine reproductive and respiratory syndrome virus 1 infection. *J. Virol.* 92, 00415–00418. doi: 10.1128/JVI.00415-18

Callaway, E. (2018). Ban on 'Gene Drives' is back on the UN's agenda - worrying scientists. *Nature* 563, 454–455. doi: 10.1038/d41586-018-07436-4

Cameron, D. E., Bashor, C. J., and Collins, J. J. (2014). A brief history of synthetic biology. *Nat. Rev. Microbiol.* 12, 381–390. doi: 10.1038/nrmicro3239

Carlson, R. (2014). *Time for New DNA Sequencing And Synthesis Cost Curves.* Available online at: https://synbiobeta.com/time-new-dna-synthesis-sequencing-cost-curves-rob-carlson/

Casini, A., Chang, F. Y., Eluere, R., King, A. M., Young, E. M., Dudley, Q. M., et al. (2018). A pressure test to make 10 molecules in 90 days: external evaluation of methods to engineer biology. *J Am Chem Soc.* 140, 4302–4316. doi: 10.1021/jacs.7b13292

Collins, J. (2018). Gene drives in our future: challenges of and opportunities for using a self-sustaining technology in pest and vector management. *BMC Proc.* 12, 37–41. doi: 10.1186/s12919-018-0110-4

Davies, J. A., and Cachat, E. (2016). Synthetic biology meets tissue engineering. *Biochem. Soc. Transac.* 44, 696–701. doi: 10.1042/BST20150289

Decoene, T., De Paepe, B., Maertens, J., Coussement, P., Peters, G., de Maeseneire, S., et al. (2018). Standardization in synthetic biology: an engineering discipline coming of age. *Crit. Rev. Biotechnol.* 38, 647–656. doi: 10.1080/07388551.2017.1380600

Dirisala, V. R., Nair, R. R., Srirama, K., Reddy, P. N., Rao, K. R. S. S., and Kumar P. G. (2017). Recombinant pharmaceutical protein production in plants: unraveling the therapeutic potential of molecular pharming. *Acta Physiol. Plant* 39, 18–26. doi: 10.1007/s11738-016-2315-3

Dolgin, E. (2018). Scientists downsize bold plan to make human genome from Scratch. *Nature* 557, 16–17 doi: 10.1038/d41586-018-05043-x

Dou, J., and Bennett, M. R. (2018). Synthetic biology and the gut microbiome. *Biotechnol J.* 13:1700159. doi: 10.1002/biot.201700159

Dunbar, C. E., High, K. A., Joung, J. K., Kohn, D. B., Ozawa, K., and Sadelain, M. (2018). Gene therapy comes of age. *Science* 359:6175 doi: 10.1126/science.aan4672

Emmanuel, M., Chapman, R., Williamson, A. L., Rybicki, E. P., and Meyers, E. (2018). Production of complex viral glycoproteins in plants as vaccine immunogens. *Plant Biotechnol. J.* 16, 1531–1545. doi: 10.1111/pbi.12963

Evangelos, T. C., and O'connor, S. E. (2016). New developments in engineering plant metabolic pathways. *Curr. Opin. Biotechnol.* 42, 126–132. doi: 10.1016/j.copbio.2016.04.012

Fletcher, E., Krivoruchko, A., and Nielsen, J. (2016). Industrial systems biology and its impact on synthetic biology of yeast cell factories. *Biotechnol. Bioeng.* 113, 1164–1170. doi: 10.1002/bit.25870

French, K. E. (2019). Harnessing synthetic biology for sustainable development. *Nat. Sustain.* 2, 250–252. doi: 10.1038/s41893-019-0270-x

Gabriele, L., Benenson, Y., and Khammash, M. (2018). Synthetic control systems for high performance gene expression in mammalian cells. *Nucleic Acids Res.* 46, 9855–9863. doi: 10.1093/nar/gky795

Gnanasekaran, T., Karcher, D., Nielsen, A. Z., Martens, H. J., Ruf, S., Olsen, C. E., et al. (2016). Transfer of the cytochrome P450-dependent dhurrin pathway from sorghum bicolor into *Nicotiana tabacum* chloroplasts for light-driven synthesis. *J. Exp. Botany* 67, 2495–2506. doi: 10.1093/jxb/erw067

June, C. H., O'Connor, R. S., Kawalekar, O. U., Ghassemi, S., Milone, M. C., et al. (2018). CAR T cell immunotherapy for human cancer. *Science* 359, 1361–1365 doi: 10.1126/science.aar6711

Karzbrun, E., Tayar, A. M., Noireaux, V., and Bar-Ziv, R. H. (2014). Synthetic biology. Programmable On-chip DNA compartments as artificial cells. *Science* 345, 829–832. doi: 10.1126/science.1255550

Koch, M., Faulon, J.-L., and Borkowski, O. (2018). Models for cell-free synthetic biology: make prototyping easier, better, and faster. *Front. Bioeng. Biotech.* 6:182 doi: 10.3389/fbioe.2018.00182

Kosuri, S., and Church, G. (2014). Large-scale *de novo* DNA synthesis: technologies and applications. *Nat. Methods* 11, 499–507 doi: 10.1038/nmeth.2918

Le Feuvre, R., and Scrutton, N. (2018). A living foundry for synthetic biological materials: a synthetic biology roadmap to new advanced materials. *Synthet. Syst. Biotechnol.* 3, 105–112. doi: 10.1016/j.synbio.2018.04.002

Libis, V., Baudoin, D., and Faulon, J. L. (2016). Expanding biosensing abilities through computer-aided design of metabolic pathways. *ACS Synthet. Biol.* 5, 1076–1085. doi: 10.1021/acssynbio.5b00225

Ljubetič, A., Gradišar, H., and Jerala, R. (2017). Advances in design of protein folds and assemblies. *Curr. Opin. Chem. Biol.* 40, 65–71. doi: 10.1016/j.cbpa.2017.06.020

Maysam, M., Strittmatter, T., and Fussenegger, M. (2019). Light-controlled mammalian cells and their therapeutic applications in synthetic biology. *Adv. Sci.* 6:1800952 doi: 10.1002/advs.201800952

Pablo, N., and de Lorenzo, V. (2018). *Pseudomonas putida* as a functional chassis for industrial biocatalysis: from native biochemistry to trans-metabolism. *Metabol. Eng.* 50, 142–155. doi: 10.1016/j.ymben.2018.05.005

Sainsbury, F., and Lomonossoff, G. (2014). Transient expressions of synthetic biology in plants. *Curr. Opin. Plant Biol.* 19, 1–7 doi: 10.1016/j.pbi.2014.02.003

Satoshi, T., Blauch, L. R., Tang, S. K. Y., Morsut, L., and Lim, W. (2018). Programming self-organizing multicellular structures with synthetic cell-cell signaling. *Science* 361, 156–162. doi: 10.1126/science.aat0271

Sauro, H. M., Hare, D., Kwiatkowska, M., Uhrmacher, A. M., Hucka, M., Mendes, P., et al. (2006). "Challenges for modeling and simulation methods in systems biology," in *Proceedings of the 2006 Winter Simulation Conference* (2006). Available online at: http://qav.comlab.ox.ac.uk/papers/winter_sim06_panel.pdf

Tait, G., Banda, A., and Watkins, A. (2017). *Proportionate and Adaptive Governance of Innovative Technologies (PAGIT): A Framework to Guide Policy and Regulatory Decision Making.* Innogen Institute. Available online at: https://www.innogen.ac.uk/reports/1222

Teixeira, P., and Fussenegger, M. (2019). Engineering mammalian cells for disease diagnosis and treatment. *Curr. Opin. Biotechnol.* 55, 87–94. doi: 10.1016/j.copbio.2018.08.008

Villarreal, F., and Tan, C. (2017). Cell-free systems in the new age of synthetic biology. *Front. Chem. Sci. Eng.* 11, 58–65. doi: 10.1007/s11705-017-1610-x

Wang, F., and Zhang, W. (2019). Synthetic biology: recent progress, biosafety and biosecurity concerns, and possible solutions. *J. Biosafety Biosecur.* 1, 22–30 doi: 10.1016/j.jobb.2018.12.003

Wang, P., Chang, A. Y., Novosad, V., Chupin, V. V., Schaller, R. D., and Rozhkova, E. A. (2017). Cell-free synthetic biology chassis for nanocatalytic photon-to-hydrogen conversion. *ACS Nano*. 11, 6739–6745. doi: 10.1021/acsnano.7b01142

Ye, H., Daoud-El Baba, M., Peng, R.-W., and Fussenegger, M. (2011). A Synthetic optogenetic transcription device enhances blood-glucose homeostasis in mice. *Science* 332, 1565–1568. doi: 10.1126/science.1203535

Zhang, R., Li, C., Wang, J., Yang, Y., and Yan, Y. (2018). Microbial production of small medicinal molecules and biologics: from nature to synthetic pathways. *Biotechnol Adv*. 36, 2219–2231. doi: 10.1016/j.biotechadv.2018.10.009

Conflict of Interest Statement: The authors declare that the research was conducted in the absence of any commercial or financial relationships that could be construed as a potential conflict of interest.

frontiers in Bioengineering and Biotechnology

ORIGINAL RESEARCH
published: 21 March 2019
doi: 10.3389/fbioe.2019.00046

ParAlleL: A Novel Population-Based Approach to Biological Logic Gates

Felipe A. Millacura, Brendan Largey and Christopher E. French**

School of Biological Sciences, Institute of Quantitative Biology, Biochemistry and Biotechnology, University of Edinburgh, Edinburgh, United Kingdom

In vivo logic gates have proven difficult to combine into larger devices. Our cell-based logic system, ParAlleL, decomposes a large circuit into a collection of small subcircuits working in parallel, each subcircuit responding to a different combination of inputs. A final global output is then generated by a combination of the responses. Using ParAlleL, for the first time a completely functional 3-bit full adder and full subtractor were generated using *Escherichia coli* cells, as well as a calculator-style display that shows a numeric result, from 0 to 7, when the proper 3 bit binary inputs are introduced into the system. ParAlleL demonstrates the use of a parallel approach for the design of cell-based logic gates that facilitates the generation and analysis of complex processes, without the need for complex genetic engineering.

Keywords: *Escherichia coli*, 3-bits, full adder, full subtractor, calculator-like display, parallel approach

OPEN ACCESS

Edited by:
Jussi Jantti,
VTT Technical Research Centre of Finland Ltd, Finland

Reviewed by:
Thomas Dandekar,
University of Wuerzburg, Germany
Chris John Myers,
The University of Utah, United States

****Correspondence:***
Felipe A. Millacura
S1647595@sms.ed.ac.uk
Christopher E. French
c.french@ed.ac.uk

Specialty section:
This article was submitted to Synthetic Biology, a section of the journal Frontiers in Bioengineering and Biotechnology

Received: *17 December 2018*
Accepted: *27 February 2019*
Published: *21 March 2019*

Citation:
Millacura FA, Largey B and French CE (2019) ParAlleL: A Novel Population-Based Approach to Biological Logic Gates. Front. Bioeng. Biotechnol. 7:46. doi: 10.3389/fbioe.2019.00046

INTRODUCTION

A major challenge in the field of synthetic biology is the construction of complex logic circuits that analyze variables as in electronics; where a single circuit accepts one or more binary inputs to generate one or more binary outputs. A cell-based logic network consists of engineered cells producing an output macromolecule only if the corresponding pattern of inputs is present. The mechanism of analysis is commonly based on the use of transcriptional regulators, transcription factors, polymerases, receptors, or recombinases (Brenner et al., 2018). Some examples of genetic circuits mimicking computational behavior are toggle switches, oscillators, boolean logic gates, feedback controllers, and multiplexers. Although there are genetic circuits that simulate computational behavior, the complex engineering of their biological chassis is affected by gene expression noise, mutation, cell death, undefined, and changing extracellular environments and improper interactions with the cellular context (Andrianantoandro et al., 2006). Furthermore, complex genetic engineering is necessary when multiple input variables are analyzed, limiting the processing capacity of the system.

Biological multiplexers analyze one or more signals over a common transmission line using interconnected transcription factors, recombinases, antisense RNA, or CRISPR-like technology (Nielsen and Voigt, 2014; Roquet et al., 2016; Brenner et al., 2018). However, complex genetic engineering is needed for wiring the basic computational units, becoming inefficient for moving beyond simple NOT or AND logic gates or for scaling to 3 bit logic circuits. The complexity of the genetic engineering required can be reduced by using distributed logic circuits, where the computation is distributed among several physically separated cellular consortia that each sense only one signal and respond by secreting a communication molecule (Regot et al., 2011). As a circuit responds to one signal, but not another, due to spatial distribution, a change in the state of the system can be triggered as response, making synthetic learning possible

(Macia et al., 2017; Shipman et al., 2017). Even though the consortium approach makes Boolean circuit design simpler, it still shows a slow response and considerable complexity since each cell needs to recognize, synthesize and secrete a wiring molecule (Macia et al., 2016).

Here we propose an alternative logic architecture, which decomposes a large circuit into a collection of small subcircuits acting in parallel (hereafter ParAlleL). Rather than having a single type of agent (such as a genetically engineered cell) doing the computation, ParAlleL has separate types of agent that each react to a different combination of inputs. A final output is then generated by combination of the responses, making all kinds of binary operation possible. As an example, here we show the implementation of this concept using cells resistant to different combinations of antibiotics, with the response indicated by growth. This is used to demonstrate a completely functional 3 bit full adder and full subtractor, as well as a calculator-style display that shows digits from 0 to 7 based on three binary input bits.

METHODOLOGY

Reagents and Stock Solution Preparations

Antibiotic stock solutions were prepared as follows: 100 mg/ml carbenicilin disodium salt (Sigma-Aldrich #C1389), 50 mg/ml kanamycin sulfate (PanReac Applichem #A1493), 20 mg/ml chloramphenicol (Acros Organics #22792), 10 mg/ml tetracycline hydrochloryde (Duchefa Biochemie #T0150), 10 mg/ml gentamicin sulfate (Melford #G0124), and 50 mg/ml spectinomycin.HCl (LKT Labs #S6018). Developing solution contained 0.1 %w/v bromothymol blue (Sigma-Aldrich #114421) and 400 mM Trizma base pH7.5 (Sigma-Aldrich #T1503).

Generation of Subcircuit Cells

E. coli JM109 was transformed with 200–300 pg of plasmid pSB4A5 (AmpR) or pSB4C5 (ChlR) (Registry of Standard Biological Parts) and selected on 100 μg/ml carbenicilin (Am) or 20 μg/ml chloramphenicol (Ch), respectively. Cells carrying the first bit plasmid were made chemically competent (Chung et al., 1989) and transformed with 200–300 pg of the 2nd bit plasmid, pSB1T3 (TetR) or pSB1K3 (KanR) (Registry of Standard Biological Parts). Selection was performed with the first antibiotic (Am or Ch) and the addition of 10 μg/ml Tetracycline (Tc) or 50 μg/ml kanamycin (Km), obtaining the two-bit combinations Km/Am (KA), Tc/Am (TA), Km/Ch (KC), and Tc/Ch (TC). This set of strains is sufficient to implement all two-bit binary operations.

The third bit layer was generated by transforming these four strains with pSEVA631 (GenR) (Silva-Rocha et al., 2012; GenBank JX560348) or pMO9075 (SpmR) (Keller et al., 2011). Resulting strains were selected on the 2-bit antibiotic combinations plus 10 μg/ml gentamicin (Gm) or 50 μg/ml spectinomycin (Sm). This gave 8 strains, designated ATG (Am/Tc/Gm), AKG (Am/Km/Gm), ATS (Am/Tc/Sm), AKS (Am/Km/Sm), CTG (Ch/Tc/Gm), CTS (Ch/Tc/Sm), CKG (Ch/Km/Gm), CKS (Ch/Km/Sm) based on their resistance markers. This set of strains is sufficient to implement all three-bit binary operations. Plasmid specifications are listed in **Figure S2**, **Tables S1, S3**, with further information about these antibiotics in **Table S2**. Plasmid sequences are available in different formats at https://doi.org/10.7488/ds/2497.

Three-Bit Logic Operations

Tests were performed in 96-well microplates by inoculating cells (1:100) in LB broth (100 μL) supplemented with 1%w/v D(+)-glucose (Fisher Chemical #G0500). Plates were incubated for 18 h at 37°C without shaking and then developed by addition of the developing solution (0.1%w/v bromothymol blue in 400 mM

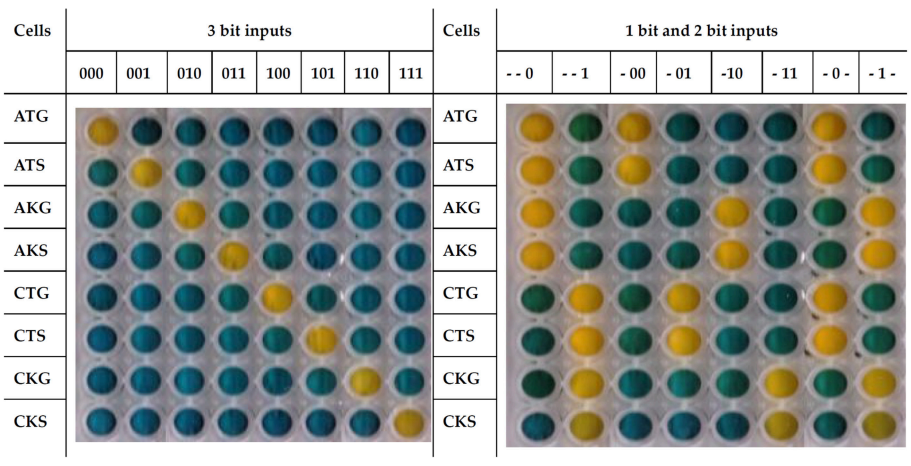

FIGURE 1 | ParAlleL responding to 1 bit, 2 bit, and 3 bit inputs. ParAlleL subcircuit cells were spatially distributed in different wells (vertically) and exposed to specified 1 bit, 2 bit, or 3 bit inputs (top of each column). Cells were inoculated (1:100) in LB supplemented with 1% w/v glucose. After 18 h of incubation at 37°C, plates were developed by addition of 0.05 volumes of the developing solution.

A Calculator-like display design

A	B	C
D	---	E
F	G	H
I	---	J
K	L	M

No. to display	A	B	C	D	E	F	G	H	I	J	K	L	M
000 (0)	ATG	ATG	ATG	ATG	ATG	ATG	----	ATG	ATG	ATG	ATG	ATG	ATG
001 (1)	----	----	ATS	----	ATS	----	----	ATS	----	ATS	----	----	ATS
010 (2)	AKG	AKG	AKG	----	AKG	AKG	AKG	AKG	AKG	----	AKG	AKG	AKG
011 (3)	AKS	AKS	AKS	----	AKS	AKS	AKS	AKS	----	AKS	AKS	AKS	AKS
100 (4)	CTG	----	CTG	CTG	CTG	CTG	CTG	CTG	----	CTG	----	----	CTG
101 (5)	CTS	CTS	CTS	CTS	----	CTS	CTS	CTS	----	CTS	CTS	CTS	CTS
110 (6)	CKG	CKG	CKG	CKG	----	CKG	CKG	CKG	CKG	CKG	CKG	CKG	CKG
111 (7)	CKS	CKS	CKS	----	CKS	----	----	CKS	----	CKS	----	----	CKS

B ParAlleL 3 bit display outputs

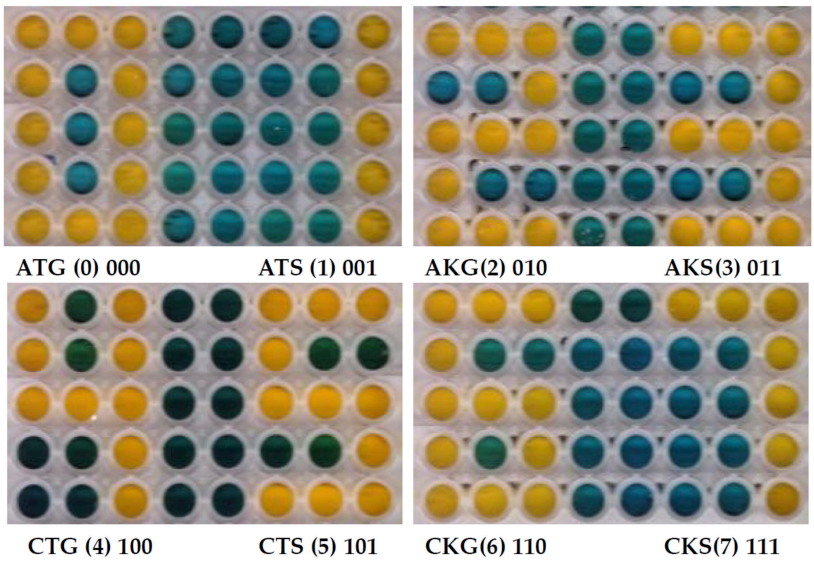

FIGURE 2 | Digital calculator-like display using 3 bit ParAlleL. Figure shows all numerals from zero to seven based on the 8 binary inputs provided. **(A)** Subcircuit cells were mixed and distributed in a 3 × 5 matrix and inoculated (1:100) in LB supplemented with 1%w/v glucose. Plate was developed after 18 h of incubation, by addition of 0.05 volumes of developing solution. **(B)** Output number results obtained by addition of each 3 bit antibiotic combination.

Tris, pH7.5) in a ratio 1:20. Images were obtained using a Kodak ESPC315 Flatbed scanner. Design of the calculator-like display, full adder, and subtractor are shown in **Figures 2**, **3** and in Supplementary material (**Figure S3**). Raw figures were deposited at https://doi.org/10.7488/ds/2497.

RESULTS

In the distributed logic system of ParAlleL each input bit has two forms, ZERO and ONE, each of which is essential to certain output agents and inhibitory to others. Thus each agent reacts only to a certain combination of input bits, allowing generation of any arbitrary pattern of outputs for any pattern of inputs. In the implementation shown here, each input bit comes in two forms, each being an antibiotic lethal to sensitive strains. In this case, bit A is represented by ampicillin for zero, chloramphenicol for one, bit B by kanamycin for zero, tetracycline for one, and bit C by gentamicin for zero, spectinomycin for one. Thus, four strains are needed to implement any operation with two input bits, and eight strains for three input bits. In contrast to other cell-based logic schemes, only very minimal genetic engineering is required, essentially transformation with 3 different antibiotic resistance markers.

Cells show a global response concordant with the behavior expected for a 1 bit, 2 bit, or 3 bit system (**Figure 1**). For instance, when the input 101 (chloramphenicol, tetracycline and spectinomycin) is added to the system growth is only observed in the corresponding CTS cells, which carry the proper resistance markers. The response time of the system is around 12 h (**Figure S1**) but plates were developed at 18 h to avoid false negatives or positives.

In order to further test the ParAlleL system, a digital calculator-like display was designed (**Figure 2A**). In this case, multiple subcircuit cells are mixed in one well and the global response displays a number from 0 to 7 when the proper binary input is applied. Numbers represent the total eight possible values encoded within 3-bit binary inputs.

				Adder				Subtractor			
C_{in}/B_{in}	B/Y	A/X	Antibiotic	C_{out}	S	C_{out}	S	B_{out}	D	B_{out}	D
0	0	0	ATG	0	0			0	0		
0	0	1	ATS	0	1			1	1		
0	1	0	AKG	0	1			1	1		
0	1	1	AKS	1	0			1	0		
1	0	0	CTG	0	1			0	1		
1	0	1	CTS	1	0			0	0		
1	1	0	CKG	1	0			0	0		
1	1	1	CKS	1	1			1	1		

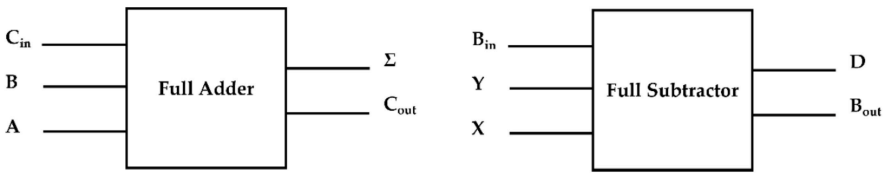

FIGURE 3 | Full adder and subtractor using the 3 bit ParAlleL system. The figure shows results of addition and subtraction using the ParAlleL for 3 bit system. Cells were mixed as shown in **Figure S3** and inoculated (1:100) in LB supplemented with 1%w/v glucose. After 18 hours of incubation, the plate was developed by addition of the 0.05 volumes of developing solution.

Input configuration versatility was proven by representing bit A in this case by gentamicin for zero, spectinomycin for one, bit B by kanamycin for zero, tetracycline for one, and bit C by ampicillin for zero, chloramphenicol for one. For instance, once input 110 represented by Ch/Km/Gm is added in the system, the number 6 is displayed (**Figure 2**).

Finally, a full adder and a full subtractor were designed. A full-adder adds three binary inputs, often denoted as A, B, and C_{in}, generating a Sum result (S) and a Carry-out (C_{out}). A full subtractor, on the other hand, has a minuend (X), a subtrahend (Y) and an additional Borrow-in (B_{in}) as inputs. The subtraction operation produces a difference (D) and a Borrow (B_{out}) (**Figure 3**).

In order to generate the full adder and subtractor, multiple subcircuit cells were mixed and distributed in two different wells (**Figure S3**). One well represents the solution (S) or difference (D) and a second one the carry (C_{out}) or borrow (B_{out}), for the adder and subtractor, respectively (**Figure 3**). A yellow color represents growth and a positive output 1, a blue color represents no growth and a binary 0 output instead.

CONCLUSIONS/DISCUSSION

Subcircuits that solve complex calculations in parallel have been extensively used for computation in order to reduce the total computation time. Translating this approach to biological systems would allow us to analyze complex processes, currently difficult in synthetic biology, as multiple simple sub-circuits.

In our proof of concept, we present a biological information processing system, ParAlleL, capable of exploiting the parallelism in mixed bacterial cultures. ParAlleL decomposes the analysis of 2 and 3 bit complex inputs, into 4 and 8 sub circuits, respectively (**Figure 1**). Each sub-circuit corresponds to a different *E. coli* strain carrying a different combination of antibiotic resistance markers (**Table S1**). As an example, in the 3 bit system the input 000 is represented by the antibiotics ampicillin, tetracycline and gentamicin (**Figure 1**). When this input is entered into the system, all cells that are not encoded for responding to 000 will die, but cells carrying the proper plasmid combination, pSB4A5, pSB1T3, and pSEVA621 will not (**Figures 1**, **2**), therefore, a live/dead response (output) is achieved in all sub circuits, the output of each well being one (growth) or zero (failure to grow) (**Figure 2** and **Figure S2**).

ParAlleL uses cellular consortia instead of a single type of cell. A similar approach has been developed by Macia et al. (2016, 2017) using eukaryotic cells, and even showing the possibility of generating transient memory. However, that approach requires a sophisticated design as it relies on a secreted intermediate molecule (hormone-like) that must be kept at the right production level, and that should be previously activated by X (Repressor) and Y (SsrA-tagged protein) degradation. Furthermore, since the output of the circuit is distributed among different consortia, the concentration of the secreted molecule

can differ according to the number of cells simultaneously producing it. This kind of multicellular approach and others based on single cells require sophisticated wiring design (Silva-Rocha and de Lorenzo, 2008; Siuti et al., 2013; Macia et al., 2016, 2017). By contrast, ParAlleL requires very minimal genetic modification and little tuning to obtain reliable outputs (**Figures 2**, **3**).

The implementation of ParAlleL presented here is simple, but its further development to useful applications presents a number of challenges. Firstly, expansion to 4 bits and beyond would require further well-behaved and non-cross-reacting antibiotic resistance markers, and would probably lead to even greater disparities in growth rate than those observed in the three-bit system (**Figure S1**). This could be addressed, and the flexibility and usefulness of the system increased, by moving away from direct use of antibiotics to a system using tightly controlled inducible promoters, each controlling a lethal "death gene," such as *ccdB,* with either the presence or absence of the inducer leading to lethality. In this way the system could be made to respond to different combinations of useful inputs, for example in the construction of multiplexed biosensors.

However, to achieve the full potential of ParAlleL, it will be necessary to generate layered systems in which the output from one layer serves as input to another layer. This might be accomplished via quorum sensing, but the implementation would be rather complex and limited. A more attractive option is to transfer the same concept, using a set of agents which each responds to a single combination of inputs, to an alternative system. For example, the concept could be implemented in a cell-free system, in which inputs may be present as small molecules interacting with transcription factors, or as DNA or RNA oligonucleotides. Outputs from the first layer, in the form of DNA or RNA molecules generated by DNA replication (e.g., PCR) or transcription, could then serve as inputs to a second layer. For example, in a PCR-based approach, one of a set of templates would be amplified based on which primer oligonucleotides were added; the output PCR product could then be processed to generate another set of oligonucleotides, or used directly to initiate priming on a second set of templates via formation of three-way junctions. Alternatively, in a transcription-based system, output RNAs from a first layer computation could act as guide RNAs directing binding of CRISPR-based transcription factors to further templates to generate a new set of guide RNAs, eventually leading to production of an output RNA such as a mRNA leading to translation of a visually detectable signal.

Another interesting aspect of ParAlleL is that, since the final output is the result of a population-based calculation, these systems may show a level of "Byzantine fault tolerance," allowing reliable outcomes even in the face of levels of noise which are unavoidable in biological systems. This would represent a new level of robustness in biological computation systems.

DATA AVAILABILITY

All datasets generated for this study are included in the manuscript and/or the supplementary files. More Data is available at https://doi.org/10.7488/ds/2497.

AUTHOR CONTRIBUTIONS

FM and CF conceived and designed the experiments. FM and BL performed the experiments. FM and CF analyzed and validated the data. FM and CF contributed reagents, materials, and analysis tools. FM and CF wrote—reviewed & edited the manuscript.

FUNDING

This work was supported by CONICYT/BC-PhD 721 70403 (FM).

ACKNOWLEDGMENTS

The authors acknowledge the valuable assistance of Dr. Louise Horsfall for supplying the pMO9075 plasmid and Dr. Aitor De las Heras for supplying the pSEVA631 plasmid. A pre-print version of the manuscript has been published on bioRxiv (Millacura et al., 2018).

SUPPLEMENTARY MATERIAL

The Supplementary Material for this article can be found online at: https://www.frontiersin.org/articles/10.3389/fbioe.2019.00046/full#supplementary-material

REFERENCES

Andrianantoandro, E., Basu, S., Karig, D. K., and Weiss, R. (2006). Synthetic biology: new engineering rules for an emerging discipline. *Mol. Syst. Biol.* 2:2006.0028. doi: 10.1038/msb4100073

Brenner, M. J., Cho, J. H., Wong, N. M. L., and Wong, W. W. (2018). Synthetic biology: immunotherapy by design. *Annu. Rev. Biomed. Eng.* 20, 95–118. doi: 10.1146/annurev-bioeng-062117-121147

Chung, C. T., Niemela, S. L., and Miller, R. H. (1989). One-step preparation of competent Escherichia coli: transformation and storage of bacterial cells in the same solution. *Proc. Natl. Acad. Sci. U.S.A.* 86, 2172–2175. doi: 10.1073/pnas.86.7.2172

Keller, K. L., Wall, J. D., and Chhabra, S. (2011). "Methods for engineering sulfate reducing bacteria of the genus *Desulfovibrio*," in *Methods in Enzymology. Vol. 497.* ed C. Voigt (California, CA: Academic Press), 503–517.

Macia, J., Manzoni, R., Conde, N., Urrios, A., de Nadal, E., Solé, R., et al. (2016). Implementation of complex biological logic circuits using spatially distributed multicellular consortia. *PLoS Comput. Biol.* 12:e1004685. doi: 10.1371/journal.pcbi.1004685

Macia, J., Vidiella, B., and Solé, R. V. (2017). Synthetic associative learning in engineered multicellular consortia. *J. R. Soc. Interface* 14:20170158. doi: 10.1098/rsif.2017.0158

Millacura, F. A., Largey, B., and French, C. E. (2018). BioLogic, a parallel approach to cell-based logic gates. *bioRxiv* [Preprint]. doi: 10.1101/303032

Nielsen, A. A., and Voigt, C. A. (2014). Multi-input CRISPR/Cas genetic circuits that interface host regulatory networks. *Mol. Syst. Biol.* 10:763. doi: 10.15252/msb.20145735

Regot, S., Macia, J., Conde, N., Furukawa, K., Kjellén, J., Peeters, T., et al. (2011). Distributed biological computation with multicellular engineered networks. *Nature* 469, 207–211. doi: 10.1038/nature09679

Roquet, N., Soleimany, A. P., Ferris, A. C., Aaronson, S., and Lu, T. K. (2016). Synthetic recombinase-based state machines in living cells. *Science* 353:aad8559. doi: 10.1126/science.aad8559

Shipman, S. L., Nivala, J., Macklis, J. D., and Church, G. M. (2017). CRISPR–Cas encoding of a digital movie into the genomes of a population of living bacteria. *Nature* 547, 345–349. doi: 10.1038/nature23017

Silva-Rocha, R., and de Lorenzo, V. (2008). Mining logic gates in prokaryotic transcriptional regulation networks. *FEBS Lett.* 582, 1237–1244. doi: 10.1016/j.febslet.2008.01.060

Silva-Rocha, R., Martínez-García, E., Calles, B., Chavarría, M., Arce-Rodríguez, A., de Las Heras, A., et al. (2012). The Standard European Vector Architecture (SEVA): a coherent platform for the analysis and deployment of complex prokaryotic phenotypes. *Nucleic Acids Res.* 41, D666–D675. doi: 10.1093/nar/gks1119

Siuti, P., Yazbek, J., and Lu, T. K. (2013). Synthetic circuits integrating logic and memory in living cells. *Nat. Biotechnol.* 31, 448–452. doi: 10.1038/nbt.2510

Conflict of Interest Statement: The authors declare that the research was conducted in the absence of any commercial or financial relationships that could be construed as a potential conflict of interest.

Advantages of publishing in Frontiers

OPEN ACCESS
Articles are free to read for greatest visibility and readership

FAST PUBLICATION
Around 90 days from submission to decision

HIGH QUALITY PEER-REVIEW
Rigorous, collaborative, and constructive peer-review

TRANSPARENT PEER-REVIEW
Editors and reviewers acknowledged by name on published articles

Frontiers
Avenue du Tribunal-Fédéral 34
1005 Lausanne | Switzerland

Visit us: www.frontiersin.org
Contact us: info@frontiersin.org | +41 21 510 17 00

REPRODUCIBILITY OF RESEARCH
Support open data and methods to enhance research reproducibility

DIGITAL PUBLISHING
Articles designed for optimal readership across devices

FOLLOW US
@frontiersin

IMPACT METRICS
Advanced article metrics track visibility across digital media

EXTENSIVE PROMOTION
Marketing and promotion of impactful research

LOOP RESEARCH NETWORK
Our network increases your article's readership